Journal of Computers

ISSN 1796-203X

Volume 9, Number 6, June 2014

Contents

REGULAR PAPERS

Statistical Analysis of Influences of ICT on Industrial Structure Changes from 1985 through 2005: The Case of Japan 1291
Ubaidillah Zuhdi, Shunsuke Mori, and Kazuhisa Kamegai

An Improved Shuffled Frog Leaping Algorithm with Single Step Search Strategy and Interactive Learning Rule for Continuous Optimization 1300
Deyu Tang, Yongming Cai, and Jie Zhao

Hardware/Software Partitioning Algorithm Based on Genetic Algorithm 1309
Guoshuai Li, Jinfu Feng, Junhua Hu, Cong Wang, and Duo Qi

Spectral Clustering with Neighborhood Attribute Reduction Based on Information Entropy 1316
Hongjie Jia, Shifei Ding, Heng Ma, and Wanqiu Xing

Evaluation of Detrending Method Based on Ensemble Empirical Mode Decomposition for HRV Analysis 1325
Chao Zeng and Xiaowen Xu

A Feature Selection Approach of Inconsistent Decision Systems in Rough Set 1333
Lin Sun, Jiucheng Xu, and Yuhui Li

Real Time Pedestrian Detection Algorithm by Mean Shift 1341
Qing Tian, Shuai Qiao, Teng Guo, and Yun Wei

Enhancing Keylogger Detection Performance of the Dendritic Cell Algorithm by an Enticement Strategy 1347
Jun Fu, Huan Yang, Yiwen Liang, and Chengyu Tan

Shape-Matching Model Optimization Using Discrete-point Sampling and Feature Salience 1355
Zongxiao Zhu and Guoyou Wang

Multi-label Classification Using Hypergraph Orthonormalized Partial Least Squares 1364
Gaofeng Luo, Tongcheng Huang, and Zijuan Shi

Research on Cloud-Based Mass Log Data Management Mechanism 1371
Fengying Yang, Huichao Liu, and Zhanping Zhao

Design of Wind-solar Complementary Power System Based on Progressive Fuzzy Control 1378
Ning Chen, Xiao Qu, Weibing Weng, and Xing Xu

Adaptive Control based Particle Swarm Optimization and Chebyshev Neural Network for Chaotic Systems 1385
Zhen Hong, Xile Li, and Bo Chen

Relay Node Scheduling Model Based on Improved Discrete Markov Chain 1391
Chaoyi Zhang, Yandong Zhao, and Junguo Zhang

Multiplexing Periodic CSI with HARQ-ACK on PUCCH Format 3 in LTE-A 1397
Dan Wang, Xuemei Deng, Xiaowen Li, and Xin Ni

Restricted Nussbaum Gain Control Method and Its Application in One Order System 1402
Jinyong Yu, Junwei Lei, Yuqiang Jin, and Hongchao Zhao

Chinese Sentiment Analysis Using Appraiser-Degree-Negation Combinations and PSO 1410
Wen Xiong, Yaohong Jin, and Zhiying Liu

Image Denoising via Robust Simultaneous Sparse Coding 1418
Lei Li, Jiangming Kan, and Wenbin Li

DDoS: Flood vs. Shrew 1426
Zhijun Wu, Guang Li, Meng Yue, and Hualong Zeng

A Dynamic Load-balancing Scheme for XPath Queries Parallelization in Shared Memory Multi-core Systems 1436
Xiaocheng Huang, Xujie Si, Xiaojie Yuan, and Chao Wang

Research on Template Computing Mode of Remote Sensing Image Based on Partition Model 1446
Gen-yuan Du, De-lan Xiong, and Huo-lin Zhang

A Novel Sink Mobility Off-line Algorithm for Avoiding Energy Hole in Wireless Sensor Network 1454
Qing-hua Li, Qiao-ming Pan, and Fu-ping Xie

A Robust and Efficient Evolutionary Algorithm based on Probabilistic Model 1462
Caichang Ding and Wenxiu Peng

Tasks Distribution Strategy based on Cluster in MWfSCC 1470
Xiuguo Wu

A P2P Traffic Management Model Based on an ISP Game 1478
Chunzhi Wang, Shuping Wang, Hui Xu, and Hongwei Chen

Study of Scraping Guide Ways Inspection 1484
Ching Wei Wu, Ying Shing Shiao, and Ching Feng Chang

Stereo Matching Using Iterative Dynamic Programming Based on Color Segmentation of Images 1491
Fuzhi Wang, Changlin Song, and Qiang Du

A SVD Feature based Watermarking Algorithm for Gray-level Image Watermark 1497
Wei Wang, Wenhui Li, Yongkui Liu, and Borut Žalik

Object Tracking via Tensor Kernel Space Projection 1503
Jiashu Dai, Tingquan Deng, Tianzhen Dong, and Kejia Yi

A Research of Image Difference Algorithm Based on the Correlation of Color Attributes 1511
Xiangyang Xu, Qiao Chen, Ziqi Zhao, Gang Zhang, and Jiang Duan

Statistical Analysis of Influences of ICT on Industrial Structure Changes from 1985 through 2005: The Case of Japan

Ubaidillah Zuhdi
Department of Industrial Administration, Graduate School of Science and Technology,
Tokyo University of Science, Noda, Japan
School of Business and Management, Institut Teknologi Bandung, Bandung, Indonesia
Email: ubaidillah.zuhdi@gmail.com

Shunsuke Mori and Kazuhisa Kamegai
Department of Industrial Administration, Tokyo University of Science, Noda, Japan
Email: sh_mori@rs.noda.tus.ac.jp and kamegai@rs.tus.ac.jp

***Abstract*—The purpose of this study is to analyze the role that information and communication technology (ICT) has played in changes of Japanese industrial structure; this analysis will be conducted by statistical analysis on input-output (IO) tables. In this study, we focus on ICT capital stock as the key driver, where ICT capital stock comprises computers (including computer accessories) and telecommunications equipment available during 1985 to 2005. Constrained multivariate regression (CMR) modeling is employed for analysis. A likelihood ratio test (LRT) is used for evaluating the statistical significance of model. At the macro level, this study analyzes the results of LRT calculations; at the micro level, this study analyzes the changes of IO coefficients. LRT calculation results confirms that the explanatory variables (computers, main parts and accessories; telecommunications equipment) induced structural changes in most (jointly, in all) Japanese industrial sectors from 1985 through 2005. The CMR model results show that the impact of these explanatory variables on the IO coefficients differed by sector. These differing effects reveal that internal factors in industrial sectors are more complex than macro-level factors and that further investigation is needed to clarify the discovered micro-level differences.**

***Index Terms*—ICT, industrial structure changes, constrained multivariate regression, likelihood ratio test, Japan**

I. Introduction

Technology is used every day by people around the world. For example, people use transportation tools, such as cars, motorcycles, and trains when they commute. Moreover, people use technology in their hobbies, too, such as photography, travel, and sports. Such examples affirm that technology is inseparable from modern daily life.

The importance of technology has also been studied by many researchers. Technology now affects, and is affected by, nearly every aspect of human life [1]. Technology is a major factor in the path of history and the shape of society [2]. For the future, green technology will have an important role in power generation as countries efforts to reduce dependence imported and polluting fuels and pursue energy independence [3].

One frequently used class of technology is information and communication technology (ICT). The use of ICT has recently become highly visible. We frequently see people using phones, both fixed line and mobile, for communicating with others, and a similar pattern can be seen in the use of the Internet. Nearly every aspect of modern society relies on the Internet. The Internet has become a powerful tool for both micro- and macro-level activities. Millions of people spend time each day accessing and creating information online [4].

ICT has been studied extensively. Ref. [5] explored the correlations between different dimensions of ICT investment and aspects of human development. Their research examined 51 countries, which were divided into three groups based on income: high, middle, and low. Ref. [6] developed the definitions and hierarchies necessary for rigorous study of ICT. Ref. [7] assessed the role of ICT in enhancing access to agricultural information for developing agriculture and agribusiness in Tanzania.

Ref. [8] examined the spatial correlation between investment in ICT and economic growth of economy by using the generalized method of moments. Their study focused on OPEC member countries from 1990 to 2007. Ref. [9] investigated the role of ICT sectors in structural changes of the Indonesian economy from 1990 to 2005 by decomposition analysis, a tool for analyzing input-output (IO) data. Ref. [10] used an IO approach to explore how to encourage the growth of ICT sectors in Indonesia.

Corresponding author: Ubaidillah Zuhdi
Email: ubaidillah.zuhdi@gmail.com

doi:10.4304/jcp.9.6.1291-1299

Ref. [11] used decomposition analysis to compare the role of ICT sectors in national economic structural changes in Japan and Indonesia. Ref. [12] employed two methods, decomposition analysis and simple output multipliers, to analyze the role of ICT sectors in the Japanese national economy from 1995 to 2005. The results of those different methods of calculation were compared to highlight alternate perspectives on the role of ICT sectors.

Statistical analysis of the role of ICT in national economies is still insufficiently studied, however. A statistical approach is important because it can quantify the influence of ICT in the economic activities of a country. Further, this kind of study can offer insight into methods for strengthening economic activity in the studied country. This study is conducted to contribute to filling the gap in the literature.

The purpose of this study is to analyze the role of ICT in changes of the industrial structure of a country; this study proceeds by statistical analysis on IO tables. The target country in this study is Japan. The period of analysis for this study is 1985 to 2005. In order to achieve the purpose, we develop a constrained multivariate regression (CMR) model and evaluate this model by using the likelihood ratio test (LRT) to calculate the statistical significance of the fitted estimators.

This paper is arranged as follows. The methodology of this study is explored in section II. Section III explains the results of calculation and analysis related to these results. Section IV describes the conclusions of this study and suggests areas for further research.

II. Methodology

In this study, ICT is represented by ICT capital stock; specifically, by computers, main parts and accessories, and telecommunications equipment. We develop a CMR model to analyze changes in industrial structure by regarding them as dynamic changes in IO coefficient vectors extracted from IO tables. The LRT method is then used to evaluate the statistical model. This study focuses on two analyses: (1) LRT calculations at the macro level and (2) IO coefficients at the micro level.

The method of this study can be summarized as follows. First, we concord the Japanese IO tables for 1985, 1990, 1995, 2000, and 2005 to equalize the number of industrial sectors. The number of sectors in the IO tables for 1985, 1990, 1995, 2000, and 2005 was 84, 91, 93, 104, and 108, respectively. There are 78 sectors after concordance; those sectors are displayed in the Appendix.

Second, we calculate the IO coefficient matrices for each year in the analyzed period. We use the following equation from [13]:

$$a_{ij} = \frac{z_{ij}}{X_j}, \tag{1}$$

where z_{ij} is the level of inter-industry sales from sector i to sector j and X_j is the total production of sector j. The right-hand side, a_{ij}, represents the IO coefficient from sector i to sector j; that is, the input needed from industry i to produce one unit of output from industry j.

Third, we use a CMR model to calculate the influences of explanatory variables used in this study—computers and telecommunications equipment—on changes in Japanese industrial structure. The data for those variables are obtained from the website of the Japanese Ministry of Public Management, Home Affairs, Posts and Telecommunications [14]. The statistical significance of the estimators in the fitted model is tested by the LRT method.

The LRT method as used in this study can be described as follows. We first index the years of analysis as *T*. In this study, we study the years (indices) 1985 (1), 1990 (2), 1995 (3), 2000 (4), and 2005 (5). Then, we can define the data representing Japanese industrial structure (i.e., the IO coefficient matrices) by *a(t)* t = 1…T. In this calculation, IO coefficients are vector entries. In other words, CMR model is applied to each industrial sector of Japan through the IO coefficient of that sector. The explanatory variables used can be described as *x(k,t)* k = 1…k. The function *a(t)* is extended in the model to

$$a(i,t) = b_0(i) + \sum_k b(i,k) \times x(k,t) + e(i,t)$$

$$a(i,t) \geq 0, \ \sum_i a(i,t) = 1.0, \tag{2}$$

where $b_0(i)$ and $b(i,k)$ are the regression coefficients of the model. Since IO coefficients are non-negative and should sum to unity by definition, constraints among estimators are imposed. The error term $e(i,t)$ describes the difference between original and estimated values. By least squares minimization, that is, by using the object function $\min\left(\sum_i \sum_t e(i,t)^2\right)$, one can obtain the parameters. Above model, actually, representing CMR model used in this study. We then formulate the data from the 5 data years and the 78 Japanese industrial sectors in the IO coefficient matrices as the function $A(t,i,j)$. The vectors of explanatory variables, $Ex\_\mathbf{x}(k,t)$, are used as a source of influences for that data.

The LRT method is based on calculating $-N(\ln S - \ln S_0)$, where N and S are the total amount of data and the results of performance function optimization, respectively. N is given by $K \times M \times T$ where K, M, and T are number of sectors which give input for discussed sector(s), number of discussed sector(s), and number of periods, respectively. The degrees of freedom is given by $(K - 1) \times M \times$(number of removed explanatory variables). The statistical significance of an explanatory variable is given by $-N(\ln S - \ln S_0)$, which follows a $\chi 2$ distribution. In this study, we take 0.05 as the level of significance. Therefore, we use the 0.05 level of $\chi 2$ distribution in applying LRT method. The degrees of freedom used in this study are $78 \times 1 \times 2 = 156$ for the explanatory variables jointly and $78 \times 1 \times 1 = 78$ for the explanatory variables separately. The cutoff scores for statistical significance in this study are $\chi 2_{0.05}$ (156) = 185.86 and $\chi 2_{0.05}$ (78) = 99.33. We use these in calculating the statistical significance of the explanatory variables for each Japanese industrial sector.

An explanatory variable significantly influences a particular sector if its calculated significance score is greater than the cutoff score.

The LRT calculations in this study are performed by the GAMS software, a system for analyzing high-level optimization models and mathematical programming [15]. We analyze the results of that calculation at the macro level. This analysis uses hypothesis testing. Three null hypotheses are used in this study.

- **Hypothesis 1:** Computers, including computer accessories, had no influence on Japanese industrial structure changes from 1985 to 2005
- **Hypothesis 2:** Telecommunications equipment had no influence on Japanese industrial structure changes from 1985 to 2005
- **Hypothesis 3:** Computers and telecommunications equipment jointly had no influence on Japanese industrial structure changes from 1985 to 2005.

We use the null model, in which the value of k is constant, as a base in testing those hypotheses.

Finally, we analyze the influences of explanatory variables used in this study at the micro level. More specifically, this analysis investigates the influences of those variables on the changes in IO coefficients, a_{ij}, for specific sectors. This part of the analysis focuses on the following sectors: (1) commerce, (2) finance and insurance, (3) broadcasting, and (4) business services and office supplies. These sectors are chosen because the ICT is expected to directly impact transactions in these sectors.

For each analyzed sector, the representation of changes in IO coefficients is chosen from the top ten sectors giving the highest input to that sector. The coefficient of variation is used to analyze the original and estimated values of the IO coefficients at the micro level. The degree of correlation between the values is also used to explore the influences of explanatory variables at the industry level. As in the macroeconomic case, microeconomic analysis is performed by using the GAMS software.

III. Results and Analysis

A. Macroeconomic Analysis

This subsection discusses the results of LRT analysis of the role of the explanatory variables used in this study, computers and telecommunications equipment, in changes in Japanese industrial structure from 1985 to 2005. The results are used to test the null hypotheses discussed earlier. Because all sectors are discussed, the analysis in this subsection is also called macroeconomic analysis.

A summary of the LRT calculations which evaluate the CMR model are seen in Table I. From information in that table, we can assert that computers significantly influenced the structure of a majority of Japanese industrial sectors from 1985 to 2005. The exceptions are (1) petroleum refinery products, (2) coal products, and (3) steel products sectors. Similar results are obtained for the influences of telecommunications equipment, which significantly influenced the structure of all Japanese industrial sectors from 1985 to 2005 except for (1) non-metallic ores, (2) basic and intermediate chemical products, and (3) gas and heat supply sectors. Because both explanatory variables significantly influence the structure changes of a majority of Japanese industrial sectors from 1985 to 2005, we reject the first and second null hypotheses.

The combination of explanatory variables used in this study significantly influenced the structure changes of all Japanese industrial sectors from 1985 to 2005. This is a stronger result than for the explanatory variables separately. We can say thus reject the third null hypothesis.

The above results show that the combination of explanatory variables used in this study played a significant role in changes in Japanese industrial structure between 1985 and 2005. For specific sectors, only one of the explanatory variable was significant; this differed by sector. For example, computers significantly influenced the non-metallic ores sector, but telecommunications equipment did not. We conclude from these results that the development of ICT broadly affected Japan during the study period.

B. Microeconomic Analysis

The previous subsection analyzed the influences of computers and telecommunications equipment at the macro level. This subsection analyzes the influences of those variables at a lower level, the IO coefficient level; as such, the analysis is at the micro level. We focus on the following sectors: (1) commerce, (2) finance and insurance, (3) broadcasting, and (4) business services and office supplies. The aim of this analysis is to investigate the influences of ICT capital stock in changes in the IO coefficients for the listed sectors. The years analyzed in this section are 1985, 1990, 1995, 2000, and 2005; these are indexed as described in Section II. The word of "original" represents pure data of IO coefficients while "estimated" represents the data of IO coefficients after receiving the influences from explanatory variables. Each selected sector is analyzed in detail below.

B.1 Commerce Sector

Fig. 1 shows the changes in one specific IO coefficient, $a_{61,59}$, which represents the input given by the real estate agencies and rental services sector, sector 61, to the commerce sector, sector 59, between 1985 and 2005. A downward trend appears in these changes. Table II compares the coefficients of variation of the original and the estimated values of that coefficient and also shows the correlation (R) of these values. From these results, we can conclude that our model results model the historical changes well. We conclude that the explanatory variables significantly influenced $a_{61,59}$ from 1985 to 2005.

TABLE I.
SUMMARY OF LRT CALCULATIONS (NULL MODEL AS A BASE)

No.	Explanatory variable	Number of sectors significantly influenced	Number of sectors not significantly influenced
1	Computers	75	3
2	Telecommunications equipment	75	3
3	Combination of 1 and 2	78	0

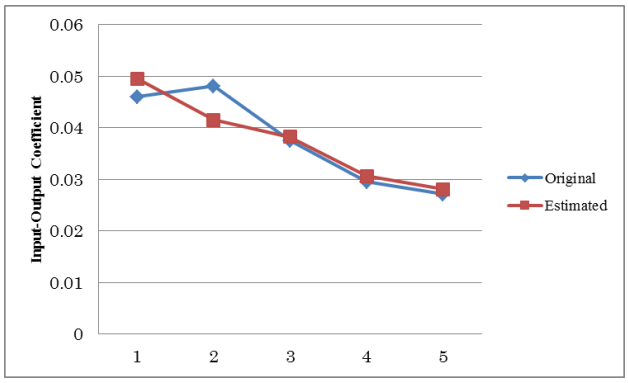

Figure 1. Changes in $a_{61,59}$ from 1985 to 2005.

TABLE II.
COEFFICIENTS OF VARIATION OF BOTH ORIGINAL AND ESTIMATED VALUES OF $A_{61,59}$ AND CORRELATION (R) OF BOTH VALUES (1985–2005)

Coefficient of variation		Correlation
Original	Estimated	0.914
0.251	0.229	

Fig. 2 shows the changes in another specific IO coefficient, $a_{70,59}$, representing input from the communication sector, sector 70, to the commerce sector, sector 59, between 1985 and 2005. An upward trend is found for this case. Table III lists the coefficients of variation of both the original and estimated values of that coefficient. This table also displays the correlation of both values. Again, we can conclude from analysis results that our model reflects historical changes, and so we can say that the explanatory variables strongly influenced $a_{70,59}$ from 1985 to 2005.

Explanatory variables used in this study affected the commerce sector differently. This difference shows that, for this sector, the microeconomic circumstances are more complex than the macroeconomic characteristic. This complexity is caused by the commerce sector itself, which uses communications media to market its products. The role of the communication sector, which is represented by its input to the commerce sector, is entwined with the activities of commerce. The strong influences of the explanatory variables used in this study and the increasing trend in estimated value from 1985 to 2005 in this relationship between commerce and communications show that ICT bolsters their relationship. This support occurs when information sharing and communication facilitate business activity between those sectors.

In contrast, the opposite phenomenon appears in the relationship between the real estate and rental services sector and the commerce sector. This relationship had a downward trend in the period between 1985 and 2005, in both original and estimated values. This decline in activity might be caused by an increase in competition between these sectors. This possibility and the strong influences of the explanatory variables in this relationship suggest that ICT weakens the relationship between these two sectors.

B.2 Finance and Insurance Sector

Fig. 3 shows the changes of $a_{61,60}$, the IO coefficient representing input from the real estate agencies and rental services sector, sector 61, to the finance and insurance sector, sector 60, between 1985 and 2005. A downward trend is seen in these changes. Table IV compares the coefficients of variation of the original and the estimated values of that coefficient as well as the correlation of these values. From these results, we conclude that our model results reflect historical changes, and so we can say that the explanatory variables significantly influenced $a_{61,60}$ from 1985 to 2005.

Fig. 4 shows the changes in $a_{77,60}$, the IO coefficient that represents input from the business services and office supplies sector, sector 77, to the finance and insurance sector, sector 60, in the period between 1985 and 2005. Here, an upward trend is observed. Table V shows the coefficients of variation of both original and estimated values of that coefficient and also shows the correlation of both values. As we did in the other cases, we conclude that our model reflects historical changes, and so we can say that the explanatory variables significantly influenced $a_{77,60}$ from 1985 to 2005.

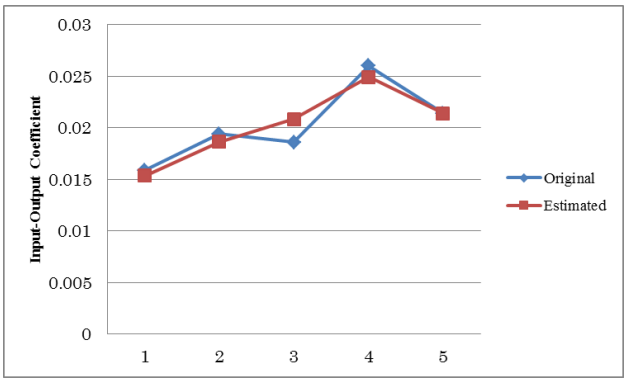

Figure 2. Changes in $a_{70,59}$ from 1985 to 2005.

TABLE III.
COEFFICIENTS OF VARIATION OF BOTH ORIGINAL AND ESTIMATED VALUES OF $A_{70,59}$ AND CORRELATION (R) OF BOTH VALUES (1985–2005)

Coefficient of variation		Correlation
Original	Estimated	0.936
0.186	0.174	

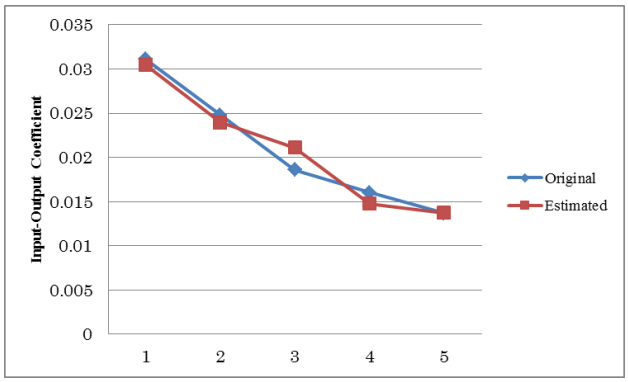

Figure 3. Changes in $a_{61,60}$ from 1985 to 2005.

TABLE IV.
COEFFICIENTS OF VARIATION OF BOTH ORIGINAL AND ESTIMATED VALUES OF $A_{61,60}$ AND CORRELATION (R) OF BOTH VALUES (1985–2005)

Coefficient of variation		Correlation
Original	Estimated	0.977
0.340	0.331	

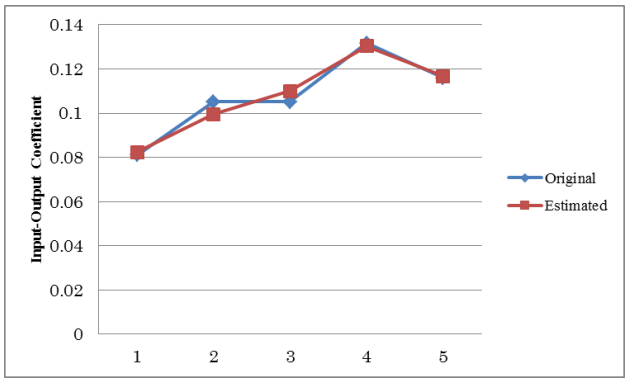

Figure 4. Changes in $a_{77,60}$ from 1985 to 2005.

TABLE V.
COEFFICIENTS OF VARIATION OF BOTH ORIGINAL AND ESTIMATED VALUES OF $A_{77,60}$ AND CORRELATION (R) OF BOTH VALUES (1985–2005)

Coefficient of variation		Correlation
Original	Estimated	0.978
0.172	0.168	

The explanatory variables affected the IO coefficients of the finance and insurance sector differently at the micro level. This difference shows, for this sector, the microeconomic circumstances are more complex than the macroeconomic characteristic. This complexity is caused by the finance and insurance sector itself; this sector needs input from the business services and office supplies sector to maintain its cash flow. That is, the role of the business services and office supplies sector, which is represented by input to the finance and insurance sector, is important for the activities of the finance and insurance sector. Strong influences from the explanatory variables and the upward trend in estimated value from 1985 to 2005 of this relationship support the contention that computers and telecommunications equipment promote the strength of this relationship. The support arises from facilities for communications and information sharing. Such activities will further accelerate business activities between the sectors.

The opposite trend appears in the relationship between the real estate agencies and rental services sector and the finance and insurance sectors. This relationship shows a downward trend in the period between 1985 and 2005, in both original and estimated values. This decline might be caused by similarity between the sectors, which would result in increased in competition between them. This possibility and strong influences from the explanatory variables clarify that these variables negatively support the existence of this relationship.

B.3 Broadcasting Sector

Fig. 5 shows changes in $a_{46,71}$, the IO coefficient that represents input from the electrical appliance sector, sector 46, to the broadcasting sector, sector 71, in the period between 1985 and 2005. A downward trend can be seen in these changes. Table VI compares the coefficients of variation of the original and estimated values of $a_{46,71}$ and the correlation of these values. From these results, we conclude that our model results reflect historical changes, and so we can say that the explanatory variables strongly influenced $a_{46,71}$ from 1985 to 2005.

Fig. 6 shows the changes in $a_{77,71}$, the IO coefficient that represents input from the business services and office supplies sector, sector 77, to the broadcasting sector, sector 71 in the period between 1985 and 2005. A different pattern appears here, where the trend is upward. Table VII shows the coefficients of variation of both original and estimated values of $a_{77,71}$, and also shows the correlation of both values. From these results, we conclude that our model results reflect historical changes, and so the explanatory variables exhibited a strong influence on $a_{77,71}$ from 1985 to 2005.

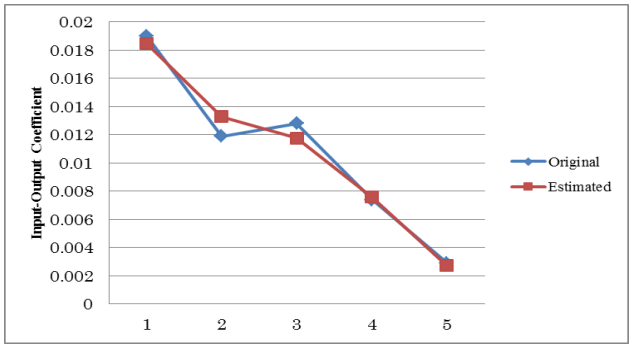

Figure 5. Changes in $a_{46,71}$ from 1985 through 2005.

TABLE VI.
COEFFICIENTS OF VARIATION OF BOTH ORIGINAL AND ESTIMATED VALUES OF $A_{46,71}$ AND CORRELATION (R) OF BOTH VALUES (1985–2005)

Coefficient of variation		Correlation
Original	Estimated	0.988
0.560	0.553	

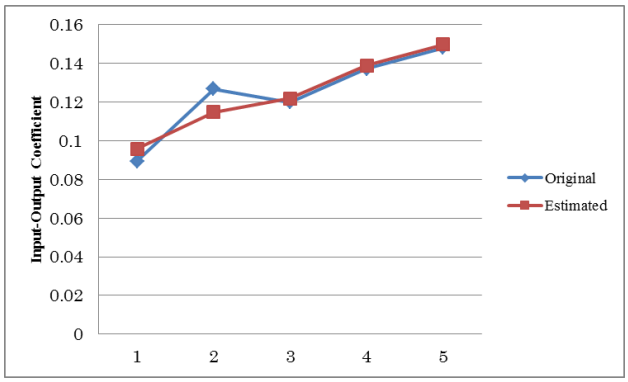

Figure 6. Changes in $a_{77,71}$ from 1985 through 2005.

TABLE VII.
COEFFICIENTS OF VARIATION OF BOTH ORIGINAL AND ESTIMATED VALUES OF $A_{77,71}$ AND CORRELATION (R) OF BOTH VALUES (1985–2005)

Coefficient of variation		Correlation
Original	Estimated	0.950
0.178	0.170	

The explanatory variables affected the IO coefficients of the broadcasting sector differently at the micro level. This difference is evidence that, for this sector, the microeconomic circumstances are more complex than macroeconomic characteristic. This complexity is caused by the broadcasting sector itself. This sector needs the information supplied by the business services and office supplies sector to conduct its activities. The role of the business services and office supplies sector, which is represented by input to the broadcast sector, is integral to the activities of the broadcasting sector. Both strong influences from the explanatory variables and the upward trend in estimated value from 1985 to 2005 suggest reasons why these variables strengthen this relationship. Communication and information sharing accelerate business activity between these sectors.

The opposite trend appears for the relationship between the electrical appliance sector and the broadcasting sector. This relationship had a downward trend in the period between 1985 and 2005, in both original and estimated values. This downward trend might be caused by preference changes in the broadcasting sector when choosing suppliers. That is, in the period between 1985 and 2005, there was a decrease in the dependence of the broadcasting sector on products from the electrical appliance sector. This change and the strong influences of explanatory variables in this relationship show that these variables negatively support the existence of this relationship.

B.4 Business Services and Office Supplies Sector

Fig. 7 shows changes in $a_{19,77,}$ the IO coefficient that represents input from the publishing and printing sector, sector 19, to the business services and office supplies sector, sector 77, in the period between 1985 and 2005. A downward trend is seen in these changes. Table VIII compares the coefficients of variation of the original and estimated values of $a_{19,77}$ and shows the correlation of these values. From these results, we conclude that our model reflects historical changes, and so we can say that explanatory variables strongly influenced $a_{19,77}$ from 1985 through 2005.

Fig. 8 shows changes in $a_{59,77}$, the IO coefficient that represents input from the commerce sector, sector 59, to the business services and office supplies sector, sector 77, in the period between 1985 and 2005. Here, an upward trend is seen. Table IX shows the coefficients of variation of both original and estimated values of $a_{59,77}$. This table also includes the correlation of both values. From these results, we conclude that our model results reflect historical changes, and so the explanatory variables used in this study strongly influenced $a_{59,77}$ from 1985 to 2005.

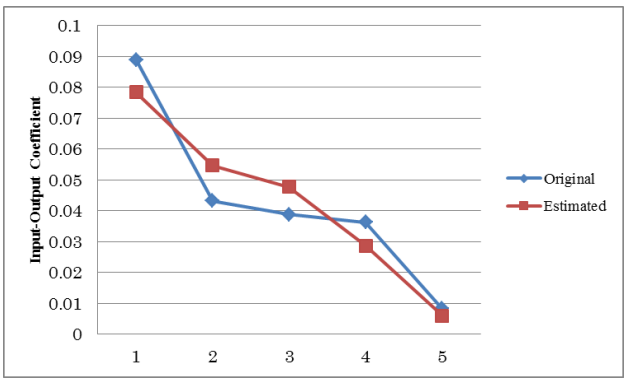

Figure 7. Changes in $a_{19,77}$ from 1985 through 2005.

TABLE VIII.
COEFFICIENTS OF VARIATION OF BOTH ORIGINAL AND ESTIMATED VALUES OF $A_{19,77}$ AND CORRELATION (R) OF BOTH VALUES (1985–2005)

Coefficient of variation		Correlation
Original	Estimated	0.941
0.674	0.634	

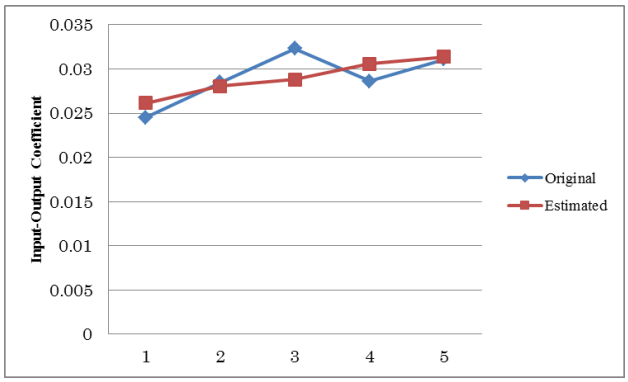

Figure 8. Changes in $a_{59,77}$ from 1985 through 2005.

TABLE IX.
COEFFICIENTS OF VARIATION OF BOTH ORIGINAL AND ESTIMATED VALUES OF $A_{59,77}$ AND CORRELATION (R) OF BOTH VALUES (1985–2005)

Coefficient of variation		Correlation
Original	Estimated	0.687
0.103	0.071	

The explanatory variables impacted the IO coefficients of the business services and office supplies sector differently at the micro level. This difference shows that, for this sector, the microeconomic circumstances are more complex than macroeconomic characteristic. This complexity is caused by the business services and office supplies sector itself. This sector relies on the activities that the commerce sector provides. In other words, the role of the commerce sector, which is represented by input to the business services and office supplies sector, is important to the activities of the business services and office supplies sector. The strong influences of the explanatory variables and the upward trend in estimated value from 1985 to 2005 in this relationship provide evidence that these variables strengthen this relationship. Communication and information sharing facilitate business activity between these sectors.

The opposite trend exists in the relationship between the publishing and printing sector and the business services and office supplies sector. This relationship exhibits a downward trend in the period between 1985 and 2005, in both original and estimated values. This weakening might be caused by an increase in competition between these sectors. Moreover, the growth in the eco-business concept in recent years might be a reason for this decline. The eco-business concept will make businesses consider environmental sustainability when conducting business activities. The publishing and printing sector uses large amounts of natural resources for its business activities. Therefore, sectors implementing the eco-business concept will tend to avoid the publishing and printing sector when making business agreements. Both the downward trend and strong influences from the explanatory variables explain that these variables negatively support the existence of this relationship.

IV. CONCLUSIONS AND AREAS FOR FURTHER RESEARCH

This study analyzed the role of ICT in changes in Japanese industrial structure from 1985 to 2005. In this study, ICT was represented by ICT capital stock, which comprises computers (including computer accessories) and telecommunications equipment. CMR modeling and LRT method were employed as an analytic tool. This study focused on two levels of analysis: (1) analysis of LRT calculation at the macro level and (2) analysis of IO coefficients at the micro level.

Hypothesis testing was used for macroeconomic analysis. The standard null hypotheses were used. The results of LRT calculation showed that both explanatory variables significantly influenced the structure of most (jointly, of all) Japanese industrial sectors from 1985 to 2005.

Microeconomic analysis focused on the (1) commerce, (2) finance and insurance, (3) broadcasting, and (4) business services and office supplies sectors. These sectors were chosen because the explanatory variables were intuitively linked to the activities of those sectors. The objective of the analysis was to investigate the influences of the explanatory variables on the IO coefficients of the chosen sectors. The results of this analysis showed that explanatory variables used in this study gave different impacts to the IO coefficients of the chosen sectors in micro level. In our analysis, the microeconomic circumstances were more complex than the macroeconomic characteristic.

This study analyzed the influences of ICT capital stock on the industrial structure changes of Japan from 1985 through 2005. The scope of this study, however, was narrow, and broader studies should be undertaken in the future. Specifically, we suggest adding other explanatory variables, such as education and export-import activities, for analyzing industrial structure changes in Japan. Additionally, further investigation to clarify microeconomic differences observed in this study would be of interest to us. More data are becoming available, and extending the period of analysis will allow deeper analysis. Extending this technique to international comparisons is also a suggested area for further research from this study. Such a comparison will show similarities and differences in the industrial structure changes of compared countries. Finally, we have made no policy suggestions in this study. We hope that our study will stimulate further research and discussion on appropriate economic policies.

REFERENCES

[1] A. Grubler, *Technology and Global Change*. Cambridge: Cambridge University Press, 1998.

[2] E. Braun, "The changing role of technology in society", http://epub.oeaw.ac.at/ita/ita-manuscript/ita_10_03.pdf, 2010, Accessed 19 October 2013.

[3] D. S. Abraham, "The battle for new resources: Minor minerals in green technologies", http://www.rieti.go.jp/jp/publications/pdp/12p005.pdf, 2012, Accessed 19 October 2013.

[4] M. Peitz and J. Waldfogel, *The Oxford Handbook of the Digital Economy: Edited by Martin Peitz and Joel Waldfogel*. NY: Oxford University Press, 2012.

[5] F. O. Bankole, F. Shirazi, and I. Brown, "Investigating the impact of ICT investments on human development," The Electronic Journal of Information Systems in Developing Countries, vol. 48, 8, pp. 1–19, 2011.

[6] C. M. Zuppo, "Defining ICT in a boundaryless world: The development of a working hierarchy," International Journal of Managing Information Technology (IJMIT), vol. 4, pp. 13–22, 2011. doi:10.5121/ijmit.2012.4302.

[7] W. P. Mtega and A. C. Msungu, "Using information and communication technologies for enhancing the accessibility of agricultural information for improved agricultural production in Tanzania," The Electronic Journal of Information Systems in Developing Countries, vol. 56, 1, pp. 1–14, 2013.

[8] E. H. Nasab and M. Aghaei, "The effect of ICT on economic growth: Further evidence," International Bulletin of Business Administration, vol. 5, pp. 46–56, 2009.

[9] U. Zuhdi, D. S. Utomo, and D. T. Alamanda, "Analyzing the role of ICT sector to the national economic structural change: The case of Indonesia," Jurnal Manajemen Teknologi, vol. 10, pp. 299–307, 2011.

[10] U. Zuhdi, N. A. R. Putranto, and A. D. Prasetyo, "Encouraging ICT sectors using input – output approach: The case of Indonesia", Adv. Sci. Lett., vol. 20, no. 1, pp. 199-202, January 2014. doi:10.1166/asl.2014.5269.

[11] U. Zuhdi, S. Mori, and K. Kamegai, "Analyzing the role of ICT sector to the national economic structural changes by decomposition analysis: The case of Indonesia and Japan," Procedia – Social and Behavioral Sciences, vol. 65, pp. 749–754, December 2012. doi:10.1016/j.sbspro.2012.11.194.

[12] U. Zuhdi, "The other perspective related to the role of ICT sectors in national economy: The case of Japan", Adv. Sci. Lett., vol. 20, no. 2, pp. 483-486, February 2014. doi:10.1166/asl.2014.5334.

[13] R. E. Miller and P. D. Blair, *Input–Output Analysis: Foundations and Extensions–2nd Ed.* NY: Cambridge University Press, 2009.

[14] Japanese Ministry of Public Management, Home Affairs, Posts and Telecommunications, "2009 White paper of information and communication: Reference", http://www.soumu.go.jp/johotsusintokei/whitepaper/ja/h21/data/html/l6c00000.html, Accessed 19 October 2013.

[15] GAMS, "Welcome to the GAMS home page!", http://www.gams.com/, Accessed 26 August 2013.

APPENDIX

JAPANESE INDUSTRIAL SECTORS USED IN THIS STUDY

1	Crop cultivation
2	Livestock
3	Agricultural services
4	Forestry
5	Fisheries
6	Metallic ores
7	Non-metallic ores
8	Coal mining, crude petroleum, and natural gas
9	Foods
10	Beverages
11	Feeds and organic fertilizer not elsewhere classified
12	Tobacco
13	Textile products
14	Wearing apparel and other textile products
15	Timber and wooden products
16	Furniture and fixtures
17	Pulp and paper
18	Paper products
19	Publishing and printing
20	Chemical fertilizer
21	Basic industrial inorganic chemicals
22	Basic and intermediate chemical products
23	Synthetic resins
24	Synthetic fibers
25	Final chemical products not elsewhere classified
26	Petroleum refinery products
27	Coal products
28	Plastic products
29	Rubber products
30	Leather, fur, skins, and miscellaneous leather products
31	Glass and glass products
32	Cement and cement products
33	Pottery, china, and earthenware
34	Other ceramic, stone, and clay products
35	Pig iron and crude steel
36	Steel products
37	Steel castings and forgings and other steel products
38	Non-ferrous metals
39	Non-ferrous metal products
40	Metal products for construction and architecture
41	Other metal products
42	General industrial machinery

43	Special industrial machinery
44	Other general machines
45	Machinery for office and service industry
46	Electrical appliance
47	Motor vehicles and repair of motor vehicles
48	Ships and repair of ships
49	Other transportation equipment and repair of transportation equipment
50	Precision instruments
51	Miscellaneous manufacturing products
52	Building construction
53	Repair of construction
54	Civil
55	Electricity
56	Gas and heat supply
57	Water supply
58	Waste management service
59	Commerce
60	Finance and insurance
61	Real estate agencies and rental services
62	House rent
63	Railway
64	Road transport (except transport by private cars)
65	Self-transport by private cars
66	Water transport
67	Air transport
68	Storage facility service
69	Services relating to transport
70	Communication
71	Broadcasting
72	Public administration and activities not elsewhere classified
73	Education
74	Research
75	Medical service, health, and social security
76	Other public services
77	Business services and office supplies
78	Personal services

Ubaidillah Zuhdi was born in Gresik, East Java, Indonesia, on 28 October 1984. He graduated from SMUN 5 Surabaya in 2003 and then entered the Department of Industrial Engineering of Institut Teknologi Bandung (ITB) in Bandung, Indonesia. He finished his bachelor's degree in 2008 and continued to his degree in Master of Science in Management, at the School of Business and Management (SBM)-ITB in 2009. In 2010, he began a double master's degree program organized by SBM-ITB and the Department of Industrial Administration of Tokyo University of Science (TUS), Noda, Japan. He received a scholarship from Japan Student Services Organization when he joined that program. He received his master's degree from SBM-ITB and TUS in 2012. His research interests include macroeconomics, microeconomics, ICT, creative industry, and input-output analysis.

On 2008, he joined a provider of data communication, Internet and value-added services in Jakarta, Indonesia, as a Junior Officer. He left this position in 2009 to continue his studies. He is currently pursuing his PhD at the Department of Industrial Administration of TUS.

Mr. Zuhdi is currently a member of the Entrepreneurship and Technology Management group at SBM-ITB and a Teaching Assistant at TUS. He is also a member of the International Input-Output Association. He received the Mahaka Media Award for Outstanding Scholar 2011 from SBM-ITB on 2011.

Shunsuke Mori was born in 1953. He received a Doctor of Engineering degree from Tokyo University in 1981. He became a Research Assistant in the Industrial Administration Department, Tokyo University of Science in 1981. He became Associate Professor in 1989 and a Professor in 1994. His research field is systems engineering, assessment of global warming, and model development for environmental technologies.

From 1981–1983, he was an Invited Researcher at the Economic Planning Agency. From 1986–1987, he was a Science Researcher at the International Institute for Applied Systems Analysis (Austria). From 1987–1993, he was an Invited Researcher at the National Institute for Science and Technology Policy. From 2002–2007, he was the Chief Researcher at the Research Institute of Innovative Technology for the Earth. He is currently Dean of the Graduate School of Science and Technology, Tokyo University of Science.

Prof. Mori has participated in Intergovernmental Panel on Climate Change (IPCC) activities in the following capacities: Lead Author (modeling team), Special Report of Emission Scenarios, Cambridge Press, 2000; Lead Author, Third Assessment Report of IPCC, WG-III, Chapter 9, Cambridge Press, 2001; Expert Reviewer, Fourth Assessment Report of IPCC, WG-III, 2006 and also Fifth Assessment Report of IPCC, WG-III, 2006. He is also a senior member of the Japan Institute of Energy.

Kazuhisa Kamegai received his PhD in Physics from the Graduate School of Science, The University of Tokyo, in 2004. He was a Postdoctoral Fellow at the Institute of Astronomy, The University of Tokyo. He worked as an Aerospace Project Research Associate at the Institute of Space and Astronautical Science (ISAS), Japan Aerospace Exploration Agency (JAXA). Currently, he is an Assistant Professor in the Department of Industrial Administration, Faculty of Science and Technology at Tokyo University of Science.

An Improved Shuffled Frog Leaping Algorithm with Single Step Search Strategy and Interactive Learning Rule for Continuous Optimization

Deyu Tang
College of Medical Information and Engineering, GuangDong Pharmaceutical University, GuangZhou, China
Email:scutdy@126.com

Yongming Cai
Dept of Computer, College of Medical Information and Engineering, GuangDong Pharmaceutical University, GuangZhou, China
Email: 78572951@qq.com

Jie Zhao
Department of information management engineering, School of Management, Guangdong university of technology, GuangZhou, China
Email: kitten-zj@163.com

***Abstract*—Shuffled frog-leaping algorithm (SFLA) is a heuristic optimization technique based on swarm intelligence that is inspired by foraging behavior of the swarm of frogs. The traditional SFLA is easy to be premature convergence. So, we present an improved shuffled frog-leaping algorithm with single step search strategy and interactive learning rule(called 'SI-SFLA'). Single step search strategy enhances exploring ability of algorithm for higher dimension and interactive learning rule strengthens the diversity of local memeplexe. The effectiveness of the method is tested on many benchmark problems with different characteristics and the results are compared with other algorithms including PSO,SFLA,DE and TLBO. The experimental results show that SI-SFLA has not only a promising performance of searching for accurate solutions, but also a fast convergence rate, which are evaluated using benchmark functions.**

***Index Terms*—shuffled frog-leaping algorithm, single stepsearch strategy, interactive learning rule, continuous optimization, swarm intelligence**

I. Introduction

Evolutionary computing (EC) is an exciting development in computer science. Over the past several decades, people have developed many optimization computation methods to solve complicated global optimization problems such as genetic algorithm (GA) inspired by the Darwinian law of survival of the fittest [1], particle swarm optimization (PSO) inspired by the social behavior of bird flocking or fish schooling [2][3]; ant colony optimization (ACO) inspired by the foraging behavior of ant colonies [4]; and biogeography-based optimization (BBO) inspired by the migration behavior of island species [5][6]; Differential Evolution (DE) [7][8] which is similar to GA with specialialized crossover and selection method; Teaching-Learning-based Optimization algorithm [9][10][11][12] which imitates the process of the teaching about teacher and students; Shuffled frog leaping algorithm (SFLA) which imitates the foraging behavior of frogs; all these algorithms can be called evolutionary algorithm or swarm intelligence optimization algorithm. Developed by Eusuff and Lansey in 2003, the shuffled frog-leaping algorithm [16] (SFLA) is a meta-heuristic optimisation method spired from the memetic evolution of frogs seeking food in a pond, which combines the advantages of the genetic-based MA [17] and the social behaviour-based particle swarm optimisation(PSO). Memetic algorithms (MAs) are a special class of heuristic searching methods that are derived from the models of adaptation in natural systems that combine the evolutionary adaptation of a population with individual learning within the lifetimes of their members. MAs are based on evolution of memes carried by the interactive individuals. The term memetic algorithm comes from 'meme', which is a transmittable information pattern that is replicated by infecting the objects 's minds and altering their behavior in a parasitic manner. The remarkable characteristic of MAs is that all memes are allowed to gain some experience through a local search before being involved in the evolutionary process.

In general, the SFLA includes two alternating processes: local exploration in the submemeplex and global information exchange among all memeplexes. Local exploration uses the search strategy of PSO and shuffled method was used for global information exchange.

In SFLA algorithm, the whole position vector of frog was updated simultaneously, rather than each

doi:10.4304/jcp.9.6.1300-1308

component of the position vector was updated independently in each iteration, so it is difficult to find the best solution in higher dimensional space. So, according to the correlation of data set, the vector can be divided into several sub-vectors, each sub-vector can be updated in cycle. At the same time, the frog analyzes the state of position before the new position was updated, then determines the updating speed of the sub-vector during the updating process.

As everyone knows, in real life, during the learning process of student in a class, in general, there are two ways. one is that the teacher guides the student to access to the new knowledge, the second method is through the interaction between the students, which can improve the learning effect. Therefore, we introduce this interactive learning method into our algorithm. One frog in the population can be associated with arbitrary two frogs in population learning from each other, which improves the global searching ability of SFLA.

In this paper, we introduce an improved SFLA algorithm with a strong searching capabilities. A singal step strategy was used to improve the local exploration and an interactive learning rule was utilized to enforce the global searching capability. The rest part of the paper is organized as follows. In Section 2, a brief introduction of SFLA is given. The improved SFLA is introduced in Section 3. In Section4, Experiments show the result of our algorithm.

II. SFLA ALGORITHM

Shuffled frog leaping algorithm simulates the process of a group of frogs looking for food. The population was classified into some memeplexes (community), in each memeplex, frogs exchange their thoughts. SFLA is a heuristic method combined with the shuffled strategy and the local search strategy. The local search strategy makes the thought of frog spread in local search space and the shuffled strategy exchanges the idea of local memeplex. In the shuffled frog leaping algorithm, a group of frogs have the same structure which is composed of solution(position) and food(fitness). According to a certain strategy, frogs of memeplex implement local search in the solution space. After the number of local search step, thought in the shuffled process was exchanged. Local search and shuffled process continue until the definition of convergence condition was satisfied [15] [16] [17].

A balance strategy of global information exchange and the local search makes the algorithm can jump out of local optimum solution and search toward the global optimum direction, which is the most important characteristics of shuffled frog leaping algorithm. In SFLA, each memeplex carry out the local search respectively, the worst individual Q_w, through the memetic evolution close to the local best individual Q_b or the global individual Q_g. When the local search is executed to a certain stage, frogs in each memeplex communicate to implement shuffled process. The basic SFLA algorithm is as follows:

a). parameter settings: population size, numbers of memeplexes, maximum of local search iterations, number of global iterations.

b). generates an initial population.

c). determine the fitness function: F(x), used to evaluate the quality of the individuals.

d). in the global iteration process, the frog was arranged in descending order by whose fitness, and determine the global optimal solution Q_g, if it meet the convergence condition, then stop the execution; otherwise, proceed to the next step.

e). frog population was divided: the frog population was divided into m memeplexes, each memeplex contains n frogs, and the number of the population meet T=m×n; then, the first frog is divided into the first memeplex, the second frog was divided into the second memeplex, ... , The M frog was divided into the M memeplex, the m+1frog was divided into the first memeplex, the m+2frog was divided into the second memeplex, and so on, until the whole frogs was division. That is:

$$Q_t = \{Q_{t+m(r-1)} \in T \mid 1 \le r \le n\},\ (1 \le t \le m) \quad (1)$$

f). each memeplex implement local search in the number of the iterations.

(1) determine Q_w, Q_b, according to the following formula to update, where $rand \in (0,1]$, r is a constant.

$$D = r \bullet rand \bullet (Q_b - Q_w) \quad (2)$$

$$Q_{w(new)} = Q_w + D, D \in [D_{\min}, D_{\max}] \quad (3)$$

(2) If a better solution was produced, then Q_w was updated by $Q_{w(new)}$;else Q_b was replaced by Q_g according to the formula (1)(2).if Q_w was not improved, then a new solution $Q'_{w(new)}$ was produced randomly, if it is better, then the Q_w was updated by $Q_{w(new)}$.

III. IMPROVED SFLA ALGORITHM

A. Single step Search Strategy

During the updating process, the traditional SFLA algorithm often changes the position of all the dimension at the same time. According to the position of the frog, it can obtain a fitness value, so as to judge the degree of adaptation. This fitness can determine the overall quality of the frog, but can not judge part dimension if it moves to the optimal direction.

For example, on three dimensional function Sphere $f_1 = x_1^2 + x_2^2 + x_3^2$, the global optimum value is (0, 0, 0), the initial value of solutions was set (10, 10, 10), the fitness value is 300. Give a random perturbation variable value (1, 0, 1), the initial value was updated to the value (11, 0, 11), and the fitness value is 242.The fitness (242) of the updated solution is less than the initial fitness value(300). So, we can see that, in the next iteration, the solution would be some extent to move toward (11, 0, 11). At this time, although the second dimension moves to the global optimum direction, but the first and third dimension move away from the global optimum. Therefore, for high-dimensional functions, general SFLA algorithm is very difficult to find the best direction of all dimension. In order to solve this problem, the search space of the frogs was divided into several low dimensional space, in specific application, according to the dependence analysis of data set, we can decide the segmentation of the data dimension. The worst frog uses a single step search strategy for each low dimensional space. If a new frog abtains a better solution than the worst frog, then the worst frog position was updated by it, else the worst frog position was updated by it with a small search step. That is as follows formula (4)(5):

$$Q_{temp} = Q_w(t) + c.rand.(Qbest(t) - Q_w(t)) \quad (4)$$

$$\begin{cases} Q_w(t+1)=Q_{temp}, Q_{temp}.fitess \le Q_w.fitness \\ Q_w(t+1)=rand.Q_{temp}, otherwise \end{cases} \quad (5)$$

B. Interactive Learning Rule

In real life, interactive learning is common. For example, students in a class often learn new knowledge through mutual discussions and exchange information for each other [9]. SFLA is a swarm intelligence algorithm. In each memeplex(community), the worst frog learns toward the best frog. In traditional SFLA, between memeplexes, the frogs were only shuffled, but they do not learn from each other. This reduces the efficiency of learning. Therefore, we use an Interactive learning rule. Firstly, we let frogs in each memeplex complete a local search; Secondly, frogs in all memeplexes learn from each other to exchange information, then was shuffled. Interactive learning method strengthens the internal information exchange, enhances the global searching ability of the algorithm. Two frogs Qa, Qbj was choosed randomly in population. The Interactive learning rule is as follows:

$$\begin{cases} Q_a(t+1)=Q_a(t)+rand.(Q_b-Q_a(t)), Q_j.fitness \le Q_i.fitness \\ Q_a(t+1)=Q_a(t)+rand.(Q_a(t)-Q_b), otherwise \end{cases} \quad (6)$$

The improved algorithm as shown in Figure 1. Figure 1 shows frog's searching process with a number of population 30. The population was divided into 5 memeplexes, each memeplex has 6 frogs. The frogs in each column of table belongs to the same memeplex. Frogs implement local search in each memeplex, for example: the first column of table with arrows shows that frogs in the same memeplex use a one-step search strategy for local search. Interactive learning rule represents the frogs among all the memeplexes (population) communicate between each other. For example, to update the position of the frog $Q_{i+m(j-1)}$, randomly choose another different frog $Q_{u+m(v-1)}$ in the whole population respectively, these two frogs communicate with each other and determine how to update it according to the formula (6). The process is as Fig.1.

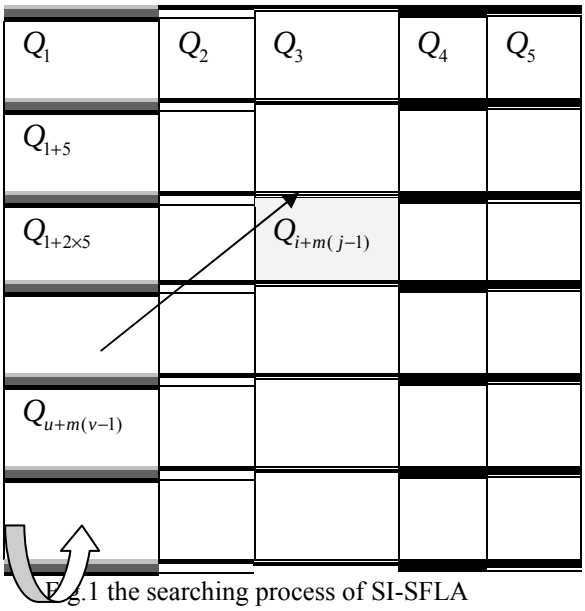

Fig.1 the searching process of SI-SFLA

The pseudo-code is as follows:

```
1.Initialize parameters:  m, n, p=m*n, etc.
  Generate population(represented by P frogs ) randomly;
2.Evaluate fitness of each frog;
3.While(  convergence criteria is satisfied)
4.{
5. Sort P frogs in descending order;
(Shuffled all frogs(construct  n groups and each groups has  m  frogs );
6.For
groups
7.{
8.Get the worst frog  Qw and the best frog Qb in this group;
9.Qtemp =Qw(t)+c.rand.(Qbest(t)-Qw(t) ) ;
10. For each Dimension
11.   If Qtemp.fitness < Qw(t).fitness
12.     Qw(t+1)= Qtemp ;
13.   Else
14.     Qw(t+1)= rand.*Qtemp ;
15.   End ;
16.end
17.get new frog using mutation;
18.if Qnew.fitness<Qw(t).fitnes
19.   Qw=Qnew;
20. end
21.}
22.For  each  frog in  population
23.{
24. get two frogs Qa, Qb randomly from population;
25. Q1=Qa(t)+rand.(Qb-Qa) ;
26. Q2= Qa(t)+rand.(Qa-Qb) ;
27. If Q1.fitness<Q(t).fitness
28.   Q(t+1)=Q1;
29. Else
30.     Q(t+1)=Q2;
31.   End
32   }
33..}
```

IV. Experiments and Results

A. Test Functions

In this paper, ten widely used benchmark continuous functions [18] shown in Table 1 with high complexity are tested. Also different benchmark problems are considered having different characteristics such as multimodality. A function is multimodal if it has two or more local optima in their solution space. Complexity increases when the local optima are randomly distributed. Moreover, complexity increases with the increase in the dimensionality.F8~F10 function are multimodality. F7 function is quartic function i.e. Noise. Initialisation dimension, search range and global optimum of these ten functions are given in **Table1**.The SI-SFLA algorithm is compared with standard PSO [2], standard SFLA [16], standard DE [7] and TLBO [9] to search for the global minima in the solution space. Details of benchmark functions are given in the appendix.

B. Initialisation Parameters Setting

The global parameter is set as follows:the population size is 50 and dimension is 30. For the basic PSO, the acceleration coefficient is set as c1 = c2 = 2, the inertia weight w decreases linearly from 0.9 to 0.4. For DE, the coefficient is set as F=0.5, CR=0.5; For the basic shuffled frog-leaping algorithm, there are 10 memeplexes, each containing 5 frogs. The local exploration in each submemeplex is executed for 5 iterations. The parameters settings for SI-SFLA are the same as those of SFLA, with the searching scale parameter *c* equal to 2.0; there is not other parameter to be set for TLBO algorithm. Especially the global iteration number is 1000 for PSO,DE and TLBO, and 200 for SFLA and SI-SFLA, because the local iteration number of SFLA and SI-SFLA are 5, then total iteration number of SFLA and SI-SFLA are 5*200=1000.

C. Test Results and Discussion

To test the performance of the improved SFLA (SI-SFLA), ten benchmark functions listed in Table 1 are used here for comparison with PSO, DE, SFLA and TLBO. We had 50 trial runs for every instance and recorded minimum of best fitness, maximum of best fitness, midian of best fitness, mean best fitness and standard deviation.

As shown in Table 2, SI-SFLA is able to evolve in a very efficient manner. Convergence rates of SI-SFLA were strikingly higher than those of PSO, DE, SFLA and TLBO. SI-SFLA also demonstrated its robustness by very consistent performances: across all of the randomly initialized runs on the same test function, SI-SFLA always showed very similar evolution speed and converged to the same point or a small region, whereas for PSO, DE SFLA and TLBO, they sometimes had very diverse behaviors resulting from the random initialization.

Because each function in f1~f7 has only a single optimal solution on origin, which usually is employed to test the local search ability of the algorithm. Thus from the result, we can see that SI-SFLA has stronger local search ability than PSO, DE, SFLA and TLBO. Especially, f3 function (Schwefel's Problem 1.2) has a flat area, so many algorithms do not easy to get its optimal solution. The result in Table2 show that SI-SFLA has a highest accuracy than PSO,DE,SFLA and TLBO.TLBO works better than PSO, DE, SFLA, but it is not stable than SI-SFLA. F8, F9 and F10 function are both multi-modal and usually tested for comparing the global search ability of the algorithm. On F8, F9 and F10 function, the SI-SFLA has better performance than PSO,DE,SFLA and TLBO algorithm; particularly, SI-SFLA can also find the optimal or closer-to-optimal solutions on the complex multimodal functions.

TABLE 1
DETAILS OF BENCHMARK FUNCTIONS

Problem	name	Dimension	Search range	Global Optimum
F1	Sphere	30	[-100,100]	0
F2	Schwefel's Problem 2.22	30	[-10,10]	0
F3	Schwefel's Problem 1.2	30	[-100,100]	0
F4	Schwefel's Problem 2.21	30	[-100,100]	0
F5	Generalized Rosenbrock's function	30	[-2.048, 2.048]	0
F6	Step function	30	[-100,100]	0
F7	Quartic function i.e. Noise	30	[-1.28,1.28]	0
F8	Generalized Griewank function	30	[-600,600]	0
F9	Generalized Rastrigin's function	30	[-5.12,5.12]	0
F10	Ackley's function	30	[-32,32]	0

TABLE 2
COMPARISISION OF RESULTS FOR THE MIN,MAX,MIDIAN,MEAN AND THE STANDARD DEVIATION FRO PSO,SFLA,DE,TLBO AND SI-SFLA.

		PSO	SFLA	DE	TLBO	SI-SFLA
F1	min	0.7101	7.0825e-005	2.2351e-011	2.5400e-015	9.1988e-093
	Max	33.9085	1.4129	2.2091e-010	14.2100	5.0804e-090
	Midian	5.6048	4.0592e-004	4.4524e-011	2.6605e-005	4.0838e-091
	Mean	7.2682	0.0610	5.8090e-011	0.4735	9.4713e-091
	SD.	6.2093	0.2302	3.8643e-011	2.2540	1.2209e-090
F2	min	0.0100	1.2102e-006	4.7970e-013	2.1934e-012	1.2287e-094
	Max	0.3256	100.0000	1.1728e-011	1.0815e+006	5.0111e-092
	Midian	0.0494	7.2865e-006	2.0384e-012	5.5212e-007	3.2693e-093
	Mean	0.0728	4.0002	2.4012e-012	2.1629e+004	5.9400e-093
	SD	0.0751	19.7948	1.9589e-012	1.5294e+005	8.2468e-093
F3	min	4.3075e+004	3.7439e+004	1.3528e+005	3.2865e-010	4.2474e-016
	Max	1.6568e+005	1.6784e+005	4.7575e+005	2.8937e+005	645.9814
	Midian	7.7664e+004	7.7712e+004	2.9498e+005	0.5759	0.5302
	Mean	8.4972e+004	8.0585e+004	2.9151e+005	1.0295e+004	48.9997
	SD	2.9328e+004	2.8036e+004	7.9253e+004	4.3603e+004	115.4962
F4	min	11.2857	3.0528	0.9726	1.0945e-007	3.1176e-072
	Max	27.6603	25.0490	2.1760	0.7453	7.6636e-070
	Midian	21.2735	14.4736	1.4421	0.0158	3.0160e-071
	Mean	20.5526	14.2677	1.4777	0.0720	6.5088e-071
	SD	3.7755	5.0859	0.3142	0.1436	1.2422e-070
F5	min	16.9985	18.6618	23.3310	28.7832	26.2041
	Max	145.7181	83.4157	25.6784	7.5675e+003	28.5672
	Midian	29.2503	28.5246	24.4105	28.9009	27.1582
	Mean	41.8042	35.0193	24.4319	179.6730	27.1621
	SD	27.6833	18.8570	0.5520	1.0661e+003	0.6455
F6	min	2	0	0	0	0
	Max	34	170	0	20	0
	Midian	11	1	0	0	0
	Mean	11.9400	5.5200	0	1.2800	0
	SD	6.6774	24.8261	0	3.3444	0
F7	min	0.0478	0.0158	0.0100	2.3995e-005	1.1186e-005
	Max	0.2660	0.2550	0.0366	0.0045	8.6906e-004
	Midian	0.1316	0.0434	0.0237	6.6088e-004	2.2484e-004
	Mean	0.1325	0.0567	0.0237	9.0397e-004	2.5737e-004
	SD	0.0453	0.0427	0.0059	8.9015e-004	1.7105e-004
F8	min	0.8571	1.4462e-004	5.4495e-011	2.0017e-013	0
	Max	1.1425	1.0344	1.0280e-007	1.3998	0
	Midian	1.0370	0.0028	3.1306e-010	1.1138e-004	0

	Mean	1.0292	0.0533	3.5514e-009	0.0915	0
	SD	0.0529	0.1674	1.5102e-008	0.2771	0
F9	min	33.4843	27.6249	98.1627	1.2260e-010	0
	Max	116.9836	226.2016	145.0373	165.9932	0
	Midian	64.3820	81.5295	134.4844	7.5345e-004	0
	Mean	65.8825	95.3020	132.0604	9.2961	0
	SD	17.8519	53.0519	9.7593	34.6402	0
F10	min	0.7373	0.0029	1.1695e-006	3.6651e-008	8.8818e-016
	Max	3.1276	4.6982	4.1530e-006	5.4371	8.8818e-016
	Midian	1.9979	0.9379	2.0644e-006	0.0028	8.8818e-016
	Mean	1.9632	1.2461	2.2340e-006	0.2293	8.8818e-016
	SD	0.6116	1.2581	7.0297e-007	0.8739	0

Fig 2 gives the comparison of convergence processes of SI-SFLA, PSO, SFLA, DE and TLBO in the above six benchmark functions (F1, F3, F7, F8, F9, F10) averaged on 50 trial runs, when the population size is 50 and the maximum generation is 1000 according to the dimension 30. For SFLA and SI-SFLA, the maximum generation=5*200. (local iteration number is 5 and global iteration number is 200). The result show that SI-SFLA has a quick convergence speed than PSO,SFLA,DE and TLBO, especially, for F1, F8, F9, F10 function, SI-SFLA obtains global solution or closer-to-global solution in iteration 100.

D. Change of Difference in Efficiency with Increasing Dimensionality

To further demonstrate its efficiency and effectiveness on high-dimensional problems, we also compared SI-SFLA with PSO, SFLA, DE and TLBO. SI-SFLA has a more smaller value of the mean and the standard deviation than PSO, SFLA, DE and TLBO, when the dimension is 10, 30 and 50 as TABLE 3~6.

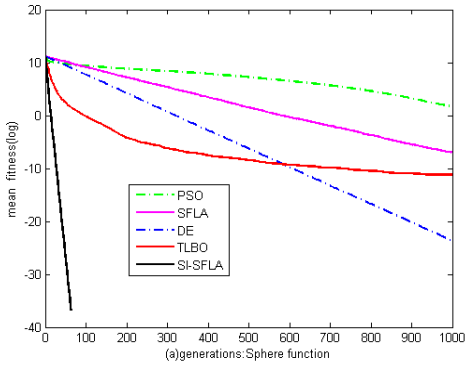

(a)Sphere

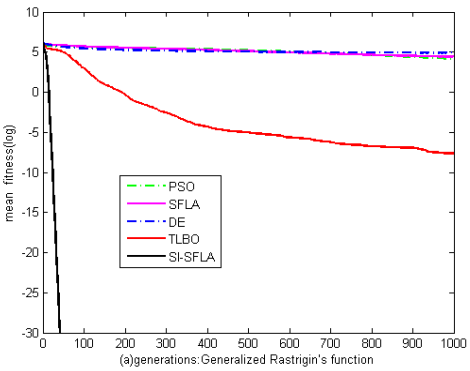

(b) Rastrigin

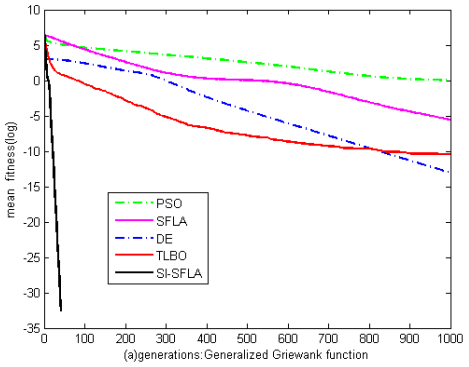

(c) Griewan

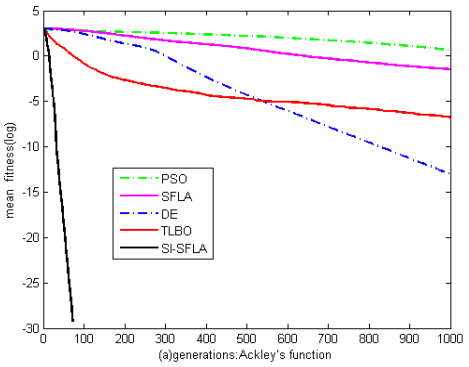

(d)Ackley

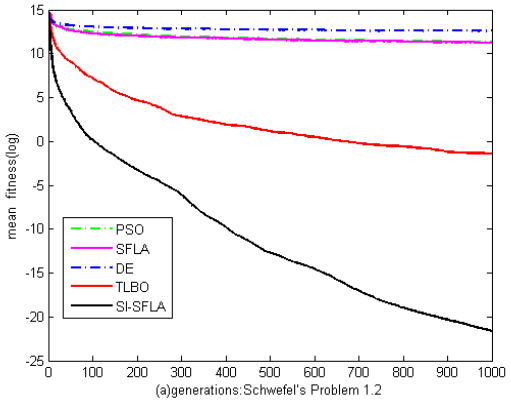

(e)Schwefel's Problem 1.2

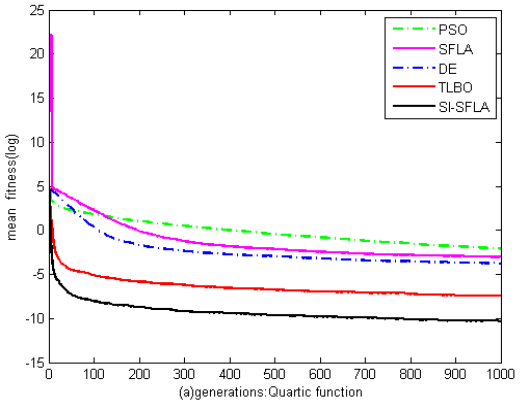

(f) Quartic function i.e. Noise

Fig 2 Convergence curve for different benchmark problems

TABLE 3
NUMERICAL EXPERIMENT RESULTS OF SPHERE FUNCTION(F1)

Dimension	PSO	SFLA	DE	TLBO	SI-SFLA
10Mean	5.7236e-012	2.7017e-025	1.2459e-045	0.0428	5.6119e-110
SD	1.3761e-011	7.7906e-025	2.5355e-045	0.1863	1.2353e-109
30Mean	7.2682	4.6363e-005	5.8090e-011	0.4735	9.4713e-091
SD	6.2093	2.8341e-004	3.8643e-011	2.2540	1.2209e-090
50Mean	524.7095	32.6081	0.0038	0.6408	4.8316e-086
SD	196.9751	92.6275	0.0013	3.4093	6.0995e-086

TABLE 4
NUMERICAL EXPERIMENT RESULS OF GENERALIZED RASTRIGIN'S FUNCTION(F9)

Dimension	PSO	SFLA	DE	TLBO	SI-SFLA
10Mean	3.2778	7.2302	3.8369e-015	2.2046	0
SD	1.6819	3.6425	1.4140e-014	5.9969	0
30Mean	65.8825	59.7707	132.0604	9.2961	0
SD	17.8519	24.0783	9.7593	34.6402	0
50Mean	195.5192	298.5764	335.7978	4.0913	0
SD	38.6663	99.2877	13.9482	19.6936	0

TABLE 5
NUMERICAL EXPERIMENT RESULTS OF ACKLEY'S FUNCTION9F(10)

Dimension	PSO	SFLA	DE	TLBO	SI-SFLA
10Mean	6.8402e-007	0.3334	4.4409e-015	0.3614	8.8818e-016
SD	6.5761e-007	0.5923	0	1.1992	0
30Mean	1.9632	1.1479	2.3458e-006	0.2293	8.8818e-016
SD	0.6116	1.2890	7.5809e-007	0.8739	0
50Mean	6.1583	3.8771	0.0154	19.6936	8.8818e-016
SD	0.8369	2.7107	0.0031	1.3180	0

TABLE 6
NUMERICAL EXPERIMENT RESULTS OF GENERALIZED GRIEWANK FUNCTION(F8)

Dimension	PSO	SFLA	DE	TLBO	SI-SFLA
10Mean	0.1129	0.0464	2.7145e-004	0.2009	0
SD	0.0711	0.0275	0.0019	0.2608	0
30Mean	1.0292	0.0533	3.5514e-009	0.0915	0
SD	0.0529	0.1674	1.5102e-008	0.2771	0
50Mean	6.0022	1.2027	0.0063	0.1114	0
SD	2.4769	0.7862	0.0037	0.3256	0

Especially, SI-SFLA has a good fitness for F8, F9, F10 function, which have many local best fitness, regardless of dimension is 10, 30 or 50. That is to say, our algorithm has a good robustness.

V. CONCLUSION

SFLA algorithm was an heuristic algorithm which combined PSO[19][20][21] with MA algorithm.This paper presents a novel improved SFLA algorithm (called SI-SFLA) to improve the stability and global search ability for high-dimensional continuous function optimisation. Single step search strategy and interactive learning rule was introduced to improved SFLA Algorithm. Single step search strategy is based on multidimensional data correlation to determine the search direction, which improved the search accuracy of SFLA algorithm, and interactive learning rule makes all the frogs find new important information which strengthen the global searching ability of the SFLA algorithm. The performance of the proposed SI-SFLA method is checked with the recent and well-known optimization algorithms such as PSO, SFLA, DE, TLBO, etc. by experimenting with different benchmark problems with different characteristics like, multimodality and dimensionality. The effectiveness of SI-SFLA method is also checked for different performance criteria, like midian, standard deviation, mean solution, average function evaluations required, convergence rate, etc. The results show better performance of SI-SFLA method over other natured-inspired optimization methods for the considered benchmark functions. This method can be used for the optimization of engineering design applications.

APPENDIX BENCHMARK FUNCTION

1. F1 Sphere

$$f_1 = \sum_{i=1}^{n} x^2{}_i$$

2. F2 Schwefel's Problem 2.22

$$f_2(x) = \sum_{i=1}^{n} | x^2{}_i | + \prod_{i=1}^{30} | x_i |$$

3. F3 Schwefel's Problem 1.2

$$f_3(x) = \sum_{i=1}^{n} (\sum_{j=1}^{i} x_j)^2$$

4. F4 Schwefel's Problem 2.21

$$f4(x) = \max\{| x_i |\}, i \in [1, n]$$

5. F5 Generalized Rosenbrock's function

$$f5(x) = \sum_{i=1}^{n-1} 100 \bullet (x_{i+1} - x_i^2)^2 + (1 - x_i)^2$$

6. F6 Step function

$$6.\ f6(x) = \sum_{i=1}^{n} (\lfloor x_i + 0.5 \rfloor)^2$$

7. F7 Quartic function i.e. Noise

$$f7(x) = \sum_{i=1}^{n} ix^4{}_i + random[0,1)$$

8. F8 Generalized Griewank function

$$f8(x) = \frac{1}{4000} \sum_{i=1}^{n} x_i^2 - \prod_{i=1}^{n} \cos(\frac{x_i}{\sqrt{i}}) + 1$$

9. F9 Generalized Rastrigin's function

$$f9(x) = \sum_{i=1}^{n} (x_i^2 - 10\cos(2\pi x_i) + 10)$$

10. F10 Ackley's function

$$f10(x) = -20\exp\left(-0.2\sqrt{\frac{1}{n}\sum_{i=1}^{n} x_i^2}\right) - \exp\left(\frac{1}{n}\sum_{i=1}^{n} \cos(2\pi x_i)\right) + 20 + e$$

ACKNOWLEDGMENT

This paper has been supported by Guangdong Province Natural Science Doctoral start-up fund project (S2011040004285); Humanities and Social Science Youth Fund project of Education Ministry (10YJCZH234); the subject of Ideological and political education in Guangdong Province (NO.2011ZZ012); Research on Guangdong Province college Party Construction, (NO.2012BKZZB12). Guangdong Province Science and technology plan project (2012B031000018)

REFERENCES

[1] D.E. Goldberg, "Genetic Algorithms in search Optimization and Machine Learning, " *Addison-Wesley*, Reading, MA, 1989.

[2] J. Kennedy, R. Eberhart, "Particle swarm optimization,"in: *Proceedings of IEEE International Conference On Neural Network, 1995*, pp. 1942-1948.

[3] Xingjuan Cai, Zhihua Cui, Jianchao Zeng, Ying Tan, "Dispersed particle swarm optimization,"*Information Processing Letters*, 105 (2008) 231-235

[4] M. Dorigo, Optimization, "Learning and Natural Algorithms,"*Ph.D. Thesis*, Politecnico di Milano, Italy, 1992.

[5] D. Simon, "Biogeography-based optimization, "*IEEE Transactions on Evolutionary Computation* (12) (2008) 702-713.

[6] D. Simon, M. Ergezer, D. Du,"Population distributions in biogeography-based optimization algorithms with elitism, "in: *IEEE Conference on Systems*, Man, and Cybernetics, 2009, pp. 1017-1022.

[7] R. Storn and K. Price, "Differential evolution - A simple and efficient adaptive scheme for global optimization over continuous spaces," *ICSI Tech. Rep.* TR-95-012 (1995).

[8] R. Storn and K. Price, "Differential evolution - A simple and efficient heuristic for global optimization over continuous spaces," *J. Global Optimization* 11 (1997) 341-359.

[9] R.V. Rao, V.J. Savsani, D.P. Vakharia, "Teaching-Learning-Based Optimization,"*Information Sciences*, 183 (2012) 1-15

[10] TaherNiknam, Rasoul Azizipanah-Abarghooee, Mohammad Rasoul Narimani, "A new multi objective optimization approach based on TLBO for location of automatic voltage regulators in distribution systems,"*Engineering Applications of Artificial Intelligence* 2012, 25, 1577-1588.

[11] R. Venkata Rao, Vivek Patel,"An improved teaching-learning-based optimization algorithm for solving unconstrained optimization problems," *Scientia Iranica*,2012.12.

[12] TaherNiknam, Rasoul Azizipanah-Abarghooee, Mohammad Rasoul Narimani, "A new multi objective optimization approach based on TLBO for location of automatic voltage regulators in distribution systems,"*Engineering Applications of Artificial Intelligence* 2012, 25, 1577-1588.
[13] M. Eusuff, K. Lansey, "Optimization of water distribution network design using the shuffled frog leaping algorithm, " *Journal of Water Resource Plan and Management* 129 (3) (2003) 10-25.
[14] Q. Y. DUAN, V. K. GUPTA, S. SOROOSHIAN, "Shuffled Complex Evolution Approach for Effective and Efficient Global Minimization, "*JOURNAL OF OPTIMIZATION THEORY AND APPLICATIONS:* Vol. 76, No. 3, (1993)MARCH.
[15] Thai-Hoang Huynh, "A modified shuffled frog leaping algorithm for optimal tuning of multivariable PID controllers," in: *Proceedings of International Conference on Information Technology (ICIT 2008),* Singapore, 2008, pp.21-24.
[16] J.P. Luo, M.R. Chen, X. Li, "A novel hybrid algorithm for global optimization based on EO and SFLA, "in: *Proceedings of the Fourth IEEE conference on Industry electronics and applications (ICIEA2009)*, Xi'an, China, 2009, pp. 1935-1939.
[17] Xia Li, Jianping Luo, Min-Rong Chen, Na Wang. "An improved shuffled frog-leaping algorithm with extremal optimisation for continuous optimisation," *Information Sciences* 192 (2012) 143-151
[18] Han Huang, Hu Qin, Zhifeng Hao, Andrew Lim. "Example-based learning particle swarm optimization for continuous optimization," *Information Sciences*. 182 (2012) 125-138.
[19] Liangyou SHU, Lingxiao YANG, "A Modified PSO to Optimize Manufacturers Production and Delivery", *JOURNAL OF SOFTWARE*, VOL. 7,pp,2325-2332,2012.
[20] Shengli Song, Yong Gan, Li Kong ,Jingjing Cheng, "A Novel PSO Algorithm Based on Local Chaos & Simplex Search Strategy and its Application, " *JOURNAL OF SOFTWARE*, VOL. 6, pp.604-611, 2011.
[21] Weitian Lin, Xingsheng Gu, Zhigang Lian, Yufa Xu,Bin Jiao, "A Self-Government Particle Swarm OptimizationAlgorithm and Its Application in TexacoGasification, " *JOURNAL OF SOFTWARE*, VOL. 8, 472-479 ,2013.

Deyu Tang was born in Jilin Province, China in 1978. He received his degree of Master in Computer software and theory in 2004 at South China University of Technology, China. Currently he is working on his doctoral degree in computer application at South China University of Technology, China. He is a Docent in College of Medical Information and Engineering at GuangDong Pharmaceutical University, Guangzhou, China. He has published at least 5 articles. Two of them has been published in Computer engineering and Applications. Three of them can be indexed by EI. His interest is in studying data mining, Bioinformatics, Swarm intelligence.

Yongming Cai was born in GuangDong Province, China in 1975. He received of Ph.D. in biomedical engineer in 2012 at Sun Yat.sen University, China. Currently, he is an associate professor in College of Medical Information and Engineering at GuangDong Pharmaceutical University, Guangzhou, China. His main research interests are data mining and bioinformatics.

Hardware/Software Partitioning Algorithm Based on Genetic Algorithm

Guoshuai Li
Aeronautics and Astronautics Engineering College, Air Force Engineering University, Xi'an, China
Email. lgsman1@163.com

Jinfu Feng, Junhua Hu, Cong Wang and Duo Qi
Aeronautics and Astronautics Engineering College, Air Force Engineering University, Xi'an, China
Email. wcsfjf@163.com, wcshjh9231@163.com, chenwang6666@126.com, wcsqd5267@163.com

***Abstract*—To solve the hardware/software(HW/SW) partitioning problem on the system that contains only one CPU, a new algorithm based on GA is studied. Firstly, the concept of hardware orientation is put forward, and then used to create the initial colony of GA and in mutation process, which reduces the randomicity of initial colony and the blindness of search. Secondly in the process of GA, crossover and mutation probability become more and more small, this not only ensures a big search space in the early, but also keeps the good solution later. Experimental statistics show that the efficiency of the proposed algorithm outperforms the algorithms in comparison by up to 23% in large-scale problem. What's more, it can obtain better solution. In conclusion, the proposed algorithm has higher efficiency and appears to be a better solution under specific conditions.**

***Index Terms*—hardware/software partitioning, hardware orientation, genetic algorithm**

I. INTRODUCTION

HW/SW partitioning technology is a crucial step in SOC HW/SW co-design and embedded systems' realization. The function of it is to decide which components of the system should be realized through hardware and which ones through software, and finally provide the best scheme for system while satisfying design constraints. Clearly, this step has dramatic impact on the cost and performance of the whole system.

Most formulations of HW/SW partitioning problem have been proved NP-hard[1], so exact algorithms tend to be quite slow for large input, hence for large partitioning problem, heuristic methods are generally applied to explore the search space in order to get the nearly optimal solutions, although they cannot guarantee the optimum solution, they comprise the majority of the research and some significant research has been done such as Genetic Algorithm(GA)[2][3], Particle Swarm Optimization(PSO)[4][5], Tabu Search(TS)[6][7], Ant Algorithm(AA)[8][9], Simulated Annealing(SA)[10] as well as some improved schemes.

GA is one of the most widely used random search techniques. It aims to obtain near-optimal partitioning by imitating the process of biological evolution. This technique has been used for HW/SW partitioning in many studies. Paper[11] expounded basic application of GA in HW/SW partitioning where some implementation methods such as coding, fitness function, selection of individuals, crossover, mutation and convergence rule were discussed in detail. Paper[12] partitioned the system into hardware and software components using GA where an enhanced resource constrained scheduling algorithm was used to determine system performance, as a result, execution time and power consumption were reduced greatly. Paper[13] proposed an Advanced Non-Dominated Sorting Genetic Algorithm (ANSGA), by introducing a removing method for building non-dominated sets (NDS) and an elitism preserving strategy for generating NDS and new sets, it not only reduced computational burden but also obtained global convergence. Paper[14] used the idea of two levels of implementation methodology, the first level provided initial solution for GA which run in the second level, results indicated that this method can improve throughput and efficiency with only a small amount of increased design space. In addition, [15][16][17] improved GA algorithm in different aspect and obtained better solution too.

To improve partitioning quality and algorithm efficiency, we propose a new partitioning algorithm based on GA. In this paper, the concept of hardware orientation is put forward and used in the process of producing initial colony and mutating, as a result, it not only avoided the blindness of creating initial colony through random method but also controlled the direction of mutation. Furthermore, we design an adaptive method for crossover/mutation probability. Experimental results demonstrate superiority of proposed approach over existing algorithms in comparison in terms of efficiency and solution quality.

This paper is organized as follows. In section 2 we introduce HW/SW partitioning problem, as well as provide the objective function in this paper. In section 3, we propose the concept of hardware orientation and its calculation. In section 4, we describe the detail of proposed hybrid algorithm based on GA. In section 5, we

doi:10.4304/jcp.9.6.1309-1315

show experimental results and analysis, and then compare proposed algorithm based on GA with existing algorithms. Finally, section 6 draws conclusions of our work and makes prediction for future work.

II. Problem Description

HW/SW partitioning is one of the most crucial steps in the design of embedded systems that typically consist of hardware and software components. Before partitioning, it's necessary to identify the construction of implementation platform. This paper discusses platform with single CPU, that is to say, the system consist of one CPU and FPGA or other reconfigurable logic module. The assignment of HW/SW partitioning is to map tasks to either CPU or hardware components while satisfying design constraints.

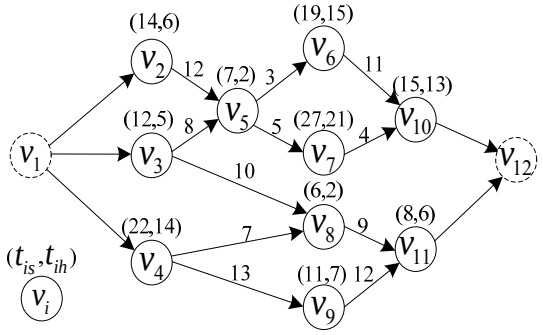

Figure1. The DAG model of system.

We now formalize the problem as follows. Tasks of system which will be partitioned are given in the form of DAG(directed acyclic graph) just as is shown in Fig 1, $G=(V,E)$ [18]. $V=\{v_1,v_2,\cdots,v_n\}$ denotes the set of nodes, while v_i denotes the i th task node, E indicates the set of edges, c_{ij} denotes communication cost between v_i and v_j, t_{is} and t_{ih} are execution time of task through software and hardware respectively, s_{is} and s_{ih} denote area cost of v_i through software and hardware, S_s, S_h and C represent software area constraint, hardware area constraint and communication constraint respectively, $T_{\cos t}$ is execution time which is defined to be the sum of processing time of all tasks. Assume that communication cost between two adjacent nodes that are all carried out through hardware or software can be overlooked, thus the objective function (1) can be formulated as the following minimization problem using the method in paper[18].

n denotes the number of nodes, x_i denotes how v_i is realized where $x_i=1(x_i=0)$ means v_i is realized through hardware(software), s_{is} and s_{ih} are area cost of v_i realized through software and hardware respectively, the sum of all the s_{is} should be less than S_s, and so is s_{ih} to S_h.

$$\begin{cases} \min\left(T_{\cos t}=\sum_1^n\left(t_{ih}x_i+t_{is}\left(1-x_i\right)\right)\right) \\ s.t.\quad \sum_1^n\left(s_{is}\left(1-x_i\right)\right)\le S_s \\ \quad\quad \sum_1^n\left(s_{ih}x_i\right)\le S_h \\ \quad\quad \sum_1^n\left(\sum_{k\in V_s}c_{ik}x_i+\sum_{k\in V_h}c_{ik}\left(1-x_i\right)\right)\le C \end{cases} \tag{1}$$

III. Calculation of Hardware Orientation

In this paper, hardware orientation is defined as superiority of implementation of one task through hardware over software, it is characterized by three metrics which are Area, Time and Communication.

A. Area-Hardware Orientation

$$S_{iorien}=\begin{cases} A\left(1-B\right)+B & , \quad S_{cons}<S_{sum} \\ 1 & , \quad S_{cons}\ge S_{sum} \end{cases} \tag{2}$$

Because the requirement of typesetting, in (2) we use A to replace $\left(S_{\max}-S_i\right)/\left(S_{\max}-S_{\min}\right)$, B to replace S_{cons}/S_{sum}. S_i denotes additional area of s_{ih} than s_{is}, while $S_{\max}$ and $S_{\min}$ indicate respectively the maximum and minimum value of S_i, S_{sum} is total area cost when the whole of the nodes are realized through hardware. In addition, S_{cons} denotes area constraint.

B. Time-Hardware Orientation

$$T_{iorien}=\begin{cases} \dfrac{\left(t_{is}-t_{ih}\right)/t_{is}-T_{1\min}}{T_{1\max}-T_{1\min}} & , \quad t_{is}>t_{ih} \\ 1-\dfrac{\left(t_{ih}-t_{is}\right)/t_{ih}-T_{2\min}}{T_{2\max}-T_{2\min}} & , \quad t_{is}\le t_{ih} \end{cases} \tag{3}$$

Here t_{is} and t_{ih} denote time cost of v_i realized through software and hardware respectively, while $\left(t_{is}-t_{ih}\right)/t_{is}$ and $\left(t_{ih}-t_{is}\right)/t_{ih}$ are performance ratio, $T_{1\max}$, $T_{1\min}$, $T_{2\max}$ and $T_{2\min}$ are the maximum and minimum value of performance ratio.

C. Communication-Hardware Orientation

$$C_{isrorien}=\sum_j\left[\left(1-D\right)\times t_{sr}+D\times t_{hr}\right]c_{ij} \tag{4}$$

$$C_{isworien}=\sum_j\left[\left(1-D\right)\times t_{sw}+D\times t_{hw}\right]c_{ij} \tag{5}$$

$$C_{ihrorien} = \sum_j \left[(1-D) \times t_{hr} + D \times t_{sr} \right] c_{ij} \quad (6)$$

$$C_{ihworien} = \sum_j \left[(1-D) \times t_{hw} + D \times t_{sw} \right] c_{ij} \quad (7)$$

$$C_{iorien} = \frac{C_{isrorien} + C_{isworien}}{C_{ihrorien} + C_{ihworien}} \quad (8)$$

t_{sr}, t_{sw}, t_{hr} and t_{hw} are reading and writing delay of hardware and software, $D=S_{iorien} \times T_{iorien}$.

Consequently, the synthesized factor of hardware orientation can be described as following.

$$Z_{iorien} = \frac{\alpha S_{iorien} + \beta T_{iorien} + \eta C_{iorien}}{S_{iorien} + T_{iorien} + C_{iorien}} \quad (9)$$

$$\alpha + \beta + \eta = 1,\ \alpha > 0,\ \beta > 0,\ \eta > 0.$$

IV. ALGORITHM

In recent years, research based on GA for solving multi-objective optimization problem makes good progress[19][20][21]. Here we mainly consider the following aspects, creation of initial colony, selection of individuals, crossover and mutation.

(1) Coding. In a number of related articles, there are two familiar coding method for GA, the binary and the decimal, by contrast, the binary-biased genetic algorithms have higher searching efficiency, less time- consumption for convergence, wider selecting domain of crossover and mutation probability and stronger robustness of optimized value than decimal-biased genetic algorithms[22]. What's more, considering that the state of the node here includes hardware realization and software realization, we choose binary as coding mechanism. $X = (x_1, \ x_2, \ \cdots, \ x_n)$ denotes a partitioning plan, $1 \le i \le n$.

(2) We make reciprocal of objective function $F(X) = 1/T_{cost}$ as fitness function in this paper.

3. Creation of initial colony. In this paper, we create initial colony on the base of hardware orientation, the bigger the hardware orientation is, the higher the probability that the node is initialized to hardware realization will be, and vice versa. Concretely, we first generate a random number $r_i \in (0,1)$, if $r_i < Z_{iorien}$, v_i will be initialized to hardware realization, otherwise to software realization. In addition, Hamming distance $H(X^i, X^j) = \sum_{k=1}^{n} \left| X_k^i - X_k^j \right|$ is adopted for the difference among individuals and $H(X^i, X^j) > 4$, X^i and X^j denote partitioning plans which are called individuals here. Repeat the operation above until we have N_X individuals.

(4) Selection of individuals. In order to prevent the precociousness phenomenon from happening, the proposed algorithm selects individuals adaptively according to the change of fitness, consequently, selection probability of x_i can be defined using the method mentioned in paper[23].

$$p_i = f'(x_i) \Big/ \sum_{i=1}^{n} f'(x_i) \quad (10)$$

$$f'(x_i) = af(x_i) + \frac{(f_{\max} - f_{\min})(e - e^{g/g_{\max}})}{e + e^{g/g_{\max}}} \quad (11)$$

$f(x_i)$ expresses fitness value of x_i, while $f_{\max}$ denotes the maximal value of $f(x_i)$ in current colony and $f_{\min}$ indicates the minimal one, g indicates the number of iterations while $g_{\max}$ indicates its maximal value, a denotes the weight of $f(x_i)$ in $f'(x_i)$, it is a constant that is greater than zero and $a = 0.75$ in this paper.

According to this selection strategy, selection probability of individuals with big fitness value can reduce greatly at the beginning of algorithm, this is beneficial for global searching, as the processing of algorithm, selection probability of individuals with big fitness value gradually grow bigger, this is beneficial for the convergence of algorithm.

(5) Crossover and mutation. In this process, some individuals($N_X/2$) are selected for crossover using two-point crossover method[18]. The selection of crossover probability P_c and mutation probability P_m will influence the whole process of genetic algorithm. In other words, the bigger the difference of colony and fitness of individual are, smaller P_c and P_m can help to protect individuals that have bigger fitness, meanwhile, the convergence speed can be improved too. The smaller the difference of colony and fitness of individual are, bigger P_c and P_m can not only help to produce excellent individuals but also prevent algorithm from entering local optimum. Experiments have shown that adaptive change of P_c and P_m can improve algorithm performance than fixed value[24]. Thus we put forward an adaptive method for crossover and mutation probability.

$$P_c = \begin{cases} p_{c1} \dfrac{f_{\max} - \max(f_i, f_j)}{f_{\max} - f_{avg}}, & \min(f_i, f_j) > f_{avg} \\ p_{c2}, & \min(f_i, f_j) \le f_{avg} \end{cases} \quad (12)$$

$$P_m = \begin{cases} p_{m1} \dfrac{f_{\max} - f}{f_{\max} - f_{avg}}, & f > f_{avg} \\ p_{m2}, & f \le f_{avg} \end{cases} \quad (13)$$

f_{avg} denotes average fitness of all the current individuals, while f denotes fitness of individual waiting for mutation, f_i and f_j are fitness of individuals that are waiting for cross, p_{c1}, p_{c2}, p_{m1} and p_{m2} are constants. If the individual fitness is smaller than f_{avg}, bigger P_c and P_m should be selected for promoting melioration of its fitness, whereas, smaller P_c and P_m should be selected for preserving the individual. Considering that individuals with bigger fitness should have smaller crossover probability, thus P_c uses $\min(f_i, f_j)$ as boundary.

(6) Termination criterion. For the sake of ending GA at appropriate time, the proposed algorithm uses dynamic termination criterion. Concretely, we define the largest number of iterations $Gene_{\max}$ and the minimum evolution rate $GeneImproRat_{\min} = 4\%$, if the evolution rate in three successive colonies is not larger than $GeneImproRat_{\min}$ or , GA will terminate.

The pseudo code of GA is as shown in Table1.

TABLE I.
GA PROCESS

Input:

Task graph G and constraints S_s, S_h, C.

Output:

The HW/SW partitioning result $X = (x_1, \quad x_2, \quad \cdots, \quad x_n)$ and runtime.

1. begin
2. Calculate the comprehensive factor of hardware orientation Z_{iorien} and set termination criterion.
3. Create initial colony on basis of Z_{iorien}, make $g = 0$, $N_{GeneImproRat_{\min}} = 0$. // $N_{GeneImproRat_{\min}}$ denotes the successive generations that evolution rate is smaller than $GeneImproRat_{\min}$.
4. Calculate fitness of individuals in $P(0)$ and average fitness.
5. Perform the operation between 6 and 21 again and again before meeting termination criterion.
6. Calculate selection probability p_i for every individual in $P(g)$.
7. for($k = 0; k < N_X; k = k + 2$)
8. {
9. Select two individuals on basis of p_i.
10. Create a random number $0 < u < 1$.
11. if($u < P_m$)
12. Perform mutation operation for selected individuals, if $Z_{iorien} > 0.9$, no matter what state of the node is, the state is set to 1, otherwise, perform the routine mutation operation, the result is put into next colony.
13. elseif($u < P_m + P_c$)
14. Perform crossover operation and put the result into next colony.
15. else
16. put the individuals into next colony without change.
17. }//end for
18. $g = g + 1$, calculate the fitness of individuals in $P(g)$ and the average fitness.
19. if($GeneImproRat_{cur} \le GeneImproRat_{\min}$)
20. $N_{GeneImproRat_{\min}} = N_{GeneImproRat_{\min}} + 1$.
21. end if
22. Output X_{GA} which has the biggest fitness value in $P(g)$ and runtime.
23. end

V. EXPERIMENT AND ANALYSIS

Creation of test set. For testing, we firstly create randomly several DAGs that have specified number of nodes and average branches, then let every node associated with one function whose cost(hardware area, software area, communication cost and runtime etal) is used to simulate task cost. Eventually, we get 6 DAGs with 30, 60, 90, 120, 200, 400 nodes respectively.

Experimental environment: (1) Pentium(R) Dual-Core 2.5GHz CPU, 2G internal storage. (2) Windows XP operating system. 3. Programming environment is Matlab R2007a.

To verify the effectiveness of proposed algorithm, we choose GA[12]and ANSGA[13] as comparison. Also, in order to make a fair comparison, all related parameters in our experiment are set on the same benchmark, initial crossover probability is set to 0.8 while initial mutation probability to 0.13.

Table3 shows partitioning results of three algorithms, it can be observed that, (1) Proposed algorithm has higher convergence speed, because hardware orientation can reduce randomicity of initial colony and affect search direction, to sum up, these two aspects reduce the number of iterations. What's more, selection strategy is also helpful to improve search speed. (2) On small-scale problem when the number of nodes is less than 60, proposed algorithm has lower efficiency than ANSGA, because the calculation of hardware orientation costs a long time. However, with the addition of scale, when the number of nodes is more than 90, the proposed algorithm can not only obtain better solution but also improve operating efficiency of nearly 23%. What's more, the larger the scale is, the bigger the improvement will be. The reason is that ANSGA must array the colony, construct non-dominated set and new groups in every iteration and this will cost much time. (3) Compared with the other two algorithms, GA has the shortest runtime, whereas it only obtains solution with lowest quality, because basic GA has great dependence on initial solution, a good initial solution could result in a good final solution, while a bad one will affect the quality of final solution.

TABLE II.
EXPERIMENTAL RESULTS

Number of nodes	S_h	S_s	C	Algorithm	T_{cost}	Cost of time
30	2850	1409	591	GA	5897	81
				ANSGA	5692	847
				Our algorithm	5685	896
60	5909	2943	1356	GA	11904	240
				ANSGA	10859	8263
				Our algorithm	10813	8379
90	8684	4308	2014	GA	17730	1158
				ANSGA	16728	57573
				Our algorithm	16347	49413
120	11611	5770	2637	GA	22493	1372
				ANSGA	21022	114437
				Our algorithm	19844	95108
200	17192	9416	3783	GA	37441	1836
				ANSGA	34739	280347
				Our algorithm	33053	224318
400	28154	15681	6539	GA	75620	2925
				ANSGA	70209	674301
				Our algorithm	66681	510302

To intuitively show experimental results, we let the three algorithms run 30 times respectively for the 6 DAGs, then calculate average value of the results for each DAG, finally we obtain the comparison between proposed algorithm and the other two algorithms on partitioning results and runtime, as is shown in Fig 3 and Fig 4.

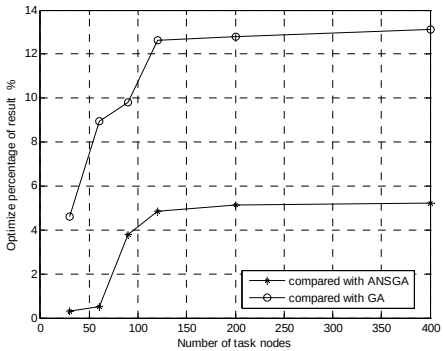

Figure 3 Optimize percentage of partitioning result

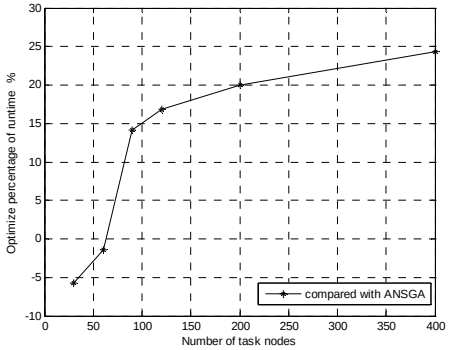

Figure4. Optimize percentage of runtime

Assume that there are 400 task nodes. We obtain initial solution using random method and hardware orientation respectively, the simulation results of ANSGA are shown in Fig 5, as can be seen, initial solution coming from hardware orientation has faster convergence rate and bring on better solution. Fig 6 shows simulation results of ANSGA and our algorithm, it intuitively illustrates the advantage of proposed algorithm on large-scale problem.

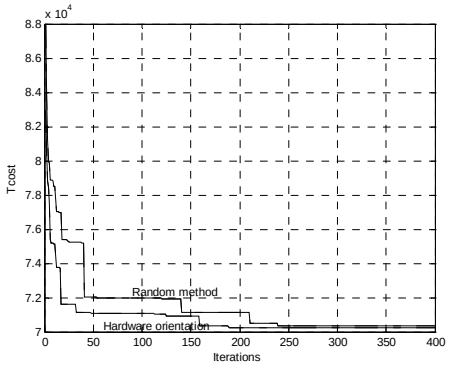

Figure 5 Simulation results of ANSGA with diffident initial solution

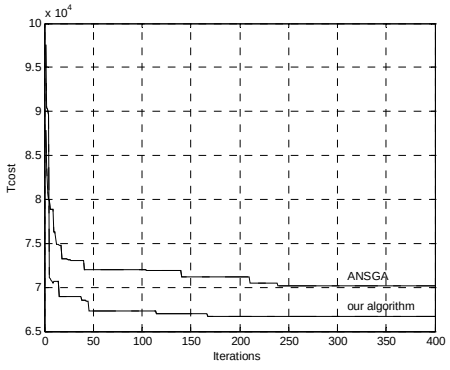

Figure6. Simulation results of proposed algorithm and ANSGA

VI. CONCLUSIONS

Based on GA, we present a simple but very efficient algorithm for solving HW/SW partitioning problem in this article. Compared with the other two algorithms, time complexity of proposed algorithm includes additional time for calculating hardware orientation except for calculating genetic operation and fitness. However, the application of hardware orientation reduces the number of iterations and it only need calculated once, as a result, the proposed algorithm can obtain higher efficiency especially on large-scale problem.

The value of crossover and mutation probability is larger than classical GA in this paper, this may induce blindness of search, but the use of hardware orientation and adaptive method prevent its occurrence. Furthermore, they increase the probability of introducing new chromosome which can increase GA's ability of local search to some extent.

In order to simplify the problem, the proposed objective function doesn't take into account power cost which may impact partitioning accuracy, our on-going work will improve the objective function.

REFERENCES

[1] Arato P, Mann ZA, Orban A. Algorithmic aspects of hardware/software partitioning, ACM Trans Des Autom Electron Syst. 2005. 10(1): pp. 136-156. doi: 10.1145/1044111.1044119.

[2] Glover F, Kelly JP, Laguna M.: Genetic algorithms and tabu search: hybrids for optimization, Computers and Operations Rsearch. 1995. 22(1): pp. 111-134. doi: 10.1016/0305-0548(93)E0023-M.

[3] Jian Pan, Guohong Mao, Jinxiang Dong.: A Web-Based Platform for Intelligent Instrument Design Using Improved Genetic Algorithm, Journal of software, 2012. 7(10): pp. 2333-2340. doi:10.4304/jsw.7.10.2333-2340.

[4] Shaobo Zhong, Zhongshi He.: Application of Particle Swarm Optimization Algorithm based on Classification Strategies to Grid Task Scheduling, Journal of software, 2012. 7(1): pp. 118-124. doi:10.4304/jsw.7.1.118-124.

[5] Shih-An Li, Chen-Chien Hsu, Ching-Chang Wong, Chia-Jun Yu.: Hardware/software co-design for particle swarm optimization algorithm, Information Sciences. 2011. (181): pp. 4582-4596. doi:10.1016/j.ins.2010.07.017.

[6] Jigang Wu, Srikanthan Thambipillai, Ting Lei.: Efficient heuristic algorithms for path-based hardware/software partitioning, Mathematical and Computer Modelling. 2010 (51): pp. 974-984. doi:10.1016/j.mcm.2009.08.029.

[7] Jigang Wu, Pu Wang, Siew-Kei Lam, Thambipillai Srikanthan.: Efficient heuristic and tabu search for hardware/software partitioning, The Journal of Supercomputing. 2013. 66(1): pp. 118-134. doi:10.1007/s11227-013-0888-9.

[8] Yu-don Zhang, Le-nan Wu, Geng Wei, Han-qian Wu, Yong-liang Guo.: Hardware/software partition using adaptive ant colony algorithm, Control and Decision. 2009. 24(9): pp. 1385-1389. doi:10.3321/j.issn:1001-0920.2009.09.021.

[9] T. He, Y. Guo.: Power consumption optimization and delay based on ant colony algorithm in network-on-chip, Engineering Review. 2013. 33(3): pp. 219-225.

[10] Henkel J, Ernst R.: An approach to automated hardware/software partitioning using a flexible granularity that is driven by high-level estimation techniques, IEEE Transactions on VLSI Systems, 2001. 9(2): pp. 273-289. doi: 10.1109/92.924041.

[11] Yun Zheng, Guo-yong Huang.: System Level Software/Hardware Partitioning by Genetic Algorithm, Journal of Computer-Aided Design & Computer Graphics, 2002, 14(8): pp. 731-734.

[12] Madhura Purnaprajna, Marek Reformat, Witold Pedrycz .: Genetic algorithms for hardware-software partitioning and optimal resource allocation, Journal of Systems

Architecture, 2007(53): pp. 339-354. doi: 10.1016/j.sysarc.2006.10.012.
[13] Sheng-qin Luo, Xiao-xiao Ma, Yi Lu .: An Advanced Non-Dominated Sorting Genetic Algorithm Based SOC Hardware/Software Partitioning, ACTA ELECTRONICA SINICA, 2009 (11):pp. 2595-2599. doi: 10.3321/j.issn:0372-2112.2009.11.043.
[14] Nithiyanantham Janakiraman, Palanisamy Nirmal Kumar.: Multi-objective module partitioning design for dynamic and partial reconfigurable system-on-chip using genetic algorithm, Journal of Systems Architecture, 2014, 60(1): pp.119-139. doi: 10.1016/j.sysarc.2013.10.001.
[15] Yan Kang, He Lu, Jing He.: A PSO-based Genetic Algorithm for Scheduling of Tasks in a Heterogeneous Distributed System, Journal of software, 2013, 8(6): pp. 1443-1450. doi:10.4304/jsw.8.6.1443-1450.
[16] Xiso-dong Guo, Ji-ren Liu, Hui Wen.: A method for hardware/software partitioning using genetic algorithm, Journal of Computer-Aided Design & Computer Graphics, 2001, 13(1): pp. 24-27. doi: 10.3321/j.issn:1003-9775.2001.01.005.
[17] Peng Liu, Ji-gang Wu, Yong-ji Wang.: Hybrid algorithms for hardware/software partitioning and scheduling on reconfigurable devices, Mathematical and Computer Modelling, 2013, (58): pp. 409-420. doi: 10.1016/j.mcm.2012.11.001.
[18] An Liu, Jin-fu Feng, Xiao-long Liang, Xiao-tian Yang.: Algorithm of hardware/Software partitioning based on genetic particle swarm optimization, Journal of Computer-Aided Design & Computer Graphic, 2010. 22(6): pp. 927-933,942.
[19] Yuan-yuan Cui, Xue-hong Qiu, Jian-xian Zhang, Rui Zhou.: SoC hardware/software partitioning algorithm for multi-performance index constraints, JOURNAL OF XIDIAN UNIVERSITY, 2013, 40(5): pp. 92-98. doi: 10.3969/j.issn.1001-2400.2013.05.015.
[20] Pankaj Kumar Natha, Dilip Dattab.: Multi-objective hardware–software partitioning of embedded systems: A case study of JPEG encoder, Applied Soft Computing, 2014 (15): pp. 30-41. doi:org/10.1016/j.asoc.2013.10. 032.
[21] Madhura Purnaprajna, Marek Reformat, Witold Pedrycz.: Hardware implementation of a novel genetic algorithm, Journal of Systems Architecture, 2007 (53): pp. 339-354. doi: 10.1016/j.sysarc.2006. 10.012.
[22] Jin Zhang, Dong-li Li, Ping Li. : Comparative study of genetic algorithms encoding mechanism, Journal of China University of Mining &Technology, 2002. 31(6): pp. 637-640. doi: 10.3321/j.issn:1000-1964.2002.06. 023.
[23] Yong-gang Peng, Xiao-ping Luo, Wei Wei.: New fuzzy adaptive simulated annealing genetic algorithm, Control and Decision, 2009.24(6): pp. 843-848. doi: 10.3321/j,issn:1001-0920.2009.06008.
[24] Yun-xiao Zu, Jie Zhou.: Cognitive radio resource allocation based on combined chaotic genetic algorithm, Acta Phys.Sin, 2011. 60(7): pp. 1-8. doi: 10.7498/aps. 60.079501.

Guoshuai Li was born in ShanDong (China) on January 1986. He received the B.E. and M.E. degrees from Aviation University of Air Force, China, in 2008 and 2011 respectively, and he is currently working toward the Ph.D. degree in School of Aeronautics and Astronautics Engineering College, Air Force Engineering University, China. His research interests mainly focus on computer aided design, system analysis and storage management system .

Jinfu Feng received the Ph.D. degrees from Nanjing University of Science and Technology, China, in 1996. He is currently a Professor and PhD Supervisor in the School of Aeronautics and Astronautics Engineering College, Air Force Engineering University, China. Her interests are in the areas of storage management system, PIM/PSM technology and computer aided design.

Junhua Hu received the Ph.D. degrees from Aeronautics and Astronautics Engineering College, Air Force Engineering University, China. He is currently a teacher in the School of Aeronautics and Astronautics Engineering College, Air Force Engineering University, China. Her interests are in the areas of PIM/PSM technology and computer aided design.

Cong Wang received the S.E. and M.E. degree from Armed Police Engineering University, China, in 2008 and 2011 respectively. He is currently working toward the Ph.D. degree in School of Aeronautics and Astronautics Engineering College, Air Force Engineering University, China. His research interests mainly focus on reliability analysis, computer aided design and system design.

Duo Qi received the B.E. and M.E. degrees from Aviation University of Air Force, China, in 2010 and 2013 respectively, and he is currently working toward the Ph.D. degree in School of Aeronautics and Astronautics Engineering College, Air Force Engineering University, China. His research interests mainly focus on computer aided design, system analysis.

Spectral Clustering with Neighborhood Attribute Reduction Based on Information Entropy

Hongjie Jia[1,2], Shifei Ding[1,2], Heng Ma[1], Wanqiu Xing[1]
1. School of Computer Science and Technology, China University of Mining and Technology, Xuzhou, China
Email: jiahongjie@cumt.edu.cn
2. Key Laboratory of Intelligent Information Processing, Institute of Computing Technology, Chinese Academy of Sciences, Beijing, 100190 China
Email: dingsf@cumt.edu.cn

***Abstract*—Traditional rough set theory is only suitable for dealing with discrete variables and need data preprocessing. Neighborhood rough sets overcome these shortcomings with the ability to directly process numeric data. This paper modifies the attribute reduction method based on neighborhood rough sets, in which the attribute importance is combined with information entropy to select the appropriate attributes. When multiple attributes have the same importance degree, compare the information entropy of these attributes. Put the attribute having the minimal entropy into the reduction set, so that the reduced attribute set is better. Then we introduce this attribute reduction method to improve spectral clustering and propose NRSR-SC algorithm. It can highlight the differences between samples while maintaining the characteristics of data points to make the final clustering results closer to the real data classes. Experiments show that, NRSR-SC algorithm is superior to traditional spectral clustering algorithm and FCM algorithm. Its clustering accuracy is higher, and has strong robustness to the noise in high-dimensional data.**

***Index Terms*—neighborhood rough sets, information entropy, attribute reduction, spectral clustering**

I. Introduction

Clustering analysis is an important method for data mining and information statistics. It can effectively find the intrinsic link between things and is able to describe the internal structure of the data set. The purpose of clustering is to divide the data set into several categories according to certain similarity measure, so that data points belonging to the same class have high similarity, while the data points belonging to different classes share low similarity [1]. k-means algorithm and FCM algorithm [2] are typical clustering methods. They are suitable for handling data sets of spherical structures, but for non-convex data set, the algorithm usually fall into local optimal. Spectral clustering algorithm is a new clustering method, which treats clustering problem as a graph partitioning problem. It can find a global optimal solution of the graph cut objective function by constructing the graph Laplacian matrix and its eigen-decomposition [3]. Compared with the conventional clustering algorithms, spectral clustering has obvious advantages that it can converge to the global optimal for the clustering on any shape of sample space, especially suitable for dealing with non-convex data set.

Spectral clustering is based on algebraic graph theory to clustering. As it has a solid theoretical foundation and good clustering results, the research in this area is very active at present. Blekas and Lagaris [4] use Newton's second law to analyze the interaction between data points, in order to obtain valuable similarity information, which can help reduce the overlap between classes and improve cluster perspicuity. Li and Guo [5] develop a new method of constructing similarity matrix according to the spread of neighbor relations. In this way, the similarities of data pairs within the same cluster will be enhanced, so the derived similarity matrix can well describe the real structure of data. Frederix and Van Barel [6] propose a novel sparse spectral clustering method. This method builds an approximation by analyzing the structure of Laplacian matrix, so that the complexity of eigen-decomposition can be reduced. Wang and Dong [7] introduce multi-level low-rank matrix approximation into spectral clustering and present an effective sampling method. This algorithm can effectively deal with the segmentation problem of high resolution images. Jiao et al. [8] exploit enhanced spectral embedding to improve the performance of semi-supervised clustering. Both the geometry information of data set and the given pairwise constraints are taken into account in this algorithm and it is robust to noise and outliers. Michoel and Nachtergaele [9] use hypergraph representations to detect communities in complex networks. It can simultaneously analyze multiple types of interactions and dynamically describe the functional part of the system. Adefioye et al. [10] develop a multi-view spectral clustering algorithm used for the classification of chemical compounds. They find that the compounds gathered together usually have very different chemical properties, which can help reveal the intrinsic relationship of these compounds. Ding et al. [11] apply spectral clustering to controlled islanding problem,

Manuscript received July 11, 2013; revised August 1, 2013; accepted September 1, 2013.
This work is supported by the National Natural Science Foundation of China (Nos.61379101), the National Key Basic Research Program of China (No. 2013CB329502), and the Natural Science Foundation of Jiangsu Province (No.BK20130209).

doi:10.4304/jcp.9.6.1316-1324

aiming to reduce the complexity of the problem and find an appropriate islanding solution to prevent the accidents of large area blackouts.

Nowadays, science and technology is growing by leaps and bounds and massive data result in "data explosion" [12]. These data are often accompanied by high dimensions. Traditional clustering algorithms are unable to meet the requirements of today's data analysis. When dealing with high-dimensional data, some clustering algorithms that perform well in low-dimensional data space are often unable to get good clustering results, and even invalid [13]. Therefore, designing and developing novel clustering algorithms for mining massive high-dimensional data, has become one of the researching hotspots at home and abroad [14]. Attribute reduction is an effective way to decrease the size of data, and it is often used as a preprocessing step for data mining. The essence of attribute reduction is to remove irrelevant or unnecessary attributes while maintaining the classification ability of knowledge base, in order to decrease the data size, reduce the computational complexity, and improve the efficiency of algorithms [15]. From an economic perspective, efficient attribute reduction not only can improve the knowledge clarity in intelligent information systems, but also reduce the cost of information systems to some extent. This reflects the business idea that "cost minimization, benefit maximization", which is of great significance for business intelligence.

In order to effectively deal with high-dimensional data, we combine attribute reduction with clustering analysis, and present a novel spectral clustering algorithm based on neighborhood rough sets reduction (NRSR-SC). This paper is organized as follows: section 2 describes some related concepts of neighborhood rough sets, and then uses information entropy to improve the attribute reduction algorithm based on neighborhood rough sets; section 3 analyzes the deficiencies of traditional spectral clustering algorithm processing high-dimensional data, and proposes NRSR-SC algorithm; section 4 verifies the effectiveness of NRSR-SC algorithm using the data sets in UCI machine learning database; finally, we summarize the main contents of this paper and discuss the priorities for future research.

II. Attribute Reduction with Neighborhood Rough Sets

Rough set theory is proposed by professor Pawlak [16] in 1982. It defines the concepts of domain, lower approximation and upper approximation etc. to describe the process of human learning and reasoning. In rough set theory, the acquired knowledge is represented by production rules, which are easy for users to understand, accept and use. As a mathematical tool for processing fuzzy and uncertain knowledge, rough set is widely used in selecting attribute subsets, finding decision rules, discovering knowledge dependency and other fields. Attribute reduction is one of the core contents of rough set knowledge discovery. It describes whether each attribute in the attribute set of information system is necessary, and how to remove unnecessary knowledge.

However, Pawlak rough set is based on the classic theory of equivalence relations and equivalence classes, so it is only suitable for handling discrete data. As for continuous data, which are widespread in the real world, should be discretized in advance. We can select appropriate division points to divide the range of continuous attribute values into a number of discrete intervals, and then use different integers to represent the attribute values in each subinterval. Such conversion will inevitably result in the loss of information and the processing results depend largely on the effectiveness of discrete. To solve this problem, Hu Qinghua et al. introduce neighborhood relations into rough set and propose neighborhood rough set model [17]. This model can directly analyze the attributes with continuous values, eliminating the process of discretization. Therefore, it has great advantages in feature selection and classification accuracy.

A. The Measurement of Neighborhood

Rough sets describe the problem to be addressed as an information system. Information system $IS = \langle U, A, V, f \rangle$, where U is a non-empty finite set of objects, called domain; A is a set of attributes, including condition attribute and decision attribute; V is the range of all attribute values; $f : U \times A \to V$ is an information function, indicating the mapping relationship between sample and its corresponding attribute values.

Definition 1. Domain $U = \{x_1, x_2, \cdots, x_n\}$ is a non-empty finite set in real space, for $x_i \in U$, the δ-neighborhood of x_i is defined as:

$$\delta(x_i) = \{x \mid x \in U, \Delta(x, x_i) \le \delta\} \tag{1}$$

where $\delta \ge 0$, $\delta(x_i)$ is called the neighborhood particle of x_i, Δ is a distance function. For $x_1, x_2, x_3 \in U$, Δ satisfies the following relations:

① $\Delta(x_1, x_2) \ge 0$, $\Delta(x_1, x_2) = 0$, if and only if $x_1 = x_2$;

② $\Delta(x_1, x_2) = \Delta(x_2, x_1)$;

③ $\Delta(x_1, x_3) \le \Delta(x_1, x_2) + \Delta(x_2, x_3)$.

For a sample set of N attributes, distance is usually calculated by P-norm:

$$\Delta_p(x_1, x_2) = \left(\sum_{i=1}^{N} \left| f(x_1, a_i) - f(x_2, a_i) \right|^p\right)^{1/p} \tag{2}$$

where $f(x,a_i)$ is the value of attributes a_i of sample x. If a_i is symbolic attribute, define:

① $\left| f(x_1, a_i) - f(x_2, a_i) \right| = 0$, if x_1, x_2 have the same value on attribute a_i;

② $\left| f(x_1, a_i) - f(x_2, a_i) \right| = 1$, if x_1, x_2 have different values on attribute a_i.

For example, domain $U = \{x_1, x_2, x_3, x_4, x_5\}$, a is an attribute of U, $f(x,a)$ represents the attribute value of sample x on attribute a. $f(x_1, a) = 1.1$, $f(x_2, a) = 1.2$,

$f(x_3,a)=1.6$, $f(x_4,a)=1.8$, $f(x_5,a)=1.9$. Set the neighborhood size $\delta=0.2$. As $|f(x_1,a)-f(x_2,a)|\le 0.2$, so $x_2\in\delta(x_1)$, $x_1\in\delta(x_2)$. Then we can derive each sample's δ-neighborhood: $\delta(x_1)=\{x_1,x_2\}$, $\delta(x_2)=\{x_1,x_2\}$, $\delta(x_3)=\{x_3,x_4\}$, $\delta(x_4)=\{x_3,x_4,x_5\}$, $\delta(x_5)=\{x_4,x_5\}$. If domain U contains multiple attributes, the δ-neighborhood of samples can be calculated in a similar way.

B. Measure Knowledge Entropy

Definition 2. Given a domain $U=\{x_1,x_2,\cdots,x_n\}$ located in real space. A represents the attribute set of U; D represents the decision attribute. If A is able to generate a family of neighborhood relationship of domain U, then $NDT=\langle U,A,D\rangle$ is called a neighborhood decision system.

For a neighborhood decision system $NDT=\langle U,A,D\rangle$, domain U is divided into N equivalence classes by decision attribute D: $X_1,X_2,\cdots,X_N$. $\forall B\subseteq A$, the lower approximation, upper approximation and decision boundary of decision attribute D about B are respectively defined as:

$$\underline{N_B}D=\bigcup_{i=1}^{N}\underline{N_B}X_i \tag{3}$$

$$\overline{N_B}D=\bigcup_{i=1}^{N}\overline{N_B}X_i \tag{4}$$

$$BN(D)=\overline{N_B}D-\underline{N_B}D \tag{5}$$

where $\underline{N_B}X_i=\{x_i\mid\delta_B(x_i)\subseteq X_i,x_i\in U\}$, $\overline{N_B}X_i=\{x_i\mid\delta_B(x_i)\cap X_i\neq\varnothing,x_i\in U\}$.

To illustrate the concept of upper and lower approximation, here we give an example of the classification of two classes. Suppose the domain U contains two equivalence classes, as shown in Figure 1. One class of samples marked with "*", and the other samples marked with "+". It can be seen from the figure that the samples in the circular neighborhood of sample x_1 are all from class "*", so x_1 belongs to the lower approximation of class "*"; the samples in the neighborhood of x_3 are all from class "+", so x_3 belong to the lower approximation of class "+"; the neighborhood of sample x_2 covers both class "*" samples and class "+" samples, so x_2 is a boundary sample. Thus, this definition is consistent with our intuitive understanding to classification problems.

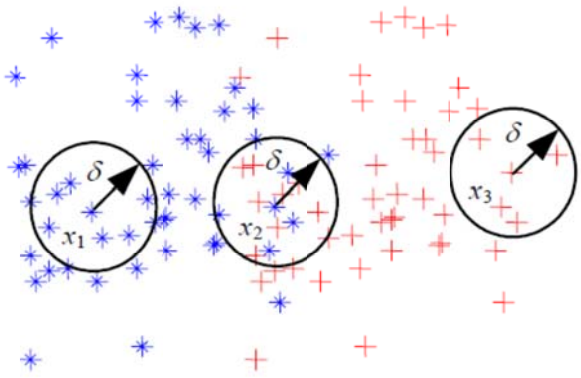

Figure 1. Neighborhood rough set model.

The lower approximation $\underline{N_B}D$ of decision attribute D is also called positive decision region denoted as $POS_B(D)$. The size of $POS_B(D)$ reflects the separable degree of domain U in a given attribute space. The greater the positive region is, means the sharper the boundaries of each class and the less overlap.

According to the nature of positive region, we can define the dependence of decision attribute D on condition attribute B:

$$\gamma_B(D)=\frac{Card(\underline{N_B}D)}{Card(U)} \tag{6}$$

where $0\le\gamma_B(D)\le 1$. $\gamma_B(D)$ represents the ratio that the samples fully contained in certain type of decision accounted for all the samples, according to the description of condition attribute B, in the sample set. Obviously, the greater the positive region $\underline{N_B}D$, the stronger the dependence of decision D on condition B.

C. Neighborhood Attribute Reduction based on Information Entropy

In a neighborhood decision system $NDT=\langle U,A,D\rangle$, $\forall B\subseteq A$, $\forall a\in B$, if $\gamma_{B-a}(D)<\gamma_B(D)$, then a is called essential to B; if $\gamma_{B-a}(D)=\gamma_B(D)$, then a is called redundant. When $\forall a\in B$ are all essential to B, then B is called independent.

Definition 3. Given a neighborhood decision system $NDT=\langle U,A,D\rangle$, If B satisfied the following two conditions, then $B\subseteq A$ is called a reduction of A.

① $\forall a\in B$, $\gamma_{B-a}(D)<\gamma_B(D)$;

② $\gamma_A(D)=\gamma_B(D)$.

The defined condition ① requires that a reduction can not contain redundant attributes, that is, the reduction must be independent; condition ② requires that of the distinguish ability of the system should remain unchanged after reduction. If $B_1,B_2,\cdots,B_k$ is the total reduction of system NDT, then $Core=\bigcap_{i=1}^{k}B_i$ is called the core of decision system.

Definition 4. Given a neighborhood decision system $NDT = \langle U, A, D \rangle$, $B \subseteq A$, $\forall a \in A - B$, then the significant degree of *a* relative to *B* is defined as:

$$SIG(a, B, D) = \gamma_{B \cup a}(D) - \gamma_B(D) \tag{7}$$

Using the attribute significance index we can design the attribute reduction algorithm based on neighborhood rough sets: first calculate the importance degree of all of the remaining attributes, and then add the attribute having the greatest importance to the reduction set; repeat the process until the importance degree of all the remaining attributes is 0, which means that adding any new attribute, the dependent function values of system are no longer changed [18]. However, sometimes several attributes may have the same greatest importance degree. Traditional reduction algorithms take the approach of randomly choosing one of the attributes, which is obviously arbitrary does not taking into account the impact of other factors on attribute selection and may lead to poor reduction results.

From the viewpoint of information theory to analyze attribute reduction can improve the reduction accuracy, and many scholars have conducted research in this area. Wang Guoyin et al. [19] propose a decision table reduction algorithm based on conditional information entropy. Ding Shouzhen et al [20] combine information entropy theory with the deterministic relationship based on positive region. It can express the probability of causation between attributes, and has strong robustness to noise data. Wu Shangzhi et al. [21] introduce mutual information into decision table to describe attribute importance, and thus obtain the relative reduction of attributes. The father of information theory Shannon noted that redundancy exists in any information [22]. The size of redundancy is related with the occurrence probability or say uncertainty of each symbol (numbers, letters or words) in information. The basic role of information is to eliminate the uncertainty of things. The greater the uncertainty, the greater the entropy value, and the larger the amount of information required to make it clear [23]. The definition of entropy is given below.

Definition 5. Given knowledge *P* and its partition $U / P = \{X_1, X_2, \cdots, X_n\}$ exported on domain *U*. The information entropy of knowledge *P* is defined as:

$$H(P) = -\sum_{i=1}^{n} p(X_i) \log p(X_i) \tag{8}$$

where $p(X_i) = |X_i| / |U|$ represents the probability of equivalence class X_i on domain *U* [24].

In this paper, we use information entropy as another criterion to evaluate attributes. When there are multiple attributes having the greatest importance degree, then compare the information entropy of these attributes and select the attribute with the minimum entropy (carrying the least uncertain information) to be incorporated into the reduction set, so that we can get better attribute reduction results. This improved attribute reduction algorithm is shown as Algorithm 1.

Algorithm 1: Neighborhood attribute reduction algorithm based on information entropy

Input: Neighborhood decision system $NDT = \langle U, A, D \rangle$.

Output: The reduced attribute set *red*.

Step 1: $\forall a \in A$, calculate the neighborhood relation N_a.

Step 2: Initialize $red = \varnothing$.

Step 3: $\forall a_i \in A - red$, calculate the importance degree of each attribute $SIG(a_i, red, D) = \gamma_{red \cup a}(D) - \gamma_{red}(D)$.

Step 4: If $\max_i(SIG(a_i, red, D))$ contains only one attribute, then select a_k so as to satisfy $SIG(a_k, red, D) = \max_i(SIG(a_i, red, D))$; otherwise, calculate the information entropy of these attributes and select a_k so as to satisfy $H(a_k) = \min_i(H(a_i))$.

Step 5: If $SIG(a_k, red, D) > 0$, put a_k into the reduction set, $red = red \cup a_k$, then go to step 3; otherwise, output *red* and the algorithm ends.

III. Spectral Clustering Algorithm based on Neighborhood Rough Sets Reduction

Spectral clustering uses the idea of graph partitioning to solve data clustering problem. Given a data set $X = \{x_1, x_2, \cdots, x_n\}$ containing *n* data points, $x_i \in R^l$. With the points of set *X*, we can construct an undirected weighted graph *G*(*V*,*E*), in which every point $x_i \in X$ being a vertex of *G* and the affinity value w_{ij} between each pair of points (x_i,x_j) being the edge weight. All the weight values constitute the affinity matrix $W \in R^{n \times n}$. The similarity between data points can be measured by angle cosine, correlation coefficient or Gaussian kernel function. Gaussian kernel function is more common in spectral clustering and its expression is:

$$w_{ij} = \exp\left(-\frac{d^2(x_i, x_j)}{2\sigma^2}\right) \tag{9}$$

where $d(x_i,x_j)$ is a distance function between two points usually described by Euclidean distance; σ is the scale parameter controlling the speed that weight value falls off with $d(x_i,x_j)$.

Since a single parameter σ is not easy to deal with multi-scale clustering problem, Manor et al. [25] proposed a self-tuning spectral clustering algorithm. Instead of using a uniform σ, this algorithm calculates an adaptive parameter σ_i for each point x_i according to their neighborhood information, where σ_i is the Euclidean distance from point x_i to its *p*-th nearest neighbor. This similarity measure is called self-tuning Gaussian kernel function, which is described by the following formula:

$$w_{ij} = \exp\left(-\frac{d^2(x_i, x_j)}{\sigma_i \sigma_j}\right) \tag{10}$$

where $\sigma_i = \frac{1}{p}\sum_{k=1}^{p} d(x_i, x_k)$. As the neighborhood information of each point is considered, self-adjusting spectral clustering can effectively separate clusters from sparse background (as shown in Figure 2). So in this paper we use self-tuning similarity measure to calculate the affinities of data points.

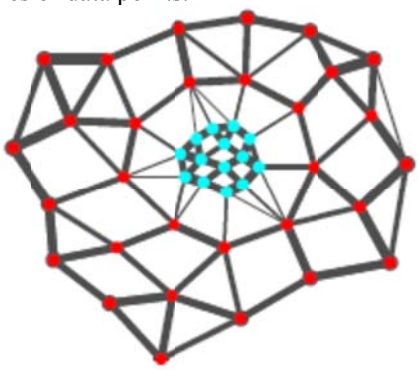

Figure 2. Local adaptive similarity measure.

Through the edge weights we can compute the degree of each vertex to compose the degree matrix $D \in R^{n\times n}$ of graph G. The degree of vertex i is denoted by d_i, which is the total weights of the edges connected to i, shown as formula (11). Thus D is a diagonal matrix with d_i being the diagonal elements and 0 being other elements.

$$d_i = \sum_{j=1}^{n} w_{ij} \tag{11}$$

According to the similarities between data points, we can create the similarity graph to describe samples points. Then the goal of clustering becomes finding an optimal partition of the graph, so that the internal nodes of the same sub-graph have greater connecting weight, while the connecting weights between different sub-graphs are much smaller. Many different graph cut methods have been proposed, for example Minimum cut, Ratio cut, Normalized cut and MinMax cut, etc. These methods typically define a number of indicate vectors to describe the attribution of data points. Given a subset of the graph, a data point is either in this subset or not, which is a discrete optimization problem. Theoretically speaking, the desired clustering results can be obtained by minimizing or maximizing the objective function of graph cut method. However, it has been proved that finding the best possible partition of a graph is an NP-hard problem [26]. With the help of spectral method, the original problem can be solved in polynomial time, and get an approximate optimal solution. Spectral method relaxes the original discrete attribution degree constraint to the real number field, so that the indicate vector may get the values in a continuous range. Then according to Rayleigh-Ritz theory, make eigen-decomposition of the Laplacian matrix, and use the resulting eigenvector to segment sub-graphs [27]. Alternatively, spectral clustering can be also interpreted from the view of random walk [28]. In random walk theory, each point on the graph may jump to the points adjacent to it in a certain probability. A probability transition matrix is composed of these jump probabilities. Dividing a graph into several sub-graphs should try to keep the random walk process among the vertices within the same sub-graph in a large probability and rarely jumping from one sub-graph to another.

Massive high-dimensional data processing has been a problem in data mining. High-dimensional data is often accompanied by the "curse of dimensionality", so traditional spectral clustering algorithms can not play to their strengths very well. Moreover, real data sets often contain noise and irrelevant features, likely to cause “dimension trap”. It would interfere with the clustering process of algorithms, affecting the accuracy of clustering results [29]. To solve this problem, we propose a spectral clustering algorithm based on neighborhood rough sets reduction (NRSR-SC). Its basic idea is: first, according to the concept of neighborhood rough set compute the importance degree of each attribute; then make reduction to the attributes based on attribute importance, removing redundant attributes and retaining the most important attribute, under the premise of ensuring the distinguish ability of the system; next measure the similarities between data points to construct the similarity matrix and Laplacian matrix; map the points of the original data set to R^k space with the largest k eigenvectors of Laplacian matrix; at last, clustering the data points in the R^k space by k-means or other conventional algorithm. The process of NRSR-SC algorithm is described in Algorithm 2.

Algorithm 2: Spectral clustering algorithm based on neighborhood rough sets reduction

Input: Data set $X = \{x_1, x_2, \cdots, x_n\}$, the number of clusters k.

Output: k divided clusters.

Step 1: Reduce the attributes of sample points according to Algorithm 1 and obtain the reduced attribute set *red*.

Step 2: On the basis of the reduction attribute set *red*, form the affinity matrix $W \in R^{n\times n}$ by Equation (10) and establish the degree matrix $D \in R^{n\times n}$ of the graph by Equation (11).

Step 3: Using the affinity matrix W and the degree matrix D to construct the Laplacian matrix $L_{sym} = D^{-1/2}(D-W)D^{-1/2}$.

Step 4: Make eigen-decomposition for Laplacian matrix L_{sym}, choosing its largest k eigenvalues and their corresponding eigenvectors $u_1, \cdots, u_k$ to form matrix $U = [u_1 \vdots \cdots \vdots u_k] \in R^{n\times k}$ by arranging these eigenvectors vertically.

Step 5: Convert each row vector of matrix U into a unit vector through normalization and get matrix Y: $y_{ij} = u_{ij} / \left[\sum_{j=1}^{n} u_{ij}^2\right]^{1/2}$.

Step 6: Every row of matrix Y can be seen as a new point in R^k space. Then we can use a certain clustering algorithm such as k-means to group these points.

Step 7: Establish a one to one relationship between the original data points and each row vector of matrix Y, and

determine the attribution of each data point in accordance with the clustering results.

IV. Experimental Analysis

A. Clustering Evaluation Method

To test the effectiveness of NRSR-SC algorithm, we select five high dimensional data sets from the UCI machine learning repository for experiments. The description of these data sets is shown in Table I.

TABLE I.
DATA SETS DESCRIPTION

Data set	Data Characteristic			
	Sample number	Condition attribute number	Decision attribute number	Class number
Ionosphere	351	34	1	2
Sonar	208	60	1	2
Small soybean	47	35	1	4
WDBC	569	30	1	2
Zoo	101	16	1	7

The merits of clustering results can be measured by many indicators. F-measure is an evaluation index based on artificial annotation, derived from information retrieval field. F-measure contains precision rate and recall rate. These two indicators describe the difference between the clustering results and the real classes from different angles. F-score calculated by the precision and recall rate, is a comprehensive index to evaluate a cluster. It gives an objective evaluation to the generated clusters [30]. Suppose there are k classes in the data set, and class i is associated with cluster i^* in clustering results. We can compute the F-score of class i using the following three formulas:

$$P(i) = N_{ii^*} / N_{i^*} \tag{12}$$

$$R(i) = N_{ii^*} / N_i \tag{13}$$

$$F(i) = \frac{2 \times P(i) \times R(i)}{P(i) + R(i)} \tag{14}$$

where $P(i)$ and $R(i)$ are respectively the precision rate and the recall rate; N_{ii^*} is the size of the intersection of class i and cluster i^*; N_i is the size of class i; N_{i^*} is the size of cluster i^*.

The total F index of the clustering results is the weighted average of each class's F-score:

$$F = \frac{1}{n} \sum_{i=1}^{k} [N_i \times F(i)] \tag{15}$$

where n is the number of sample points; k is the class number of data set; N_i is the size of class i. $F \in [0,1]$, the greater the F index is, means the clustering results of the algorithm is closer to the real data category.

B. Experimental Results and Discussion

Using the real world data sets, NRSR-SC algorithm is compared with the traditional spectral clustering (SC) and FCM algorithm in the experiment. The clustering results of these three algorithms on each data set are shown in Figure 3 to Figure 7. The horizontal axis of the figure is the class label of obtained clusters, and the vertical axis is their F-scores.

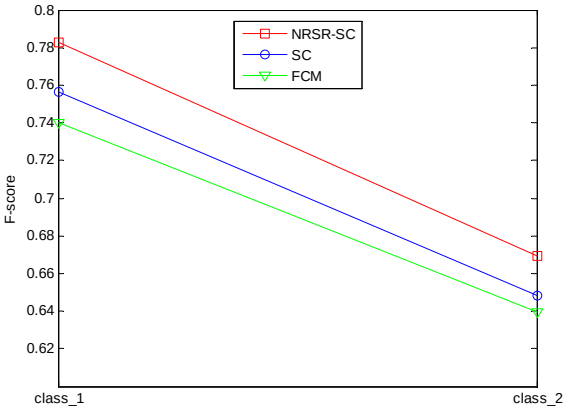

Figure 3. Clustering results on Ionosphere dataset.

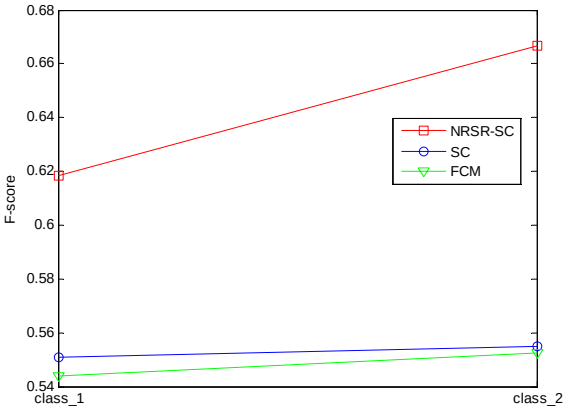

Figure 4. Clustering results on Sonar dataset.

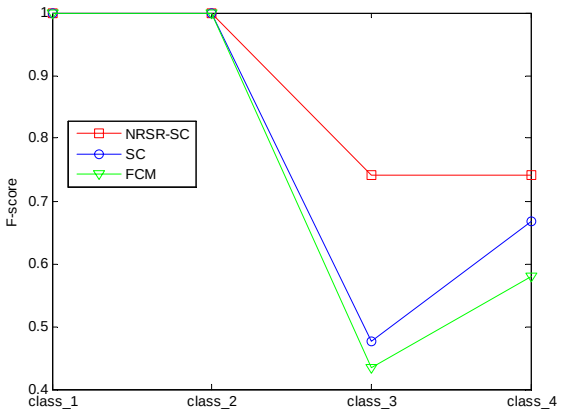

Figure 5. Clustering results on Small soybean dataset.

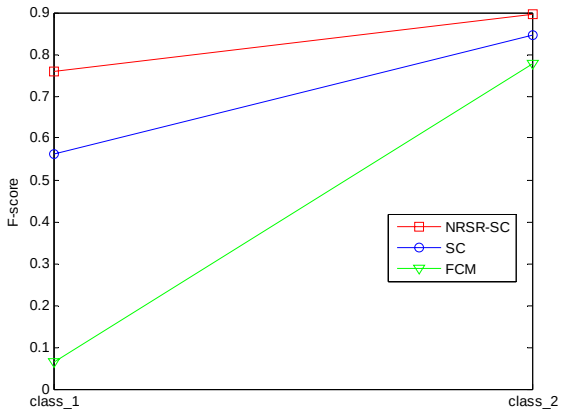

Figure 6. Clustering results on WDBC dataset.

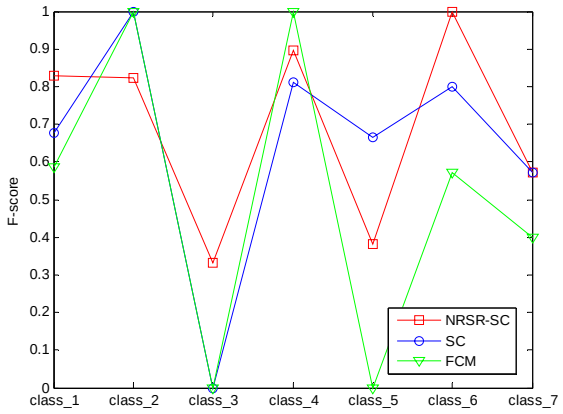

Figure 7. Clustering results on Zoo dataset.

In the above figures, the F-score of FCM algorithm is relatively low. This is mainly due to that in FCM algorithm, the initialization of cluster centers is a random process. Improper cluster centers would cause a greater impact on the clustering results. Moreover, FCM algorithm does work well with multi-scale clustering problem, easily dropping into local optimum. As spectral clustering algorithm, the indexes of NRSR-SC and SC algorithm are much higher. They turn clustering problem into graph partitioning problem. Using the spectral method and Laplace transform, the algorithm may find the global optimum solution, resulting in a more balanced class division. But the curve of SC algorithm is slightly below the proposed NRSR-SC algorithm. Because the information in each attribute of the samples is different, and they also make different contributions to clustering. Traditional spectral clustering algorithm does not take this into account, susceptible to the interference of noise and irrelevant attributes, so the clustering performance is not very well. For further comparison, the number of condition attributes as well as the overall F index of each data set processed by NRSR-SC algorithm, SC algorithm and FCM algorithm are given below, as shown in Table II and Table III.

TABLE II.
CONDITION ATTRIBUTE NUMBER OF DATA SETS

Data set	Number of condition attributes	
	NRSR-SC	SC and FCM
Ionosphere	6	34
Sonar	8	60
Small soybean	2	35
WDBC	7	30
Zoo	5	16

TABLE III.
OVERALL F INDEX OF ALGORITHMS

Data set	Algorithm		
	NRSR-SC	SC	FCM
Ionosphere	0.7421	0.7177	0.7040
Sonar	0.6442	0.5530	0.5483
Small soybean	0.8511	0.7680	0.7281
WDBC	0.8443	0.7411	0.5113
Zoo	0.7822	0.7239	0.6496

From the experimental data in Table 2 and Table 3 we can see that compared with FCM algorithm and conventional spectral clustering algorithm, NRSR-SC algorithm can better handle high-dimensional data, and generate more accurate clustering results. NRSR-SC algorithm uses neighborhood rough sets to optimize data samples, removes non-related properties and retains the attributes contributing the most to clustering, so that the sample points within the same cluster are more compact, while the sample points of different clusters are more separate, thus improving the accuracy of clustering. The neighborhood attribute reduction based on information entropy diminishes the negative impact of noise data and redundant attributes on the clustering. Not only reduce the complexity of problem solving, but also can better describe the approximate relationship between data points, and play the advantages of spectral clustering algorithm to enhance its robustness and generalization ability.

V. CONCLUSION

Spectral clustering is based on algebraic graph theory and can effectively solve many practical problems. However, suffering from the interference of noise and irrelevant attributes, traditional spectral clustering algorithm does not work well on high-dimensional data. In order to reduce the computational complexity and weaken the negative impact of noise data and redundant attributes on clustering, this paper propose a spectral clustering algorithm based on neighborhood rough sets reduction (NRSR-SC). Information entropy is introduced into the neighborhood rough sets in this algorithm, so that redundant attributes can be removed and the attributes making the greatest contribution to clustering can be reserved, under the premise of maintaining the ability to

distinguish different kind of samples. Then, based on the reduced attribute collection, the similarities between sample points are calculated to construct the affinity matrix and Laplacian matrix. At last, use spectral method to get the final clustering results. Experiments show that, when dealing with high-dimensional data, NRSR-SC algorithm has a strong anti-jamming ability and the efficiency and accuracy has improved significantly. In the future, we will study how to use NRSR-SC algorithm to process large data problems, and consider its application to web data mining, image retrieval and other fields.

REFERENCES

[1] Sun JG, Liu J, Zhao LY. Clustering Algorithms Research. Journal of Software, 2008, 19(1): 48-61.

[2] Jiang HF, Gu JF, Liu YJ, et al. Study of Clustering Algorithm based on Fuzzy C-Means and Immunological Partheno Genetic. Journal of Software, 2013, 8(1): 134-141.

[3] Nascimento MCV, de Carvalho ACPLF. Spectral methods for graph clustering - A survey. European Journal of Operational Research, 2011, 211(2): 221-231.

[4] Blekas K, Lagaris IE. A Spectral Clustering Approach Based on Newton's Equations of Motion. International Journal of Intelligent Systems, 2013, 28(4): 394-410.

[5] Li XY, Guo LJ. Constructing affinity matrix in spectral clustering based on neighbor propagation. Neurocomputing, 2012, 97: 125-130.

[6] Frederix K, Van Barel M. Sparse spectral clustering method based on the incomplete Cholesky decomposition. Journal of Computational and Applied Mathematics, 2013, 237(1): 145-161.

[7] Wang LJ, Dong M. Multi-level Low-rank Approximation-based Spectral Clustering for image segmentation. Pattern Recognition Letters, 2012, 33(16): 2206-2215.

[8] Jiao LC, Shang FH, Wang F, Liu YY. Fast semi-supervised clustering with enhanced spectral embedding. Pattern Recognition, 2012, 45(12): 4358-4369.

[9] Michoel T, Nachtergaele B. Alignment and integration of complex networks by hypergraph-based spectral clustering. Physical Review E, 2012, 86(5): 056111.

[10] Adefioye AA, Liu XH, Moor BD. Multi-view spectral clustering and its chemical application. International Journal of Computational Biology and Drug Design, 2013, 6(1-2): 32-49.

[11] Ding L, Gonzalez-Longatt FM, Wall P, Terzija V. Two-Step Spectral Clustering Controlled Islanding Algorithm. IEEE Transactions on Power Systems, 2013, 28(1): 75-84.

[12] Li H, Ding SF. Research and Development of Granular Neural Networks. Applied Mathematics & Information Sciences, 2013, 7(3): 1251-1261.

[13] Xu L, Ding SF, Guo FF. A Rough Kernel Clustering Algorithm Based on Improved Attribute Reduction. Journal of Guangxi Normal University (Natural Science Edition), 2011, 29(3): 105-109.

[14] Li XW. A New Text Clustering Algorithm Based on Improved K-means. Journal of Software, 2012, 7(1): 95-101.

[15] Zhu H, Ding SF, Zhao H, et al. Attribute Granulation Based on Attribute Discernibility and AP Algorithm. Journal of Software, 2013, 8(4): 834-841.

[16] Pawlak Z. Rough sets [J]. International Journal of Computer and Information Sciences, 1982, 11(5): 341-356.

[17] Hu QH, Yu DR, Xie ZX. Numerical Attribute Reduction Based on Neighborhood Granulation and Rough Approximation. Journal of Software, 2008, 19(3): 640-649.

[18] Hu QH, Zhao H, Yu DR. Efficient Symbolic and Numerical Attribute Reduction with Neighborhood Rough Sets. Pattern Recognition and Artificial Intelligence, 2008, 21(6): 732-738.

[19] Wang GY, Yu H, Yang DC. Decision Table Reduction based on Conditional Information Entropy. Chinese Journal of Computers, 2002, 25(7): 759-766.

[20] Ding SZ, Sang L, Zhu QY, et al. Attribute reduction in rough set based on information entropy and it's application. Computer Engineering and Applications, 2007, 43(35): 245-248.

[21] Wu SZ, Gou PZ. Attribute Reduction Algorithm on Rough Set and Information Entropy and Its Application. Computer Engineering, 2011, 37(7): 56-61.

[22] Shannon CE. A Mathematical Theory of Communication. Bell System Technical Journal, 1948, 27: 379-423, 623-656.

[23] Ding SF, Zhu H, Xu XZ, Shi ZZ. Entropy-Based Fuzzy Information Measures. Chinese Journal of Computers, 2012, 35(4): 796-801.

[24] Jia WK, Ding SF, Xu XZ, et al. Factor Analysis Feature Extraction Algorithm Based on Shannon Entropy. Pattern Recognition and Artificial Intelligence, 2011, 24(3): 327-331.

[25] Zelnik-Manor L, Perona P. Self-tuning spectral clustering. In Proceeding of NIPS, 2005: 1601-1608.

[26] Li JY, Zhou JG, Guan JH, et al. A survey of clustering algorithms based on spectra of graphs. CAAI Transactions on Intelligent Systems, 2011, 6(5): 405-414.

[27] Jia HJ, Ding SF, Zhu H, et al. A feature weighted spectral clustering algorithm based on knowledge entropy. Journal of Software, 2013, 8(5): 1101-1108.

[28] Zhang XC, You QZ. An improved spectral clustering algorithm based on random walk. Frontiers of Computer Science in China, 2011, 5(3): 268-278.

[29] Wang XZ, Wang TT, Zhai JH. An Attribute Reduction Algorithm Based on Instance Selection. Journal of Computer Research and Development, 2012, 49(11): 2305-2310.

[30] Tao XM, Song SY, Cao PD, et al. A Spectral Clustering Algorithm Based on Manifold Distance Kernel. Information and Control, 2012, 41(3): 307-313.

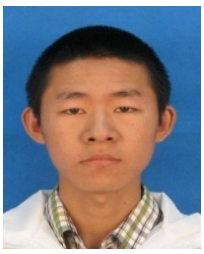

Hongjie Jia is currently a graduate student now studying at School of Computer Science and Technology, China University of Mining and Technology, and his supervisor is Prof. Shifei Ding. He received his B.Sc. degree in computer science from China University of Mining and Technology in 2011. His research interests include pattern recognition, machine learning, and spectral clustering et al.

Shifei Ding is a professor and Ph.D. supervisor at China University of Mining and Technology. His research interests include intelligent information processing, pattern recognition, machine learning, data mining, and granular computing et al. He has published 3 books, and more than 150 research papers in journals and international conferences. He received his B.Sc., M.Sc. degree in

mathematics and computer science in 1987, 1998 respectively from Qufu Normal University, received Ph.D. degree in computer science from Shandong University of Science and Technology in 2004, and received post Ph.D. degree in computer science from Key Laboratory of Intelligent Information Processing, Institute of Computing Technology, and Chinese Academy of Sciences in 2006.

Heng Ma is currently a graduate student now studying in School of Computer Science and Technology, China University of Mining and Technology, and his supervisor is Prof. Shifei Ding. He received her B.Sc. degree in computer science from China University of Mining and Technology in 2013. His research interests include cloud computing, feature selection, pattern recognition, machine learning et al.

Wanqiu Xing is currently a graduate student now studying in School of Computer Science and Technology, China University of Mining and Technology, and her supervisor is Prof. Shifei Ding. She received her B.Sc. degree in computer science from China University of Mining and Technology in 2012. His research interests include cloud computing, feature selection, pattern recognition, machine learning et al.

Evaluation of Detrending Method Based on Ensemble Empirical Mode Decomposition for HRV Analysis

Chao Zeng[1, 2]
[1] School of Geosciences and Info-physics, Central South University, Changsha, Hunan, 410083, China
[2]College of Information Science and Technology, Shihezi University, Shihezi, 832003,China
Email: zengc_bme@csu.edu.cn

Xiaowen Xu[1*]
[*1] School of Geosciences and Info-physics, Central South University, Changsha, Hunan, 410083, China
Email: xuxiaowencn@163.com

***Abstract*—Heart rate variability (HRV) is a key indicator for assessing autonomous nervous system activity. Because nonstationary and slow trends which can cause distortion to HRV analysis are usually occurred in HRV signals, detrending scheme is necessary before HRV analysis. Ensemble empirical mode decomposition (EEMD), which offers the ability to break down signals into a set of intrinsic mode functions and acts as a high-pass filter through partial reconstruction, is proposed for HRV detrending. Experiment results show that the detrending method based on EEMD can achieve better performance than the smoothing priors approach (SPA), which is one of the most widely used method.**

***Index Terms*—Ensemble Empirical Mode Decomposition; Heart Rate Varibility; Detrending; Smoothing Priors Approach**

I. INTRODUCTION

The variation of time interval between heart beats, which is usually determined by the consecutive RR intervals of ECG recordings, is known as heart rate variability. As it reflects the function of the automatic nervous system, HRV has attracted much attention in biomedical and clinical research during the past few decades [1-2]. Consequently, a number of methods, such as time domain, frequent domain and nonlinear methods have been proposed to quantify the fluctuation in heart rate [1]. However, the slow linear or more complex trends in HRV signals will affect significantly the accuracy of analysis results. To obtain reliable results of HRV analysis, it is essential to extract the trends in HRV signals and remove them by subtraction before analysis [3-5].

Several methods have been proposed to deal with the problem of the extraction of trends which is usually considered to be nonstationary [6]. Fist-order [7, 8] and higher order [8] polynomial models have been used before analysing HRV. The polynomial filter is very sensitive to the choice of polynomial order and the duration [9]. To avoid these problems the Smoothness prior approach (SPA) was purposed [6], it is more widely adopted [3, 5, 10] in HRV analysis. The SPA acts as a time-varying finite impulse high-pass filter and addresses directly the phenomenon of nonstationarity [10]. The effects of SPA on linear and nonlinear analysis of HRV in estimation of the depth of anesthesia have been studied in [3].

Empirical mode decomposition, introduced by Huang et al [11], provided new insight in nonlinear and nonstationary signals. The method locally decomposes signals into oscillating components, which are called intrinsic mode functions (IMFs). Due to its properties of adaptive and fully-data driven, it is very attractive in the biomedical signal processing filed. Its ability for removing the baseline wander in ECG [12] and detrending in HRV [9, 13] has been reported. The major disadvantage of EMD is the mode mixing effect. Mode mixing indicates that oscillations of different time scales coexist in a given IMF, or that oscillations with the same time scale have been assigned to different IMFs. Recently, a variation of EMD, named ensemble EMD (EEMD) [14] has been developed. It performs the EMD over an ensemble of the signal plus Gaussian white noise and thus overcomes the "mode mixing" problem in EMD [14-15]. It is reasonably to infer that this variation would perform better than EMD, and this fact has been proved in a lot of problems [16-17]. However, to the best of our knowledge, no work has been reported for trend extraction in HRV signals using EEMD method.

In this paper, we demonstrated a quantitative comparison study of the detrending methods between SPA and EEMD. Firstly, the simulated HRV signals [18] containing artificial trends [8] were employed in the tests. The performance of the two methods on the simulated

*Corresponding author: Xiaowen Xu, Email: xuxiaowencn@163.com.
This work is supported by the National Natural Science Foundation of China (No.21105127), and the Science Foundation of Hunan Province, China (No. 12JJ6061).

doi:10.4304/jcp.9.6.1325-1332

HRV signals is evaluated in terms of three standard metrics. The evaluation of the detrending performance on real HRV signals is also important. However, it is impossible to be directly made by the above mentioned metrics because there is no universally formal justification of the recognition of the "real trend". Statistics comparison of HRV index derived from HRV signals may be an alternative and indirect way to compare the performance of detrending methods. Since HRV index has the ability to distinguish between young and elderly groups [19-20], statistical comparison is then made to evaluate the effects of detrending methods imposed on HRV index in terms of their ability for the separation of the two groups. Secondly, an advanced detrending procedure based on EEMD is presented. The performance of SPA and EEMD methods for detrending is compared with the simulated and real HRV signals. The metrics for evaluation the detrending performance are discussed in details. Finally, the results of the SPA and EEMD methods in simulated and real HRV signals are given.

II. Methods and Materials

A. SPA Method for Detrending

SPA [4] [6] [10] is applied in evenly sampled series. The HRV signal is derived from the RR interval series evenly re-sampled by cubic spline interpolation. It is denoted by z and considered to consist of two components:

$$z = z_{stat} + z_{trend} \tag{1}$$

where z_{stat} is the nearly stationary component, and z_{trend} is the trend component. The trend component can be modeled as

$$z_{trend} = H\theta + \upsilon \tag{2}$$

where H is the observation matrix, υ is the observation error, and the regression parameters θ can be estimated by

$$\hat{\theta}_\lambda = \arg\min_\theta \{\|H\theta - z\|^2 + \lambda^2 \|D_d(H\theta)\|^2\} \tag{3}$$

where λ is the smoothing parameter, D_d is the discrete approximation to the dth derivative operator. By choosing H as the identity matrix, and d =2, the estimated trend which we want to remove can be written in the form

$$\hat{z}_{trend} = (I + \lambda^2 D_2^T D_2)^{-1} z \tag{4}$$

And the detrended nearly stationary component of HRV signals can be written as

$$\hat{z}_{stat} = (I - (I + \lambda^2 D_2^T D_2))^{-1} z \tag{5}$$

The smoothing parameter λ =500 is set as default in [4], with re-sampling rate of 4Hz for HRV signals, and thus is accepted in this contribution. Under this circumstance, the SPA method corresponds to a high-pass filter with a cutoff frequency of 0.035Hz.

B. EEMD Method for Detrending

The standard EMD algorithm [11] utilizes an iterative shifting process as follows:

(1) Identify all the extreme (maxima and minima) peaks of the signal $s(t)$;

(2) Generate the upper and lower envelope by the cubic spline interpolation of the extreme peaks, then calculate the mean function of the upper and lower envelopes $m(t)$;

(3) Subtract the local mean from the signal $s(t)$, $d(t) = s(t) - m(t)$;

(4) If the stop criterion of shifting is satisfied, stop the iteration of this process and denote $d(t)$ as $c(t)$ for output. Otherwise, replace $s(t)$ with $d(t)$ and go to step (1);

The shifting process will never stop until the stop criterion of shifting is satisfied.

After the introduction of shifting process, the standard EMD algorithm [14] can be described as follows:

(1) For the input signal $s(t)$, perform shift process and get its output $c(t)$, then denote it by $c_i(t)$ (i=1,2, ⋯), where it is the ith time repeat of this step.

(2) Calculate the residual signal $r(t) = s(t) - c_i(t)$;

(3) If the stop criterion of EMD algorithm is satisfied, receive $c_i(t)$ (i=1,2, ⋯) and $r(t)$ as the outputs of EMD algorithm; Otherwise replace $s(t)$ with $r(t)$, then go to step (1).

EEMD is a variant of EMD in that it gets the $c_i(t)$ and $r(t)$ as the mean of the corresponding $c_i(t)$ and $r(t)$ obtained by EMD over an ensemble of trials, generated by adding different realizations of white noise to the signal $s(t)$. The EEMD algorithm can be described as follows:

(1) Add white noise generated randomly to the targeted signal;

(2) Decompose the signal containing white noise using EEMD algorithm, get its outputs $c_i(t)$ and $r(t)$, and denote them as $c_{ij}(t)$ and $r_j(t)$ respectively, where it is the jth repeat of this step;

(3) Repeat step (1) and (2) if the pre-defined repeat times is not satisfied; otherwise compute $c_i(t) = \frac{1}{n}\sum_{j=1}^{n} c_{ij}(t)$ and $r(t) = \frac{1}{n}\sum_{j=1}^{n} r_j(t)$ as outputs, where n is the pre-defined repeat time.

In some EMD algorithm, the process will stop if $d(t)$ satisfied the two conditions: 1) the number of extreme and the number of zero crossing is equal or differ at most by one; and 2) the mean value of the upper and lower envelope is zero everywhere. The stop criterion of EMD algorithm commonly accepted is that it will stop if the residual signal $r(t)$ is a monotonic function. In this contribution, however, the repeat time is selected as stop criterion both in shifting process and EMD algorithm, and the selected time is 10 and K for shift process and EMD algorithm, respectively, and K is calculated by

$$K = fix(log_2 N) - 1 \tag{6}$$

where N is the length of the signal, and $fix(X)$ is the function to round the elements of X to the nearest integer.

After the HRV signal z is decomposed by EEMD, its stationary component and trend component can be denoted by:

$$\hat{z}_{state} = \sum_{i=1}^{D} c_i(t) \quad (7)$$

$$\hat{z}_{trend} = \sum_{i=D+1}^{K} c_i(t) + r(t) \quad (8)$$

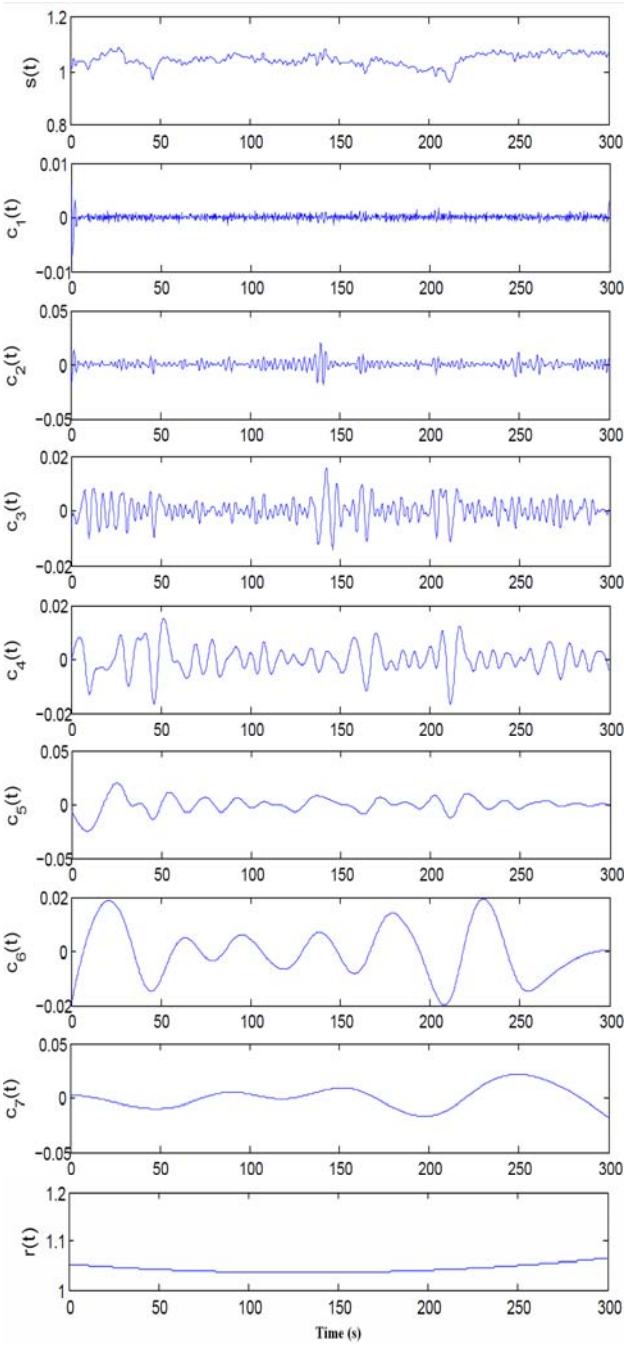

Figure 1 EEMD for HRV signal. From top to bottom are the HRV signal, $c_1(t)$-$c_9(t)$, and r(t), respectively

In this contribution, the effect of the decomposition using the EEMD method is investigated with D=5, 6, 7. Fig.1 illustrates the decomposition of real HRV signal. The effects of the decomposition using the EEMD are that the added white noise series cancel each other in the final mean of the corresponding IMFs; the mean IMFs stay within the natural dyadic filter windows and thus significantly reduce the chance of mode mixing and preserve the dyadic property.

C. HRV Analysis

Time domain, frequency domain and nonlinear methods are employed for HRV analysis. The RR interval time series data is used for time domain analysis and nonlinear analysis, and the evenly re-sampled signal is used for frequency domain.

The time domain indices are: 1) SNDD, the standard deviation of the RR intervals; 2) RMMSD, the root mean square of the differences of successive RR intervals; 3) NN50, the number of consecutive RR intervals with absolute difference more than 50ms; 4) pNN50: the percentage value of NN50 with respect to all RR intervals.

In the frequency domain analysis, the power spectrum density (PSD) estimation is calculated from the HRV signal with fast Fourier transform (FFT) based on Welch's periodogram method. The commonly used frequency bands are very low frequency (VLF, 0~0.04Hz), low frequency (LF, 0.04~0.15Hz), and high frequency (HF, 0.15~0.4Hz). The frequency domain indices investigated here are: 1) VLF, absolute power of VLF band; 2) LF, absolute power of LF band; 3) HF, absolute power of HF band; 4) LF/HF, ratio between LF and HF band powers.

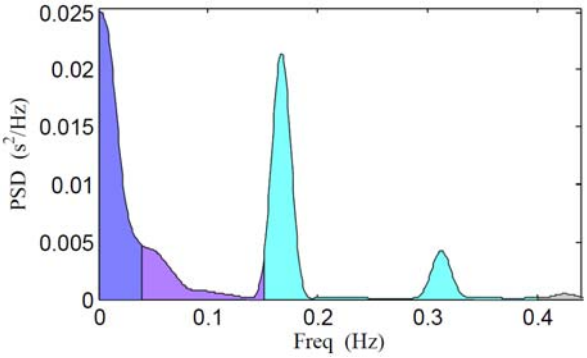

Figure 2 Power spectrum density of HRV signal

Poincaré plot is a commonly used nonlinear analysis method for HRV analysis. By plotting RR_{i+1} as a function of RR_i, the graph could reveal the correlation between successive RR intervals (see Fig.2). An ellipse is fitted on the graph, and two indices could be derived: 1) SD1, the standard deviation of the points perpendicular to the line of symmetry; 2) SD2, the standard deviation of the points along the symmetry.

D. Validation

Both artificial HRV signal and real HRV signal are employed for validation, making contribution for

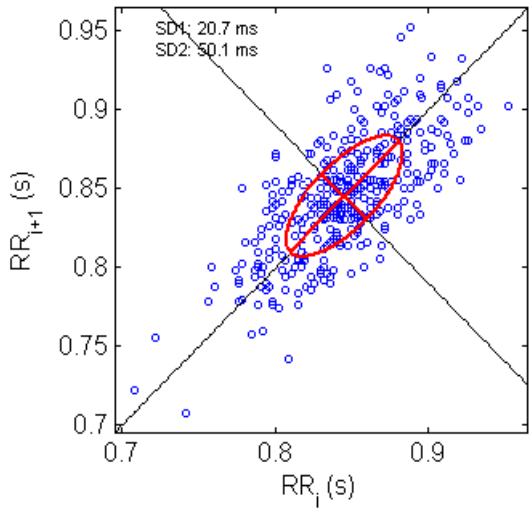

Figure 3 Poincaré plot analysis of RR intervals

providing a comparison of the effect between SPA and EEMD detrending methods.

In the generation of simulated HRV signals, four patterns of trends are considered as follows:

(1) The line pattern trend is denoted by

$$trend_1(t) = -\frac{a}{2} + \frac{a}{L} \cdot t, \ 0 \le t \le L \tag{9}$$

where the parameter a =0.15 is chosen, and L is the duration of the trend.

(2) The Gaussian pattern trend is denoted by

$$trend_2(t) = a \cdot e^{-c(t-L/2)^2}, \ 0 \le t \le L \tag{10}$$

where the parameters a =0.15, and c=5×10^{-4} are chosen.

(3) The break pattern trend is denoted by

$$trend_3(t) = \begin{cases} a/2, & 0 \le t \le L/3 \\ a - \dfrac{6a}{L}(t - L/3), & L/3 < t < 2L/3 \\ -a/2, & L/3 \le t \le 2L/3 \end{cases} \tag{11}$$

where a =0.15 is chosen.

(4) The cosine pattern trend

$$trend_4(t) = \frac{a}{2}\cos(2\pi f_{tr} t), \ 0 \le t \le L \tag{12}$$

where f_{tr} =0.02 is chosen.

The process of generation of the artificial RR interval series mixed with trend is described as follows:

(1) An expression for the heart rate (HR) is firstly written as:

$$HR(t) = HR_0 + A_l \sin(2\pi f_l t) + A_h \sin(2\pi f_h t) \tag{13}$$

where the parameters HR_0=60bpm, A_l=2, A_h=2.5, f_l =0.095Hz and f_h =0.275Hz are selected.

(2) The high frequency HRV signal is then formed by sampling

$$RR(t) = \frac{60s}{HR(t)} + trend \tag{14}$$

at a relative high frequency $f_s = 2000Hz$ such that $t_n = \dfrac{n}{f_s}$ where $n = 1, 2, \cdots, N$.

(3) The simulated RR interval series is unevenly re-sampled from $RR(t)$ in the way as follows: Record the first data point pair, $(t_1, RR(t_1))$ as the first time stamp and RR interval pair (t_1', RR_1), Then proceed through each sample, t_i, until $x_n \ge t_i - t_1'$; if $x_n - t_i \le x_{n-1} - t_{i-1}$, $(t_2' = t_i, RR_2 = RR(t_i))$ is selected as the second RR interval, otherwise, $(t_2' = t_{i-1}, RR_2 = RR(t_{i-1}))$ is selected. This is generated for the length of the simulated RR interval series is satisfied.

At the end of this process, a sequence

$$z = (RR_1, RR_2, \cdots, RR_n), \ n = 1, 2, \cdots N_1$$

is get as a simulated RRI series with exactly known stationary and trend components.

Following [17], three metrics, SNR improvement (SNR_{imp}) in decibel, mean squared error (MSE), and percent distortion (PRD) are used to quantify the detrending performance:

$$SNR_{imp} = 10\log_{10}\frac{\sum_{n=1}^{N}(z[n] - z_{stat}[n])^2}{\sum_{n=1}^{N}(\hat{z}_{stat}[n] - z_{stat}[n])^2} \tag{15}$$

$$MSE = \frac{1}{N}\sum_{n=1}^{N}(\hat{z}_{stat}[n] - z_{stat}[n])^2 \tag{16}$$

$$PDR = 100\sqrt{\frac{\sum_{n=1}^{N}(\hat{z}_{stat}[n] - z_{stat}[n])^2}{\sum_{n=1}^{N} z_{stat}^{\ 2}[n]}} \tag{17}$$

For a detrending method, the larger the SNR_{imp} is, and the smaller the MSE and PRD are, a better performance of the detrending could be achieved.

In real HRV experiment, the ECG signals from MIT-BIH Fantasia database are used. 19 young and elderly subjects with 5 minutes' segments of RRI series with normal beats only are derived for the experiment. The segments are derived without any beats overlapped. In the database, ECG signals were collected from healthy subjects undergoing 120 minutes of supine resting, and digitized at 250Hz, and R peaks were detected automatically and verified by visual inspection. In this way, 95 segments of RRI series are available both in the young and elderly group for the further experiment.

Statistical comparison between the indices of HRV signal calculated from young and elderly groups was performed by using independent t-test. All the data were expressed as mean±SD (standard deviation). The values of HRV indices were also compared between the two methods.

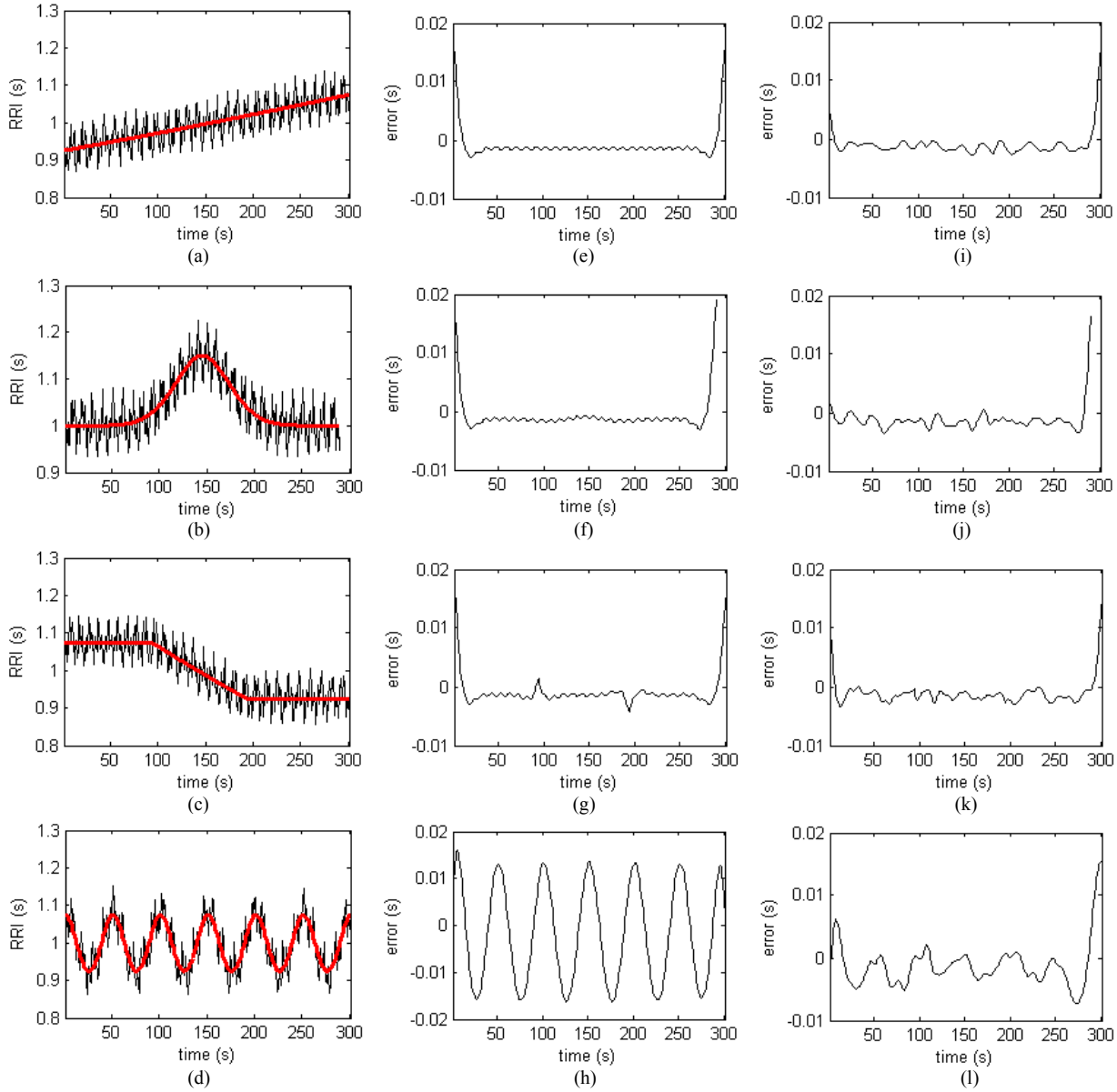

Figure 4 Trend filtering performance: (a)~(d) are simulated HRV signals with line, gauss, break, cosine pattern trend respectively; (e)~(h) are error traces corresponding to (a)~(d) using SPA method with λ=500 for detrending; (i)~(l) are error traces corresponding to (a)~(d) using EEMD method with D=5 for detrending.

TABLE I.
COMPARING OF SPA AND EEMD METHODS FOR DETRENDING IN SIMULATED HRV SIGNALS

	Line			Gauss			Break			Cosine		
	SNR_{imp} (db)	MSE ($s^2\times 10^{-5}$)	PRD (%)	SNR_{imp} (db)	MSE ($s^2\times 10^{-5}$)	PRD (%)	SNR_{imp} (db)	MSE ($s^2\times 10^{-5}$)	PRD (%)	SNR_{imp} (db)	MSE ($s^2\times 10^{-5}$)	PRD (%)
SPA	23.3	0.89	0.3	25.8	1.03	0.32	26.4	1	0.32	14	11.16	1.06
EEMD1	26.2	0.45	0.21	30.7	0.33	0.18	30.1	0.43	0.21	0.2	271	5.21
EEMD2	25.5	0.53	0.23	30	0.39	0.2	28.9	0.56	0.24	25.9	0.72	0.27
EEMD3	13.4	8.65	0.93	13.9	15.86	1.26	12	27.58	1.66	12.1	17.23	1.31

TABLE II.
COMPARISON OF INDICES DERIVED FROM HRV SIGNALS OF YOUNG AND ELDERLY GROUPS DETRENDED BY SPA METHOD.

Indices (unit)	young group (n=95)	elderly group (n=95)	p value
SDNN (ms)	54.0±23.1	22.8±11.3	1.06×10^{-22}
RMSSD (ms)	57.3±30.8	23.7±12.6	2.61×10^{-17}
NN50	84.7±57.8	11.7±18.3	2.73×10^{-21}
pNN50 (%)	29.4±22.2	4.84±8.93	1.43×10^{-17}
VLF (ms^2)	158.8±251.2	79.8±132.1	7.50×10^{-3}
LF (ms^2)	1655±1691	285.4±416.6	9.28×10^{-12}
HF (ms^2)	1381±1463	173.6±173.5	2.95×10^{-12}
LF/HF	2.17±2.85	2.23±2.07	0.87
SD1 (ms)	40.5±21.8	16.7±8.88	2.61
SD2 (ms)	64.0±26.2	27.2±14.0	1.36×10^{-23}

TABLE III
COMPARISON OF INDICES DERIVED FROM HRV SIGNALS OF YOUNG AND ELDERLY GROUPS DETRENDED BY EEMD METHOD.

Indices (unit)	indices	young group (n=95)	elderly group (n=95)	p value
SDNN (ms)	SDNN	50.3±21.5	19.4±10.0	1.22×10^{-24}
RMSSD (ms)	RMSSD	57.0±30.6	23.3±12.4	1.87×10^{-17}
NN50	NN50	84.7±57.8	11.3±18.1	3.55×10^{-21}
pNN50 (%)	pNN50	29.4±22.1	4.70±8.81	1.26×10^{-17}
VLF (ms^2)	VLF	22.1±32.3	4.91±7.61	1.92×10^{-6}
LF (ms^2)	LF	1349±1295	192.3±305.6	1.63×10^{-13}
HF (ms^2)	HF	1381±1464	173.8±173.7	2.97×10^{-12}
LF/HF	LF/HF	1.86±2.68	1.36±1.33	0.11
SD1 (ms)	SD1	40.3±21.7	16.5±8.73	1.87×10^{-17}
SD2 (ms)	SD2	57.9±23.5	21.6±11.8	6.07×10^{-27}

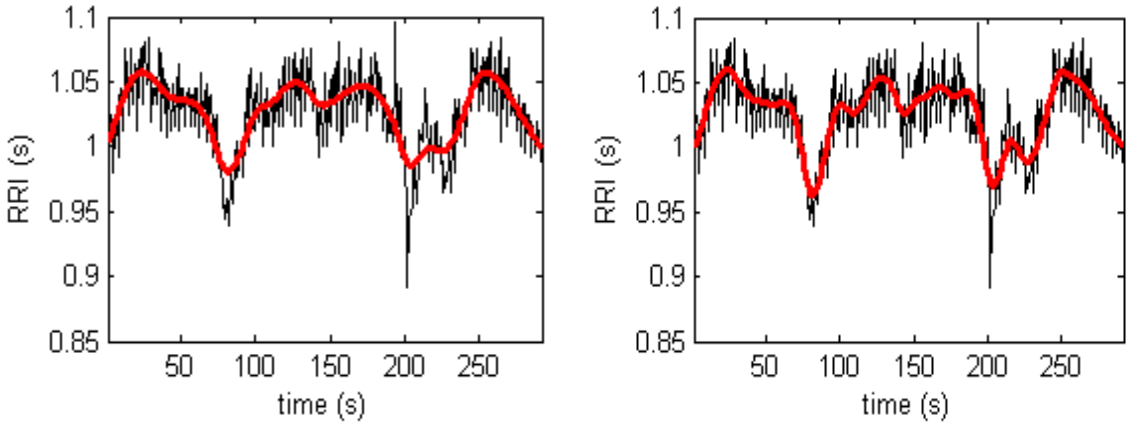

Figure 4 Trend exaction performance: (a) is a real RR interval series and its trend extrated by SPA method withλ=500; and (b) is the same RR interval series and its trend extracted by EEMD method with D=6.

III. RESULTS AND DISCUSSION

The detrending performance in simulated RR interval series with trends using SPA method and EEMD method is shown in Fig. 3. Fig. 3 (a) ~ (d) shows simulated series with four patterns of trends: line, gauss, break, and cosine trends, respectively. The error trace, i.e. the difference between pure simulated series and detrended RRI is shown in Fig. 3 (e) ~ (h) using SPA method. The mean relative errors of them reduced after detrending, which show that the trends could influence the HRV analysis. Therefore, it is necessary to remove the trend before analysis. Fig 3 (i) ~ (l) shows error traces using EEMD method with D=5 for detrending. The EEMD method shows excellent performance for the line and gauss trends. Thus the EEMD method shows a better performance than the SPA method.

Table 1 further illustrates the performance of SPA method and EEMD method with D=5, 6, and 7 using three metrics: SNR_{imp}, MSE, PRD. EEMD1, EEMD2, EEMD3 denotes the EEMD detrending method with D=5, 6, 7, respectively. In the case of cosine pattern trend, the EEMD method with D=6 shows obviously better performance. Table 1 shows that the EEMD method with D=6 performs better than SPA method, especially when dealing with cosine pattern trend.

The comparison of trend extraction in real RR interval series by SPA method and EEMD method is illustrated in Fig. 4.

The HRV time domain, frequency domain, and poincaré plot indices derived from real RR interval series using SPA method and EEMD detrending method are presented in Table 2 and Table 3, respectively, to show the difference in young and elderly groups.

RR interval series are derived from R peaks in ECG. It should be noted that this unevenly spaced time series is unusual in that both axes of the signal are time intervals, and related to each other. The value of the signal at the current point is horizontal distance between the current and the previous adjacent point. This propriety hasn't been emphasized in simulated HRV signals in [3, 9, 13]. However, we have paid much attention in this aspect of RR interval series, hoping to get more precise results for evaluating the detrending methods. Visual inspection in Fig. 3 reveals that both SPA and EEMD methods have satisfactorily removed the four pattern trends from the simulated RR interval series, and the error traces of the two methods illustrated that in line, gauss and break trend added HRV signals, the two methods acts generally comparable. However, in the case of cosine pattern trend,

the EEMD method with D=6 shows obviously better performance. Table 1 quantitatively shows that the EEMD method with D=6 is better than SPA method, especially when dealing with cosine pattern trend. This conclusion is again confirmed by real HRV signals in Fig. 4. The trend from 200s to 250s shown in Fig. 4 is more or less a cosine pattern, and the EEMD method gets a better trend exaction. As D=6 provides a compromise result in four situations in Table 1, this value is selected for further investigation when using EEMD method. Besides, the distortion of data end points could be observed for SPA method (see Fig. 1 (e) ~ (h)), and this problem can be relieved when using EEMD method [9].

Comparing the p value in Table 2 and Table 3, we can found that the HRV indices derived from RR interval series detrended by the EEMD method show more significant difference between the young and elderly groups, since a lower p value is received, indicating a better performance of EEMD method indirectly.

The numerical analysis for the performance of the EEMD detrending method for HRV analysis is presented using simulated HRV signals with trends, and compared with the SPA method. However, a theoretical study is still desired to be explored. The detrending method is used in HRV analysis related to age. Results show that most of the HRV indices derived from the HRV signals detrended by the EEMD method can improve the ability for distinguishing between young and elderly groups except the index HF. For our future work, we shall conduct more experiments to evaluate the influence of the EEMD detrending method in HRV indices, especially in terms of HF.

Ⅳ. Conclusion

In this paper, comparison results of the EEMD and SPA detrending methods show that the EEMD is superior to SPA in detrending RR interval series. The main advantage of the EEMD method, compared to SPA method is that EEMD can partly relieve the adverse end point effect, and more importantly, EEMD method shows an excellent performance in extraction of cosine pattern trends. The conclusion is not restricted to HRV analysis only, but can also be applied to other physiological signals, such as blood pressure variability and detrending of EEG signals in EEG analysis.

Acknowledgment

This work was supported by the National Natural Science Foundation of China (No.21105127), and the Science Foundation of Hunan Province, China (No. 12JJ6061).

References

[1] Task Force of the European Society of Cardiology the North American Society of Pacing Electrophysiology. Heart Rate Variability: Standards of Measurement, Physiological Interpretation, and Clinical Use. Circulation, 1996, 93(5):1043-1065.

[2] Li H, Kwong S, Yang L, Huang D, Xiao D. Hilbert-Huang transform for analysis of heart rate variability in cardiac health. IEEE/ACM Trans Comput Biol Bioinform. 2011, 8(6):1557- 167.

[3] Yoo C S, YI S H. Effects of detrending for analysis of heart rate variability and applications to the estimation of depth of anesthesia. Journal of the Korean Physical Society, 2004, 44(3):561-568.

[4] Tarvainen M P, Niskanen J P. Kubios HRV User's Guide.[2013-5-8]. http://kubios.uef.fi/media/Kubios_HRV_2.1_Users_Guide.pdf.

[5] Wen Feng, HE Fang-tian. An efficient method of addressing ectopic beats: new insight into data preprocessing of heart rate variability analysis. Journal of Zhejiang University-SCIENCE B (Biomedicine & Biotechnology), 2011,12(12): 976-982.

[6] Tarvainen M P, Ranta-aho P O, Karjalainen P A. An Advanced Detrending Method With Application to HRV Analysis. IEEE TRANSACTIONS ON BIOMEDICAL ENGINEERING, 2002,49(2):172-175.

[7] Litvack D A, Oberlander T F, Carney L H, Saul J P. Time and frequency domain methods for heart rate variability analysis: a methodological comparison. Psychophysiology, 1995, 32(5):492-504.

[8] Mitov I P. A method for assessment and processing of biomedical signals containing trend and periodic components. Medical Engineering & Physics, 1998, 20(9), 660~668.

[9] Shafqat K, Pal S K, Kyriacou P A. Evaluation of two detrending techniques for application in Heart Rate Variability// 29th Annual International Conference of the IEEE Engineering in Medicine and Biology Society. IEEE: Lyon, 2007: 22-26.

[10] Eleuteri A, Fisher A C, Groves D, Dewhurst C J. An Efficient Time-Varying Filter for Detrending and Bandwidth Limiting the Heart Rate Variability Tachogram without Resampling: MATLAB Open-Source Code and Internet Web-Based Implementation. [2013-5-8]. http://www.hindawi.com/journals/cmmm/2012/578785/.

[11] Huang N E, Shen Z, Long S R, Wu M C, Shih H H, Zheng Q, Yen N C, Tung C C, Liu H. The empirical mode decomposition and the Hilbert spectrum for nonlinear and non-stationary time series analysis. Proc. R. Soc. Lond. A, 1998, 454(1971):903-995.

[12] Kabir M A, Shahnaz C. Denoising of ECG signals based on noise reduction algorithms in EMD and wavelet domains. Biomedical Signal Processing and Control, 2012, 7(5):481-489.

[13] Li Liping, Li Ke, Liu Changchun, Liu Chengyu. Comparison of Detrending Methods in Spectral Analysis of Heart Rate Variability. Research Journal of Applied Sciences, Engineering and Technology, 2011,3(9): 1014-1021.

[14] Wu Z, Huang, N E. Ensemble empirical mode decomposition: a noise-assisted data analysis method. Advances in Adaptive Data Analysis. 2009, 1(1):1-41.

[15] Torres M E, Colominas M A, Schlotthauer G, Flandrin P. A complete ensemble empirical mode decomposition with adaptive noise. // 2011 IEEE International Conference on Speech and Signal Processing. IEEE:Acoustics, 2011:22-27.

[16] Mhamdi F, Poggi J, Jaidane M. Trend extraction for seasonal time series using ensemble empirical mode decomposition. Adaptive Data Analysis, Theory and Applications, 2011, 3(3), 363-383.

[17] Chang K M, Liu S H. Gaussian Noise Filtering from ECG by Wiener Filter and Ensemble Empirical Mode Decomposition. J Sign Process Syst 2011, 64:249-264.
[18] Clifford G D. Signal Processing Methods for Heart Rate Variability. Oxford: Oxford University, 2002.
[19] Abhishekh A H, Nisarga P, Kisan R, Meghana A, Chandran S, Raju T, Sathyaprabha T N. Influence of age and gender on autonomic regulation of heart. J Clin Monit Comput, 2013, 27(3):259-264.
[20] Voss A, Heitmann A, Schroeder R, Peters A, Perz S. Short-term heart rate variability-age dependence in healthy subjects. PHYSIOLOGICAL MEASUREMENT, 2012,33(8):1289-311..

Chao Zeng was born in Yiyang, China in August, 1982. He received his B.S. from Xiangtan University in 2005. He is now a Ph.D. candidate in Central South University, Changsha, China. He is also a lecture in Shihezi University, Shihezi, China since 2010. His major field of study covers biomedical image and biomedical signal processing techniques.

Xiaowen Xu was born in Jiangsu, China in May, 1978. He received his Ph.D degree from Changchun Institute of Optics, Fine Mechanics and Physics, Chinese Academy of Science in 2004. He is now an associate professor in Central South University. His major field of study covers biomedical signal processing and instrumentation.

A Feature Selection Approach of Inconsistent Decision Systems in Rough Set

Lin Sun
College of Computer & Information Engineering, Henan Normal University, Xinxiang 453007, P. R. China
Engineering Technology Research Center for Computing Intelligence and Data Mining, Henan Province, China
International WIC Institute, Beijing University of Technology, Beijing 100124, P. R. China
Email: linsunok@gmail.com

Jiucheng Xu, Yuhui Li
College of Computer & Information Engineering, Henan Normal University, Xinxiang 453007, P. R. China
Engineering Technology Research Center for Computing Intelligence and Data Mining, Henan Province, China
Email: xjc@htu.cn

***Abstract*—Feature selection has been widely discussed as an important preprocessing step in data mining applications since it reduces a model's complexity. In this paper, limitations of several representative reduction methods are analyzed firstly, and then by distinguishing consistent objects form inconsistent objects, decision inclusion degree and its probability distribution function as a new measure are presented for both inconsistent and consistent simplified decision systems. New definitions of distribution reduct and maximum distribution reduct for simplified decision systems are proposed. Many important propositions, properties, and conclusions for reduct are drawn. By using radix sorting and hash techniques, a heuristic distribution reduct algorithm for feature selection is constructed. Finally, compared with other feature selection algorithms on six UCI datasets, the proposed approach is effective and suitable for both consistent and inconsistent decision systems.**

***Index Terms*—feature selection, rough set, decision system, decision inclusion degree, distribution reduct**

I. INTRODUCTION

Rough set theory, originated by Pawlak [1] in 1980s, is a powerful mathematical tool to deal with inexact, uncertain, and vague knowledge in information systems [2-5]. It has been widely used for feature selection because it is completely data-driven and does not require any auxiliary information [6]. The selection of relevant and significant features is an important problem particularly for data sets with large number of features [7-9]. But those irrelevant features can deplete the storage space, deteriorate the computational performance, and even decrease the generalization power of the induced patterns [2, 3, 6, 7]. It is, thus, desirable to search for a feature subset that has the same predictive capability as that of the original feature set.

In the last two decades, as an important successful application of rough set models in a variety of problems such as artificial intelligence, machine learning, data mining, and so on, feature selection or attribute reduction in information systems has been drawing wide attention [2, 3, 10]. There are many techniques for feature selection developed in rough set theory [2-12]. These types of feature selection have been proposed in the analysis of information systems, each of which aimed at some basic real-world requirements. Unfortunately, it has been proved that finding all reducts or finding an optimal reduct (a reduct with the least number of attributes) is an NP-complete problem [13]. Many researchers devote themselves to finding an efficient reduct by optimization techniques [2-20]. A distribution reduct [21] was a subset of the feature set that preserved the degree to which every object belonged to each decision class. Kryszkiewicz [22] described two methods of knowledge reduction for inconsistent decision systems, namely assignment reduction and distribution reduction. In an inconsistent decision system, assignment reduction maintains unchanged with the possible decisions for arbitrary object. In comparison, distribution is characterized by preserving the class membership distribution and is a more complete knowledge reduction for all objects in an inconsistent decision system. In other words, the distribution reduction preserves not only all of the deterministic information but also the non-deterministic information of an inconsistent decision system. Yao and Zhao [23] thought that the partition based on the membership distribution vector was more complex, which allowed the distribution reduction to preserve the quality of the decisions. However, it can be a concern that the distribution reduction has strict requirements, and the decision rules derived from distribution reduction are usually less compact and more complicated. For this reason, the maximum distribution reduction in [24] proposed by Zhang et al. remains unchanged with the maximum decision classes for all of the objects in a decision system, which is a good compromise between the compactness of derived rules and the capability of preserving information with respect to decisions. Mi et al. [25] introduced β-reduct on the basis of variable precision rough set model. This type of reduct preserved the sum of objects in the β lower approximations of all decision classes. Wu et al. [26] proposed the concepts of β lower

doi:10.4304/jcp.9.6.1333-1340

distribution reduct and β upper distribution reduct. Ye et al. [27] presented an algorithm for finding a maximum distribution reduct of an inconsistent decision system. Liu et al. [28] introduce a new type of reducts called the λ-Fuzzy-Reduct. However, some of these current algorithms for feature selection have still their own some limitations. Based on the mutual information, Miao and Hu [29] constructed a heuristic algorithm costing time complexity $O(|C||U|^2)$ + $O(|U|^3)$. Hence, the main disadvantage of these methods is much time-space cost. Xu et al. [30] designed a new and relatively reasonable formula for an efficient reduction algorithm, whose worst time complexity was cut down to Max($O(|C||U|)$, $O(|C^2|U/C|)$). Liu et al. [31] presented a hash-based algorithm to calculating positive region, and its time complexity decreased to $O(|U|)$, and a reduction algorithm with twice-hash was presented, whose time complexity was $O(|C|^2|U/C|)$. So far its efficiency is fortunate. However, because of various factors such as noise in the data, lack of critical knowledge, compact representation, and prediction capability, most of decision systems are inconsistent. Inconsistent decision system is a common information system in realistic decision analysis problems, as well as is the focus of study in information systems reduction processing [32]. Discernible matrix that was used for seeking core attribute set of inconsistent decision system in [33] is defective [34]. It may not obtain the right attribute set. Moreover, when several reductions are achieved, their advantages and disadvantages of every reduction cannot be compared in actual applications. Algorithms in [35] used for seeking core attribute set with discernible matrix for incompatible decision system are also defective. Distribution reduction of both consistent and inconsistent decision systems were defined in [33], and their equivalent forms were discussed there. But there was no further study for these two kinds of knowledge reduction methods. Qin et al. [36] proved conditional information entropy reduction in [34] and distribution reduction in [37] were equivalent, and they cannot only ensure decision-making ability of invariant consistent decision rules, but also can guarantee decision-making ability of invariant inconsistent decision rules. Although the heuristic approaches above can avoid the exponential computation in exhaustive methods, they still suffer from intensive computation of either discernibility functions or partitions of universe. Therefore, it is necessary to propose an effective heuristic feature selection algorithm in inconsistent decision systems with less time-space complexity. This paper focuses on creating such a solution.

The remainder of this paper is structured as follows. In Section II, some basic concepts are recalled. In Section III, some concepts, properties and propositions about decision inclusion degree and probability distribution function are presented for both inconsistent and consistent simplified decision systems. An effective heuristic distribution reduct algorithm for feature selection is put forward in Section IV. Section V gives the applications and experimental evaluations. Finally, the conclusions are described in Section VI.

II. Preliminaries

In this section, we review briefly some notions and results related to information systems and decision systems in rough sets. Detailed description of concepts can be found in [1, 2, 5, 10].

The notion of information system (*IS*) has been studied by many authors as a simple knowledge representation method. Formally, an information system is a quadruple $IS = (U, A, V, f)$, where U is a finite nonempty set of objects indicating a given universe; A is a finite nonempty set of features; V is the union of feature domains such that $V = \bigcup_{a\in A} V_a$ for V_a denoting the value domain of feature a; $f: U \times A \to V$ is an information function which associates a unique value of each feature with every object belonging to U, such that for any $a \in A$ and $u \in U$, $f(u, a) \in V_a$. Also, $IS = (U, A, V, f)$ can be written more simply as $IS = (U, A)$.

With every subset $P \subseteq A$, there is an associated indistinguishable relation $IND(P)$ as follows:

$$IND(P) = \{(u, v) \in U \times U \mid \forall a \in P, f(u, a) = f(v, a)\}.$$

It can be easily shown that $IND(P)$ is an equivalence relation on the set U and $IND(P) = \bigcap_{a\in P} IND(\{a\})$. For $P \subseteq A$, the equivalence relation $IND(P)$ partitions U into some equivalence classes given by $U/IND(P) = \{[u]_P \mid u \in U\}$, for simplicity, $U/IND(P)$ will be replaced by U/P, where $[u]_P$ denotes the equivalence class (block) determined by u with respect to P, i.e., $[u]_P = \{v \in U \mid (u, v) \in IND(P)\}$. Each $[u]_P$ is viewed as an information granule consisting of indistinguishable elements.

We define a partial order on all partition sets of U. Let P and Q be two equivalence relations of U, $U/P = \{P_1, P_2, \ldots, P_m\}$ and $U/Q = \{Q_1, Q_2, \ldots, Q_n\}$ be partitions of the finite set U. Then, we define that the partition U/P is finer than the partition U/Q (or the partition U/Q is coarser than the partition U/P), denoted by $P \preceq Q$ (or $Q \succeq P$), between partitions by $P \preceq Q \Leftrightarrow \forall P_i \in U/P, \exists Q_j \in U/Q \to P_i \subseteq Q_j$. If $P \preceq Q$ and $P \succeq Q$, then we say that $P = Q$. If $P \preceq Q$ and $P \neq Q$, then we say that U/Q is strictly coarser than U/P (or U/P is strictly finer than U/Q) and write $P \prec Q$ (or $Q \succ P$).

An information system $IS = (U, A)$ is also called a decision system (*DS*) if $A = C \cup D$, and $C \cap D = \emptyset$, where C is the finite set of condition features and D is the finite set of decision features. Obviously, the previous properties derived hold for $DS = (U, A = C \cup D, V, f)$. The quadruple $DS = (U, A = C \cup D, V, f)$ is usually denoted by a triple (U, C, D) for short, that is, $DS = (U, C, D)$.

Theorem 1. Let $DS = (U, C, D)$ be a decision system with $P, Q \subseteq C \cup D$. If $Q \subseteq P$, then $P \preceq Q$.

Proof. Suppose $U/P = \{P_1, P_2, \ldots, P_m\}$, $U/Q = \{Q_1, Q_2, \ldots, Q_n\}$, for any $P_i = [x]_P \in U/P$, since $Q \subseteq P$, then one has that $P_i = [x]_P = \{y \mid f(x, a) = f(y, a), \forall a \in P\} \subseteq Q_j = [x]_Q = \{y \mid f(x, a) = f(y, a), \forall a \in Q\}$. Hence, since each P_i selected randomly, then $P \preceq Q$ holds. This completes the proof.

Let $DS = (U, C, D)$ be a decision system with $P \subseteq C$. For any $x_i, x_j \in U$, x_i and x_j conflict with each other from P to D if and only if $f(x_i, a) = f(x_j, a)$ for any $a \in P$, and $f(x_i, d) \neq f(x_j, d)$, where $d \in D$. An instance $x \in U$ is a consistent instance in the DS if and only if there does not exist an instance $y \in U$, which conflicts with $x \in U$. Hence, we have the conclusion that the DS is a consistent decision system if and only if each instance $x \in U$ is a consistent instance.

Let $DS = (U, C, D)$ be a decision system with $X \subseteq U$ a subset of universe, attribute subsets P, $Q \subseteq C \cup D$, then $\underline{P}(X) = \cup \{[x]_P | [x]_P \subseteq X\}$ is called P-lower approximation of X. The P-positive region of Q is denoted by

$$POS_P(Q) = \cup \{\underline{P}(X) \mid X \in U/Q\}.$$

Let $DS = (U, C, D)$ be a decision system with any attribute subsets $P \subseteq C \cup D$, to make $a \in P$, and a in P is dispensable for D, if $POS_P(D) = POS_{P-\{a\}}(D)$. Otherwise a is necessary. Then, P is independent relative to D, if every element in P is indispensable for D.

Let $DS = (U, C, D)$ be a decision system. The elements in $POS_C(D)$ are regarded as the objects of consistent set, and the elements in $U - POS_C(D)$ are regarded as the objects of inconsistent set [20].

Let $DS = (U, C, D)$ be a decision system with $U/(C \cup D) = \{[U'_1]_{C \cup D}, [U'_2]_{C \cup D}, \ldots, [U'_n]_{C \cup D}\}$, where $U = \{U_1, U_2, \ldots, U_m\}$, $n \leq m$, and $U'_i \in U$, then $U' = \{U'_1 \cup U'_2 \cup \ldots \cup U'_n\}$. Then (U', C, D) is called a simplified decision system (*SDS*). It is obvious that by virtue of this technology of simplicity lots of redundancy information is deleted, and then the space complexity of the DS is decreased [5].

Theorem 2. Let $SDS = (U', C, D)$ be a simplified decision system. If there exists $IND(C) \subseteq IND(D)$, then the *SDS* is referred to as a consistent simplified decision system (*CSDS*). Otherwise, the *SDS* is referred to as an inconsistent simplified decision system (*ISDS*).

Proof. It is straightforward.

Theorem 3. Let $SDS = (U', C, D)$ be a simplified decision system. If $POS_C(D) = U'$, then we say that the S is consistent, otherwise the S is inconsistent.

Proof. It can be derived directly from the definition of positive region and Theorem 2.

Let $DS = (U, C, D)$ be a decision system with P, $Q \subset C \cup D$, $U/P = \{X_1, X_2, \ldots, X_n\}$, $U/Q = \{Y_1, Y_2, \ldots, Y_m\}$, then the conditional information entropy of knowledge Q with reference to P in [39] is denoted by

$$H(Q \mid P) = -\sum_{i=1}^{n} \frac{|X_i|}{|U|} \sum_{j=1}^{m} \frac{|Y_j \cap X_i|}{|X_i|} \log \frac{|Y_j \cap X_i|}{|X_i|}.$$

III. Decision Inclusion Degree

A. Limitations of Representative Reduction Methods

Firstly, it is known that matrix theory is the core content in advanced algebra. Many of ideas and methods in matrix theory have greatly enriched algebraic theory of mathematics. With deepening of people researching in science, application of matrix theory becomes wider. However, in classical reduction methods, core attribute set can be found by discernible matrix method, and then matrix elements containing core attributes are deleted from discernible matrix. Then, matrix elements free of core attributes with disjunctive form are turned into conjunctive form expression. At last, one makes reduction in this expression, and then it becomes a disjunctive normal form. But the process of transforming conjunctive normal form into disjunctive normal form is very complicated, and it always causes that the time complexity of discernible matrix method does exponential growth with the increase of system size. Each of disjunctive normal form with core attribute set is reduction of decision systems, such that all reducts can be obtained. However, it is unnecessary to compute all reductions in practical problems because people usually only concern about how to find minimum reduction. Therefore, it is concluded that matrix methods in classical rough set theory cannot search the minimum or suboptimal reduction effectively.

Secondly, in a decision system $DS = (U, C, D)$, a reduct of the *DS*, named as a positive region reduct for convenience, is presented in [30, 38] as follows: for any $P \subseteq C$ and $D = \{d\}$, if $POS_P(D) = POS_C(D)$ and $POS_Q(D) \neq POS_C(D)$ for any $Q \subset P$, then P is a positive region reduct of the *DS*. That is, whether or not any condition attribute is redundant depends on whether or not the positive region is changed. Thus, these presented algorithms in [30, 38] only reflect whether or not the prediction of deterministic decision rules has change after reduction [5]. Therefore, if new inconsistent objects are added to the *DS*, it is not considered whether the probability distribution generated by the primary inconsistent objects is changed in their corresponding decision blocks.

Thirdly, in a decision system $DS = (U, C, D)$, a reduct of the *DS*, named as an information entropy reduct for convenience, is presented in [39] as follows: for any $P \subseteq C$ and $D = \{d\}$, if $H(D|P) = H(D|C)$ and $H(D|Q) \neq H(D|C)$ for any $Q \subset P$, then P is an information entropy reduct of the *DS*. That is, whether or not any condition attribute is redundant depends on whether or not the conditional information entropy value of decision system is changed. However, in practical application, there exist new added and primary inconsistent objects in decision blocks, hence, if their probability distribution is changed [5]. Thus, the main criterions of algorithms in [30, 38, 39] in evaluating decision ability only think about the change of certainty factor for all decision rules after reduction.

B. Decision Inclusion Degree and Probability Distribution Function

Inclusion degree is a kind of soft computing method to deal with fuzzy and uncertain knowledge [40]. Data analysis based on inclusion degree is one of main application technologies in rough set theory, which is mainly used to analyze rough classification, attribute dependency, attribute significance, and so on. Uncertainty reasoning methods can be summed up in a special kind of inclusion degrees [20, 40]. Set X is a universe, A and B are two subsets of X. Degree of collection A included in

set B is $D(B/A)$ which is called inclusion degree. In the meantime, knowledge acquisition from a large number of cases for some rules, and rules of the before and after parts relationship is also a kind of actually closed inclusion, so you can use inclusion degree theory to study uncertain rules. In decision systems, decision rules can be extracted. Certain rules can be extracted from consistent decision systems, but uncertain rules or possible rules only can be extracted from inconsistent decision systems.

Theorem 4. Let $SDS = (U', C, D)$ be a simplified decision system with $P, Q \subseteq C$, $U'/D = \{D_1, D_2, \ldots, D_m\}$. Then $POS_P(D) = POS_Q(D)$ if and only if $\underline{P}(D_i) = \underline{Q}(D_i)$, where $i = 1, 2, \ldots, m$.

Proof. Suppose that $\underline{P}(D_i) \neq \underline{Q}(D_i)$, $i = 1, 2, \ldots, m$, if $POS_P(D) = POS_Q(D)$, it follows from the definition of positive region that one has $\underline{P}(D_i) = \underline{Q}(D_i)$. This yields a contradiction. Thus, $POS_P(D) = POS_Q(D) \Leftrightarrow \underline{P}(D_i) \neq \underline{Q}(D_i)$, where $i = 1, 2, \ldots, m$. This completes the proof.

In a simplified decision system $SDS = (U', C, D)$, suppose that $D_0 = U' - POS_C(D)$, it follows that $\underline{C}D_0 = D_0$. That is, all inconsistent objects $U' - POS_C(D)$ detached form the unattached set D_0. Then, suppose that $\underline{C}D_i \neq \emptyset$, one has another decision partition $\{\underline{C}D_0, \underline{C}D_1, \underline{C}D_2, \ldots, \underline{C}D_m\}$ of C on U, and then a new equivalent relation can be constructed, denoted by R_D. Similar to [17], it follows that there exists $U'/R_D = \{\underline{C}D_0, \underline{C}D_1, \underline{C}D_2, \ldots, \underline{C}D_m\}$. It can be concluded that the presented decision partition U'/R_D has not only detached consistent objects from different decision blocks in U, but also distinguished consistent objects from inconsistent objects.

Definition 1. Let $ISDS = (U', C, D)$ be an inconsistent simplified decision system with $P \subseteq C$, $U'/D = \{D_1, D_2, \ldots, D_m\}$, $U'/R_D = \{\underline{C}D_0, \underline{C}D_1, \underline{C}D_2, \ldots, \underline{C}D_m\}$, and $\forall u \in U'$. The decision inclusion degree is denoted by $D(\underline{C}D_i/[u]_P)$, is defined as

$$D(\underline{C}D_i / [u]_P) = \frac{|\underline{C}D_i \cap [u]_P|}{|[u]_P|},$$

where $i = 1, 2, \ldots, m$.

Definition 2. Let $ISDS = (U', C, D)$ be an inconsistent simplified decision system with $P \subseteq C$, $U'/D = \{D_1, D_2, \ldots, D_m\}$, $U'/R_D = \{\underline{C}D_0, \underline{C}D_1, \underline{C}D_2, \ldots, \underline{C}D_m\}$, and $\forall u \in U'$. The probability distribution function P with respect with u in U' is denoted by $\mu_P(u)$, is defined as

$$\mu_P(u) = \left(\frac{|\underline{C}D_0 \cap [u]_P|}{|[u]_P|}, \frac{|\underline{C}D_1 \cap [u]_P|}{|[u]_P|}, \ldots, \frac{|\underline{C}D_m \cap [u]_P|}{|[u]_P|}\right).$$

From Definition 2, it can be obtained the following property immediately.

Property 1. Let $ISDS = (U', C, D)$ be an inconsistent simplified decision system with $\forall u, v \in U'$. Then

$$\forall u, v \in [u]_P \Rightarrow \mu_P(u) = \mu_P(v).$$

Property 1 states that in an inconsistent simplified decision system $ISDS = (U', C, D)$, for any $X \in U/C$, the probability distribution function of each equivalence class X only need to be calculated.

Let $DS = (U, C, D)$ be a decision system and $P \subseteq C$. If $U/P = \{X_1, X_2, \ldots, X_n\}$, $D = \{d\}$, $U/D = \{Y_1, Y_2, \ldots, Y_m\}$, and $U/R_D = \{\underline{C}Y_0, \underline{C}Y_1, \underline{C}Y_2, \ldots, \underline{C}Y_m\}$, then let $H(R_D|P)$ denote the conditional rough entropy of D with reference to P of DS in [17] as follows

$$H(R_D \mid P) = \sum_{i=1}^{n} \frac{|X_i|}{|U|} \sum_{j=0}^{m} \frac{|\underline{C}Y_j \cap X_i|}{|X_i|} \log_2 \frac{|X_i|}{|\underline{C}Y_j \cap X_i|}.$$

Theorem 5. Let $ISDS = (U', C, D)$ be an inconsistent simplified decision system with $P \subseteq C$, $U'/P = \{X_1, X_2, \ldots, X_n\}$, $U'/C = \{Y_1, Y_2, \ldots, Y_k\}$, $U/D = \{D_1, D_2, \ldots, D_m\}$, $U'/R_D = \{\underline{C}D_0, \underline{C}D_1, \underline{C}D_2, \ldots, \underline{C}D_m\}$, and $\forall u \in U'$. $H(R_D \mid P) = H(R_D \mid C) \Leftrightarrow \forall u \in U' \Rightarrow \mu_P(u) = \mu_C(u)$.

Proof. ($\Rightarrow$) Suppose that $P \subseteq C$, it follows from the above partial order that $C \preceq P$. Then, it can draw from Proposition 10 in [17] that $H(R_D|C) \leq H(R_D|P)$. For $\forall u \in U'$, when $H(R_D|P) = H(R_D|C)$, assume that $\mu_P(u) = \mu_C(u)$ is not true, then there exists u_0 such that $\mu_P(u_0) \neq \mu_C(u_0)$. Thus one has that

$$\left(\frac{|\underline{C}D_0 \cap [u_0]_P|}{|[u]_P|}, \frac{|\underline{C}D_1 \cap [u_0]_P|}{|[u]_P|}, \ldots, \frac{|\underline{C}D_m \cap [u_0]_P|}{|[u]_P|}\right) \neq$$
$$\left(\frac{|\underline{C}D_0 \cap [u_0]_C|}{|[u]_C|}, \frac{|\underline{C}D_1 \cap [u_0]_C|}{|[u]_C|}, \ldots, \frac{|\underline{C}D_m \cap [u_0]_C|}{|[u]_C|}\right).$$

Hence, it can be obtained that $[u_0]_P \neq [u_0]_C$. One has that $[u_0]_C \subset [u_0]_P$ from the above partial order. Assume that $[u_0]_P = \bigcup \{[u_i]_C \mid u_i \in U', i = 0, 1, 2, \ldots, l, \text{ and } 1 \leq l \leq |U'|\}$, for $\forall s \neq t$ ($s, t \in \{0, 1, 2, \ldots, l\}$), and $[u_s]_C \cap [u_t]_C = \emptyset$. Then there exist at least $s_0, t_0 \in \{0, 1, 2, \ldots, l\}$ and $s_0 \neq t_0$ such that $\mu_C(u_{s_0}) \neq \mu_C(u_{t_0})$, otherwise $\mu_P(u_0) = \mu_C(u_0)$. Thus one has that

$$\left(\frac{|\underline{C}D_0 \cap [u_{s_0}]_C|}{|[u_{s_0}]_C|}, \frac{|\underline{C}D_1 \cap [u_{s_0}]_C|}{|[u_{s_0}]_C|}, \ldots, \frac{|\underline{C}D_m \cap [u_{s_0}]_C|}{|[u_{s_0}]_C|}\right) \neq$$
$$\left(\frac{|\underline{C}D_0 \cap [u_{t_0}]_C|}{|[u_{t_0}]_C|}, \frac{|\underline{C}D_1 \cap [u_{t_0}]_C|}{|[u_{t_0}]_C|}, \ldots, \frac{|\underline{C}D_m \cap [u_{t_0}]_C|}{|[u_{t_0}]_C|}\right).$$

It can be obtained from Proposition 8 in [17] that for $\forall X_i, X_j \in U'/P$, $X_i \neq X_j$, $\forall \underline{C}D_k \in U'/R_D$, if $X_i \bigcup X_j \in U'/C$ and $\frac{|X_i \cap \underline{C}D_k|}{|X_i|} = \frac{|X_j \cap \underline{C}D_k|}{|X_j|}$ always holds, then $H(R_D|P) = H(R_D|C)$. Thus, it is obvious from $\mu_C(u_{s_0}) \neq \mu_C(u_{t_0})$ that $H(R_D|P) > H(R_D|C)$, which contradicts with the above hypothesis that $H(R_D|P) = H(R_D|C)$. Therefore, it can be obtained that $\forall u \in U' \Rightarrow \mu_P(u) = \mu_C(u)$. ($\Leftarrow$) Suppose that $P \subseteq C$, if $\forall u \in U' \Rightarrow \mu_P(u) = \mu_C(u)$, it follows from the above partial order that $C \preceq P$, and then one has that $[u]_P = [u_1]_C \bigcup [u_2]_C \bigcup \ldots \bigcup [u_l]_C$, where $u_1, u_2, \ldots, u_l \in U'$, $1 \leq l \leq |U'|\}$, $\forall s \neq t$ ($s, t \in \{0, 1, 2, \ldots, l\}$), and $[u_s]_C \cap [u_t]_C = \emptyset$. Thus, it can be obtained that $\mu_P(u_1) = \mu_P(u_2) = \ldots = \mu_P(u_l)$. It follows from Definition 4 in [17] that

$$\sum_{i=1}^{l} \frac{|[u_i]_C|}{|U|} \sum_{j=0}^{m} \frac{|\underline{C}D_j \cap [u_i]_C|}{|[u_i]_C|} \log_2 \frac{|[u_i]_C|}{|\underline{C}D_j \cap [u_i]_C|}$$
$$= \sum_{i=1}^{l} \frac{|[u_i]_C|}{|U|} \sum_{j=0}^{m} \frac{|\underline{C}D_j \cap [u]_B|}{|[u]_B|} \log_2 \frac{|[u]_B|}{|\underline{C}D_j \cap [u]_B|}$$

$$= \frac{|[u_1]_C \cup [u_2]_C \cup ... \cup [u_l]_C|}{|U|} \sum_{j=0}^{m} \frac{|\underline{C}D_j \cap [u]_B|}{|[u]_B|} \log_2 \frac{|[u]_B|}{|\underline{C}D_j \cap [u]_B|}$$
$$= \frac{|[u]_B|}{|U|} \sum_{j=0}^{m} \frac{|\underline{C}D_j \cap [u]_B|}{|[u]_B|} \log_2 \frac{|[u]_B|}{|\underline{C}D_j \cap [u]_B|}.$$

Hence, one has that

$$H(R_D \mid C) = \sum_{i=1}^{k} \frac{|Y_i|}{|U|} \sum_{j=0}^{m} \frac{|\underline{C}D_j \cap Y_i|}{|Y_i|} \log_2 \frac{|Y_i|}{|\underline{C}D_j \cap Y_i|}$$
$$= \sum_{i=1}^{n} \frac{|X_i|}{|U|} \sum_{j=0}^{m} \frac{|\underline{C}D_j \cap X_i|}{|X_i|} \log_2 \frac{|X_i|}{|\underline{C}D_j \cap X_i|}$$
$$= H(R_D \mid P),$$

Thus, $H(R_D|P) = H(R_D|C)$ holds. This completes the proof.

Theorem 5 shows that in an inconsistent simplified decision system $ISDS = (U', C, D)$, the conditional rough entropy of D with reference to $P \subseteq C$ has the same discriminating capability as the probability distribution function P with respect with u in U' when their equations hold.

IV. Feature Selection Of Inconsistent Decision Systems

A. Decision Inclusion Degree-based Distribution Reduction

Distribution reduction which is based on inclusion degree [40] can obtain all reducts of a decision system, and we can always use discernible matrix method to find core attribute set in both consistent and inconsistent decision system. Since core and reduction are the most important concepts of knowledge reduction in decision systems and the main goal of using discernible matrix is also for calculating core and reduction, but both time complexity and space complexity of existing methods on the basis of discernible matrix for core are not ideal. In order to overcome the limitations of these above methods which seek core and reduction through discernible matrix to improve operational efficiency, it is necessary to find a new heuristic method. Attribute significance based on positive region in classical rough set theory only makes a quantitative description for positive region cardinality, while attribute significance based on conditional information entropy only describes separation of objects belonging to different decision classes in equivalence classes of condition attribute subset without considering separation of consistent and inconsistent objects that have the same decision attribute values. Due to inconsistent objects in inconsistent decision systems, the existing methods based on positive region and conditional information entropy cannot equally express knowledge reduction [5, 17, 30, 39]. Then, if all inconsistent objects are separated from consistent objects, it is helpful to search for the minimum or suboptimal reduction.

Definition 3. Let $ISDS = (U', C, D)$ be an inconsistent simplified decision system with $P \subseteq C$, $U'/D = \{D_1, D_2, \ldots, D_m\}$, $U'/R_D = \{\underline{C}D_0, \underline{C}D_1, \underline{C}D_2, \ldots, \underline{C}D_m\}$. For $\forall u_i \in U'$, $\mu_P(u_i) = (\underline{C}D_0^P(u_i), \underline{C}D_1^P(u_i), ..., \underline{C}D_m^P(u_i))$, and $\gamma_P(u_i) = \{\underline{C}D_h \mid \underline{C}D_h^P(u_i) = \underset{0 \le j \le m}{Max} \underline{C}D_j^P(u_i)\}$, where $\underline{C}D_j^P(u_i) = \frac{|\underline{C}D_j \cap [u_i]_P|}{|[u_i]_P|}$, $j = 1, 2, \ldots, m$. Then

(1) P is called a distribution set of the $ISDS$ if $\mu_P(u_i) = \mu_C(u_i)$ for $i = 1, 2, \ldots, |U'|$. P is called a distribution reduct of the $ISDS$ if and only if $\mu_P(u_i) = \mu_C(u_i)$ for $i = 1, 2, \ldots, |U'|$, and for $\forall P' \subset P$, there exist $u_j \in U'$ such that $\mu_{P'}(u_j) \neq \mu_C(u_j)$.

(2) P is called a maximum distribution set of the $ISDS$ if $\gamma_P(u_i) = \gamma_C(u_i)$ for $i = 1, 2, \ldots, |U'|$. P is called a maximum distribution reduct of the $ISDS$ if and only if $\gamma_P(u_i) = \gamma_C(u_i)$ for $i = 1, 2, \ldots, |U'|$, and for $\forall P' \subset P$, there exist $u_j \in U'$ such that $\gamma_{P'}(u_j) \neq \gamma_C(u_j)$.

Definition 3 states that in an inconsistent simplified decision system $ISDS = (U', C, D)$, if attribute subset $P \subseteq C$ is a distribution reduct of an inconsistent decision system, then rules coming from P and C have the same reliability. Then, from Definition 3, it can be obtained the following property immediately.

Property 2. Let $CSDS = (U', C, D)$ be a consistent simplified decision system. Since $D_0 = U' - POS_C(D) = \emptyset$, one has that $\underline{C}D_0 = \emptyset$, then the probability distribution function P with respect with u in U' degenerates into the general probability distribution function, and the conditional rough entropy degenerates into the conditional information entropy in [39].

Property 2 illustrates that the probability distribution function in consistent decision systems is a special instance of that in inconsistent decision systems. This means that the definition of probability distribution function in consistent decision systems is a consistent extension in inconsistent decision systems. It follows that the decision inclusion degree in an inconsistent decision system is suitable for measuring the uncertainty of both inconsistent and consistent decision systems. Therefore, the distribution reduct and the maximum distribution reduct are suitable for both inconsistent and consistent decision systems. In what follows, the inconsistent or consistent simplified decision systems can be unified into the simplified decision systems.

Definition 4. Let $SDS = (U', C, D)$ be a simplified decision system with $P \subseteq C$. For $\forall a \in P$ and $\forall u \in U'$, the significance measure of a in P with reference to D is denoted by $SIG^{inner}(a, P, D)$, defined as

$$SIG^{inner}(a, P, D) = \frac{\{\forall u \in U' \mid \mu_{P-\{a\}}(u) \neq \mu_P(u)\}}{|U'|}.$$

Definition 5. Let $SDS = (U', C, D)$ be a simplified decision system with $P \subseteq C$. For $\forall a \in C - P$ and $\forall u \in U'$, the significance measure of a in P with reference to D is denoted by $SIG^{outer}(a, P, D)$, defined as

$$SIG^{outer}(a, P, D) = \frac{\{\forall u \in U' \mid \mu_{P \cup \{a\}}(u) \neq \mu_P(u)\}}{|U'|}.$$

According to Definitions 4 and 5, it can be obtained the following properties immediately.

Property 3. $0 \le SIG^{inner}(a, P, D) \le 1$.

Property 4. $0 \le SIG^{outer}(a, P, D) \le 1$.

Property 5. when $P = C$, $SIG^{outer}(\ , C, D) = 0$.

Property 6. $\forall\ a \in C - P$ is a dispensable attribute if and only if $SIG^{outer}(a, P, D) = 0$.

Definition 5 shows that the significance measure $SIG^{outer}(a, P, D)$ indicates the importance of attribute a added to $P \subseteq C$ with reference to D in a simplified decision system $SDS = (U', C, D)$, offering the powerful reference to the decision. Furthermore, the bigger the significance measure of attribute is, the higher its position in the decision system is, otherwise the lower its position is. Thus, all the definitions above are used as heuristic information for feature selection algorithm to select a reduct from consistent or inconsistent data sets. It is known that the intersection of all attribute reducts is said to be indispensable and is called the core in a decision system. Each attribute in the core must be in every attribute reduction of the decision system. Then, the significance measures above can be used to find the core attributes. The following properties are of interest with this regard.

Property 7. Let $SDS = (U', C, D)$ be a simplified decision system with $P \subseteq C$. $\forall\ a \in P$ is indispensable in P with reference to D if and only if $SIG^{inner}(a, P, D) > 0$.

Property 8. Let $SDS = (U', C, D)$ be a simplified decision system. For $\forall\ a \in C$, if $SIG^{inner}(a, C, D) > 0$, then a is a core attribute of the SDS, i.e., $CORE = \{a \in C \mid SIG^{inner}(a, C, D) > 0\}$.

Theorem 6. Let $SDS = (U', C, D)$ be a simplified decision system with $P \subseteq C$. P is a distribution reduct of C relative to D if $\mu_P(u) = \mu_C(u)$ for $\forall\ u \in U'$ and $SIG^{inner}(a, P, D) > 0$ for $\forall\ a \in P$.

Proof. It can be derived directly from Definition 3 and Properties 6 and 7.

B. Feature Selection Algorithm of Inconsistent Decision Systems

In the following, we focus on how to improve computational efficiency of a heuristic feature selection algorithm. Then we introduce the idea of radix sorting in [30] and hash in [31] to calculate equivalence blocks and positive region effectively. The main advantage of this approach stems from the fact that this framework is able to characterize the granulation structure using a granulation order. Thus, through the decomposition of $SIG^{outer}(a, P, D)$, it can be seen easily that every time to calculate any attribute a with the maximum of $SIG^{outer}(a, P, D)$ is in fact to calculate that with the maximum of $\mu_{P\cup\{a\}}(u)$, because $\mu_P(u)$ is a constant when we calculate $SIG^{outer}(a, P, D)$. Therefore, we only need calculate $\mu_{P\cup\{a\}}(u)$ except $\mu_P(u)$. Thus, the above policies will help to reduce the quantity of computation and the time-space of search. Formally, we can now construct a distribution reduct algorithm, also called an efficient feature selection algorithm based on decision inclusion degree (FSDID) for inconsistent decision systems as follows.

Algorithm 1. FSDID

Input: An inconsistent decision system $IDS = (U, C, D)$, where $C = \{c_1, c_2, \ldots, c_{|C|}\}$, and $D = \{d\}$

Output: *reduct*, a reduct of *IDS*

(1) Let $CORE = \emptyset$, $R = \emptyset$

(2) Calculate U/C, U/D and $U/(C \cup D)$ incrementally to get U' by radix sorting, and obtain $POS_C(D)$ and $U' - POS_C(D)$ by hash, then get U'/R_D

(3) Calculate $\mu_C(u)$ and $\mu_{C-\{c_i\}}(u)$ to get $CORE = \{c_i \in C \mid SIG^{inner}(a, C, D) > 0\}$ for $\forall\ u \in U'$ and $i = 1, 2, \ldots, |C|$, then let $R = CORE$ and go to (5)

(4) Select a_i with $max\{\mu_{P\cup\{a_i\}}(u)\}$ by radix sorting to put a_i into H, where $\forall\ a_i \in C - R$
// Select a_i with $max\{SIG^{outer}(a_i, P, D)\}$
(4.1) If $|H| \ne 1$, select $a_i \in H$ with $min\{|U/(P \cup \{a_i\})|\}$
(4.2) If the selected is not only, then select the front
(4.3) $R = R \cup \{a_i\}$

(5) If $\mu_R(u) \ne \mu_C(u)$, then go to (4), else
(5.1) Let $R = R - CORE$;
(5.2) $t = |R|$;
(5.3) For ($i = 1$; $i \le t$; i++)
(5.3.1) $a_i \in R$;
(5.3.2) $R = R - \{a_i\}$;
(5.3.3) If $\mu_{R\cup CORE}(u) \ne \mu_C(u)$, then $R = R \cup \{a_i\}$

(6) $reduct = R \cup CORE$

(7) End

Remark. The above steps for feature selection algorithm of distribution reduct should be of reference in obtaining the maximum distribution reduct in both inconsistent and consistent decision systems. It can be easily seen that Step 5 in FSDID algorithm ensures that the distribution reduct is complete, which can ensure that the final reduct will be obtained. By calculation and analysis, the total worst time complexity of FSDID algorithm is $O(|C||U|) + O((|C| - 1)|U|) + O((|C| - 2)|U|) + \ldots + O(|U|) = O(|C|^2|U|)$, which is below the time complexity of these methods in [22, 24, 27-29, 32, 33, 35, 38, 39]. After comparison, it can be easily known that the algorithm proposed in this paper is effective and available. Furthermore, the worst space complexity of FSDID algorithm is $O(|C||U|)$.

V. Experimental Results

In this section, we apply the proposed approach and other feature selection approaches in several data sets from the UCI Repository of machine learning databases, to evaluate the proposed approach. In the following, their advantages and disadvantages can be further found easily through comparing roundly the Algorithm 4 in [38] and the Algorithm CEBARKCC in [39] with the proposed FSDID algorithm, shortly denoted by Alg_a, Alg_b, and Alg_c, respectively. Here we choose six discrete databases from UCI datasets and use three algorithms above to do more experiments on PC (Inter(R) Pentium(R) D CPU 3.4 GHz, 2 GB memory, Windows XP). Then the comparison results of three feature selection algorithms are outlined in Table I.

TABLE I.
COMPARISON RESULTS FOR DIFFERENT FEATURE SELECTION ALGORITHMS

NO.	Dataset	Objects	Attributes	Consistent or not	Selected attributes		
					Alg_a	Alg_b	Alg_c
1	Liver-disorders	345	7	Yes	3	3	3
2	Zoo	101	17	No	10	9	8
3	Vehicle	946	20	Yes	4	4	4
4	Mushroom	8124	23	Yes	5	4	3
5	Voting-records	435	17	Yes	10	9	9
6	Breast cancer-wisconsin	683	10	Yes	5	4	4

VI. CONCLUSIONS

Dataset dimensionality is one of the primary impediments to data analysis areas. An important step prior to constructing a classifier for a very large data set is feature selection. In this regard, by distinguishing consistent objects form inconsistent objects, the decision inclusion degree, the probability distribution function, the distribution reduct and the maximum distribution reduct are presented for both inconsistent and consistent simplified decision systems. Furthermore, many important properties and propositions are discussed as well. An effective heuristic feature selection algorithm in inconsistent decision systems with less time-space complexity are put forward as a distribution reduct. The theoretical analyses show that the time complexity of this method is lower than that of existing representative feature selection methods. Meanwhile, the experiment results are consistent with our theoretical analysis. In sum, the proposed method is an effective means of feature selection for both inconsistent and consistent decision systems, especially large ones.

ACKNOWLEDGMENT

We are highly grateful to the anonymous reviewers, referees and Editor-in-Chief for their valuable comments and hard work.

This work was supported by the National Natural Science Foundation of China (Nos. 60873104, 61370169), the Key Project of Science and Technology Department of Henan Province (No. 112102210194), the Science and Technology Research Key Project of Educational Department of Henan Province (Nos. 12A520027, 13A52 0529), and the Education Fund for Youth Key Teachers of Henan Normal University.

REFERENCES

[1] Z. Pawlak, *Rough Sets: Theoretical Aspects of Reasoning about Data*, Dordrecht: Kluwer Academic Publishers, 1991.

[2] J. C. Xu, L. Sun, and Q. Q. Zhang, *Theories and Methods of Granular Computing and Its Uncertainty Information Measures*, Beijing: Academic Press, 2013.

[3] L. Sun, J. C. Xu, and Y. Tian, "Feature selection using rough entropy-based uncertainty measures in incomplete decision systems", *Knowledge-Based Systems*, vol. 36, pp. 206−216, 2012.

[4] L. Sun, J. C. Xu, S. Q. Li, X. Z. Cao, and Y. P. Gao, "New approach for feature selection by using information entropy", *Journal of Information and Computational Science*, vol. 8, pp. 2259−2268, 2011.

[5] L. Sun, J. C. Xu, Z. A. Xue, and J. Y. Ren. "Decision degree-based decision tree technology for rule extraction", *Journal of Computers*, vol. 7, pp. 1769−1779, 2012.

[6] Z. C. Lu, Z. Qin, Y. Q. Zhang, and J. Fang, "A fast feature selection approach based on rough set boundary regions", *Pattern Recognition Letters*, vol. 36, pp. 81−88, 2014.

[7] L. Sun and J. C. Xu, "A granular computing approach to gene selection", *Bio-Medical Materials and Engineering*, vol. 24, pp. 1307−1314, 2014.

[8] L. Sun, J. C. Xu, J. Y. Ren, and T. H. Xu, "Granularity partition-based feature selection and its application in decision systems", *Journal of Information and Computational Science*, vol. 9, pp. 3487−3500, 2012.

[9] L. Sun, J. C. Xu, Y. W. Hu, and L. N. Du, "Granular space-based feature selection and its applications", *Journal of Software*, vol. 8, pp. 817−826, 2013.

[10] G. Y. Wang, Y. Y. Yao, and H. Yu. "A survey on rough set theory and its application", *Chinese Journal of Computers*, vol. 32, pp. 1229−1246, 2009.

[11] L. Sun and J. C. Xu, "Feature selection using mutual information based uncertainty measures for tumor classification", *Bio-Medical Materials and Engineering*, vol. 24, pp. 763−770, 2014.

[12] L. Sun, J. C. Xu, Z. A. Xue, and L. J. Zhang, "Rough entropy-based feature selection and its application", *Journal of Information and Computational Science*, vol. 8, pp. 1525−1532, 2011.

[13] S. K. M. Wong and W. Ziarko, "On optimal decision rules in decision tables", *Bulletin of the Polish Academy of Sciences*, vol. 33, pp. 693−696, 1985.

[14] J. C. Xu and L. Sun, "Knowledge entropy and feature selection in incomplete decision systems", *Applied Mathematics & Information Sciences*, vol. 7, pp. 829−837, 2013.

[15] J. C. Xu and L. Sun, "A new knowledge reduction algorithm based on decision power in rough set", *Transactions on Rough Sets*, vol. 12, pp. 76−89, 2010.

[16] L. Sun, J. C. Xu, and Y. P. Song, "Information quantity-based decision rule acquisition from decision tables", *Journal of Convergence Information Technology*, vol. 7, pp. 57−67, 2012.

[17] L. Sun, J. C. Xu, and L. J. Zhang, "Approaches to knowledge reduction of decision systems based on conditional rough entropy", *International Journal of Advancements in Computing Technology*, vol. 3, pp. 129−139, 2011.
[18] L. Zhang and B. Zhang, "The quotient space theory of problem solving", *Fundamenta Informaticae*, vol. 59, pp. 287−298, 2004.
[19] L. Sun, J. C. Xu, C. Wang, T. H. Xu, and J. Y. Ren, "Granular computing-based granular structure model and its application in knowledge retrieval", *Information Technology Journal*, vol. 11, pp. 1714−1721, 2012.
[20] L. Sun, J. C. Xu, and Y. Y. Ma, "New reduction method based on inclusion degree in inconsistent decision table", *Chinese Computer Engineering and Applications*, vol. 43, pp. 166–168, 2007.
[21] M. Beynon, "Reducts within the variable precision rough sets model: a further investigation", *European Journal of Operational Research*, vol. 134, pp. 592−605, 2001.
[22] M. Kryszkiewicz, "Comparative study of alternative type of knowledge reduction in inconsistent systems", *International Journal of Intelligent Systems*, vol. 16, pp. 105−120, 2001.
[23] Y. Y. Yao and Y. Zhao, "Attribute reduction in decision-theoretic rough set models", *Information Sciences*, vol. 178, pp. 3356−3373, 2008.
[24] W. X. Zhang, J. S. Mi, and W. Z. Wu, "Approaches to knowledge reductions in inconsistent systems", *International Journal of Intelligent Systems*, vol. 18, pp. 989−1000, 2003.
[25] J. S. Mi, W. Z. Wu, and W. X. Zhang, "Approaches to knowledge reductions based on variable precision rough sets model", *Information Sciences*, vol. 159, pp. 255−272, 2004.
[26] W. Z. Wu, M. Zhang, H. Z. Li, and J. S. Mi, "Knowledge reduction in random information systems via dempster-shafer theory of evidence", *Information Sciences*, vol. 174, pp. 143−164, 2005.
[27] D. Y. Ye, Z. J. Chen, and C. Y. Yu, "A novel maximum distribution reduction algorithm for inconsistent decision tables", in *Proceedings of International Conference on Knowledge Science, Engineering and Management*, J. Lang, F. Z. Lin, and J. Wang, Eds., Lecture Notes in Computer Science, vol. 4092, 2006, pp. 548−555.
[28] Q. Liu, L. T. Chen, J. Z. Zhang, and F. Min, "Knowledge reduction in inconsistent decision tables", in *Proceedings of International Conference on Advanced Data Mining and Applications*, X. Li, O. R. Zaïane, and Z. H. Li, Eds., Lecture Notes in Computer Science, vol. 4093, 2006, pp. 626–635.
[29] D. Q. Miao and G. R. Hu, "A heuristic algorithm for reduction of knowledge", *Chinese Journal of Computer Research and Development*, vol. 36, pp. 681–684, 1999.
[30] Z. Y. Xu, Z. P. Liu, B. R. Yang, et al., "A quick attribute reduction algorithm with complexity of max ($O(|C||U|)$,$O(|C|^2|U/C|)$)", *Chinese Journal of Computers*, vol. 29, pp. 391–399, 2006.
[31] Y. Liu, R. Xiong, and J. Chu, "Quick attribute reduction algorithm with hash", *Chinese Journal of Computers*, vol. 32, pp. 1493–1499, 2009.
[32] J. S. Mi, W. Z. Wu, and W. X. Zhang, "An approach to approximation deduction in inconsistent decision tables", in *Proceedings of Rough Sets, Fuzzy set, Data Mining, and Granular*, 2003, pp. 283–286.
[33] K. Li, Y. S. Liu, and L. Wang, "An attribute reduction algorithm of rough set", *Chinese Computer Engineering and Applications*, vol. 38, pp. 15–16, 2002.
[34] G. Y. Wang, "The calculation method of core properties in decision table", *Chinese Journal of Computers*, vol. 26, pp. 611–615, 2003.
[35] T. Bin and L. L. Li, "The discussion about attribute reduction algorithm based on clear matrix", *Chinese Computer Engineering and Applications*, vol. 40, pp. 184–186, 2004.
[36] K. Y. Qin, P. Zheng, and W. F. Du, "The relationship among knowledge reduction approaches", in *Proceedings of International Conference on Fuzzy Systems and Knowledge Discovery*, Changsha, China, 2005, pp. 1232–1241.
[37] W. X. Zhang, Y. Leung, and W. Z. Wu, *Information System and Knowledge Discovery*, Beijing: Science Press, 2003.
[38] S. H. Liu, Q. J. Sheng, B. Wu, et al., "Research on efficient algorithms for rough set methods", *Chinese Journal of Computers*, vol. 26, pp. 524–529, 2003.
[39] G. Y. Wang, H. Yu, and D. C. Yang, "Decision table reduction based on conditional information entropy", *Chinese Journal of Computers*, vol. 25, pp. 759–766, 2002.
[40] W. X. Zhang, W. Z. Wu, J. Y. Liang, and D. Y. Li, *Rough Set Theory and Methods*, Beijing: Science Press, 2001.

Lin Sun works at College of Computer & Information Engineering, Henan Normal University. He is currently a Ph.D. Candidate at Beijing University of Technology. He received his B.S. and M.S. degree in Computer Science and Technology, Henan Normal University in 2003 and 2007, respectively. His main research interests include rough set, granular computing, bioinformatics, and data mining.

Real Time Pedestrian Detection Algorithm by Mean Shift

Qing Tian
College of Information Engineering, North China University of Technology, Beijing, China
Email: tianqingncut@yeah.net

Shuai Qiao
College of Information Engineering, North China University of Technology, Beijing, China

Teng Guo
College of Information Engineering, North China University of Technology, Beijing, China

Yun Wei
Beijing Urban Engineering Design and Research Institute Beijing, China

***Abstract*—Conventional moving objects detection algorithm associated with visible image is often affected by the change of moving objects' shapes, illumination conditions and is also influenced by complex backgrounds, shadow of moving objects, moving objects of self-occlusion or mutual-occlusion phenomenon. This paper presents a method of human detection by mean shift based on depth map. By analyzing and comprehensively applying segmentation method based on height information to extract moving target and remove the background information from depth map, the region of interest (ROI) with moving target should be found, then through mean shift method the goal of real-time objects (pedestrian) detection can be achieved eventually. In this paper, using the depth image pattern recognition is a good way to overcome the difficulties that visible light image pattern recognition often encounters. The depth image pixel value is only related to the distance from the surface of the object to the view window plane. Therefore, depth image has nothing to do with color space and does not suffer from the factors such as illumination, shadow effect. In addition, the mean shift targets detection method with high efficiency and fast speed features can solve the problems of low identification efficiency and poor real-time performance based on traditional pedestrian detection system to a certain extent. Our algorithm using mean shift method based on depth information has been tested on several image sequences and shown to achieve robust and real-time detection.**

***Index Terms*—human detection, depth image, height division, mean shift**

I. Introduction

In recent years with the functions of intelligent monitoring system more and more powerful, the demand for intelligent video monitoring system increases rapidly and it is gradually being applied in almost all walks of life. However, pedestrian detection is the kernel of these monitoring systems. Many methods have been offered for moving objects tracking in image sequences so far. Mean shift algorithm is one of the noted methods [1]. Due to the mean shift target detection tracking algorithm with the advantages of a good real-time performance, low computations, independence of turning and transformation [2], this paper proposed a mean shift method based on depth image to detect Pedestrians. Mean shift algorithm is a kind of statistical probability density gradient algorithm which utilizes kernel function histogram model of rotation and has no sensitive to the edge of blocks, background movement, the target rotation and deformation. Besides, mean shift algorithm has fast and effective characteristics and can also well solve the matching problem between two frames of moving targets. Fukunaga [3] put forward the concept of mean shift for the first time in an essay about probability density gradient function such as estimates in the literature in 1975. But at the beginning of this concept proposed, mean shift was not noticed by people, not mention to the use of actual needs. Yizong Cheng [4] published an important literature about mean shift in 1995. This text did supplements to the basic mean-shift algorithm in two aspects: define a set of kernel functions, which makes the magnitude of contributions of offsets to the mean shift vector follow with the distances from the sampling point to the center of mass; cited a weight coefficient, which leads to different sample points have different importance to the mean shift vector, thus making mean shift algorithm extend the limits of application. Comaniciu [5] and others put mean shift tracking method into practical application and opened the door of mean shift applications in target tracking. Yuan Xiao [6] utilized a single histogram to describe the color characteristics of the object and combined with mean shift algorithm to track moving people. To improve theoretic limitation of mean shift, Zhu Sheng-li [7] proposed an algorithm using mean shift and Kalman filter for fast tracking motion objects. On the basis of this, Baohong Yuan [8] came up

doi:10.4304/jcp.9.6.1341-1346

an improved algorithm and overcame the defect of occlusion in the process of tracking moving object well.

Using the depth image for moving targets detection is a rising technology in recent years. Especially after the Prime Sense Company of Israel launched Kinect (Xbox 360 special external equipment based on 3D measurement technology) for Microsoft in April 2010. More and more scholars pay attention to this new field. Because the depth image pixel value only related to the distance from the surface of the object to the view window plane, it can effectively break through the problems and bottlenecks of optical image recognition. In a certain space range, it can be used to represent the object coordinates in the 3D space [9]. Joshua Fabian [10] developed a "VU-Kinect" block and showed the utility of both the VU-Kinect block and the Kinect itself through a simple 3D object tracking example, which helps fully realize the Kinect' s potential. Junping Zhang [11] described a system for predicting pedestrian counts that significantly extended the utility of statistical learning algorithms.

In this paper, we first use the Kinect motion-sensing camera to obtain depth image. Because there is no shadow in the depth image and it is not affected by illumination change factors of interference, we employ segmentation method based on distance information to remove background and extract the moving object. In terms of the human body detection, we use the mean shift method for detection. Mean shift algorithm is an algorithm based on density gradient rise, which has advantages of low computational complexity, simple implementation and also can ensure the real-time performance of the system [12]. Mean shift pedestrian detection method based on the depth image can not only effectively solve the problem of interference light changes and occlusion, but also receive good detection effect while applying to the high density passenger flow detection in complex environment.

The paper is organized as follows: pedestrian detection method by mean shift algorithm based on depth image is introduced in section 2. Section 3 shows the efficiency and accuracy of the algorithm through the experimental results. Section 4 is the conclusion.

II. Pedestrian Detection Method Based on Depth Image and Mean Shift

Moving target detection technology based on the video has been one of hot topics in the field of computer vision. The target detection is the analysis of video sequences, looking for moving targets in ROI, and making judgments about the targets' location, size, speed and other motions in video sequences so that gaining the moving target real-time state information. It also serves as an initial step of the research on pose estimation, tracking, trajectory analysis, calculation of passengers flow density and speed or activity recognition.

In this paper, we reconstruct target states directly by existing information of target detection in video sequence, finding moving target preliminary location (region of interest) which uses the method of image segmentation based on the distance information, then using mean shift pedestrian detection method to detect moving targets. Our algorithm not only utilizes depth information, but also combines with mean shift pedestrian detection algorithm to obtain faster and more accurate detection results. Fig. 1 shows the whole algorithm flow chart.

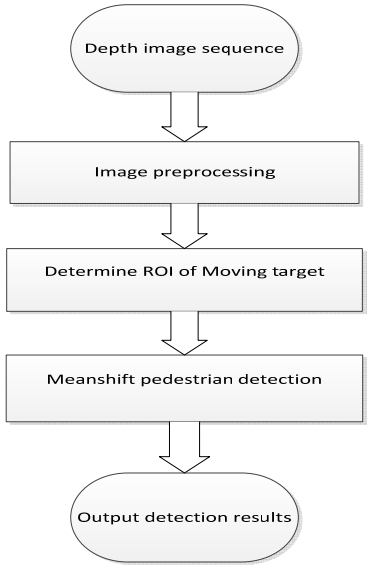

Figure 1. The whole algorithm flow chart

A. Image Preprocessing

Actual image pretreatment process is the process of removing useless information so that improving the algorithm efficiency and speed. It directly affects the computation complexity of next processes. So it is essential to do some pretreatments for raw image sequences. In our algorithm, we firstly smooth the image by median filter. The main purpose is to eliminate noise in image so that improving the image quality and facilitating the subsequent processing and analysis. Median filter [15] is a nonlinear processing method for noise suppression, the basic principle of median filter is using at various points in the field of a point at which the value of the median instead a digital image or the value of the point in the sequence, let the surrounding pixel values close to the real value, thereby eliminating isolated noise points.

For the pixel x, Assuming that there is n neighborhood pixels, put these n pixel gray values in accordance with the order from small to large, then obtain sorted sequence p_1 , p_2 , … , p_n . The gray value of pixel x is set to $p_{\frac{n+1}{2}}$ (n is an odd number)or $\frac{p_{n/2} + p_{n+1/2}}{2}$ (n is an even number), that is:

$$x = med(p_1, p_2, \ldots, p_n) = \begin{cases} p_{\frac{n+1}{2}} & (n\%2 \neq 0) \\ \frac{p_{n/2} + p_{n+1/2}}{2} & (n\%2 = 0) \end{cases} \quad (1)$$

B. Find out the ROI with the Moving Target

This paper removes the background based on segmentation method of height information, and then finds out the ROI with moving targets. For the convenience of data processing, we convert actual distance data to the actual pixel values of depth map for processing, and the camera maximum acquisition range is a known parameter which divides the gray image pixel information into 0 to 255 gray scales, so we can divide effective distance into 255 equal parts, which is corresponding to each pixel level of depth image. After that, the actual depth information is able to be represented by gray values in depth image. We usually get through the practical application scene to determine the camera construction height, and then estimate the distance from pedestrian's head and shoulder to the camera. After that, the next step is to set gray threshold value through conversion relationship of the actual distance and the gray value of depth map. On the assumption that gray value of a height for S:

$$S = H/L_{\max} * 255 \tag{2}$$

The H is the distance from the surface of the object to the view window plane, and $L_{\max}$ is the maximum effective distance of camera. In order to make gray values consistent with the height of pedestrian, we take a reverse operation for pixel values of depth map. After that, if src (x,y) (Original pixels) > threshold; dst(x,y) (Target pixels) = src (x, y), if src (x,y) (Original pixels) < threshold, dst (x,y) (Target pixels) = 0. Through this operation, moving targets can be separated from the background. Supposing filtering gray information under 1000 mm (high threshold), we can convert high threshold to gray threshold through formula (2), and then obtain the image which only contains potential targets. Through this method, interference images in complex background would be removed by setting right height threshold. Then it can determine ROI of depth image (moving target area).

C. Mean shift Pedestrian Detection

Mean shift algorithm's application range is considerably wide, such as in the image smooth aspect, image segmentation aspect and target tracking aspect. Due to the advantages of target histogram features stable, easy to calculate, we choose target gray histogram as the search feature, and through continuous iterative mean shift vector let algorithm converges to the true location of the target, so as to achieve the purpose of detection. Mean shift algorithm based on histogram can not only track the target accurately, but also solve the problem of tracking lost partially caused by occlusion to a certain extent. In addition, it also has good robustness and high efficiency. Assuming that a given Euclidean space R^d , n sample points are x_i (i=1… N), the basic form of the mean shift vector at the x point is defined as:

$$M_h(x) = \frac{1}{k} \sum_{x_i \in S_h} (x_i - x) \tag{3}$$

S_h is an area of a high dimensional ball whose radius is h, and it is an assemblage of y points satisfying the following relations:

$$S_h(x) \equiv \left\{ y : (y-x)^T (y-x) \le h^2 \right\} \tag{4}$$

k represents that at these n point samples x_i ,there are k points in the region S_h . $(x_i - x)$ is the offset vector of the sample points x_i and x . The definition of the mean shift vector $M_h(x)$ in Eq. 3 is to offset vector summation and then average of k sample points (fall into the region S_h) relative to the point x . If sample points x_i are sampled from a probability density function $f(x)$, due to the non-zero probability density gradient direct to the larger probability density direction, the sample points in the area of S_h more fall on the direction of probability density gradient. Therefore, the mean shift vector $M_h(x)$ should point to the direction of probability density gradient.

As is shown in Fig. 2, the range of big circle is, small circles represent sample points falling into the area of S_h ($x_i \in S_h$), and black spot x is the benchmark for the mean shift, the arrows represent offset vectors that the reference point x relative to sample points. Obviously, the average deviation vector will point the area of most samples distributed where it is the gradient direction of probability density function.

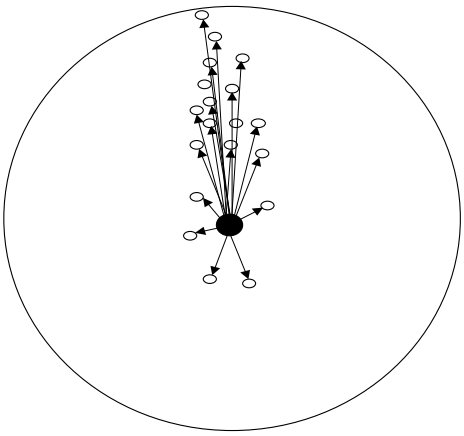

Figure 2. Mean shift schematic plot

During the execution of mean shift pedestrian detection algorithm based on the depth map, our algorithm firstly finds out potential target area (ROI) through background segmentation method based on the height information, then utilizes a rectangular box to calibrate the ROI which is kernel function impact on. In the process of target detection, the first step is selecting the gradient as a feature of target, setting up the target model at the determined target area in the image frames, then the specific method is to calculate the probability of each characteristic value in the feature space of target zone, establish a target model, and then calculate each Eigen value of the feature space in the target area which may exist in subsequent frames, After that, the candidate target model is established. The next step is using mean

shift algorithm to detect targets. In mean shift algorithm, kernel function must satisfy such requirements:

$$\int_{R^d} k(x)dx = 1 \tag{5}$$

$$\int_{R^d} xk(x)dx = 0 \tag{6}$$

$$\lim_{\|x\|\to\infty} \|x\|^d \; k(x) = 0 \tag{7}$$

Epanechnikov kernel [13] is usually selected as kernel function. Eq. (8) shows the expression of this kernel function.

$$K(x) = \begin{cases} \frac{1}{2} c_d^{-1}(d+2)(1-\|x\|^2), & \|x\| < 1 \\ 0 \quad , & others \end{cases} \tag{8}$$

where c_d represents the volume of a unit ball, $\|x\|$ is the norm of x.

After that, the next step of this algorithm is calculating similarity degree current frame between the candidate target model and target model by using the similarity measure function, after a finite time the target in the current will converge to the its true location eventually by iterative calculating the mean shift vector. Specific steps are as follows:

1. The establishment of target model

Make m_0 represents the center of the target area, $\{m_i\}_{i=1,2,\cdots,n}$ represent n pixels fallen into the target zone, n is the number of eigenvalue interval, the target model can be expressed as the following vector form:

$$\hat{k}_n = S\sum_{i=1}^{n} w(\left\|\frac{m_0 - m_i}{h}\right\|^2)\varsigma[t(m_i) - \mu] \tag{9}$$

Among them, S is the corresponding normalization constant, making $\sum_{n}^{a} k_n = 1$, the definition is as follows:

$$S = 1\Big/\sum_{i=1}^{n} w(\left\|\frac{m_0 - m_i}{h}\right\|^2) \tag{10}$$

$w(x)$ is the selected outline function of kernel function. The $w(x)$ assigns a largest value to the center pixel points, but a small weight value far away from the center pixel. Due to the pixels near the center of target model are more reliable than far away from the center point, it has certain inhibitory effect to occlusion and the influence of background. h is the width of window. We use $\left\|\frac{m_0 - m_i}{h}\right\|$ to eliminate the influence of different target calculation in the kernel function of target dimension size change, and we should raise the value of h when increasing the target, on the other hand, lower the value of h. $\varsigma(x)$ is Kronecker function, $\varsigma[t(x_i) - \mu]$'s role is to determine whether pixel color values of x in the target area belong to the n eigenvalue interval, If the pixel belongs to the area the value is 1，Otherwise, the value is 0.

2. The establishment of candidate model

For motion image sequence, the adjacent frames similarity is very large, therefore, in the second frame and other subsequent frames, we usually choose the testing results v_0 of the previous frame as the under test area center, $\{m_i\}_{i=1,2,\cdots,n}$ represent all pixels fallen in the this area, however bandwidth is still h, the target model can be converted to:

$$\bar{r}_n = S_h \sum_{i=1}^{n_i} w(\left\|\frac{v_0 - m_i}{h}\right\|^2)\varsigma[t(m_i) - \mu] \tag{11}$$

Among them, $S_h = 1\Big/\sum_{i=1}^{n} w(\left\|\frac{v_0 - m_i}{h}\right\|^2)$ is the normalized constant, n_i represents the number of target points in candidate regions.

3. The similarity detection

In the ideal situation, the similarity degree of candidate target model and target model should reach 100%. But in the actual application, due to noise and influence of lights, the change of targets' shape, it is not able to guarantee that the two models completely match. Although there are lots of similarity functions, Bhattacharyya coefficient is superior to other similarity function in the mean shift algorithm [14]. Bhattacharyya similarity expression is shown as follows:

$$\hat{\rho}(v) \equiv \rho(\hat{p}((v), \hat{k}_n)) = \sum_{n=1}^{a} \sqrt{\hat{p}(v)\hat{k}_n} \tag{12}$$

Bhattacharyya similarity value's range is [0, 1], and the value represents the similarity degree between two models. The more similar between target model and candidate model, the larger of the coefficient is. Through iteration calculating the Bhattacharyya coefficient of mean shift vector in the current frame, the last candidate region of making maximum can be thought as the final location of target in the frame.

4. The target positioning

In order to calculate the final location of the target in a frame, mean shift algorithm first makes the location of v_0 in the previous frame as the original target center of current frame, then searches for the optimal matching target location since from v_0 . Let v represents the current target center, then calculate the candidate target model character description $\hat{\rho}(v_0)$. We make Taylor series expansion for equation (12) at the position $\hat{\rho}(v_0)$, the Bhattacharyya coefficient can be expressed as:

$$\rho(\hat{p}(v),\hat{k}) = \frac{1}{2}\sum_{n=1}^{a}\sqrt{\hat{p}_n(v_0)\hat{k}_n} + \frac{S_h}{2}\sum_{i=1}^{n_h} z_i w(\left\|\frac{v-m_i}{h}\right\|^2) \quad (13)$$

Among them, $z_i = \sum_{n=1}^{a}\sqrt{\frac{\hat{k}_n}{\hat{p}_n(v_0)}}\varsigma[t(m_i)-\mu]$ is defined as weight coefficient in the process of calculation. As it can be seen from equation (13), the first part is independent of v , and only the second part is concerned with v . The second part can also be represented as a kernel density estimation that the weight is z_i and the expression is shown as the following:

$$f_{n,w} = \frac{S_h}{2}\sum_{i=1}^{n} z_i w(\left\|\frac{v-m_i}{h}\right\|^2) \quad (14)$$

Only Bhattacharyya coefficient is greater than a certain threshold, it can be ensured to take the maximum value, and mean shift vector can be calculated and work out the best corresponding position. The process of looking for maximum value of Bhattacharyya coefficient can be done by an iteration of mean shift vector. Candidate regional centers moving to the real target area v vector can be defined as the following form:

$$d_{h,G}(m) = v_1 - v_0 = \frac{\sum_{i=1}^{n_h} m_i z_i g(\left\|\frac{\hat{v}_0 - m_i}{h}\right\|^2)}{\sum_{i=1}^{n_h} z_i g(\left\|\frac{\hat{v}_0 - m_i}{h}\right\|^2)} - v_0 \quad (15)$$

Among them, $g(m) = -w(m)'$, $d_{h,,G}(m)$ is the mean shift vector which represents the target center moving from the initial point v_0 to the direction of v , thus it can be seen, through an iterative process, mean shift vector is from the initial point v_0 moving towards the direction where the colors of two models are the most similar. This direction is also same as the density gradient direction.

III. The Experimental Results Analysis

In our experiment, we first utilize Kinect camera to collect real-time video which contains depth information of objects, and the image resolution is 640 × 480. In order to maintain the real-time requirements of video image collection and transmission frames rate keeping at 20-30 fps, we use MPEG-4 as image coding and decoding standard. The experiment is performed on PC with Intel(R) Core(TM) i7-2600 CPU 3.4GHz master frequency, 8 thread, 8G memory and windows7 pro-OS. From the experimental results, we know that when the moving targets appear less (0-3) in detection area，each image processing time is between 15 and 40 ms, and when the moving target more (more than 5), each image processing time is around 40-100 ms, which basically satisfies the requirement of real-time.

Our detection system was set up at the top of a teaching building hall. There are many pedestrians in this actual application occasion, so it has a high demand for real-time accuracy of the detection system. The experimental results are shown in Fig. 3.

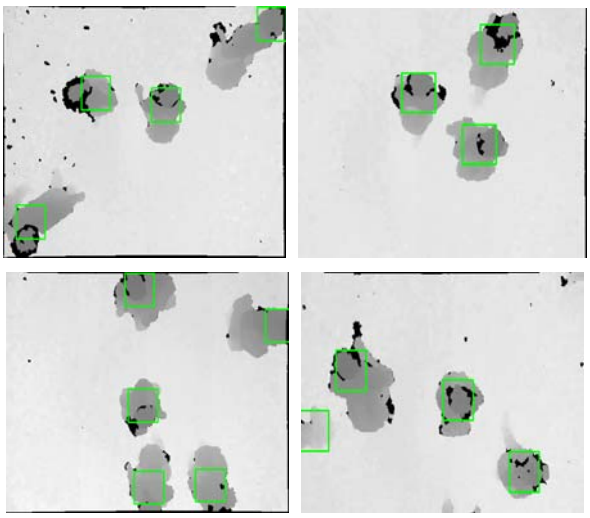

Figure3. The detection results of our algorithm

Then we calculate the detection rate and accuracy through the following formulas:

$$Detection\ rate = \frac{TruePos}{TruePos + FalsePos} \quad (16)$$

$$Accuracy = \frac{TruePos + TrueNeg}{TruePos + TrueNeg + FalseNeg + FalsePos} \quad (17)$$

From the formula (16) (17), the TruePos substitutes for the number of correct detections for pedestrian targets, the FalsePos substitutes for the number of false detections for pedestrian targets, the TrueNeg represents the number of correct pedestrian detections for non pedestrian targets (always 0), the FalseNeg represents the false pedestrian detections for non pedestrian targets. Table I shows the experimental results of our algorithm.

From the experimental results, our algorithm achieves good performance on accuracy and also satisfies requirements of real-time. Especially, comparing with algorithms based on color features, our algorithm can effectively address the case of interference light changes and occlusions.

TABLE I.
THE ACCURACY OF OUR ALGORITHM

Detection result	TruePos	TrueNeg	FalsePos	FalseNeg
	200	0	13	4
Precision	97%			
Accuracy	92.16%			

IV. SUMMARY

This paper mainly introduces a kind of target detection technology by mean shift based on depth image. Because mean shift tracking algorithm just calculates the pixel values of the probability density in target area, and only compares the Bhattacharyya coefficient between target model and candidate target model, the calculation of our algorithm is relatively simple. Besides, the algorithm only counts pixel values in ROI which further reduces the complexity of calculation. Especially, the algorithm just counts pixel values and does not care about changes of target shapes, rotation, small occlusions and so on, so the thesis algorithm has good robustness. Due to pixel gray values in depth image only concerned with the distance between viewing window plane and object surface, depth image has the unique characters which is different from characters of color space: there is no shadow in depth image; it is not affected by illumination change factors interference, so using depth information of image to detect moving targets can overcome some occlusion and overlap problems successfully. At last, through several experiments, the detection algorithm is proved that can be well applied to complex scenes of high density passenger flow detection with great efficiency and accuracy.

ACKNOWLEDGMENT

This work is sponsored by Project of Beijing Municipal Commission of Education (No.KM201210009008) and Natural Science Foundation of China (No. 61103113).

REFERENCES

[1] D. Comaniciu, P. Meer, "Mean Shift Analysis and Applications", *Proc. Seventh International Conference on Computer Vision*, pp. 1197-1203, Sept. 1999.

[2] M. J. Deilamani, R. N. Asli, "Moving Object Tracking Based On Mean Shift Algorithm and Features Fusion", *International Symposium on Artificial Intelligence and Signal Processing*, pp. 48-53, June 2011.

[3] K. Fukunage, L. D. Hostetler. "The estimation of the gradient of a density function with application in pattern recognition", *IEEE Trans. Information Theory*, vol.14, no.3, pp. 32-40, 1975.

[4] Y.Cheng. "Mean shift, mode seeking and clustering", *IEEE Transactions on Pattern Analysis and Machine Intelligence*, vol. 17, no.8, pp. 790-799, 1995.

[5] D.Comaniciu, V.Ramesh and P.Meer. "Kernel-based Object Tracking", *IEEE Transactions on Pattern Analysis and Machine Intelligence*, vol.24, no.3, pp. 564-577, 2003.

[6] Yuan Xiao,Wang Liping, "Tracking Moving People Based on the Mean Shift Algorithm", *Computer Engineering & Science*，vol. 30, no. 4, pp. 46-49, 2008.

[7] Zhu Shengli, Zhu Shanan and LI Xuchao, "Algorithm for tracking of fast motion objects with Mean shift" , O*pto-Electronic Engineering,* vol.33, no.5, pp. 66-70, 2006.

[8] Yuan Baohong, Zhang Dexiang, Fu Kui and Zhang Lingjun, "Video tracking of human with occlusion based on Mean Shift and Kalman filter"，*Electronic System-Integration Technology Conference (ESTC)*, pp.148-151, Sept 2012.

[9] Lin Peng. "Body Part Recognition Based on Depth Image by Learning". School of Electronic Information and Electrical Engineering, Master thesis, 2012.

[10] J. Fabian, T. Young, J. C. P. Jones, G. M. Clayton, "Integrating the Microsoft Kinect With Simulink: Real-Time Object Tracking Example", *IEEE/ASME Transactions on Mechatronics*, vol.99, pp.1-12, 2012.

[11] Zhang Junping , Tan Ben, Sha Fei, and He Li. "Predicting Pedestrian Counts in Crowded Scenes With Rich and High-Dimensional Features", *IEEE Transactions on Intelligent Transportation Systems,* vol.12, no.4, pp.1037-1046, 2011.

[12] Erik Lilienblum, Bernd Michaelis, "Optical 3D Surface Reconstruction by a Multi-Period Phase Shift Method", *Journal of Computers,* vol. 2, no. 2, pp.73-83, 2007.

[13] Wang Shuai, "A Research of Object Tracking Based on Mean Shift", Shandong University, Master thesis, 2011.

[14] Peng Zhaoyi,, Zhou Yu, Zhu Yanhui, Wen Zhiqiang, "Application of an Improved Mean Shift Algorithm in Real-time Facial Expression Recognition", *Journal of Software,* vol. 6, no.1, pp. 100-107, 2011.

[15] H. L. Eng and K. K. Ma, "Noise adaptive soft-switching median filter", *IEEE Transactions on Image Processing*, vol. 10, no. 2, pp. 242-251, 2011.

Qing Tian received his PhD degree in electronic science and technology from institute of electronics, Chinese academy of science, Beijing, China, in 2010. He is a distinguished lecturer at North China University of Technology, Beijing, China. His research interests include electrical engineering, intelligent transportation systems, pattern recognition and computer vision.

Shuai Qiao is currently working toward the master's degree in Electronic Science and technology at the College of Information Engineering, North China University of Technology, Beijing, China.

Teng guo is currently working toward the master's degree in Electronic Science and technology at the College of Information Engineering, North China University of Technology, Beijing, China.

Yun Wei received his PhD degree in intelligent transportation systems from Southeast University, Nanjing, China. He is a researcher at Beijing Urban Engineering Design and Research Institute, Beijing. His research interests include intelligent transportation systems and computer vision.

Enhancing Keylogger Detection Performance of the Dendritic Cell Algorithm by an Enticement Strategy

Jun Fu and Huan Yang
The 28th Research Institute of China Electronics Technology Group Corporation, Nanjing 210007, China
Email: {doctorfj, happyfairy106}@163.com

Yiwen Liang and Chengyu Tan
Computer School, Wuhan University, Wuhan 430079, China
Email: ywliang@whu.edu.cn, nadinetan@163.com

***Abstract*—Evasive software keyloggers hide their malicious behaviors to defeat run-time detection. In this paper, based on the analysis of the evasion mechanisms used by common software keyloggers, we established a framework for their detection. Using an enticement strategy, the framework we built could induce keyloggers exhibited more obvious malicious activities by mimicking user keystrokes. These 'amplified' activities are then correlated by the dendritic cell algorithm (an immune-inspired algorithm) to final determine the existence of a keylogger in a host. Preliminary experimental results showed that the framework could improve the performance of keylogger detection and hard to evade.**

***Index Terms*—keylogger, keystroke simulation, dendritic cell algorithm (DCA), correlation**

I. Introduction

With the development of e-commerce and online games, software keyloggers which steal confidential information by monitoring a user's keyboard actions are becoming a new trend for malware [1] [2]. They intercept and log all keystrokes, and transmit this information to profit-driven attackers. Unlike other types of malicious programs, keyloggers are designed to capture what is done on a PC without attracting the attention of users and present no threat to the system [3]. This makes them largely undetectable by most anti-virus and anti-keylogger applications [4] [5].

To overcome the problems above, security experts are trying to use behavior-based detection techniques that analyze API calls of a process to classify it as keylogger or not [6][7]. However, these methods all have some shortcomings to some extent. Detection [6] relies on single behavior (setting Windows hooks) has a high rate of false positives (FP) [7]. Though correlation of multiple behaviors (keystroke tracking, file access and network communication) reduces the FP rate, it seems that the detection is prone to be evaded when specified time window and simple correlation algorithm are used [7].

For the purpose of improving the detection performance, Fu [8] uses an immune-inspired algorithm - dendritic cell algorithm (DCA) to correlate the behaviors mentioned by [7]. As an algorithm, the DCA performs multi-sensor data fusion on a set of input signals, and these signals are correlated with potential 'suspects', leading to information which will state not only if an anomaly is detected, but in addition the culprit responsible for it. By using variable time windows and time sequence of the different behaviors, the DCA improves the detection performance to a certain degree. But every coin has two sides. The correlating feature of the DCA can be exploited by crafty attackers to evade detection by reducing the frequency of the malicious behaviors [9]. The experimental results of [8] support the above claim.

Man-to-machine interfaces cannot be ignored when fight against keyloggers [3]. In this paper, we analyzed the evasion mechanisms used by common software keyloggers. We discovered that the keystroke (especially keystroke of the special key, such as '*Enter*' key) frequency is an important trigger for keyloggers to log and send captured information. As a result, we built an induction-correlation framework for keylogger detection. In this framework, we synthesized man-to-machine interactions by implementing a keystrokes simulation program. The program can induce keyloggers to exhibit more malicious activities without disturbing normal applications. Then, the 'amplified' behaviors are correlated by the DCA in order to identify the keylogger as early as possible. Experiments were conducted to test capabilities of our framework to improve the detection rate and reduce the possibility of successful evasion.

II. Related Work

There are only a few existing techniques for software keylogger detection. Most of these techniques use signature-based approaches. Since signature-based detection has nothing to do against keylogger variants [10], security experts are now focusing their attentions to

doi:10.4304/jcp.9.6.1347-1354

behavior-based detection techniques that analyze API calls of a process to classify it as benign or malicious.

Some approaches based on API calls focus on searching only those APIs that can be used to intercept keystrokes, either statically [6] or dynamically [11] [12]. Unfortunately, these APIs are also used by legitimate applications, which makes these approaches heavily prone to false positives.

Rather than relying on single type of API (keylogging APIs), Al-Hammadi and Aickelin [7] detects keylogging activities with correlations between multiple types of API (keystroke tracking, file access and network communication APIs), that is detecting when both interception and leakage of keystrokes are taking place. Although the technique has a relatively low false positive rate, the detection rate is not high because specified time windows and simple correlation algorithm (an algorithm using Spearman's Rank Correlation [13]) are used.

Based on the work above, Fu [8] uses an immune-inspired algorithm - dendritic cell algorithm (DCA) to correlate multiple types of API described in [7]. The DCA is based on an abstract model of the behaviors of dendritic cells which are natural intrusion detection agents of the human body. These cells collect antigens and signals (environmental conditions of the antigens), and combine the evidence of damage (signals) with the collected suspect antigen to provide information about how 'dangerous' a particular antigen is. The DCA performs multi-sensor data fusion on a set of input signals and antigens, leading to information which states not only if an anomaly is detected, but in addition the culprit responsible for it [14]. More information about the DCA please refers to [15].

The input signals defined in [8] are derived from the frequency of invocations of keystroke tracking functions (PAMPs and safe signal-2), the time difference between two consecutive *WriteFile* calls (danger signal-1), the relation between different categories of function calls (danger signal-2) and the time difference between two outgoing consecutive communication functions (safe signal-1). The process (identified by Process ID) which causes the calls is defined as antigens [8]. The DCA correlates these antigens with input signals, resulting in a pairing between signal evidences and antigen suspects, and the identification of the keylogger process in the end. However, as the DCA distinguishes between normal and potentially malicious antigens on the basis of neighboring antigens, the crafty attackers can exploit this correlating feature to evade detection by reducing the 'concentration' of antigens in DCs [9].

The experimental results of [8] confirmed the above conclusion. The keylogger they used in experiments hid its behaviors by logging and sending keys only when enough keystrokes were intercepted or special keys (such as '*Enter*' key) were pressed. In experiments that long sentences were entered, the frequency of the malicious activities generated by the keylogger decreased significantly compared to the one observed in short sentence scenarios. The same trends were also found in detection performances of the DCA because of the reducing of the 'concentration' of the malicious antigens. In the real world, we believe users keystroke patterns are similar with the long sentence scenarios described in [7] and [8]. This challenges the DCA to detect keyloggers in the real environment.

III. Keylogger Analysis

In this paper, we analyzed the source code of some typical open source keyloggers running on *Windows NT* operating systems, such as *Keymail V0.7*, *Spybot V1.2* and *Morsa-Keylogger V1.8*. Then we compiled and executed these source codes to find their run-time features. Based on the static and dynamic analysis, we discovered the relationships between different behaviors generated by these keyloggers, and revealed the evasion mechanisms often used by them.

Through static analysis, we found that all keyloggers worked in a similar manner. They all firstly tracked keystrokes and then wrote them to a file or/and send them to a destination across the Internet (via Email, FTP and etc.). The most important difference between these keyloggers was the timing that triggered file access and communication activities. These activities were performed when:

1) intercepted every keystroke;
2) the keystrokes intercepted reached a certain amount;
3) special keys (such as '*Enter*' key) were pressed.

After running the compiled source codes, we found the keyloggers (such as *Keymail*) using the 1) trigger condition generated more file access and communication behaviors. However, these behaviors were relatively rarely observed when the keyloggers (such as *Spybot* and *Morsa-Keylogger*) with the 2) and the 3) trigger conditions were executed. So we could make a conclusion that it is the 2) and the 3) trigger conditions that gave keyloggers capabilities to evade the correlation-based detection (such as the DCA).

Fortunately, the evasion mechanism above is a double-edged sword. Besides hiding keylogger behaviors, it greatly exposes the existence of the keylogger when high frequency of keystrokes (especially special keystrokes) is encountered. That is why we use the keystroke simulation to enhance the detection performance of the DCA.

IV. Induction-Correlation Framework

We assume that the host to be monitored is infected with a keylogger without a user's awareness. The installed keylogger logs and sends the captured information when a user types his/her privacy via keyboard. In this paper, we propose an enhanced approach to detect software keyloggers on a host. The approach consists of two steps: 1) the induction of the keyloggers, 2) the correlation of the behaviors exhibited by them. We emphasize on the first step, describing how it improves the performance of the second step. The framework of our approach is shown in fig. 1.

Because the frequency of keystrokes in real environment is not high, the behaviors of the keylogger are not evident enough [8]. Therefore, we design a

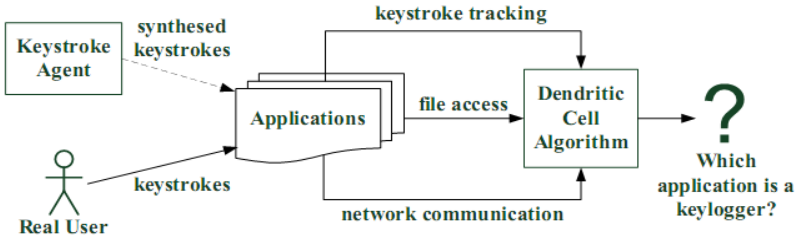

Figure 1. The induction-correlation framework for software keylogger detection by the DCA.

keystroke agent application to frequently generate random keystrokes, hoping that these keystrokes will be seen by the keylogger, but will not affect normal applications. As a result, the behavior of the keylogger will be more obvious in the stimulation of a large number of random keystrokes in a short time. Meanwhile, the keystroke agent holds the simulated keystrokes within a hidden application it creates to avoid them passing to the other applications. Thus the normal applications will not be affected by the simulated keystrokes since they only focus on the keystrokes passed to them.

We also focus on keystroke tracking, file access and network communication behaviors exhibited by applications. By correlating API calls generated by these behaviors, the DCA can classify the application running in a host as a keylogger or not. For example, file access shortly after the keystroke tracking strongly indicates that there exist keylogging activities. The more active the application is in that period, the more likely it is a keylogger.

A. Induction Phase

In the induction phase, we synthesize random keystrokes to induce keyloggers. In order to find a way to simulate keystrokes which will be seen by a keylogger, we must understand how an operating system generates and handles keyboard events. We also must be clear that how a keylogger intercepts keystrokes in this process.

As in fig. 2, a *Windows NT* operating system generates a keyboard interrupt when a key was pressed. Then the keyboard driver transforms the interrupt to a system-defined message and puts it into the '*system level message queue*'. Tracking the focused application at the time when the keyboard interrupt was generated, the operating system passes the message to the '*application level message queue*' of that specific focused application. Now it's the responsibility of that application to handle this key accordingly. If the operating system does not find any specific focused application, it simply discards that key. In this process, keyloggers employ very low level operating system calls [14], such as *GetKeyboardState* or *GetAsyncKeyState*, to intercept keystroke messages or detect keyboard interrupts directly. So the keyloggers see everything whenever a key is pressed.

In this paper, we design a keystroke agent according to the mechanisms described above. By invoking system kernel (*keybd_event*), the agent simulates keyboard event completely. Because a keylogger tracks keystrokes from all applications (including keystroke agent application) in order to log sensitive data entered in them, it could see the simulated keystrokes since they are the same with the real keystrokes. But the keylogger doesn't understand what it sees and it can't tell the keystrokes generated by real users via keyboard from the ones generated by phantom users via our keystroke agent. When we simulate keystrokes frequently, in order to log and send these plentiful keys, the keylogger has to perform more file access and communication behaviors.

In this case, the keystroke stream generated by the keystroke agent can be described as follows:

$$KeystrokeStream(N, T_L, T_I, f) \quad (1)$$

The keystroke stream can be modeled as a sequence of N samples with a uniform time interval T_I. Each sample lasts for a particular length of time T_L, and synthesizes keystrokes with an rate changes according to function $f(t) : (0, T_L) \rightarrow (0,+\infty)$. $f(t)$ determines the pattern of a sample. In this paper, we design the following patterns:

1) Fixed Square Wave. All samples synthesize keystrokes with a fixed rate R_0. This pattern attempts to minimize the variability of the keystroke rate.
2) Random Square Wave. All samples synthesize keystrokes with a rate uniformly distributed over the range [0, R_0]. This pattern attempts to maximize the variability of samples.
3) Sawtooth Wave. Each sample linearly increases the rate based on an initial rate R_0. This pattern explores the effect of constant increments in the rate.

On the other hand, the simulated keystrokes must not affect normal applications. Before starting to simulation, the agent creates a hidden window and sets the current active window to it. Then the simulated keystrokes are generated and passed to the hidden window which simply discards the keys received. After the simulation, the active window is set back to the active window before simulation. The keystroke agent regularly performs the procedure above. Since the execution time of this process is very short, the active window switches are almost imperceptible to users.

B. Correlation Phase

In this paper, we use the dendritic cell algorithm (DCA) to correlate API calls generated by all running applications to identify keylogger applications. In order to obtain the API calls, we implement a hook program to monitor three types of function calls:

1) **Keyboard Tracking**: *GetKeyboardState*, *GetAsyncKeyState* and *GetKeyNameText* [17].

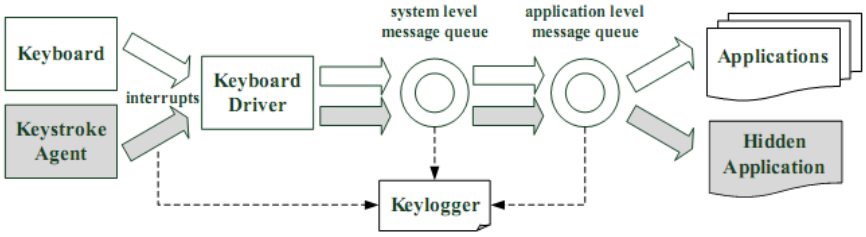

Figure 2. How keystrokes are handled by a *Windows NT* operating system and intercepted by a keylogger.

2) **File Access**: *CreateFile*, *OpenFile*, *ReadFile* and *WriteFile* [18].
3) **Communication**: *socket*, *send*, *recv*, *sendto* and *recvfrom* [19].

These API functions are often employed by keyloggers to implement their keylogging and other features, but also may form part of legitimate usage. Therefore, an intelligent correlation method such as the DCA is required to determine if the invocations of such functions are indeed anomalous. Signals and antigens are vital input to the DCA. To facilitate comparison, we use the same definitions of the signal and antigen described in [7].

Five signals, namely one PAMP signal (PAMP), two danger signals (DS) and two safe signals (SS), are used for the input of the DCA. They are derived from the API calls captured, and then analyzed by the DCA, following a signal normalization process.

PAMP is a signature based signal. This signal is derived from the rate (r) of keyboard tracking function calls. A large number of these function calls indicate the potential existence of a keylogger. Let the signal value be 100 (danger) when $r > N_{ph}$ and be 0 (not danger) when $r < N_{pl}$ ($N_{pl} < N_{ph}$). We normalize the PAMP base on these values by applying linear scale between 0 and 100.

Danger signal is a measure of an attribute which increases in value to indicate an abnormality. Low values of this signal may not be anomalous.

DS-1 is derived from the time difference (Δt_1) between two consecutive *WriteFile* function calls. Because a keylogger saves the keystrokes captured to log files continuously, a small Δt1 will be observed. In contrast, a normal application will have a higher value of Δt_1 between writing activities. Let the signal value be 0 (not danger) when $\Delta t_1 > N_{d1h}$ and be 100 (danger) when $\Delta t_1 < N_{d1l}$ ($N_{d1l} < N_{d1h}$). We normalize DS-1 base on these values by applying linear scale between 0 and 100.

DS-2 is derived from the correlation between different categories of function calls. Based on the behavioral characteristics of keyloggers, we generate this signal when file access or communication functions are invoked shortly after the invocations of keyboard tracking functions. The value of the signal lies on the sum of the number of the file access and communication function calls within specified time-window. Let the signal value be 100 (danger) when this sum exceeds N_{d2h}. DS-2 is normalized base on this value by applying linear scale between 0 and 100.

Safe signal is a confident indicator of normal or steady-state system behavior. This signal is used to counteract the effects of PAMP and danger signals.

SS-1 is derived from the time difference (Δt_2) between two outgoing consecutive communication functions including *send*, *sendto* and *socket* functions. This is needed as keyloggers send information to attackers after the keylogging activity. In normal situation, we expect to have a large Δt_2 between two consecutive functions. In comparison, we expect to have a short period of this action when the keylogger sends information to the attacker. Let the signal value be 100 (not danger) when the $\Delta t_2 \geqslant N_{s1h}$ and be 0 (danger) when the $\Delta t_2 < N_{s1l}$ ($N_{s1l} < N_{s1h}$). We normalize SS-1 base on these values by applying linear scale between 0 and 100.

SS-2 is derived from the small amount of the keyboard tracking function calls within a specified time-window. As legitimate applications such as *notepad* or *wordpad* invoke much fewer keyboard tracking functions than keyloggers. So, small amount of invocations is considered to be safe in the host. Let the signal value be 0 (danger) when this amount exceeds N_{s2l}. SS-2 is normalized base on this value by applying linear scale between 0 and 100.

Antigens are potential culprits responsible for any observed changes in the status of the system. As any process executed one of the selected API functions, the process id (PID) which causes the calls and thus generates signals is defined as antigens. Observing which processes are active when signal context is danger, the DCA can find the existing keylogger in the system.

V. EXPERIMENS

The aim of our experiments is to verify that the keystroke simulation can enhance the visibility of a keylogger's behaviors, and thus can improve the detection performance of the DCA. To achieve this goal, we chose the same keylogger instance (*spybot*) and benign instances (*notepad* and *mirc* [20]) used in the experiments in [8], and set up the same environment for their running.

The experiments are divided into two groups to show the detection performance differences between the DCA with the keystroke agent (E2) and the DCA without (E1) the keystroke agent. The agent works in Fixed Square Wave pattern ($R_0 = 200$, $T_I = 5$s, $T_L = 50$ms), synthesizing some random (numbers and letters) and special keys ('*Enter*' key). Each experiment was repeated for 10 times and lasted 600 seconds. Without any operations in the

first 60 seconds, we used *notepad* and *mirc* to input sentences for 180 seconds respectively with an interval of 60 seconds. We had no operations in the final 120 seconds.

In both groups of experiments, we monitor two scenarios of typing. We type short sentences in one scenario (E1.1 and E2.1) and long sentences in the other (E1.2 and E2.2). The sentence ends with '*Enter*' key. By monitoring two typing scenarios, we are able to show the effects of different keystroke patterns on our detection scheme and the effects of keystroke simulation in different input mode.

In [8], the contents of the sentences are random, and the lengths of the sentences are not mentioned. To get closer to real user keystroke patterns, we collect 200 commonly used English sentences: 100 long (19-48 characters) and 100 short (9-23 characters) sentences, and type them one by one in corresponding scenarios. Because of the changes in typing mode, we adjust the signal threshold values used in [8]: N_{ph} = 1301(times/s), N_{pl} = 1105(times/s), N_{d1l} = 7000(ms), N_{d1h} = 20000(ms), N_{d2h} = 2(times/s), N_{s1l} = 5000(ms), N_{s1h} = 10000(ms), N_{s2l} = 55(times/s). They are set based on the statistical results of the frequency of API calls. Take keyboard tracking API calls for example, the average frequency generated by *spybot* is 1203(times/s), the standard deviation is 88(times/s). And the max frequency concerning *notepad* or *mirc* is 55(times/s). Therefore, we set N_{ph} = 1203 + 88 = 1301(times/s), N_{pl} = 1203 − 88 = 1105(times/s), N_{s2l} = 55(times/s). The maliciousness of keyboard tracking API calls is depend on whether they are in a high frequency (greater than N_{ph}) or a low frequency (less than N_{s2l}). The population of DCs is set to 100, the DCA chooses 10 DCs every time an antigen or a signal is arrived for their storage. The fuzzy migration threshold value of DCs is between 1500 and 2000. The weight matrix is the same with [7].

A. Results

We first give a look at the frequency of API calls generated by all applications in E1 and E2. The x-axis represents time in seconds while the y-axis represents the normalized value of API call frequencies. The normalized API call frequency values represent the total value we get during 10 seconds divided by the maximum value of the whole period (600 seconds).

Keystroke agent does not interfere with normal applications by design. This means that normal application instances are not affected by simulated keystrokes, as shown in Fig. 3 (take *mirc* program for example). From Fig. 3, we notice that the difference between the API call frequencies of *mirc* instance in E1.1 and E2.1 is very small. When *mirc* program is used for online chatting (301-480 seconds), most of the values of the keyboard tracking and communication API call frequencies are in the range of (0.2-0.3) and (0.1-0.2) respectively in both experiments. When *mirc* program is idle, we also notice that there is a burst in the network traffic in both experiments. This burst is generated due to *mirc* program which sends a bulk of words to its servers every specified time intervals.

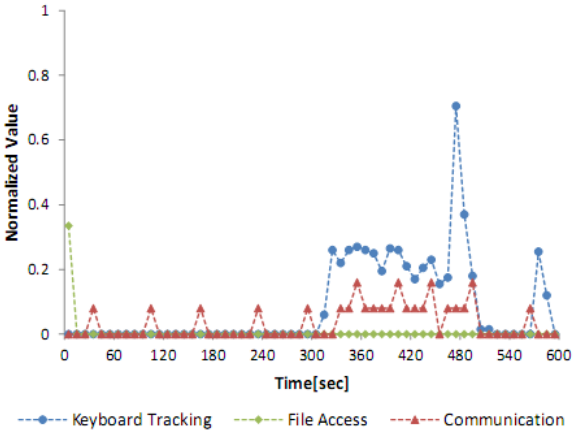

(a) API functions invoked by *mirc* in E1.1

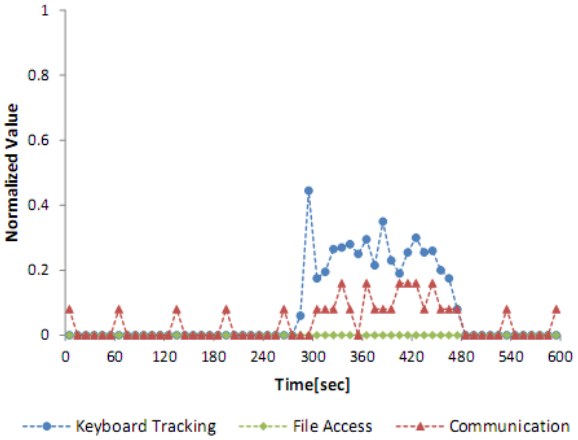

(b) API functions invoked by *mirc* in E2.1

Figure 3. API functions invoked by *mirc* in E1.1 (without keystroke simulation) and E2.1 (with keystroke simulation). The *mirc* program is executed at the beginning of the experiments and is used for online chatting during 301-480s.

For *spybot* instance, the results from E1 and E2 show that there are significant differences between API call frequency without keystroke simulation and the one with keystroke simulation in both two typing scenarios, as depicted in Fig. 4 and Fig. 5.

From Fig. 4(a) and Fig. 4(b), we can see that although the keyboard tracking API calls generated by *spybot* maintain a high frequency in both E1.1 and E2.1, the frequencies of file access and communication API calls in E2.1 are much higher than the ones in E1.1, especially when short sentences for text editing (using *notepad* from 61 to 240 second) or online chatting (using *mirc* from 301 to 480 second) are typed. The same differences are also shown in Fig. 5(a) and Fig. 5(b) when long sentences are entered. Therefore, we can conclude that the keystroke agent does have the ability to amplify the malicious behavior exhibited by *spybot*.

The intercepted API calls invoked by *spybot*, *notepad* and *mirc* are used to generate corresponding signals using the method described in section IV-B. The DCA then processes and analyzes these signals to determine which

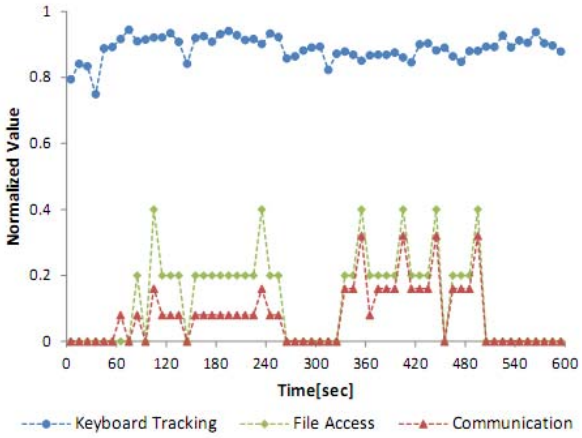

(a) API functions invoked by *spybot* in E1.1

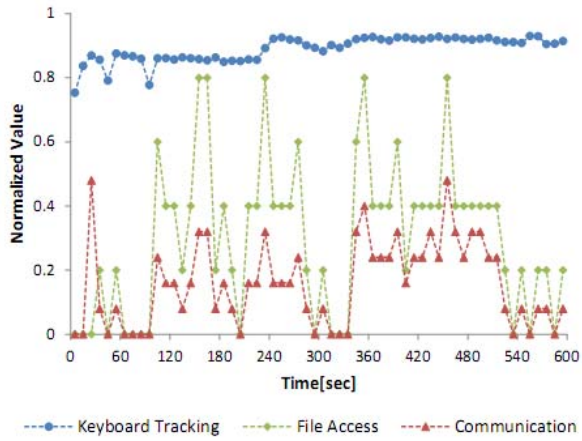

(b) API functions invoked by *spybot* in E2.1

Figure 4. API functions invoked by *spybot* in long sentences scenarios (E1.1 and E2.1). We use *notepad* program for text editing during 61-240s and *mirc* program for online chatting during 301-480s.

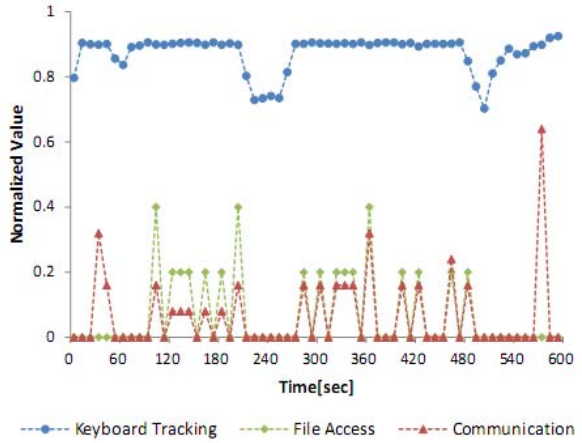

(a) API functions invoked by *spybot* in E1.2

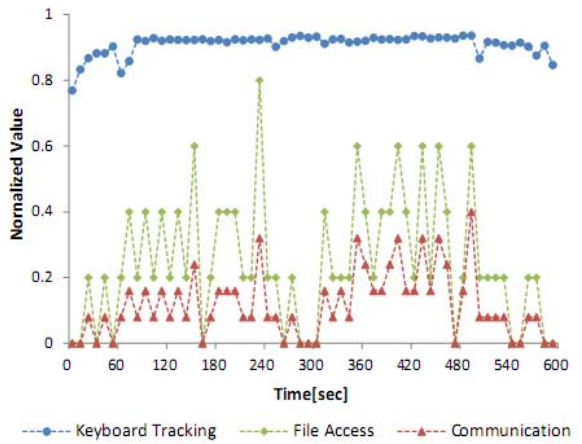

(b) API functions invoked by *spybot* in E2.2

Figure 5. API functions invoked by *spybot* in long sentences scenarios (E1.2 and E2.2). We use *notepad* program for text editing during 61-240s and *mirc* program for online chatting during 301-480s.

process has keylogger behaviors. Table I gives the results from the DCA. The values in the last two columns are the mean values and standard deviation values (in parentheses) in 10 repeated experiments.

A threshold (T) is applied to *MAC* to make the final classification decision. The process whose *MAC* is higher than T is termed malicious, and vice-versa. Because the dataset contains one malicious instance and two benign instances, we can define $T = 1 / (1+2)$. So the process with $MAC > 1/3$ is considered to be a keylogger process. From the table, we observe that the DCA detects the keylogger process in all scenarios except in E1.2. This means that the keylogger is more difficult to be detected when user inputs long sentences. However, with the help of the keystroke agent, the DCA detects keylogger process with no false negatives no matter which input mode is used. It is also noteworthy that no false positives are generated in all scenarios.

B. Discussions

From the results of the experiments, we can find that although the *MAC* values in Table I are relatively low compared to the results from the experiments in [8], the basic experimental conclusions do not change:

- Keystroke simulation can enhance the visibility of keylogger behaviors, and thus can improve the detection performance of the DCA.
- Keystroke patterns have an obvious impact on the detection performance of the DCA. And the effects of keystroke simulation vary in different input mode.

Fig. 4 and Fig. 5 demonstrate that the keystroke agent we implemented can induce *spybot* to perform more file access and communication behaviors. And the simulation method improves the *spybot* detection performance of the DCA to some extent in the same environment, as depicted in Table I. The *MAC* value increases by about 58% and 11% in average when we type long sentences (E1.2 and E2.2) and short sentences (E1.1 and E2.1) respectively. In 20 experiments without simulation (E1.1 and E1.2), only 10 experiments detects *spybot*, detection rate is 50%. In contrast, all 20 experiments report *spybot* detection when keystroke agent is used.

TABLE I.
RESULTS FROM THE DCA

Scenario	Process Name	The Number of Antigens	MAC
E1.1	spybot notepad mirc	6767(23.0) 1470(0) 1804(3.8)	0.540(0.0049) 0.087(0.0022) 0.087(0.0027)
E1.2	spybot notepad mirc	5164(35.5) 1140(0) 1795(5.9)	0.271(0.0111) 0.024(0.0020) 0.037(0.0030)
E2.1	spybot notepad mirc	8045(23.2) 1520(0) 1718(1.4)	0.599(0.0065) 0.064(0.0030) 0.109(0.0024)
E2.2	spybot notepad mirc	6819(43.4) 1640(0) 1804(5.4)	0.427(0.0060) 0.056(0.0033) 0.071(0.0029)

The improvement of detection efficiency in long sentences scenarios is much higher than short sentences scenarios. That may because the *spybot* behaviors are already obvious enough since the '*Enter*' key is typed frequently when the user type short sentences. So there is not much room for improvement in short sentences scenarios.

The keystroke agent passes synthesized random keys to a hidden window created by it. The keylogger not only can intercept these keys, but also can know the destination of them (We find *spybot* has this ability in experiments). As a result, the keylogger can defeat the keystroke agent by the way that not to handle the keys send to the hidden window created by the agent. The future work will find a possible way to solve it.

In addition, only Fixed Square Wave pattern keys are generated by the keystroke agent in experiments because we are more concerned about the feasibility of our approach and it is easy to be implemented and analyzed. In future work, we will further analyze the effects of the other two patterns so as to identify the application range of these patterns.

VI. CONCLUSION

The success of any keylogger is determined by its ability to evade detection. In this paper, we analyzed the evasion mechanisms used by common software keyloggers and proposed an induction-correlation framework for keylogger detection. In this framework, keystrokes simulation raises the frequency of the keystrokes, and thus induces keyloggers produce more malicious behaviors to deal with these synthesized keystrokes. Then the 'amplified' behaviors are correlated by the DCA in order to find the keylogger process as early as possible to reduce the loss of privacies. Experimental results showed that the framework we built can improve the keylogger detection rate and reduce the possibility of successful evasion.

ACKNOWLEDGMENT

This work was supported by the Defense Industrial Technology Development Program of PR China (GrantNo. A1420080183).

REFERENCES

[1] N. Patterson and M. Hobbs, "Virtual World Security Inspection", *Journal of Networks*, Vol. 7, No. 6, 2012, pp. 895–907.

[2] T. Holz, M. Engelberth, and F. Freiling, "Learning More about the Underground Economy: A Case-Study of Keyloggers and Dropzones", in *Proc. of 14th European Symposium on Research in Computer Security*, 2009, pp. 1–18.

[3] S. Sagiroglu and G. Canbek, "Keyloggers", *Technology and Society Magazine*, Vol. 28, No. 3, 2009, pp. 10–17.

[4] M. Baig and W. Mahmood, "A Robust Technique of Anti Key-Logging Using Key-Logging Mechanism", in *Proc. of Digital EcoSystems and Technologies Conference*, 2007, pp. 314–318.

[5] W. Luo, N. Li, and Y. Tang, "Reverse Analysis of Malwares: A Case Study on QQ Passwords Collection", *Journal of Software*, Vol. 7, No. 8, 2012, pp. 1706–1712.

[6] M. Aslam, R. Idrees, M. Baig, and M. Arshad, "Anti-Hook Shield against the Software Key Loggers", in *Proc. of the National Conference on Emerging Technologie*s, 2004, pp. 189–191.

[7] Y. Al-Hammadi and U. Aickelin, "Detecting Bots Based on Keylogging Activities", in *Proc. of the 3rd International Conference on Availability, Reliability and Security*, 2008, pp. 896–902.

[8] J. Fu, Y. Liang, C. Tan, and X. Xiong, "Detecting Software Keyloggers with Dendritic Cell Algorithm", in *Proc. of the International Conference on Communications and Mobile Computing*, 2010 , pp. 111–115.

[9] S. Manzoor, M. Shafiq, S. Tabish, and M. Farooq, "A Sense of 'Danger' for Windows Processes", in *Proc. of the 8th International Conference of Artificial Immune System*, 2009, pp. 220–233.

[10] S. Qi, M. Xu, and N. Zheng, "A Malware Variant Detection Method Based on Byte Randomness Test", *Journal of Computers*, Vol. 8, No. 10, 2013, pp. 2469–2477.

[11] M. Xu, B. Salami, and C. Obimbo, "How to Protect Personal Information against Keyloggers", in *Proc. of the 9th International Conference on Internet and Multimedia Systems and Applications*, 2005, pp. 275–280.

[12] K. Nasaka, T. Takami, T. Yamamoto, and M. Nishigaki, "A Keystroke Logger Detection Using Keyboard-Input-Related API Monitoring", in *Proc. of 14th International Conference on Network-Based Information Systems*, 2011, pp. 651–656.

[13] G. Bancroft and G. O'Sullivan, *Maths and Statistics for Accounting and Business Studies*, 2nd ed., McGraw-Hill, 1988.

[14] J. Greensmith, U. Aickelin, and G. Tedesco, "Information Fusion for Anomaly Detection with the Dendritic Cell Algorithm", *Information Fusion*, Vol. 11, No. 1, 2010, pp. 21–34.

[15] L. Ding, F. Yu, and Z. Yang, "Survey of DCA for Abnormal Detection", *Journal of Software*, Vol. 8, No. 8, 2013, pp. 2087–2094.

[16] C. Herley and D. Florencio, "How to Login from an Internet Cafe without Worrying about Keyloggers", in *Proc. of Symposium on Usable Privacy and Security*, Vol. 6, 2006, pp. 1–2.

[17] MSDN-Keyboard Input. http://msdn2.microsoft.com/en-us/library/ms645530.aspx.
[18] MSDN-File Management Functions. http://msdn2.microsoft.com/en-us/library/aa364232.aspx.
[19] MSDN-Winsock Functions. http://msdn2.microsoft.com/en-us/library/ms741394.aspx.
[20] mIRC client application. http://www.mirc.com

Jun Fu received a PhD. degree on computer software and theory from Wuhan University in 2011. Now he is an engineer of the 28th Research Institute of China Electronics Technology Group Corporation. His research interests include artificial immune system, network security and stealthy malware detection.

Huan Yang received a PhD. degree on computer software and theory from Wuhan University in 2012. Now she is an engineer of the 28th Research Institute of China Electronics Technology Group Corporation. Her research interests are in the field of software reliability, artificial immune system, and software health management. Currently, she focuses on applying the AIS on web server aging.

Yiwen Liang is currently a Professor and Ph.D. advisor in Computer School, Wuhan University. His research interests include artificial immune system and anomaly detection. He has been awarded three NSFC research funding as principal investigator on topics including AIS, Network Security and Anomaly Detection. Prof. Liang is an associate Secretary General of the Natural Computing Committee of Chinese Association for Artificial Intelligence (CAAI), a member of the council of the IEEE education association China sub-commission.

Chengyu Tan is currently an associate professor and master advisor in Computer School, Wuhan University. She received a B.E. (1990) and a M.S. (1996) degrees from Wuhan University of Hydraulic and Electrical Engineering, and completed a PhD in software and theory at Wuhan University in 2007. Her research interests include artificial immune system and natural computation.

Shape-Matching Model Optimization Using Discrete-point Sampling and Feature Salience

Zongxiao Zhu
Huazhong University of Science and Technology, Wuhan, China
South-Central University for Nationalities, Wuhan, China
Email: zhuzongxiao@gmail.com

Guoyou Wang
Huazhong University of Science and Technology, Wuhan, China
Email: gywang@mail.hust.edu.cn

***Abstract*—The component classification and potential fault region locating in the full-automatic inspection system of a freight train require a computer vision method with the ability of classifying quickly and locating precisely, addressing anti-nonlinear deformations, and being able to perform extensible learning. Inspired by these requirements, this paper specifically optimizes the three elements of a shape-matching model, including the scene map, the shape template, and the matching. Our method uses a discrete-point sampling map (DPSM) as an intermediate representation, to enhance the stability of the scene maps, uses the criterion function based on feature salience to select a better shape-template group, and matches hand-sketches with regions in DPSMs to reduce the difficulty of the matching calculation. Based on our optimized shape-matching model, we set up a new procedure for component classifications and potential fault region locating in the full-automatic inspection system for freight trains, which has been applied successfully on more than 10 parts of freight train cars in the railway for more than 2 years. The results of anti-noise testing in laboratory and daily operation at several inspecting stations show that our method has a strong ability to survive with nonlinear deformations, and has a good extensibility to be used with different parts, which meet application demands for the full-automatic inspection system.**

***Index Terms*—TFDS; shape matching, discrete-point sampling, shape template, feature salience**

I. Introduction

The research in this paper is inspired by a series of bottleneck problems that occur when Chinese freight train car inspections are changed from half-automatic mode to full-automatic mode. Currently, most freight car inspections are half-automatic with a substantial manual portion. The "Trouble of Freight Car Detection System" [1]-[2] （TFDS, official name） that is equipped in

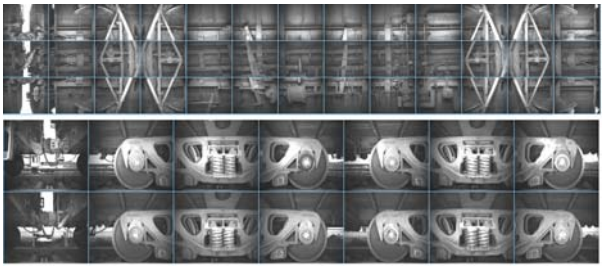

Figure 1. Fifty-three photos from Chinese trouble of freight car detection system.

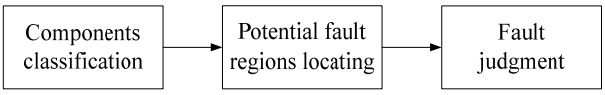

Figure 2. The basic procedure of inspection on freight cars

Chinese railways uses five cameras to take 53 part photos (sized 1400 × 1024) from the two sides and bottom of one freight car, where faults might emerge. Among these photos, two cameras from each side take 7 photos each, and three cameras from the bottom side take 13 photos each, as Fig. 1 shows. When these photos are taken, the freight train is running normally, and the size, distance, angle, and shooting time for each part's photos are relatively unified. There will be 2000-3000 photos that are taken from one freight train according to the number of cars that it drives. All of these photos will be examined, and fault judgments will be made in 10 minutes by 4 freight train surveyors in a detecting office. If any fault is found, then the surveyors are to report it without delay. If the fault is severe enough to endanger the running safety of the freight train, then the freight train should be stopped, and outdoor surveyors will be sent for further detection to confirm the fault and to handle it. Full-automatic inspection attempts to use computer vision partly or completely instead of the work of the four freight train surveyors, to reduce their labor intensity, improve the detection quality and efficiency, and better ensure the security and celerity of the railway transport.

Manuscript received August 1, 2013.
This work was supported by Wuhan Huamu Science and Technology Company.
Guoyou Wang is the corresponding author.

doi:10.4304/jcp.9.6.1355-1363

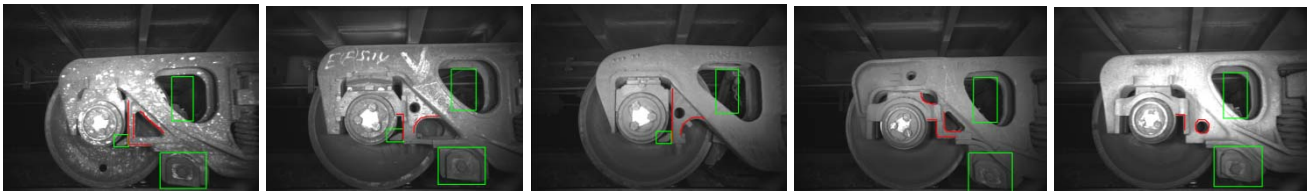

(a) (b) (c) (d) (e)

Figure 3. The component's type and its corresponding potential fault regions. Among which there are square frames with potential fault regions; the red lines are salient hand-sketches that will be discussed later. (a) Wheel component I; (b) wheel component II; (c) wheel component III; (d) wheel component IV; (e) wheel component V.

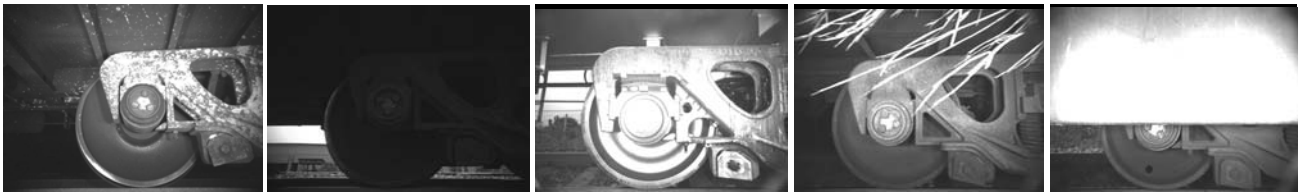

(a) (b) (c) (d) (e)

Figure 4. Several common interference happen to wheel parts. (a) Abundant stains; (b) insufficient illumination; (c) blazing; (d) foreign body shelter; (f) part shelter.

Regardless of whether the half-automatic inspection with manual work or full-automatic inspection with computer vision is used, their basic procedures are the same one shown in Fig. 2. For different components, one part might correspond to different fault regions and types, and the component type in the current parts photo should be recognized first. Next, one or more potential fault regions are located, and a fault judgment will be performed with these potential fault regions. The bottleneck problems mentioned above are the component classification and the locating of potential fault regions, which can be divided into the following three aspects:

A. Classifying Precisely and Locating Quickly

Because the railway transportation in China is developing very quickly, many different ages and types of freight cars, with different component types, run at the same time. New components with new fault regions and types are used every year. Before freight train surveyors in offices were using TFDS to detect faults manually, they were outside surveyors who have been inspecting and repairing all types of freight car faults for more than five years. These surveyors were very familiar with all the potential fault regions in every type of freight car and its components. As a result, component classification and the locating of potential fault regions in the current parts photos can be accomplished quickly and precisely with a single glance at the photo, which ensures that thousands of photos can be inspected in 10 minutes. Fig. 3 shows five types of components in the wheel parts; it can been observed that different types of components might correspond to different locations and that there could be different numbers of potential fault regions, while the faults and their judgment methods could be the same. If computer vision can classify components quickly and can locate potential fault regions as precisely as human do, then the accuracy of fault detection will improve greatly with a decrease of the missing recognition rate and the false acceptance rate.

B. Robustness to All Kinds of Interference

The relative unified shooting conditions of the TFDS guarantees that there will be no large geometric transformations (e.g., translation, rotation, scaling) with the components in the photos. However, after running in the open for a long time, factors such as noise, all types of spots, strong reflected light, articulations and occlusions make the details of the photos from the same component of the same part different from one another, and no identical photos can be found, although they retain a general similarity. The trained surveyors have strong adaptability to such nonlinear deformations, which are much more challenging for computer vision than for geometric transformations [3]. Fig. 4 shows several common nonlinear deformations types applied to wheel parts.

C. Easy to Extend

Humans have an excellent capacity for extensible learning. If there is a new component with a new potential fault region, then the surveyors can quickly master it within a short training time. While for a computer vision system that has been operated in the field, such a change could mean that the system should be ended and sent back to its developer for updates and re-debugging before operating it again, which poses an obstacle to popularizing a full-automatic inspection system for freight trains. In fact, most of the faults in a new potential fault region that correspond to a new component are old and detectable faults. If the method for component classification and potential fault region locating can be extended to be compatible with a new component type and a new potential fault region, then the fault can be judged by the available judging program. Thus, the method of components classification and potential fault region locating in a full-automatic inspection system of a freight train should also be good at extensible learning, to quickly adapt to a freight train's component upgrading.

In summary, component classification and potential fault region locating in the full-automatic inspection system of a freight train require a computer vision method with the ability of classifying quickly and locating precisely, addressing anti-nonlinear deformations, and being able to perform extensible learning. Inspired by these requirements, this paper specifically optimizes the three elements of a shape-matching [4]-[5] model, including the scene map, the shape template, and the matching. Based on our optimized shape-matching model, we set up a new procedure for component classifications and potential fault region locating in a full-automatic inspection system for freight trains, which has been applied successfully on more than 10 parts of freight train cars in the railway for more than 2 years. The experiments using random noise and salt noise added to wheel parts repeatedly prove that our method has a robust ability to address anti-nonlinear deformations. In addition, our shape-template drawing and learning method is simple and convenient and can be adjusted by various detecting offices according to the actual situation of the passing freight cars. Thus, our method has an excellent capability for extensible learning.

This paper is organized as follows. Section II presents related studies. Section III introduces our optimization of a shape-matching model. Section IV describes the results of our experiments. Section V offers our discussion and conclusions.

II. Related Studies

Shape matching, which uses object regions or boundary information to retrieve and locate an object, is in best agreement with how the human eye recognizes and distinguishes objects. Thus, this problem has been widely studied by many scholars in the fields of image processing and computer vision for a long time. There are mainly two categories of shape matching: edge-based methods [6] and region-based methods [3]. Edge matching traditionally requires explicit edge correspondence, while edge detection is a difficult classification decision that is also sensitive to noise and illumination changes. Region matching gives edge matching with no need for point-to-point edge correspondence and is more robust to local-shape distortions and occlusions. However, many important shape details are absent, and it is difficult to extract a shape reliably and to represent or match shapes precisely when complex shapes are present. Because regions have closed boundaries, they do not adapt easily when matching open image curves.

Geometric transformations (e.g., translation, rotation, scaling) and nonlinear deformations (noise, articulation and occlusions) are the main problems that make shape matching difficult. Currently, many studies focus on how to improve the invariant ability of shape templates with geometric transformations, while there is less research on nonlinear deformations. Deformable template [7] achieves invariance to location, rotation, and moderate scale changes by a parameterized transformation that is applied to the prototype to deform it; this technique is widely used in the representation and recognition of handwritten digits [8], vehicle segmentation and classification [9], and object tracking [10]. Wang [3] proposed a novel shape descriptor by computing the height functions of the sample points of a given contour, which is not only invariant to geometric transformations but also insensitive to nonlinear deformations because of noise and occlusion. Ferrari [11] used grouped edge fragments as intermediate representations. These grouped curves have more specificity and fewer potential matches than individual edge fragments yet are still relatively easy to match, and they occur often enough to survive occlusions and detection failures. Wang [6] avoids point-to-point edge correspondence by matching shapes in an over-segmentation map, which leads the system to be robust to small shape variations and spatial shifts.

Unlike edge matching between edges or region matching between regions, in this paper, out shape template is a hand-sketch and our matching is conducted between the hand-sketch and a region in a discrete-point sampling map (DPSM) [12]-[13] that is obtained by sparse sampling [14], which brings robust and efficiency to the classification and locating while sacrificing a small amount of accuracy of the locating. Traditionally, sparse sampling in shape matching is performed with a shape template, which reduces the search space but also decreases the overall accuracy of the shape description and adds a risk of aliasing [6]. Our sparse sampling is conducted on scene maps, and the DPSM using this approach corresponds more to the intuitive impression of an initial image in human brains, which can automatically accentuate the basic information and reject the abundant details such as noise, texture and uneven illumination conditions. Matching between a hand-sketch and a region combines the advantages of local edge representations and global region robustness and has sufficient shape description accuracy for classification, which not only can be robust to small shape variations and spatial shifts but also can have strong toleration for nonlinear deformations.

To improve the accuracy of the classification, the feature saliency [15]-[16] of each shape template should be measured, and the more discriminative shape template should be selected. The terminology ‘more discriminative’ in this paper includes two meanings. First, the system should tolerate the geometric differences of objects from the same category, and at the same time, the system should allow for discriminating objects that are from different shape classes. If there are multiple objects to be classified, then each category requires a shape template that has a strong discriminative ability. The feature salience of this series of shape templates should be measured, and then, a better template group for classification can be found. Feature salience can be divided into two categories, structural salience and probabilistic salience [17]. Taking intra- and inter-cluster distances as measurements, structural salience selects features by a criterion function with small intra-cluster distances and larger inter-cluster distances. Probabilistic salience selects a salience feature that has a minimal

judgment error statistically, using the minimum classification error criterion. Learning based on structural salience can be easily conducted with a small number of samples, while the correcting rate of classification is less than probabilistic salience. Probabilistic salience can make a better correcting rate of classification with a large number of learning samples in every class. In this paper, we define a criterion function that is based on structural salience and that has values from 0 to 1, which makes salience measurement values from different shape templates clear compared. With our method, the shape templates that have a better discriminating ability can be selected simply and efficiently, which can satisfy the demand for extensible learning.

If there are serious geometrical transformations with objects of interest, such as rotation, scaling and translation, it is difficult to find point-to-point edge correspondences. Thus, some complex algorithms, such as dynamic programming [3], binary search tree structure of weak classifiers [5], and generic probabilistic algorithms based on random sampling [4] are used to improve the accuracy of the matching. For shapes that have small distortions and spatial shifts, the difficulty of finding high quality point-to-point shape correspondences decreases, which makes shape matching easier. For example, Chamfer matching [17] and Hausdorff-distance [18] matching compute edge correspondences that are purely based on the Euclidean distance between the edge points. However, these approaches are that they rely on the completeness and accuracy of edge detection, which cannot be guaranteed for factors such as unknown objects that occur, occlusions, movement, background changes and noise interference. The method proposed in this paper is based on a DPSM. If there is a region in a specific map that could contain a specific shape template (or a hand-sketch), then the initial image could contain this shape template with a high probability, and the similarity calculated by the density is higher, which greatly accelerates the process of classification and locating, while accommodating to some of the nonlinear deformations.

In conclusion, there are three main factors that should be considered with a shape-matching model: the stability of the scene maps, the discrimination of the shape templates, and the difficulty of matching. Our method uses the DPSM from sparse sampling as an intermediate representation, to enhance the stability of the scene maps, uses the criterion function based on feature salience to select a better shape-template group, and matches hand-sketches with regions in DPSMs to reduce the difficulty of the matching calculation. Our method can be used broadly in applications where there are abundant nonlinear deformations but small geometrical transformations, such as all kinds of automatic assembly line inspection, machine part detection, and vehicle-type classification.

III. Optimization Methods

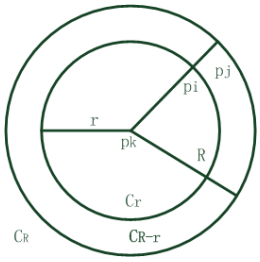

Figure 5. Diagram of the discrete-point sampling model

A. Sparse Sampling

The discrete-point sampling model is defined in [13] as Fig.5 and formula (1), (2) shows.

$$U(P_k)=\left(\frac{1}{C_{R-r}}\sum_{P_j\in C_{R-r}} g_j-\frac{1}{C_r}\sum_{P_i\in C_r} g_i\right)\Big/\left(\frac{1}{C_r}\sum_{P_i\in C_r} g_i+\varepsilon\right) \quad (1)$$

$$T(p_k)=\begin{cases}1 & U(p_k)>\xi\\ 0 & U(p_k)\le\xi\end{cases} \quad (2)$$

here are three parameters in the discrete-point sampling model: the sampling radius r, the external circle radius R, and the Weber-Fechner ration ξ. The sampling radius r has an effect on three factors: the density of the discrete points in a DPSM, the map's ability to describe the detailed information that is contained in the initial gray images, and the difficulty of subsequent matching or grouping based on the map. When we increase the sampling radius r, the discrete-point sampling map will become sparser and will have less detailed information and sampling time, and it will become more difficult to match or grouping. The external circle radius R determines how strongly the curvilinear structures can be enhanced in a DPSM, with an effect on its sampling time and its ability to suppress interference from noise and texture. The larger its value is, the farther away from the real edge is the discrete points that are generated and the more salient is the curvilinear structure that is gathered by these points, which is more beneficial for curve shape matching and curvilinear structure detection. Meanwhile, formula (1) can be perceived as a mean filter, and the external radius R can be perceived as the window's size. The larger its value, the better is its inhibiting ability toward interfering noise and textures, and the larger the amount of time that is needed for calculating the discrete points. The sampling time grows linearly with the external circle radius R, while the number of sampling points does not, which means that the effect of filtering is enhanced. Taking all of these factors into account, including the salient level of the curvilinear structures, the difficulty of the shape matching, and its sampling time, we use r=2 and R=15 in this paper for calculating a DPSM, in which the subsequent shape matching is mainly conducted. The Weber-Fechner ratio ξ affects the describing ability of the details in an initial image by a DPSM and its inhibiting ability toward interfering noise and textures. These two abilities restrict each other. The larger the value of ξ is, the weaker its ability is for describing the details in the initial images with a better inhibition ability. In practice, there is no need to select a Weber-Fechner ratio ξ that corresponds to the human

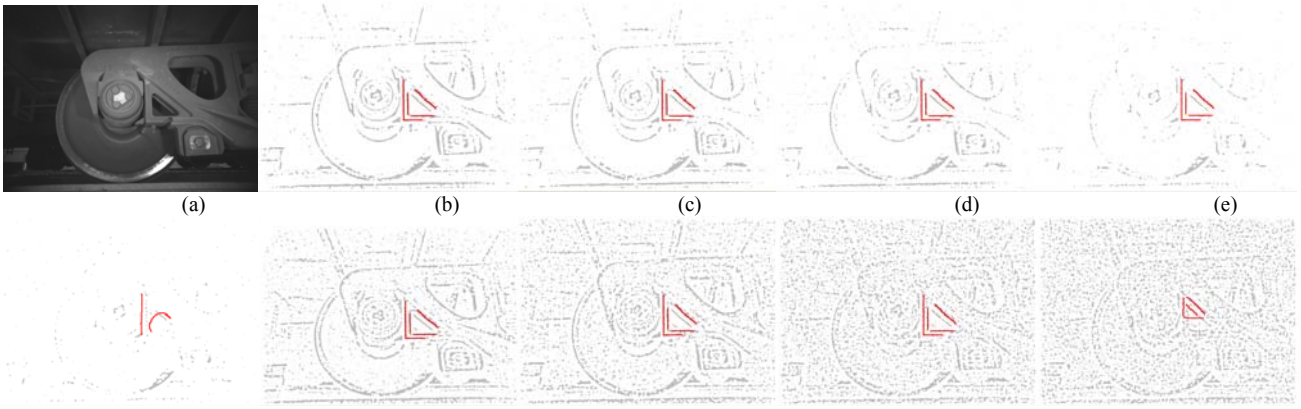

Figure 6. Shape matching test with different lever of noise. (a) Initial image (1400×1024); (b) no noise added, λ=0.970827; (c) random noise 22 dB, λ= 0.935170; (d) random noise 18 dB, λ= 0.760130; (e) random noise 15 dB, λ=0.350081; (f) random noise 14 dB, matching failed; (g) salt noise 21 dB, λ= 0.857374; (h) salt noise 18 dB, λ= 0.816856; (i) salt noise 15 dB, λ= 0.670989; (j) salt noise 14 dB, matching failed.

eyes exactly. If the entire photograph is too dark to identify the details, then ξ can be decreased to increase the detailed information, which is contrary to the physiological properties of the human eye. If the photograph has too many details and contains a substantial amount of noise, then ξ can be increased to reduce unnecessary information. By experimentation, we choose ξ=0.05 for all of the subsequent applications in this paper, which corresponds to the human eye in a circumstance that has a very high or very low brightness.

B. Shape Matching

Shape matching will be conducted with hand-sketches in DPSMs from sparse sampling, and similarities are calculated among them by density estimations [33]. The introduction of prior shape information helps to detect objects in the presence of strong occlusions and, at the same time, helps to reject undesired contours, while it has a stronger immunity to noise and blurring. Meanwhile, DPSMs are quite fit for performing density estimation with hand-sketches. If there is a belt-shaped region that has clustered discrete points in the map can contain a hand-sketched shape, this shape is more likely to exist in its initial image. We define a similarity operator for performing density estimation with hand-sketches in DPSMs, as formula (4) shows.

$$\lambda = \frac{N}{M} = \frac{\sum_{k=1}^{M} S(p_k)}{M} \tag{4}$$

In formula (4), M is the total number of points in a hand-sketch, p_k is the present point in the hand-sketch, and N is the total number of points in the hand-sketch that have responses with the belt-shaped region in the DPSM. The response is defined by the density function S, as follows:

$$S(p_k) = \begin{cases} 1 & I(p_k) = 1 \quad or \quad C_8(p_k) \geq 2 \\ 0 & else \end{cases} \tag{5}$$

where $I(P_k)=1$ means that there is a pixel that corresponds to p_k in the DPSM, and $C_8(p_k) \geqslant 2$ means that there are two pixels that are located at 8 connected directions around the position that corresponds to p_k. Both of these two situations can be considered to have corresponding points with p_k in the DPSM.

By this definition, our method avoids the requirement of explicit point to point correspondence by edge matching and has a strong immunity to small deformations and noise. To prove this concept, we add random noise and salt noise at different levels in Fig. 3 (a) and test our shape-matching method by recording the similarity λ. The effects of random noise and salt noise with DPSMs are shown in Fig. 6 (b)-(j). Only when the noise-signal ratio is decreased to less than 15 dB from these two types of noise will the shape matching fail, which means that our shape matching method has a strong anti-noise ability.

In this paper, a hand-sketch's data are stored as follows: the absolute coordinate of the starting point (4 Bytes) + the extended direction of the starting point (2 Byte) + the extended lengths of the starting point (2 Byte) + the relative coordinates of the sequence of the hand-sketch (4Byte × (M-1), where M is the total number of points in the hand-sketch). When a hand-sketch is drawn, its starting point must be selected carefully because its extended direction and the extended length is a necessary matching requirement, then a large number of unrelated areas can be excluded and the matching speed improves significantly.

By setting up the corresponding relationship between the shape-matching position and the potential fault region position, the potential fault region of one category of component is also located, and the results of matching and locating are shown in Fig. 3.

C. Template Optimization

As mentioned above, the difficulty of shape matching is decreased in DPSMs, while a higher discrimination of the shape template is required. Different hand-sketch's feature salience should be measured, to allow a group of better hand-sketches to be selected for matching. Every hand-sketch can be perceived as an observer that

determines a matching feature *t*. In this section, the method of hand-sketch selection based on the matching feature *t*'s structural salience will be set up.

1. Structural salience measurement for bi-object classification with one template's matching features

If there are two types of objects, called ω_i and ω_j, and the goal of the template's matching feature *t* is to distinguish them, then a structural salience measurement S_{ij}^t for ω_i and ω_j with feature *t* is defined in formula (6), as follows:

$$S_{ij}^t = 1 - e^{-a\left(\frac{(m_i - m_j)^2}{\sigma_i^2 + \sigma_j^2 + C}\right)^b}, 0 < a < 1, 0 < b < 1 \quad (6)$$

In formula (6), m_i and m_j are the mean values that correspond to the template's matching feature *t*, and σ_i^2 and σ_j^2 are the variances of *t*. Formula (6) indicates that the larger the value between the class variances and the smaller the within-class variances, the larger the S_{ij}^t, which means that the more salient the feature *t* is, the higher the ability is to distinguish ω_i and ω_j. The role of the natural logarithm *e* in this formula (6) is to adjust S_{ij}^t between 0 and 1, which makes it more convenient to compare features with different value ranges. The '*a*' is a proportional adjustment coefficient, and the '*b*' is an exponential adjustment coefficient, and with their cooperation, the different values of S_{ij}^t can be adjusted to be easily distinguished. *C* is a notably small constant to keep the denominator from being 0. By experiments we found that when *a=0.3*, *b=0.7*, the value discrimination of S_{ij}^t is larger; thus, we use *a=0.3*, *b=0.7*, and *C=0.0000001* in our method.

2. Structural salience measurement for multiple object classifications with one template's matching features

If there are *n* categories of objects, and the goal of the template's matching feature t is to distinguish ω_i from the other *n-1* categories, then a structural salience measurement $S_i^{t_i}$ for ω_i with feature *t* is defined as formula (7) shows:

$$S_i^t = \frac{1}{n-1}\sum_{j=1}^{n} S_{ij}^t, \quad j \neq i \quad (7)$$

Formula (7) indicates that the larger the $S_i^{t_i}$, the more salient the feature *t* is, and the higher the ability is to distinguish ω_i from the other *n-1* categories.

(a) (b) (c) (d)

Figure 7. Four hand-sketches of wheel component type I with the structural salience measurements. (a) Hand-sketch I, S_1^{t1}=0.994; (b) hand-sketch II, S_1^{t2}=0.944; (c) hand-sketch III, S_1^{t3}=0.765; (d) hand-sketch IV, S_1^{t4}=0.860 It can be perceived that among these four hand-sketches, S_1^{t1} from hand-sketch I is the highest, and hand-sketch I can best distinguish wheel type I from the other wheel types in theory. All of these results are based on 1000 wheel part images, with five types randomly taken from a TFDS station, with each type having 200 images.

(a) (b) (c) (d) (e)

Figure 8. A salient hand-sketch group for the wheel part's five component types. (a) Wheel component I's hand-sketch, S_1=0.994; (b) wheel component II's hand-sketch, S_2=0.881; (c) wheel component III's hand-sketch, S_3=0.684; (d) wheel component IV's hand-sketch, S_4=0.626; (e) wheel component V's hand-sketch, S_5=0.486. The image database is the same as in Fig. 9.

3. Salient feature group T for multiple objects

If there are several templates, and all of the matching features $t_1, t_2, \cdots, t_k$ can distinguish ω_i from the other *n-1* categories, then every structural salience measurement $S_i^{t_i}$ with t_i for ω_i is calculated, and we take the feature that corresponds to $S_i = \max(S_i^{t_k})$ to be the better feature for ω_i, which is written as t^i. If this method is used for every category of object to select a better matching feature, then a more salient feature group T for multiple objects can be obtained. Formula (8) shows this construct:

$$T = \{t^1, t^2, \cdots t^n\} \quad (8)$$

4.Example of hand-sketch template optimization

The problem of component classifications and potential fault region locating with one TFDS image can be solved by shape matching that is based on hand-sketch templates, while the key point is how to improve these hand-sketch templates' qualities, which make them perform better at distinguishing the present category of components from other categories.

In this paper, we take the wheel component I in Fig. 3 (a) as an example to illustrate our detailed method. For a special component type, more than one hand-sketch can be drawn, as Fig. 7 shows, and formula (7) is used to calculate the structural salience measurement for this component type. The hand-sketch with the highest $S_i^{t_i}$ is chosen as the shape template, and the accuracy of the component classifications and potential fault region locating can be improved by this way.

We use the same method with every wheel's type, and a salient hand-sketch group can be obtained, as Fig. 8 shows. Based on this salient hand-sketch group, a shape-template library is established, and the similarity λ_i of every hand-sketch is calculated with every testing image, using formula (4). The type of wheel component and its potential fault region in the present image are determined by the hand-sketch with the highest similarity λ_i.

IV. Experiments and Results

In this section, we will compare our method with several classical template matching methods, and we will test its performances in classifying and locating, addressing noise. We will use four experiments, including matching comparison, classification test, anti-noise test and extensibility test. Our test environment utilizes an Intel Core i5-2540 2.60GHz CPU， 4 GB RAM, and VC++2010.

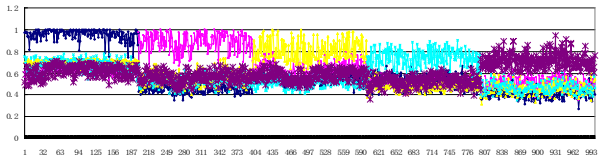

Figure 9. Similarity results on five types of hand-sketches. The image database is the same as in Fig. 7.

Fig. 9 shows the calculated results for the similarity λ_i using the five types of hand-sketches of the wheel components in Fig. 8. It can be perceived that these five types of hand-sketches have a strong discriminative ability, which can classify wheel components by directly comparing their similarity λ_i.

Using the method proposed in section 3 of this paper, we conduct a classification test with 7382 wheel part images from 143 freight cars passing through a TFDS station on a single day. The matching area is restricted to a 256×128 region around the absolute coordinate of each hand-sketch's starting point, which not only decreases significantly the computational complexities of generating DPSMs and shape matching but also provides some adaptation for geometric transformations from varying the speed, camera vibration and different shooting times.

The test results are recorded in table II, where the total classification accuracy is 99.39%, and the average time for each image is no more than 40 ms, which means that 25 frames per second can be achieved. From the analysis of table II, we can see that, with the five templates in Fig. 10, the recall and accuracy rate of the components of types I, II, and III, which hold 90% of all of the types of

TABLE II
Classification Results of a Wheel Part Based on Our Method

Detected / Real	Type I	Type II	Type III	Type IV	Type V	Real Sum	Recall (%)	Proportion (%)
Type I	5004	0	3	5	0	5012	99.84	68.01
Type II	0	1398	0	0	1	1399	99.93	18.98
Type III	0	0	216	0	0	216	100.00	2.93
Type IV	0	1	0	226	2	229	98.69	3.11
Type V	0	19	3	11	480	513	93.58	6.96
Detected Sum	5004	1418	222	242	483	7369		100.00
Accuracy (%)	100.00	98.59	97.30	93.39	99.38	99.39		

TABLE III
Classification Results with Random Noise and Salt Noise

Noise Type	Recall (%)_ Type / Accuracy (%) / SNR (dB)	Type I	Type II	Type III	Type IV	Type V	Total Accuracy (%)
Random noise	∞	100.0_100.0	100.0_100.0	100.0_100.0	100.0_100.0	100.0_100.0	100.0
	26	99.5_98.5	100_99.5	99.0_99.5	98.0_97.5	97.0_98.0	98.7
	21	97.5_100	99.5_98.0	98.0_99.0	99.0_94.7	96.5_99.0	98.1
	18	94.5_99.5	97.5_96.5	97.0_96.5	98.5_91.6	94.5_98.4	96.4
	16	84.5_97.1	92.5_92.5	87.5_87.0	97.0_76.4	81.0_94.7	88.5
Salt noise	∞	100.0_100.0	100.0_100.0	100.0_100.0	100.0_100.0	100.0_100.0	100.0
	22	99.0_100.0	99.5_98.5	99.0_99.5	100.97.1	97.5_100	99.0
	18	98.5_94.7	98.0_94.7	96.5_98.5	99.9_95.7	95.5_99.0	97.5
	16	94.0_99.5	93.5_92.1	93.0_92.5	98.5_91.6	93.0_96.9	94.4
	15	92.0_100.0	92.0_92.5	93.0_91.2	98.5_88.7	91.0_95.7	93.3

components, are above 99.8%, while the recall and accuracy rate of the components of types IV and V, which hold 10% of all of the types of components, are lower. In the future, the accuracy of these two components can be further improved by drawing supplementary distinguishable sketches of component types IV and V and calculating the combined similarity with one component's two hand-sketch templates.

To further prove our method's robustness to noise, we choose another five categories of components in the wheel parts, with 200 images each, which can be classified correctly without adding noise. Random noise and salt noise with different signal-to-noise ratios are placed into these images individually, and the anti-noise ability is checked by calculating the recall and accuracy rates. The test results in table III show that our method has a very strong anti-interference ability with random noise and salt noise, especially with salt noise, which means that our method can have excellent performance with many types of interference as shown in Fig. 4. Our field tests also have proven this conclusion.

V. Discussion and Conclusions

The whole automation of freight car fault detection requires computer vision for the ability to classify quickly and perform locating precisely, to address anti-nonlinear deformations and to accomplish extensible learning, similar to what human inspectors are capable of. Traditional methods mainly include region matching and edge matching. When regions have closed boundaries, they do not adapt easily when matching open-image curves. To avoid explicit edge correspondence, edge matching introduces complex methods, such as edge grouping or segmentation averaging, to adjust the possible corresponding areas into a more appropriate level and to perform distance calculations or dynamic searches. Many researchers focus on how to improve the robustness of a template with geometric transformations, while seldom analyzing and evaluating its separability. Extensible learning of a new category is not considered sufficiently, and research on nonlinear deformations is relatively non-satisfactory.

In this paper, the three elements of a shape-matching model, including the scene map, the shape template, and the matching, are all optimized to solve the problems mentioned above. For scene maps, this paper establishes a sparse sampling operator that is based on the Weber-Fechner law, which reflects how human eyes perceive brightness differences and change a gray image into a DPSM as an intermediate representation. In a DPSM, large-scale structural features are enhanced as belt-shaped regions, and details of noise and textures are inhibited. Compared with the typically used thresholding segment map and edge map, a DPSM corresponds more to the intuitive impression of an initial image in human brains, which can automatically accentuate the basic information and reject many details regarding noise, texture and uneven illumination. In essence, the sparse sampling in our method is a fixed grid sampling with a local scale parameter. The Weber-Fechner ratio ξ is the local scale parameter that improves the stability of a DPSM under different illumination and blurs conditions. Fixed grid sampling extracts both edges and their surroundings, which also enhances the stability of the intermediate representations.

For a shape template, this paper selects the template that can best represent its pattern and that differs from other patterns by drawing contours in a learning sample's DPSM. Our method calculates their feature salience to find better templates , which imitates the initiation and improving procedures in the human brain and improves the accuracy and efficiency of classifying multiple objects.

For matching, our matching is between a hand-sketch and a region. A shape template is placed into a DPSM directly to obtain density estimation. If there is a region in the DPSM that contains the shape template, then the shape template is more likely to be in the initial image, and the calculated density estimation is higher. Our method increases the speed of classification and locating, improves the ability of addressing anti-nonlinear deformations, and is robust to small shape variations and spatial shifts.

For such applications as TFDS, the same component's edges in a large number of images are distributed in specific areas. These edges are not fixed, are not standard, might not be continuous, and are also with no many geometric transformations caused by scaling or rotation. By artificially selecting the parts that have salient separability in a learning sample's DPSM, and drawing a component's contours in these parts as hand-sketches, those hand-sketches can be projected into test sample's DPSM. Our shape matching is a process of finding regions that might have a hand-sketch, which makes classification very quickly with enough locating precision. The results of anti-noise testing in laboratory and daily operation at several TFDS stations show that our method has a strong ability to survive with nonlinear deformations and has a good extensibility to be used with different parts, which meet application demands for TFDS stations.

Acknowledgment

This work was supported in part by the Natural Science Foundation of China under Grant 60975021.

References

[1] Z.H. Liu, D.Y. Xiao and Y.M. Chen, "Displacement fault detection of bearing weight saddle in TFDS based on hough transform and symmetry validation," in *9th International Conference on Fuzzy Systems and Knowledge Discovery (FSKD)*, pp. 1404-1408, Chongqing, China, May. 2012.

[2] X.D. Yang, L.J. Ye and J.B. Yuan, "Research of Computer Vision Fault Recognition Algorithm of Center Plate Bolts of Train," in *1st International Conference on Instrumentation, Measurement, Computer, Communication and Control*,pp.978-981, Beijing, China, Oct. 2011.

[3] J.W. Wang et al., "Shape matching and classification using height functions," *Pattern Recognition Letters*, vol. 33, no.2, pp. 134-143, Jan. 2012.

[4] Deng, Lawrence Y., et al. "Real-time hand gesture recognition by shape context based matching and cost matrix." *Journal of Networks* 6.5 (2011): 697-704.
[5] Chu, Jun, and Guimei Zhang. "Match Planar Curve Based on Affine Invariant." *Journal of Software* 7.1 (2012): 9-16.
[6] H.Z. Wang and J. Oliensis, "Rigid Shape Matching by Segmentation Averaging," *IEEE Trans. Pattern Anal. Mach. Intell.*, vol. 32, no. 4, pp. 619-635, Apr. 2010.
[7] A.K. Jain, Z. Yu and S. Lakshmanan, "Object matching using deformable templates," *IEEE Trans. Pattern Anal. Mach. Intell.*, vol. 18, no. 3, pp. 267-278, Mar.1996.
[8] A.K. Jain and D. Zongker, "Representation and recognition of handwritten digits using deformable templates," *IEEE Trans. Pattern Anal. Mach. Intell.*, vol. 19, no. 12, pp. 1386-1390, Dec.1997.
[9] Qi X, Ji J, Han X. Vehicle Type Classification by Acoustic Waves with Dimension Reduction Technique[J]. *Journal of Computers*, 2013, 8(3): 685-692.
[10] Yu Zhong, A.K. Jain and M.P. D. Jolly, "Object tracking using deformable templates," *IEEE Trans. Pattern Anal. Mach. Intell.*, vol. 22, no. 5, pp. 544-549, May.2000.
[11] V. Ferrari, et al., "Groups of Adjacent Contour Segments for Object Detection," *IEEE Trans. Pattern Anal. Mach. Intell.*, vol. 30, no. 1, pp. 36-51, Jan.2008.
[12] Zhu, Zongxiao, Guoyou Wang, and Jianguo Liu. "Object detection based on multiscale discrete points sampling and grouping." *Sixth International Symposium on Multispectral Image Processing and Pattern Recognition*. International Society for Optics and Photonics, YiChang, China,2009.
[13] Zhu, Z., et al., "Fast and Robust 2D-Shape Extraction Using Discrete-Point Sampling and Centerline Grouping in Complex Images". *Image Processing, IEEE Transactions on*, 2013. 22(12): p. 4762-4774.
[14] T.V. Pham and A.W.M. Smeulders, "Sparse representation for coarse and fine object recognition," *IEEE Trans. Pattern Anal. Mach. Intell.*, vol. 28, no. 4, pp. 555-567, Apr. 2006.
[15] Wang H, Dang Y, Ke H, et al. A Method of Target Region Detection Based on Multi-channel Weighted Visual Attention[J]. *Journal of Computers*, 2013, 8(10): 2478-2482.
[16] Tie Liu, et al., "Learning to Detect a Salient Object," *IEEE Trans. Pattern Anal. and Mach. Intell.*, vol. 33, no. 2, pp. 353-367, Feb. 2011.
[17] Zhen-Xue Chen, et al., "Automatic License-Plate Location and Recognition Based on Feature Salience," *IEEE Trans. Veh. Techno.*, vol. 58, no. 7, pp. 3781-3785, Sep. 2009.
[18] G. Borgefors, "Hierarchical chamfer matching: a parametric edge matching algorithm," *IEEE Trans. Pattern Anal. Mach. Intell.*, vol. 10, no. 6, pp.849-865, Nov.1988.
[19] Dong-Gyu Sim, Oh-Kyu Kwon and Rae-Hong Park, "Object matching algorithms using robust Hausdorff distance measures," *IEEE Trans. on Image Process.*, vol. 8, no. 3, pp.425-429, Mar.1999.
[20] J.H. Shen, "On the foundations of vision modeling I. Weber's law and Weberized TV restoration," *Physica D Nonlinear Phenomena*, vol. 175, no. 3-4, pp. 241-251, Feb. 2003.
[21] A.M. Peter and A. Rangarajan, "Maximum Likelihood Wavelet Density Estimation With Applications to Image and Shape Matching," *IEEE Trans. on Image Process.*, vol. 17, no. 4, pp. 458-468, Apr. 2008.

Zongxiao Zhu received the BS degree and the MS degree in electrical and electronic engineering from Xi'an Jiaotong University, Xi'an, China in 2000 and 2003, respectively. He is currently pursuing the Ph.D. degree in control science and engineering at the Institute for Pattern Recognition and Artificial Intelligence, Huazhong University of Science & Technology, Wuhan China.

From 2003 to 2004, he was an engineer with SuZhou Shihlin Electric&Engineering Co., where he was in charge of designing small power converters (on the market in 2004). Since 2004, he has been a faculty of College of computer Science, South-Central University for Nationality (SCUN), Wuhan, China. In 2007, he founded the Information Processing Laboratory for Minority Language (IPLML) in SCUN and began to manage a multidisciplinary research team aiming at using information technology to salvage, protect and broadcast endangered minority cultures. His research interests include image processing, object detection, and endangered minority culture's protection with information technology.

Mr. Zhu is a member ACM and a member of Chinese computer federation (CCF).

Guoyou Wang received BS degree in Electronic Engineering and the MS degree in pattern recognition and intelligent system from Huazhong University of Science and Technology., Wuhan, China in 1988 and 1992, respectively. He is currently a professor with the Institute for Pattern Recognition and Artificial Intelligence, Huazhong University of Science & Technology, Wuhan China. His research interests include image processing, image compression, pattern recognition, artificial intelligence, and machine learning.

Multi-label Classification Using Hypergraph Orthonormalized Partial Least Squares

Gaofeng Luo
Hunan Provincial Key Laboratory of Information Service in Rural Area of Southwestern Hunan, Shaoyang University, Shaoyang 422000, China
E-mail: luogfeng@yeah.net

Tongcheng Huang and Zijuan Shi
Hunan Provincial Key Laboratory of Information Service in Rural Area of Southwestern Hunan, Shaoyang University, Shaoyang 422000, China
E-mail: luogfeng@yeah.net

***Abstract* — In many real-world applications, human-generated data like images are often associated with several semantic topics simultaneously, called multi-label data, which poses a great challenge for classification in such scenarios. Since the topics are always not independent, it is very useful to respect the correlations among different topics for performing better classification on multi-label data. Hence, in this paper, we propose a novel method named Hypergraph Orthonormalized Partial Least Squares (HOPLS) for multi-label classification. It is fundamentally based on partial least squares with orthogonal constraints. Our approach takes into account the high-order relations among multiple labels through constructing a hypergraph, thus providing more discriminant information for training a promising multi-label classification model. Specifically, we consider such complex label relations via enforcing a regularization term on the objective function to control the model complexity and balance its contribution. Furthermore, we show that the optimal solution can be readily derived from solving a generalized eigenvalue problem. Experiments were carried out on several multi-label data sets to demonstrate the superiority of the proposed method.**

***Index Terms*—Partial least squares; Orthogonal constraints; High-order relations; Regularization; Multi-label learning**

I. INTRODUCTION

Multi-label learning has gained increasing popularity from both the academia and the industry in recent years [1, 2, 3, 4]. It focuses on the data each of which is associated with more than one label. Such problems are omnipresent in many real-world applications, such as image annotation, video indexing and music style categorization [5, 6]. For example, an image might contain 'road' and 'house' at the same time since a road has a high probability to appear surrounding a house. For a video clip on Youtube, it might has several annotations, e.g., 'comedy', 'American' and 'humor'. In modern music information retrieval systems, the contents of the music refer to various styles, e.g., 'urban', 'country', 'jazz' and 'pop'. It can be easily observed from the above examples that there exist positive relations among the semantic topics, which can be explored to better address the multi-label problems.

In practice, multi-label data often reside in a high-dimensional space, where some noises or redundancy would affect the classification performance [23]. Therefore, it is of vital importance to learn a low-dimensional subspace which preserves the primary energy or components of the original data. In this work, we study extracting a latent subspace shared by all labels for multi-label classification. This is different from conventional methods, which construct the binary classifier for each label and neglect the label relations. In the low-dimensional data space, the performance of multi-label classification is expected to be significantly improved. Essentially, this problem can be called dimensionality reduction or feature extraction [26], which is a classical problem in machine learning and data mining. Thus, traditional unsupervised methods can be directly employed for multi-label problems, since none of the label information is required in this fashion, such as Principal Component Analysis (PCA) [7]. An obvious drawback is they fail to employ the label information, which plays a critical role in deriving a well-structured subspace. For supervised methods, we can achieve feature extraction on multi-label data from the perspective of maximizing the correlation or the covariance between the features and the labels, such as Canonical Correlation Analysis (CCA) [8] and Partial Least Squares (PLS) [9, 25] in this paper, we concentrate on a variant of PLS, named Orthonormalized Partial Least Squares (OPLS) [10], which imposes the orthogonal constraints onto the projected vectors. However, none of them have probed into the intrinsic relationships among the multiple labels, thus not capturing the decoupled effects from label relations.

To address this issue, we propose to encode the high-order label relations by a hyper-graph [11] to capture the correlated discriminant information for a better preserved structure in the projected data space. Hence, we present a novel method called Hyper-graph Orthonormalized

doi:10.4304/jcp.9.6.1364-1370

Partial Least Squares (HOPLS) for multi-label classification. In particular, each data point is treated as a vertex, and each label indicates a hyper-edge including all data points sharing a common label. With this method, the projection from the high-dimensional data space into a low-dimensional space is guided by the high-order relations among multiple labels, thus achieving improved multi-label classification performances. We formulate this model as a generalized eigenvalue problem, which can be readily solved. As a consequence, the extracted subspace is spanned by the eigenvectors corresponding to the leading eigenvalues from solving the eigenvalue decomposition problem. Since we take into account the complex label relations of multiple labels, as a result, the low-dimensional data space is able to characterize the discriminating power and approach the intrinsic data structure.

It is worthwhile to highlight the main contributions of this work as follows.

- A novel method is proposed for multi-label classification, i.e., Hypergraph Orthonormalized Partial Least Squares (HOPLS). This approach makes use of a hypergraph to encode the high-order label relations to guide the projection, so that the obtained low-dimensional data space characterizes a well preserved structure approaching the intrinsic one. Meanwhile, thanks to the supervised information, the derived data subspace has more discriminating power, leading to improved multi-label classification performances.
- We show this established model can be mathematically formulated as a generalized eigenvalue problem, which can be easily solved by eigenvalue decomposition technique. Thus, a set of eigenvectors corresponding to the leading eigenvalues span a subspace in the low-dimensional data space, where the multi-label classification are performed.
- To examine the performance of the proposed method, we conducted some interesting experiments on several real-world multi-label data collections. Results have demonstrated that our approach outperforms some competing alternatives.

The remainder of this work is structured as follows. Section II reviews some related works. We introduce the proposed Hypergraph guided Orthonormalized Partial Least Squares method in Section III. Experimental results are reported in Section IV with rigorous analysis. Finally, the concluding remarks are provided in Section 5.

II. Related Works

In this section, we give a brief review on recent works related to our method. Multi-label learning has gained increasing attention in the last decade, due to its widespread applications in many areas, e.g., image annotation, video retrieval and webpage categorization. A latest comprehensive review on multi-label learning algorithms can be referred to [12]. In these applications, the dimensionality of multi-label data is often very high, which is computationally expensive. Therefore, it is very meaningful to reduce the dimension of multi-label data prior to further processing them.

Heuristically, we can directly employ unsupervised methods in single-label learning, e.g., PCA[7]. Besides, we can use matrix factorization methods to obtain the low-dimensional representations, such as manifold kernel concept factorization [13] and discriminant orthogonal nonnegative matrix factorization [14]. But it is a common fact that the dimensionality reduction can be better performed while guided by supervised information, such as pairwise constraints or labels themselves. This poses a challenge for multi-label data since several labels might be associated with each data point. If we treat each label set as an individual, the number of label combinations is always too huge to handle and the label correlations are neglected as well. To this end, a number of methods have emerged to address this issue for regression and classification [8, 15, 16, 17, 18]. Among these methods, Partial Least Squares (PLS) [9] and Canonical Correlation Analysis (CCA) [8] are two representative ones, which are used for finding the relationships between two sets of variables.

Partial least squares maximizes the covariance along the maximum direction while canonical correlation analysis finds the directions of maximum correlation [10]. Specifically, PLS is shown to be useful when the number of observed variables is much larger than that of observations. Generally, PLS maximizes the covariance between different sets of variables to obtain orthogonal score vectors or components. Orthornormalized PLS (OPLS) is one of its variants to be studied in this work. Essentially, there exists a close connection between PLS and CCA in discrimination and the equivalence relation between OPLS and CCA has been proved [10]. Both of them can be naturally applied to multi-label data, in the sense that the label set with multiple dimensions caters to a set of multi-dimensional variables for CCA and PLS. They can be also performed in reproducing kernel Hilbert space by using kernel tricks [19]. Besides, some researchers attempt to extend the Linear Discriminant Analysis (LDA) to multi-label scenario by considering the label relations in the between-class and within-class scatter matrices [20]. In addition, some works try to maximize the dependence between the data features and the labels through using Hilbert-Schmidt Independence Criterion (HSIC) for multi-label dimensionality reduction [20]. Nevertheless, the label correlations still remain unclear thus requiring further explorations.

Hypergraph is employed to address this point in recent works for multi-label classification [21, 11]. In particular, a hypergraph is able to capture high-order relations among different categories in multi-label data. Each vertext represents an instance and each hyperedge includes all instances sharing the same label. Empirical studies have shown the effectiveness of hypergraph in revealing the intrinsic label relations, which inspires us to impose the hypergraph regularization onto orthonormalized partial least squares. Details are narrated in the following section.

III. Our Methods

In this section, we introduce the proposed Hypergraph Orthonormalized Partial Least Squares (HOPLS) algorithm for multi-label classification. We begin with the problem formulation.

A. Problem Formulation

Given a set of training multi-label data points $\{x_1,...,x_n\}$, each of which is stacked in the column of a data matrix $X \in \mathbb{R}^{m\times n}$. In other words, these data points reside on am-dimensional Euclidean space. Each data point might be associated with more than one labels and the maximum number of the labels is c. Thus, the corresponding label matrix can be denoted by $Y \in \mathbb{R}^{c\times n}$,which is an indicator matrix, where $Y_{ki}=1$ holds if x_i belongs to the $k-th$ class c_k, otherwise $Y_{ki}=-1$. In this work, both the data matrix and the label matrix are assumed to be centered, such that the cumulative column-wise sum in the data space is zero. Note that throughout this paper I is the identity matrix and $\mathrm{A}^{\dagger}$ denotes the pseudo-inverse of the matrix A.

Our goal is to learn a projection matrix $W \in \mathbb{R}^{m\times d}$ from the training data and the label matrix. By using this projection matrix, the original high-dimensional data points can be mapped onto a ddimensional data space, which suffices to $d \ll m$. In this way, the unseen data (e.g., out-of-sample problem) can be projected onto a much lower-dimensional data space via this transformation matrix W, such that the most prominent components are preserved for discrimination, thus benefitting multi-label classification.

B. Hypergraph

Hypergraph [6] is a generalization of traditional graph and yet it has some nice merits, namely the high-order relations among different objects can be captured for further analysis.

Mathematically, we define a hypergraph $G=(v,\varepsilon)$ where v is the vertex set containing the data points each of which acts as a vertex, and ε denotes the set of the hyperedges. Each hyperedge includes all samples sharing the same label, i.e., each label has an affiliated hyperedge e. Suppose that each hyperedge is assigned a weight $w(e)$ and the number of vertices in e is denoted by $\delta(e)$, i.e., the degree of a hyperedge. Thus, the degree in a conventional simple graph remain 2. The degree $d(v)$ of a vertex v is

$$d(v)=\sum_{v\in e, e\in\varepsilon} w(e) \tag{1}$$

The vertex-edge incidence matrix $J \in \mathbb{R}^{|V|\times|E|}$ is defined as

$$J(v,e)=\begin{cases}1, & if\ v\in e\\ 0 & otherwise\end{cases} \tag{2}$$

As a result, we obtain

$$d(v)=\sum_{e\in\varepsilon} W(e)J(v,e) \tag{3}$$

$$\delta(e)=\sum_{e\in v} J(v,e) \tag{4}$$

The diagonal matrix forms for $d(v)$, $\delta(e)$ and $w(e)$ are respectively D_e, D_v and W_h. The Laplacian matrix from a traditional graph has been widely used to learn from graphs [11, 24]. It is clear that graph Laplacian is the discrete analog of the Laplace-Beltrami operator on compact Riemannian manifolds, which reflect the intrinsic structure of the data. In this work, we utilize a commonly used Clique Expansion algorithm to construct our hypergraph Laplacian.

Note that we add a subscript to the above notations for discrimination in clique expansion. Thus, the edge weight $w_c(u,v)$ of G_c is defined by

$$w_c(u,v)=\sum_{u,v\in e, e\in\varepsilon} w(e), \tag{5}$$

whose matrix form can be written as

$$W_c = HWH^T \tag{6}$$

We define

$$D_c(u,u)=\sum_{v} w_c(u,v), \tag{7}$$

then the combinatorial Laplacian L_c is shown as

$$L_c = D_c - W_c \tag{8}$$

Usually, we make use of its normalized version, i.e.,

$$L_n = D_c^{-1/2} L_c D_c^{-1/2} \tag{9}$$

In clique expansion, the similarity between two data points is positively proportional to the weights of their common labels, thus capturing the intrinsic relationship among different classes. This motivates us to enforce hypergraph as a regularizer to orthonormalized partial least squares in the following part.

C.Orthonormalized PLS with hypergraph regularization

Different from CCA that maximizes the correlation of two sets of variables in the transformed space, Orthonormalized PLS (OPLS) attempts to find the principal directions of maximum variance with orthogonality constraints. Formally, OPLS computes the orthogonal score vectors for X by solving

$$\max_{w}\ T_r(W^T XY^T YX^T W),$$
$$s.t.\quad W^T XX^T W = I, \tag{10}$$

Algorithm 1 Hypergraph Orthonormalized Partial Least Squares (HOPLS)

Input:

A collection of training data points $\left[x_{1,\cdots,}x_n\right]=X\in\mathbb{R}^{m\times n}$ the label matrix $Y\in\mathbb{R}^{c\times n}$ the constant parameters $a,\lambda>0$

Output:

The projection matrix $W\in\mathbb{R}^{m\times d}$.

1: Initialize the weights $w(e)$ for the hyperedges.

2: Compute the normalized graph Laplacian matrix L_n for the hypergraph using Clique Expansion as shown in (9).

3: Compute the matrix $S=I-L_n$.

4: Optimize the objective function in (11) by solving the generalized eigenvalue problem in (13).

5: Construct the projection matrix W by the eigenvectors corresponding to the top d eigenvalues.

where W is a projection matrix for learning a low-dimensional data representation. Inspired by the success of hypergraph in multi-label learning [11], we impose it onto the objective function in (10) as a regularization term, thus additionally capturing the high-order relations among different labels. Now, we can readily formulate the proposed HOPLS algorithm as

$$\max_{w}\ T_r[W^TX(Y^TY+\alpha S)X^TW],$$
$$s.t.\quad W^TXX^TW=I, \tag{11}$$

Where $S=I-L_n$ captures the high-order label relationships and $a>0$ is a tradeoff parameter for balancing the contribution of the hypergraph regularizer to the objective function. Thus, the proposed method is able to maximize the relation between the data points and the corresponding labels as well as to respect the high-order relations among different class labels. Note that the matrix $\hat{S}=Y^TY+aS$ is symmetric and semi-definite positive. If we assume $\hat{S}$ is full-rank, then it is a well-defined matrix having the inverse.

Observing the objective function in (11), we find it is a generalized eigenvalue problem given by

$$X\left(Y^TY+aS\right)X^Tw=\eta XX^Tw \tag{12}$$

Where η is the eigenvalue variable and w is the corresponding eigenvector. Therefore, the optimal projection matrix W can be derived from solving this eigen-decomposition problem. The eigenvectors corresponding to the topdeigenvectors spans the row space of W.

Furthermore, it is commonly believed that regularization is a popular technique to penalize the complexity of a learning model and regularized CCA is shown to have natural statistical interpretations [10]. Hence, we can directly show the regularized HOPLS by adding a regularization term to XX^T, leading to the following formulation:

$$X\left(Y^TY+aS\right)X^Tw=\eta\left(XX^T+\lambda I\right)w, \tag{13}$$

Where λ is positive constant to avoid overfitting and also control the model complexity.

In summary, the complete procedures of our approach is structured clearly in Algorithm 1.

Moreover, we provide the whole framework of our proposed HOPLS method using MLKNN as the classifier in Fig.2.

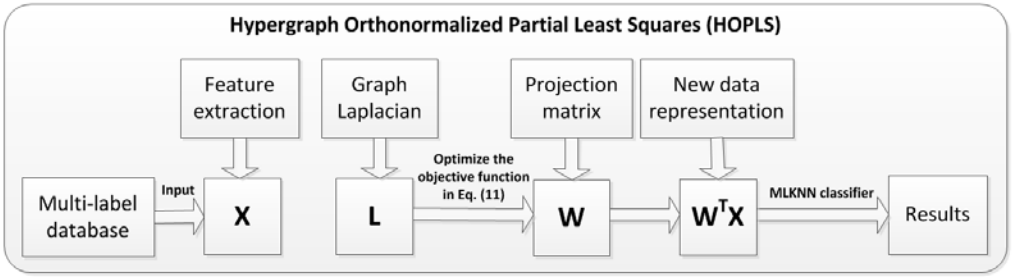

Fig.2 Framework of HOPLS using MLKNN as the classifier

IV. EXPERIMENTS

We have conducted a number of experiments on several multi-label data sets to justify the proposed method as compared to the competitive alternatives. For all algorithms, we use MLKNN[4] as the base classifier to predict the possible label sets in a lower-dimensional data space. For each data set, they are randomly divided into two parts, leading to 70% as the training data and the rest as the test data. Parameter settings are as follows. We set the number of nearest neighbor for MLKNN to 10 as default. The number of projected components is set to the number of classes in the data set. The regularization parameters are searched from the grid $\{10^i\,|\,i=-3:3\}$ and the best parameters are derived from cross-validation on the training data. The hyperedge weights of HOPLS are set as in [6]. Note that we tuned the tradeoff parameters in smaller bins, i.e., $[0.1:0.1:1]$, for better performance. To eliminate the bias, we repeat the experiments ten times, and report the averaged values.

A. Data Sets

In this test, we collect four multi-label data sets to investigate the performance of our approach from various domains, including music (emotions), image (scene), gene expression (genbase) and text document (medical). They are available at http://mlkd.csd.auth.gr/multilabel.html.

The music data emotions contains 593 songs, each of which has 72 features, and can be affiliated with 6 different styles. The scene data consists of 2407 images and refers to six scenarios, where each image is represented as a 294 dimensional vector. The biology data genbase is composed of 662 instances that are associated with at most 27 labels. The medical data includes 978 documents with 1449 features, covering 45 different topics. We summarize the statistics of these data in Table 1.

TABLE I.
SUMMARY OF STATISTICS OF THE DATA SETS.

Data set	domain	instances	features	labels	cardinality	density	distinct
emotions	music	593	72	6	1.869	0.311	27
scene	image	2407	294	6	1.074	0.179	15
genbase	biology	662	1185	27	1.252	0.046	32
medical	text	978	1449	45	1.245	0.028	94

B. Performance Evaluation

We make use of macro F1-score, precision and recall[3] as the evaluation criteria to examine the performance of the proposed HOPLS method and all the compared algorithms in the following.

- Principal Component Analysis (PCA) [7].
- Locality Preserving Projection (LPP) [22].
- Canonical Correlation Analysis (CCA) [8].
- Multi-label informed Latent Semantic Indexing (MLSI) [16].
- Multi-label Dimensionality reduction via Dependence Maximization (MDDM) [20].
- Orthonormalized Partial Least Squares (OPLS) [10].

Among the above methods, PCA and LPP are unsupervised methods while the rest are all supervised methods. Multi-label classification were conducted in the lower-dimensional data space derived from these approaches.

TABLE II.
THE F1-SCOREON DIFFERENT COMPARISON METHODS

Data set	PCA	LPP	CCA	MLSI	MDDM	OPLS	HOPLS
emotions	0.4282	0.4831	0.6158	0.4208	0.6421	0.6479	**0.6615**
scene	0.6277	0.6331	0.6313	0.6423	0.6358	0.6445	**0.6538**
genbase	0.9230	0.9287	0.9065	0.9520	0.9488	0.9509	**0.9569**
medical	0.6338	0.6317	0.6776	0.7178	0.6964	0.7205	**0.7352**

TABLE III.
THE PRECISIONON DIFFERENT COMPARISON METHODS

Data set	PCA	LPP	CCA	MLSI	MDDM	OPLS	HOPLS
emotions	0.6162	0.6045	0.6834	0.6211	0.6888	0.6971	**0.7127**
scene	0.7006	0.7077	0.7023	0.7073	0.6972	0.7087	**0.7290**
genbase	0.9896	0.9905	0.9888	0.9916	0.9958	0.9947	**0.9972**
medical	0.7624	0.7559	0.7128	0.7688	0.7426	0.7635	**0.7748**

TABLE IV
THE RECALLON DIFFERENT COMPARISON METHODS

Data set	PCA	LPP	CCA	MLSI	MDDM	OPLS	HOPLS
emotions	0.3305	0.4022	0.5613	0.3225	0.6020	0.6074	**0.6369**
scene	0.5678	0.5668	0.5740	0.5886	0.5847	0.5914	**0.6114**
genbase	0.9008	0.9103	0.8915	0.9109	0.9062	0.9109	**0.9147**
medical	0.5437	0.5479	0.6468	0.6738	0.6561	0.6826	**0.6984**

C. Results and Analysis

Experimental results are reported in Table 2 to Table 4. The best performances on each data set are highlighted in boldface. To examine the classification performances with the varied size of training data, we depict the curves of the three evaluation metrics onemotionswith increasing ratios of training samples in Fig. 1.

A number of interesting points can be observed from these results.

- The proposed HOPLS algorithm systematically and consistently outperforms other competing methods. We attribute this to the fact that a hypergraph is utilized as a regularizer in HOPLS to encode the high-order relations among different labels, thus capturing the intrinsic label structure for more discriminating power of the model. This justifies our theoretical analysis.

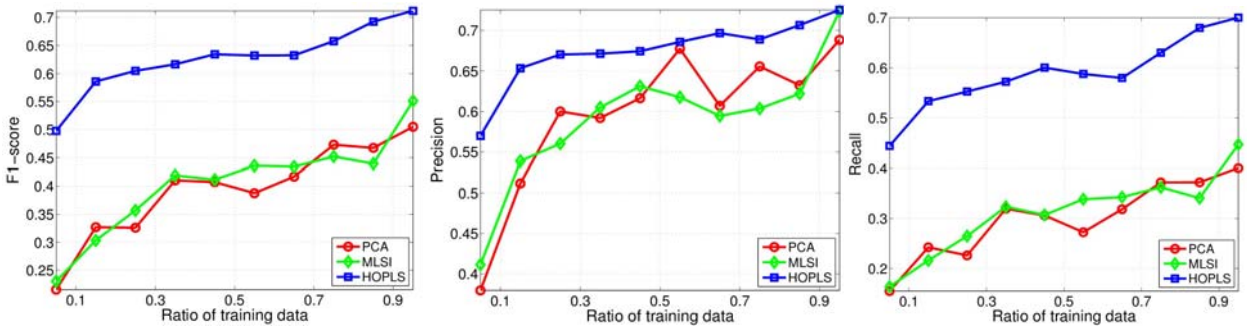

Fig.1: Multi-label classification performance with increasing ratios of training data onemotions. Results are averaged over five test runs.

- Mostly supervised methods perform better than unsupervised methods (i.e., PCA and LPP), which confirm that projection under the guidance of label information will lead to a more discriminant low-dimensional data space, thus improving the multi-label classification performance.
- With the increase of the training data points, the classification performance would be boosted gradually regardless of supervised or unsupervised methods. The reason for this is that more data points lead to a more robust and discriminating model for learning a betterstructured data space.

V. Conclusion

This paper presents a novel method for multi-label classification, i.e., Hypergraph Orthonormalized Partial Least Squares (HOPLS). Essentially, it is strongly motivated by the success of hypergraph to encode the high-order relations among different labels. In this work, we incorporate the intrinsic label information into the orthonormalized partial least squares, which has been shown to have satisfying performance on multi-label problems. To consider the complex label relations, we impose the hypergraph regularizer onto the objective function of OPLS, leading to a generalized eigenvalue problem. Empirical studies on some multi-label data sets have shown more promising performances by the proposed method in comparison with others.

Acknowledgment

The authors would like to thank the anonymous reviewers for their helpful advices to improve this paper. This work was supported in part by a grant from the Construction Program of the Key Discipline in Hunan Province of China and the Key Scientific Research Program of Department of Education of Human Province (NO.13A091).

References

[1] X. Feng, H. Zhang, H. Ji, S. Zhang, “TMLLC: Transductive multi-label learning based on local correlation”, *Journal of Information & Computational Science*, 10(1), 2013, 297-311

[2] H. Li, Y. Guo, M. Wu, P. Li, Y. Xiang, “Combine multi-valued attribute decomposition with multi-label learning”, *Expert Systems With Applications*, 37(12), 2010, 8721-8728

[3] G. Tsoumakas, I. Katakis, I. Vlahavas, “Mining multi-label data”, Data mining and knowledge discovery handbook, Springer, 2010, 667-685

[4] M. Zhang, Z. Zhou, Ml-knn: “A lazy learning approach to multi-label learning”, *Pattern Recognition*, 40(7), 2007, 2038-2048

[5] G. Qi, X. Hua, Y. Rui, J. Tang, T. Mei, H. Zhang, “Correlative multi-label video annotation”, in *MM’07: Proc. of the 15th International Conference on Multimedia*, ACM, 2007, 17-26

[6] F. Wang, X. Wang, B. Shao, T. Li, M. Ogihara, “Tag integrated multi-label music style classification with hypergraph”, in *ICMIR’09: Proc. of the 10th International Conference of Music Information Retrieval*, 2009, 363-368

[7] H. Abdi, L. Williams, “Principal component analysis”, Wiley Interdisciplinary Reviews: *Computational Statistics*, 2(4), 2011, 433-459

[8] L. Sun, S. Ji, J. Ye, Canonical correlation analysis for multilabel classification: “A least-squares formulation, extensions and analysis”, *IEEE Transactions on Pattern Analysis and Machine Intelligence*, 33(1), 2011, 194-200

[9] C. M. Bishop, N. M. Nasrabadi, “Pattern recognition and machine learning”, *Springer*, New York, 2006

[10] L. Sun, S. Ji, S. Yu, J. Ye, “On the equivalence between canonical correlation analysis and orthonormalized partial least squares”, in IJCAI’09: *Proc. of the 21st International Joint Conference on Artificial Intelligence*, 2009, 1230-1235

[11] L. Sun, S. Ji, J. Ye, “Hypergraph spectral learning for multi-label classification”, in KDD’08: *Proc. Of the 14th*

International Conference on Knowledge Discovery and Data mining, ACM, 2008, 668-676

[12] M. Zhang, Z. Zhou, "A review on multi-label learning algorithms", *IEEE Transactions on Knowledge and Data Engineering, in press*, 2013, doi : http://dx.doi.org/10.1109/TKDE.2013.39

[13] P. Li, C. Chen, J. Bu, "Clustering analysis using manifold kernel concept factorization", *Neurocomputing*, 87, 2012, 120-131

[14] P. Li, J. Bu, Y. Yang, R. Ji, C. Chen, D. Cai, "Discriminative orthogonal nonnegative matrix factorization with flexibility for data representation", *Expert Systems With Applications*, in press, 2013, doi: http://dx.doi.org/10.1016/j.eswa.2013.08.026

[15] G. Tsoumakas, I. Katakis, "Multi-label classification: An overview". *International Journal of Data Warehousing and Mining*, 3(3), 2007, 1-13

[16] K. Yu, S. Yu, V. Tresp, "Multi-label informed latent semantic indexing", in SIGIR'05: *Proc. of the 28th ACM SIGIR Conference on Research and Development in Information Retrieval, ACM*, 2005, 258-265

[17] H. Li, P. Li, Y. Guo, M. Wu, "Multi-label dimensionality reduction based on semi-supervised discriminant analysis", *Journal of Central South University of Technology*, 17, 2010, 1310-1319

[18] P. Li, H. Li, M. Wu, "Multi-label ensemble based on variable pairwise constraint projection", *Information Sciences*, 222, 2013, 269-281

[19] J. Arenas-Garc´\u305Xa, G. Camps-Valls, "Efficient kernel orthonormalized pls for remote sensing applications", *IEEE Transactions on Geoscience and Remote Sensing*, 46(10), 2008, 2872-2881

[20] Y. Zhang, Z. Zhou, "Multilabel dimensionality reduction via dependence maximization", *ACM Transactions on Knowledge Discovery from Data*, 4(3), 2010, issue 14

[21] G. Chen, J. Zhang, F. Wang, C. Zhang, Y, Gao, "Efficient multi-label classification with hypergraph regularization", in CVPR'09: *Proc. of the International Conference on Computer Vision and Pattern Recognition, IEEE*, 2009, 1658-1665

[22] X. He, P. Niyogi, "Locality preserving projections", *Advances in Neural Information Processing Systems*, 16, 2004, 153-160

[23] Wenbin Zheng, Yuntao Qian, Minchao Ye. "A Grouped Structure-based Regularized Regression Model for Text Categorization". *Journal of Software*, Vol 7, No 9 (2012), 2119-2124.

[24] Wencheng Wang, Faliang Chang. "A Multi-focus Image Fusion Method Based on Laplacian Pyramid". *Journal of Computers*, Vol 6, No 12 (2011), 2559-2566.

[25] Zhengguang Xu, Jinxia Wu, Shoude Qu. "Prediction Model based on Moving Pattern". *Journal of Computers*, Vol 7, No 11 (2012), 2695-2701.

[26] Shi Qu, Ronghuan Yu, Yingmei Wei, Lingda Wu. "Gaussian Process Latent Variable Models for Inverse Kinematics". *Journal of Multimedia*, Vol 6, No 1 (2011), 48-55

Gaofeng Luo received the M.S. degree in Information and Communication Engineering from Central South University, China, in 2010. He is currently a lecturer in Shaoyang University, China. Also, he is the Office Director of the Key Laboratory of Southwest Hunan Rural Information Service, Hunan Province. His research interests include Internet of things and artificial intelligence.

Tongcheng Huang received the PhD degree in Information and Communication Engineering from Shanghai University, China, in 2008. Before that, he received the M.S. degree from National University of Defense Technology, China, in 2000. He is currently a Professor and Master supervisor in Shaoyang University, China. Also, he is the Leading Director of the Key Laboratory of Southwest Hunan Rural Information Service, Hunan Province. His research interests include Intelligent Information Processing and artificial intelligence.

Research on Cloud-Based Mass Log Data Management Mechanism

Fengying Yang
School of Information Engineering, Huanghuai University, Zhumadian, China
Email: yfyinghh@yeah.net

Huichao Liu and Zhanping Zhao
School of Information Engineering, Huanghuai University, Zhumadian, China
Email: yfyinghh@yeah.net

***Abstract*—In this paper, we study the file management mechanism of large-scale cloud-based log data. With the rise of big data, there are more and more the Hadoop-based applications. Log analysis is an important part of network security management, but the existing network log analysis system can't deal with huge amounts of log data, or only use offline mode which with a longer response delay. Therefore, building the online Hadoop-based log processing system is necessary. However, how to effectively manage vast amounts of log data have become the key problems of such system. To this end, this paper puts forward a new hierarchical file archiving (HFA) mechanism which can realize the hierarchical and sorted storage of massive amounts of log data. In addition, some feasible methods for the mechanism are also proposed. Through the HFA mechanism, the traditional log analysis mode and Hadoop-based offline analysis mode can be combined to achieve the online Hadoop-based log analysis system, which have good scalability that can effectively store and handle the massive log data, and faster response speed for user request to meet the requirements of online processing. The feasibility and effectiveness of the HFA mechanism have been verified by the experiment of a small log process system.**

***Index Terms* —Network security, Log analysis, Hadoop, File management, Hierarchical file archiving mechanism, Online system**

I. INTRODUCTION

With the rise of big data, the number of Hadoop-based application and research continues to increase [1-6], and the application areas also keep expanding [7-9]. Conventional log data processing models cannot deal with the massive amount of log data for large network systems, so Hadoop-based log analysis systems are emerged [10-14]. However, almost all of the current Hadoop-based log analysis systems use offline processing mode, which means that the raw log data should be merged and clean in advance into the large data files which already have the clear structure and reasonable layout, and the analysis system only need to focus on business processes, and don't need to care about the complex log file management issues. Moreover, the response time of log analysis to user request is also not strict.

But in order to build online Hadoop-based log analysis system, the more complex situations will be faced [15]. On the one hand, the requirements of response time to process user requests in online log analysis system will be higher. The system must efficiently handle the various query and analysis requests in time or even in real-time. In addition, the response contents generated by system also should include the processing of the latest log data. On the other hand, log data are the stream data. Therefore, online log system must timely receive numerous log records from various log sources, and meanwhile, split the data stream into separated log file for appropriate size to store in the HDFS. For a large network system, the amount of log data that need to be store can be up to tens of TB or PB level [16]. If the size of log file is set too small, a large number of small files will be produced which could seriously impact the performance of Hadoop. Otherwise, if the size is too large, the update cycle of log file will be very long, that could result in the response for user request cannot contain the latest data.

Based on the above analysis, the online Hadoop-based log analysis system must have the high performance and massive storage capacity. Moreover, it also must have a valid file organization and management mechanism with good scalability. On the one hand, the scale of small file should be controlled reasonably in order to reduce the impact on system performance [17]. On the other hand, some effective methods should be taken for organizing the historical log data to meet the needs of business process, and remaining the relatively stable for file system structure when increasing the amount of log data to ensure the stability of system performance. Therefore, build a good organization and management mechanism of the log data is the key for online Hadoop-based log analysis system.

Hadoop platform also provides some mechanisms and tools for the processing of small files, such as HAR, SequenceFile and CombineFileInputFormat et al. But they all have some limitations. In addition, the literatures [18-21] have introduced some solutions for some kinds of specific application environment (such as WebGIS, Bluesky courseware delivery system and the Chinese font engineering). These works solve the problem of small file by adding a small file processing module above the

doi:10.4304/jcp.9.6.1371-1377

original HDFS file system. The design idea of the small file processing module is to archive some related small files into one large file firstly, and then create an index file for these small files for quick access.

In this paper, a hierarchical file archiving mechanism is proposed for the log data management based on the characteristic of online log analysis system, and some feasible methods of this mechanism are also present. The basic idea of hierarchical file archiving mechanism is to save the log data into different files which have different levels that are consistent with the access frequency of the log data. The data with higher access frequency will be saved in a relatively smaller file; otherwise, the larger file will store the data which has less access frequency. Thereby, this will form a pyramid and inverted pyramid hierarchy for log files and data storage structure respectively. The hierarchical file archiving mechanism can effectively solve the problem of small files through reducing the file size and maintaining reasonable file number to organize the global data space. The system which using this mechanism can maintain the good scalability, and improve the system performance and user experience.

Organization of the rest of this paper is as follows. The Hadoop environment is briefly reviewed in Section II. In Section III, the hierarchical file archiving mechanism and some feasible methods are proposed. The implement architecture of the mechanism is introduced in section IV. In Section V, a simple experiment for the mechanism is taken, and the results are given. Finally, the work is concluded in Section VI.

II. Hadoop File System

The Hadoop is a framework that allows for the distributed processing of large data sets across clusters of computers using simple programming models [14]. It is designed to scale up from single servers to thousands of machines, each offering local computation and storage. Hadoop is designed to detect and handle failures at the application layer, so delivering a highly-available service on top of a cluster of computers. Hadoop includes many important modules, but the basis of which are HDFS (Hadoop Distributed File System), which is a distributed file system that provides high-throughput access to application data, and MapReduce, which is a system for parallel processing of large data sets.

A. Read and Write Operation of HDFS

Hadoop Distributed File System (HDFS) is the default and widely used file system of the Hadoop platform. The main operation supported by HDFS are read, write and append, while the alter operation is not provided.

The procedure to read a file is indicated in Fig. 1, which include two main steps:

1) Client sends the read command to NameNode. If the file is not existence, error information will be returned. Otherwise, the blocks corresponding to the file and its position in DataNode will be sent to Client.

2) After receive the position information of the blocks, Client will connect to different Datanode, and get the data in parallel.

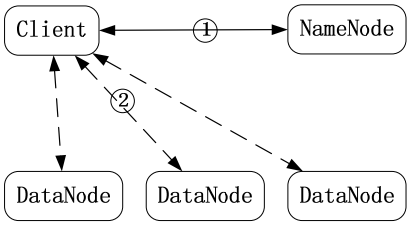

Figure 1. Read operation of HDFS.

Fig. 2 shows the procedure of the write operation, in which four steps are included:

1) Client sends the write file command. NameNode checks the file to see if the file exists. If it is, the error information will be return directly. Otherwise, NameNode will send a useful DataNode node list to Client.

2) Client splits the file into some blocks, and sends each block concurrently to different DataNode. When the sending complete, Client send message to NameNode and DataNode.

3) When receiving the message from Client, NameNode send a confirmation message to DataNode.

4) After receiving the confirmation messages from NameNode and Client, DataNode submits the write operation, and completes the file storage process.

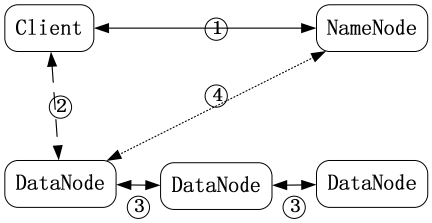

Figure 2. Write operation of HDFS.

B. Hadoop File Merging Mechanism

Hadoop also offers several file merging solutions for the problem of small file process. They are Hadoop Archive, Sequence file, CombineFileInputFormat and Append operation [17, 22].

Hadoop Archive or HAR is a new file system above the Hadoop file system, and also an efficient archiving tool that can package a number of small files into a HAR file and store it in some whole HDFS blocks. HAR mechanism can save the storage of HDFS, reduce the usage of memory in NameNode, and support the transparent access for those small files. Creating a HAR file is actually to run a Mapreduce job on a Hadoop cluster. In addition, once a HAR file is created, it cannot be changed. It must be re-created when add or remove the contents of the HAR file.

Sequence file consists of a series of binary Key/Value pairs. Hence the large numbers of small files can be merged into one large sequence file by setting the file name to the Key, and save the contents of the small file to the Value.

CombineFileInputFormat is a new format of Inputformat, used to combine multiple small files into a single split when running a Mapreduce job. In addition, the store locations of these small files are also taken into account for using.

The HDFS append operation has been redesigned and implemented in Hadoop 1.0 to fix some defects existed in previous versions. The new HDFS append operation is more complex for involving many interactions between Client, Namenode and Datanode. From the Client perspective, appending new data to an existed file need to call the append operation of *DistributedFileSystem* firstly, which will return an *FSDataOutputStream* stream object, namely *out*. Then the function *out.write*() should be called to append data to the file. Finally, the function *out.close*() should be executed to close the file.

C. Existed Small Files Handling Systems

Hadoop platform is designed for large data processing, and there is no universal system-level solution for the problem of small files so far. However, the small file problem is existed widely in many application fields, and some solutions have been proposed in some works. Literature [18] utilizes the data dependencies feature in WebGIS system to merge the small files which stored in adjacent location into one large file, and then creates an index file for these small files for quick access. Literature [19] proposed an HDFS small file storage solution base on the characteristics of Bluesky system. First, the files that belong to the same courseware will be archive into a large file in order to improve the storage efficiency of small files in HDFS. Second, the two-level pre-fetching mechanisms are proposed to enhance the reading efficiency of small files, which includes both the index file pre-fetching and data file pre-fetching. When using index file pre-fetching to access a file, the index file corresponding to the block which contains the small files will be loaded into memory firstly, so that the Client no longer need to interact with NameNode when access the other files. When using data file pre-fetching, all the files concern to the same courseware will be loaded into memory, so the access speed will be significantly improved when access the other files.

These works attempt to add a small file processing module base on the original HDFS to process the small files. Firstly, the module merges many small files which have some relevance into a large file. And then an index file is created for these small files for quick access. The mergence can not only increase the storage efficiency, but also improve the speed of application processing.

III. HIERARCHICAL FILE ARCHIVING MECHANISM

A. File Management Requirements

If the file stored in HDFS is not closed, the existence of the file cannot be observed by Client. But the user response in online log analysis system requires the processing of latest log information. This makes the online log analysis system must cut the log stream in time when receiving log data, and form separate log files which contains the received small amount of log information in short time. This approach can significantly reduce the data update cycle, and improve the real-time effect of log analysis. The timeliness of the response is undoubted a very important indicator for an online log analysis system, but it also will produce a large number of small files.

Too many small files would seriously affect the performance of Hadoop. Hadoop is designed to handle the large files, and the file storage unit is block which default size is 64M. If the size of file is less than the default size of block, the file will still take up a separate block for storage. Therefore, Excessive number of small files will significantly reduce the system storage efficiency. In addition, the metadata information of each file is stored in Namenode and resides in memory. If the number of small files is too many, the file namespace and memory cost will be very large in NameNode, and the processing cost for each request will be very time consuming. The Hadoop may also be crash due to the memory limitations in some case. If the problem of small file cannot be solved effectively, to build the online log analysis system is pointless.

Using the file merge methods provided by Hadoop to solve the small file problem is not a feasible idea. On the one hand, these files merge methods have some drawbacks which could result the merge cost or file access cost is too high. On the other hand, the primitive merge idea of these methods is also not suitable for the application features of online log analysis system. In which the distribution of log data is too concentrated will also produce some serious system performance issues. In the online log system, not all businesses are required of all data sets. Instead, only a few operations need to manipulate large data sets. Large number of operations is focus on the current or recent data. The longer of the historical data, the access frequency of the log data will be lower. If the data is too centralized, each business will involve a lot of useless data processing, which is bound to improve the system processing performance.

Therefore, the appropriate file management mode must be selected to solve the problem of small file by organizing the system data effectively, and make the system not only has better scalability, but also have better performance to meet the needs of user response time.

B. The Ideas of Hierarchical Archiving

Hierarchical file archiving mechanism is proposed based on the application characteristics of online log analysis system. This mechanism need to firstly set the different archiving levels in accordance with certain archiving criteria. When the lower-level file reaches the archiving standard, the mechanism will be started to merge the lower-level files into one upper-level file, and empty the old files meanwhile. When after a certain time, the lower-level files could reach the archiving standards again, and the archiving program will also be started. The similar methods will be used to archive the upper-level files to more high-level file when the file archiving standards is arrived. So after the cycle of step by step, the finished system file structure and storage structure will form a pyramid and inverted pyramid structure, shown in

Figure 3. Log analysis system splits log stream by the first-level file standard, and forms the bottom-level log file. Within the file structure of the system, the higher of the level, the less of the files number, and vice versa, thereby a positive pyramid structure is formed. However, in the storage structure, the lower level, the less amount of stored data, so an inverted pyramid structure is formed.

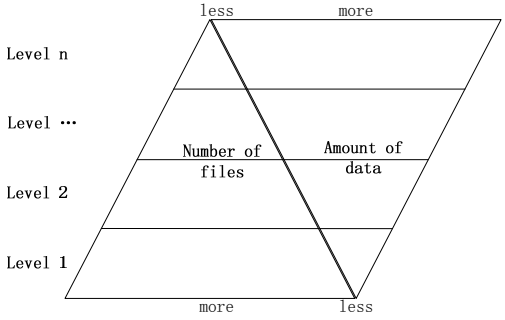

Figure 3. File and storage structure.

A good file archiving mechanism should have the following characteristics:

1) File merging frequency must be low. If the file merges too often, it will increase the burden of the system undoubtedly.

2) Average file merge cost should be small. This requires reducing the bigger cost merge operation as far as possible.

3) File system should have good scalability. Files number in the system should remain relatively stable, could not have a greater change with the increase of the amount of log data.

4) File structure should meet the needs of application. The partitions of file should fit the application needs of the data set, and minimize the chance of cross-file operations.

C. Hierarchical File Archiving Mechanism

Since the log data structure is relatively simple, just consisted by the text log record, so the log file has better divisibility. Therefore, the mergence or reorganization for log files has greater flexibility, which only needs to keep the integrality of the log record. For different application needs, it can be specified by different hierarchical archiving standards, such as archiving by content attributes, by file size, by files number, by time attribute of log data, by comprehensive multiple factors and so on.

1) Archiving by files size

First of all, the standards of file size should be set for different levels of the archiving mechanism. Log system splits log stream and forms log file according to the first-level archive file size. When the data size of lower-level file is greater than or equal to the higher-level file size standard, then the system will start archiving process and merge the lower-level files into a upper-level file. For example, setting the first-level file size is 64MB, the file size of the second and third level is 1GB and 1TB respectively. When the number of first-level file reaches 16 (16 * 64MB = 1GB), the system starts the archiving program to form a second-level file. When the number of 1GB file reaches 1024, they will be merged into the third-level file.

Hierarchical archiving by the file size has the advantage that it can translate the large data process in log analysis system into a series of sub-operation. When processing a query, the system can be firstly carried out the sub-operations on lower-level file. Because the small data size of lower-level file, the system can complete and return the response in a shorter time. While the user to process the returned results, the system could start a new search for higher-level file. This enables the user processing and system processing in parallel. Furthermore, if the user has found the result of the needed, the subsequent sub-operations should be abort. Using this file organization model can not only ensure that the system can respond faster, but also to process all log data gradually.

Achieving by file size can guarantee that the file size in every level is constant. For the predictable data size, the maximum amount of files needed to maintain by system can be easily calculated. Therefore, the scalability of the file system is very good, and the maximum number of files changed very little as the data size increasing. With this mechanism, the archiving opportunity of system performing is uncertain. When the log flow is large, the period to formation equal size file will be short, and the times for file archiving will be more. And vice versa, the chance of archiving file will be decreased when the data flow is small. But because of the network log flow has its periodicity, and the amount of log data files with different level is different, the higher-level file will have the smaller effect by the changing of data flow.

2) Archiving by number of files

Firstly, the desired levels and the number of files standard for each archiving level need to be set. When the number of current-level files accumulates to the archiving standards for next-level files, system will start the file archiving operations to form a higher-level file. Assume that the number of files for every archiving level is set to 400, when the number of files reaches 400 for each level, the lower-level file will be archived into an upper-level file.

Archive by the number of files has the similar effect with the archiving by file size. The system processes each file step by step, which can ensure the response speed, and improve the user experience.

However, there are some differences between the two methods: archiving by the number of files can ensure the regularity of archived files within the same time interval. But it cannot guarantee the uniformity of size of each merged file. When the log flow enlarges, the size of the log file archived within the interval will be very large. On the contrary, the size of the file may be smaller. But this effect mainly occurred in the low-level file, the more upper-level file the smaller of the influence on it.

3) Archiving by log time

The frequencies of use of log data will become less with its time growing. Users are always taking more interested in current or recent log data, even though the historical data also is valuable. Therefore, we can make different

archiving time standards according to different application environments. Equidistant time standards are one of the feasible methods, such as one week, two weeks, three weeks, etc. Non-equidistant time standard is another good choice, such as one day, one week, one month, one quarter and more than one year and so on. In the latter for instance, system archives the accumulated data within one day to form a daily log file. The weekly archived data was formed by merging the log data accumulated in a week. And so on, log files within different time periods can be created.

Time is an important attribution for the log query. Therefore, the data within some time interval is more suitable for some application. Archiving by time could allow the system to process user request confined to the specific data set, rather than the all of the data, which can significantly improve system performance.

4) Archiving by log priority

The log messages generated by various kind of network equipment are all have the priority tag, typically which are debug, informational, notice, warning, critical, alert, emergency and so on. Log message with different priority represents different important level which could result in the different probability of being requested or processed in practice. Using this method, the log messages with same priority will archive into the same log file. Therefore, when processing the user requests, only the interested datasets need to access, which can reduce the amount of log data, and in favor of improving the process efficiency.

5) Archiving by comprehensive strategies

Two or more strategies can be used together to form a more careful and reasonable file archiving mechanism. For example, the log message priority and time can be combined to form a new archiving method which first to merge log messages with different priority into different log files. Then achieve each log file by different level time standard. The log time and file size method also can be combined, the low-level file can be archived with file size standard, and the formed high-level log file can be processed by time standard.

The general principle of selecting multiple strategies is beneficial to show the advantages of each strategy, and overcome their disadvantages. Comprehensive strategies can not to undermine the scalability of the log storage system, and should be helpful to improve system performance.

D. Solving the Archiving Singularity

Archiving singularity refers to the lower-level archiving operation triggers on a series of upper-level archiving operations in the archiving process. In this case, the archiving operation would rise like the dominoes extension. Concentrated archiving operation will undoubtedly bring greater impact on system performance, while resulting in major changes of the file structure. This could deviate from the original design of hierarchical archiving mechanism.

The time delay mechanism can be taken to resolve the archiving singularity problem. One way is to set the delay interval for continuous archiving operation, and the successive archiving operations must be conducted outside the specified delay interval. This separates the archiving operation artificially. Delay interval should reference the average interval of each archiving level, it is best to set the number coprime with all archiving levels. Another method is to set the system to perform high-level archiving in spare time. The probability of upper-level archiving is already very low, so perform the archiving mechanism when the system is idle can avoid the archiving singularity problem effectively.

IV. The Implement Architecture

In order to apply this mechanism better in practice, this section discusses the implementation architecture of the hierarchical file archiving mechanism in detail. Fig. 4 shows the simple deployment architecture of the Hadoop-based log analysis system. There are three major characters in this architecture: log source, log server and Hadoop cluster. The range of log source is very wide, which could be the computers (such as workstation, application server et al.), network devices (such as router, switcher, firewall and many others) and so on. During the running of the log source, some events may be occurred. The log process on log source captures the event and forms the log message. Then, these log messages will be sent to log server in the form of stream. The number of these log messages from different log source will be very huge. So, the log server should put them into different queue. Then, these log messages will be do some pretreatment, such as format conversion, removing the useless field, adding some default fields and so on. Then the log will be saving to a local log buffer file. When the local log file reaches the predefined conditions, they will be sent to the Hadoop cluster, saved into the DataNode and indexed in NameNode.

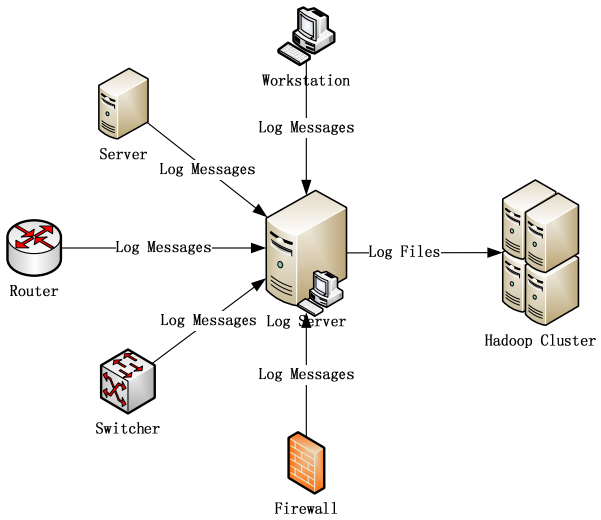

Figure 4. The deployment architecture of log system.

Obviously, the log server occupies the core position in the whole system. We should understand how log server works. Fig. 4 indicates the process procedure of log

information within the log server. In order to store a log message to the cloud system, there are seven steps that need to be performed.

Step1: log server uses some threads to receive the log message, and put them in the appropriate queue.

Step2: log server does some pretreatment, such as discarding the useless or repeated log information, adding or removing some fields and so on. Finally, the log information also should be classified.

Step3: log server stores the classification data into the local log buffer file, which according to bottom level of the hierarchical file archiving mechanism.

Step4: log server checks the size of the saved log buffer file. If the file meets the predefined size, then the flow continues, otherwise, the flow will go to step 6.

Step5: merges the saved local log files into a single log file, and save it to Hadoop cluster, and then delete all the local log buffer files.

Step6: check the conditions of the hierarchical file archiving mechanism. If the conditions are met, step 7 will be taken to perform the hierarchical file archiving mechanism; otherwise, step 8 will be performed.

Setep7: run the MapReduce programs on the Hadoop cluster. Archive the low-level log file to the upper-level log file, and then delete namespace of the low-level files in Namenode.

Step8: check whether the exit condition is met. If so, the flow will be exited. Otherwise, the flow will be go to setep1, and start the next loop.

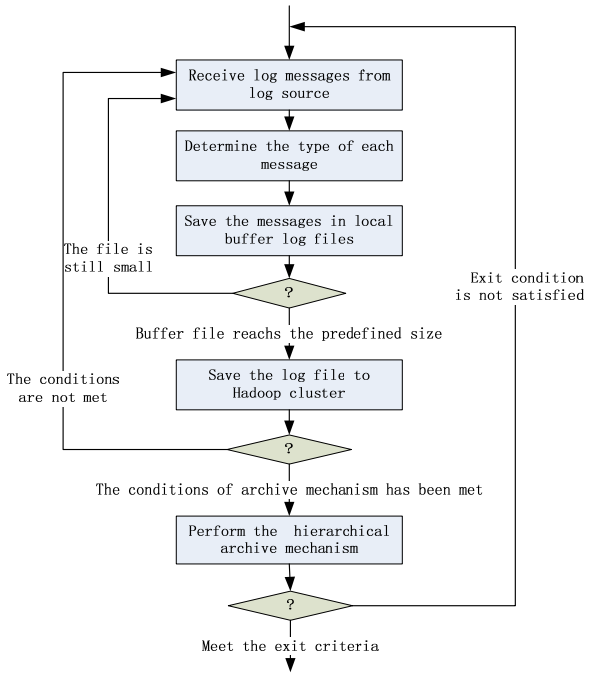

Figure 5. Log processing flow of log server

V. Experimental Analysis

In order to verify the feasibility of proposed hierarchical file archiving mechanism, here take a simple experiment, in which the 1T log data was processed to compare the processing performance in a hierarchical and non-hierarchical system. Hierarchical mechanism used the method of archiving by file size, and the archiving standards for level 1 to level 4 were set to 64MB, 1GB, 16GB and 256GB. The amount of log data allocated for each level are 1GB, 15GB, 240GB and 768GB. The hardware platform contains 4 servers, one acts as the NameNode, the remaining 3 servers are the DataNode. The data processing time in hierarchical and non-hierarchical case are shown in Table I and Table II.

From Table I and Table II, it can be seen that, the total data processing time of the system with hierarchical file archiving mechanism is slightly more than the system with non-hierarchical mechanism for the same amount of log data. But the response time of system with hierarchical file archiving mechanism is in the large lead of the other system, which is a crucial indicator for the online log analysis system. In addition, since most user requests do not need to access the entire data set, so the processing time of hierarchical archiving data could far fewer than non-hierarchical data in practice.

TABLE I.
PROCESSING COSTS

Item/data	Non-hierarchical	Hierarchical			
File size	1T	64M	1G	16G	256G
Data size	1T	1G	15G	240G	768G
Files number	1	16	15	15	3
Time	12760	63	547	4923	9716

TABLE II.
PERFORMANCE COMPARISON

Item/data	Non-hierarchical	Hierarchical
Total processing time	12760	15249
First response time	12760	63

VI. Conclusion

Aim at the application characteristics and needs of the online log analysis system, this paper analyzes the necessity of using the hierarchical file system to manage the log data, and proposes the hierarchical file archiving mechanism and some specific archiving methods. Furthermore, one or more suitable archiving methods can be selected to form the more complete solution in the practical application. Simulation experiments show that after taking the hierarchical file archiving mechanism, the system response time can be significantly shortened. Hierarchical archiving mechanism is also beneficial to the system for selecting the appropriate data sets to process, which can avoid useless data operate, and improve the processing speed and system performance.

Acknowledgment

This work was supported by Henan Province Science and Technology R&D Program (No.: 122102310474), Henan Province Basic and Frontier Technology Research Projects (No.: 122300410071) and Zhumadian Municipal Science and Technology Research Projects (No.: 11314).

REFERENCES

[1] T. A. Sang. "Log-based approach to make digital forensics easier on cloud computing," *Proc. of the 2013 3rd Inter. Conf. on Intelligent System Design and Engineering Applications, ISDEA2013*, pp. 91-94, 2013.

[2] D. Wang, J. Chen, W. B. Zhao. "A Task Scheduling Algorithm for Hadoop Platform," *Journal of Computers*, vol. 8, no. 4 (2013), pp. 929-936, Apr 2013.

[3] S. B. Ren, D. Muheto. "A Reactive Scheduling Strategy Applied On MapReduce OLAM Operators System," *Journal of Software*, vol. 7, no. 11 (2012),pp. 2649-2656, Nov 2012.

[4] S. Chen, N. An, L. Li, Y. W. Wu, W.M. Zheng, L. Sun. "Human dynamics revealed through log analytics in a cloud computing environment," *Lecture Notes in Computer Science* , vol. 7923 LNCS, pp. 58-63, 2013.

[5] J. H. Lee, M. W. Park, J. H. Eom, T. M. Chung. "Multi-level intrusion detection system and log management in cloud computing," *Inter. Conf. on Advanced Communication Technology, ICACT*, pp. 552-555, 2011.

[6] R. R. Bhandari, N. Mishra. "Encrypted IT auditing and log management on cloud computing," *Inter. Journal of Computer Science Issues*, vol. 8, no. 55-1, pp. 302-305, Sep. 2011.

[7] M. Cheng, H. P. Chen. "Weblog Mining Based on Hadoop," *Computer Engineering*, vol. 37, no. 11, pp. 37-39, 2011.

[8] F. Y. Yang, H. C. Liu. "Research in HDFS based on Campus Network Environment," *Proc. of 2011 International Conference on Image Analysis and Signal Processing*. Wuhan, China, 2011, pp. 648-652

[9] C. B. Huang, J. L. Wang, H. J. Deng, J. Chen. "Mining Web Logs with PLSA Based Prediction Model to Improve Web Caching Performance," *Journal of Computers*, vol. 8, no. 5 (2013), pp. 1351-1356, May 2013.

[10] J. G. Lou, Q. Fu, Y. Wang, J. Li. "Mining dependency in distributed systems through unstructured logs analysis," *Operating Systems Review (ACM)*, vol. 44, no. 1, pp. 91-96, 2010.

[11] M. Philippe, N. Syed et.al. "A monitoring and audit logging architecture for data location compliance in federated cloud infrastructures," *IEEE International Symposium on Parallel and Distributed Processing Workshops and Phd Forum*, 2011, pp. 1510-1517.

[12] W. Xu, L. Huang et.al. "Detecting large-scale system problems by mining console logs," *Proc., 27th International Conference on Machine Learning*. Haifa, Israel, 2010, pp. 37-44.

[13] H. Y. Yu, D. Sh. Wang. "Mass log data processing and mining based on Hadoop and cloud computing," *Proceedings of 2012 7th International Conference on Computer Science and Education*, Melbourne, Australia, 2012, pp. 197-202.

[14] J. Therdphapiyanak, K. Piromsopa. "Applying Hadoop for Log Analysis toward Distributed IDS," *Proceedings of the 7th International Conference on Ubiquitous Information Management and Communication*, Kota Kinabalu, Malaysia, 2013.

[15] W. Zhou, J. F. Zhan, D. Meng, Zh. H. Zhang. "Online Event Correlations Analysis in System Logs of Large-Scale Cluster Systems," *Proceedings, International Conference on Network and Parallel Computing*. Zhengzhou, China, 2010, LNCS6289, pp. 262-276.

[16] C. J. Jiang. "The Function of Log Analysis in Network Security," *New Technology of Library and Information Service*, vol.20, no. 12, pp. 58-60, 2004.

[17] X. C. Dong "HDFS small file problems and solutions", *http://dongxicheng.org/mapreduce/hdfs-small-files-solution/*.

[18] W. B. Chen, X. J. Zhang, L. LI, J. Tang. "A distributed system of log analysis based on Hadoop," *Journal of Guangxi University (Natural Science Edition)*, no. S1, pp. 339-342, 2011.

[19] G. M. Hu, L. Zhou, L. X. KE. "Research on Hadoop-based Network Log Analysis System," *Computer Knowledge and Technology*, no. 22, pp. 6163-6164+6185, 2010.

[20] A. Q. Song. "Design and completment of Hadoop-based log analysis system," *Beijing: China University of Geosciences*, 2012

[21] The Apache Software Foundation, "HDFS 0.21 Documentation," http://hadoop.apache.org/hdfs/docs/r0.21.0/.

[22] White T. *Hadoop: The Definitive Guide, 2nd Edition.* O'Reilly Media / Yahoo Press, 2010.

Fengying Yang was born in 1978. She received the M.S. degree in computer technology from Wuhan University in 2011. She is a lecturer at Huanghuai University, Zhumadian, China. Her research interests include cloud computing and computer network.

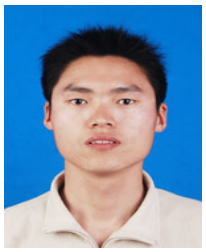

Huichao Liu was born in 1982. He received the M.S. degree in computer technology from Wuhan University in 2011. He is a lecturer at Huanghuai University, Zhumadian, China. His current research interests are cloud computing and intelligent computation.

Zhanping Zhao was born in 1965. He received his Ph. D. degree in probability and mathematical statistics from Yunan University in 2008. He is a professor, master tutor in department of economic management of Huanghuai University, Zhumadian, China. His current research interests include bayesian inference and computer techenolog.

Design of Wind-solar Complementary Power System Based on Progressive Fuzzy Control

Ning Chen
School of Mechanical and Automotive Engineering, Zhejiang University of Science and Technology, Hangzhou, China
Email: nelching@163.com

Xiao Qu
School of Automation and Electrical Engineering, Zhejiang University of Science and Technology, Hangzhou, China
Email: quxiao@zust.edu.cn

Weibing Weng and Xing Xu
School of Mechanical and Automotive Engineering, Zhejiang University of Science and Technology, Hangzhou, China
Email: xuxing1332@163.com

***Abstract*—In order to make a wind-solar complementary power system be a self-intervention controller, a new fuzzy control approach to hybrid power generation in wind and solar co-generation system is developed in this paper. Firstly, a new kind of structure of wind-solar complementary power system is designed. The method of double-fed brushless wind turbine sets is adopted, based on the principle of nonlinear control theory, according to the external excitation caused by the nonlinear changes of wind forces and wind speeds, for the purpose of capturing the wind power in the greatest degree. Meanwhile, the idea of extensional adaptive control on solar cells is adopted, also in order to transform the renewable energy to electrical power to the most degree. Secondly, according to the analysis on the characteristics of the multi-input and multi-output of the distributed wind-solar complementary power system, a progressive fuzzy control algorithm based on fuzzy control method and adaptive control theory is put forward to control the loading and unloading process congruously among the wind turbines, the solar cells and the grid. Finally, the simulation study is carried out. It is shown that the new kind of wind-solar complementary power system can achieve the balance quite well between the supply and the demand of the electrical energy automatically according to the load of system, under the premise of improving the utilization rate of renewable resources as much as possible.**

***Index Terms*—renewable energy, wind-solar complementary power system, nonlinear control, algorithm of progressive fuzzy control, extensional adaptive control, double-fed brushless wind turbine, congruous loading and unloading process, self-intervention controller**

I. INTRODUCTION

With the growing world energy shortage and the requirements of environmental protection, wind power generation technology and solar power generation technology have respectively made considerable development in recent years[1]. More and more wind power and solar power has been applied as the substitute for fossil fuels. But, whether wind power generation technology or solar power generation technology has its great limitation when they are applied independently[2]. Thus, a new power generation style named wind-solar complementary power system has been developed, which can help wind power generation and solar power generation to compensate for each other so as to supply a stable output of electrical power[3,4].

In the future, a wind-solar complementary power system could guarantee a great certain percentage of power supply all the year, reduce the exhaust of diesel fuel, and realize the sufficient use of the natural renewable resources. But nowadays, the technology has not been perfect enough[5,6]. There are several key problems urgently need to be resolved, such as the incongruous loading and unloading process among the wind generators and the solar cells and the grid, the bad stability of the system, the lack of self-intervention and adaptability, and so on.

In order to promote the technology of wind-solar complementary power generation to practical progress, some scientists threw themselves into the relevant studies and researches. Boroyevich D. et al put forward a optimal sizing method for wind-solar-battery hybrid power system[7], Dufo-López R, et al. established a multi-mode energy control and management model for wind-solar hybrid power generation[8], Gelik, A.N. [9] and Billinton R, et al[10] developed respectively a coordination control algorithm for wind-solar hybrid power system, Mingliang Li[11] and Yifeng Wang et al [12] designed a new type wind-solar hybrid generator respectively. Although some technical items about wind-solar complementary power generation system were solved quite well with those researches above, some were left hanging in the air, especially how to control the loading and unloading process congruously. In addition, almost all researches

Manuscript received May 19, 2013; revised November 22, 2013; accepted December 19, 2013.
Xing Xu is the corresponding author to this work.

doi:10.4304/jcp.9.6.1378-1384

above focus on the off-net household wind-solar complementary power system. The knack about how to achieve the balance between the supply and the demand of the electrical energy automatically according to the load of system and the grid has not been under the scientific exploration yet. It's necessary to develop a new design of wind-solar complementary power system, which is a self-intervention controller according to the supply and the demand of the system and the grid, and can achieve a congruous loading and unloading process among the wind generators and the solar cells and the grid.

A new design of wind-solar complementary power system based on fuzzy control theory combining with extensional adaptive control idea and adaptive control method was established in this paper, so as to achieve the balance between the supply and the demand of the electrical energy automatically according to the load of system, under the premise of improving the utilization rate of renewable resources as much as possible.

II. A New Structure Of Wind-solar Complementary Power System

A typical wind-solar complementary power system consists of wind generator, solar units, batteries, charge controllers, inverters, system monitoring system, etc.[13] Because of no evaluation about the impact of the load on the power output, this type of structure is not smart enough to link into the power grid.

In order to solve the above problems, a new kind of structure of wind-solar complementary power system is designed, shown in Fig.1. The wind generator employs a special design which means a double-fed brushless wind turbine, and the solar units are composed of a group of pollution-free solar panels attached with a certain dry battery groups. Both the rectified currents from solar units and wind turbine paralleled on the side of direct current will pass through a charge-discharge controller to charge the solar battery groups. After that, the rectified currents will go through an inverter to charge or to drive the alternating load linked to the power grid. In this structure, a power quality controller will take its responsibility when the alternating load has a higher requirement about power output, or the power grid need to be charged. Then, the wind-solar complementary power system can not only run independently but also incorporate into the electrical power grid.

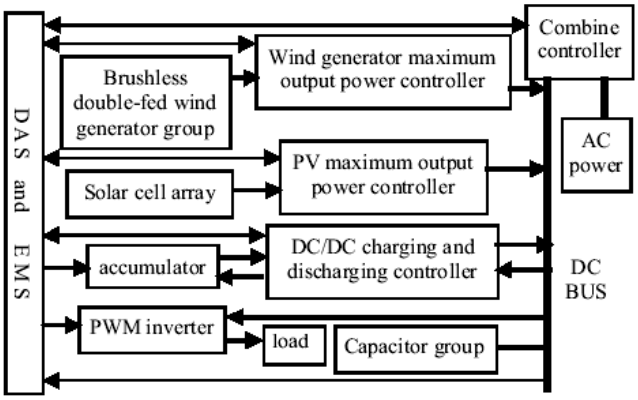

Figure 1. The schematic diagram about the new structure of the wind-solar complementary power system

In order to decrease the costs of electronic components and to eliminate the replacement of the electric brush, the ratio of the *loop-circuit power* to *control loop-circuit power* of double-fed brushless wind turbine in this new structure is set to be at an even/odd number. Furthermore, a lower control loop-circuit power is employed.

For the purpose of controlling the frequency changes dynamically as well as avoiding the occurrence of harmonic, frequency conversion circuit is put to use on controlling the double-fed brushless wind turbine to develop a passive control on frequency error of the wind-solar complementary power system. After that, the nonlinear characters of the external excitation caused by the nonlinear changes of wind forces and wind speeds are inputted into the anti-disturbance controller based on the adaptive theory, which consists of tracking differentiator, extended state observer, and feedback device for nonlinear state error. Tracking differentiator can provide the generalized differential signal without any noise. Extended state observer can take the real-time measurement on the internal systematic state as well as the external disturbance, so that the ascertainment of feedback and linearization of dynamic feedback can be achieved. Feedback device for nonlinear state error can ensure the perfect dynamic performance of the generation system with good robustness, and big swing.

III. Design Of The Progressive Fuzzy Control System

Although it is an exponential relationship between regulation totality and input variables in a general fuzzy controller, the linear relationship can be achieved in a progressive fuzzy controller (PFC) based on fuzzy control method and adaptive control theory. If the nonlinear system has more than one input variable, PFC can effectively reduce the dimensions of fuzzy controlling rules' database and can simplify the instructions of practical operation of the controller.

As shown in Fig.1, the input of the PFC is

$$y = f_3(x_4, f_2(x_3, f_1(x_2, x_1))) \tag{1}$$

In which the i th output is

$$f_i(y_{i-1}, x_{i+1}) = \frac{\sum_{p=1}^{n_i}\sum_{q=1}^{m_i} h_i(y_{i-1}, x_{i+1})[\mu_{ip}(y_{i-1})\mu_{iq}(x_{i+1})]}{\sum_{p=1}^{n_i}\sum_{q=1}^{m_i}[\mu_{ip}(y_{i-1})\mu_{iq}(x_{i+1})]}$$

$$i = 1, 2, 3, 4 \tag{2}$$

Where, n_i is the number of the (i-1)th output fuzzy set titled y_{i-1}, and m_i is the number of ith input fuzzy set titled x_{i+1}. The block diagram of PFC in the wind-solar complementary power system is shown in the Fig. 2.

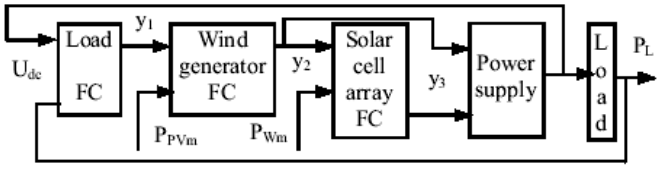

Figure 2. The block diagram of PFC in the wind-solar complementary power system

In our design, the wind generation set is composed of 5 wind turbines on 12kW class, so that the total output power of the generation set ranges from 0kW to 60kW. The solar generator set consists of 5 solar cell units on 6kW class, and the total output power of the solar generator set would swing from 0kW to 30 kW, meanwhile the load power changes from 0kW to 90kW.

The prerequisite of a safe, stable, and efficient power supply system is to keep the balance of the electrical power supply and the demand from the load. Because the load is always powered by DC voltage through inverter, the DC voltage stability will directly determine the quality of the power used to drive the load. The DC generatrix voltage titled U_{dc}, working from 198V to 242V, is taken as passive control variable in the design and its rated voltage is 220V. In order to simplify the structure, the inputs of energy control system are chosen as U_{dc}, P_{Wm} (maximal output power of wind generator set), P_{PVm} (maximal output power of solar generator set), and P_L (the demand of load). The outputs are *KW* (utilization ratio of wind generator set output power), K_{PV} (utilization ratio of solar generator set output power), and K_S (switch function: when K_S=1, the generation system could be connected into the power grid; when K_S=0, the generation system is disconnected from the power grid). In our design, $KW, K_{PV} \in [0,0.2,0.4,0.6,0.8,1]$.

According to the operation characteristic, system control regulations include fuzzy control rules and precise control rules.

Fuzzy control: It not only monitor the wind turbines, solar units, DC generatrix voltage and the load, but also control the former two components and maintain the balance between the supply and demand of the electric power. When the system can not generate sufficient power, the public grid will compensate the shortfall; once the supplement exceeds, it will break off automatically from the public power grid.

$$D_1(t) = \frac{1}{2}(1 + \frac{u_m}{V_{tri}}) \tag{3}$$

$$K_{\mathrm{PWM}} = \frac{U_i(s)}{U_m(s)} = \frac{E}{V_{tri}} \tag{4}$$

$$G(s) = \frac{U_o(s)}{U_i(s)} = \frac{\frac{1}{Cs}//R}{\frac{1}{Cs}//R + Ls + R_L} = \frac{1}{LCs^2 + (\frac{L}{R} + R_L C)s + \frac{R_L}{R} + 1} \tag{5}$$

$$P(s) = \frac{U_o(s)}{U_m(s)} = \frac{U_o(s)}{U_i(s)}\frac{U_i(s)}{U_m(s)} = \frac{1}{LCs^2 + (\frac{L}{R} + R_L C)s + \frac{R_L}{R} + 1}\frac{E}{V_{\mathrm{tri}}} \tag{6}$$

Precise control:

When U_{dc}<198V, K_S=1; when U_{dc}>220V, K_S=0; and when U_{dc}>242V, cut off the power supply from wind-solar complementary power system, until U_{dc} less than 220V.

$$|\frac{P(s)}{1 + k_f P(s)}\frac{Q(s)}{P(s)}e^{-Ts}| < 1 \tag{7}$$

$$P(s) = \frac{U_o(s)}{U_m(s)} = \frac{U_o(s)}{U_i(s)}\frac{U_i(s)}{U_m(s)} = \frac{1}{LCs^2 + R_L Cs + 1}\frac{E}{V_{\mathrm{tri}}} \tag{8}$$

$$|1 + k_f P(s)| > |Q(s)| \tag{9}$$

In our design, the most influential variables to system are chosen as the first-level rule sets system variables, and the less ones are chosen as the second-level rule sets system variables, and so on. We can set fuzzy subset variables as *Z*(Zero), *S*(Small), *Sr*(Smaller), *M*(Middle), *Br*(Bigger), *B*(Big), *N*(Negative), *L*(Low), *M*(Middle), *H*(High).It is recommended by our research that it is better to reduce the number and complexity of the fuzzy control subsets for keeping higher precision. Besides, when there are some changes of power supply and power demand, each on-off action would not switch frequently, so that the wavy input variable should be designated as a fuzzy subset to avoid the bad fluctuation of controlling output. Based on above principles, U_{dc} would be working from 198V to 242V, and relevant fuzzy subset would be [L, M, H], and P_L would be from 0kW to 75kW, and relevant fuzzy subset would be [Z, S, Sr, M, Br, B], as well as P_{Wm} would be from 0kW to 75kW, and relevant fuzzy subset would be [S, Sr, M, Br, B], and P_{PVm} would be from 0kW to 15kW, and relevant fuzzy subset would be [Z, S, Sr, M, Br, B]

A. Design of the First-step Fuzzy Controller

In the wind-solar complementary power system, DC voltage is the critical factor for system stability. The relationship between DC voltage and load power determines the subsequent controlling of energy management system. Thus, we take P_L and U_{dc} as the first-level inputs, and take energy intensity y_1, which is the load relatively to the system, as the output. The membership's function of the first-step fuzzy controller is shown in Table I, and the control rules are shown in Fig. 3.

The variable set of y_1 is defined as [Z, S, Sr, M, Br, B], and the relevant de-fuzzy precise variable set is deduced out as [0, 0.1, 0.3, 0.5, 0.7, 0.9].

TABLE I.
THE FIRST-STEP FUZZY RULES SET

U_{dc} \ P_L	Z	S	Sr	M	Br	B
L	S	Sr	M	Br	B	B
M	Z	S	Sr	M	Br	B
H	Z	S	Sr	M	Br	B

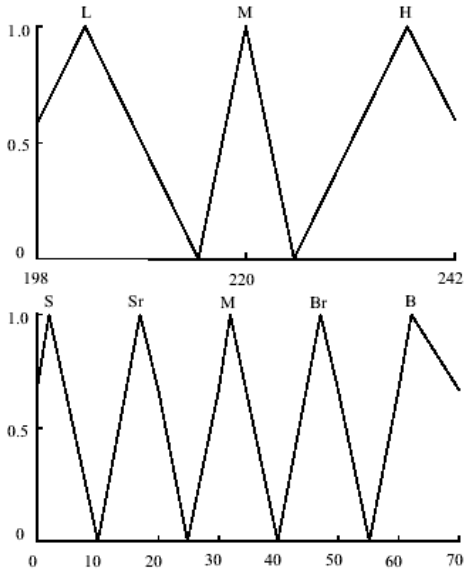

Figure 3. The membership function of P_L and U_{dc}

B. Design of the Second-step Fuzzy Controller

In our research, we take y_1 and P_{Wm} as the inputs, and take y_2, which is defined as the percentage of wind power supplied to system, as output. The memberships function named P_{Wm} is shown in Table 2, and the rules for the second-level control are shown in Fig. 4. The fuzzy variable set of y_2 is defined as [Z, S, Sr, M, Br, B], and the relevant de-fuzzy precise variable set is deduced out as [0, 0.2, 0.4, 0.6, 0.8, 1.0]. Besides, the wind turbines set used is defined as [0,1, 2, 3, 4, 5].

TABLE II.
THE SECOND-STEP FUZZY RULES SET

y1 \ P_{Wm}	S	Sr	M	Br	B
Z	Sr	S	S	Z	Z
S	M	Sr	Sr	S	S
Sr	B	M	M	Sr	Sr
M	B	B	Br	Br	M
Br	B	B	B	B	Br
B	B	B	B	B	B

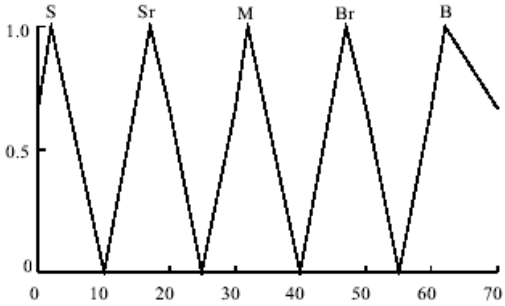

Figure 4. The membership function of P_L (the same as P_{Wm})

C. Design of the Third-step Fuzzy Controller

In our research, we take x_4 and P_{PVm} (x_4=75 y_2- y_3P_{Wm}) as the inputs, and take y_3, which is defined as the percentage of solar power supplied to system, as the output. The memberships function of x_4 and P_{PVm} are shown in Table 3, as well as the second-step control rules are shown in Fig 5.

TABLE III.
THE THIRD-STEP FUZZY RULES SET

P_{PVm} \ x_4	N	S	Sr	M	Br	B
Z	Z	B	B	B	B	B
S	Z	Br	B	B	B	B
Sr	Z	M	B	B	B	B
M	Z	Sr	M	M	B	B
Br	Z	S	Sr	M	Br	B
B	Z	S	Sr	M	Br	B

In our research, we found that the de-fuzzy variable of y_3 equals to y_2. And the terms of $5y_2$ and $5y_3$ separately means the total number of the wind turbines set and the solar units, which supply the power to the system together.

When P_L and U_{dc} are changed, the system would perform the real-time control function automatically, through gradually fuzzy control steps, so as to progressively approach the object function.

IV. SIMULATING RESEARCH AND THE ANALYSES

For the purpose of validating the feasibility of the system, we designed a simulation model of energy management system based on progressive fuzzy control, which is established by the power demand and supply from 8:00 to 20:00 in a certain day.

The power of the entire output of the wind turbines set and the solar units fluctuates in a comparatively large range, as well as the load power does. The output power curves are shown in Fig. 6. Obviously, the electrical power grid will be unstable if there don not have any control.

The relationship between the load power and the maximal output power of hybrid power generation in

wind-solar complementary power system is shown in Fig. 7, where the term of (P_{Wm}+P_{PVm}) means the maximal output power, and the term P_L means the load power.

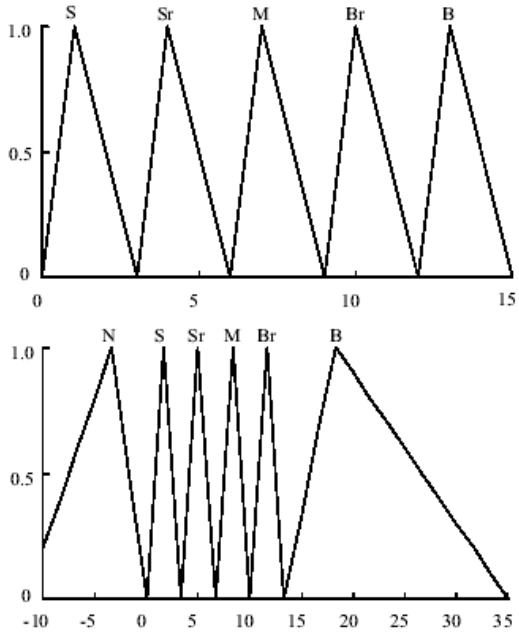

Figure 5. The membership function of x_4 and P_{PVm} (x_4=75y_2-y_3P_{Wm})

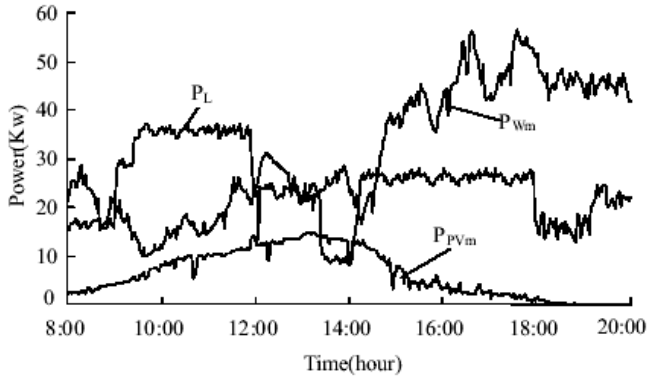

Figure 6. Output power curves of wind turbines unit and solar cells unit as well as the power curve of the load

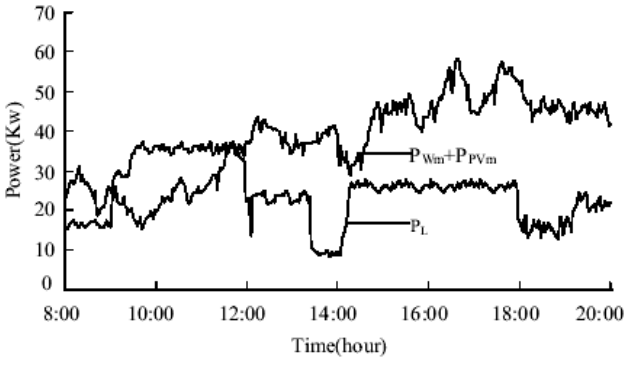

Figure 7. The maximum output power curves of wind turbines unit and solar cells unit as well as the power curve of the load

From Fig.7, it can be seen that the load power sometimes would be away from totally hybrid power, so that the direct current generatrix voltage would like to be fluctuant without control. Thus, the system would not work properly.

Figure 8 gives the relationship curve between load power and real output power of hybrid power generation in wind-solar complementary power system under fuzzy control without connecting into the grid. The term of (P_W+P_{PV}) means the real power supplied by hybrid power generation in wind-solar complementary power system. If the maximal output power of reproducible resources is less than the load power, the output power of reproducible resources would equal the number of (P_{Wm}+P_{PVm}), that is to say that the reproducible resources are adequate enough to use. Otherwise, the output power of reproducible resources would equal the number of the load power, which means that the system can load or unload the solar cells group and wind turbines unit according to the load power.

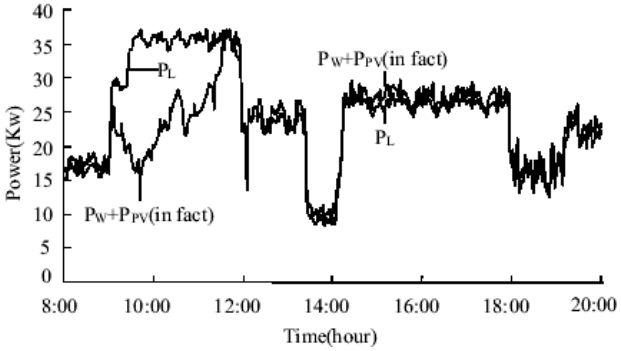

Figure 8. The real output power curves of wind turbines unit and solar cells unit as well as the power curve of the load

When the total output power of the wind-solar complementary power system is less than the load power, leading to that the direct current voltage drops to the threshold value (192V) preset on the system, the grid will supplement the insufficiency on the basis of fully utilizing the output power of the wind-solar complementary power system, in order to maintain the DC voltage at 192V. It is shown in Fig.9

The load power curves compared to the total power supplied after the algorithm of progressive fuzzy control was used on the wind-solar complementary power system

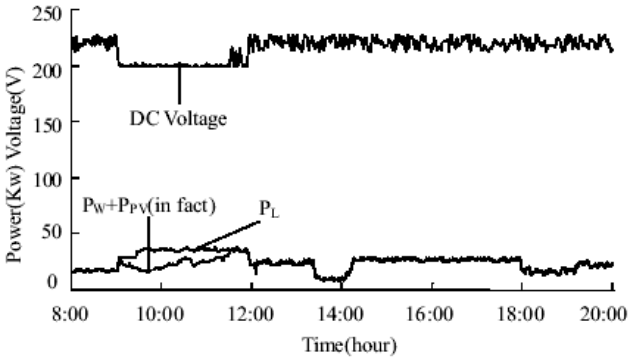

Figure 9. The curves of DC voltage if the load power partly more than the output power of the wind-solar complementary power system

were shown in Fig.10. It is seen that the power supply system can do self-intervention according to its load, so that the balance between supply and demand will be achieved.

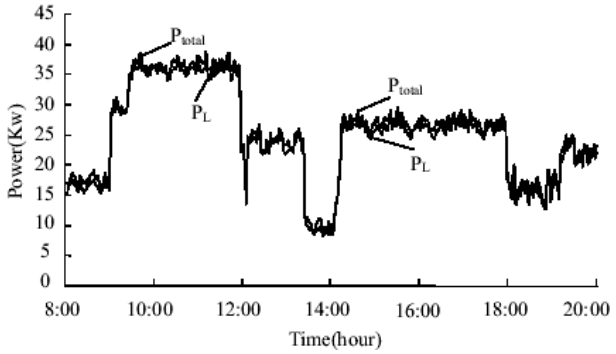

Figure 10. The power curves of the total supply and the load

Some experiments were held and the results indicate that the wind-solar complementary power system based on the progressive fuzzy control can automatically load or unload from the grid according to the load demand. So that the purpose of utilizing wind resources and solar resources efficiently is accomplished.

IV. CONCLUSION

In order to make the wind-solar complementary power system be a self-intervention controller, a new fuzzy control approach to hybrid power generation in wind-solar complementary power system is developed in this paper. Firstly, a new kind of structure of wind-solar complementary power system is designed. The method of double-fed brushless wind turbines set and the idea of extensional adaptive control on solar cells unit are adopted, based on the external excitation caused by the nonlinear changes of wind forces and wind speeds, for the purpose of capturing the wind power and the solar power in the greatest degree. Secondly, according to the analysis on the characteristics of the multi-input and multi-output of the distributed hybrid power system, an algorithm of progressive fuzzy control is put forward to control the loading and unloading process congruously among the distributed wind-solar complementary power system. Finally, the simulation study is carried out. It is shown that the wind-solar complementary power system can achieve the balance between the supply and the demand of the electrical energy automatically according to the load of system, under the premise of improving the utilization rate of renewable resources as much as possible.

ACKNOWLEDGMENT

The authors wish to thank the reviewers for their valuable comments on this paper. Our thanks would also go to Ms. Bingjing Xiang for her sage advices to this work.

The work is supported in part by National Natural Science Foundation of China(Grant No.61273240), and by Key Project of Chinese Ministry of Education (Grant No.211070), as well as by Zhejiang Provincial Natural Science Foundation of China (Grant No. LY12F03024).

REFERENCES

[1] Wang Bo, Wu Jie, Yang Jin-ming, Zhao Shi-wei, "Wind and PV hybrid power power management systems based on fuzzy control". *Proceedings of the Annual Academic Meeting of Power System Dispatching Automation &Simulation Technology in 2003*. Chengdu(China): 2003, pp. 404-409.

[2] Michio Sugeno, Takahino Yasukawa. "A fuzzy-logic based approach to qualitative modeling. Fuzzy Systems, *IEEE Transactions on Systems*, Feb. 1993, vol. 1, pp. 7-31.

[3] G.V.S,.Raju,Jun Zhou. "Adaptive Hierarchical Fuzzy Controller". *IEEE Transactions On Systems, Man, and Cybernetic*, 1993, vo1. 23, no.4, pp.973-980.

[4] Prats M A M , Carrasco J M , Galvan E , et a1. "Improving Transition between Power Optimization and Power Limitation of Variable Speed , Variable Pitch Whad Turbines Using Fuzzy Control Techniques". *Industrial Electronics Society (IECON'00)* , Nagoya , Aichi , Japan , 2000:pp.1497-1502 .

[5] Tan Guan-zheng , Zeng Qing-dong , He Sheng-jun , et a1. "Adaptive an d Robust Design for PID Co ntroller Based on Ant System Algorithm". *Advances in Natural Computation Lecture Notes in Computer Science ,* 2005 , vol. 36, No. 5,pp.915—924

[6] Bimal K. Bose. "Energy, environment, and advances in power electronics", *IEEE Trans. Power Electronics*. 2000 , Vol.15 , No.4 , pp.688-701

[7] Boroyevich D, Cvetković I, Dong D, et al. "Future electronic power distribution system:A contemplative view", *Proceedings of the 12th International Conference on Optimization of Electrical and Electronic Equipment.* Brasov, Romania: IEEE , 2010, pp.1369 -1380

[8] Dufo-López R, José L，Agustín B, et al. "Multi-objective optimization minimizing cost and life cycle emissions of stand-alone PV-wind-diesel systems with batteries storage", *Applied Energy.* 2011, Vol.88, No.11, pp.4033-4041

[9] Gelik, A.N. "Techno-economic analysis of autonomous PV-wind hybrid energy systems using different sizing methods", *Energy Conversion and Management*. 2003, Vol. 44, No. 12, pp.1951-1968

[10] Billinton R, Wangdee W. "Reliability-based transaction reinforcement planning associated with large-scale wind farms", *IEEE Trans on Power Systems*. 2007, Vol.22, No.1, pp.34-41.

[11] Mingliang Li, Cong Wang. "Research on optimization of wind and PV hybrid power systems", *Proceedings of 7th World Congress on Intelligent Control and Automation.* Chongqing, China, 2008, pp.6429-6432

[12] Yifeng Wang, Jian Wu, Junmin Xu, et al. "Wind/Photovoltaic hybrid power generator based on fuzzy control", *Proceedings of IEEE 6th International Power Electronics and Motion Control Conference.* Wuhan, China: IEEE, 2009, pp.2284-2287

[13] Mohamed O, Youssef M Z, Jain P K. "Investigation of self-excited induction generators for wind turbine applications". *Electrical and Computer Engineering Conference*. Canada. 2004,4, 4: pp.1853-1856

Ning Chen received the Ph.D. degree in mechanical engineering from Zhejiang University in 2004. Currently, he is an Associate Professor at Zhejiang University of Science and Technology, and the fellow of Chinese Association on Mechanical Engineering. His research interests include Intelligent Transport System(ITS) and Logistics Engineering. He has published 33 papers around mechanical engineering, transportation engineering, and logistics engineering. His work has been supported by the National Natural Science Foundation of China as well as other academic originations.

Xiao Qu received the Master degree in automation engineering from Zhejiang University in 1999. Currently, she is an associate professor at Zhejiang University of Science and Technology. Her interests are in urban transportation system control design and information processing.

Xing Xu received the Ph.D. degree in mechanical engineering from Zhejiang Sci-Tech University in 2013. Currently, he is an assistant professor at Zhejiang University of Science and Technology. His interests are in urban transportation system control design and information processing.

Weibing Weng received the Ph.D. degree in Logistics Engineering from Dortmund University of Technology in 2011. Currently, he is an assistant professor at Zhejiang University of Science and Technology. His interests are in logistics technologies and equipments.

Adaptive Control based Particle Swarm Optimization and Chebyshev Neural Network for Chaotic Systems

Zhen Hong*
Faculty of Mechanical Engineering & Automation, Zhejiang Sci-Tech University, Hangzhou, China
Email: zhong@zstu.edu.cn

Xile Li
Faculty of Mechanical Engineering & Automation, Zhejiang Sci-Tech University, Hangzhou, China
Email: yizhikuaileo@126.com

Bo Chen
College of Information Engineering, Zhejiang University of Technology, Hangzhou, China
Email: bchen@aliyun.com

***Abstract*—The control approach for chaotic systems is one of the hottest research topics in nonlinear area. This paper is concerned with the controller design problem for chaotic systems. The particle swarm optimization (PSO) algorithm is firstly proposed to search for the weights of the Chebyshev neural networks (CNNs), and then an adaptive controller for the chaotic systems is designed based on the PSO and CNNs. Moreover, it is proved that the designed controller can guarantee the stability of chaotic systems. Numeral simulation shows the effectiveness of the proposed method in the Logistic chaotic system.**

***Index Terms*—adaptive control, particle swarm optimization, Chebyshev neural networks, chaotic systems**

I. Introduction

Since the control approach for the chaotic systems was firstly proposed in [1], controlling chaotic system has become a hot research topic in nonlinear areas. Therefore, there are many approaches solving the control problem of chaotic systems, such as feedback control of chaotic system, adaptive control of chaotic system, state feedback law [2-4]. These methods are required to control all states of the system. However, in the actual engineering system, some state variables cannot be controlled directly. To overcome these drawbacks, it is interesting and important for finding the suitable practical control method in engineering application.

The neural network can learn and approach any nonlinear and uncertain system dynamics model with arbitrary precision, thus it provides new ideas and methods to solve the control problem for chaotic systems. In this case, the chaotic control methods designed by using neural networks have made some achievements [5-12]. On the other hand, the studies in [13] show that the neural network with the orthogonal polynomial function has global approximation properties for approaching continuous function on any compact set with arbitrary precision. Particularly, when the orthogonal polynomial function is taken as Chebyshev polynomial, the performance of the designed neural networks is optimal. The reason is that the connection weights of Chebyshev neural networks (CNNs) is determined by the unidirectional gradient method, which is easy to make the objective function into local optimal impacting the efficiency of such neural network. Additionally, the particle swarm optimization (POS) adopts the speed-displacement search model, where the computational complexity is low, and the optimal solution is obtained by the cooperation and competition between particles. In this sense, the weights of the neural networks (NNs) are trained by using POS, which can give full play to the global optimization capability and rapid local convergence advantages for the PSO. Moreover, the PSO algorithm can also improve the generalization and learning capability of neural network [14]. These advantages of the PSO algorithm and CNNs motivate us to develop a control approach based on the PSO and CNNs for chaotic systems. Furthermore, to be best of the author's knowledge, few results have been reported on this issue.

Motivated by the aforementioned analysis, the PSO algorithm is utilized to determine the connection weights of the CNNs, thus a novel CNN algorithm based on the PSO is proposed. In this case, we use the proposed algorithm to design an adaptive controller for the chaotic system. Since the convergence interval of Chebyshev basis function is in [-1, 1], an *S*-type function is introduced to extend its input range $[-\infty, +\infty]$, which

Manuscript received November 16, 2013; revised December 25, 2013; accepted January 5, 2014.
* Corresponding author: Zhen Hong (zhong@zstu.edu.cn).

doi:10.4304/jcp.9.6.1385-1390

expends the scope of application of such neural network. It is proved that the model of neural networks has good approximation performance for the multivariate polynomial. Finally, the one-dimensional Logistic chaotic system is given to demonstrate the effectiveness of the proposed method.

II. CNN Learning Algorithm from PSO

A. Improved CNNs

First, the Chebyshev orthogonal polynomials [15] can be expressed as:

$$T_n(x) = \cos(n \arccos(x)), \quad |x| \le 1 \tag{1}$$

where $T_0(x)=1$, $T_1(x)=x$, and the recurrence formula is:

$$T_{n+1}(x) = 2xT_n(x) - T_{n-1}(x) \tag{2}$$

Since the range of x is $[-1,1]$, and this condition will restrict the applications of CNNs, we introduce the following *S*-type function:

$$g(x) = \frac{2}{1+e^{-\alpha x}} - 1 \tag{3}$$

where the domain of the Eq.(3) is $[-\infty, +\infty]$, but the range of $g(x)$ is $[-1,1]$. Meanwhile, the variable α in the function $g(x)$ is a tunable parameter. Then substituting Eq.(3) into Eq.(1) yields:

$$\begin{aligned} C_n(x) &= T_n(g(x)) = \cos(\arccos g(x)) \\ &= \cos\left(n \arccos\left(\frac{2}{1+e^{-\alpha x}} - 1 \right) \right) \end{aligned} \tag{4}$$

where $C_0(x) = 1$, $C_1(x) = \frac{2}{1+e^{-\alpha x}} - 1$, and $C_n(x)$ is orthogonal polynomial satisfying

$$C_{n+1}(x) = 2\left(\frac{2}{1+e^{-\alpha x}} - 1 \right) C_n(x) - C_{n-1}(x) \tag{5}$$

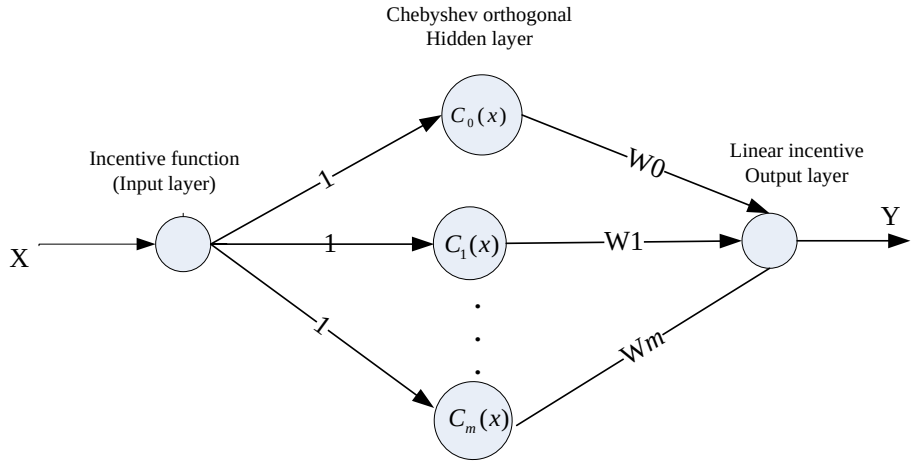

Figure 1 A neural network model of Chebyshev basis function

It can be seen from Fig.1 that the output of the model is:

$$y = \sum_{j=0}^{m} \mathrm{W}_j C_j(x) \tag{6}$$

where the improved Chebyshev function $C_j(x)$ is determined by (5). It is assumed that the desired output is y_d, then the error function is defined by $e_l \triangleq y_d - y$. Under this condition, the objective function of optimization problem is:

$$\varepsilon = \frac{1}{2}\sum_{l=1}^{r} e_l^2 = \frac{1}{2}\sum_{l=1}^{r} (y_d - y)^2 \tag{7}$$

where r denotes the number of training samples. It follows from the gradient descent method that the learning rule of W_j is:

$$\frac{\partial \varepsilon}{\partial \mathrm{W}_j} = \frac{\partial \varepsilon}{\partial e_l}\frac{\partial e_l}{\partial y}\frac{\partial y}{\partial \mathrm{W}_j} = e_l C_j(x)$$

As mentioned before, one has

$$\mathrm{W}_j(t+1) = \mathrm{W}_j(t) + \eta e_l C_j(x) \tag{8}$$

where η is the learning rate, and $0 < \eta < 1$.

B. Optimized Connection Parameters based on PSO

Since the connection weights of CNNS from section II(A) is determined by single-point gradient method, it is easy to fall into local minimum value. When the learning rate in formula (8) is hard to accurately given, it is hard to make the neural network algorithm converge under certain conditions. In the optimization process, each particle of the PSO algorithm updates themselves through their own experience and group experience, and the convergence rate is fast. In this sense, adopting the PSO algorithm for optimizing network connection weights can

improve the efficiency of neural network algorithm, and the convergence performance can be improved. In what follows, we firstly give the detailed mathematical description of the PSO:

Suppose that $\Omega \subset \mathrm{R}^n$ is a target search space of *n*-dimension, and a group $X = \{x_1, x_2, \cdots, x_n\}$ is composed by *n* particles. Then the velocity and position of the i_{th} particle is defined by:

$$v_i(k) \triangleq [v_{i1}(k) \quad v_{i2}(k) \quad \cdots \quad v_{in}(t)]^{\mathrm{T}},$$
$$x_i(k) \triangleq [x_{i1}(k) \quad x_{i2}(k) \quad \cdots \quad x_{in}(k)]^{\mathrm{T}}$$

And the current individual optimal solution of the i_{th} particle is:

$$\mathrm{pbest}_i(k) \triangleq (p_{i1}(k) \quad p_{i2}(k) \quad \cdots \quad p_{in}(k))$$

The current group optimal solution is:

$$\mathrm{gbest}(k) \triangleq (g_{g_1}(k), g_{g_2}(k), \cdots, g_{g_n}(k))$$

where *k* is the number of current evolution generation.

According to the theory of optimal particle tracking, the particle x_i updates its velocity and position according to the following formula:

$$\begin{aligned} v_{id}(k+1) &= w(k) v_{id}(k) \\ &+ c_1 \cdot \mathrm{rand}(0,1) \cdot (\mathrm{pbest}_i(k) - x_{id}(k)) \\ &+ c_2 \cdot \mathrm{rand}(0,1) \cdot (\mathrm{gbest}_g(k) - x_{id}(k)) \quad (i = 1, 2, \cdots, n) \end{aligned} \tag{9}$$

$$x_{id}(k+1) = x_{id}(k) + v_{id}(k+1) \tag{10}$$

where the Eq.(9) and Eq.(10) describe the update mode of particles' velocity and position, respectively. The parameters c_1 and c_2 are the accelerated constant, and their selected values are in [0, 2]. $w(k)$ is a linear inertia weight index. If the value of $w(k)$ is relatively large, the global convergence will be better. Otherwise, the local convergence is better. $w(k)$ is taken as:

$$w(k) = 0.9 - \frac{k}{\mathrm{MaxNumber}} \cdot 0.5$$

Where the "MaxNumber" is the maximum iterations.

For the neural network model in Section II(A), we make the connection weights W_j of CNNs as the position vector *x* in the PSO algorithm. We also determine the fitness function in particle swarm optimization according to the Eq.(7). Given a set of initial velocity randomly, and using the PSO algorithm to conduct iteration training, when the fitness function is less than the given error range, $f_i < \varepsilon_0$, the algorithm is suspended.

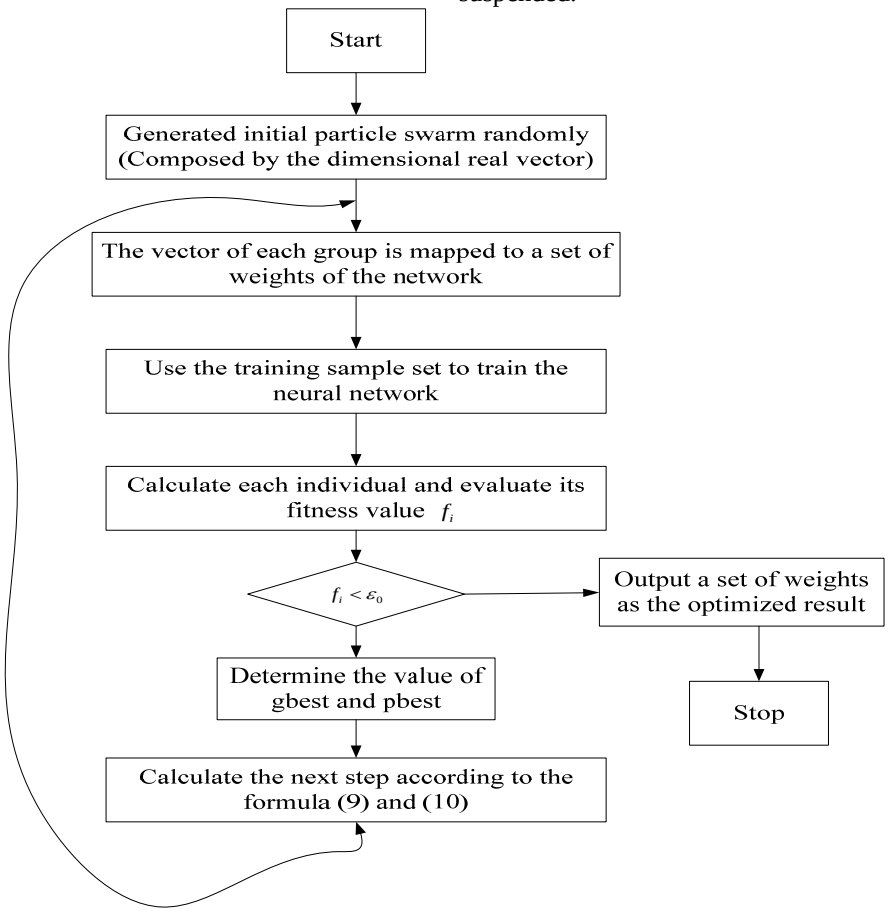

Figure 2 A optimized connection weights of the PSO

III THE CONTROLLER DESIGN BASED ON CNNS AND PSO

Considering the following chaotic system:

$$x(k+1) = f(x(k), p) \tag{11}$$

where $x \in \mathrm{R}^n$ is the system status, and p is the system parameter.

Using the neural network learning algorithm based on the PSO to simulate the input-output relationship of chaotic model (11), one has

$$\hat{x}(k+1) = \hat{f}(x(k), p) \tag{12}$$

According to the system stability theory, the controller can be taken as:

$$u(k) = -\hat{f}(x(k), p) + x_d(k+1) + \beta(x(k) - x_d(k)) \tag{13}$$

where x_d is the desired target track, β is the parameter. Then combining Eq.(12) and Eq.(13) yields:

$$\begin{aligned} x(k+1) = {} & f(x(k), p) - \hat{f}(x(k), p) \\ & + x_d(k+1) + \beta(x(k) - x_d(k)) \end{aligned} \tag{14}$$

If the proposed neural network can approach the system (11), then the error system is described by

$$e(k+1) = \beta(x(k) - x_d(k)) = \beta e(k) \tag{15}$$

where $e(k+1) = x(k+1) - x_d(k+1)$.

According to the system stability theory, we assume $|\beta| < 1$, which guarantees the error system (15) is asymptotically stable. It is easy to prove that when the system (11) is applied to control, it can track the controlled objective. So the approximation performance of the neural network is particularly important. In what follows, we will discuss the demands of the fuzzy Chebyshev basis function neural network to the chaotic system control accuracy.

Definition 1 Suppose $\forall X \in R^n$, $x^n \in [a,b]$, $g(X)$ is an n-polynomial and $\| g(X) \|$ is bounded or integral in the domain, and if $g(X)$ satisfies the following inner product relationship:

$$\begin{aligned} (g_l(X), g_k(X)) &= \int_{[a,b]}^{n} \rho(X) g_l(X) g_k(X) dX \\ &= \begin{cases} 0, & l = k \\ \int_{[a,b]}^{n} \rho(X) g_l^2(X) dX, & l \neq k \end{cases} \end{aligned} \tag{16}$$

Then $g_n(X)$ sequence is called multivariate orthogonal polynomial, and the weights are $\rho(X)$.

For the n-dimensional vector $X = [x_1, x_2, \cdots, x_n]^{\mathrm{T}}$, n-arid function $f(X)$ and multiple integral symbols, we make the convention as:

$\forall x_i \in X, x_i \in [a,b]$ is recorded as $x^n \in [a,b]$, $\underbrace{\int_a^b \int_a^b \cdots \int_a^b}_{n\uparrow}$ is recorded as $\int_{[a,b]}^{n}$, $dx_1 \cdots dx_n$ is recorded as dX.

Considering the multivariate polynomial composed by orthogonal polynomial, one has

$$g_i(X) = \prod_{j=1}^{n} C_i(X) \tag{17}$$

On the other hand, Chebyshev orthogonal polynomial satisfies the following inner product relationship:

$$\begin{aligned} (C_l(x), C_k(x)) &= \int_{-1}^{1} \rho(x) T_l(x) T_k(x) dx \\ &= \begin{cases} 0, & l = k \\ \int_{-1}^{1} \rho(x) T_l^2(x) dx, & l \neq k \end{cases} \end{aligned} \tag{18}$$

where $x \in R$.

Substituting Eq.(17) into Eq.(18) yields:

$$\begin{aligned} (g_l(X), g_k(X)) &= \int_{[-1,1]}^{n} \rho(X) g_l(X) g_k(X) dX \\ &= \int_{[-1,1]}^{n} \rho(X) \prod_{j=1}^{n} C_l(x_j) \prod_{j=1}^{n} C_k(x_j) dX \end{aligned} \tag{19}$$

Since the orthogonal polynomial $C_0(x)$, $C_1(x)$, …, $C_n(x)$ is linearly independent, the integral order of the Eq.(19) can be changed, then:

$$\begin{aligned} (g_l(X), g_k(X)) &= \int_{[-1,1]}^{n} \rho(X) g_l(X) g_k(X) dX \\ &= \begin{cases} 0, & l = k \\ \int_{[-1,1]}^{n} \rho(X) g_l^2(X) dX, & l \neq k \end{cases} \end{aligned} \tag{20}$$

Obviously, Eq.(20) satisfies the condition in Definition 1, which is a multivariate orthogonal polynomial, and $x^n \in [-1,1]$.

Definition 2 For a given function $f(X)$ which the range is $x^n \in [-1,1]$, using the polynomial $y(X) = \sum_{k=1}^{n} W_k g_k(X)$ to make the optimization mean square approximation and find out the value $W_i (i = 1,2,\cdots n)$ to make the function $\| f(X) - y(X) \|_2^2 = \int_{[-1,1]}^{n} \rho(X) [f(X) - y(X)] dX$ is the minimum.

Lemma 1 [13] A neural network based on the orthogonal polynomial possesses the global approximation property for arbitrary precision approaching continuous function on any compact set.

Theorem 1 According to Eq.(11), utilizing the input-output relationship of the CNN learning algorithm

based on the PSO, we can get the neural network model (12) for the chaotic system. Using the controller designed by Eq.(13) to chaotic system (11), then there exists a positive constant $\sigma(\sigma>1)$ such that $|e(k)|<\sigma|f_e(k)|$, where $e(k)$ and $f_e(k)$ denotes the tracking error and model error, respectively.

Proof: Let us denote $\gamma_1=\sup_k|e(k)|$ and $\gamma_2=\sup_k|f_e(k)|$. If we want to prove $|e(k)|<\sigma|f_e(k)|$, we just need to prove $\gamma_1\le\sigma\gamma_2$.

It follows from Eq.(14) that

$$e(k+1)=f_e(k)+\beta e(k).$$

Taking the absolute value on both sides of the equation above, one has:

$$|e(k+1)|=|f_e(k)+\beta e(k)|\le|f_e(k)|+|\beta e(k)| \qquad (21)$$

Taking the maximum on both sides of the Eq.(21), one has

$$\gamma_1\le\gamma_2+|\beta|\gamma_1$$

where $|\beta|<1$.

Consolidating the above equations yields

$$\gamma_1\le\frac{1}{1-|\beta|}\gamma_2$$

Then we denote $\sigma=\frac{1}{1-|\beta|}$, one has

$$\gamma_1\le\sigma\gamma_2$$

where it is obvious that $\sigma>1$, which implies that $|e(k)|<\sigma|f_e(k)|$.

Remark**:** Theorem 1 denotes that the tracking error cannot be less than the model error. Therefore, the model error on the stability of the system is an extremely important role that the higher accuracy of the model, the higher accuracy of the control.

IV THE NUMERICAL SIMULATION

We use the Logistic chaotic system to check the effectiveness of the chaos control method. The details are as follows.

Logistic mapping system is:

$$x(k+1)=\lambda x(k)(1-x(k)) \qquad (22)$$

where $x\in[0,1]$ and λ is a positive constant. When $\lambda=4$, the system is in a chaotic state. Supposing $\eta=0.05$, $\alpha=0.01$, and using the fuzzy Chebyshev neural network learning algorithm (22), we can get a model as follows:

$$\hat{x}(k+1)=\hat{f}(x(k))$$

According to the Eq.(13), a desired controller is as follows:

$$u(k)=-\hat{f}(x(k))+x_d(k+1)+\beta(x(k)-x_d(k))$$

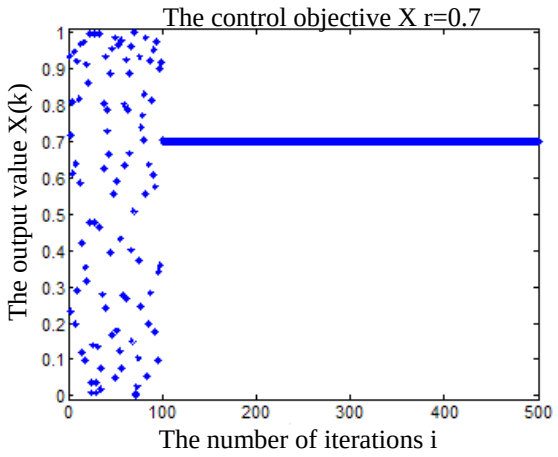

Figure 3

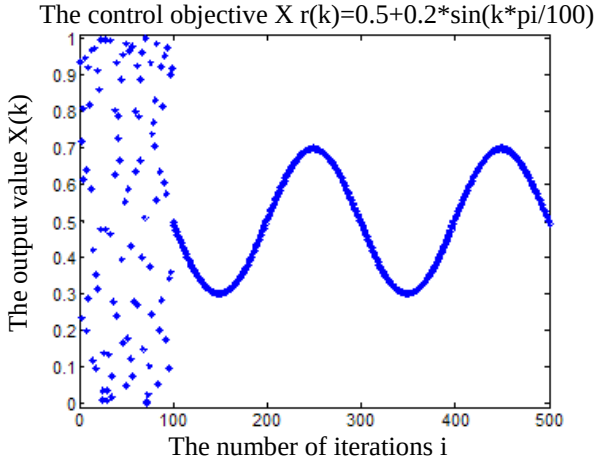

Figure 4

When the control is exerted, the system (22) is changed as:

$$x(k+1)=\lambda x(k)(1-x(k))+u(k) \qquad (23)$$

When $\lambda=4,\beta=0.02$, the designed control targets are $x_r(k)=0.7$ and $x_r(k)=0.5+0.2\sin(k\pi/100)$.

When the control is exerted at the 100th step, the control results are showed in figure 3 and figure 4, respectively.

V CONCLUSION

An adaptive control method based PSO and CNNs is proposed for chaotic systems. The PSO algorithm is mainly used to search for the weights of the CNNs. Then, an adaptive controller for the chaotic systems is designed using the approach which is combined with PSO and CNNs. Furthermore, we prove that the designed controller can guarantee the stability of chaotic systems.

Finally, the Logistic chaotic system is given to demonstrate the effectiveness of the proposed method.

ACKNOWLEDGMENT

This work was supported by National Natural Science Foundation of China (61304256), Zhejiang Provincial Natural Science Foundation of China (LQ13F030013), project of Education Department of Zhejiang Province (Y20132700), Ningbo Natural Science Foundation (2012A610016) and Science Foundation of Zhejiang Sci-Tech University (1202815-Y).

REFERENCES

[1] E. Ott, C. Grebogi, and J. A. Yorke, "Chaos control," *Physical Review Letters*, vol. 64, no. 11, pp. 1196-1199, 1990.
[2] G. Chen, "Controlling chaos and bifuractions in engineering systems", *CRC press*, 2000.
[3] W. Sanum, and B. Srisuchinwong, "Highly complex chaotic system with piecewise linear nonlinearity and compound structures," *Journal of Computers*, vol. 7, no. 4, pp. 1041-1047, 2012.
[4] X J Li, W X Xiao, Z Liu, W L Wan, and T S Hu, "A new fractional order chaotic system and its compound structure," *Journal of Software*, vol. 8, no. 1, pp. 126-133, 2013.
[5] P. M. Alsing, A. Gavrielides, "Using neural networks for controlling chaos," *Physical Review E*, vol. 49, pp. 1225-1231, 1994.
[6] C. T Lin, "Controlling chaos by GA-based reinforcement learning neural networks," *IEEE Transactions on Neural Networks*, vol. 10, no. 4, pp. 846-859, 1999.
[7] C. F Hsu, "Intelligent control of chaotic systems via self-organizing Hermite-polynomial-based neural network," *Neurocomputing*, vol. 123, pp. 197-206, 2014.
[8] P. Yadmellat, S. K. Y. Nikravesh, "A recursive delayed output-feedback control to stabilize chaotic systems using linear-in-parameter neural networks," *Communications in Nonlinear Science and Numerical Simulation*, vol. 16, no. 1, pp. 383-394, 2011.
[9] S. C. Jeong, D. H. Ji, J. H. Park, S. C. Won, "Adaptive synchronization for uncertain chaotic neural networks with mixed time delays using fuzzy disturbance observer," *Applied Mathematics and Computation*, vol. 219, no. 11, pp. 5984-5995, 2013.
[10] L S Yin, Y G He, X P Dong, and Z Q Lu. "Multi-step prediction algorithm of traffic flow chaotic time series based on volterra neural network," *Journal of Computers*, vol. 8, no. 6, pp. 1480-1487, 2013.
[11] W Tan, Y N Wang, Z R Liu,and S W Zhou, "Controlling chaotic system by RBF neural networks nonlinear compensator," *Control Theory & Applications*, vol. 20, no. 6, 951-954, 2003. (In Chinese)
[12] D Liu, H P Ren, and Z Q Kong, "Control of chaos solely based on RBF neural network without an analytical model," *Acta Physica Sinica*, vol. 52, no. 3, pp. 533-535, 2003. (In Chinese)
[13] X J Wu, S T Wang, J Y Yang, and Q Y Cao, "The study on the orthogonal polynomials-based neural networks and its properties," *Computer Engineering and Application*, vol. 39, no. 9, 25-27, 2002. (In Chinese)
[14] J. R Zhang, J Zhang, T. M Lock, and M. R. Lyu, "A hybrid particle swarm optimization—back-propagation algorithm for feedforward neural network training," *Applied Mathematics and Computation*, vol. 185, pp. 1026-1037, 2007.
[15] V Basios, A. Yu. Bonushkina, and V. V. Ivanov, "On a method for approximatin one-dimensiona functions," *Computer and Mathematics with Applications*, vol. 34, pp. 687-693, 1997.

Zhen Hong received both B.S. degrees from Computer Science & Technology at Zhejiang University of Technology, Hangzhou, China and Computing at University of Tasmania, Australia, respectively. He received Ph. D. degree in Control Theory and Control Engineering at the College of Information Engineering, Zhejiang University of Technology, Hangzhou, China, in 2012. He is currently working as a lecturer at Faculty of Mechanical Engineering & Automation, Zhejiang Sci-Tech University, Hangzhou, China.

His main research interests include wireless sensor networks, optimization, adaptive control and intelligent transportation.

Xile Li received the B.S. degree in Measurement Technology and Instrument at Faculty of Mechanical Engineering & Automation, Zhejiang Sci-Tech University, Hangzhou, China, in 2012. She is currently a Master student in Faculty of Mechanical Engineering & Automation, Zhejiang Sci-Tech University, Hangzhou, China.

Her main research interests include wireless sensor networks, topology control.

Bo Chen received the B.S. degree in Information and Computing Science from Jiangxi University of Science and Technology, Ganzhou, China, in 2008. He is currently working toward the Ph.D. degree in Control Theory and Control Engineering at the College of Information Engineering, Zhejiang University of Technology, Hangzhou, China.

His main research interests include information fusion, distributed estimation, and time-delay systems.

Relay Node Scheduling Model Based on Improved Discrete Markov Chain

Chaoyi Zhang
School of Science and Technology, Beijing Forestry University, Beijing 100083, China
Email: drzhangchy@yeah.net

Yandong Zhao and Junguo Zhang
School of Science and Technology, Beijing Forestry University, Beijing 100083, China
Email: drzhangchy@yeah.net

***Abstract*—This paper focuses on relay node scheduling method which is based on an improved discrete Markov chain. It presents a single relay node's existing state, analyzes its access behavior, and summarizes various linear system design, according to our present balanced equations and form state transition probability, nodes are scheduled in relay network, the improved discrete time Markov chain is used to reduce destination noise, improve channel's SNRs performance. The simulation shows that the Markov chain-based relay distribution scheduling model is better than the tradition similar relay network methods, and the result is consistent with the theoretical analysis.**

***Index Terms*—relay system, node scheduling, Markov chain, state transition, balance equations**

I. Introduction

The relay network is one of the most promising architectures for future wireless networks. The users, who share the antenna with each other, can bring about the space diversity, so the multipath fading of wireless channel can be restrained effectively. The single-source relay systems are well studied [1]. The research of relay network demonstrates that simultaneous using relay nodes can extend the cell coverage and enhance the system capacity. In wireless sensor networks, several relay nodes can be utilized to support multiple source-destination pairs simultaneously as a virtual spatial multiplexing (SM) mode [1-3].

In traditional cellular system, with the data increasing, 3GPP defines a variable data rate cellular system [2-3]. For the data services, the power sharing concept, which is used in voice service, no longer keeps the effectiveness, the reason is that the purpose of data service transmission system is to maximize throughput. In addition, the variable data rate cellular system does not use the power control mechanism on its downlink data access, and the data rate which Mobile Terminal (MT) obtained will be changed with the user's location movement. Therefore, the users who are close to the base station will receive a higher downlink transmission rate, and the users who are at the cell edge will obtain a lower downlink transmission rate. Base-station scheduling or modulation technique can be used to solve this problem. If the scheduling mechanism provides fair downlink transmission rate for each user, and regardless the user's location, the system throughput will be reduced [4-5]. However, when the scheduling mechanism is used to maximize the system throughput, the fairness will be difficult to allocate. So it is necessary to find a new solution to provide fairness service for each user, meanwhile, the network resources are used efficiently.

There are plenty of patterns of relay collaboration, J N Laneman had summarized it in [6], he grouped these relays into fixed relay, selective relay and incremental relay coordination, present and proved that the frequency spectrum efficiency of incremental relay coordination is better than the others, and the incremental relay coordination is a low complexity, high-efficiency wireless relay model.

How to distribute and manage the relay nodes is a key technology in cooperative communication. Because the network mobility of each node causes the link failure, and the relay synergistic effect may be influenced, this will increase the system cost, the previous research [7] focuses on the outage probability, frame error rate, power and other performance parameters. However, whether the state of relay node itself should be considered --- when to work? Will it sleep? how collaboration's probability? There are many relay cooperative patterns [8-10].

At present, some researches focus on some scheduling mechanism which the discrete time Markov chain (DTMC) present, [11] Markov fluid model is used in establishing the model of the wireless channel state, and obtained the effective expression of the system capacity, [12] used the Markov features to solve the different priority of access service, established the scheduling model, and proposed the corresponding performance analysis. Most previous researches were based on the node itself state to schedule. In the wireless relay system, the Markov features are not taken into the system model, which includes the data arriving and data sending .

Inspired by the above introduction, this paper presents a new Markov chain-based relay distribution scheduling model (MRDSM). Based on the relay node working state, the Markov process is able to describe the state transition,

doi:10.4304/jcp.9.6.1391-1396

and the system equilibrium equations are obtained through the state transition probability. Nodes scheduling model is used, and the calculation is taken into this model finally, the simulation results show the correctness and effectiveness of theoretical analysis.

II. System Model

One cellular access situation is considered. The network topology which uses the relay station is shown in Fig.1. The BS is the base station, the RS is the relay station, the SS is the user terminal. Because the distance between the terminal nodes and the base station, it leads to the performance differences in data transmission rate, time-delay and so on, to solve this, the cellular can be divided into different coverage areas. It can be seen from the figure that the circular area covered by the base station is the network basic coverage layer, which in the centre of base station with the circle in solid line in Fig.1. The relay station's position should be on the edge of the base station coverage area, its coverage includes the district's "blind spot" areas, and has a ringlike overlapping with the base station's coverage area, which is in the centre of relay station with the dashed circle line in Fig.1. The relay station's service area is far less than the base station coverage, it is mainly used to supply the coverage (i.e. SS1~SS6 in Fig.1), it can also reduce the inter-cell interference, and the terminals in the ringlike overlapping area can be provided the diversity gain (i.e. SS7~SS8 in Fig.1). A terminal can be connected with the base station through the relay station (i.e. SS1 ~ SS6), and it also can be connected with the base station directly (i.e. SS7, SS8).

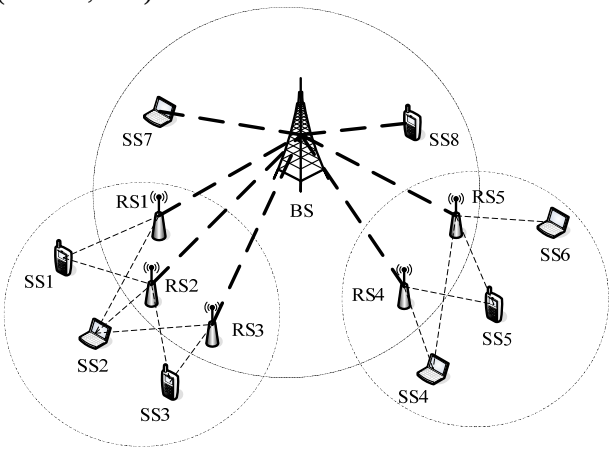

Figure 1. Network system model

Resource allocation and scheduling are both controlled and managed by the base station. Using one hop relay station, that means the hop count from the base station to the terminal is 1, the multi-hop relay will be considered when the network needs to extend. And all nodes have to maintain the time consistency; this can make the nodes wake up from the sleep state at the same time.

III. Node Access Behavior Modeling

In the actual network environment, the nodes state can be approximated considered that it is only related with the last time, so this process can be seen as a discrete time Markov chain (DTMC), and influenced by other nodes.

A. Node Status Description

The node R generally can be divided into two states: working state (W) and sleep state (D). Because the nodes state has Markov character, so the random process of node state transition can be described as follows:

$$P\{X_{n+\Delta t}=D \mid X_n=W_n, X_{n-1}=W_{n-1},\cdots, X_1=W_1\} = P\{X_{n+\Delta t}=D \mid X_n=W_n\} \quad (1)$$

When the node is in the working state, elapsed time Δt , then entering into the next state's probability (transition probability), is not only related with the next state W, but also related with the time Δt . Δt is the residence time in which the node stay a certain state, i.e. the node's probability distribution in the state W. From the discrete-time Markov character, we can know that T_i is a non-memory distribution function, so the probable distribution of equation (1) can be expressed as:

$$P\{X_{n+\Delta t}=D \mid X_n=W_n\}=P\{T_i<\Delta t\} \ =1-\exp(-q\Delta t) \quad (2)$$

Here we use the non-memory character of exponential distribution. Taking equation (2) into Taylor expansion, we acquire :

$$P\{X_{n+\Delta t}=D \mid X_n=W_n\}=q\Delta t+o(\Delta t) \quad (3)$$

Where q is the exponential distribution parameter, and q is also the state transition probability, $o(\Delta t)$ is a infinitely small variable. Equation (3) shows that the node state transition probability from W to S is proportional to the time interval Δt , and the transition probability is q . These transition probabilities constitute the transition probability matrix, as follows:

$$q_{iiz}=\sum_{i\neq j}^{n} q_{ij} \ , \sum_{j=1}^{n} q_{ij}=0 \ , i=1,2,\cdots,n \quad (4)$$

The above process can be expressed as Fig.2.

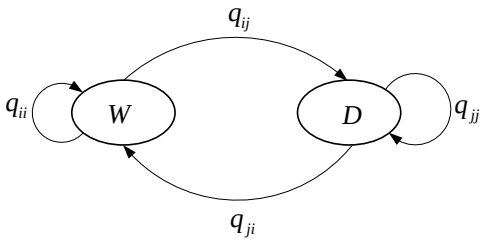

Figure 2. A single node's working state transition

Because every node's state is different, the data transmission process will cause data collision in a certain probability. Therefore, if we want the data to be successfully sent, the relay node has to take a logical estimate of the previous hop node, next hop node working state and sleep state, then the base station can schedule the system resources and avoid conflict effectively.

B. Markov state Transition Model Description

The system nodes scheduling process under Markov model is a doubly stochastic process, this is expressed as the user communicating with the base station through a

certain relay node or direct is all random, the relay node working state or sleep state is also random in the network. So we can use the Markov theory to establish the node's scheduling model and describe such random process.

According to the system structure in Fig.1, the cellular has one base station, M relay nodes, K users, i relay nodes and j users in the working state. Then state space S of the two-dimensional discrete Markov chain can be expressed as:

$$S=\{(i,j)\,|\,i=1,2,\cdots,M,\ j=1,2,\cdots,K\} \tag{5}$$

The relay nodes and users' data receiving and sending process are complied with the Poisson distribution, and their arrival rate are λ_1 and λ_2 respectively, data sending rate or service rate are μ_1 and μ_2. Here, λ_1, λ_2, μ_1 and μ_2 's dimension are the call number of arriving or sending in one second. Thus, the system node access model which based on Markov model can be expressed as:

$$\phi=(S,Q,P) \tag{6}$$

S means the state space. Q means the transition probability matrix, $Q=[q_{(c,d)}^{(a,b)}]$, $(a,b)、(c,d)\in S$, matrix element $q_{(c,d)}^{(a,b)}$ means the probability of system state from (a,b) transfer to (c,d). P is the distribution vector when the system reaches the steady-state, $P=[P(i,j)]$.

From the nature of transfer probability matrix in equation (4), we can get:

$$P^TQ=0,\ P^T\cdot 1=1 \tag{7}$$

Under normal circumstances, the state (i,j) transition situation in Fig.3 is considered. It can be seen from the figure, in the time interval Δt, only one node state causes changes, then it can be transfered to the next state in the system; when two or more nodes state have changed, the system will occur blocking phenomenon. And the system also can change state if the blocking occurs, then the system state will be transferred from (i,j) to $(i-m,j+1)$ under the blocking conditions, where m means the number of relay nodes which from working state to sleep state in time interval Δt, $0\le m\le M$.

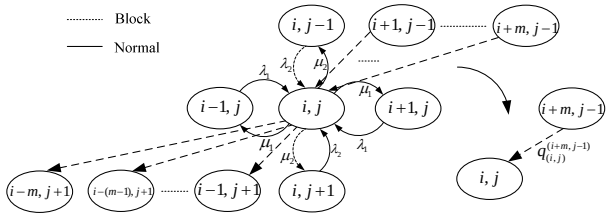

Figure 3. Network node's state transition

Based on the above process, the system equilibrium equation under the general situation is considered. The system state is transferred from (i,j) to $(i-m,j+1)$, that also means the m relay nodes which from working state to sleep state in time interval Δt, thus it causes the system blocking and operating failure. The remaining $i-m$ relay nodes are still communicated with $K-j-1$ users. From the calculation of transition probability according to the Markov theory, we can get the transition probability of m relay nodes state have in time interval Δt:

$$P_{(i-m,j+1)}^{(i,j)}=\frac{C_M^m C_{K-j-1}^{i-m}}{C_{k-j}^i} \tag{8}$$

In addition, the system stay time in the state (i,j) is related to the time interval Δt and the user's call arrival rate λ_1 and $\Delta t=1/\lambda_1$, so the system transition probability, from state (i,j) to $(i-m,j+1)$, is:

$$q_{(i-m,j+1)}^{(i,j)}=P_{(i-m,j+1)}^{(i,j)}/\Delta t=\lambda_1 C_M^m C_{K-j-1}^{i-m}/C_{k-j}^i \tag{9}$$

By the constraint conditions (7) and (9), the equilibrium equation of system state (i,j) can be achieved according to Fig.3:

$$\begin{aligned}&[j\mu_1+i\mu_2+\lambda_2+\sum_{m=0}^{M}q_{(i-m,j+1)}^{(i,j)}]P(i,j)=\\&\lambda_1P(i-1,j)+(j+1)\mu_1P(i,j+1)+(i+1)\mu_2P(i+1,j)+\\&\sum_{m=0}^{M}q_{(i,j)}^{(i+m,j-1)}P(i+m,j-1)\end{aligned} \tag{10}$$

And the nature of steady-state probability

$$\sum_{i=0}^{M}\sum_{j=0}^{K}P(i,j)=1,\ 0<i<M,0<j<K; \tag{11}$$

And

$$i<0,\ j<0,\ P(i,j)=0 \tag{12}$$

C. Work Process

The above section shows that, when two or more nodes have changed status, the nodes which have caused the state transition will enter into the blocking state and can not transmit data, until the time interval Δt is over, then they continue the working state. According to the number m, we get the state transition probability, and obtain the system state balance equation. Based on this, we present a new Markov chain-based relay distribution scheduling model (MRDSM). MRDSM's main idea is: first, the state model of the relay nodes is needed to establish and calculate; second, the nodes state transition probability is constructed, and the state transition probability matrix is obtained; third, through scheduling the probability of node work or sleep state, it can save the system resources. This method is as follows:

Every node has a state information table which stores the transition probability and time interval, the table records each node's own occurrence transition probability and time interval Δt. The power and time information should be recorded when RTS / CTS frame are sent, for example, the relay node i detects the RTS signal which is sent from user k. The node power values are translated into the probability statistic values [13], then put into the state information table, and the time t of receiving RTS is recorded as well. At this moment, if the state information table is not empty, the node will be at working state, otherwise, the system will block. By these steps, the system working steps are as follows:

1) Each node takes the cooperation of detecting the channel's handshake signal power values, and calculates the probability values, then stores these values into the state information table.

2) Each node records the time values, and also stores them into the table.

3) The system state (i, j) transfer situation should be scheduled according to the system equilibrium equation which presented in section 3.2. If the state information table is empty, it indicates that the node is blocked, after a time interval Δt, we change this node to re-work state, and update the state information table.

4) The state information table is updated continually, and the nodes are re-scheduled, then repeat the process.

According to the above algorithm, we can get the system transition probability which based on Markov model and the final steady-state probability of each node.

IV. Simulation Results And Analysis

A. Bandwidth Utilization and Forced Outage Probability

This paper builds a honeycomb cell model, the simulation environment is as follows: there has 3 relays, users number K is set 8, the system bandwidth is $B = 11MHz$, assuming in the transmit power of base station, relay node and user node is the same, the signal to noise ratio (SNR) of signals arriving destination node is equal $SNR = 2dB$, Rayleigh channel model is used. The average outage probability and ergodic capacity are considered as the criterion, and they are defined as:

$$P_{out} = \frac{1}{N_S}\sum_{i=1}^{N_S} \Pr(\gamma_i < \gamma_{th}), \gamma_{th} = 1 \tag{13}$$

$$C = \sum_{i=1}^{N_S} E[\log_2(1+\gamma_i)] \tag{14}$$

The simulation assumes that $N_R = 4$, $N_S = N_D = 2$, $\rho_{SR} = \rho_{RD}$. The traditional relaying protocol is shown as "non SCM" in the simulation results, "SCMP" means the spatial channel matching matrix which based on permutation, "SCMM" means Markov chain-based relay distribution scheduling model method.

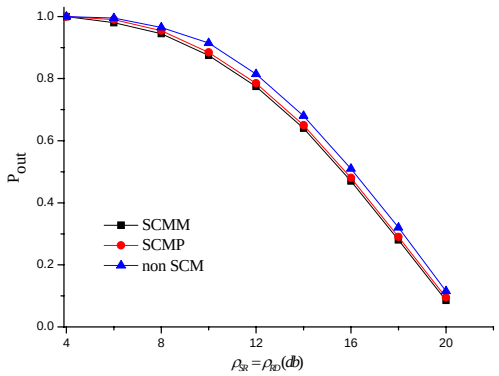

Figure 4. System outage probability comparison

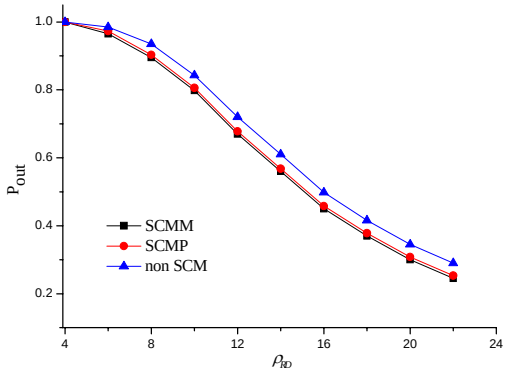

Figure 5. System outage probability comparison

The outage probability performance of spatial channel matching and mapping matrix is shown in Fig.4. The matrix reduces the outage probability, and enhances the system reliability. As for what is mentioned before, the unitary matrix has a more extensive, it includes the permutation matrix, so the performance of spatial channel mapping matrix is better than the matching matrix, but there is little difference between them. When $\rho_{SR} = \rho_{RD}$, the spatial channel mapping matrix has about 0.3dB/0.2dB gain in outage probability performance, which compared with the traditional ZF relaying protocol. With ρ_{SR} and ρ_{RD} increasing, the effect of the spatial channel mapping matrix is gradually weakened, finally, three curves are overlapped. When ρ_{SR} is fixed, the outage probability curve is flattened with the ρ_{RD} increasing, as shown in Fig.5.

It can be seen from the simulation results that the Markov chain-based relay distribution scheduling model is better than the spatial channel matching that based on permutation matrix. However, the performance difference between these two methods is not obvious. The spatial channel matching (mapping) reduces the relay transmitting signal's noise, and it can be used in multiple single-antenna destination nodes or one multiple-antennas destination node to improve the relay system effectiveness and reliability.

B. System Capacity and Blocking

Here it still uses the above section's parameters, and the different is: the *SNR* is set as $16dB$, and average power allocation algorithm is used on each node, this can compare these two group simulation performance clearly. In this section, ergodic capacity is considered as the criterion, and it is defined as:

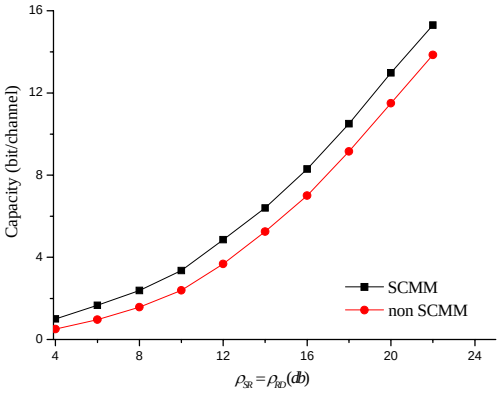

Figure 6. Capacity and call arrival rate

Fig.6 shows the relationship between the system capacity and the call arrival rate. It can be seen from the figure, the system capacity will increase with the call increasing, because the call increasing can lead to the frequency spectrum utilization effective. At the same time when the call grows to a certain extent, the system capacity will slowly levelling off, because with the call increasing, the system outage probability will also tend flattening, then the system may reach a state of equilibrium eventually. From the figure, the parameters λ and μ can cause greater differences of the two simulation scenarios, and they are two important parameters which controlling the service speed of Markov model. The figure shows that, if the system capacity want to be having a greater improvement, the service rate of relay nodes needs to be strengthened.

V. CONCLUSIONS

This paper focuses on relay node scheduling method based on discrete time Markov chain. It presents a single relay node's existing state, and analyses its access behaviour, and summarizes various linear system designs, according to some equation, nodes are scheduled in relay network. The improved discrete time Markov chain is used to reduce destination noise and improve the SNRs performance. The simulation shows the performance changed under using the spatial channel mapping matrix, and the result is consistent with the theoretical analysis.

ACKNOWLEDGMENT

This work was supported by Fundamental Research Funds for the Central Universities (NO.TD2013-3) and the project of Beijing Municipal Education Commission for building scientific research and scientific research base No.2008BJKY01.

REFERENCES

[1] Xiaoqing Yu, Pute Wu, Ning Wang, Wenting Han, Zenglin Zhang. "Development of a New Wireless Sensor Network Communication," *Journal of computers*, Vol. 8, No. 10, Oct 2013.

[2] Ding Zhiguo, Leung Kin K., Goeckel Dennis L. "A relay assisted cooperative transmission protocol for wireless multiple access systems," *IEEE Transactions on Communications*, vol. 58, no. 8, pp. 2425-2435, 2010.

[3] 3GPP TS 26.234 V5.6.0: "Transparent end-to-end Packet-switched; Streaming Service (PSS); Protocols and codes (Release 5) ," *http://3gpp.org/*, 2003, 09.

[4] Yuan Quan, Cardei Ionut, Wu Jie. An efficient prediction-based routing in disruption-tolerant networks. *IEEE Transactions on Parallel and Distributed Systems*, vol. 23, no. 1, pp. 19-31, 2012.

[5] Shi Xiaomeng, Médard Muriel, Lucani Daniel E.Whether and where to code in the wireless packet erasure relay channel. *IEEE Journal on Selected Areas in Communications*, vol. 31, no. 8, pp. 1379-1389, 2013.

[6] Laneman J. Nicholas, Tse David N. C., Wornell Gregory W. "Cooperative diversity in wireless networks: Efficient protocols and outage behavior," *IEEE Transactions on Information Theory*, vol. 50, no. 12, pp. 3062-3080, December 2004.

[7] Nazir Sajid, Stankovic Vladimir, Attar Hani, Stankovic Lina, Cheng Samuel. Relay-assisted rateless layered multiple description video delivery. *IEEE Journal on Selected Areas in Communications*, vol. 31, no. 8, pp. 1629-1637, 2013.

[8] Mahbubul Syeed M.M., Hammouda Imed, Systä Tarja. "Evolution of open source software projects: A systematic literature review," *Journal of Software*, vol. 8, no. 11, pp. 2815-2829, 2013.

[9] Maham B., Hjrungnes A. "Differential space-time coded cooperation for decode-and-forward-based wireless relay networks," *IET Communications*, vol. 4, no. 6, pp. 631-638, 2010.

[10] Sun Li, Zhang Taiyi, Lu Long, Niu Hao. "On the combination of cooperative diversity and multiuser diversity in multi-source multi-relay wireless networks," *IEEE Signal Processing Letters*, vol. 17, no. 6, pp. 535-538, 2010.

[11] Vianello Valerio, di Flora Cristiano, Prehofer Christian. "A comparison of GIS architectures for implementing indoor location-based services," *Journal of Software*, vol. 4, no. 7, pp. 664-674, Sep 2009.

[12] Tadayon Navid, Wang Honggang, Kasilingam Dayalan, Xing Liudong. Analytical modelling of medium-access delay for cooperative wireless networks over rayleigh fading channels. *IEEE Transactions on Vehicular Technology*, vol. 62, no. 1, pp. 349-359, 2013.

[13] Witwicki Stefan J., Witwicki Stefan J. "Commitment-based service coordination," *International Journal of Agent-Oriented Software Engineering*, vol. 3, no. 1, pp. 59-87, 2009.

[14] Gu Bo, Hong Xiaoyan, Wang Pu. Analysis for bio-inspired thrown-box assisted message dissemination in delay tolerant networks. *Telecommunication Systems*, vol. 52, no. 1, pp. 217-227,Jan 2013.

[15] Liu Ke. Applied Markov Decision Process. Beijing: *Tsinghua University Press*, 2004.

[16] MPR-MIB Users Manual (Revision A) [Online], available: *http://www.xbow.com*, June 6, 2007.

Chaoyi Zhang born in December 1985, received his Bachelor's degree in Measurement control technology and instruments from Beijing University of Posts and Telecommunications, Beijing, China, at 2003~2007, received his Master and Ph.D degree in Communication and Information System from Beijing University of Posts and Telecommunications, Beijing, China, at 2007~2012. Since July of 2012 he worked in Beijing Forestry University as a Lecturer. His research interests include cooperative communication, relay transmission, signal processing, communication theory, and he has great interest in 4G technologies.

E-mail：drzhangchy@yeah.net

Address: School of Technology, Beijing Forestry University, No.74 Mailbox, 35# Qinghua East Road Haidian District, Beijing, China

Post Code: 100083

Yandong Zhao born in 1965, Ph.D degree, professor at Beijing Forestry University. She is interested in researching control theory and control engineering, frozen soil research, wireless sensor network and plant water detection technology.

Junguo Zhang born in 1978, Ph.D degree, associate professor at Beijing Forestry University. He is interested in researching control theory and control engineering, wireless sensor network and wild animal detection technology.

Multiplexing Periodic CSI with HARQ-ACK on PUCCH Format 3 in LTE-A

Dan Wang[1, 2]
1.School of Communication and Information Engineering, Chongqing University of Posts and Telecommunications, Chongqing, China
2.College of Communication Engineering, Chongqing University, Chongqing, 400044, China
Email: drwangdan@yeah.net

*Xuemei Deng, Xiaowen Li and Xin Ni
School of Communication and Information Engineering, Chongqing University of Posts and Telecommunications, Chongqing, China
Email: drwangdan@yeah.net

***Abstract* — In order to avoid dropping the periodic CSI report frequently in case of collision between a periodic CSI report and HARQ-ACK feedback in LTE-Advanced system, this paper gives two coding schemes for multiplexing periodic CSI (Channel State Information) with HARQ-ACK (Hybrid Automatic Repeat request Acknowledgement) feedback on PUCCH (Physical Up Control Channel) format 3. The result of simulation shows that both of the two coding schemes can effectively support simultaneous transmission periodic CSI and HARQ-ACK feedback on PUCCH format 3. What's more, with joint coding scheme, periodic CSI and HARQ-ACK feedback have the same performance, while HARQ-ACK feedback has better performance than periodic CSI with separate coding scheme. Hence through the separate coding scheme, we can not only enhance simultaneous transmission of periodic CSI and HARQ-ACK feedback, but also guarantee the similar performance of HARQ-ACK feedback as transmitting it alone.**

***Index Terms* — Periodic CSI, HARQ-ACK, Multiplexing, PUCCH format 3**

I. INTRODUCTION

Along with the 4rd generation mobile communication technology appearance, the LTE-Advanced is researched and standardized by 3GPP organization. One of the most important technologies introduced in LTE-Advanced is the carrier aggregation (CA) of multiple Component Carriers (CCs) [1, 2], which is introduced to LTE-Advanced to support peak data rates of 1 Gbps in the downlink and 500 Mbps in the uplink, facilitate efficient use of fragmented spectrum and support heterogeneous networks. However, some technical challenges for implementing CA technique in LTE-Advanced [3] system still remain highlighted. One of the challenges is the HARQ-ACK bits with huge increase compared with LTE [4, 5] system. In carrier aggregation, a UE (User Equipment) have to feedback HARQ-ACK bits for all configured downlink CCs [6-8] on uplink PCC (Primary Component Carriers) which can be as much as 90 bits at most. However, LTE was not designed to carry such large numbers of HARQ-ACK bits from multiple downlink CCs. In order to solve this problem, PUCCH format 3 [9, 10] is applied in LTE-Advanced in support of carrier aggregation.

The PUCCH format 3 supports transmission of 48 coded bits. The actual number of bits of HARQ-ACK is determined from the number of configured CCs, the configured transmission modes on each of them, and, in TDD, the HARQ-ACK bundling window size (the number of downlink subframes associated with a single uplink subframe). For TDD, PUCCH format 3 supports a HARQ-ACK payload size of up to 20 bits. If the number of HARQ-ACK bits to be fed back for multiple downlink subframes from multiple CCs is greater than 20, 'spatial bundling' of the HARQ-ACK bits corresponding to the two codewords within a downlink subframe is performed for each of the configured CC to reduce the HARQ-ACK bits. Thus, the HARQ-ACK bits may be less than 20 bits and can be fed back on PUCCH format 3. However, a UE not only need to feedback HARQ-ACK bits from multiple downlink CCs, but also should report CSI about each configured CC. So, when HARQ-ACK bits collide with CSI [11, 12], a new challenge appears.

For TDD and for a UE that is configured with one CC and with PUCCH format 3, in case of collision between a periodic CSI report and an HARQ-ACK feedback [13-15] in the same subframe without PUSCH, if we drop the periodic CSI report, the system performance will be degraded. As more configured CCs are aggregated, its dropping will occur more frequently and thus lead non-negligible downlink throughput loss [16, 17]. Therefore, to avoid downlink throughput loss, it should be considered that simultaneous transmission of HARQ-ACK feedback and periodic CSI on PUCCH format 3 is introduced for LTE-Advanced.

This paper focuses on the feasibility and application scenarios of multiplexing periodic CSI with HARQ-ACK

*Corresponding Author.

doi:10.4304/jcp.9.6.1397-1401

feedback on PUCCH format 3, then proposes two channel coding schemes, such as joint coding scheme and separate coding scheme, for simultaneous transmission periodic CSI and HARQ-ACK feedback on PUCCH format 3. Simulation results demonstrated that with joint coding scheme the performance of periodic CSI and HARQ-ACK feedback are similar whereas the performance of HARQ-ACK feedback [18] is better than it of periodic CSI and close to it of HARQ-ACK feedback as transmitting it alone with separate coding scheme. Thus through the separate coding scheme, we can not only enhance simultaneous transmission of periodic CSI and HARQ-ACK feedback, but also guarantee the similar performance of HARQ-ACK feedback as transmitting it alone.

The rest of this paper is organized as follows. In Section Ⅱ, the feasibility and application scenarios of multiplexing periodic CSI with HARQ-ACK feedback on PUCCH format 3 are discussed. Two coding schemes to realize it are described in detail in Section Ⅲ. Simulation results are presented and discussed in Section Ⅳ. This paper is concluded in Section Ⅴ at last.

II. Feasibility and Application Scenarios

A. Feasibility

From 3GPP Rel-11, the maximum payload size carried by PUCCH format 3 is 22 bits in TDD, this corresponds to 21 HARQ-ACK bits plus 1 SR bit where the SR is appended to the HARQ-ACK bits [10]. According to Rel-11, the periodic CSI report is 11 bits at most. If there is up to 10 HARQ-ACK bits plus 1 SR bit, the PUCCH format 3 can in principle be used for multiplexing HARQ-ACK bits with any of the PUCCH periodic CSI reporting modes. For example, this could be done by using a dual $(32, O)$ RM coding for a total of 22 payload bits. However, we should expect the number of configured downlink CCs for a UE to be less than the nominal maximum of 5 CCs for many cases. If the number of the HARQ-ACK bits is more than 10 bits and the SR need to be transmitted in the same subframe, a much simpler approach for this case is to drop the periodic CSI report on the PUCCH format 3.

B. Application Scenarios

For TDD, it's feasible to multiplex periodic CSI report with HARQ-ACK feedback on PUCCH format 3 [13]. However, we should not increase PUCCH overhead and complicate the PUCCH format 3 too much. So it is not preferred to use PUCCH format 3 for simultaneous transmission of periodic CSI and HARQ-ACK if extra resource for PUCCH format 3 is needed. For example, for the case that PUCCH format 1b with channel selection is used for HARQ-ACK only feedback and PUCCH format 2 is configured for periodic CSI only reporting, eNB (evolved Node Base) needs to assign extra resource for PUCCH format 3 to support simultaneous transmission of periodic CSI and HARQ-ACK on PUCCH format 3, which will increase the PUCCH overhead. Thus, multiplexing periodic CSI report with HARQ-ACK bits on PUCCH format 3 has the following two possible application scenarios.

(1) Scenario 1: PUCCH format 3 is used for HARQ-ACK only feedback but not configured for periodic CSI only reporting.
(2) Scenario 2: PUCCH format 3 is configured for periodic CSI only reporting.

III. Two Channel Coding Schemes

With simultaneous transmission of periodic CSI and HARQ-ACK on PUCCH format 3, the channel coding scheme needs to be simple, flexible and effective. According to this, we propose two coding schemes for periodic CSI and HARQ-ACK feedback on PUCCH format 3.

A. Joint Coding of Periodic CSI and HARQ-ACK

In joint coding scheme, periodic CSI bits are concatenated next to HARQ-ACK bits, and then the concatenated bits are encoded by Reed-Muller (RM) code and rate matching. The processing is the same as in the case if there are only HARQ-ACK bits on PUCCH format 3. An example for the case of dual RM code is shown in Fig. 1.

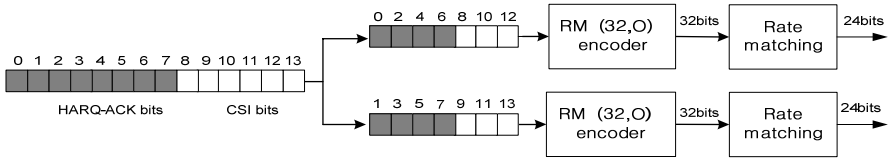

Figure 1. An example for joint coding scheme

The coding processing of this scheme is the same as in the case if there is only HARQ-ACK feedback without CSI. So it is fully compatible with the earlier version and can be implemented with little modification. However, in joint coding scheme, the HARQ-ACK bits and periodic CSI bits are treated like the same. Thus the performance of HARQ-ACK and periodic CSI is always the same. From Fig. 1, both of them are punched by rate matching, so the performance of them will be all degraded.

As we known, the HARQ-ACK feedback has the higher priority than periodic CSI bits. As the communication environment getting worse, the performance of HARQ-ACK will be serious degraded, which will inevitably decrease downlink throughput heavily. So, it is not necessary to sacrifice the performance of HARQ-ACK for periodic CSI. Thus, periodic CSI and HARQ-ACK feedback should be treated differently.

B. Separate Coding of Periodic CSI and HARQ-ACK

To multiplex periodic CSI with HARQ-ACK and control their performance separately, it is preferred to use separate coding scheme. The processing of separate coding scheme is shown in Fig. 2.

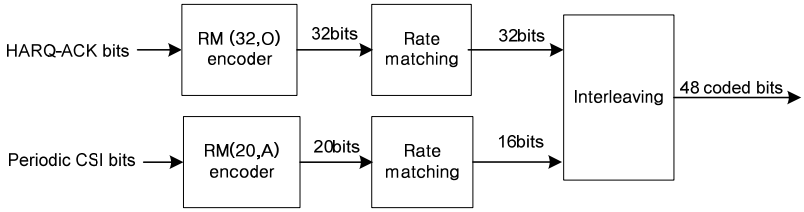

Figure 2. Basic processing for separate coding

In separate coding scheme, HARQ-ACK and periodic CSI are encoded by RM $(32, O)$ encoder and RM $(20, A)$ encoder separately. As HARQ-ACK and periodic CSI are coded separately, the performance of HARQ-ACK and periodic CSI can be controlled. To make the performance of the HARQ-ACK bits better than periodic CSI, rate matching is adopted. Interleaving of the coded bits from the encoders is needed to obtain time and frequency diversity gain for both HARQ-ACK and periodic CSI. The processing of separate coding scheme is as follows.

(1) Encoding: HARQ-ACK is encoded by RM $(32, O)$ encoder and periodic CSI is encoded by RM $(20, A)$ encoder separately. The HARQ-ACK sequence and periodic CSI sequence are $a_0, a_1, \cdots, a_{N_{A/N}-1}$ and $o_0, o_1, \cdots, o_{N_{CSI}-1}$ respectively. The output bit sequences of encoders are $\tilde{b}_0, \tilde{b}_1, \cdots, \tilde{b}_{31}$ and $\tilde{\tilde{b}}_0, \tilde{\tilde{b}}_1, \cdots, \tilde{\tilde{b}}_{19}$ respectively, as Fig. 2 shows.

(2) Rate matching: PUCCH format 3 can carry 48 coded bits, which are distributed among the HARQ-ACK and periodic CSI. One or multiple parameter(s) signaled by eNB can be used to adjust the coding rate. In this paper, among the 48 encoded bits, 32 bits are distributed to HARQ-ACK and 16 bits are distributed to periodic CSI. The output bit sequences of rate matching are $\tilde{b}_0, \tilde{b}_1, \cdots, \tilde{b}_{31}$ and $\tilde{\tilde{b}}_0, \tilde{\tilde{b}}_1, \cdots, \tilde{\tilde{b}}_{15}$ respectively, as Fig. 2 shows.

(3) Interleaving: Both the HARQ-ACK coded bits and periodic CSI coded bits should be mapped to both slots. So as to obtain time and frequency diversity gain. In this paper, the interleaving is executed as follows: every four HARQ-ACK bits, there should be two periodic CSI bits. The output bit sequence of interleaving $b_0, b_1, \cdots, b_{B-1}$ where $B=48$ is obtained by the concatenation of the bit sequences $\tilde{b}_0, \tilde{b}_1, \cdots, \tilde{b}_{31}$ and $\tilde{\tilde{b}}_0, \tilde{\tilde{b}}_1, \cdots, \tilde{\tilde{b}}_{15}$, the processing is shown in Fig. 3.

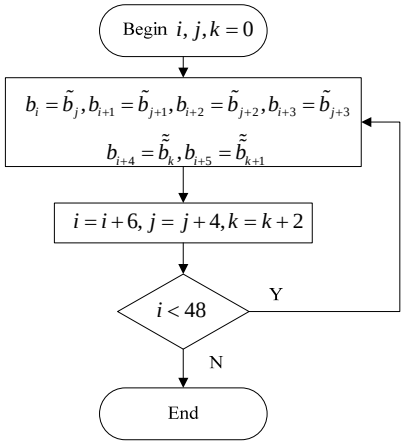

Figure 3. Basic processing of interleaving

From Fig. 2, it is obvious that the basic processing for separate coding scheme is a little bit complicated than joint coding and has more impact on the specification and implementation. But it is more flexible in controlling the performance of HARQ-ACK feedback and periodic CSI separately to meet the different performance requirements of periodic CSI and HARQ-ACK. Through rate matching, only CSI will be punched heavier than the joint coding scheme but HARQ-ACK not need to be punched. Obviously, we can obtain better HARQ-ACK performance.

With separate coding scheme, the performance of HARQ-ACK feedback will be very close to the case of transmitting it alone. At the same time, it can enhance simultaneous transmission of periodic CSI and HARQ-ACK feedback. As a result, periodic CSI dropping will be avoided and thus downlink throughput will be increased without sacrificing the performance of HARQ-ACK feedback too much.

IV. SIMULATIONS

In order to demonstrate the feasibility of multiplexing the periodic CSI report with HARQ-ACK bits on PUCCH format 3 and the effectiveness of the two coding schemes under different moving speed of user equipment, simulations will be provided in this section. In this paper, the extended typical urban model (ETU) [19] is chosen as the channel model, and the Doppler frequency cases are 200 Hz and 300 Hz, corresponding moving speed of user equipment are $105km/h, 160km/h$ respectively. The performance is represented by bit error rate (BER). PUCCH format 3 adopts SORTD transmit diversity [20, 21], and both of the length of HARQ-ACK bits and

periodic CSI report are 10. The simulation parameters are listed in Table Ⅰ.

TABLE I.
SIMULATION PARAMETERS

Parameters	Values
Carrier frequency	2GHz
Bandwidth	5MHz
Cyclic prefix	Normal
FFT size	2048
MIMO configuration	2T×2R
Channel model	ETU
Length of HARQ-ACK/periodic CSI bits	10/10
Number of simulations for each SNR	1000
Mobile speed	105/160 Km/h

In Fig. 4 and Fig. 5, both the BER of simultaneous transmitted periodic CSI and HARQ-ACK feedback with the two coding schemes are shown respectively. What's more, the BER of transmitted HARQ-ACK feedback alone is also studied. From them, if joint coding has been adopted, no significant difference is observed between the BER of periodic CSI and HARQ-ACK feedback, whereas if separating coding scheme has been adopted, the BER of HARQ-ACK feedback is bigger than it of the periodic CSI significantly. Due to code the periodic CSI and HARQ-ACK feedback independently in separate coding scheme, the BER of periodic CSI is worse than the it with joint coding scheme and the BER of HARQ-ACK feedback is better than it with joint coding scheme at all range of SNR. The most impressive achievement of separate coding scheme is that the BER of HARQ-ACK feedback with separate coding scheme is very close to the BER of HARQ-ACK feedback as transmitting it alone.

Comparing Fig. 4 with Fig. 5, it can be concluded that Doppler frequency 200 and Doppler frequency 300 have little impact to the BER of periodic CSI and HARQ-ACK feedback in the two coding schemes. The BER of periodic CSI and HARQ-ACK feedback with two coding schemes in the environment of Doppler frequency of 200 Hz are almost the same as the BER in the environment of 300 Hz respectively at each SNR.

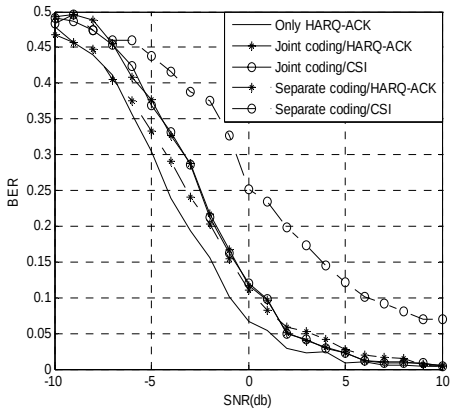

Figure 4. Simulation performance of Doppler frequency 200 Hz

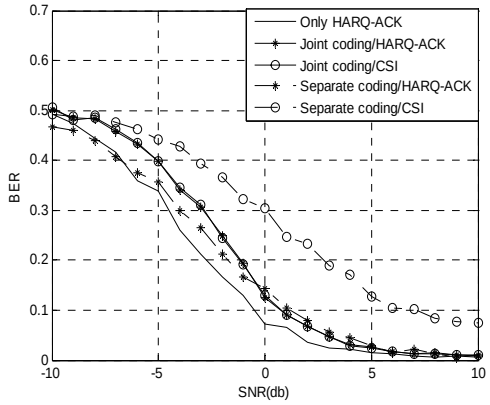

Figure 5. Simulation performance of Doppler frequency 300 Hz

V. CONCLUTION

In this paper, the feasibility and application scenarios of multiplexing periodic CSI with HARQ-ACK feedback are introduced first. Then two coding schemes to realize simultaneous transmission of periodic CSI and HARQ-ACK feedback are described in detail. The simulation results indicate that both of the two coding schemes can effectively support simultaneous transmission periodic CSI and HARQ-ACK feedback on PUCCH format 3. But from joint coding, periodic CSI and HARQ-ACK feedback have the same performance while from separate coding, HARQ-ACK feedback has better performance than periodic CSI. Furthermore, the performance of HARQ-ACK feedback with separate coding scheme is very close to the performance of HARQ-ACK feedback as transmitting it alone. Hence through the separate coding scheme, we can not only enhance simultaneous transmission of periodic CSI and HARQ-ACK feedback, but also guarantee the similar performance of HARQ-ACK feedback as transmitting it alone.

ACKNOWLEDGMENT

This work is supported by two of the Sciences Youth Funded Projects for Chongqing University of Posts and Telecommunications (No. A2012-89 and A2012-91).

REFERENCES

[1] Le-xiang LIN, Yuan-an LIU, Fang LIU, and Gang XIE, "Resource scheduling in downlink LTE-advanced system with carrier aggregation," The Journal of China University of Posts and Telecommunications, vol 19(1), pp.44-49, February 2012.

[2] Zukang Shen, Aris Papasakellariou, and Juan Montojo, "Overview of 3GPP LTE-advanced carrier aggregation for 4G wireless communications," IEEE Communications Magazine, vol. 50, pp.122-130, February 2012.

[3] Wen'an Zhou, Yiju Zhang, Pei Qin, and Wei Chen, "Jiont Scheduling Algorithms for LTE-A CoMP System," Journal of Computers, vol. 8, No. 11, pp. 2795-2801, November 2013.

[4] Shih-Jung Wu, Jen-Chih Lin, and Lin Hui, "Apply HIP to Handover Procedures in Hybrid Access Mode LTE Femtocells," Journal of Software, vol.8, No. 9, pp.2114-2121, October 2013.

[5] Dan Wang, Shizhong Yang, Yong Liao, and Yu Liu, "Efficient Receiver Sheme for LTE PUCCH," IEEE communications letters, vol. 16, No. 3, pp. 352-355, March 2012.

[6] Jia Zhang, Dongfeng Yuan, and Haixia Zhang, "On Stochastic Cell Association Scheme Over Carrier Aggregated Heterogenous Networks," Journal of Computers, vol.8, No. 11, pp. 2895-2901, November 2013.

[7] Yang Lu, Liu Liu, Mingju Li, and Lan Chen, "Uplink Control for Low Latency HARQ in TDD Carrier Aggregation," IEEE 75th Vehicular Technology Conference, vol. 10, pp. 1-5, May 2012 [IEEE 75th Vehicular Technology Conf. pp.1-5, May 2012].

[8] Yun Rui, Peng Cheng, and Mingqi Li, "Carrier aggregation for LTE-advanced: uplink multiple access and transmission enhancement features," IEEE Wireless Communications, vol. 20, pp.101-108, Aug. 2013.

[9] S.Sesia,I.Toufik,and M.Baker, "LTE-The UMTS Long Term Evolution: From Theory to Practice SECOND EDITION," 2009 John Wiley&Sons,Ltd.ISBN:978-0-470-69716-0.

[10] 3GPP TS 36.213 v11.4: "Evolved Universal Terrestrial Radio Access(E-UTRA)", Physical channels and modulation.(Release 11)," 2013-09.

[11] Borade, S., and Lizhong Zheng, "Writing on Fading Paper, Dirty Tape With Little lnk: Wideband Limits for Causal Transmitter CSI," Information Theory, IEEE, vol. 58, No. 8, PP. 5388-5397, Aug.2012.

[12] Xiongbin Rao, Liangzhong Ruan, and Lau,V.K.N, "CSI Feedback Reduction for MIMO Interference Alignment," IEEE Transactions on Signal Processing, vol.61, No. 18, PP. 4428-4437, Sep. 2013.

[13] R1-120122, "Motivations on UL signalling enhancement," Huawei, HiSilicon, Dresden, Germany, February 6- 10, 2012.

[14] R1-113904, "Simultaneous transmission of HARQ-ACK and CSI on PUCCH Format 3," LG Electronics, San Francisco, USA, November 14- 18, 2011.

[15] R1-113924, "Multiplexing CSI and A/N using PUCCH F3," Inter Digital Communications, LLC, San Francisco, USA, November 14- 18, 2011.

[16] Chen Chen, Lin Bai, Bo Wu, and Jinho Choi, "Downlink Throughput Maximization for OFDMA Systems With Feedback Channel Capacity Constraints," IEEE Transactions on Signal Processing, vol.59, No.1, PP. 441-446, Jan. 2011.

[17] Ameen, A.S. , Mellios, E. , Doufexi, A. , Dahnoun, N., and Nix, A.R., "LTE-advanced downlink throughput evaluation in the 3G and TV white space bands," IEEE 24th International Symposium on Personal, Indoor and Mobile Radio Communications: Fundamentals and PHY Track, 2013, vol. 10, pp.771-775 [IEEE 24th International Symposium on Personal, Indoor and Mobile Radio Communications: Fundamentals and PHY Track].

[18] Demin Zhang, and Jiang Zhongjun, "Research and development of designing HARQ in LTE Systems," 2012 2nd International Conference on Consumer Electronics, Communications and Networks (CECNet), vol.05, pp.2773-2776, April 2012 [2nd International Conference on Consumer Electronics, Communications and Networks (CECNet)].

[19] Prabagarane Nagaradjane, Prasaanth Muralidharan, "Multi-user transmitter preprocessing assisted uplink multi-cell multiple-input multiple-output system with base station cooperation over frequency-selective channels," Computers and Electrical Engineering, Vol.39 (06), pp.1016-1025, October, 2013,.

[20] Ahmed Attia, Ahmad EIMoslimany, "MIMO Vehicular Networks: Research Challenges and Opportunities," Journal of Communications, Vol.7 (06), pp.500-513, November, 2012.

[21] Chaitanya, T.V.K., and Larsson, E.G, "Improving 3GPP-LTE uplink control signaling by repetition across frequency bands ," *2013 IEEE international Conference on Communications Workshops (ICC)*, vol.8, pp. 1243-1248.

Dan Wang received the B.S. degree from Southwest Normal University, Chongqing, China, in 2003, and the M.S. degree in circuits and system from Chongqing University, Chongqing, China, in 2006.

From 2006 to 2009, she joined Chongqing University of Posts and Telecommunications. She has worked on a wide array of wireless communication technologies including TD-SCDMA, GSM, and LTE. Since 2009, she has been an engineer in communication engineering, Chongqing University of Posts and Telecommunications and studying for Ph.D. in communication engineering in Chongqing University, researching on LTE physical layer technology now.

Xuemei Deng is receiving her bachelor degree in Communication and Information Engineering from Chongqing University of Posts and Telecommunications, Chongqing, China.

Restricted Nussbaum Gain Control Method and Its Application in One Order System

Jinyong Yu[A]
[A] Department of Control Engineering, Naval Aeronautical and Astronautical University, Yantai, China
Email: yujinyong1024@126.com

Junwei Lei[B]
[B] Department of Control Engineering, Naval Aeronautical and Astronautical University, Yantai, China
Email: leijunwei@126.com

Yuqiang Jin[C] and Hongchao Zhao[D]
[C] Department of Trainning, Naval Aeronautical and Astronautical University, Yantai, China
[D] Department of Static Engineering, Naval Aeronautical and Astronautical University, Yantai, China
Email: {jinyuqiang1024[C], zhaohongchao1024[D]}@126.com

***Abstract*—The unknown control direction is one of the most open difficult question in nonlinear control theory. A new kind of restricted Nussbaum method is proposed to solve the unknown control direction problem without using high gain feedback. Although High gain has some advantages for improving the dynamic performance of a control system such as it can improve the quickness of the system and it can make the steady state error as small as possible. But now experienced engineers also realized that it causes many problems such as make the system unstable for big signal or high frequency noise. A kind of restricted Nussbaum gain method is firstly proposed to solve the problem. And simulation results show that it has better control effect compared with the traditional Nussbaum gain method. What is worthy pointing out is that the robustness of the Nussbaum gain strategy is improved obviously.**

***Index Terms*—Nussbaum gain; Unknown control direction; Stability; Uncertainty; Adaptive**

I. INTRODUCTION

Since there are typical results for linear system control, more and more researchers are interesting in control of nonlinear system [1-3]. The main difficulties for nonlinear control lie to the uncertainties and nonlinearity. Also there are some special method is proposed to solve special nonlinear systems; such as special controller [4, 5] designed for a kind of strict feedback nonlinear systems. Or the controller is designed based on differential geometric approach theory[6], Neural-network method [7], Robust control theory[8,9,10], linear feedback[11], sliding mode method[12,13,14,15]. But the unknown control direction is one of the most open difficult questions in nonlinear control theory.

Since Nussbaum first proposed the Nussbaum gain method [16, 17], the unknown control direction problem has arouse many researchers' interests. And Nussbaum gain method was applied in first order system and achieved obvious effect. Adaptive methods used by DING Z[18] to solve unknown control direction problem, and this problem can also be called without a priori knowledge of control direction[19,20] or with unknown virtual control coefficients. Xuedong Ye [21] considered the over parameterization problem during coping unknown control directions. NN method is applied to solve this problem and simultaneously the input constraint is considered by Weisheng Cheng [22]. And T.P.Zhang [23] also use adaptive neural method to solve this problem with dead-zones.

Also unknown control direction with discrete time, time varying , time-delay and output feedback problems are studied by Yang C[24] and Ge, S. S[25,26] and Liu Yunguang [27]. There are some similar problems such as unknown high frequency gains or unmodeled dynamics are research by KE Hai-sen [28] and M. Krstic[29]. Since there is no clear line among those problems so methods for unknown high frequency and unmodeled dynamics can also be used in solve unknown control direction problem.

The Nussbaum gain method can deal with the unknown control direction problem, which is discussed in many papers recently. But it is also has some problems when this method is applied in real engineering control object. The first problem is how to design a proper gain for the system.

It is very common for real physical systems that the gain is not allowed being too big. Also the experienced engineers will be very care to choose a proper gain for every loop. In fact, the big gain can make the system have better performance, such as high response speed, small steady state error and so on. But the problem is that high gain can also cause a lot of problems. First one is that it can make the system too sensitive to noise and also make the system unstable in some special situation. The second disadvantage is that it is too expense to realize a high gain device or it is impossible to realize the high gain system in some situation.

doi:10.4304/jcp.9.6.1402-1409

So it is always important to choose a proper gain for every system with any control method. Nussbaum gain control is a kind of complex nonlinear adaptive method. It should also obey the above principle. In fact, some Nussbaum gain algorithms can be unstable in some situation and the main reason is that the Nussbaum gain is not proper, or in most situations it is too big. In this paper, a new kind of restricted Nussbaum method is proposed to solve the above problem.

II. Problem Description

Considering a typical one order system with unknown control direction

$$\dot{x} = f(x) + bu \ . \tag{1}$$

Where x is the state of system and u is the controller or input, $f(x)$ is the known nonlinear function and b is the unknown control direction or it can be called control coefficient.

The control objective of restricted Nussbaum gain method is to design a control $u = q(x,k)$ and $|k| \le k_{sat}$, where k_{sat} is the restriction of the system gain condition, such that system state x can track desired value x^d even if the sign of control b is changed from positive to negative or from negative positive.

The solution of restricted gain problem is based on the traditional Nussbaum gain method since it is effective for the unknown control direction problem. But to make the gain is bounded; a bounded gain function is introduced. With a design of double bounded gain layer, the restriction of the gain is realized; also the whole system signals can be guaranteed to be bounded.

III. Assumption

For above systems, five assumptions are proposed to make the following design easier.

Assumption 1: The given gain k_{sat} is big enough and it satisfies the energy need of the physical system.

Assumption 2: Without loss of generality, assume the desired value to be constant so $\dot{x}^d = 0$.

Assumption 3: The control direction b is bounded and its value is in an unknown field $I = [l_1^-, l_1^+]$ where $0 \notin I$, so the sign of b is unknown.

Assumption 4: The bound of b is known, so there exists a known constant $b_{\max}$ such that $|b| \le b_{\max}$.

Assumption 5: The number of the sign change of b is not infinite.

IV. Design of Restricted Nussbaum Gain

Design a new error variable as $z = x - x^d$, the error of the system can be written as

$$\dot{z} = f(x) + bu \, . \tag{2}$$

Use the poles placement method to design the virtual control as

$$u^d = -f(x) - k_1 z - k_2 \int z dt \ . \tag{3}$$

Considering the unknown control direction problem, design the Nussbaum gain control as:

$$u = -N(k)u^d \ . \tag{4}$$

Then

$$\dot{z} = -k_1 z - k_2 \int z dt - bN(k)u^d - u^d \ . \tag{5}$$

Design the turning law of Nussbaum gain as

$$\dot{l} = k_l z u^d \ . \tag{6}$$

Design a bounded gain function as

$$k = f_s(l) \ . \tag{7}$$

Where $f_s(l)$ can be chosen as triangular functions.

The error function can be written as:

$$z\dot{z} = -k_1 z^2 - k_2 z \int z dt - \frac{1}{k_l}(bN(k)+1)dl \ . \tag{8}$$

Construct a type of integral Lyapunov function as follows:

$$V = \frac{1}{2}z^2 + \frac{k_1}{2}\int z^2 dt + \frac{k_2}{2}(\int z dt)^2 \ . \tag{9}$$

Solve the derivative of Lyapunov function as

$$k_l \dot{V} = -(bN(k)+1)dl \ . \tag{10}$$

With integration in both sides of the equation, it holds:

$$\begin{aligned} k_l V(t) - k_l V(0) &= \int -(bN(k)+1)dl \\ &= \int_{l(0)}^{l(t)} -bN(k)dl + l(0) - l(t) \end{aligned} \ . \tag{11}$$

To make it simple, choose the restricted Nussbaum gain as $k = 10\sin(l)$, Nussbaum, and choose the Nussbaum gain function as $N(k) = k^2 \sin k$.

It is obvious that the system gain satisfies below restrictions with the above design:

$$N(k) = k^2 \cos k < 100 \ . \tag{12}$$

Also different restriction can be chosen to meet the different demand of real systems.

With the proof below, the system can be proved to be stable and the control law can adapted to the disturbance of control direction change.

First, assume the gain l is unbounded. Without loss of generality, consider the situation $l \to +\infty$, divide by l on both side of the equation it holds:

$$\frac{k_l V(t) - k_l V(0) + l(0)}{l} = \frac{1}{l}\int_{l(0)}^{l(t)} -bN(k)dl - 1 \ . \tag{13}$$

Since $-bN(k)$ is bounded, there exist positive constants ε_1 and ε_2 such that

$$-\varepsilon_1 \le \frac{1}{l}\int_{l(0)}^{l(t)} -bN(k)dl - 1 \le \varepsilon_2 \ . \tag{14}$$

It is obvious that if $k_l > 0$, it holds:

$$-\frac{l}{k_l}\varepsilon_1 \le V(t) \le \frac{l}{k_l}\varepsilon_2 \ . \tag{15}$$

If $k_l < 0$, it holds:

$$\frac{l}{k_l}\varepsilon_2 \le V(t) \le -\frac{l}{k_l}\varepsilon_1 . \quad (16)$$

Assume that the limit of above integration exists:

$$\lim_{l\to\infty}\frac{1}{l}\int_{l(0)}^{l(t)} -bN(k)dl = \varepsilon + 1 . \quad (17)$$

So it always has

$$V(t) = \varepsilon k_l l . \quad (18)$$

It is obvious that contradiction will appear if $k_l > 0$ or $k_l < 0$ because it will make $V(t) \le 0$.

Also if the integration does not exist, so there exists a t such that

$$\lim_{l\to\infty}\frac{1}{l}\int_{l(0)}^{l(t)} -bN(k)dl = \varepsilon_3 . \quad (19)$$

where

$$-\varepsilon_1 \le \varepsilon_3 \le \varepsilon_2 . \quad (20)$$

So whether ε_3 is positive or negative, there exists $k_l > 0$ or $k_l < 0$ such that $V(t) \le 0$, then contradiction appears.

Now, it is easy to prove that $l(t)$ is bounded. Also $V(t)$ is bounded and $z(t)$ is bounded. Finally, u^d is proved to be bounded. Because of the construction of integral type Lyapunov function, it is easy to prove that $z(t) \to 0$.

V. Numerical Simulation

Take a simple one order system with unknown control direction as an example, the model can be written as

$$\dot{x} = 3x\sin x + bu . \quad (21)$$

Where the unknown control direction b is designed as:

$$b = \begin{cases} 1 & 0 < t < 3 \\ -2 & 3 < t < 6 \\ 2 & t > 6 \end{cases} . \quad (22)$$

Choose the initial value of Nussbaum gain as $l(0) = 1$, the initial condition as $x(0) = 0$, set the desired value of state as $x^d = 2$, set the simulation step as 0.001s and do the simulation with Eular method , the simulation result can be show as below figures.

Figure 1 shows the state of x1 and at time 3s and 6s, the state x is disturbed by the change of control direction. But it can be stabled by Nussbaum gain law successfully.

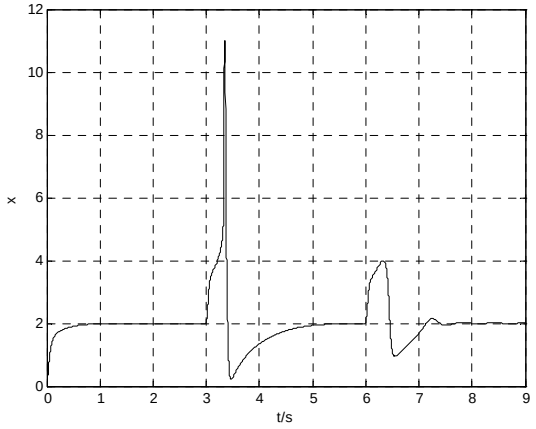

Figure 1. Curve of state x.

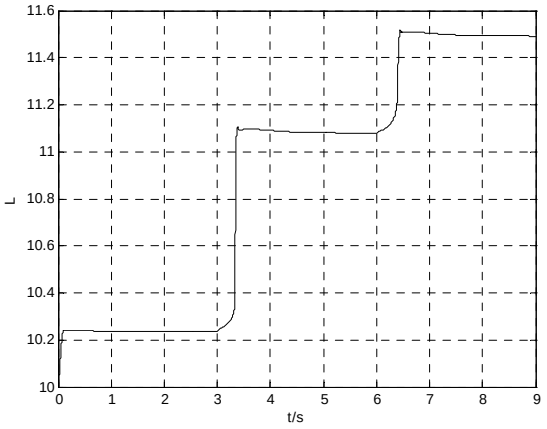

Figure 2. Curve of Gain L

Figure 2 shows the restricted Nussbaum Gain L and it is clear that the Nussbaum gain can adapt to a proper gain after the disturbance of control direction.

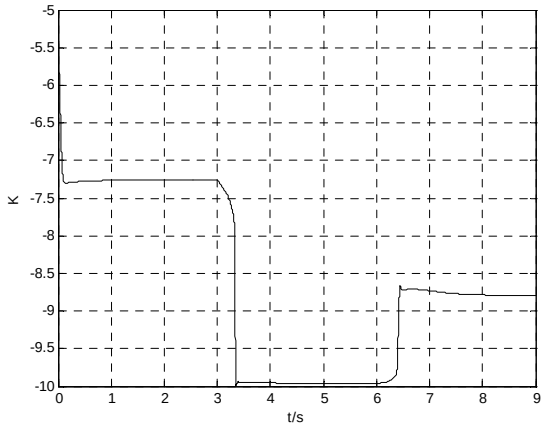

Figure 3. Curve of Gain K.

Figure 3 shows the real Nussbaum Gain K and it is obvious that the Nussbaum gain can adapt to the unknown change of control direction.

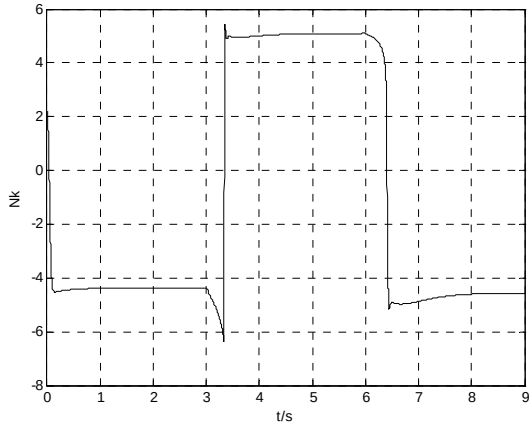

Figure4. Curve of Gain Nk

Figure 4 shows the real gain of control and it can follow the change of control direction very quickly.

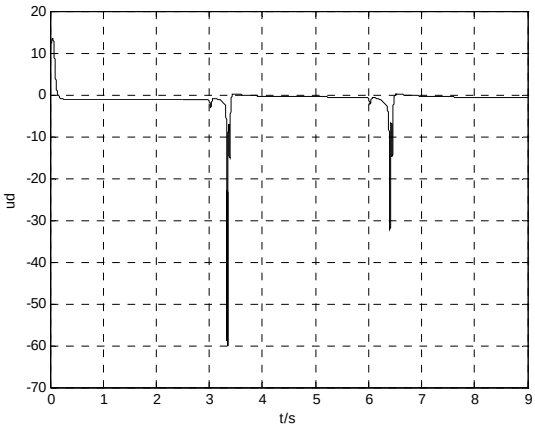

Figure 5. Ideal control Ud.

Figure 5 shows the ideal control and the overshoot is obvious at the time when control direction is changed.

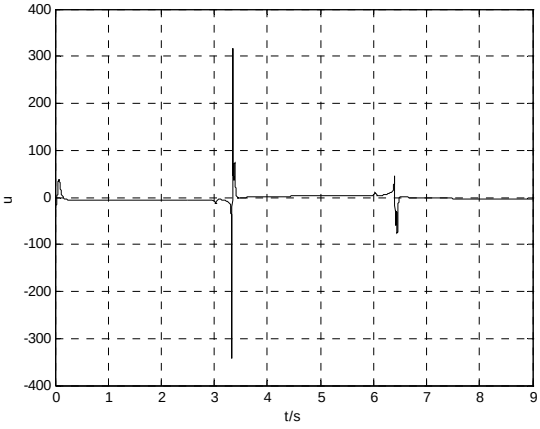

Figure6. Curve of Control U

Figure 6 shows the real control and it shows that at the time the control direction changes the control law need enough energy to make the system stable.

In order to test the robustness of this limit Nussbaum gain method under different initial gain value, we done a simulation assume that the initial gain is $l(0)=10$, and simulation result is show as below.

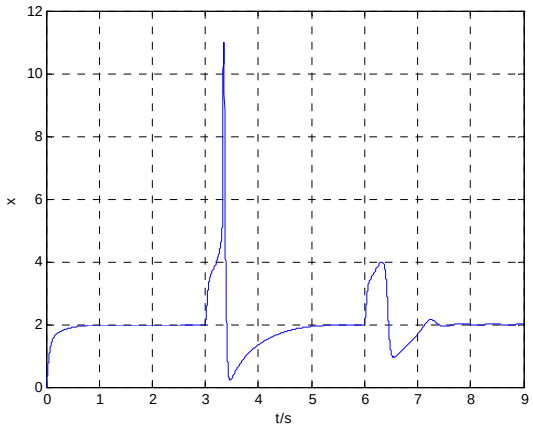

Figure 7. Curve of state x.

Figure 7 shows the state of x1 and at time 3s and 6s, the state x is disturbed by the change of control direction.

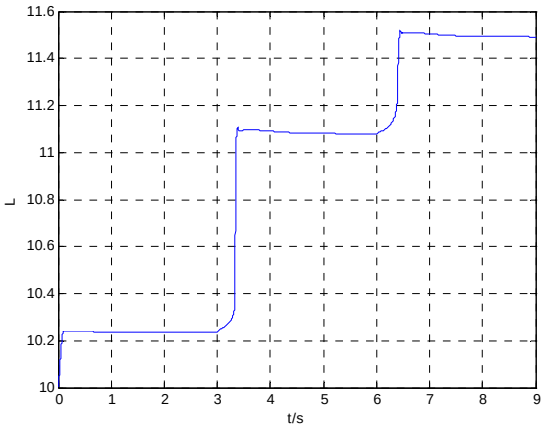

Figure 8. Curve of Gain L

Figure 8 shows the restricted Nussbaum Gain L and the initial value is set to 10.

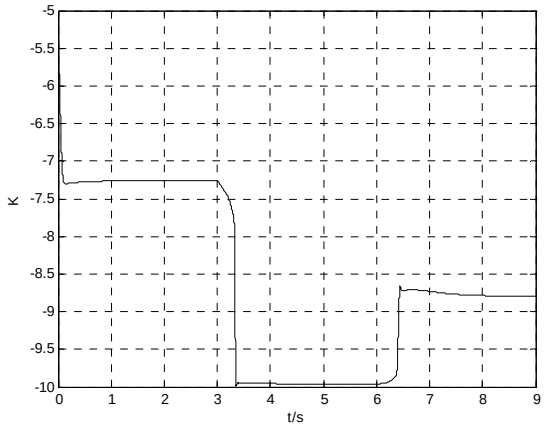

Figure 9. Curve of Gain K

Figure 10 shows the real Nussbaum Gain K and it is begin from -5.5 and adapt to the unknown change of control direction and finally stop at about -9.5.

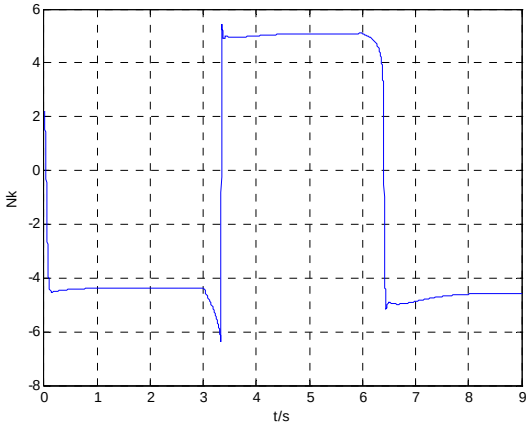

Figure 10. Curve of Gain Nk

Figure 11 shows the ideal gain of control and it can follow the change of control direction very quickly.

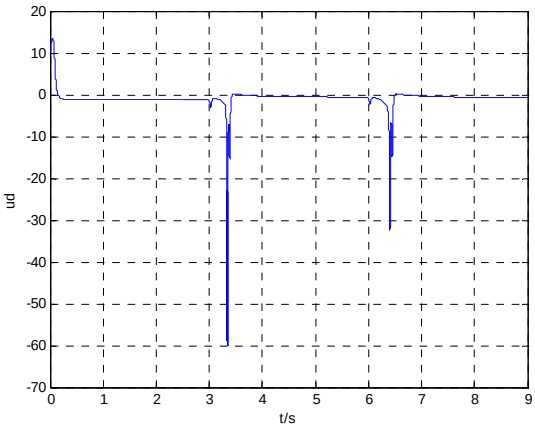

Figure 11. Ideal control Ud

Figure 12 shows the ideal control and the overshoot. We can make a conclusion from above simulation results that the restricted Nussbaum gain method is effective and robust under different initial gain value.

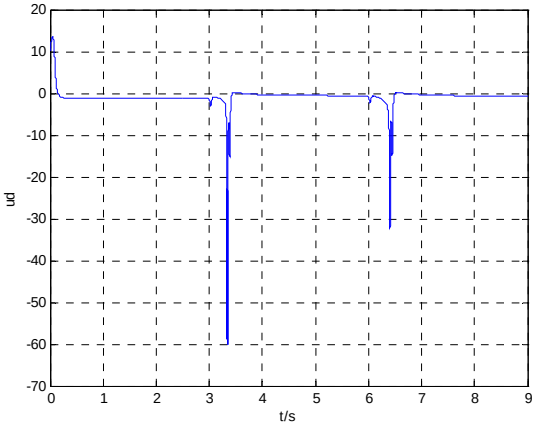

Figure 12. Curve of real control U

To test the robustness of the restricted Nussbaum method under different initial value of system state, we done a simulation and assume that the initial value the first order system is $x(0) = 5$. And the simulation result is shown as below.

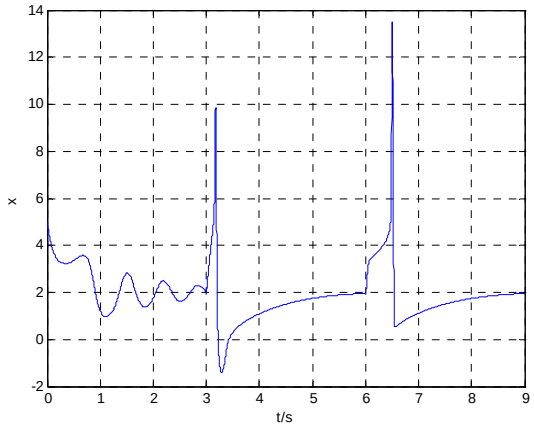

Figure 13. Curve of state x.

Figure 13 shows the state of x1 and at time 3s and 6s, the state x is disturbed by the change of control direction, and the initial state is 5.

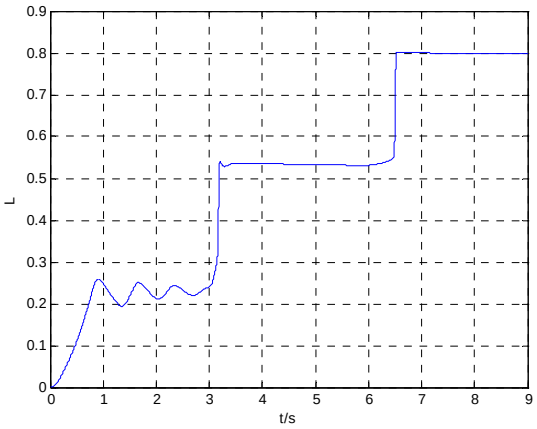

Figure 14. Curve of Gain L

Figure 14 shows the restricted Nussbaum Gain L and the initial value is set to 10.

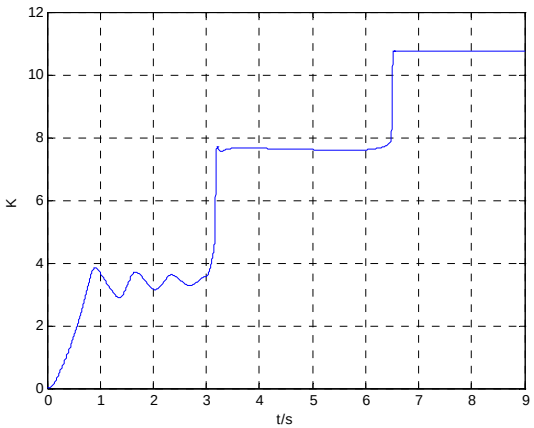

Figure 15. Curve of Gain K

Figure 15 shows the real Nussbaum Gain K and it is begin from 0 and adapt to the unknown change of control direction and finally stop at about 10.8.

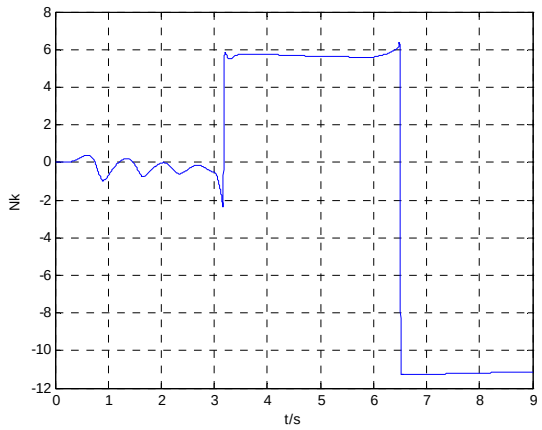

Figure 16. Curve of Gain Nk

Figure 16 shows the ideal gain of control and it can follow the change of control direction very quickly.

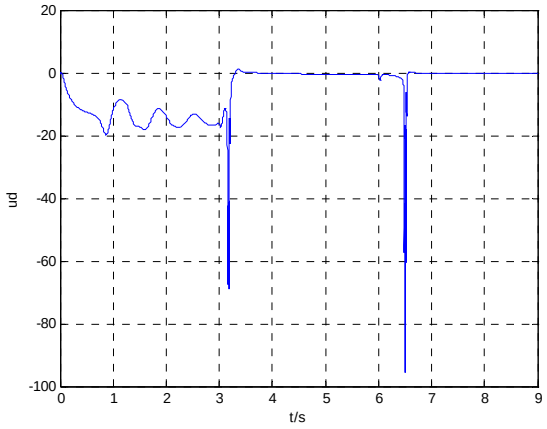

Figure 17. Ideal control Ud

Figure 17 shows the ideal control and the overshoot and Figure 18 shows the real control of the Nussbaum gain method. We can make a conclusion from above simulation results that the restricted Nussbaum gain method is effective and robust under different initial system state.

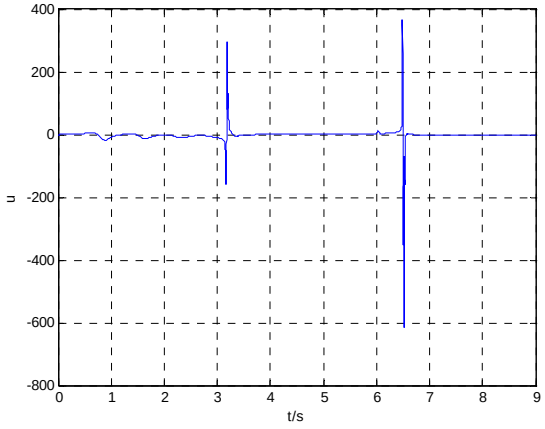

Figure 18. Curve of real control U

Also choose another initial value as $x(0) = 6.6$, it is the biggest initial value the proposed restricted method can cope. And compared with common Nussbaum gain method, this value is improved. And the simulation result is shown as below.

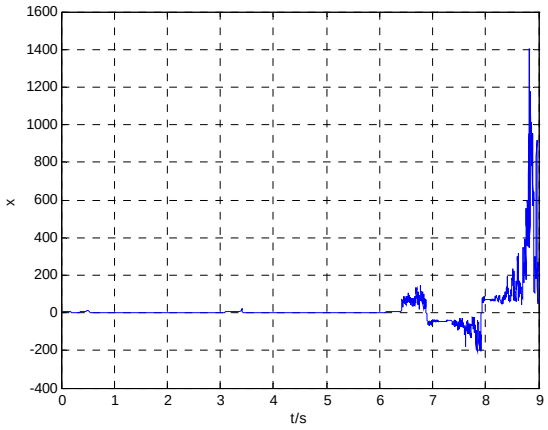

Figure 19. Curve of state x

Figure 19 shows the state of x1 and at time 3s and 6s, the state x is disturbed by the change of control direction. It is obvious that the system is unstable since the initial value of the system state is too big.

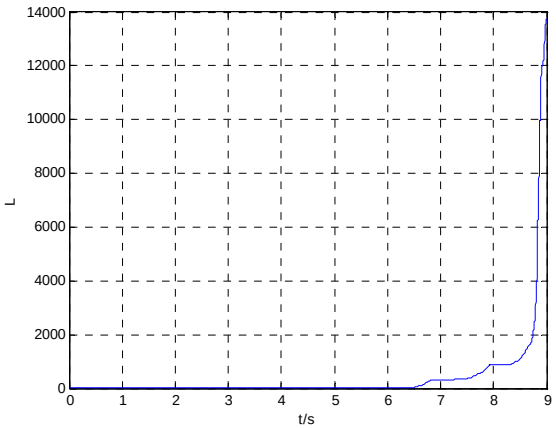

Figure 20. Curve of Gain L

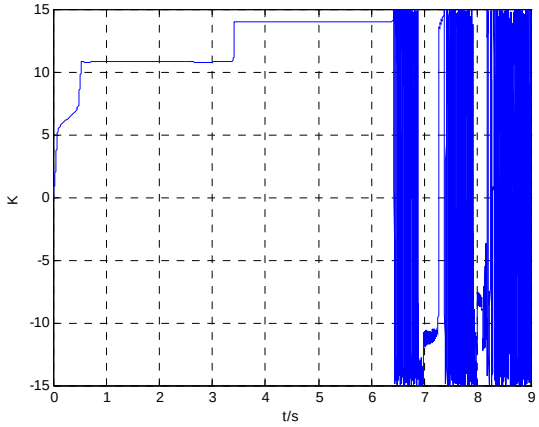

Figure 21. Curve of Gain K

VI. CONCLUSIONS

A kind of restricted Nussbaum gain method is proposed in this paper. It can be used to solve the complex unknown control direction problem. The advantage of this method is that the gain of controller is limited. It can also improve the traditional Nussbaum gain design that it makes the Nussbaum gain strategy more stable since the gain is restricted. Also the stability is proved in this paper that it is not affected by the limit gain.

Figure 20 shows the restricted Nussbaum Gain L and the initial value is set to 0, and figure 21 shows the Nussbaum gain K and it is restricted from -15 to 15. Both gain K and L is unstable as time increase.

So we can make a conclusion that the restricted Nussbaum can improve the system stability compared with common Nussbaum gain method. But it is still can not guarantee the system is always stable if the initial value is too big. That is mainly because the Nussbaum gain is a nonlinear control law and the stability is not global. And also because the simulation step is not small enough on some point the gain of the system is too big.

ACKNOWLEDGMENT

The author wish to thank his friend Heidi in Angels (a town of Canada) for her help , and thank his classmate Amado in for his many helpful suggestions. This paper is supported by Youth Foundation of Naval Aeronautical and Astronautical University of China, National Nature Science Foundation of Shandong Province of China ZR2012FQ010, National Nature Science Foundations of China 61174031, 61004002, 61102167, Aviation Science Foundation of China 20110184 and China Postdoctoral Foundation 20110490266.

REFERENCES

[1] RYAN E P.A universal adaptive stabilizer for a class of nonlinear systems. Systems & Control Letters, 1991, 16(3): 209-218.
[2] Qian, C., & Lin, W. (2002). Output feedback control of a class of nonlinear systems: A nonseparation principle paradigm. IEEE Transactions on Automatic Control, 47, 1710-1715
[3] RYAN E P. A nonlinear universal servomechanism. IEEE Trans on Automatic Control, 1994, 39(4): 753-761.
[4] GE Shuzhi Sam, WANG J. Robust adaptive neural control for a class of perturbed strict feedback nonlinear systems. IEEE Trans on Neural Networks, 2002, 13(11): 1409- 1419.
[5] Charalampos P. Bechlioulis, George A. Rovithakis, adaptive control with guaranteed transient and steady state tracking error bounds for strict feedback systems , Automatica 45(2009)532-538
[6] C. C. Fuh and P. C. Tung, “Controlling Chaos Using Differential Geometric Approach,” Physical Review Letters, vol. 75, no. 16, pp. 2952-2955, 1995.
[7] Jagannathan S, He P. Neural-network-based state-feedback control of a nonlinear discrete-time system in nonstrict feedback form. IEEE Transactions on Neural Networks 2008; 19(12):2073-87.
[8] Polycarpou, M. M., Ioannou, P. A. A robust adaptive nonlinear control design. Automatica, Vol. 32. No. 3 (1996) 423-427
[9] Seung-Hwan Kim, Yoon-Sik Kim, Chanho Song, A robust adaptive nonlinear control approach to missile autopilot design, Control engineering practice, 12(2004) pp. 149-154
[10] Sahjendra N. Singh, Marc Steinberg, Robert D. Digirolamo, Variable Structure Robust Flight Control System for the F-I4, IEEE transactions on aerospace and electronic systems vol. 33, No. 1 , 1997
[11] Tsinias, J. (1991). A theorem on global stabilization of nonlinear systems by linear feedback. System and Control Letters, 17, 357-362
[12] Xu H J and Mirmirani M.Robust adaptive sliding control for a class of MIMO nonlinear systems [A].In: AIAA Guidance,Navigation,and Control Conference and Exhibit. Montreal, Canada, AIAA 2001-4168.
[13] Yuqiang Jin, Junwei Lei, Yong Liang, Tracking of super chaotic system with static uncertain functions and unknown parameters, Journal of Computers, 2012:7(12),2853-2860
[14] Jingjing Du, Chunyue Song, Multi-PI control for block-structured nonlinear systems, Journal of Computers,2012:7(12),3052-3059
[15] Guoqiang Liang, Junwei Lei, Yong Liang, Research on the robustness of PISS integral sliding mode control of supersonic missiles, Journal of Computers, 2012:7(8),1943-1950
[16] Nussbaum, R. D. (1983). Some remarks on the conjecture in parameter adaptive control. Systems and Control Letters, 3(3), 243-246
[17] MARTENSSON B. Remarks on adaptive stabilization of first order nonlinear systems. Systems & Control Letters, 1990, 14(1): 1-7
[18] DING Z. Adaptive control of nonlinear systems with unknown virtual control coefficients. Int J of Control Signal Processing, 2000, 14(4): 505 - 517.
[19] YE X, JIANG J. Adaptive nonlinear design without a priori knowledge of control directions. IEEE Trans on Automatic Control, 1998, 43(11): 1617 -1621.
[20] YE X D. Asymptotic regulation of time-varying uncertain nonlinear systems with unknown control directions. Automatica, 1999, 35(5): 929 - 935.
[21] Xuedong Ye, Global adaptive control of nonlinear systems with unknown control directions nonover-parameterization

design, Journal of China Jiliang University, Jan, 2005 Vol.14,No,1
[22] Weisheng Chen, Adaptive NN control for discrete-time pure-feedback systems with unknown control direction under amplitude and rate actuator constraints, ISA Transactions 48 (2009) 304-311
[23] T.P.Zhang , S.S.Ge Adaptive neural control of MIMO nonlinear state time-varying delay systems with unknown dead-zones and gain signs, Automatica 43(2007) 1021-1033
[24] Yang C, Ge SS, Xiang C, Chai TY, Lee TH. Output feedback NN control for two classes of discrete-time systems with unknown control directions in a unified approach. IEEE Transactions on Neural Networks 2008; 19(11):1873-86.
[25] Ge, S. S., & Wang, J. (2003). Robust adaptive tracking for time-varying uncertain nonlinear systems with unknown control coefficients. IEEE Tran-sactions on Automatic Control, 48(8), 1463-1469.
[26] Ge, S. S., Hong, F., & Lee, T. H. (2004). Adaptive neural control of nonlinear time-delay system with unknown virtual control coefficients. IEEE Transactions on Systems, Man, and Cybernetics-PartB: Cybernetics, 34(1), 499-516.
[27] Liu Yunguang, Output-feedback Adaptive Control for a Class of Nonlinear Systems with Unknown Control Directions, ACTA AUTOMATICA SINICA, Vol. 33, No. 12, 1306-1312
[28] KE Hai-sen, YE Xu-dong, Robust adaptive controller design for a class of nonlinear systems with unknown high frequency gains, Univ SCIENCE A 2006 7(3):315-320
[29] M. Krstic, J. Sun, and P. V. Kokotovic, “Control of Feedback Linearizable Systems with Input Unmodeled Dynamics,” Proc. of the 33rd Conference on Decision and Control, Lake Buena Vista, FL, pp. 1633-1638, 1994

Jinyong Yu (1977-) was born in Haiyang city of Shandong province of China and received his Doctor degree in Guidance, Navigation and Control in 2006 from Naval Aeronautical and Astronautical University, Yantai of China.

He became a vice professor of this school in 2008 and now he is the director of drone teaching team of control engineering department. Now his current interest is aircraft control and navigation.

Junwei Lei (1981-) was born in Chibi of Hubei province of China and received his Doctor degree in Guidance, Navigation and Control in 2010 from Naval Aeronautical and Astronautical University, Yantai of China. Her present interests are control theory, chaotic system control, aircraft control and adaptive control.

He was promoted to be a lecture of NAAU in 2010. His typical book named Nussbaum gain control technology of supersonic missiles was published in 2013 in China.

Chinese Sentiment Analysis Using Appraiser-Degree-Negation Combinations and PSO

Wen Xiong[1,2]
[1] Institute of Chinese Information Processing, Beijing Normal University,
19#, WaiDa St., XinJieKou, HaiDian Area, Beijing, China
[2] China Patent Information Center,
25#, BeiTaiPingZhuang Road, HaiDian Area, Beijing, China
Email: xiongwen@cnpat.com.cn

Yaohong Jin and Zhiying Liu
Institute of Chinese Information Processing, Beijing Normal University,
19#, WaiDa St., XinJieKou, HaiDian Area, Beijing, China
Email: {jinyaohong, liuzhy}@bnu.edu.cn

***Abstract*—To recognize effectively the polarity of Chinese sentences using Chinese appraisers, degree adverbs, and negations, this article presents a new rule-based method. First, the method combines three types Chinese words into the pre-defined rules; it employs the word distances of those rules as constraints; it utilizes the strengths of appraisers and degree adverbs as items of the rules. Then, it utilizes the particle swarm optimization (PSO) to obtain the optimal parameters of the rules, such as the thresholds of constraints and the adjustments of the strengths. Furthermore, it uses Chinese lexicon HowNet as the resources of Chinese sentiment. Experiments show that the method realizes higher precision, recall, and F1 than the baseline of C-support vector classification (C-SVC) on two real-world applications. Moreover, it obtains the second rank for the task 2 of Chinese opinion analysis and evaluation (COAE) in 2011, indicating the availability of the method.**

***Index Terms*—sentiment analysis, text mining, particle swarm optimization, support vector machine**

I. Introduction

The researches for sentiment analysis are concerned more and more, which are especially with growing requirements in multiple fields for commercial organizations and governmental departments. Public response for emergent events and consumers' feedback need the tools used for text sentiment classification (TSC) and opinion mining to analyze the sentiment polarity of texts, which can help to discover the problems and the requirements. Thus, TSC becomes a sub task in text mining (TM), and a necessary method for sentiment analysis and opinion mining.

The methods of sentiment analysis can be divided into multiple categories, such as sentiment classification using sentiment phrases (SCSP) [1], sentiment classification using the methods of machine learning (SCML) [2], and sentiment classification using scoring functions (SCSF) [3].

There are methods using phrases or semantic triples as basic constituents for the analysis of the sentence sentiment, which are based on dependency parser, and semantic parser. However, these methods are dependent on the corpus, which are tagged manually to form a training data set. The performance of the parser can be influenced when running in the practical texts due to that the coverage ratio from the training data set is limited. On the other hand, those methods using algorithms of machine learning are influenced due to not tackling sentiment words. In this paper, we propose a rule-based method to analyze the sentence sentiment using sentiment words, and optimize those parameters in the rules using particle swarm optimization (PSO).

The rest of the paper is organized as follows: in Section 2, we describe the role of appraisers, degree adverbs, and negations in the sentiment analysis. Then, we propose the scoring rules using the combinations of appraisers, and the degree adverbs (ADA) and appraisers, degree adverbs, and negations (ADAN) in Section 3. And then, we propose a method combining appraisers, degree adverbs, and negations (ADN) in Section 4, followed by the parameter optimization using PSO. In Section 5, we show the experiments on multiple data sets, such as an open data set, a manually constructed data set, and an evaluative data set used for Chinese opinion analysis and evaluation (COAE)[1]. Section 6 introduces the related work, and Section 7 gives the conclusions.

II. Role Analysis of Sentiment Words

A. Appraiser Roles

Some Chinese words have clear appraisive meaning. Therefore, these words express the main sentiment in the sentence. Due to their different types in part of speech

Manuscript received October 18, 2013; revised October 22, 2013.
Corresponding author: Wen Xiong; email to: xiongwen@cnpat.com.cn

[1] http://ir-china.org.cn/coae2011.html

doi:10.4304/jcp.9.6.1410-1417

(POS), we provide their roles in the sentiment analysis according to their POS as follows:

1) Positive appraiser verbs:

Positive appraiser verbs increase the positive sentiment of Chinese sentences. For example, “Ta Zhenxi Yu Taren Jiaoliu De Jihui (he cherished the opportunity to communicate with others.)” Here are a few words, such as Zhenxi (to cherish), Baojiang (to praise and to honor), and Fenli (to make a long arm).

2) Negative appraiser verbs:

Negative appraiser verbs increase the negative sentiment of Chinese sentences. For example, “Ta Mushi Yu Taren Jiaoliu De Jihui (he ignored the opportunity to communicate with others.)” Here are a few words, such as Moshi (to ignore), Aichi (to lament), and Anhai (to murder).

3) Positive appraiser nouns:

Positive appraiser nouns express the positive sentiment of Chinese sentences. For example, “Ta Yinwei Nuli Gongzuo Huode Liao Biaoyang (he works hard to gain recognition.)” Here are a few words, such as Aimu (adoration), Anhao (ease), and Anggui (costliness).

4) Negative appraiser nouns:

Negative appraiser nouns express the negative sentiment of Chinese sentences. For example, “Ta Kan Qilai Xiang Ge Baichi (he looks like an idiot.)” Here are a few words, such as Angzhang (dinginess), Anggui (costliness), and Baichi (idiot).

5) Positive appraiser Adjectives:

Positive appraiser adjectives increase the sentiment of the modified noun. For example, “Ta Shi Yi Ge Hao Nanren (he is a good man.)” Here are a few words such as Anquan (safe), Bang (good), and Biyao (essential).

6) Negative appraiser adjectives:

Negative appraiser adjectives increase the sentiment of the modified nouns. For example, “Ta Shi Yi Ge Huai Nanren (he is a bad man.)” Here are a few words, such as Buan (unsafe), Zhaogao (bad), and Duoyu (redundant).

7) Positive appraiser adverbs:

Positive appraiser adverbs increase the sentiment of the modified verbs. For example, "Ta Cengken Di Shuo (he said honestly.)" Here are a few words, such as Anshi (schedule), Buchuo (correctly), and Cengzhi (cordially).

8) Negative appraiser adverbs:

Negative appraiser adverbs increase the sentiment of the modified verbs. For example, “Ta Baibai di Huafei Liao Shijian (he spent time in vain.)” Here are a few words, such as Anzhong (secret), Aoman (haughtily), and Baibai (in vain).

9) Positive appraiser idioms:

Positive appraiser idioms express the positive sentiment of Chinese sentences. For example, “Renmen Anjuleye (people live and work in peace and contentment.)” Here are a few words, such as Aibushishou (fondle admiringly), and Anjuleye (live and work in peace and contentment).

10) Negative appraiser idioms:

Negative appraiser idioms express the negative sentiment of Chinese sentences. For example, “Tamen Renwei Ta Aishouaijiao (they think he is in a hindrance.)” Here are a few words, such as Eyufengcheng (greasiness), Aishouaijiao (be in a hindrance), and bamianlinglong (be smooth and slick).

B. Degree Adverb Roles

Chinese degree adverbs can reinforce the sentiment of the modified appraisers, though degree adverbs do not have a negative meaning or positive meaning. They can be divided into six levels by empirically. Therefore, we assigned the degree adverbs of level 1 with weight 10, level 2 with weight 8, level 3 with weight 6, level 4 with weight 4, level 5 with weight -3, and level 6 with weight -1. The positive weight means reinforcement. The bigger weight the stronger reinforcement has a degree adverb. On the other hand, the negative weight means weakening the modified words, the bigger absolute weight the weaker modification has a degree adverb.

We describe their roles as follows:

1) Degree adverbs with reinforcement:

a) Words of level 1 (such as Duo (excessively), Guo (over), and Qiang (strongly)) reinforce the sentiment strength with weight 10.

b) Words of level 2 (such as BaiFenzhibai (absolutely), Jidu (to the utmost), and chongfen (plenty)) reinforce the sentiment strength with weight 8.

c) Words of level 3 (such as Cen (deep), Chuqi (unusually), and hao (well)) reinforce the sentiment strength with weight 6.

d) Words of level 4 (Geng (still), Gengjia (much more), and Nayang (in that way)) reinforce the sentiment strength with weight 4.

2) Degree adverbs with weakening:

a) Words of level 5 (Buda (not too), Liao (a little), and Xiangdui (rather)) weaken the sentiment strength with weight -3.

b) Words of level 6 (Haosheng (properly), Huoduohuoshao (more or less), and Man (quite)) weaken the sentiment strength with weight -1.

C. Negation Roles

Negations reverse the sentiment of appraisers, for example, “Ta Bushi Huai Nanren (he is not a bad man.)” Here are a few words, such as Bingfei (no), Meiyou, (without), and Bugou (not enough).

III. Scoring Rules

A. Rules for ADA

In fact, the strength of appraisers is a fuzzy number, and the number of appraisers is big. Therefore, we can assign a weight 0.4 to the positive appraisers, and a weight -0.4 to the negative appraisers by empirically. On the other hand, the combination of words with different roles has a decisive role for the sentiment polarities.

For example, a Chinese *ADA* combination can be a form as ‘$da_1\ da_2\ ap\ldots\ da_n$’ with modifications ($0 \le n \le 4$), where ‘*da*’ is the degree adverbs, and ‘*ap*’ is the appraisers. For example, BaiFenzhibai Zhenxi ‘absolutely cherishes’, Fenwai Chuqi Zhenxi ‘especially unusually cherishes’, and Zhenxi De Budeliao ‘cherishes extremely’.

We developed rules to score an *ADA* by combining both appraisers' weight and degree adverbs' weight for different *ADA*s. The thresholds of the word distances (from t_1 to t_3) are the number of words between two words plus one. When the distance exceeds a threshold, e.g., four, the constraints between two words are treated as invalid. Furthermore, we introduced adjustable integer values for the appraisers and the degree adverbs due to the optimization purpose, which reflects the adjustment amount of constraints of the rules.

$$\begin{aligned}&\text{if } (num(da)=0 \text{ and } polarity(ap)=positive)\Rightarrow\\ &\quad score=weight(ap).\end{aligned} \tag{1}$$

Where the *score* shows the sentiment of Chinese sentences when the number of *da* (*num (da)*) is zero.

$$\begin{aligned}&\text{if } (num(da)=1 \text{ and } polarity(ap)=positive)\Rightarrow\\ &score=\begin{cases}weight(ap), \text{ if } dist(da,ap)>t_1\\ weight(ap)\cdot(1+weight(da)/c_1), \text{ otherwise.}\end{cases}\end{aligned} \tag{2}$$

Where *dist(da, ap)* is the word distance between *da* and *ap*; t_1 is the threshold of the word distance. C_1 is the adjustable integer mentioned above for the modification of the positive appraiser. Therefore, this rule shows *da* reinforces the score of the *ap* when only one *da* (*num (da) = 1*) appears, with the distance between them less than t_1.

$$\begin{aligned}&\text{if } (num(da)=2 \text{ and } polarity(ap)=positive)\Rightarrow\\ &score=\begin{cases}weight(ap)\cdot(1+weight(da_1)/c_1),\\ \quad \text{if } pos(da_1)<pos(ap) \text{ and } dist(da_1,ap)\le t_1\\ score+weight(ap)\cdot(1+weight(da_2)/c_1),\\ \quad \text{if } pos(da_2)<pos(ap) \text{ and } dist(da_2,ap)\le t_1.\end{cases}\end{aligned} \tag{3}$$

Where *pos(w)* is the position of the word *w*. Therefore, this rule shows *da*s reinforce the score of the *ap* when two *da*s precede *ap* with the distances between them less than t_1.

$$\begin{aligned}&\text{if } (num(da)>2 \text{ and } polarity(ap)=positive)\Rightarrow\\ &score=weight(ap)\cdot(1+(weight(da_1)+weight(da_2))/\\ &\qquad c_1\cdot num(da)/2).\end{aligned} \tag{4}$$

Equation (4) shows *da*s reinforce the score of the *ap* with the number of the *da*s greater than two.

$$\begin{aligned}&\text{if } (num(da)=0 \text{ and } polarity(ap)=negative)\Rightarrow\\ &\quad score=-weight(ap)-c_2.\end{aligned} \tag{5}$$

Wherein: c_2 is the adjustable integer for the negative appraiser.

$$\begin{aligned}&\text{if } (num(da)=1 \text{ and } polarity(ap)=negative)\Rightarrow\\ &score=\begin{cases}-weight(ap)-c_2, \text{ if } dist(da,ap)>t_1\\ -weight(ap)-(weight(ap)+c_3)\cdot\\ \quad weight(da)/c_1, \text{ otherwise.}\end{cases}\end{aligned} \tag{6}$$

Wherein: c_3 is the adjustable integer for the negative appraiser when the *da* modifies the *ap*. Therefore, this rule shows *da* reinforces the negative score of the *ap* when only one *da* appears, with the distance between them less than t_1.

$$\begin{aligned}&\text{if } (num(da)>2 \text{ and } polarity(ap)=negative)\Rightarrow\\ &score=-weight(ap)-(weight(ap)+c_3)\cdot\\ &\quad (weight(da_1)+weight(da_2))/c_1\cdot num(da)/2.\end{aligned} \tag{7}$$

Equation (7) shows that *da*s reinforce the negative score of the *ap* with the number of the *da*s greater than two.

$$\begin{aligned}&\text{if } (num(da)=2 \text{ and } polarity(ap)=negative)\Rightarrow\\ &score=\begin{cases}-weight(ap)-(weight(ap)+c_3)\cdot weight(da_1)/c_1,\\ \quad \text{if } pos(da_1)<pos(ap) \text{ and } dist(da_1,ap)\le t_1,\\ score-weight(ap)-(weight(ap)+c_3)\cdot weight(da_2)/c_1,\\ \quad \text{if } pos(da_2)<pos(ap) \text{ and } dist(da_2,ap)\le t_1\end{cases}\end{aligned} \tag{8}$$

Equation (8) shows *da*s reinforce the negative score of the *ap* when two *da*s precede the *ap* with the distances between them less than t_1.

B. Rules for ADAN

An *ADAN* is a sequence of words: "w_1 w_2 w_3 w_4 *ap* w_5 w_6 … w_8," where the w_i $(1\le i\le 8)$ is degree adverbs or negations, e.g., "Wei Baifenzhibai Zhenxi (not absolutely cherishes)", and "Wei Zhenxi De Budeliao (not cherishes extremely)".

We developed rules to score an *ADAN* by combining appraisers' weight, degree adverbs' weight, and negations' reversion. Those rules for *ADAN*s are as follows.

$$\begin{aligned}&\text{if } (num(ne)=1 \text{ and } num(da)=0 \text{ and}\\ &polarity(ap)=positive)\Rightarrow\\ &score=\begin{cases}weight(ap), \text{ if } dist(ne,ap)>t_2\\ -weight(ap)-c_2, \text{ otherwise.}\end{cases}\end{aligned} \tag{9}$$

Wherein: *ne* is a negation, and t_2 is the threshold of word distance between *ne* and *ap*. Therefore, the rule shows that the negation reverses the sentiment polarity of the original appraiser with the conditional threshold t_2.

$$\begin{aligned}&\text{if } (num(ne)=1 \text{ and } num(da)=1 \text{ and}\\ &\quad polarity(ap)=positive)\Rightarrow\\ &\quad \text{if } (dist(ne,da)\le t_3 \text{ and } pos(da)>pos(ne))\\ &\qquad score=\begin{cases}weight(ap), \text{ if } dist(ne,ap)>t_2\\ -weight(ap)+(1-weight(ap)-c_2)\cdot\\ weight(da)/c_1, \text{ otherwise}\end{cases}\\ &\quad \text{elseif } (dist(ne,da)\le t_3 \text{ and } pos(da)<pos(ne))\\ &\qquad score=\begin{cases}weight(ap), \text{ if } dist(ne,ap)>t_2\\ -weight(ap)-(weight(ap)+c_3)\cdot\\ weight(da)/c_1, \text{ otherwise}\end{cases}\\ &\quad \text{else}\\ &\qquad score=\begin{cases}weight(ap), \text{ if } dist(ne,ap)>t_2\\ -weight(ap)-c_2, \text{ otherwise.}\end{cases}\end{aligned} \tag{10}$$

Equation (10) shows the reinforcing role of *da*, which is either after or before *ne* with the thresholds of t_2 and t_3, when only one *ne* and one *da* appears.

$$\begin{aligned}&\text{if } (num(ne)=2 \text{ and } ((pos(ne_1)>pos(ap)\\&\text{and } pos(ne_2)>pos(ap)) \text{ or } (pos(ne_1)<pos(ap)\\&\text{and } pos(ne_2)<pos(ap))) \text{ and } polarity(ap)=positive)\Rightarrow\\&score=\begin{cases}weight(ap), \text{ if } num(da)=0\\weight(ap)\cdot(1+weight(da)/c_1),\\\text{if } num(da)=1.\end{cases}\end{aligned} \tag{11}$$

Equation (11) shows that the two *ne*s must be either prior or posterior the appraiser together.

$$\begin{aligned}&\text{if } (num(ne)=1 \text{ and } num(da)=0 \text{ and } polarity(ap)=negative)\Rightarrow\\&score=\begin{cases}-weight(ap)-c_2, \text{ if } dist(ne,ap)>t_2\\weight(ap), \text{ otherwise.}\end{cases}\end{aligned} \tag{12}$$

Equation (12) is an allelomorph of (9), indicating the reverse role of the *ne* with the threshold t_2.

$$\begin{aligned}&\text{if } (num(ne)=1 \text{ and } num(da)=1 \text{ and } polarity(ap)=negative)\Rightarrow\\&\text{if } (pos(da)>pos(ne) \text{ and } dist(ne,da)\le t_3)\\&score=\begin{cases}-weight(ap)-c_2, \text{ if } dist(ne,ap)>t_2\\weight(ap)-(weight(ap)-c_4)\cdot\\weight(da)/c_1, \text{ otherwise}\end{cases}\\&\text{elseif } (pos(da)<pos(ne) \text{ and } dist(ne,da)\le t_3)\\&score=\begin{cases}-weight(ap)-c_2, \text{ if } dist(ne,ap)>t_2\\weight(ap)\cdot(1+weight(da))/c_1, \text{ otherwise}\end{cases}\\&\text{else}\\&score=\begin{cases}-weight(ap)-c_2, \text{ if } dist(ne,ap)>t_2\\weight(ap), \text{ otherwise.}\end{cases}\end{aligned} \tag{13}$$

Equation (13) is an allelomorph of (10), indicating the reinforcing role of *da*. *Da* is either after or before *ne*, where only one *ne* and one *da* appear, with a threshold t_2 or t_3, and with an adjustable integer c_4 for *ne*.

$$\begin{aligned}&\text{if } (num(ne)=1 \text{ and } num(da)>1 \text{ and } polarity(ap)=negative)\Rightarrow\\&score=-weight(ap)-c_5.\end{aligned} \tag{14}$$

Equation (14) is a complementary rule for (12) and (13), and c_5 is an adjustable integer for this case.

$$\begin{aligned}&\text{if } (num(ne)=2 \text{ and } ((pos(ne_1)>pos(ap)\\&\text{and } pos(ne_2)>pos(ap)) \text{ or } (pos(ne_1)<pos(ap)\\&\text{and } pos(ne_2)<pos(ap))) \text{ and } polarity(ap)=negative)\Rightarrow\\&score=\begin{cases}-weight(ap)-c_5, \text{ if } num(da)=0\\-weight(ap)-(weight(ap)+c_6)\cdot\\weight(da)/c_1,\\\text{if } num(da)=1.\end{cases}\end{aligned} \tag{15}$$

Equation (15) is an allelomorph of (11). C_6 is an adjustable integer for this case.

IV. METHODS

To compare our method with machine learning based method for sentiment analysis of Chinese sentences, we used a support vector machine (SVM) method as the baseline classifier, e.g., C-support vector classification (C-SVC) with linear kernel [4].

A. SVM for Sentiment Analysis

The data set can be represented as: $\{x_i, y_i\}$, $y_i \in \{-1,1\}$, $x_i \in R^d$, i=1,…,n, where d is the dimension of word vector, and n is the number of sentences. We formulate SVM solution for nonlinear machines on non-separable data set as follows:

$$\begin{aligned}&\max_{\alpha}\Big(\sum_{i=1}^{n}\alpha_i-\frac{1}{2}\sum_{i=1}^{n}\sum_{i=1}^{n}\alpha_i\alpha_j y_i y_j K(\mathbf{x}_i,\mathbf{x}_j)\Big)\\&\text{s.t. } \sum_{i=1}^{n}y_i\alpha_i=0,\\&0\le\alpha_i\le C,\ i=1,...,n.\end{aligned} \tag{16}$$

Where *K()* is a kernel function, and α_i is a Lagrange multiplier. *C* is a constant. The decision function can be expressed as follows:

$$\begin{aligned}&f(\mathbf{x})=\text{sgn}\Big(\sum_{i=1}^{n}y_i\alpha_i K(\mathbf{x}_i,\mathbf{x})+b^*\Big)\\&\text{s.t. } b^*=y_j-\sum_{i=1}^{n}y_i\alpha_i^* K(\mathbf{x}_i,\mathbf{x}_j),\ 0<\alpha_j^*<C.\end{aligned} \tag{17}$$

We used the bag-of-word (BOW) model to form sentence vectors, and employed term frequency and inverse document frequency (TF-IDF) as the feature values of the vector, which can be expressed as follows:

$$TF\text{-}IDF(t,d)=(1+\log(tf(t,d)))\cdot\log(N/df(t)). \tag{18}$$

Where $tf(t, d)$ is a frequency of term t in a document d, and $df(t)$ is a document frequency of term t. N is the total number of documents.

B. ADN-Scoring for Sentiment Analysis

Based on the rules from (1) to (15), we offer a new method called ADN-scoring to calculate the sentiment polarities of Chinese sentences. The processing steps of the method are as follows:

ADN-scoring algorithm for Chinese sentences:

1. Divide paragraphs into sentences according to the Chinese punctuations, e.g., full stop, exclamatory mark, and question mark;

2. Divide those sentences into clauses according to other Chinese punctuations, e.g., comma, semicolon, pause mark;

3. For each clause:

3.1 Segment it using forward maximum segmentation to obtain word vector and position of words;

3.2 For each word in the word vector:

3.2.1 If the word is an *ap*, check other words in the word vector;

3.2.1.1 When the word is a *ne*, record the position of the *ne* if the number of the *ne*s is less than three; otherwise, do not record it;

3.2.1.2 When the word is a *da*, record the position and weight of the *da* if the number of the *da*s is less than four; otherwise, do not record them;

3.2.2 If the word is a positive *ap*:

3.2.2.1 When no *ne* appears in the word vector, calculate the score of the clause according to the rules from (1) to (4);

3.2.2.2 When only a *ne* appears in the word vector, calculate the score of the clause according to the rules from (9) to (10);

3.2.2.3 When two *ne*s appear in the word vector, calculate the score of the clause according to (11);

3.2.3 When the word is a negative *ap*:

3.2.3.1 When no *ne* appears in the word vector, calculate the score of the clause according to the rules from (5) to (8);

3.2.3.2 When only a *ne* appears in the word vector, calculate the score of the clause according to the rules from (12) to (14);

3.2.3.3 When two *ne*s appear in the word vector, calculate the score of the clause according to the rule (15);

4. Accumulate the scores of the clauses to form the score of the sentence;

5. Return the score of the sentence.

C. Parameter Optimization Using PSO

As mentioned above, the rules from (2) to (15) use parameters: c_1 … c_6, t_1, t_2, and t_3. If those parameters are determined manually, uncertain factor will be introduced in them. Therefore, we can use PSO algorithm to optimize those parameters.

PSO was proposed by Kennedy and Eberhart in 1995 [5], simulating the behavior mechanism of swarm, e.g. bird swarm. When bird swarm migrates, or searches food, birds adjust themselves adaptively to obtain optimal targets according to their individual and social knowledge.

Each bird is called a particle, which is treated as an agent. It consults the optima found earlier, and that found by its neighbors, searching the optimal targets by adjusting its position and its velocity in flight.

The PSO algorithm integrates information from the current, the historical, and the neighboring of every particle, forming a stochastic, uniform, and adaptive behavior mechanism.

The particle changes its velocity when it moves, which can be expressed as follows:

$$v_{p,d} = w \cdot v_{p,d} + c_1 \cdot r_1 \cdot (pb_{p,d} - x_{p,d}) + c_2 \cdot r_2 \cdot (gb_d - x_{p,d}). \quad (19)$$

Where $v_{p,d}$ is the velocity of particle p in dimension d, and w is the weight for the original velocity. $x_{p,d}$ is the position of the particle p in dimension d. $pb_{p,d}$ is the personal-best position, and the $gb_{p,d}$ is the global-best position found by the swarm. c_1 and c_2 are two constants for the convergence of swarm; r_1 and r_2 are two random values.

After the update of the velocity, particle changes its position too, which can be expressed as follows.

$$x_{p,d} = x_{p,d} + v_{p,d}. \quad (20)$$

Due to that the velocity and position of each particle can be out of the range of the solution's space, we used a function clamping them, which can be expressed as follows.

$$\begin{aligned} &\text{if } (x_{p,d}^{\max} < x_{p,d})\ x_{p,d} = x_{p,d}^{\max},\ v_{p,d} = 0 \\ &\text{if } (x_{p,d} < x_{p,d}^{\min})\ x_{p,d} = x_{p,d}^{\min},\ v_{p,d} = 0. \end{aligned} \quad (21)$$

V. Experiments

We used three data sets from the real-world applications to examine the validity of the proposed ADN-scoring algorithm. First data set was collected manually[2] about a movie called 'Slumdog Millionaire'. We extracted the first paragraph from 566 different Chinese reviews. Then, we filtered the neutral Chinese sentences to form the data set (No.1). The characteristic of the data set is summarized in Table 1.

TABLE I.
CHARACTERISTICS OF DATA SET (NO.1)

Positive Sentence	Negative Sentence	Total
493	296	789

To cover more Chinese sentences using appraisers, we extracted more appraisers from Chinese news Website[3] to extend the appraiser lexicon from HowNet[4]. The characteristic of the appraiser lexicon is summarized in Table 2.

TABLE II.
CHARACTERISTICS OF LEXICON AND EXTENSION

lexicon	Positive appraiser	Negative appraiser
HowNet	4566	4370
extended	3288	4407

Furthermore, we extracted 29 representative Chinese negations manually, which are listed in Table 3.

TABLE III.
CHINESE NEGATIONS EXTRACTED

Negations			
Mei	Bingfei	Meiyou	Bu
Bugou	Buqu	Buhui	Buneng
Bukeneng	Bingbu	Congwei	Fei
Hebu	Buyu	Bushi	Haobu
Bushi	Benbu	Haowu	Shiqu
Juebu	Juefei	Juebu	Meishen mo
Wei	Wu	Yaobu	Yongbu
Yuanfei	-	-	-

We used the popular measures to evaluate the ADN-scoring algorithm, such as precision, recall, and F1, which are expressed as follows:

$$\begin{aligned} precision &= tp/(tp+fp) \\ recall &= tp/(tp+fn) \\ F_1 &= \frac{2 \cdot recall \cdot precision}{recall + precision} = \frac{2 \cdot tp}{2 \cdot tp + fn + fp}. \end{aligned} \quad (22)$$

[2] http://movie.mtime.com/80325/comment.html

[3] http://news.sina.com.cn

[4] http://www.keenage.com

Where:

1) *tp* is true positive, equaled to the number of positive cases judged to positive category;

2) *fp* is false positive, equaled to the number of negative cases judged to positive category;

3) *fn* is false negative, equaled to the number of positive cases judged to negative category.

The sentiment is positive when the score is greater than zero, and is negative when the score is less than zero.

We ran PSO algorithm five times to determine the parameters of the PSO as follows:

1) Each of particles has nine dimensions, corresponding to the nine parameters of the ADN-scoring algorithm, i.e., $c_1 \ldots c_6, t_1, t_2, t_3$.

2) Each run has 20 iterations.

3) The w is 0.6893, and the c_1 and c_2 of the PSO algorithm are 1.

4) The r_1 and r_2 are uniform random numbers in the range $[0, w]$.

5) The fitness of particle is F1.

Cross-validation (CV) is a popular evaluative method in the training and the test procedures. We used data set No.1 as the training data set, and 3-fold CV to calculate the F1 values.

In our method, the size of the neighbor is the size of the swarm. The position of every particle is initialized to a uniform random value in the solution's space. Similarly, the velocity of every particle is also initialized to another uniform random value within the range between 0 and half of the maximum value of the position.

After running ADN-scoring algorithm, we attained the optimal parameters as follows:

(a) t_1 is 2; (b) t_2 is 5; (c) t_3 is 3; (d) c_1 is 17; (e) c_2 is 0.177074; (f) c_3 is 0.074365; (g) c_4 is 1; (h) c_5 is 0.622489; (i) c_6 is 0.657678.

The results of SVM baseline and ADN-scoring using the 3-fold CV on the data set No.1 are listed in Table 4.

TABLE IV.
RESULTS OF SVM AND ADN ON DATA SET NO.1

Method	Precision	Recall	F1
SVM	0.8746	*0.8579*	0.8662
ADN	*0.9227*	0.8414	*0.8799*

From Table 4, ADN-scoring algorithm realized slightly better than SVM baseline.

We extracted three typical examples, in which SVM classifier failed, but ADN method succeeded as follows.

1) Yiyang de pin (they are similarly poor.) The length of the Chinese sentence is short, where 'pin' is a negative appraiser. SVM algorithm failed in this short sentence due to the word is not existed in the training data set, but ADN method recognized successfully the appraiser 'pin', which is included in the lexicon.

2) Zhuduo jiangxiang, sihu youxie yanguoqishi (many awards, it seems some exaggeration.) In this Chinese sentence, 'yanguoqishi' is a negative appraiser (a Chinese idiom). Many words in this sentence do not appear in the training data. Therefore, SVM algorithm failed in this case, but ADN method successfully recognized the idiom due to having a large lexicon, including that idiom.

3) Wo juede meiyou bu gei manfen de liyou (there is no reason not to give full points.) In this sentence, 'meiyou' and 'bu' are two negations, and 'manfen' is a positive appraiser. The double negations only can be recognized by rules. Although SVM algorithm failed in this case, ADN succeeded due to that the lexicon includes those negations.

Furthermore, we adopted more complicated data sets called corpus-sentiment[5]. The characteristics of the data sets are summarized in Table 5.

TABLE V.
CHARACTERISTICS OF DATA SETS (NO.2)

Data set	Positive articles	Negative articles	Total articles
Hotel	2000	2000	4000
Notebook	2000	2000	4000
Book	2000	2000	4000

Each article in the data sets can have both positive and negative sentences, which increases the difficulty of sentiment classification. We calculated the sum of sentiment polarities of those sentences in the article as the final polarity. Thus, we ran the SVM baseline and ADN-scoring algorithm on this data set (No. 2) using 3-fold CV with the parameters optimized on the training data set (No. 1). The results are as follows.

TABLE VI.
RESULTS OF SVM AND ADN-SCORING METHOD ON DATA SETS NO.2

Method	Data set	Precision	Recall	F_1
ADN	Hotel	0.7550	*0.815*	*0.7838*
	Notebook	*0.7333*	*0.8675*	*0.7948*
	Book	*0.7332*	*0.808*	*0.7688*
SVM	Hotel	*0.8212*	0.5071	0.6267
	Notebook	0.7203	0.5462	0.6209
	Book	0.6840	0.5280	0.5953

From table 6, the results of ADN-scoring are better than that of the SVM baseline.

We guessed that the noise in the data reduced the performance of SVM due to that an effective attribute selection or feature extraction was not adopted before using SVM baseline, which is normally an important pre-processing step for SVM method.

Furthermore, we used the closest data set of evaluation task two in COAE to evaluate, and calculated the macro-

[5] www.searchforum.org.cn/tansongbo/corpus-senti.htm

and micro-evaluation results for the three fields (digital, entertainment, and finance). The results are as follows.

TABLE VII.
RESULTS FOR CLASSIFICATION OF OPINION SENTENCES

Method	Macro Evaluation			Micro Evaluation		
	Prec	Recall	F1	Prec	Recall	F1
HITSZ	*0.5347*	*0.7234*	*0.5414*	*0.4945*	0.6544	*0.6254*
ADN	0.3315	0.7195	0.4086	0.3994	*0.7618*	0.5241
Suda	0.3706	0.4054	0.3840	0.3652	0.5048	0.5089

From table 7, we see that the ADN approach attained better results than the Suda method which obtained the second rank.

VI. RELATED WORK

Sentiment and subjectivity classification can be run on two levels: document, and sentence [6]. The former mostly uses supervised learning methods. Naive Bayesian and SVM are such algorithms used for the sentiment classification. Moreover, feature selection can improve the performance of these algorithms [7]. The latter are normally treated as a middle procedure of the former. Supervised learning methods are also can be used for the latter [8]. Meantime, the methods of semi-supervised learning [9] and the methods of opinion word collection [10] have also been effective. Especially, the context has been influential too [11], such as negations and contraries. In [12], the strength of opinion and types of subjectivity are classified to neutral, low, medium, or high using deeply nested clauses within a sentence. Another target of sentiment classification is discovering the objects of opinion first, and then deciding their sentiment polarities [13].

The model of sentiment composition [14] can classify the sentiment of the grammatical constituents, which used a quasi-compositional way, and was implemented as a post-process of lexical parsing, interpreting the output of a dependency parser. In this paper, instead of acquiring the linguistic constituents on the grammatical levels, we used constraints existed in between the words closed to each other, and expressed those constraints by using word distances, where the appraisers are the center of sentence sentiments.

An analytical approach to assess text sentiment was proposed in [15]. The method processed the semantics, followed by employing rules to assign contextual valences to the linguistic components. Instead of acquiring the valences of Chinese linguistic components, we calculated the sentence sentiment directly using three types of words, and utilizing constraints, combinations, and rules with their adjustable parameters.

The method learning with compositional semantics was presented in [16], which incorporated structural inference, and motivated by integrating the compositional semantics into learning procedure. Experiments showed the performance was better (90.7%) than that using simple heuristics based on compositional semantics (89.7%), and that using learning-based methods without compositional semantics (89.1%). In the method, the constraints of word distance were ignored.

A method of sentiment classification for Japanese and English sentences was proposed in [17], which was based on conditional random fields (CRF) with hidden variables and dependency tree to compute the polarity of the entire sentence, where the cooperation of the hidden variables was considered.

AVA method [18] analyzed the sentiment strength of English sentences using adjectives, verbs, and adverbs with their combinations, where two AVAC-scoring algorithms have been developed.

In the paper, the method is different from the AVA. First, it processed sentences in Chinese instead of that in English. Second, it used appraises, degree adverbs, negations, and their combinations, where those appraisers included multiple POSs, such as verbs, nouns, adjectives, adverbs, and idioms, and those degree adverbs were only part of the whole adverbs. Third, the method employed word distance constraints, Chinese lexicons from HowNet, weighted adjustments, and parameterized rules.

A method called Elastic Net was proposed for online sentiment classification [19], which used character-level, word-level n-grams, and different combinations of them to improve the interpretability. Experiments showed that it outperformed semantic-oriented approaches according to the accuracy of sentiment classification. The top-ranked features were selected, which had strong sentiment polarities, and had significant implications for markets.

In [20], a framework was introduced for Chinese documents, which combined context-sensitive sentiment lexicon and sentiment words from Hownet to improve the performance of opinion mining.

In [21], a new method of opinion mining was proposed, which used hierarchical fuzzy domain sentiment ontology to define a space of product features and opinions. Therefore the user experience was improved, and the experimental results showed that the polarity of many sentiment expressions was automatically identified by the approach.

VII. CONCLUSIONS

We present a ADN-scoring method in the paper, which used appraisers, degree adverbs, negations, and their combinations for the sentiment analysis of Chinese sentence. Furthermore, We utilized PSO algorithm to optimize the parameters of the rules for the method. When those parameters are determined by the PSO algorithm on the training corpus, the performance of the sentiment classification for new sentences and texts will be improved. The experimental results indicate the improvement on new test data sets. The model can be extended to new applications. For example, it can be applied to the social media, such as Blog and Micro-Blogging.

The sentiment words used in this article came from general fields. Therefore, those words can be used in other fields. However, there are a few sentiment words for specific fields not including in our lexicons. On the other hand, some words' sentiment will change in different contexts and situations. For example, the Chinese word Laji 'junk' can be ambiguous. When it used for a certain person, it is a negative term meaning as 'bad person'. Otherwise, it is a neutral term meaning as 'void items.' Those ambiguous words are useful for special fields. Furthermore, the lexicons in the method can be expanded. How to integrate the fields into the lexicons to identify a certain sentiment in those fields more precisely will be the future work.

ACKNOWLEDGMENT

This work is supported by "863: the Hi-Tech Research and Development Program of China (No. 2012AA011104)."

REFERENCES

[1] P. Turney, "Thumbs up or Thumbs down? Semantic Orientation Applied to Unsupervised Classification of Reviews," Proc. The Meeting of the Association for Computational Linguistics (ACL'02), pp. 417-424, 2002.
[2] B. Pang, L. Lee, and S. Vaithyanathan, "Thumbs up? Sentiment Classification Using Machine Learning Techniques," Proc. The EMNLP. pp. 79-86, 2002.
[3] K. Dave, S. Lawrence, and D. Pennock, "Mining the Peanut Gal-lery: Opinion Extraction and Semantic Classification of Product Reviews," Proc. The 12th Intl. World Wide Web Conference (WWW'03), pp. 519-528, 2003.
[4] C.C. Chang and C.J. Lin, "LIBSVM: A Library for Support Vector Machines," Available at http://www.csie.ntu.edu.tw/~cjlin/libsvm, 2001.
[5] J. Kennedy, and R. Eberhart," Particle Swarm Optimization," Proc. ICNN. vol. 4, pp. 1942-1948, 1999.
[6] Bing Liu. "Sentiment Anlaysis and Subjectivity." Invited Chapter for the *Handbook of Natural Language Processing*, Second Edition (editors: N. Indurkhya and F. J. Damerau), March, 2010.
[7] B. Pang and L. Lee, "Opinion Mining and Sentiment Analysis." *Foundations and Trends in Information Retrieval*, 2(1-2), pp. 1–135, 2008.
[8] H. Yu and V. Hatzivassiloglou, "Towards Answering Opinion Questions: Separating Facts from Opinions and Identifying the Polarity of Opinion Sentences," Proc. The Conference on Empirical Methods in Natural Language Processing (EMNLP), 2003.
[9] M. Gamon, A. Aue, S. Corston-Oliver, and E. Ringger, "Pulse: Mining Customer Opinions from Free Text," Proc. The International Symposium on Intelligent Data Analysis (IDA), pp. 121–132, 2005.
[10] S.-M. Kim and E. Hovy, "Determining the Sentiment of Opinions," Proc. The International Conference on Computational Linguistics (COLING), 2004.
[11] T. Wilson, J. Wiebe, and P. Hoffmann, "Recognizing Contextual Polarity in Phrase-level Sentiment Analysis," Proc. The Human Language Technology Conference and the Conference on Empirical Methods in Natural Language Processing (HLT/EMNLP), pp. 347–354, 2005.
[12] T. Wilson, J. Wiebe, and R. Hwa, "Just How Mad are You? Finding Strong and Weak Opinion Clauses," Proc. AAAI. pp. 761–769, 2004.
[13] B. Liu, M. Hu, and J. Cheng, "Opinion Observer: Analyzing and Comparing Opinions on the Web," Proc. WWW. 2005.
[14] K. Moilanen and S. Pulman, "Sentiment Composition," Proc. The Recent Advances in Natural Language Processing International Conference (RANLP 2007), pp. 378–382, 2007.
[15] M. Al Masum Shaikh, H. Prendinger, and M. Ishizuka, "An Analytical Approach to Assess Sentiment of Text," Proc. ICCIT. 2007.
[16] Y. Choi and C. Cardie, "Learning with Compositional Semantics as Structural Inference for Subsentential Sentiment Analysis," Proc. EMNLP. pp. 793-801, 2008.
[17] T. Nakagawa, K. Inui, and S. Kurohashi, "Dependency Tree-Based Sentiment Classification using CRFs with Hidden Variables," Proc. ACL: HLT, 2010.
[18] V.S. Subrahmanian and D. Reforgiato, "AVA: Adjective-Verb-Adverb Combinations for Sentiment Analysis," *IEEE Intelligent System*, vol. 23, no. 4, pp. 43-50, 2008.
[19] L. Fan, Y.L. Zhang, and H.C. Chen, "Sentiment Analysis on Chinese Web Forums using Elastic Nets: Features, Classification and Interpretation," FCB Working Paper Series, 2011.
[20] L. Liu, M. Lei, and H. Wang, "Combining Domain-Specific Sentiment Lexicon with Hownet for Chinese Sentiment Analysis." *Journal of Computers*, vol. 8, no. 4, pp. 878-883, 2013.
[21] H. Wang, X. Nie, L. Liu, and J. Lu, "A Fuzzy Domain Sentiment Ontology based Opinion Mining Approach for Chinese Online Product Reviews," *Journal of Computers*, vol. 8, no. 9, pp. 2225-2231, 2013.

Wen Xiong was born in Wuhan City, Hubei Province, in 1968. He received the Ph.D. degree in signal and information processing from Beijing University of Posts and Telecommunications, Beijing, China, in 2011. From January 2011 to April 2013, he was a postdoctoral fellow with the Institute of Chinese Information Processing, Beijing Normal University, Beijing, China. Since May 2013, he has been an employee at China Patent Information Center, and CPIC-BNU joint laboratory of machine translation. His research interests include machine translation, natural language processing, artificial intelligence, affective computing, and data mining.

Yaohong Jin received the MA and Ph.D. degrees from Chinese Academy of Sciences, P. R. China. He is a professor at the Institute of Chinese Information Processing, Beijing Normal University, China. Previously, he was an associate professor of Chinese Academy of Sciences. His research interests include natural language processing, machine translation and search engine, in which areas he has published more than 20 papers in international journals and conference proceedings.

Image Denoising via Robust Simultaneous Sparse Coding

Lei Li
School of Technology, Beijing Forestry University, Beijing 100083, P. R. China
Email:Lilei7760@163.com

Jiangming Kan
School of Technology, Beijing Forestry University, Beijing 100083, P. R. China
Email:kanjm@bjfu.edu.cn

Wenbin Li
School of Technology, Beijing Forestry University, Beijing 100083, P. R. China
Email:leewb@bjfu.edu.cn

***Abstract*—Simultaneous sparse coding (SSC) has shown great potential in image denoising, because it exploits dependencies of patches in nature images. However, imposing joint sparsity might neglect the sight difference between patches. In this paper, we propose an image denoising algorithm based on robust simultaneous sparse coding (RSSC). In our algorithm, the sparse coefficient matrix is decomposed into two parts. One coefficient matrix is imposed on the joint sparse regularizer which exploits self-similarities of image patches while the other matrix is imposed by the elementwise sparse regularizer which considers the subtle differences between patches. Experiments on the benchmark data show the superior performance over the state-of-art algorithms.**

***Index Terms*—Image denoising, robust simultaneous sparse coding, regularization, accelerated proximal gradient (APG)**

I. Introduction

In recent years, affordable hardware has made it possible for digital cameras to capture images of very high resolution. However, images are often corrupted by noise during the procedures of both image acquisition and transmission. An efficient denoising algorithm becomes very important to the performance of image processing techniques. Hence, denoising of images remains one of the most fundamental tasks of image processing. As follows, for an origin image $\mathbf{x} \in \mathbf{R}^N$ and its degraded image $\mathbf{y}$ the problem of denoising can mathematically be defined as the following observation model:

$$y_i = x_i + \eta_i \tag{1}$$

where x_i is the original pixel intensity of the y_i pixel observed as after being corrupted by zero mean independent identically distributed additive noise η_i .

Corresponding author: Jiangming Kan, Email: kanjm@bjfu.edu.cn, Tel: 8610-62337736.

recently,Many proposed denoising methods are based on image patches. Decomposing the origin image into overlapping patches, the data model can be written as

$$\mathbf{y}_i = \mathbf{x}_i + \boldsymbol{\eta}_i \tag{2}$$

where $\mathbf{x}_i$ is the original image patch intensities with the i -th pixel at its center written in a vectorized format and $\mathbf{y}_i$ is the observed patch corrupted by a noise vector $\boldsymbol{\eta}_i$. Denoising an image is thus solving the inverse problem to estimate pixel intensities $\mathbf{x}_i$.

In the past several decades, image denoising has been extensively studied and many algorithms [1] [2] [12] [13] have been proposed, leading to state-of-the-art performances. Of these various approaches, Non-Local Means (NLM) algorithm [1] recently proposed by Buades *et al*. assumes that the noise is zero-mean and uncorrelated across locations. Thanks to the presence of repeating structures in a given image, performing a weighted averaging of pixels with similar neighborhoods can suppress the noise. Inspired by the idea of NLM, Dabov *et al*. [2] proposed an effective algorithm named BM3D. BM3D performs denoising by utilizing similar patches across the image in the transform domain rather than in the origin image space.

Recently, using redundant representations and sparsity for denoising of signals have drawn a lot of research attention [3] [4] [14]. In [3], Elad and Aharon applied the K-SVD algorithm to learn the optimal over-completed dictionaries for the observed noisy image. Each image patch can be sparsely represented by the learned dictionary and denoising is carried out by coding each patch as a linear combination of only a few atoms in the dictionary. Mairal *et al*. [4] extended the K-SVD algorithm to the color image denoising.

However, in [3] [4], image patches are sparsely represented independently, which ignores self-similarities

doi:10.4304/jcp.9.6.1418-1425

in natural images as NLM did. Mairal *et al*. [5] argued exploiting similarities can improve the denoising performance. And he grouped image patches into a few groups and argued patches in the same group have similar sparse decomposition. And the simultaneous sparse coding (SSC) is applied to learn the sparse representation matrix. Experiments show the superior performance over the K-SVD algorithm. Dong *et al*. [6] propose a new denoising algorithm based on clustering-based sparse representation (CSR), which incorporates the dictionary learning and structural clustering into a unified variational framework.

However, there is a key problem that similar patches corrupted by noises might not share the same structure and imposing joint sparse regularizer as done in [5] may degrade the denoising performance [7] [8]. To overcome this problem, in this paper, we propose our image denoising algorithm based on robust simultaneous sparse coding (RSSC). As shown in Fig.1, in our algorithm, the sparse coefficient matrix $\mathbf{A}$ is decomposed into two parts $\mathbf{P}$, $\mathbf{Q}$. A joint sparse regularizer is imposed on $\mathbf{P}$, corresponding to the shared structure while an elementwise sparse regularizer is imposed on $\mathbf{Q}$ which corresponds to the non-shared features. The joint-sparsity exploits the similarities between patches while the elementwise sparsity considers the differences of patches. Experiments with images corrupted by synthetic noise show that the proposed method outperforms the state of the art algorithms in image denoising.

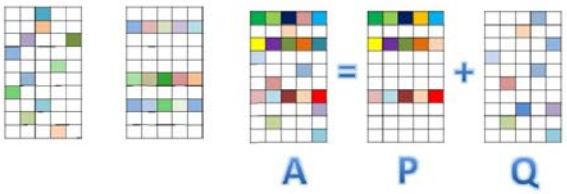

Figure 1. Illustration of sparsity vs. joint sparsity vs. robust joint sparsity: color squares represent nonzero values in the coefficient matrix.

The rest of this paper is organized as follows. In Sec.2, our new image denoising algorithm is described in detail. Experimental results and comparison with other state-of-the-art approaches are presented in Sec.3. Our work is summarized in Sec.4.

II. ROBUST SPARSE REPRESENTATION MODEL

A. Image Denoising Model

Various image restoration tasks based on sparse coding can be formulated into the following minimization problem:

$$\boldsymbol{\alpha}_i = \arg\min_{\boldsymbol{\alpha}_i} \left\|\mathbf{y}_i - \mathbf{D}\boldsymbol{\alpha}_i\right\|_2^2 + \gamma\left\|\boldsymbol{\alpha}_i\right\|_1 \qquad (3)$$

where $\mathbf{y}_i = \mathbf{R}_i\mathbf{x}$ denotes an degraded image patch of size $\sqrt{n}\cdot\sqrt{n}$ extracted at location i, $\mathbf{R}_i$ is the matrix extracting patch $\mathbf{y}_i$ from $\mathbf{y}$ at location i and $\mathbf{D}\in\mathbf{R}^{n\times K}$ is a fixed dictionary and K is its size, $\boldsymbol{\alpha}_i\in\mathbf{R}^K$ is the reconstruction coefficients, γ is the penalty to control the sparsity of $\boldsymbol{\alpha}_i$. After determining sparse coefficients $\boldsymbol{\alpha}_i$, we estimate the original image $\mathbf{x}$ by solving the following over-determined system:

$$\mathbf{x} = \arg\min_{\mathrm{x}} \lambda\left\|\mathbf{y}-\mathbf{x}\right\|_2^2 + \sum_{ij}\left\|\mathbf{R}_{ij}\mathbf{x}-\mathbf{D}\boldsymbol{\alpha}_{ij}\right\|_2^2 \qquad (4)$$

This above quadratic equation has a straightforward solution:

$$\mathbf{x} = \left(\lambda\mathbf{I} + \sum_{ij}\mathbf{R}_{ij}^T\mathbf{R}_{ij}\right)^{-1}\left(\lambda\mathbf{y} + \sum_{ij}\mathbf{R}_{ij}^T\mathbf{D}\boldsymbol{\alpha}_{ij}\right) \qquad (5)$$

A major drawback of (3) is that image patches are sparsely represented independently and dependencies between patches are ignored. The self-similarities among patches can be used to improve learned sparse models [5]. The basic idea is to group a set of similar patches $\mathbf{Y}=\left[\mathbf{y}_1,\mathbf{y}_2,\cdots,\mathbf{y}_m\right]\in\mathbf{R}^{n\times m}$ and imposing a grouped-sparsity regularizer on the matrix $\mathbf{A}=\left[\boldsymbol{\alpha}_1,\boldsymbol{\alpha}_2...,\boldsymbol{\alpha}_m\right]$ and (3) is reformulated as follows:

$$\mathbf{A} = \arg\min_{\mathrm{A}} \frac{1}{2}\left\|\mathbf{Y}-\mathbf{D}\mathbf{A}\right\|_F^2 + \lambda\left\|\mathbf{A}\right\|_{p,q} \qquad (6)$$

where m is the number of similar patches and $\left\|\cdot\right\|_{p,q}$ is the pseudo-matrix norm defined as

$$\left\|\mathbf{A}\right\|_{p,q} = \sum_{i=1}^{n}\left\|\boldsymbol{\alpha}^i\right\|_q^p \qquad (7)$$

where $\boldsymbol{\alpha}^i=\left[\alpha_{i1},...,\alpha_{im}\right]$ denotes the i-th row of matrix $\mathbf{A}$. In this paper, we choose the pair (p, q) with the values (1, 2). From (6), we can see that simultaneous sparse coding encourages similar patches to be represented by the same atoms and this can exploit the dependencies between patches.

However, due to image patches corrupted by noise, similar patches may not fall into a single shared structure [7] and block ℓ_{12} regularization might perform worse than simple separate elementwise ℓ_{11} regularization. Therefore, to deal with this problem, we propose our image denoising model based on robust sparse coding (RSC) as follows:

$$\begin{aligned}\mathbf{P},\mathbf{Q} = \arg\min_{\mathbf{P},\mathbf{Q}} &\frac{1}{2}\left\|\mathbf{Y}-\mathbf{D}\left(\mathbf{P}+\mathbf{Q}\right)\right\|_F^2 \\ &+\lambda_1\left\|\mathbf{P}\right\|_{1,2}+\lambda_2\left\|\mathbf{Q}\right\|_{1,1}\end{aligned} \qquad (8)$$

where $\mathbf{P}$ is a group sparse component which reflects the same structure shared by similar patches and $\mathbf{Q}$ is an elementwise component which reflects the difference between patches. That is, we decompose the coefficient matrix into two components and impose different regularizer on them. This exploits the similarities between patches while considering their differences.

B. Optimization Algorithm

In this section, we show how to solve the robust image denoising model in (8) efficiently. Denote

$$\begin{aligned} \mathrm{F}(\mathbf{P},\mathbf{Q}) &= \frac{1}{2}\left\|\mathbf{Y}-\mathbf{D}(\mathbf{P}+\mathbf{Q})\right\|_F^2 \\ \mathrm{G}(\mathbf{P},\mathbf{Q}) &= \lambda_1\left\|\mathbf{P}\right\|_{1,2}+\lambda_2\left\|\mathbf{Q}\right\|_{1,1} \end{aligned} \tag{9}$$

where $\mathrm{F}(\mathbf{P},\mathbf{Q})$ is the empirical loss function and $\mathrm{G}(\mathbf{P},\mathbf{Q})$ is the regularization term. Obviously, the object function in Problem (8) is a composite model, which is consist of a differential term $\mathrm{F}(\mathbf{P},\mathbf{Q})$ and a non-differential term $\mathrm{G}(\mathbf{P},\mathbf{Q})$. And it can easily be proved $\mathrm{F}(\mathbf{P},\mathbf{Q})$ is jointly convex and $\mathrm{G}(\mathbf{P},\mathbf{Q})$ is also convex with respect to all their variables. Therefore, the global solution can be obtained. We propose a method based on the accelerated proximal gradient (APG) methods [9] [10] to solve the optimization problem.

In the APG method [9] [10], at every iteration k, we need optimize the following problem:

$$(\mathbf{P}^k,\mathbf{Q}^k)=\arg\min_{\mathbf{P},\mathbf{Q}} \mathrm{T}_{\mathbf{P}^k,\mathbf{Q}^k,L_k}(\mathbf{P},\mathbf{Q})+\mathrm{G}(\mathbf{P},\mathbf{Q}) \tag{10}$$

where

$$\begin{aligned} \mathrm{T}_{\mathbf{P}^k,\mathbf{Q}^k,L_k}(\mathbf{P},\mathbf{Q}) &= \frac{1}{2}\mathrm{T}(\mathbf{P}^k,\mathbf{Q}^k)+\left\langle\frac{\partial \mathrm{T}(\mathbf{P},\mathbf{Q})}{\partial \mathbf{P}},\mathbf{P}-\mathbf{P}^k\right\rangle \\ &+\frac{L_k}{2}\left\|\mathbf{P}-\mathbf{P}^k\right\|_F^2+\left\langle\frac{\partial \mathrm{T}(\mathbf{P},\mathbf{Q})}{\partial \mathbf{Q}},\mathbf{Q}-\mathbf{Q}^k\right\rangle+\frac{L_k}{2}\left\|\mathbf{Q}-\mathbf{Q}^k\right\|_F^2 \end{aligned} \tag{11}$$

L is the Lipschitz constant of $\frac{\partial \mathrm{T}(\mathbf{P},\mathbf{Q})}{\partial \mathbf{P}}$ and $\frac{\partial \mathrm{T}(\mathbf{P},\mathbf{Q})}{\partial \mathbf{Q}}$. And the initial $L=L_0=100$ and is updated $L_k=\tau L_{k-1}$ given $\tau > 1$. The composite object function in Problem (8) has two nonsmooth functions. However, because they are separable, Problem (10) can be solved efficiently as the following two separate problems:

$$\begin{aligned} \mathbf{P}^{k+1} &= \frac{1}{2}\left\|\mathbf{P}-\left(\mathbf{P}^k-\frac{1}{L_k}\nabla_{\mathbf{P}}\mathrm{F}\right)\right\|_F^2+\frac{\lambda_1}{L_k}\left\|\mathbf{P}\right\|_{1,2} \\ \mathbf{Q}^{k+1} &= \frac{1}{2}\left\|\mathbf{Q}-\left(\mathbf{Q}^k-\frac{1}{L_k}\nabla_{\mathbf{Q}}\mathrm{F}\right)\right\|+\frac{\lambda_2}{L_k}\left\|\mathbf{Q}\right\|_{1,1} \end{aligned} \tag{12}$$

where $\nabla_{\mathbf{P}}\mathrm{F}$ and $\nabla_{\mathbf{Q}}\mathrm{F}$ is the partial derivatives of $\mathrm{F}(\mathbf{P},\mathbf{Q})$ with respect to $\mathbf{P}$ and $\mathbf{Q}$ at $(\mathbf{P}^k,\mathbf{Q}^k)$. The above problems admit closed form solutions:

$$\begin{aligned} \left(\mathbf{P}^{k+1}\right)^i &= \max\left(0,1-\frac{\lambda_1}{L_k\left\|\left(\mathbf{u}^k\right)^i\right\|}\right)\left(\mathbf{u}^k\right)^i,\forall i=1:n \\ \mathbf{Q}^{k+1} &= \mathrm{sign}\left(\mathbf{V}^k\right)\max\left(0,1-\frac{\lambda_2}{L_k}\right)\mathbf{V}^k \end{aligned} \tag{13}$$

Where $\mathbf{U}^k=\mathbf{P}^k-\frac{1}{L_K}\nabla_{\mathbf{P}}\mathrm{F}$, $\mathrm{V}^k=\mathrm{Q}^k-\frac{1}{L_k}\nabla_{\mathrm{Q}}\mathrm{F}$.

In [11], it has been proved the APG method achieves an $\mathrm{O}\left(\frac{1}{k^2}\right)$ residual from the optimal solution after k iterations. Finally, the algorithm for solving Problem (8) is given in Algorithm1.

Algorithm 1 Optimization for Problem (8)

- Input: $\mathbf{D}$ and $\mathbf{Y}$.
- Output: Optimal solution $(\mathbf{P}^*,\mathbf{Q}^*)$.

(1).Set
$\mathbf{P}^1=\mathbf{P}^0=0$, $\mathbf{Q}^1=\mathbf{Q}^0=0$, $t_0=0$, $t_1=1$, $k=1$, $L=L_0=100$, $\eta=1.05$, $\lambda_1=0.3$, $\lambda_2=0.01$.
(2). while not converged do
(3). Compute the proximal points:

$$\mathbf{P}_v^k=\mathbf{P}^k+\frac{t^{k-1}-1}{t^k}\left(\mathbf{P}^k-\mathbf{P}^{k-1}\right);$$

$$\mathbf{Q}_v^k=\mathbf{Q}^k+\frac{t^{k-1}-1}{t^k}\left(\mathbf{Q}^k-\mathbf{Q}^{k-1}\right);$$

(4). Calculate the gradient $\nabla_{\mathbf{P}}\mathrm{F}$, $\nabla_{\mathbf{Q}}\mathrm{F}$;
(5). Calculate $\mathbf{P}^{k+1}$, $\mathbf{Q}^{k+1}$ via (13);
(6).If $\mathrm{F}_{\mathbf{P}^{k+1},\mathbf{Q}^{k+1}} > \mathrm{T}_{\mathbf{P}^k,\mathbf{Q}^k,L_k}$,update $L_k=\tau L_{k-1}$ and go to Step 5;
(7). Stepsize update:

$$t^{k+1}=\frac{1+\sqrt{4\left(t^k\right)^2+1}}{2}$$

(8). end while

III. IMAGE DENOISING EXPERIMENTS

We have implemented the proposed RSSC denoising algorithm under MATLAB. In all experiments, the block-size $n = 64$, the penalties on sparsity λ_1, λ_2 are set as 0.5, 0.01 respectively. The dictionary is trained on patches from nature images and is shown in Fig 2. And the size of the dictionary $K = 256$.

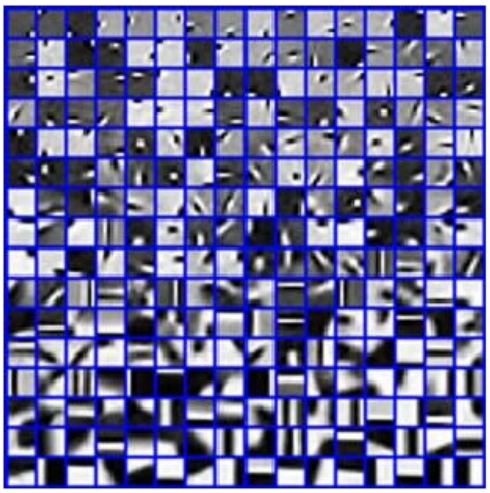

Figure 2.The dictionary used in our denoising algorithm

We first compare the proposed RSSC denoising algorithm and two leading methods for removing additive white Gaussian noise: K-SVD [3], BM3D [2]. The denoising results of all benchmark schemes are generated from the source codes or executables released by their authors. The PSNR performance of three competing denoising algorithms are reported in Table 1 (the highest PSNR value is in Italic).

From Table 1, we can see that our RSSC outperforms the other two algorithms on all tested images except that BM3D achieves better performances on Barbara at the noise level $\theta_n = 15, 25$. Especially, when images are corrupted by $\theta_n = 35$ level Gauss noise, our algorithm achieves the best results on all test images in the three ones. Therefore, we can conclude that RSSC outperforms the other two benchmark methods.

The visual comparison of the denoising methods is shown in Figs. 3-8. Fig. 5 presents visual results of different methods for Peper image with the noise level $\theta_n = 25$. We can observe that all methods can remove the noise effectively and our RSSC which exploits the similarities between patches and considering their differences provides an important improvement over the K-SVD method which considers each patch independently. The proposed method also outperforms over the BM3D method.

Fig. 6 gives the results of our algorithm on the corrupted image House. We can see that our RSSC method shows better visually quality result. The K-SVD method generates many visually disturbing artifacts in the denoised image. The BM3D method loses many details compared our RSSC method.

VI. CONCLUSION

In this paper, we propose a robust image denoising algorithm based on the robust simultaneous sparse coding. We decompose the sparse coefficient matrix into two halves. Joint sparsity regularizer is imposed on one matrix and elementwise sparsity regularizer is imposed on another. This makes our algorithm exploit the dependencies between patches while considering the differences between them. Experiments on the benchmark data show the superior performance over the state-of-art algorithms.

TABLE 1.
QUANTITATIVE COMPARASION. THE GAUSS NOISE LEVEL ΘN=15, 25, 35 AND THE PSNR ARE CHOSEN AS THE PERFORMANCE MEASURE. BEST RESULTS ARE SHOWED IN ITALIC.

θn	Method	House	Peppers	Barbara	Boat	Lena
	KSVD	34.33	32.11	34.53	34.49	34.98
15	BM3D	36.14	33.36	*35.35*	34.82	35.33
	RSSC	*37.13*	*35.20*	35.09	*35.13*	*35.48*
	KSVD	32.08	29.71	30.38	30.29	30.35
25	BM3D	32.03	30.14	*30.68*	29.82	30.03
	RSSC	*32.30*	*30.31*	30.59	*30.43*	*30.77*
	KSVD	31.08	28.91	28.94	29.09	29.15
35	BM3D	31.13	29.18	29.47	29.11	29.21
	RSSC	*31.20*	*29.45*	*29.59*	*29.33*	*29.40*

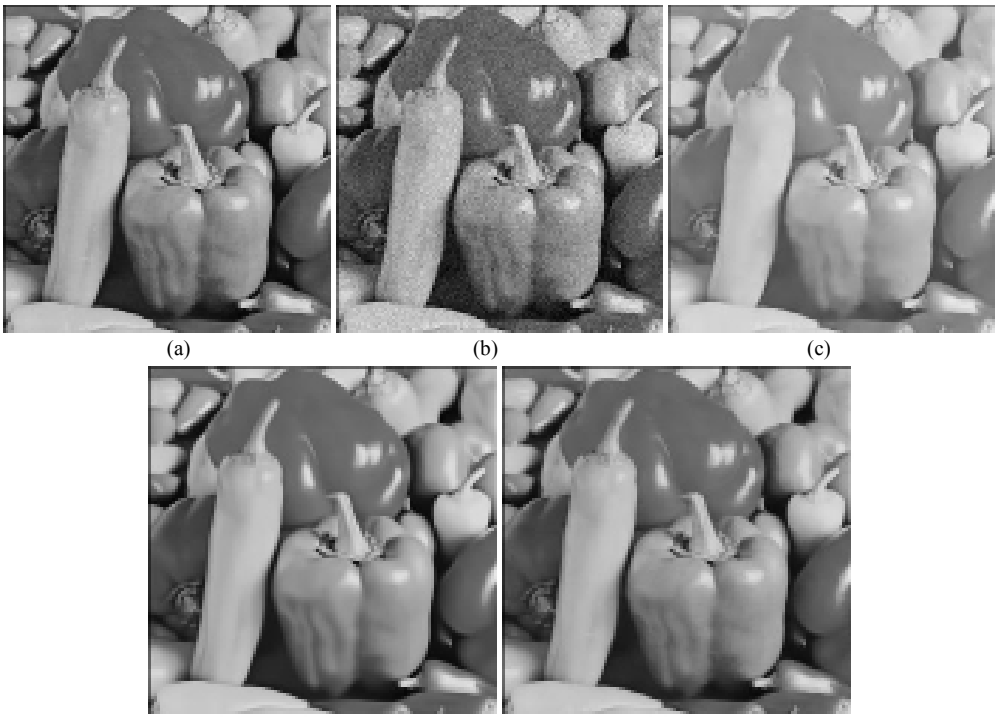

(a) (b) (c)

(d) (e)

Figure 3. Denoising performance comparison for Barbara image at Gauss noise level θn = 15.
From the left to right, the original image, noising image, KSVD, BM3D, RSSC.

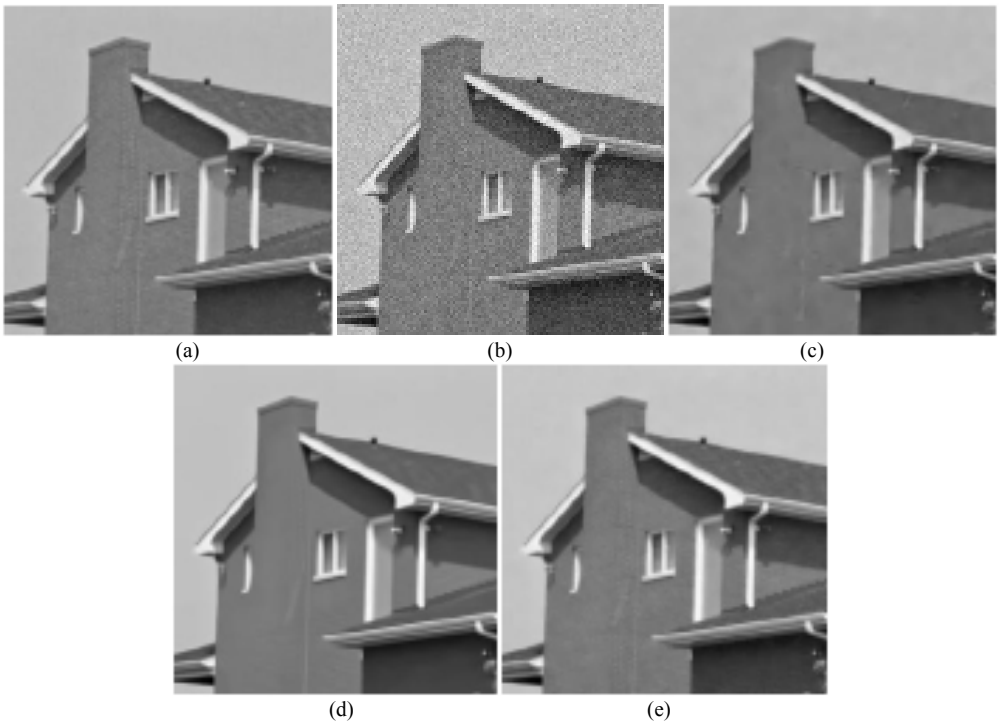

(a) (b) (c)

(d) (e)

Figure 4. Denoising performance comparison for Boat image at Gauss noise level θn = 15.
From the left to right, the original image, noising image, KSVD, BM3D, RSSC.

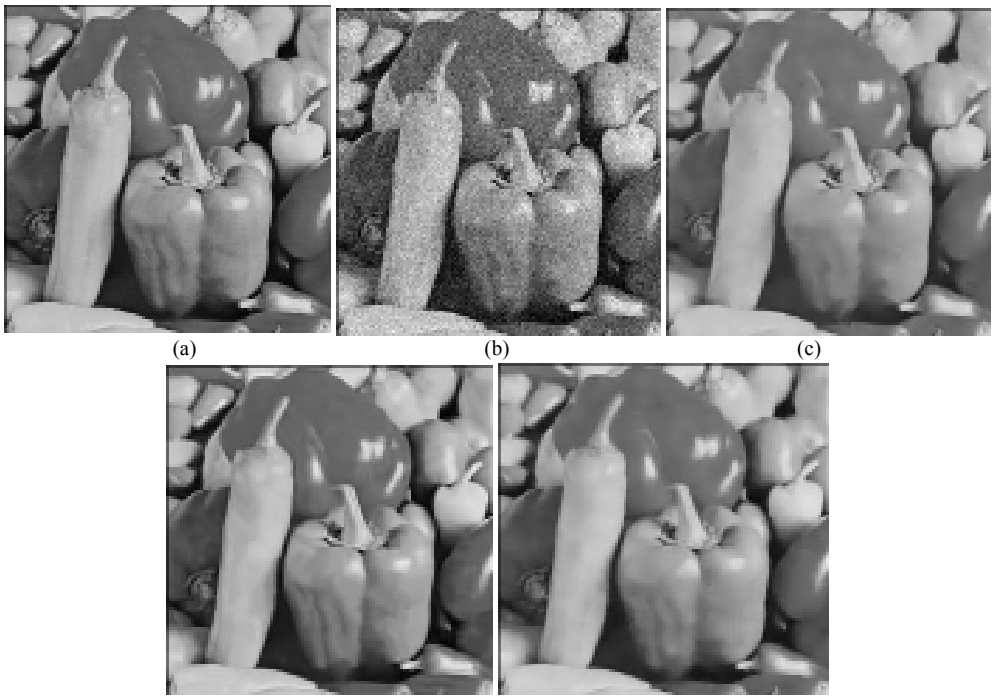

(a) (b) (c)

(d) (e)

Figure 5. Denoising performance comparison for Peppers image at Gauss noise level θn = 25.
From the left to right, the original image, noising image, KSVD, BM3D, RSSC.

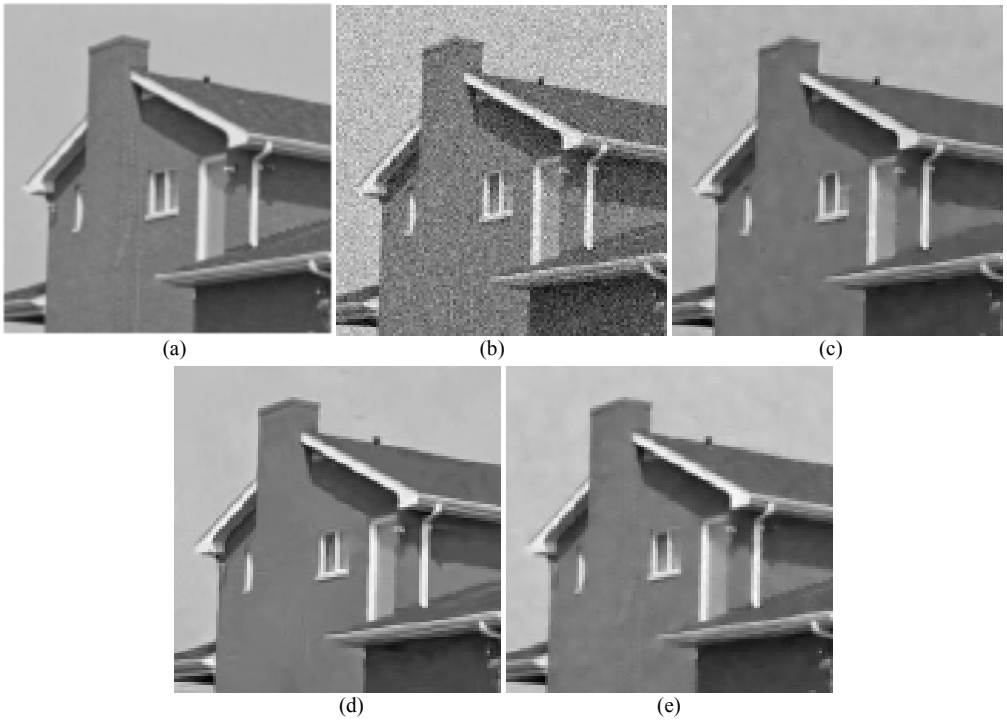

(a) (b) (c)

(d) (e)

Figure 6. Denoising performance comparison for House image at Gauss noise level θn = 25.
From the left to right, the original image, noising image, KSVD, BM3D, RSSC.

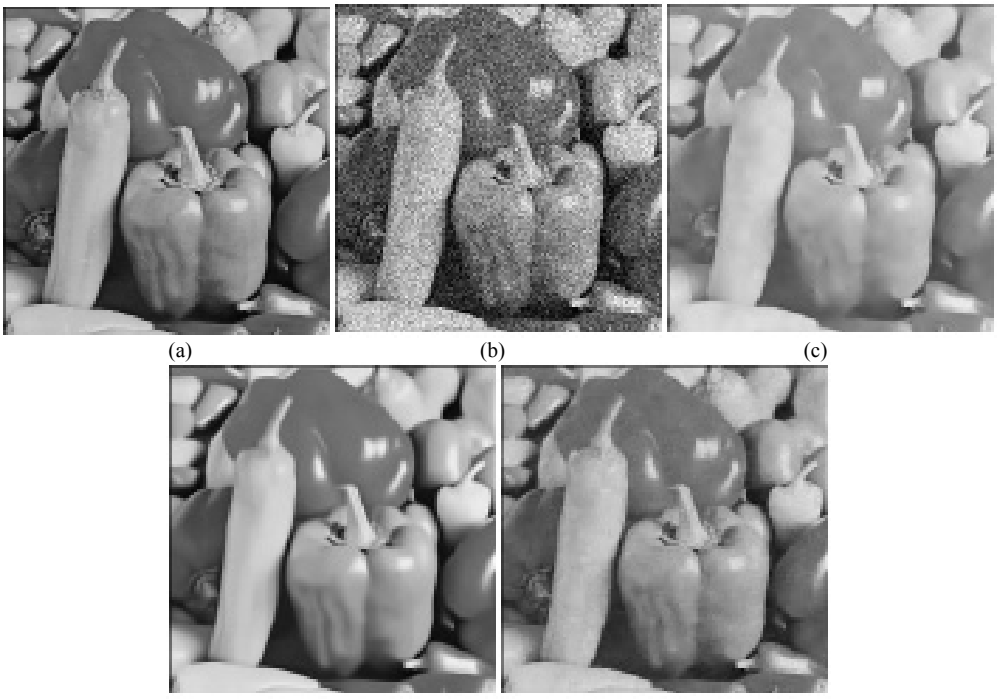

Figure 7. Denoising performance comparison for Peppers image at Gauss noise level θn = 35.
From the left to right, the original image, noising image, KSVD, BM3D, RSSC

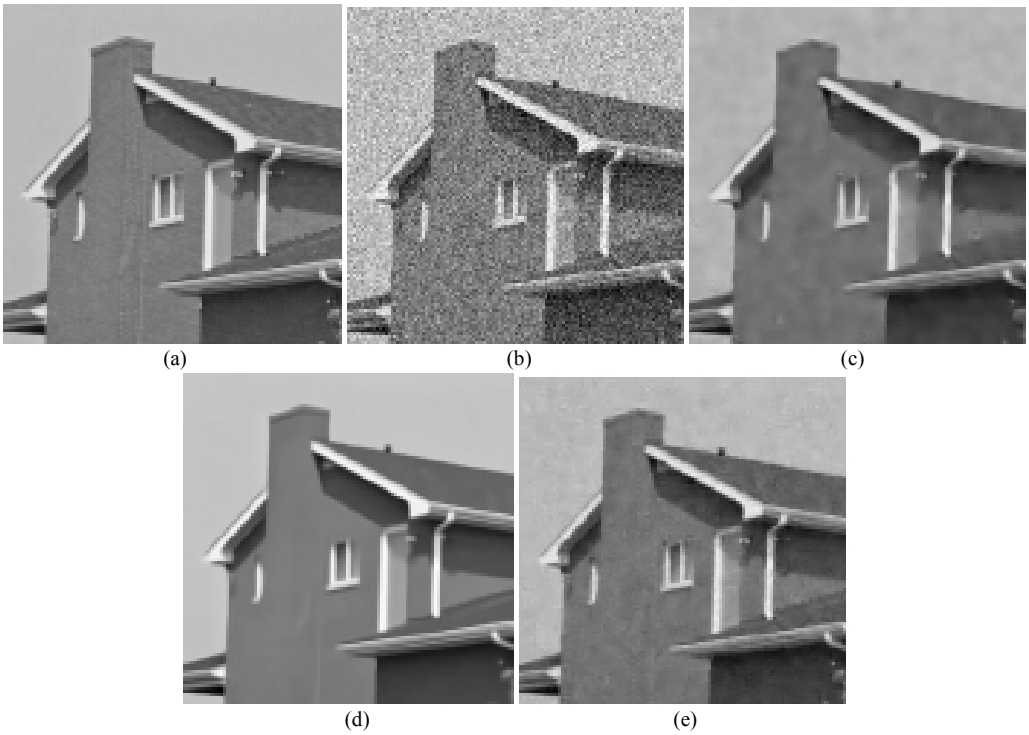

Figure 8. Denoising performance comparison for House image at Gauss noise level θn = 35.
From the left to right, the original image, noising image, KSVD, BM3D, RSSC

ACKNOWLEDGMENT

This work was supported by the Fundamental Research Funds for the Central Universities (Grant No. BLYX200905 and TD2013-4) and National Natural Science Foundation of China (Grant No. 30901164).

REFERENCES

[1] A. Buades, B. Coll, and J. Morel, "A review of image denoising algorithms, with a new one," *Multiscale Modeling and Simulation*, vol. 4, no. 2, pp. 490–530, 2005.
[2] K. Dabov, A. Foi, V. Katkovnik, and K. Egiazarian, "Image denoising by sparse 3-d transform-domain collaborative filtering," *IEEE Trans Image Processing,* vol. 16,no. 8, pp. 2080–2095, 2007.
[3] M. Elad and M. Aharon, "Image denoising via sparse and redundant representations over learned dictionaries," *IEEE Trans Image Processing,*, vol. 15, no. 12, pp.3736–3745, 2006.
[4] J. Mairal, M. Elad, and G. Sapiro, "Sparse representation for color image restoration," *IEEE Trans Image Processing,*, vol. 17, no. 1, pp. 53–69, 2008.
[5] J. Mairal, F. Bach, J. Ponce, G. Sapiro, and A. Zisserman, "Non-local sparse models for image restoration," in *Computer Vision*, IEEE 12th International Conference on. IEEE, 2009, pp. 2272–2279.
[6] W. Dong, X. Li, D. Zhang, and G. Shi, "Sparsity-based image denoising via dictionary learning and structural clustering," in *Computer Vision and Pattern Recognition(CVPR)*, 2011 IEEE Conference on, 2011, pp. 457–464.
[7] A. Jalali, P. Ravikumar, S. Sanghavi, and C. Ruan, "A dirty model for multi-task learning," *Advances in Neural Information Processing Systems*, vol. 23, pp. 964–972, 2010.
[8] S. Negahban and M. J. Wainwright, "Joint support recovery under high-dimensional scaling: Benefits and perils of l1,-regularization," *Advances in Neural Information Processing Systems*, vol. 21, pp. 1161–1168, 2008.
[9] P. Tseng, "On Accelerated Proximal Gradient Methods for Convex-Concave Optimization," unpublished.
[10] S. Ji and J. Ye, "An accelerated gradient method for trace norm minimization," in *International Conference on Machine Learning*. ACM, 2009.
[11] P. Gong, J. Ye, and C. Zhang, "Robust multi-task feature learning," in *Proceedings of the 18th ACM SIGKDD international conference on Knowledge discovery and data mining*, New York, NY, USA: ACM, pp. 895–903. 2012.
[12] G. Liu, J. Liu, Q. Wang, W. He, "The Translation Invariant Wavelet-based Contourlet Transform for Image Denoising," *Journal of Multimedia*, North America, 7, jun. 2012.
[13] H. Fan, Y. Wang, J. Li, "Image Denoising Algorithm Based on Dyadic Contourlet Transform," *Journal of Software*, North America, 6, jun. 2011.
[14] J. Hu, Y. Pu, J. Zhou, "A Novel Image Denoising Algorithm Based on Riemann-Liouville Definition," *Journal of Computers*, North America, 6, jul. 2011.

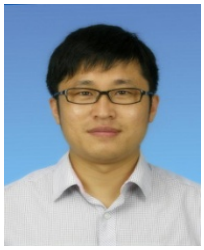

Lei Li was born in JiLin Province, China, in 1980. He studies in Technology Beijing Forestry University, and separately gained a bachelor's degree in 2005 and a master's degree in 2008. Now, he is a doctorate candidate in the same university. His research interests mainly include information security, image processing image compression.

Jiangming Kan received in PhD degree in forestry engineering from Beijing Forestry University, P.R.China in 2009. Currently, he is an associate professor in Beijing Forestry University. His research interests include computer vision and intelligent control.

Wenbin Li received M.S. and Ph.D. degrees in Shizuoka University and Ehime University, Japan, in 1987, and 1990, respectively. Starting 1992, he was a faculty with the School of Technology, Beijing Forestry University and was promoted to be a professor in 1996, Ph.D. supervisor. His current research interests include forest machinery automation and intelligent.

DDoS: Flood vs. Shrew

Zhijun Wu, Guang Li, Meng Yue, Hualong Zeng
Tianjin Key laboratory for Advanced Signal Processing, Civil Aviation University of China, Tianjin, 300300, China
Email: {zjwu, myue}@cauc.edu.cn

***Abstract*—Distributed Denial of Service (DDoS) attack is one of the greatest threats to connectivity, continuity, and availability of the Internet. In this paper, two typical types of DDoS attacks, high-rate (Flood) and low-rate (Shrew), are studied on their generation principles, mechanism utilizations, behaviors, signatures, and attack performances. Experiment results show that: (I) high-rate DDoS sends a large amount of traffic to destroy the victim but it is easy to be detected. (II) low-rate DDoS organizes a small quantity of traffic to degrade the service quality at the victim end and it is easy to escape from detection. Comparison of flood with shrew is helpful to detect and defend DDoS attacks efficiently.**

***Index Terms*—DDoS, High-Rate, Low-Rate, Flood, Shrew**

I. INTRODUCTION

Nowadays, more and more computers connect with each other to compose a huge and complex system throughout the Internet. The situation of system security is not improved greatly for a long time. One of the primary reasons is that there are massive and aggressive behaviors in network system. As a typical destructive behavior, Distributed Denial of Service (DDoS) appeared as early as the birth of Internet. From the viewpoint of economic loss, investigation report from Arbor shows that the DDoS attack is the secondary rank of threat to Internet (Botnet ranks the first) [1]. It is very difficult to defense against DoS attack, and the reason is that the flows generated by DoS attacks are natural and normal.

After more than ten years' experience, DDoS attack generates many forms and can be divided into different types. From the viewpoint of data rate, DDoS attack includes two categories: high-rate and low-rate.

The high-rate DDoS attack (Flood type DDoS, denoted as FDDoS) sends continuously large volume data packets to victims and consumes the victim's limited resources, such as network links or operating systems, to make the victim refusal to provide effective services for legitimate users. The high-rate DoS attack is very similar to flood to destroy a target in the attack form. Hence, high-rate DDoS attack is usually called Flood DDoS. The classical high-rate DoS attacks have SYN, ACK, TCP and UDP Flood [2], etc..

The low-rate DDoS attack (Shrew type DDoS, denoted as LDDoS) launches a sequence of cycle pulse with a certain period, width, and amplitude to victim and degrades the quality of service (QoS) at the end of victim without being sensed. Low-rate DDoS attack was firstly detected on Internet Abilene in 2001 and presented on SigComm conference in 2003 by Kuzmanovic[3]. Low-rate DDoS has a relatively low data rate to elude being detected. The behavior of low-rate DDoS attack likes a shrew can defeat an elephant. Hence, low-rate DDoS attack is called Shrew in early. Because the waveform of low-rate DDoS attack is a series square pulses, someone call low-rate DDoS attack as Pulse DoS (PDoS) attack. The purpose of low-rate DDoS attack is not to tear down the target, but to degrade the quality of service (QoS). So, low-rate DDoS attack has another name of Degrading QoS attack.

Low-rate DDoS attack is quite different from traditional flood-based attacks in behavior, attack effect and vulnerabilities mechanism exploitation. Low-rate DDoS attacks only send attack packets within a specific time interval with a relatively low rate, so that it can hide in normal network traffic. Hence, low-rate DDoS attack is characterized as intermittent attack[4].

Most available researches focus on the detection and defense against DDoS attacks, and little concern is paid on the attack performance (destructive). This paper focuses on the attack performance of high-rate and low-rate DDoS attacks for the purpose of understanding their degree of harm to victim. This paper makes three contributions. First, it describes a DDoS attack model that has been created for exploring the DDoS attack organization techniques. The model consists of four elements, attacker, handlers or masters, daemon agents or zombie hosts, and victim. Second, this paper develops a testbed that has been created for evaluating DDoS attack performance. The testbed consists of a software-defined real-time phase-coherent DDoS attack traffic simulator capable of carrying out sophisticated simulated attacks, a real-time software-defined attack sink that plays the role of victim,

Manuscript received September 17, 2013; revised October 27, 2013; accepted November 15, 2013.

Part of this paper was first appeared in 'Research on the Comparison of Flood DDoS and Low-rate DDoS', which is published on the proceedings of the 2nd International Multimedia Technology Conference (ICMT2011).

This work was supported by National Natural Science Foundation of China under grant 61170328 and U1333116, Natural Science Foundation of Tianjin under grant 12JCZDJC20900, and the Fundamental Research Funds for the Central Universities of CAUC under grant 31122013P007, 3122013D003, and 3122013D007.

Co-author: WU Zhijun Email: zjwu@cauc.edu.cn

doi:10.4304/jcp.9.6.1426-1435

and post-processing versions of both the attacker and victim. Third, it presents results of simulated attacks against throughput of network, including the comparing of flood-type DDoS with shrew-type DDoS.

II. DDoS Strategy

There are a variety of DoS attacks. The most common DoS attacks use a reasonable request to take up too many resources, so that legitimate users can not get a response from the service. The lack of effective authentication of the network makes it difficult to verify whether the packet is issued by the packet source IP address, resulting in a very easily to forge the source IP address and network attacks; and most of the access side of the bandwidth should be far less than the core side bandwidth, such as the core backbone of 40Gbps, while most of the access bandwidth is less than 1Gbps. The aggregate traffic from the core backbone link is easy to block the access link.

We make an assumption using knowledges of signal processing [5] to descript the process of DDoS attack. First, the *Attacker* generates attack signal, denoted by $Attack(t)$. After a certain delay time, it arrives at *Handler* and stimulates the *Handler* to produce a first-step response signal, denoted by $Handle(t)$. Second, the first-step response signal takes a certain delay time to arrive at the *Agent* and generate a second-step response signal $Agent(t)$. Third, the second-step response signal undergoes a delay time and finally reaches the Victim. Then we can summarize the process of this system to form a mathematical model as shown in Fig.1[6].

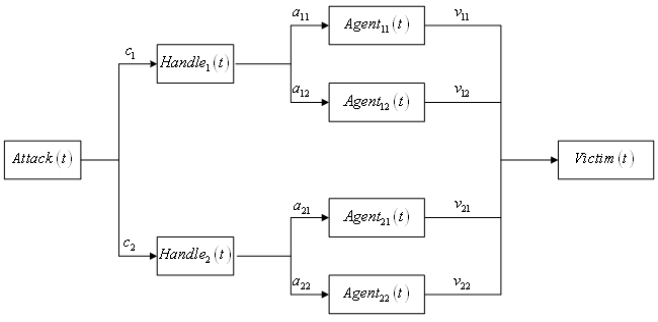

Figure 1. Attack system model.

In Fig.1, $Attack(t)$ represents the behavior of the *Attacker*, c_1, c_2 show the delay time between *Attacker* and *Handler*. $Handle(t)$ represents the system function of the *Handler*. $a_{11}, a_{12}, a_{21}, a_{22}$ show the delay time between *Handler* and *Agent*. $Agent(t)$ denotes the system function of the *Agent*. v_{11}, v_{12}, v_{21}, v_{22} show the delay time between Agent and Victim. $Victim(t)$ means the waveform at the end of *Victim*.

We can derive the following system transfer function from Fig.1. Equation (1) indicates the response function of the attack system model.

$$h(t)=\sum_{j=1}^{2}\sum_{i=1}^{2}\delta(t-c_i)*Console(t) \\ *\delta(t-a_{ij})*Agent(t)*\delta(t-v_{ij}) \tag{1}$$

Where, $\delta(t-c_i)$, $\delta(t-a_{ij})$, $\delta(t-v_{ij})$ represent the transfer function of the link delay.

Actually, since the number of the *Handler* and *Agent* is very large, we extend the i and j starting from 1 to infinite, as illustrated in equation (2).

$$h(t)=\sum_{j=1}^{}\sum_{i=1}^{}\delta(t-c_i)*Console(t) \\ *\delta(t-a_{ij})*Agent(t)*\delta(t-v_{ij}) \tag{2}$$

Where, $i=1,2\cdots, j=1,2\cdots$, i is a variable which represents the number of the Handlers, while j is a variable which represents the number of Agents attached to the every Handler.

Normally, the *Attacker* gives the orders at a moment, so we can deem it as an impulse signal, denoted by $Attack(t)=\delta(t)$. From receiving the top orders to making next orders, the *Handler* need a certain time for machine reaction, denoted as by τ_i, to a certain extent，we can also deem it as a delay system. Both τ_i and c_i are delay systems, we combine them, totally denoted by c_i, as long as modify the definition that c_i is the time slice between the *Attacker* giving the top orders and the *Handler* giving the second orders. Then, the behavior of the *Handler* can be represented as $Handle(t)=\delta(t)$. The $Agent(t)$ represents concrete waveforms, e.g. rectangle, hackle or trapezoid (speed change). This paper mainly analyses the power, attack duration, periodic or non-periodic of the waveforms as described in Fig.2. Finally, the signals aggregate in the Victim after v_{ij} delay.

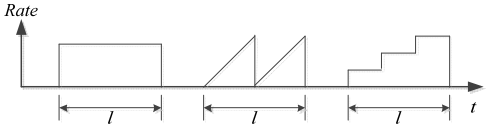

(a) Typical FDDoS waveforms

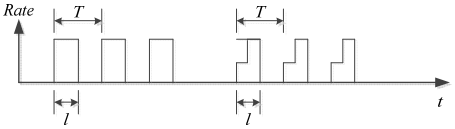

(b)Typical LDDoS waveforms

Figure 2. Typical FDDoS and LDDoS waveforms.

So, the whole system can be illustrated as equation (3).

$$
\begin{aligned}
&Victim(t) = \delta(t) * h(t) \\
&= \delta(t) * \sum_j \sum_i \delta(t - c_i) * Console(t) \\
&\qquad * \delta(t - a_{ij}) * Agent(t) * \delta(t - v_{ij}) \qquad (3) \\
&= \delta(t) * \sum_j \sum_i \delta(t - c_i) * \delta(t) * \\
&\qquad \delta(t - a_{ij}) * Agent(t) * \delta(t - v_{ij}) \\
&= \sum_j \sum_i Agent(t - c_i - a_{ij} - v_{ij})
\end{aligned}
$$

III. TRAFFIC ANALYSIS

Since DDoS attack is in a form of distribution, it must have issues of time synchronization and flow aggregation. If these two problems remain unsolved, the attack can't achieve its purpose efficiently. Derived from equation (3), different attack flow has different delay, so we modify equation (3). Let $k = i \times j$, $Agent(t - c_i - a_{ij} - v_{ij})$ is denoted by $Agent(t - t_k)$, $k = 0,1,2\cdots$, then equation (3) can be converted to equation (4).

$$Victim(t) = \sum_k Agent(t - t_k) \qquad (4)$$

A. Flood DDoS

Let $Agent(t)$ be rectangle waveform, the time synchronization and flow aggregation can be illustrated by a schematic diagram in Fig.3.

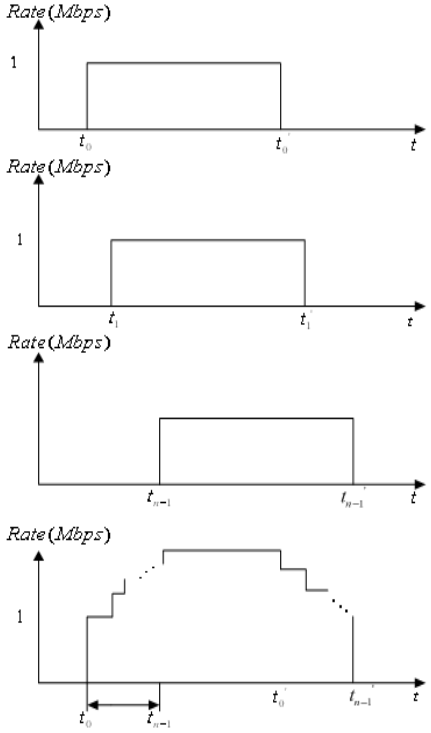

Figure 3. Time synchronization and flow aggregation in FDDoS

In Fig.3, $t_0, \cdots, t_{n-1}$ denote the every point of n attack flows arriving at victim; we define the metrics $\Delta\tau = t_{n-1} - t_0$ as the performance of synchronization. The smaller $\Delta\tau$, the better synchronization and the higher aggregation in the beginning of the attack is. So the attack effect is better. And it's a big challenge for the detection and defence system.

B. Shrew DDoS

A low-rate TCP attack is essentially a periodic burst which exploits the homogeneity of the minimum retransmission timeout (RTO) of TCP flows. Consider a router with capacity C (in bits/s). One form of attack is a periodic square wave as described in [7]. The period of the square wave is denoted by T , which is approximately one second so as to force other TCP flows to enter the retransmission state effectively. Within each period, the square wave has a magnitude of zero except for l units of time ($l \geq \max\{RTT_i\}$). During this time, the square wave has a magnitude of a normalized burst of R . The average bandwidth of this periodic square wave is Rl/T . Again, the objective of the low-rate attack is that for a short duration l , the attack packets will fill up the buffer of a victim router so that packets of any TCP flows are discarded by the router. The packet loss will force, if not all, most TCP flows to enter the retransmission state. And we note that it is considered to be a low-rate TCP attack, whose average rate has to be small. Otherwise, system administrators can easily detect an attack by its high traffic volume.

A general model of a low-rate TCP attack can be described by these parameters (R, l, T) . Fig.4 illustrates an example of low-rate TCP attack traffic [7].

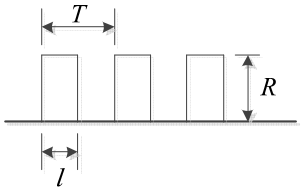

Figure 4. LDDoS attack traffic with parameters (R, l, T)

The time synchronization and flow aggregation of LDDoS attack is shown in Fig.5.

In Fig.5, $t_0, \cdots, t_{n-1}$ denote the every point of n attack flows arriving at victim. We define the metrics $\Delta\tau = t_{n-1} - t_0$ as the performance of synchronization. Normally, the duration l is about of the order of 100ms, and if $\Delta\tau$ is relatively big for l , it will extend the l and weaken the power of attack aggregation, unlike FDDoS only affecting the attack beginning, it will affect the LDDoS attack all the time .

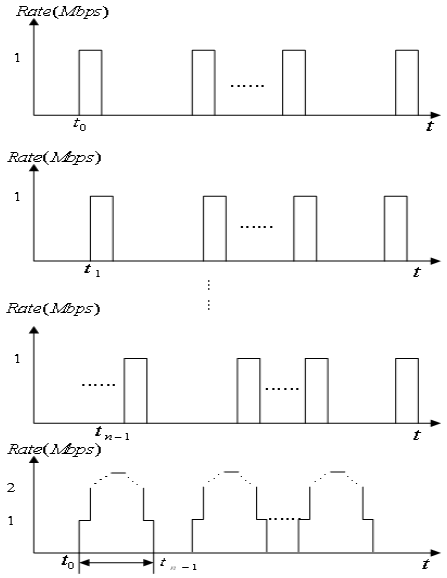

Figure 5. Time synchronization and flow aggregation in LDDoS

Equation (4) is also suitable for LDDoS. The mainly difference is the attack duration.

IV. Simulation and Experimentation

An experimental environment is built in NS-2 platform to test the performance of LDoS attack. The experimental network topology is a dumbbell as shown in Fig.6.

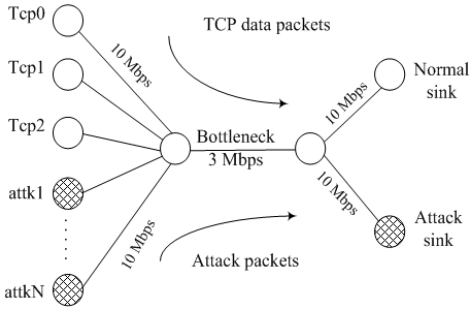

Figure 6. The simulation network topology

In Fig.6, the bandwidth for bottleneck is 3Mbps, which is the link of router R1 and R2, and the other links bandwidth is uniform 10Mbps, which are used for normal TCPs and attacks connecting with R1, and R2 connecting with Normal Sink and Attack Sink. There are three Normal TCP clients and N attacks in this topology. In experiments, the N is selected as 1, 3, 5, and 8 individually in order to sample a large number of flows for the purpose of traffic analysis. Routes use Drop Tail scheme. There are 3 legitimate TCP flows traversing through the bottleneck link, all of which are based on TCP New Reno, and their RTTs range from 20ms to 120ms. The minRTO of each flow is equal to 1s. All the simulation experiments were performed in the NS-2 2.34 environment. The queue size (QS) is 100 packets. All the attack flows begin at 20s and end at 110s[8][9].

A. Comparison of FDDoS and LDDoS as well as Normal TCP Traffic in Time-Frequency Domain

This part will reveal the differences between FDDoS and LDDoS in time domain and frequency domain. The traffic within the time slice between 20s and 30s is chosen to analyse. Vertical axis of time domain represents the number of arrivals within every ten milliseconds and the frequency domain is the FFT transform of the arriving packet number sequence in the time slice.

Without attack, normal traffic uses FTP traffic generator, setting package with size 1000B. As illustrated in Fig.7, the simulation results of normal traffic TCP flow.

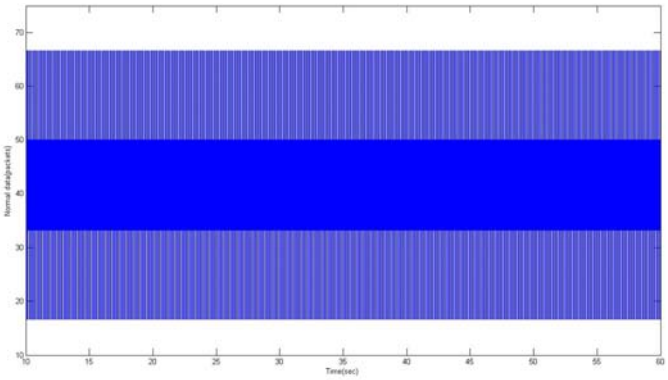

(a) Normal tcp in time domain

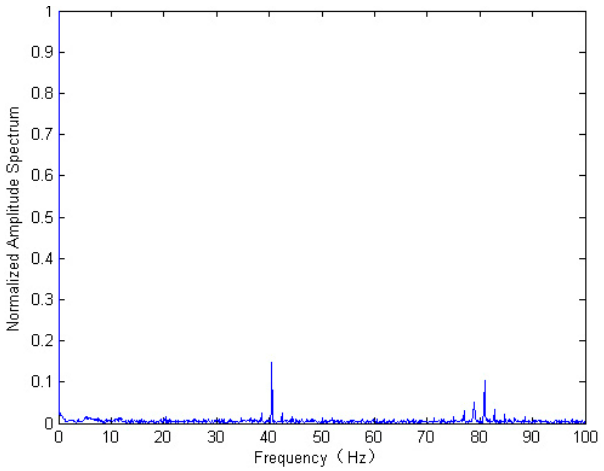

(b)Normal tcp in frequency domain

Figure 7. Normal tcp traffic

Note that the mean number of arrivals is about 1.25. We can approximately calculate the traffic by 1.25*1000*8/100=1Mbit/s. As there are 3 TCPs flow, so the total TCP flow is 3Mbit/s in general corresponding with the bottleneck bandwidth, which proves the rationality of the simulation. In the frequency domain, there is a rather big value at 0HZ. We all know that 0HZ presents the direct current, which is consistent with the mean arrivals fluctuating above and below 1.25. The rest of frequency components are very small and well-proportioned[10].

FDDoS adopts UDP FLOOD attack, using CBR (Constant Bit Rate) traffic generator. Setting rate as 3Mb/s and package size as 50B, the traffic of FDDoS is shown in

Fig.8. From the frequency domain, the obvious feature is that there is a very large value at 0 HZ and little value in the rest frequency, due to FDDoS keeping a high traffic for a rather long time.

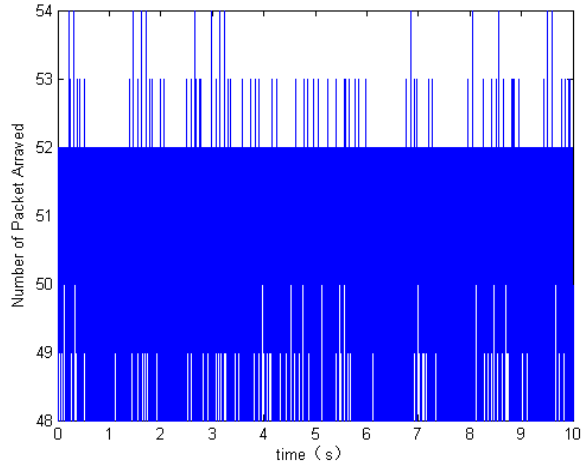

(a) FDDoS time domain

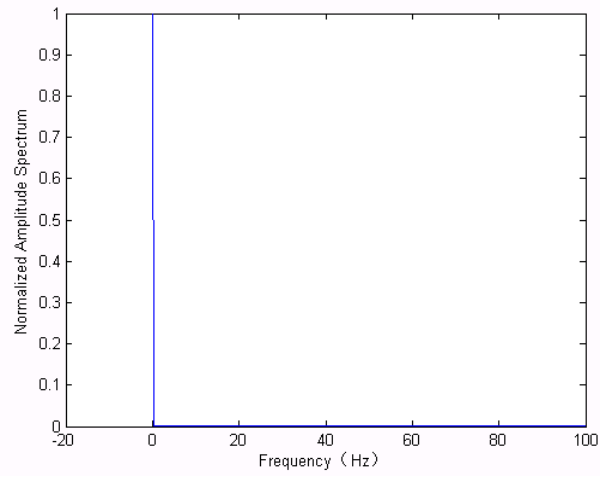

(b)FDDoS frequency domain

Figure 8. FDDoS traffic

LDDoS attack sends 8 UDP rectangle pulses, with period 1.1s, pulse length 0.1s and peak rate 0.375Mb/s, packet size 50B. Then we can get simulation results as depicted in Fig.9.

Note that in the time domain, after the short pulses, normal TCP traffic is very low or even zero, certifying the effect of the LDDoS. In the frequency domain, the most important character is that the signal energy mainly focus on [0,20]HZ, due to the low-rate period[10].

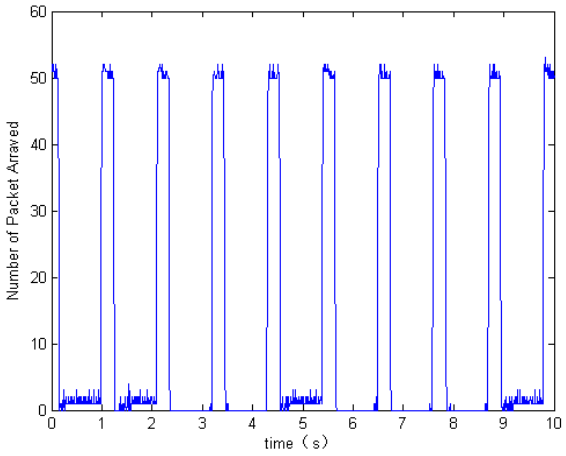

(a) LDDoS time domain

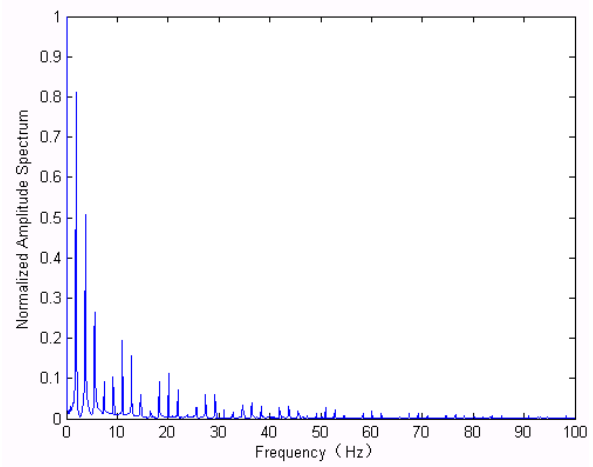

(b) LDDoS frequency domain

Figure 9. LDDoS traffic

TableI gives the energy distribution in each frequency slice.

TABLE I.
ENERGY DISTRIBUTION IN PERCENT

Item	Normal TCP	FDDoS	LDDoS
0	92.42	99.995	41.31
(0-20]	1.16	0.001	56.80
[20-40]	0.68	0.001	1.55
[40-60]	2.73	0.001	0.24
[60-80]	1.05	0.001	0.07
[80-100]	1.96	0.001	0.03

Energy distribution shows that 90% energy of normal traffic and FDDoS traffic focus on 0 HZ, which means they have a rather steady direct current without much fluctuation. As to LDDoS, the fluctuation is much higher, and only 41% energy focus on 0HZ, 97% energy is in the range of [0,20]HZ.

B. Network QoS Analysis

This paper evaluates the impact of FDDoS attacks and LDDoS attacks on two metrics: packet dropping rates and throughput.

All the following experiments are based on the NS-2 environment as mentioned above.

a) packet dropping rates

The experimental environment and parameters are the same as mentioned above except for the parameter of power.

The situation of dropping rate changes with different attack power is shown in TableII. With different power, the numbers of dropping packets are basically similar, but the numbers of total received packets are much distinct. So, we can draw a conclusion that stronger attack power does not indicate higher dropping rate.

TABLE II.
PACKET DROPPING PROBABILITY

Item		Total received numbers	Dropping packets numbers	Dropping rate
Normal TCP		3784	6	0.16%
FDDoS	3Mbps	578	149	25.78%
	2Mbps	592	150	25.34%
	1.5Mbps	925	159	17.19%
	1Mbps	2038	156	7.65%
SDDoS	3Mbps	1792	264	14.73%
	2Mbps	2517	298	11.84%
	1.5Mbps	2435	297	12.20%
	1Mbps	3326	206	6.20%

b) Throughput

Then, in order to analyse the throughput of FDDoS and LDDoS, the Normal, DoS and LDoS attacks are added into the experiments.

As we all know, single flow FDDoS is FDoS, and single flow LDDoS is LDoS. Here, we define the rate of DoS and LDoS as the bottle neck bandwidth, which is 3Mbps. Besides, we mainly study the beginning 10s of attack by statistics of the total cumulative TCP throughput.

In experiments, the LDoS attack is configured with a period of 100ms and pulse length of 200ms. The LDoS attack lasts for 25s, which starts at 25s and ends at 50s. All LDoS attack flows are sampled during 25s. Two types of LDDoS attacks, synchronous and asynchronous, are used to generate the attack traffic. The synchronized LDDoS attack is all LDoS attacks from different domain start attacking at the same time. The asynchronous LDDoS attack is organized to start all LDoS attacks one by one with a time separation of 20ms.The attack rate for single attack flow is different configured with the number of attacks, as shown in Table III.

TABLE III.
CONFIGURATION OF ATTACKS

Number of Attacks N	1	3	5	5	8
Attack rate of single flow R (mbps)	3	1	0.6	1	0.375

Multi-LDoS attacks with different attack rates are expressed in LDoS N-M. Here, N is the number of LDoS attacks, and M is the attack rate for single LDoS attack. The traffic are sampled in NS-2 platform and analyzed by using MATALB to draw the performance curve, in which the x-axis is time in second, range of 25s-50s, and the y-axis is the accumulative value of normal TCP flow though the bottleneck link under the LDoS attack during 25s-50s.

Fig.10 is the experiment result of normal TCP, single LDoS, and Multi-LDoS N-M attacking in the performance of network throughput. In order to analyze the performance, the interested part in Fig.10 is zoomed in Fig.11.

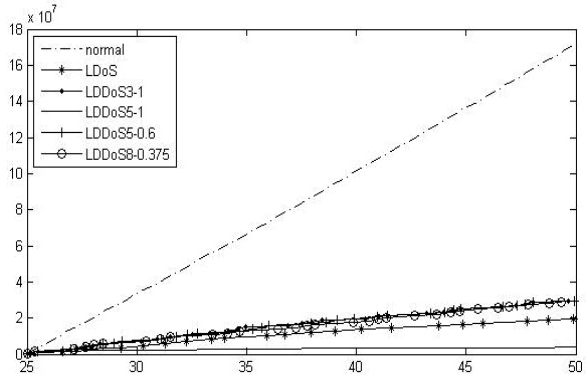

Figure 10. Thought of normal TCP under single LDoS, and Multi-LDoS N-M attacking

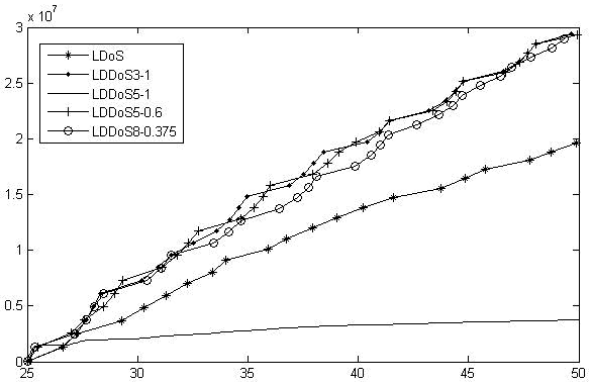

Figure 11. Part enlarge of LDoS N-M attack

Fig.10 and Fig.11 show that the throughput of normal TCP increases linearly, but it degrades badly when the LDoS attacks are added. (I) When the network suffers from single LDoS attack with a rate of 3Mbps, the network throughput has a drop of 89% approximately. (II) Increase the number of LDoS attacks from 1 to 3 and assign the bottleneck bandwidth of 3Mbps to 3 LDoS attacks averagely, hence, each of three LDoS attack has a rate of 1Mbps. This kind attack is denoted as LDoS 3-1. The attack effect of LDoS 3-1 is not better than the single LDoS attack. (III) Increase the number of LDoS attacks from 1 to 5 and assign 5Mbps to each LDoS attack, denoting this kind attack as LDoS 5-1. Because 5Mbps is bigger than the bottleneck bandwidth of 3Mbps, hence, the attack effect is much better than single LDoS attack. (IV) Increase the number of LDoS attacks from 1 to 5 and assign 3Mbps to each LDoS attack, denoting this kind attack as LDoS 5-0.6. The attack effect of LDoS 5-0.6 is almost the same with LDoS 3-1. (V) Increase the number of LDoS attacks from 1 to 8 and assign 3Mbps to each LDoS attack, denote this kind attack as LDoS 8-0.375. The attack effect of LDoS 5-0.375 is almost the same with LDoS 3-1 and LDoS 5-0.6.

Analysis shows that if a certain bandwidth is assigned to

a number of single LDoS attack averagely, this kind attack is called as LDoS N-M. LDoS N-M is compared with single LDoS attack in the attack effect, and result shows LDoS attack is better than LDoS N-M. But, LDoS N-M has relative lower rate than LDoS attack, hence, LDoS attack is easier to be detected than LDoS N-M, which is a covered attack can elude traditional detection. For example, the LDoS 5-1 attack is concealable even through it has a bigger attack rate of 5Mbps than the bottleneck bandwidth of 3Mbps.

The experiment result of normal TCP under single LDoS, and LDDoS attack is shown in Fig. 12.

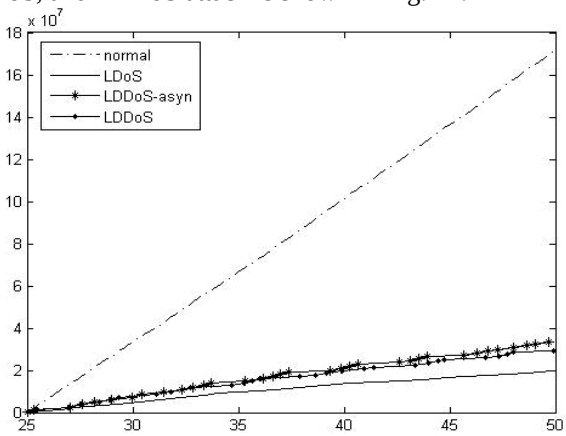

Figure 12. Thought of normal TCP under single LDoS, and LDDoS attacking

LDoS and LDDoS attacks have the same attack rate. Asynchronous LDDoS attack is composed of many LDoS attacks from different domains. These LDoS attacks start one by one with a 20ms time dely. From the viewpoint of attack performance, single LDoS attack is the best. It is obvious that the attack effect of asynchronous LDDoS attack is not good as that of single LDoS and LDDoS attack. Because the attack rate is shared by all LDoS attacks, which are the elements of asynchronous LDDoS attack.

The experiment result of FDoS attack is shown in Fig.13. DDoS N-M means N single DoS attack with rate of M. Fig.13 shows that the network throughput degrades to about zero, and the whole network refuses to offer all service. For the purpose of analysis, the interested part in Fig.13 is enlarged.

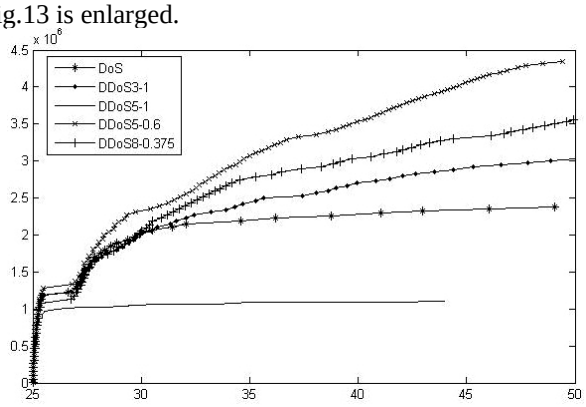

Figure 13. Thought of normal TCP under single DoS, and Multi-DoS N-M attacking

The differences between LDDoS and DDoS on attack performance are analyzed as follow. The attack effects are shown in Fig.14, in which the single LDoS/DoS and LDDoS/DDoS attacks are involved, and the dotted line donates the throughput of normal TCP traffic.

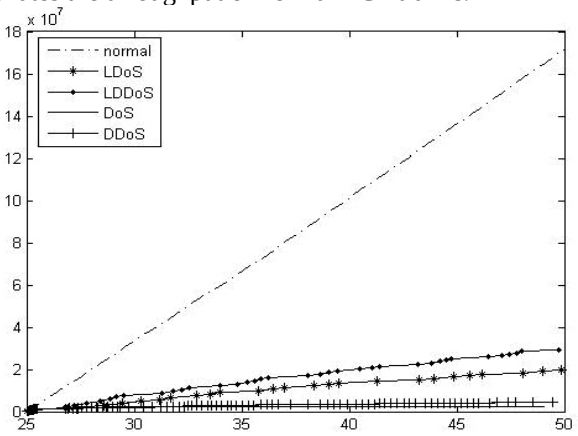

Figure 14. Attack effects

Fig.14 shows that the total throughput under attacks is lower than the normal throughput. In general, the attack effect of DoS is better than that of LDoS. The best is DDoS attack, and the worst is LDoS attack. This result is reasonable, because the intent of DDoS attacks is to tear down the victim machine while LDoS attack is to degrade the quality of service at the end of victim.

In order to get more clear observation on the attack effects, remove the throughput of normal traffic and enlarge the part of interest in Fig.14. Partial enlarged cavers are shown in Fig.15.

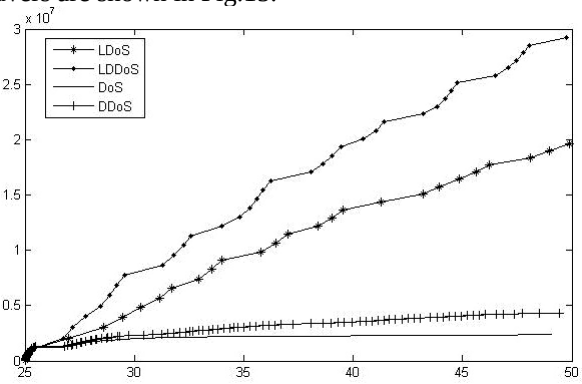

Figure 15. Enlarged attack effect

For understanding the attack effects better, the comparative analysis is performed by statistical on the cumulative value of the throughput within 25 seconds, as shown in Table IV.

C. Firewall Experiment

In this part, six typical software firewalls are used to test the detection and defence against DDoS in real environment, as shown in Table V.

The parameter configuration for LDDoS attack is 300ms-10M and 200ms-3.3M. It is different from FDDoS. Note that if LDDoS attacks of 300ms-10M cannot be intercepted by firewalls, then the LDDoS attacks of 200ms-3.3M scarcely have the probability to be stopped.

Additionally, the LDDoS attacks are configured to attack only on the servers, and it is able to achieve the effect of reduce service without being detected [9].

Table IV indicates that all the firewalls have the function of detecting FDDoS, but not all of them can detect LDDoS attacks.

TABLE IV.
CUMULATIVE VALUE OF THE THROUGHPUT WITHIN 25 SECONDS

Attacks	Cumulative value of the throughput
Without Attack	100%
LDoS	11.4%
LDoS3-1	17.0%
LDoS5-1	2.0%
LDoS5-0.6	17.0%
LDoS8-0.375	17.2%
DoS	1.2%
DoS3-1	1.8%
DoS5-1	0.6%
DoS5-0.6	2.5%
DoS8-0.375	2.1%

D. Web Service Experiments

Firstly, Web service test is performed. The test-bed topology is shown in Fig.16. The Victim is a Web server; Routers are CISCO-XM 2621. The bottleneck bandwidth we set is 10Mbit/s (about 1.25MB/s)[11].

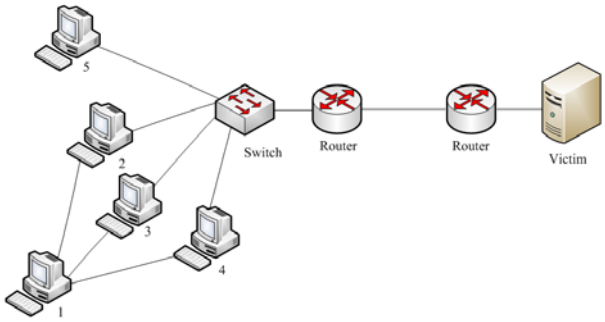

Figure 16. Test-bed network topology

Loadrunner is software that can be used to simulate Internet traffic, for example, http traffic.

LDDoS Attack is a UDP LDDoS attack tool embedded in zombies. LDDoS Control is a control tool which controls the LDDoS Attack to attack the victim with certain parameters.

TABLE V.
TEST OF FIREWALL

Type	Name	User	Default UDP Traffic Threshold (Packets Number/s)	Attack Parameter			Detecting	
				L (ms)	R (Mbps)	T (s)	Yes	No
General Firewall	KASPERSKY	PC	500	200	3.3	1.1	Yes	No
	SkyNet	PC	None	300	10	1.1	Yes	No
	Zone ALARM	PC	None	300	10	1.1	Yes	No
Professional FDDoS Firewall	Bing Dun	Server	2000	200	3.3	1.1	Yes	No
	Tian Ao	Server	10000	300	10	1.1	Yes	No
	Ao Dun	Server	8000	300	10	1.1	Yes	No

Set the parameter of LDDoS Attack in each zombie as follow[10][11][12]:

(I) pulse period T=1.1s.

(II) length of burst L=200ms.

(III) pulse peak rate R=40Mb/s.

The setup for DDoS attack are:

(I) DDoS Attack is a SYN-FLOOD attack tool embedded in zombies.

(II) DDoS Control is a control tool that controls the DDoS Attack to attack the victim.

The parameter of SYN-FLOOD doesn't need to set, because it will try its most best to send a large number of packets.

Run the Loadrunner tool to simulate 10 users visiting the web site "www.cauc.edu.cn". The size of the web page is 60KB.

The configuration of test environment is shown in Table VI.

TABLE VI.
TEST-BED HOST CONFIGURATION

Number of host	IP Address	Role	Operating System	Software
1	10.0.20.214	controller	Fedora core 4	LDDoSControl /DDoSControl
2	10.0.20.215	zombie	RedHat 9.0	LDDoSAttack /DDoSAttack
3	10.0.20.216	zombie	RedHat 9.0	LDDoSAttack /DDoSAttack
4	10.0.20.217	zombie	RedHat 9.0	LDDoSAttack /DDoSAttack
5	10.0.20.218	normal host	Windows XP	Loadrunner
Victim	10.1.30.223	target host	Fedora core 4	Apache

As shown in Fig 17, 00:00- 00:00, there is only legitimate http traffic. At 01:00, zombies start attacking, and at 01:30 (about 30min later), attacks stop. During 00:00 to 01:00, the response time is about 0.135s. While during 01:00 to 01:30, response time changes from 1.0s to

8.8s. At 01:30, attacks end, response time gradually recovers to 0.135.

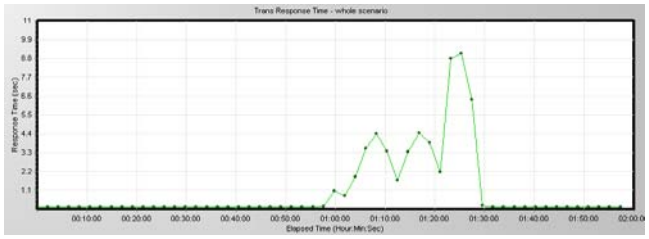

Figure 17. Record of Transaction Response Time under LDDoS

Test data shows that LDDoS attacks lower the quality of service. It is verified that LDDoS attacks are harmful for legitimate Internet applications.

In Fig 18, 00:00- 01:00, there is only legitimate http traffic. At 01:00, zombies start attacking, and at 01:30, attacks stop. During 00:00 to 01:00, the response time is about 0.135s. At 01:00-01:30, there is no dot between this time slice. The response time is none, that is to say, the normal visiting are totally refused. At 01:30, attacks end, and response time gradually recovers to about 0.135s.

By comparing LDDoS with DDoS, result shows that DDoS attack has fatal harm.

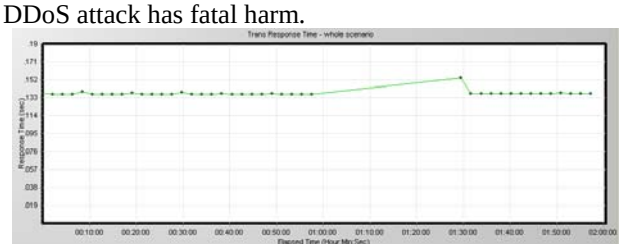

Figure 18. Record of Transaction Response Time under DDoS

E. FTP Service Experiments

The test-bed network topology is shown in Fig.16, which is used to test FTP throughput, and here the victim provides FTP service. At the beginning, host 5 downloads a file from FTP server, and after the normal FTP traffic is steady, we start attacking with T=1.1s, L=200ms, R=40Mbps.

As shown in Fig.19, before attack, the **Normal** in Fig.19(a) represents the client's normal download traffic recorded in host 5, and the Normal in the Fig.19(b) is the server's upload traffic recorded in FTP server, they are approximately equal. The Hybrid represents the combination of the upload and downloads in the client or server, and the **Abnormal** is the attack traffic.

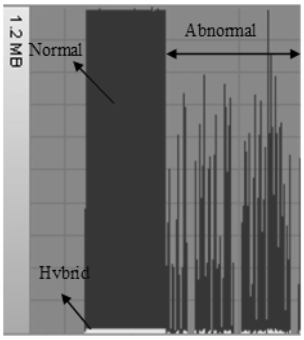

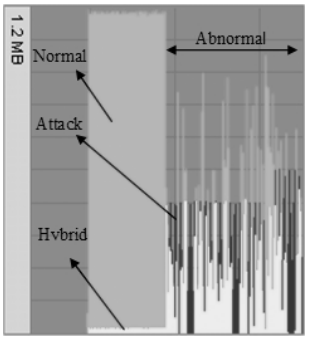

(a) Download (b)Upload

Figure 19. Traffic with LDDoS attacks

During LDDoS attacks, download traffic and upload traffic are lower than normal state and fluctuate strongly. In Fig.19(b), the **Attack** represents the attack traffic from zombies. We can see that the rate of LDDoS attacks is even lower than the attacked FTP traffic.

In Fig.20, the **Hybrid** also represents the combination of the upload and download in the client or server.

In Fig. 20(a), during DDoS attacks, download traffic in normal host 5 is none; the ftp service is totally down, absolutely denial of service. In Fig. 20(b), there is no upload traffic during DDoS, all of the traffic remained in the server is DDoS attack traffic from zombies.

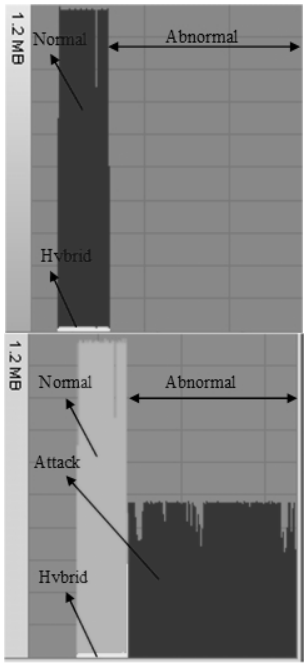

(a) Download (b)Upload

Figure 20. Traffic with DDoS attacks

V. CONCLUSION

The comparison of FDDoS with LDDoS shows that they are different in some aspects, such as volume of traffic and behavior. LDDoS attack is stealthy with low enough flows, likes a shrew can beat an elephant. While FDDoS is manic with large volume traffic, likes a behemoth swallowing the victims.

FDDoS attacks do not need time to synchronize and aggregate flow to send a large amount of packets to targets during a certain time independently. There is no coordinate mechanism in FDDoS attacks. What the controller of FDDoS attacks does is just to set up the start and end time, then send the start instruction. Of course, before the attack, the controller should make a decision on how many zombies are used in this attack. The more zombies, the bigger attack traffic will be sent, and the better attack effect will be observed.

Ideally, LDDoS attacks need time synchronization and flow aggregation to send average low rate of packets in a periodic pulses, forming big volume of flows at the end of target. It is very difficult to generate synchronous and aggregated LDDoS attacks in real wide network. Because it needs to be coordinated to reach the state of time synchronization and flow aggregation. Additionally, network RTT and RTO are required to be estimated in synchronous and aggregated LDDoS attacks. If multiple LDoS attacks from different domains are simply put together according to their arrival time at the end of target, they are neither synchronous nor aggregated. The attack effect of multiple LDoS attacks is appreciably improved than a single LDoS attack even the number of attacks increases largely. But, if multiple LDoS attacks from different domain are coordinated carefully to form a big volume of attack flow, the attack effect will be improved obviously every time when a new LDoS attack is added in the attack.

In the future, the researches will focus on the control mechanism for Flood DDoS attacks and the time synchronization and flow aggregation for multiple LDoS attacks.

REFERENCES

[1] Steve Ragan, “Arbor Networks targeted after DDoS report (Update),” Dec 16 2010, 18:47.. http://www.thetechherald.com/article.php/201050/6571/Arbor-Networks-targeted-after-DDoS-report-Update

[2] Khanna, S., Venkatesh, S.S., Fatemieh, O., Khan, F., and Gunter, C.A., "Adaptive Selective Verification: An Efficient Adaptive Countermeasure to Thwart DoS Attacks", IEEE/ACM Transactions on Networking, 2012, 20(3):715-728.

[3] Kuzmanovic. A, Knightly. E. W, “Low-rate TCP-targeted denial of service attacks,” Proceedings of ACM SIGCOMM 2003, Karlsruhe, Germany, 2003: 75- 86.

[4] Aleksandar. Kuzmanovic, Edward W. Knightly, “Low-Rate TCP-Targeted Denial of Service Attacks and Counter Strategies,” IEEE/ACM Transactions on Networking. 2006,14(4): 683-696.

[5] M. Salagean and I. Firoiu, “Anomaly detection of network traffic based on Analytical Discrete Wavelet Transform,” 2010 8th International Conference on Communications (InfoComm), 2010: 49-52.

[6] Zhang Yong Zheng, Xiao Jun, Yun Xiao Chun, "DDoS Attacks Detection and Control Mechanisms". Journal of Software, 2012, 23(8): 2058-2072.

[7] Macia-Fernandez. G, Diaz-Verdejo. J.E, Garcia-Teodoro. P, “Mathematical Model for Low-Rate DoS Attacks Against Application Servers,” IEEE Transactions on Information Forensics and Security, 2009, 4(3): 519 -529.

[8] Mohammed Alenezi, and Martin J Reed, “Traceback of DoS over Autonomous Systems”, International Journal of Network Security & Its Applications (IJNSA), 2013, 5(2):132-142.

[9] Mitko Bogdanoski,Tomislav Shuminoski, and Aleksandar Risteski, "Analysis of the SYN Flood DoS Attack", I. J. Computer Network and Information Security, 2013, 8:1-11.

[10] Chen. Y, Hwang. K, “Collaborative detection and filtering of shrew DDoS attacks using spectral analysis,” Journal of Parallel and Distributed Computing, 2006, 66(9):1137-1151.

[11] Wu Zhijun, Yue Meng, “Research on the performance of low-rate attack,” Journal of Communications, 2008, 29(6): 87-93.

[12] Zhi-jun Wu, Minghua Wang, Haitao Zhang, Xingchen Liu, “Correlation-based Detection of LDoS Attack”, Journal of Software, 2012, 7 (10): 2341-2348.

ZhijunWu born in 1965, China. He received BS degree and Master Degree in Signal Processing from Xidan University, Xian city, China, in 1998 and 1996 individually. He received PhD degree in Cryptography and Network Security from Beijing University of Posts & Telecommunications. His main research field is Network Security, with special focus on denial of service (DoS) attacks, intrusion detection, and defense.

He is professor in College of Electronics & Information Engineering, Civil Aviation University of China (CAUC), Tianjin, China.

Guang Li was born in TianJin, 1988. He is a master candidate at Communication and Information System, Civil Aviation University of China (CAUC). His research interests include network and information security.

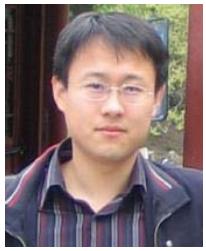

Meng Yue was born in Hebei province, China at July, 1984. He received the M.A., degree in communication and information system from Civil Aviation University of China (CAUC) in 2009.

He is currently with College of Electronics & Information Engineering Civil Aviation University of China (CAUC), Tianjin, China. In 2008, he studied in China Education & Research Network Engineering Center, Tsinghua University, China. His research was initially focused on information security and cloud computing, with special focus on denial of service attacks, intrusion detection, and defense.

Hualong Zheng was born in Henan province, China, 1985. He received master degree in Communication and Information System from Civil Aviation University of China (CAUC) in 2011. His research interests include network and information security

A Dynamic Load-balancing Scheme for XPath Queries Parallelization in Shared Memory Multi-core Systems

Xiaocheng Huang
Department of Computer Science, Nankai University, Tianjin 300071, China
Email: huangxiaocheng@dbis.nankai.edu.cn

1Xujie Si, 2Xiaojie Yuan and 2Chao Wang+
1, Department of Electrical Engineering and Computer Science, Vanderbilt University, USA
Email: sixujie@gmail.com
2, Department of Computer Science, Nankai University, Tianjin 300071, China
Email: {yuanxiaojie, wangchao}@dbis.nankai.edu.cn

***Abstract*—Due to the rapid popularity of multi-core processors systems, the parallelization of XPath queries in shared memory multi-core systems has been studied gradually. Existing work developed some parallelization methods based on cost estimation and static mapping, which could be seen as a logical optimization of parallel query plan. However, static mapping may result in load imbalance that hurts the overall performance, especially when nodes in XML are not evenly distributed. In this paper, we solve the problem from another view using parallelizing techniques. We use dynamic mapping to improve XPath query performance, which can achieve better load balance no matter what XML document is queried. Compared with static mapping, dynamic mapping is a more general method. We first design a parallel XPath query algebra called PXQA (ParallelXPath Query Algebra) to explain the parallel query plan. And second, using PXQA we extract the task-dependence graph to define which operations can be executed in parallel and help analyze the overheads of dynamic mapping. At last, we discuss how to do the data partition based on dynamic mapping in accordance with the runtime situations adaptively. Experimental results show that the adaptive runtime XPath queries parallelization achieves a good performance in shared memory multi-core systems.**

***Index Terms*—XPath, Query Parallelization, Shared Memory**

I. INTRODUCTION

XML's emergence as the *de facto* standard for encoding tree-oriented, semi-structured data has brought significant interoperability and standardization benefits. Meanwhile, XPath [15] as an expression language based on XML attracts many researchers. When XML document becomes large and recursive, time cost in XPath querying becomes unbearable. How to accelerate the query speed of XPath becomes a hot topic. Due to the rapid popularity of multi-core processors systems, it is being studied to execute XPath in parallel.

One viable option is to modify existing query algorithms from single-core to multi-cores. However, these methods cannot be applied widely. As a solution, [2] proposes data and query partition which are independent on certain query algorithms. Despite these, there still are some problems to be solved. Existing work focus on optimizing the plan logically, such as partition point chosen. In this paper, we'll optimize the plan physically using the parallelizing techniques.

In this study, we develop a dynamic load-balancing scheme to accomplish better performance. Towards the goal, we first design a parallel query algebra called PXQA. PXQA is based on set theory and takes great advantage of the properties of XPath. It defines a data model, four operators and three rules to generate parallel plan. What's more, according to PXQA, task-dependency graph is extracted. Task-dependency graph plays an important role in task mapping when designing parallel algorithms. Using task-dependency graph, we analyze the overheads of parallelization and make it clear why dynamic mapping leads to load balance. At last, we build dense index among tasks in work pool, which aims to reduce the task mapping overhead caused by exclusive lock and increase the concurrency. Experimental results reveal that, compared with static mapping, dynamic mapping decreases query time greatly when load distribution is uneven in the XML tree and does not hurt performance when load distribution is balanced.

The core contributions of this paper are summarized as follows:

- We design a parallel algebra called PXQA to address the parallel plan. Further, task-dependency graph can be extracted for dynamic mapping.
- Compared with static mapping, we propose a general mapping method adapted to any XML document or any XPath query. We analyze the disadvantages of static

+Corresponding author: Chao Wang

doi:10.4304/jcp.9.6.1436-1445

mapping and show how dynamic mapping leads to load balance.

• We do our experiments in a realistic dataset XStu. Experimental results demonstrate that the dynamic load-balancing scheme works well and has a good scalability.

II. Related Work

There are many studies in how to optimize the performance of a single XPath by improving its traversal pattern or structural join method, such as [12] [16] [17] [19]. However recently, some researchers explore other methods using parallelization, since multi-core systems have become commodity hardwares. It is possible to execute XPath in parallel.

Due to the wide-spread availability of commodity multi-core processors, XML parsing and XPath queries in shared memory multi-core system are being studied these years. Ref. [6] investigates the seemingly quixotic idea of parsing XML in parallel on a shared memory multi-core computer. It preparses XML document to determine the logical tree structure of the document and then use the logical tree to divide the document into chunks. As an improvement, [7] presents a stealing-based parallel XML processing model, using which the load balance among the threads is dynamically controlled. Compared with [7], [11] gives a static load-balancing scheme for parallel XML parsing on multi-core CPUs. It uses a static, global approach to reduce synchronization and load-balancing overhead to improve performance.

Besides XML parsing, XML query in shared-memory multi-core system has been studied meanwhile. There are many studies about parallelization of XML query algorithm. These studies aim to change traditional single-thread XPath query evaluation algorithms to multi-threads. Ref. [5] is based on structural join algorithm. It partitions elements into buckets and then evaluates XPath step (Parent-Child or Ancestor-Descendant relationship) of every buckets. Ref. [3] is based on twig queries. It proposes an efficient parallel PathStack algorithm for processing XML twig queries. In addition, [8] [9][10] aim to execute holistic twig joins in parallel. Ref. [8] proposes a grid metadata model for XML that gives a conceptual view to partition XML data, specifically for holistic twig joins processing. Ref. [9] [10] try to improve workload balance on both static data distribution and dynamic data distribution.

Meanwhile, Parallelization of XPath queries using multi-core processors has been studied. It's quite different from the previous research. The evaluations are based on the scenario where an XPath processor uses multiple threads to concurrently navigate and execute individual XPath queries on a shared XML document. Ref. [2] raises the problem and lists some parallelization issues, such as storage model, cost estimation and load balance. The most important contribution is that it proposes three strategies for parallelizing individual XPath queries: Data partitioning, Query partitioning, and Hybrid (query and data) partitioning. Ref. [1] proposes a parallelization algorithm that uses the statistics together with several heuristics to find and select parallelization points in an XPath query. It describes the statistics-based model used to estimate the running time of different parallel execution strategies. It also shows that query partitioning is involved in semantic of XPath and hardly get better performance than data partitioning.

III. Parallel XPath Query Algebra (PXQA)

In order to explain the parallelization of XPath query, we design a parallel XPath Query Algebra, PXQA. In this paper, PXQA mainly focuses on the presentation of XPath query process. What's more important, the task-dependency graph extracted from PXQA plays an essential role in parallelization analysis. Due to space constraint, more content about PXQA optimization is not included and will occur in future work.

A. Data Model, Operators and Plan Generating

An XML document on which XPath operates is a tree (Figure 3). An abstract data set called the XML Information Set (Infoset) is recommended by W3C in [14]. An XML document's information set consists of a number of information items. Information items include the document information item, element information item, attribute information item, etc. PXQA is based on XML Infoset.

There are three operators in PXQA, i.e.

ψ: query processing. $\psi_{xpath}(infoset)$ returns the query result of $xpath$ on the context nodes $infoset$. The query result is an infoset too.

σ: data partition. σ means choosing part of the infoset.

op: the common operations on sets, such as union $(\cup)$, intersection $(\cap)$.

Note that, during the partition, the document order of infoset may be messed up. So we need to reform document order of results. In the following statement, we will use infoset to represent XML document and intermediate results. Using $\psi, \sigma, op, infoset$, all parallel query plans generated are based on the following three rules where the rule 1 focuses on the infoset and the rule 2 and 3 focus on the XPath.

1. If $infoset = infoset1\ op\ infoset2$ then

$$\psi_{xpath}(infoset) = \psi_{xpath}(infoset1)\ op\ \psi_{xpath}(infoset2)$$

2. An XPath query can be rewritten as

$$\psi_{xpath}(infoset) = \psi_{xpath1}\left(\psi_{xpath2}(infoset)\right)$$

The result of $\psi_{xpath2}(infoset)$ is an infoset, which is the context nodes of $xpath1$.

3. From [15], productions of OrExpr and AndExpr of XPath are:

$$OrExpr ::= AndExpr("or" AndExpr)^*$$

AndExpr ::=

ComparisonExpr("*and* "*ComparisonExpr*)*

The instances of *OrExpr* and *AndExpr* can be rewritten as

$$\psi_{xpath}(infoset) = \psi_{xpath1}(infoset)\ op\ \psi_{xpath2}(infoset)$$

To illustrate how to generate a plan, we list two examples using data partition and (or) query partition.

Data partition proposed by [2] means executing the same (sub)query on different sections of the same XML document, for which we use σ. An instance using data partition is:

Example 1: If we want to execute the XPath */FILE/EMPTY//NP* on a XML document, for example, *treebank.xml* , using two processes while partitioning the data on EMPTY half, the query plan is

$$\begin{aligned}&\psi_{/FILE/EMPTY//NP}(treebank.xml)\\ &=\psi_{//NP}(\psi_{/FILE/EMPTY}(treebank.xml))\ //\ rule2\\ &=\psi_{//NP}(\sigma_{part}(\psi_{/FILE/EMPTY}(treebank.xml)))\bigcup\\ &\quad\sigma_{part}(\psi_{/FILE/EMPTY}(treebank.xml)))\ //\ data\ partition\\ &=\psi_{//NP}(\sigma_{part}(\psi_{/FILE/EMPTY}(treebank.xml)))\bigcup\\ &\quad\psi_{//NP}(\sigma_{part}(\psi_{/FILE/EMPTY}(treebank.xml)))\ //\ rule1\end{aligned}$$

Proposed by [1], *EMPTY* here is called **Partition Point**.

Another instance, using query partition, which is also proposed in [2], meaning executing different (sub)queries on the same XML document, is:

Example 2: If we want to execute XPath */FILE/EMPTY* [*count*(.//*NP*)>1 *and count*(.//*VP*)>1] while partitioning the query into two subqueries */FILE/EMPTY*[*count*(.//*NP*)>1]and */FILE/EMPTY*[*count*(.//*VP*)>1], the query plan is:

$$\begin{aligned}&\psi_{/FILE/EMPTY[count(.//NP)>1\ and\ count(.//VP)>1]}(treebank.xml)\\ &=\psi_{/FILE/EMPTY[count(.//NP)>1]}(treebank.xml)\cap\\ &\quad\psi_{/FILE/EMPTY[count(.//VP)>1]}(treebank.xml)\ //\ rule3\end{aligned}$$

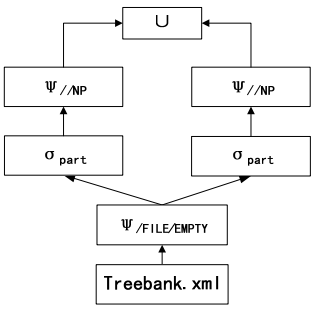

Figure 1 Task-dependency Graph of Example 1

Any plan should be deduced in terms of the three operators and the three rules above. As a counterexample, we do not provide extra operators. If we want to partition the query */FILE/EMPTY//NP* into two single queries: *query*1: */FILE/EMPTY* and *query*2: *//NP*, and then choose the nodes from query2 who are descendent of nodes in query1, this kind of plan is not accepted by PXQA, because PXQA does not provide the operator of choosing descendent nodes.

B. Plan Choosing

Given a XPath query, there are many candidate plans. e.g. Given a long XPath */FILE/EMPTY/S// VP*[*count*(.//*NP*)>1], the candidate plans could be:

candidate plan1:

$$\begin{aligned}&\psi_{/FILE/EMPTY/S//VP[count(.//NP)>1]}(treebank.xml)\\ &=\psi_{//VP[count(.//NP)>1]}(\sigma_{part}(\psi_{/FILE/EMPTY/S}(treebank.xml)))\\ &\bigcup\psi_{//VP[count(.//NP)>1]}(\sigma_{part}(\psi_{/FILE/EMPTY/S}(treebank.xml)))\end{aligned}$$

candidate plan2:

$$\begin{aligned}&\psi_{/FILE/EMPTY/S//VP[count(.//NP)>1]}(treebank.xml)\\ &=\psi_{/S//VP[count(.//NP)>1]}(\sigma_{part}(\psi_{/FILE/EMPTY}(treebank.xml)))\\ &\bigcup\psi_{/S//VP[count(.//NP)>1]}(\sigma_{part}(\psi_{/FILE/EMPTY}(treebank.xml)))\end{aligned}$$

Note that, the main difference of the two plans is the different partition points. Diverse query plans lead to diverse performances. It has been studied to decide the best partition point in [1]. [1] proposed a cost-estimation model based on query specifics and data statistics. We will apply the algorithm of [1] to optimize the plan. Nevertheless, given the best partition point, the query plan cannot be optimized logically any more. So we optimize the query plan from physical perspective by executing it in parallel.

IV. Parallel Execution of Plan

A. Task-dependency Graph Extraction

Given a plan, first we extract its task-dependency graph. A task-dependency graph is a directed acyclic graph in which nodes represent tasks and directed edges indicate the dependencies amongst tasks. A task-dependency graph determines which tasks can run in parallel and which must be executed serially, i.e. to distinguish independent and dependent tasks. This extraction phase is simple. Task-dependency graphs of ***Example*1** and ***Example*2** can be quickly extracted as Figure 1 and Figure 2. The data stream flowing across the operators is infoset.

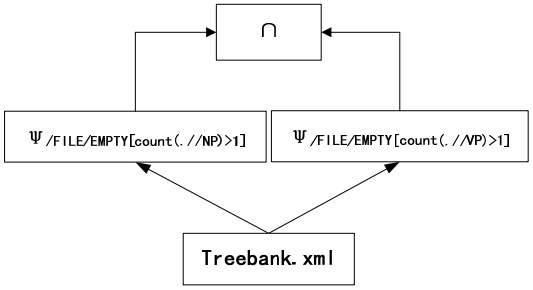

Figure 2 Task-dependency Graph of Example 2

We can see from Figure 1 that $\psi_{//NP}$ depends on $\psi_{/FILE/EMPTY}$ and different $\psi_{//NP}$ are independent of

each other. It's similar from Figure 2 that $\psi_{/FILE/EMPTY[count(.//NP)>1]}$ is independent of $\psi_{/FILE/EMPTY[count(.//VP)]>1}$ and $\cap$ depends on both $\psi_{/FILE/EMPTY[count(.//NP)>1]}$ and $\psi_{/FILE/EMPTY[count(.//VP)]>1}$ This kind of dependency and independency is helpful for the analysis of load-balancing design below. The experiments in [2] show that query partition is harder to get good performance than data partition. So in this paper we focus on data partition.

B. Overhead Analysis of Parallelization

Formerly, [1] constructs a cost model to evaluate the expense considering the data distribution or the complexity of XPath query. The model recommends the partition method (data or query or hybrid partition) and partition point. Then using static mapping, distributes tasks evenly among processes, which may subsequently cause load imbalance. It is a bottleneck to obtain the optimal performance under the given best partition point. So in this paper, we try to accomplish load balance to accelerate XPath query.

To achieve the shortest execution time, the overheads of executing the tasks in parallel must be minimized. For a given task decomposition, there are two key sources of overhead. One is inter-process interaction. The other is processes idle. Processes idle is caused by a variety of reasons. Considering executing XPath query in share-memory system, there are some problems to take into account. As is known, in the shared-memory system, for consistency, thread interactions are in form of synchronization between concurrent tasks. Talking about parallel XPath query using data partition, the overhead of interactions is so small to be ignored. That's because that in parallel phase, the execution of several ψ are independent from each other.

In the contrast, the cost of processes being idle plays an important role on query performance. Uneven load distribution may cause some processes to finish much later than others. It reduces the efficiency of CPUs and results in a bad performance. It is especially true when executing XPath query in parallel in share-memory systems. On one hand, task decomposition typically is coarse-grained. Consider **Example 1**, the tasks to be executed in parallel are thousands of sub-trees rooted by EMPTY, shown as Figure 3. Each sub-tree rooted by EMPTY is a task. However, the structures of all these sub-trees may vary seriously. Some have a large quantity of descendant nodes, while the others do not. Consequently, even task distribution leads to uneven load distribution, which will impact overall performance significantly. On the other hand, it is hard to construct a general model to estimate the cost of tasks that is adapted to any query. A model may fit for some queries and datasets, but not for others. Load-imbalance always occurs.

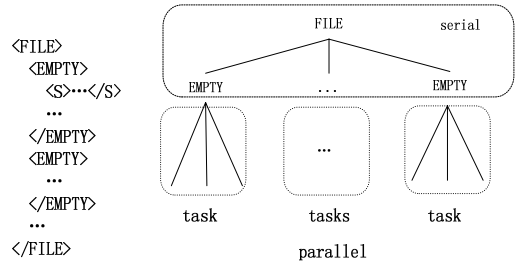

a. treebank.xml b. Data Access Model

Figure 3 Data Access Model of Example 1

As mentioned, even task distribution may cause uneven load distribution when using static mapping. So we try to accomplish load balance by dynamic mapping. The core point is to schedule tasks at runtime.

C. Dynamic Mapping

We use the work pool [4] model. The model is characterized by a dynamic mapping of tasks onto processes in which any task may potentially be performed by any process. In our scenario, the total tasks are known as a priori, i.e. that there is no task produced dynamically during executing parallel tasks. So the work pool shrinks monotonously as processes fetch tasks to execute continuously.

Initially, all processes are idle and all tasks in work pool are in unplayed state. Then, idle process applies a certain amount of tasks from work pool and then executes the tasks. After the process accomplishes the tasks, it becomes idle again. So it repeats the procedure until the work pool becomes empty. This way of self-scheduling turns out to be very useful in parallel XPath query in share-memory system. In our design, every time process applies the same amount of additional tasks, so-called chunk. Here, chunk is the granularity of dynamic mapping. Proper granularity selection is an important factor to the performance of dynamic mapping. Too coarse granularity may cause load imbalance like static mapping. Too fine granularity will cause heavy extra interaction overhead.

The biggest overhead of dynamic mapping is caused by task application and assignment, which is exclusive lock overhead in work pool model. To minimize this overhead, we build a dense index on all sub-trees as shown in Figure 4. There is an index pool containing the indices of all tasks in the work pool. An exclusive lock is used for index pool to guarantee consistency when concurrent task applications are issued by multiple processes. Therefore, task assignment and execution are completely independent. That is, when some processes fetch tasks from index pool serially, other processes execute their tasks simultaneously on the work pool. This

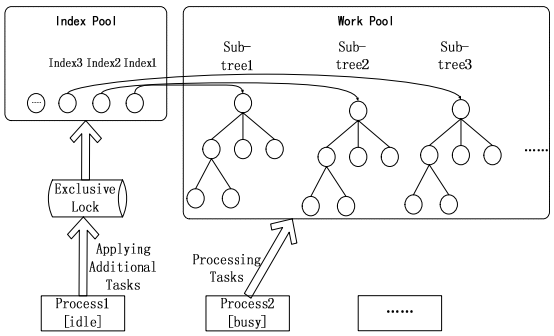

Figure 4 Processing of Dynamic Mapping

model increases concurrency obviously. In addition, our experimental evaluation show that even interaction overhead of extreme fine granularity is too light to impact performance perceptibly.

D. Performance Analysis

In this subsection, we will show that our dynamic scheme will get much better load balance compared with static mapping, especially when the problem size is large. Analytically, we pay much attention to the parallel phase after data partitioning, which is the core difference between dynamic and static mapping. As shown in Subsection 4.1, ψ in different processes are independent of each other, so we first assume there is no extra overheads in parallel phase.

We denote by n the number of tasks in work pool, and g the mapping granularity. So there are $\lceil n/g \rceil$ chunks to be assigned to threads.

LEMMA 1. For two threads i and j, let p_1, p_2 ... p_{k_i} and q_1, q_2 ... q_{k_j} be two chunk sequences which are assigned to the two threads and run on them sequently, respectively. Let t_p be the execution time of task p, t_g be the largest execution time among those of $\lceil n/g \rceil$ chunks and T_i denote the running time of thread i. Using the scheduling strategy described in the last subsection,

$$\left|T_j - T_i\right| \le t_g$$

PROOF. First, we prove $T_i \ge T_j - t_{q_{k_j}}$ by contradiction. WLOG, suppose that $T_i < T_j - t_{q_{k_j}}$. After the p_{k_i} finishes, thread i will no longer get scheduled by any chunk. It must be true that at the very moment when p_{k_i} finishes, there is no unfinished chunk. Obviously, $T_i < T_j - t_{q_{k_j}}$ implies that at least one chunk, q_{k_j}, remains unprocessed after p_{k_i} finishes, which is a contradiction. So there is $T_i \ge T_j - t_{q_{k_j}}$. As the same, $T_j \ge T_i - t_{p_{k_i}}$. Since $t_{p_{k_i}} \le t_g \; and \; t_{q_{k_j}} \le t_g$, $\left|T_j - T_i\right| \le t_g$.

With Lemma 1 we know that, for any two processes, the difference of their final running time cannot be larger than the longest execution time of a single chunk. So, with appropriate g, the load is well balanced. What's more, $\left|T_j - T_i\right| \le t_g$ is irrelevant of n, i.e. when n becomes large, the absolute load difference does not rise.

Now consider the overheads involved in dynamic scheduling. As mentioned, we use index pool to reduce the cost of lock. There are $\lceil n/g \rceil$ times exclusive lock acquirements and releases in total. Assuming the cost of lock and chunk assignment of every chunk with mapping granularity g is $C_{lg} + C_{ag}$, so overhead of our algorithm is estimated as $\lceil n/g \rceil * \left(C_{lg} + C_{ag}\right)$. The overhead will rise as n becomes large. Actually, we observe in our experiments that $\left(C_{lg} + C_{ag}\right)$ is too small compared with the computation time. The overhead is acceptable.

There are a few of performance metrics for parallel algorithms. Like serial algorithms, the execution time is an important metric. The parallel runtime T_p is the time that elapses from the moment a parallel computation starts to the moment the last processing element finishes [4]. Suppose that each thread gets at least one task chunk, we estimate the worst case of the parallel time:

$$T_p = n * t_c / p + t_g + \left(\lceil n/g \rceil - p + 1\right) * \left(C_{lg} + C_{ag}\right)$$

where t_c denotes the maximum execution time of a single task.

The speedup S and the efficiency E are metrics specific for parallel algorithms. The speedup is defined as the ratio of sequential time T_s to parallel time T_p to measure how much performance gain is achieved by parallelizing a sequential algorithm [4]. The efficiency measures how efficient the processing elements are employed that is defined as the ratio of speedup to the number of processing elements p [4].

Another important metric is isoefficiency function for scalability [4]. If a parallel algorithm can keep the efficiency fixed by increasing both problem size W and the number of processing elements p simultaneously, it is scalable. Isoefficiency function quantifies scalability by describing how faster W must be increased with respect to p to keep the efficiency fixed. Slower growing isoefficiency function means higher scalability. Following the method described in [4], we get the isoefficiency function of our algorithm $W = KT_o = K\left(t_g + \left(\lceil n/g \rceil - p + 1\right) * \left(C_{lg} + C_{ag}\right)\right)$ where T_o denotes the total overhead, and K is a constant. Since W is actually the amount of computation of the problem, we can express it using the sequential time, $W = T_s = nt_c$. Solve the above isoefficiency function, we get

$$W = O(p)$$

which implies that our algorithm is perfectly scalable.

V. EXPERIMENTS

A Experimental Design

We have performed extensive experiments on several types of XPath queries over many XML datasets. In this section, we describe our experiments and present a representative subset.

Prototype Implementation. To afford the XPath queries, we choose Xerces-C and XALAN DOM APIs [13], since DOM APIs have been proved to be a very useful standard for XML query. We use the XALAN interfaces as the

operator ψ, and we implement the other operators in PXQA. To afford the parallel computing, we use pthread to create more than one threads to compute in parallel. The experiments are performed on TYAN FT72-B7015, a 4U server with two Intel Xeon 5520 quad-core processors. It supports up to eight physical threads. The server has 12GB of memory running Federo 12.

Experimental Schemes. We design our experiments from the following four aspects. First, we show that the mapping granularity affects the performance of dynamic mapping. We will compare coarse-grained and fine-grained scenarios to determine an appropriate granularity. Second, we present load balance and faster query speed accomplished by dynamic mapping when the dataset is not even-distributed. In addition, third, we show that dynamic mapping does not hurt the good performance achieved by static mapping when dataset is already even-distributed. At last, we validate the scalability of our dynamic scheme.

Datasets and Queries. We experiment with several typical datasets, such as DBLP, Treebank. These datasets are all even-distributed, so the results are similar. Though Treebank is not very large, it is deeply recursive. The queries in Treebank are more complex. We just show the results of Treebank on behalf of these typical datasets. What's more, we experiment with a realistic dataset, XStu, from a college. XStu is a set of realistic data, which collects the records of students' personal information and course details. XStu is wide and deeply recursive. Due to space constraint, we show part structure of XStu in Figure 5. The original XStu is 663 MB from Table 2. But as said above, to measure the scalability of dynamic mapping, we need datsets of different size. So we extract part of XStu to form XStu-2 and XStu-3, which are much smaller than XStu, see also Table 2. XStu collects information of 35778 students, while XStu-2 collects 1517 students and XStu-3 collects 12274 students. These three datasets are uneven-distributed and will lead to load-imbalance, which we will show next.

The characteristics of the datasets are shown in Table 2. In addition to the real XStu data, we also use XPath expressions extracted from a real-world query workload provided by the college. Table 2 lists the representative XPath queries over the two XML datasets. We have tested many queries, the results are similar. We show only two representative queries. Query TB is from [2], and query XS is a real query.

Comparing Arguments. Given a data partition point and threads, we test our dynamic mapping algorithm with the plain static mapping algorithm as the control group. Besides the common performance metrics for parallel algorithms, the parallel time, speedup, isoefficiency function (described in Subsection 4.4), we also use a dedicated metric for this problem, the load gap among the threads, denoted by d.

TABLE 1
QUERIES AND PARTITION POINTS

Dataset		Key	Query	$T_s(s)$	Partition Point	Number of tasks
TreeBank		TB	/FILE/EMPTY/S//VP[count(.//NP)>1]	29	EMPTY	52851
XStu-2		XS2	/totalstudents/s//sc[./FinalExamScore/text()>=60]	6.39	s	12274
XStu-3		XS3	/totalstudents/s//sc[./FinalExamScore/text()>=60]	130.57	s	1517
XStu		XS	/totalstudents/s//sc[./FinalExamScore/text()>=60]	371.6	s	35778

TABLE 2
CHARACTERISTICS OF TREEBANK AND XSTU

	Treebank	XStu-2	XStu-3	XStu
Size(MB)	84	86.9	334	663
Number of Elements	9 Million	2 Million	34 Million	68 Million
Max Depth	36	7	7	7
Avg Depth	7.87	7	7	7

To evaluate the load distribution among threads, the running time of all threads are collected to indicate the load of threads. If load in a thread is higher, the running time of the thread is longer. We define d as:

$$d = \left(Max\left(T_1, T_2 ... T_p\right) - Min\left(T_1, T_2 ... T_p\right)\right) / Min\left(T_1, T_2 ... T_p\right)$$

$$T_i : the\ running\ time\ of\ the\ i^{th}\ process$$

The higher d is, the more imbalanced load is.

TABLE 3
EFFICIENCY OF DIFFERENT PARAMETERS

	p=2	p=4	p=6	p=8
XS2	4.38	4.32	3.83	2.66
XS3	22.43	22.2	22.19	13.37
XS	32.25	32.02	27.67	19.2

B Evaluation1: Mapping Granularity

The query XS, based on XStu, returns all passed course selections. In the data partitioning strategy, original query is split into two subqueries: /*totalstudents*/*s* (*serial*), and .//*sc*[./*FinalExamScore*/*text*()>=60] (*parallel*).

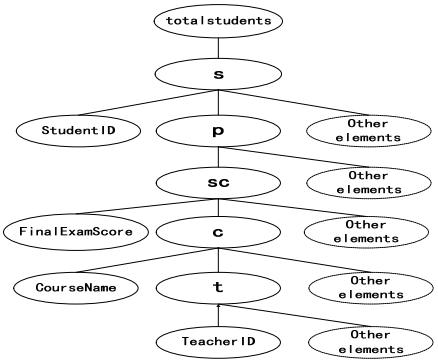

Figure 5 Part Structure of XStu

Using four threads, the plan is:

$$\psi_{/totalstudents/s//sc[./FinalExamScore/text()>=60]}(XStu.xml)$$

$$=\psi_{//sc[./FinalExamScore/text()>=60]}\left(\sigma_{part}\left(\psi_{/totalstudents/s}(XStu.xml)\right)\right)$$

$$\cup\psi_{//sc[./FinalExamScore/text()>=60]}\left(\sigma_{part}\left(\psi_{/totalstudents/s}(XStu.xml)\right)\right)$$

$$\cup\psi_{//sc[./FinalExamScore/text()>=60]}\left(\sigma_{part}\left(\psi_{/totalstudents/s}(XStu.xml)\right)\right)$$

$$\cup\psi_{//sc[./FinalExamScore/text()>=60]}\left(\sigma_{part}\left(\psi_{/totalstudents/s}(XStu.xml)\right)\right)$$

At the beginning, $\psi_{/totalstudents/s}(XStu.xml)$ is executed serially. After serial phase there are 35778 unprocessed tasks (sub-trees rooted by s) in work pool. And next, we experiment dynamic mapping with different mapping granularity. We test from fine mapping granularity 1 to coarse mapping granularity 10000, shown in Figure 6. The curve is flat when mapping granularity is in [1, 100], which implies that tasks applying and assignment overhead is negligible. Index pool mechanism is the most important reason for this. Then, the curve rises slowly when mapping granularity is between 100 and 2000 and rises sharply when mapping granularity is beyond 2000. It is reasonable, for the mapping granularity is too coarse. In the next statement, we will always experiment with mapping granularity 100.

C. Evaluation2: Comparison between Dynamic Mapping and Static Mapping

Table 1 presents a set of XPath queries used for the experimental evaluation. The two queries include those with long chains of child steps, path predicates, functions such as text() and count() and different axes. The two instances TB and XS stand for the two aspect of dynamic mapping. For one thing, when the data is well-distributed, an instance using static mapping causes load balance, like TB, by coincidence. Then we will show dynamic mapping will not reduce the good performance. The extra overhead of dynamic mapping can be made up. For another thing, when the data is uneven-distributed, an instance using static mapping leads to load-imbalance such as XS. Consequently, the execution time of XPath query is long. Yet, we will show dynamic mapping will gain a good load distribution and accelerate the query speed.

The query TB (Table 1), based on Treebank, returns all elements labeled VP, who have more than one descendants labeled NP. In the data partitioning strategy,

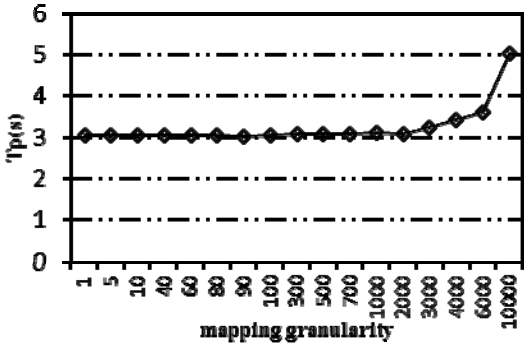

Figure 6 Mapping Granularity

EMPTY as partition point, is chosen according to [1]. Original query is split into two subqueries: /*FILE*/*EMPTY*(*serial*), and ./*S*//*VP*[*count*(.//*NP*)>1](*parallel*). Using four threads, the plan is:

$$\psi_{/FILE/EMPTY/S//VP[count(.//NP)>1]}(treebank.xml)$$

$$=\psi_{/S//VP[count(.//NP)>1]}\left(\sigma_{part}\left(\psi_{/FILE/EMPTY}(treebank.xml)\right)\right)$$

$$\cup\psi_{/S//VP[count(.//NP)>1]}\left(\sigma_{part}\left(\psi_{/FILE/EMPTY}(treebank.xml)\right)\right)$$

$$\cup\psi_{/S//VP[count(.//NP)>1]}\left(\sigma_{part}\left(\psi_{/FILE/EMPTY}(treebank.xml)\right)\right)$$

$$\cup\psi_{/S//VP[count(.//NP)>1]}\left(\sigma_{part}\left(\psi_{/FILE/EMPTY}(treebank.xml)\right)\right)$$

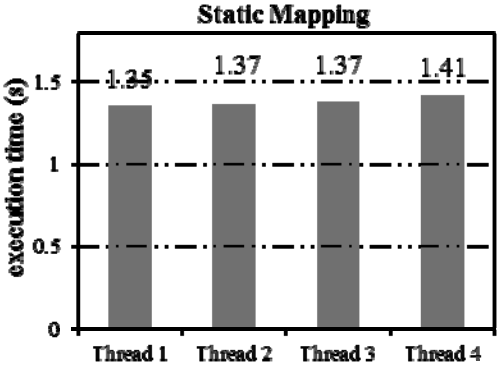

Figure 7 Load Balance Distribution of TB with 4 threads (Static)

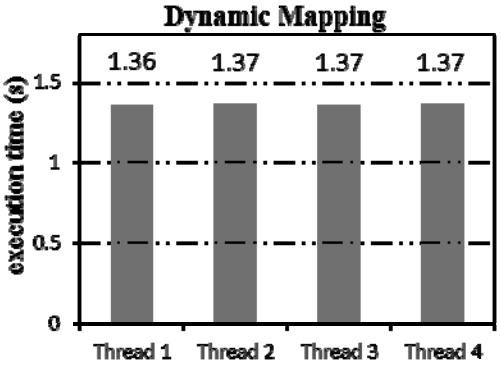

Figure 8 Load Balance Distribution of TB with 4 threads (Dynamic)

At the beginning, $\psi_{/FILE/EMPTY}(treebank.xml)$ is executed serially. As shown in Table 1, after serial phase there are 52851 unprocessed tasks (sub-trees rooted by EMPTY) in work pool. And then, we experiment two kinds of mapping methods in parallel phase, static mapping and dynamic mapping. Figure 7 shows the

running time of four threads about TB using static mapping in [1]. Using static mapping, three threads get $\lfloor 52851/4 \rfloor = 13212$ tasks and the forth gets 13215 tasks. The running time of four threads are 1.355s, 1.365s, 1.374s, 1.414s respectively. The load of four threads are more or less the same with d = 4.35%. So, using static mapping, TB does not cause load imbalance with $T_p = 1.414s$.

Correspondingly, Figure 8 presents the performance of TB using dynamic mapping. In this case, the running time of four threads are 1.362s, 1.367s, 1.365s and 1.373s, with d = 0.8%, when mapping granularity is 100. Compared with static mapping, dynamic mapping has smaller d, which means dynamic mapping gains a little better load balance. But the imperfect thing is that the execution time is not much better than static mapping. Figure 11 presents the execution time (T_p) of dynamic mapping with different mapping granularity. The first point stands for static mapping and other points stand for dynamic mapping with certain mapping granularity. It's seen that dynamic mapping does not always gain better performance than static mapping. That's because static mapping has already gained good load balance and dynamic mapping costs some time in overheads, such as lock cost. However, it is acceptable. In a word, dynamic mapping does not hurt the performance when load distribution is even.

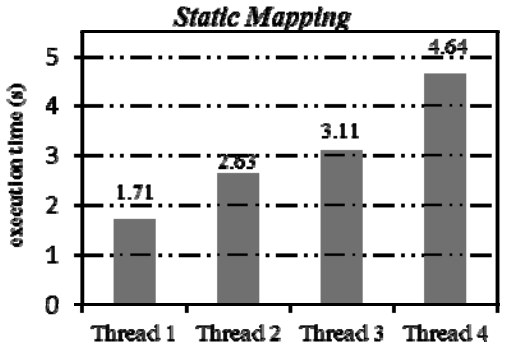

Figure 9 Load Balance Distribution of XS with 4 threads (Static)

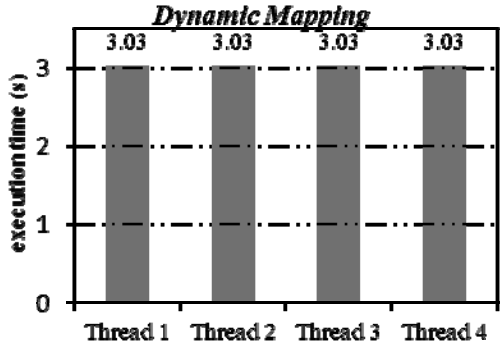

Figure 10 Load Balance Distribution of XS with 4 threads (Dynamic)

The execution of XS is similar with TB. $\Psi_{/totalstudents/s}(XStu.xml)$ is executed serially at first. After serial phase there are 35778 unprocessed tasks in work pool. And next, we experiment static mapping and dynamic mapping.

Figure 9 shows the running time of XS using four different threads in static mapping. It is clear that loads among threads are quite different from others, as 1.711s, 2.629s, 3.107s, 4.645s. d reaches 171.48%. There is a serious load-imbalance. It is not surprising of this load imbalance if looking inside the structure of XStu. As mentioned above, XStu is about the students' personal information and selected courses. Naturally, the elements labeled s are ordered by StudentID. Smaller StudentID means the student having higher grade, which indicates he chooses more courses. As a result, the thread allocated too many s with higher StudentID will last long and vice versa. Load-imbalance takes place in this case. In contrast, Figure 10 gains load balance clearly with d = 0.17% when using dynamic mapping with mapping granularity 100. As a result, the total execution time decreases from 4.657s to 3.048s. It accelerates the query speed by 34.5%. It is a great achievement.

D. Evaluation3: Scalability Evaluation

Our dynamic scheme for load balance is designed and tested for smaller datasets on fewer processing elements. However, the real datasets we want to solve may be much larger, and the computers may contain larger number of processing elements, such as cluster system. So in this evaluation, we investigate the scalability of our scheme.

As mentioned in Subsection 4.4, there are two factors to be taken into account when evaluating scalability. One is problem size. As shown in Table 2, we extract part of XStu to form XStu-2 and XStu-3, which have different problem size from each other. XStu-2 is 86.9 MB and XStu-3 is 334 MB while XStu is 663 MB. We experiment the same query *./totalstudents/s//sc*[*./FinalExamScore/text*()>=60] with partition points on XStu, XStu-2 and XStu-3. To distinguish, XS, XS2,XS3 are in use. It is only true for part of parallel algorithms that the efficiency increases with increasing problem size and fixed number of processing elements. The other factor is the number of processing elements (threads). We experiment dynamic mapping of XS, XS2, XS3 using 2, 4, 6, 8 threads respectively. All parallel algorithms will show efficiency degradation with increasing number of processing elements and fixed problem size. If a parallel algorithm can keep constant efficiency by increasing both system size and problem size, we say it is scalable. When mapping granularity is 100, the efficiency is shown in

Table 3.

Note that our dynamic mapping algorithm achieves super-linear speedup, that is, an efficiency greater than 1. This is because XALAN algorithm is cache sensitive. Multi-thread means multiplying cache size, so improves performance dramatically.

As shown in

Table 3, with fixed number of threads, the efficiency increases remarkably as problem size increases. This implies that our algorithm can make better use of the processing elements as the problem size increases. On the other hand, with the fixed problem size, the efficiency remains the same when p increases from 2 to 4, and

decreases slowly when p increases to 6 and 8. We can see that, the efficiency remains fixed (even increases significantly) as both the problem size and the number of processing elements increases. This result shows the good scalability of our algorithm.

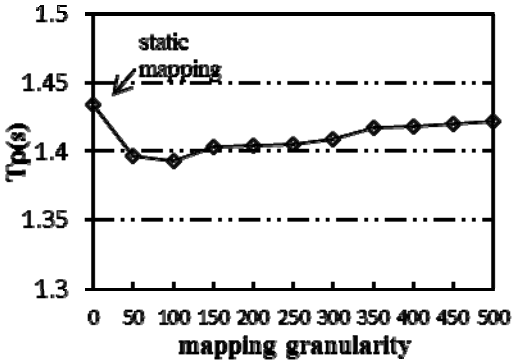

Figure 11 Comparison of Static and Dynamic Mappings on TB

VI Conclusions and Future Work

Motivated by the emergence of multi-core processors in commodity systems, this paper presents that dynamic mapping improve performance by up to 34.5% when static mapping can not distribute load evenly among threads. Meanwhile, it shows the good scalability of the dynamic mapping algorithm agreeing well with our theoretical analysis. This means that the algorithm can efficiently deal with large datasets on large systems. In this paper, we implement dynamic mapping algorithm in the multi-core shared memory system. However, our algorithm is platform-independent. It can easily be ported to Message Passing platforms such as clusters. The work pool (index pool) is implemented as a main process rather than a global object. Task assignment consistency is implemented by message passing between processes instead of exclusive lock. Certainly, the overhead of message passing is higher than shared object access. An important future work is to minimize this overhead.

It would be very interesting to consider the scenario where the dataset is too large to fit in the main memory. Besides, the optimization of PXQA and granularity chosen automatically need to be studied more. In addition, GPU is becoming the most promising platform for high performance computing. Design and implementation of our algorithm on GPU is also planned.

Acknowledgment

This work is partly supported by the grants from the National High-Tech Research and Development Plan of China (No.2013AA013204); the Doctoral Fund of Ministry of Education of China (No.20120031120038), and Natural Science Foundation of Tianjin, China (No.13JCQNJC00100 and No.3ZCZDGX02200).

References

[1] Rajesh Bordawekar, Lipyeow Lim, Anastasios Kementsietsidis, and Bryant Wei-Lun Kok. “Statistics-based Parallelization of XPath Queries in Shared Memory Systems.” In EDBT, pages 159–170, New York, NY, USA, 2010.

[2] Rajesh Bordawekar, Lipyeow Lim, and Oded Shmueli.“Parallelization of XPpath Queries Using Multi-core Processors: Challenges and Experiences”, in EDBT, pages 180–191, New York, NY, USA, 2009.

[3] Jianhua Feng, Le Liu, Guoliang Li, Jianhui Li, and Yuanhao Sun. “An Efficient Parallel Pathstack Algorithm for Processing XML Twig Queries on Multi-core Systems.” Database Systems for Advanced Applications, volume 5981 of Lecture Notes in Computer Science, pages 277–291, 2010.

[4] Ananth Grama, George Karypis, Vipin Kumar, and Anshul Gupta. Introduction to Parallel Computing (2nd Edition). Addison Wesley, 2 edition, 2003.

[5] Le Liu, Jianhua Feng, Guoliang Li, Qian Qian, and Jianhui Li. “Parallel Structural Join Algorithm on Shared-memory Multi-core Systems”, in WAIM, pages 70–77, Washington, DC, USA, 2008.

[6] Wei Lu, Kenneth Chiu, and Yinfei Pan. “A Parallel Approach to XML Parsing”, in GRID, pages 223–230, Washington, DC, USA, 2006.

[7] Wei Lu and Dennis Gannon. “Parallel XML Processing by Work Stealing”, in SOCP, pages 31–38, New York, NY, USA, 2007.

[8] Imam Machdi, Toshiyuki Amagasa, and Hiroyuki Kitagawa. “GMX: An XML Data Partitioning Scheme for Holistic Twig Joins”, in iiWAS, pages 137–146, 2008.

[9] Imam Machdi, Toshiyuki Amagasa, and Hiroyuki Kitagawa. “XML Data Partitioning Schemes for Parallel Holistic Twig Joins”, IJWIS, 5(2):151–194, 2009.

[10] Imam Machdi, Toshiyuki Amagasa, and Hiroyuki Kitagawa. “XML Data Partitioning Strategies to Improve Parallelism in Parallel Holistic Twig Joins”, in ICUIMC, pages 471–480, 2009.

[11] Yinfei Pan, Wei Lu, Ying Zhang, and Kenneth Chiu. “A Static Load-balancing Scheme for Parallel XML Parsing on Multicore CPUs”, in Cluster Computing and the Grid, IEEE International Symposium on, 0:351–362, 2007.

[12] Jens Teubner, Torsten Grust, Sebastian Maneth, and Sherif Sakr. “Dependable Cardinality Forecasts for XQuery”, in PVLDB, 1(1):463–477, 2008.

[13] http://www.w3.org/DOM/.

[14] http://www.w3.org/TR/xml-infoset/.

[15] http://www.w3.org/TR/xpath20/.

[16] Xiaojie Yuan, Xin Lian, Ya Wang, Xiangyu Hu, Haiwei Zhang, "DPIX: A Dynamic Path Index for XML Data in Relational Database", JDCTA, Vol. 7, No. 5, pp. 434 ~ 442, 2013

[17] LEAGUE, C., ENG, K..“Schema-Based Compression of XML Data with Relax NG” in Journal of Computers, North America, 2, dec. 2007

[18] Husheng Liao, Weifeng Shan, Hongyu Gao, “Automatic Parallelization of XQuery Programs” in Journal of Software, North America, 2013

[19] LI, R., LUO, J., YANG, D., HU, H., CHEN, L. “A Scalable XSLT Processing Framework based on MapReduce” in Journal of Computers, North America, 8, sep. 2013.

Xiaocheng Huang is a Ph.D. candidate in Computer Science of Nankai University. Her research interests are broadly in the areas of data and information management, including XML query/update, and keyword search/query on scientific workflows (context-free graph grammars).

Xujie Si is a Ph.D. candidate in Computer Science, Vanderbilt University.

Xiaojie Yuan is a professor and dean of College of Computer and Control Engineering in Nanakai University. Her research focuses on data management, including database and information retrieval.

Chao Wang is a Ph.D. candidate in Computer Science of Nankai University.

Research on Template Computing Mode of Remote Sensing Image Based on Partition Model

Gen-yuan Du
International School of Education, Xuchang University, Xuchang Henan 461000, China
Email: xcdgy@163.com

De-lan Xiong
International School of Education, Xuchang University, Xuchang Henan 461000, China
Email: xiongdelan@aliyun.com

Huo-lin Zhang
International School of Education, Xuchang University, Xuchang Henan 461000, China
Email: chouchu20@163.com

***Abstract*— As the amount of data rises and application needs expand, the efficient organization and management of remote sensing data has become a bottleneck restricting the application of remote sensing technology. The Global Partition Theory (GPT) and high performance computing provide an approach to solve the above mentioned problems. GPT studies how the Earth's surface is split into different levels of thickness seamless mesh and how to organize and manage it. Thus, rapid integration of mass remote sensing data of different sources, different types and different resolution can be achieved. Meanwhile, there is a natural segmentation of regional location and distributed storage features in spatial data in the partition organization framework, which makes remote sensing images computing model based on partition inherently parallel attributes. Combing a partition model of the Extended Model Based on Mapping Division (EMD), the researchers study the partition facet of remote sensing image, and propose the conceptual model and data model of partition facet template. Combing with parallel processing framework in high-performance computing of remote sensing image, the researchers design the template-based computing mode of partition facet and the partition process of spatial data. Through analyzing spatial relationship of partition facets, such as containment relationship, neighboring relationship and direction relationship, the researchers propose the basic calculation modes of partition template. There are aggregation, division in longitudinal and extend, conversion in transverse. This research paper is of great significance for expanding the application of GPT, improving the remote sensing technology speed, accelerating spatial information visualization analyzing and decision making speed. It also provides valuable guidance for studying high-performance remote sensing image processing in the future.**

***Index Terms*— Remote Sensing, EMD Partition Model, Partition Facet, Template Data Model, Computing Mode**

Corresponding author, Du Gen-yuan, xcdgy@163.com, +86 374 2968725.

I. INTRODUCTION

Remote Sensing refers to the technology to measure, analyze and determine the nature of the target through certain sensor device in the distance, but not in direct contact the target [1]. Data obtained by remote sensing technique has the following advantages, such as high real-time, covering-widely and rich information-. So it has been widely used in many military and civilian fields like aviation, aerospace, military reconnaissance, disaster forecasting and environmental monitoring. With the development of sensors, remote sensing platforms, data communications technology, spatial data obtained by remote sensing is expanding rapidly, which results into the situation of "the production and transmission capacity of spatial data is far greater than its analysis capabilities" (Deren LI). At the same time, many applications have increasingly higher requirements of timeliness, accuracy and reliability of remote sensing images. The efficient organization and management of spatial data and its processing speed have become a bottleneck affecting the quick application of remote sensing images. These questions result in high-performance processing methods and technology developing of remote sensing images.

As remote sensing applications research and theoretical exploration deepens, especially after "Digital Earth" proposed, remote sensing image processing is faced with some new questions of global continuous, multi-level and dynamic environment resources and social information. The traditional grid system gradually exposed limitations of projection complex, lacking of multi-scale data integration and management. The Global Partition Theory (GPT) is put forward in this circumstance. Division in earth science refers to the partitioning method of geospatial location. The GPT is based on spatial partition organizational framework, which divides the earth into discrete facets with similar shapes ,rules and clear levels. It can realize massive global data storage, extraction and analysis, and ensure

doi:10.4304/jcp.9.6.1446-1453

spatial data application services in global harmonization organization, sphere-plane integrated expression and rapid integration of multi-source spatial data [2, 3]. So it can solve a series of bottlenecks that restrict quickly retrieval, efficient integration and sharing of geospatial information. It achieves that the multi-source, multi-scale, multi-temporal spatial information can be integrated into organizations, open-sharing, interoperability and rapid distribution and so on.

The paper will introduce GPT and a partition model of the Extended Model Based on Mapping Division (EMD), and study the partition facet of remote sensing image. Besides, the conceptual model and data model of partition facet template will be proposed, and subdividing process of spatial data will be designed. And we propose a kind of facet computing model of partition template. Through analyzing spatial relationship of partition facets, such as containment relationship, neighboring relationship and direction relationship, we propose basic calculation modes of partition template. There are aggregation, division in longitudinal and extend, conversion in transverse. This research will provide the possibility and a base for remote sensing templates parallel processing.

II. Global Partition Theory

Global Partition Theory (GPT) is a kind of multi-levels, multi-scale data organization. It is based on global grid division, and has unique advantages in expression and management of spatial information [4-6]. It studies on how to divide the Earth into levels of facets with regular shape and small deformation. It has equal spatial distribution and fusion spatial indexing mechanism, which can support multi-resolution and multi-scale transformation. So it is considered as a new seamless open hierarchical spatial data management framework. It can achieve to store, extract and analyze massive data in global scale. It can solve the existing limitations of traditional data models that manage multi-scale, hierarchical global data. It's ensuring that the global spatial data will be expressed in a global, continuous, hierarchical and dynamic model [7-9].

Partition model is the key of GPT, it researches on how to subdivide the Earth, what shape of subdivided facets is and how to code the facets. At present, there are three kinds of partition models in China and abroad. They are latitude and longitude grid model, equal regular polyhedron grid model and adaptive grid model [10]. The partition methods can be classified into polyhedral division, experience division and wavelet division. Typical partition models include QTM [11], STQIE [12], SIMG [13] and so on. The partition model generally adopts quadtree structure and partition code to organize facets, and achieve interrelated global remote sensing system in different levels and different facets at the same level. But some partition models have questions of computing complex and facets reshape, so it can't adapt to high efficient requirements of spatial information processing.

Based on integrating advantages of various partition models, Professor Cheng Chengqi in Peking University proposed a new partition model of the Extended Model Based on Mapping Division (EMD) [14-16]. The main idea of EMD is using regular polyhedral triangles partition method in high latitudes, while using equal latitude and longitude grid basing mapping division in low and middle latitudes [14]. The EMD model is the subset of mapping division system, and its development. It can realize unified organization and management of remote sensing, survey and map data. Except the similar advantages of other partition model, the EMD model has simple and clear correspondence with existing space data and coordinate system. Through integrating basic survey technology, present space data can be easily merge into this organization system. So it has strong practicability. At the same time, the system of EMD has unified record baseline, data association method and efficient data organization method of calculating for spatial data. So it can reflect the spatial characteristics of the data to the maximum extent. It can achieve unified organization and management of multi-type, multi-scale and large amount of spatial data, and support multi-scale transformation, centralized services and distributed services across the region [17, 18].

In the EMD model, partition is done according to topographic maps division from four to six levels. The forth level partition facets are gotten by dividing the third level facet into four equal parts, their size is 3°×2°.

Divide the forth level facet into four equal parts, the fifth level facets will be gotten, and each one is 1°30'×1°. The sixth level equal part facets are gotten by dividing the fifth level facet into nine equal parts, its size is 30'×20'. The three levels facets are corresponding with division maps range of 1:500000, 1:250000 and 1:100000 scale.

From the seventh level in the EMD model, partition is recursively done by quadtree partition with equal latitude and longitude difference. The seven to ten facets are corresponding with 1:50000, 1:25000, 1:10000, 1:5000 division map ranges. The other levels partition and the polar partition method are shown in Ref. [16].

The facet coding model in the EMD model includes middle-low and high latitude coding method. The middle-low latitude (0°-88°) coding is using sequence encoding from the first to sixth level, and using Hilbert curve for seventh and above level. The high latitude (88°-90°) coding is using QTM encoding. The coding structure and code generation method are also shown in Ref. [16].

III. Partition Facet Template of Remote Sensing Image

A. Partition Facet Template Conceptual Model

Partition facet is a multi-scale segmentation unit with regular shape and small deformation, which is divided by certain partition model. Each partition facet has accurate geospatial position range, regular geometric shape, distinct hierarchical structure, and a unique identification code. The main parameters of partition facet are code, dividing level, corner coordinates, location coordinates, area, length, position, curvature, projection area and

conversion accuracy. The code is a globally unique mark, and it can be converted into other common coordinate system easily.

Partition facet template of remote sensing image (called partition facet template) is a spatial feature set of partition facets. It may be extracted from high resolution remote sensing image. It may also be other spatial data related to partition facet. Actually, partition facet template is a data sample of remote sensing image that corresponded with certain range of partition facet. Usually, the data is orthophoto remote sensing with obvious features. It contains spatial feature set, geographical features set and control point data of partition facet. So it inherits all the advantages of partition facet, and can establish association between abstract partition model and specific remote sensing images. Using partition facet template, an unknown remote sensing image can be quickly identified which one belongs to which partition facet. According to different data processing requirement, many kinds of templates can exist for different applications. Each template is corresponding to a specific algorithm of partition data processing.

B. Partition Facet Template Data Model

Partition facet templates consist of facet information, template type and template data. Facet information includes code, level, shape, area, geographic location and projection transformation of partition facet. Template type corresponds to specific partition processing algorithms, which can be created by template management module, and use to manage template metadata information. Template data refers to basic sensing image information corresponding to certain partition facet. It includes resolution, coordinate, pixel information, and color, texture, shape feature of spatial entities. Template metadata includes data format, data type, data files algorithm interface, data processing algorithm interface. Here, the data files algorithm is responsible for generating and parsing data files. the data processing algorithm is responsible for spatial data processing using template data.

Operation Defination Layer	Registration	Projection Transformation	Image Mosaic	Object Retrieval	Landform Analysis
Data Model Layer	Referenced Image Data	Control Points Data	Features Data	Altimetric Data	
Concept Model Layer	Template Code	Altimetric Data Partition	Features Recombination	Control Points Measure	

Figure 1. Data model of partition facet template

The data model of partition facet template is shown in Figure 1.

The conceptual model layer describes uniform interface and abstract model of partition facet template. It is the basis for designing various template types. The data model includes reference remote sensing image data and all kinds of template data. The operation definition layer consists of specific algorithms of various types of templates in data layer. It can customize operations according to the data type in data layer.

C. Rapid Generation Process of Partition Facet Template

Figure 2 shows the subdivided generation processing flow for geospatial data.

When geospatial data goes into partition system, preprocessing is the first work to do. Then it needs to determine the partition level according to resolution or scale of the metadata in spatial data. And determine the location of partition facet according to the data center of latitude and longitude coordinates. After that, spatial data partition processing will be done according to it's upper-left and lower-right latitude and longitude coordinates and the size of the facet. This step can determine the facets range of data and decide whether the data is in one partition unit. If so, partition code will be obtained and reorganize the spatial data basing partition facet. And if not, overlay and analyze the image data and facet set. Then, analyze the contain relationship between partition facet and trimmed image data. Through encoding the partition facet according the theory of GPT, organize image data according to facet codes, and geospatial data organized by partition facet will be gotten at last [19].

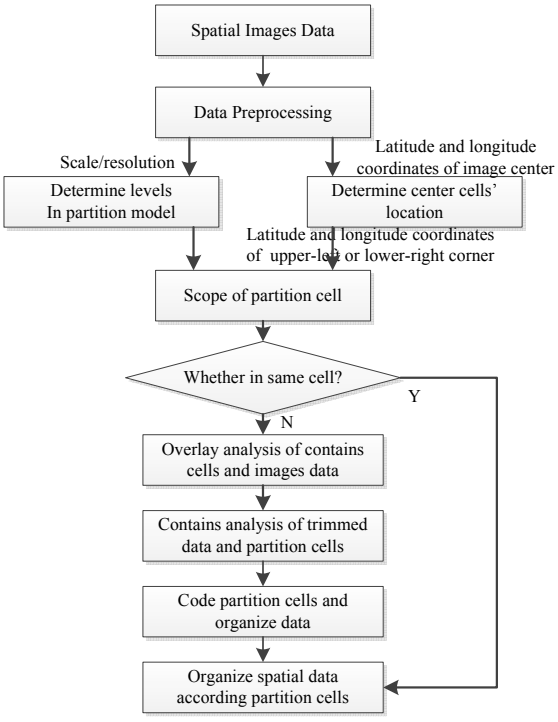

Figure 2. Partition processing flow of spatial data

IV. TEMPLATE-BASED COMPUTING MODE FOR REMOTE SENSING IMAGES PARTITION FACET

In the organized framework of the earth partition, arbitrary geospatial data becomes part of the partition data after higher accurate registration with the reference data. For each precision reference image of partition facets, extracting the control points and other spatial characteristics, it can be made templates. Then we can make parallel processing on the multiple facets of a large area image using partition templates. With the frame and

storage cluster of partition, we can achieve high-performance parallel processing of template.

Template-based parallel processing is using the advantages of partition facet template to achieve parallel processing for massive remote sensing image data. The overall framework of it can be shown in Figure 3.

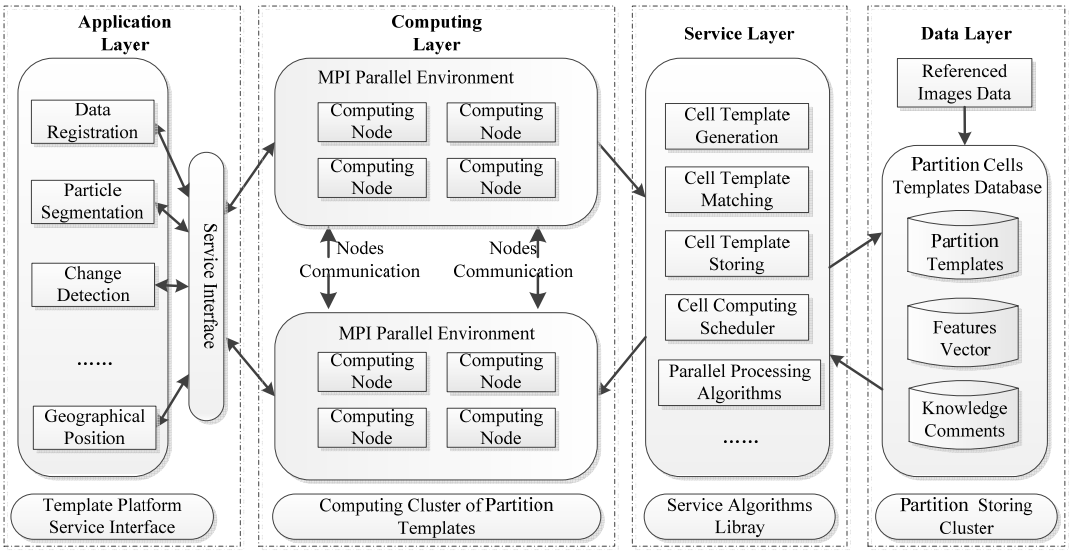

Figure 3. Overall framework of template-based parallel processing for partition data

A..Advantages of Templates Parallel Processing Mechanism

Currently, template parallel processing mechanism has already become one of the most effective ways to improve the speed and efficiency of remote sensing processing. High-performance cluster processing mechanism, which is based on parallel processing and cell processing mechanism and mass distribution processing, is the main method adopted by high-performance remote sensing processing [20, 21]. At the same time, high-performance cluster, distributed computing system and specialized hardware devices are widely adopted in the field of high-performance remote sensing processing. People rely high-performance cluster processing mechanism on the platform and use parallel processing to improve speed [22, 23].

Partition facet template of remote sensing image has many distinct advantages in parallel processing.

- Facilitate to realize multi-source remote sensing images quickly match. The global multi-source remote sensing images are unified organized according to regions of partition facets. So all remote sensing images of the same region can be quickly obtained just by facet codes. Using distributed storage can directly parallel process remote sensing image, and greatly save overhead and improve overall efficiency.
- Favor to multi-scale freedom granular partition spatial image data. Since there are nested hierarchies among levels of partition facets in partition organization, the remote sensing images can partition into different levels of sub-data corresponding to partition facet. So remote sensing images' multi-scale freedom granular dividing is completed.
- Realize efficient geographical location and access of partition data. The partition data is stored according to a certain level and sequence. You can quickly access any location partition data blocks using the association of code, storage location and actual region. And if using distributed parallel storage, retrieval efficiency will be greatly improved.

B. Template-Based Partition Facets Parallel Processing Mechanism

Template-based partition facets parallel processing mechanism is backed by the lower-facet data model, thus it is suitable for efficiently processing mass data. The geographical segmentation feature of the partition data supports parallel data processing. Partition template provides the global spatial data with efficient storage and organization methods. After parallel processing, people can attain geographical division of the spatial data of different regions and provide guarantee for multi-regional parallel calculation. Template-based partition facets parallel processing mechanism not only improves the processing speed by parallel model, but also conducts regional storage and parallel calculation according to the geographical attributes of the spatial data. Thus, it is able to realize multi-facet data processing. Partition data storage model provides support for efficiently accessing and processing the distributed data. People can use uniform partition data form to obtain the data of different sizes within the documents, thus realizing parallel processing of the single data document.

C. Computing Mode of Partition Facet

The main idea of template-based computing mode of partition facet is: consider template as basic unit of partition facet computing, establish baseline image with the unit of partition facet in an appropriate level and range, create partition template according to facet information, image information and special application. When processing the data in any zone, the partition image facet template will be extracted from template database for computing. Thus, remote sensing image fast partition parallel processing is achieved. It can provide support for relevant application.

The EMD partition model has nature of point and surface relationship, and each partition level is relatively uniform in local area. Because of space continuity and distributed storage of spatial data, the partition facets can easily implement concurrent execution in many parallel compute nodes. Because partition data has record storage and internal organization format, the parallel processing within one computer node can be easily achieved.

The architecture of partition template computing is shown in Figure 4.

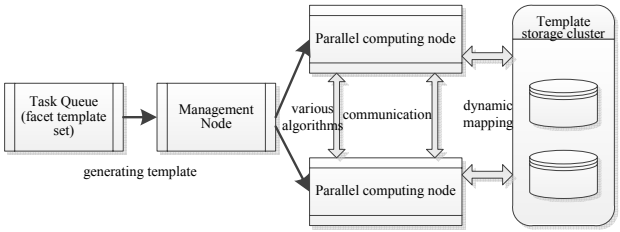

Figure 4. Architecture of partition template computing

Partition facet based on the template parallel processing mode is shown in Figure 5.

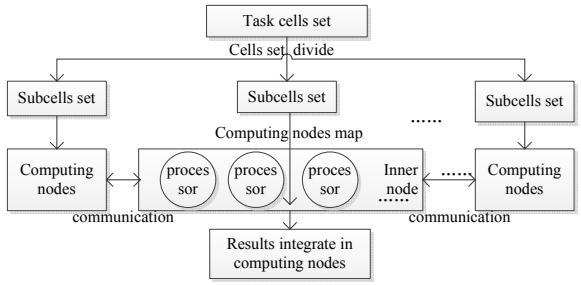

Figure 5. Template-based partition facets parallel processing mode

Structural model of partition images is a key and base of partition facet computing. Remote sensing image data is organized by GPT, so the image data block, pixel and partition facet have certain relationship. Using partition framework of structure facet, the remote sensing image can be expressed as structure partition data set. Because of multi-scale partition facet and global uniqueness of partition code, the data unit can directly index and compute combining pyramid image and space filling curves. Constructing partition image structure model mainly considers layering and partitioning strategies. Hierarchical strategy can be flexible depending on the data source. There is greater flexibility in choosing multi-source data for pyramid image, which can ensure image accuracy and reduce data calculation. Block strategy is to improve I/O access efficiency of image data. Generally, choose $2^n \times 2^n$ pixels as the standard data block of image. And at the same time, record the block code and geographic coordinate range for each image block [15].

Template-based partition facet computing mode comprises two directions calculated in the longitudinal direction of the facet polymerization, splitting and other operations, and in the transverse direction of the facet extension, shrinkage and other operations. Wherein the polymerization represents a number of same level facets gathered to get a high-level facet, mainly involving the combination of positional relationship of same level facets, facet data structure adjustment, etc. Split represents a high-level facet split into several low-level facets, mainly related to facets split, control point adjustment, high precision image selection and so on. Extended operation represents the same level of adjacent facets directly spliced, mosaic, composed of large temporary view.

VI. Template-based Partition Facet Computing Examples

A. Spatial Relationship of Partition Facet

The spatial relation of partition facet is caused by its pure geometry location. It is the basis and premise for parallel processing of partition facet. There are three primary spatial relationships among partition facets. They are measure relation, location relation and topological relation [16]. The measure relation is used to describe the distances and sizes among facets, and it mainly contains space distance model and measurement accuracy. The location relation is used to express orientation relationship among facets, such as front or back, up or down, left or right, corner angle. The topological relation refers to some invariants under topological transformation, and it is the key feature information for partition template storing and computing. In EMD model, the topological relationship among facets is the base of quick transforming and adjusting images in several levels. The facets in the same level have relations of apart, neighbor, and equal, and the facets in different levels have relations of inclusion.

1) Inclusion Relation

Using partition code, the inclusion relation in different levels can be described as follows. Suppose M_A and M_B are the binary code of codes of facet A and B, and their lengths are L_A and L_B respectively. If $L_A<L_B$, and the L_A front bits of M_B are consistent with M_A, we say A contains B. That is:

$$A \supset B \Leftrightarrow \{L_A < L_B, M_A \otimes M_B(0, L_A) = 0\} \quad (1)$$

In this format, the mark $\otimes$ expresses XOR operation, the expression $M_B(0,L_A)$ means that the code bit from *0* to L_A of M_B.

2) Neighborhood Relation

Since the facet code is the globally unique identifier of partition facet, it also corresponds to a geographical

area in real world. The continuity of geographical area can be reflected by neighborhood relations of partition facets in same level. The neighborhood relationship also can be computed by their codes' binary operations. For example, the partition facets *A* and *B* have four kinds of neighborhood relationships, they are described as:

$$Neighboring-\mathrm{Re}lationship(A,B)\Leftrightarrow\begin{pmatrix} L_A=L_B,|M_A-M_B|=1 \\ L_A>L_B,\&M_A(i)=0,M_A(1,L_B)-M_B=1 \\ L_A>L_B,\&M_A(i)=1,M_B-M_A(1,L_B)=1 \\ L_A<L_B,\&M_B(i)=0,M_B(1,L_A)-M_A=1 \\ L_A<L_B,\&M_B(i)=1,M_A-M_B(1,L_A)=1 \end{pmatrix} \tag{2}$$

Here, $M_A(i)$ represents the bit i in code M_A of facet A, $M_A(i,j)$ represents the bit i to j of M_A, "-" represents binary subtraction, "&" represents binary union operation of bit.

3) Separation Relation

Using the previous method to discriminate on the two facets, if they are neither inclusion nor neighborhood relations, then the two facets will be for the separation relationship.

4) Experiments

Aiming at the above computing mode of remote sensing images, we carried out a verification experiment. Four facets aggregation results are shown in Figure 6.

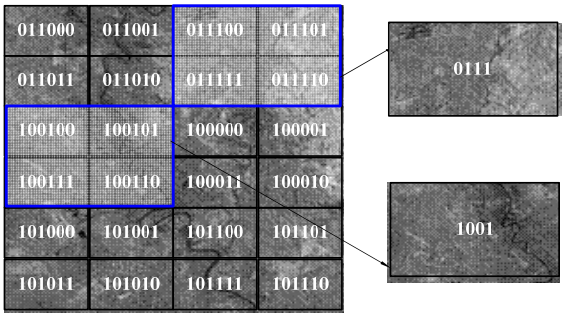

Figure 6. Four facets aggregation results

The results show that the proposed method can make use of partition facet template and achieve quick processing of remote sensing image. It will simplify computing task of remote sensing images, and easy to express and recognize the typical objects in remote sensing images. The computing mode is not dependent on vector structure, and it can directly analyze spatial relations using uniform partition codes. So it can improve the speed of browsing or displaying remote sensing images. But present experiment was done in single computer with four cores; we will focus on its efficiency in parallel processing computing cluster environment in further study.

B. Remote Sensing Template-based Partition Facet Computing

Partition template has characteristics and advantages of partition facet, and also has basic information of original remote sensing images. According to the applied requirements of EMD model and remote sensing images in different regions, many kinds of templates can be designed, such as control point templates for matching and feature templates for target retrieval.

The computing mode for images data is defined by partition facet template. It is based on basic spatial relations of inclusion, neighboring, apart, distance and corner-angle. It refers to some operations of remote sensing images in unit of facet, such as moving, changing, resizing, rotating, and restructuring and so on. It mainly includes operations in two directions; they are aggregation or split in longitude and extension or conversion in transverse.

1) Longitude computing mode

Aggregation operation means several facets in the same level gathered into a high-level facet. It mainly involves facets' position recombination and data structure adjustment. Splitting operation means a high-level facet is splitted into several facets of low-level. It mainly involves facet's segmentation, sub-facets rearrangement, high-precision images selection.

Suppose the number of facets is N, the number of facets' code will have bits of $logN$. So, the facets of A_1, A_2, ..., A_i $(i<=N)$ aggregate into one facet B, it can be described as:

$$\begin{aligned} L_B &= \mathrm{Min}\ (L_A(\mathrm{i}))-\log(\mathrm{N}) \\ M_{Bi} &= \&M_B, M_A(i)\oplus(j) \end{aligned} \tag{3}$$

Here, the mark $\oplus$ represents EXOR operation in binary. This formula can be repeated recursively by bit. The operation of one facet B split into A_1 , A_2, ..., A_i can be looked as reverse operation of it.

2) Transverse computing mode

Transverse computing mode is mainly among facet in the same level. It provides browsing and retrieval operations for remote sensing images. Extension operation represents facets directly stitching or mosaic and is composed of large temporary views. Conversion operation is corresponding to the specific operation of remote sensing images for moving, rotating, cropping.

3) Application Examples

Template-based partition facet parallel processing technology is based on the following typical technologies: partition processing of remote sensing data; forming

partition facet set; forming corresponding template according to partition facet; storing template; satisfying specialized needs. The typical applications include image retrieval, image real-time processing, and information fast compilation.

The application flow is shown in Figure 7.

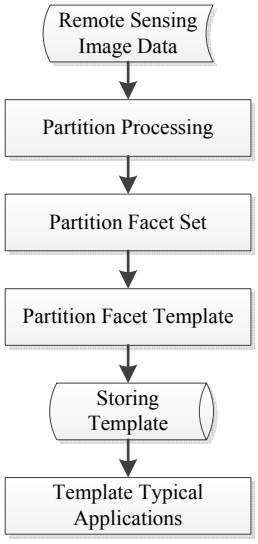

Figure 7. Partition template computing mode application flow

Based on the above information, people attempt to research the remote sensing data of the tourist sites by the template-based partition facet processing mechanism. They propose some typical applications. In the Ubuntu 12.04 server environment, people can use 5 DELL machines of quad cores to build small-scale parallel processing platform. People can select the remote sensing image of 2.5M, 5M, 10M as the original image data. People can process the remote images by partition and feature extraction, then forming partition-based template database. They can attain user interface design by VC++. Compared with other remote sensing image processing system, this small-scale application system has the advantages of fast image display and intuitive feature information. Meanwhile, it can be used for retrieving and presenting the original template in the regional images of different areas.

V. Conclusion

Remote sensing image data has been widely applied in many military and civilian fields. As the amount of data rises and application needs expand, the efficient organization and management of remote sensing data has become a bottleneck restricting the application of remote sensing technology. In this paper, we discussed GPT and EMD partition model, and proposed the conceptual model and data model of partition facet template. In addition, the template-based parallel processing flow was introduced and computing mode of partition facet was designed. We also emphasized how to realize special computing mode of remote sensing images basing basic spatial relation of subdivision facets. These operations are aggregation, split, extension and conversion. They provide underlying computing foundation and implementation premise for parallel computing of remote sensing image. This research paper plays an important role in speeding up visualization expressing, and target detecting, identifying and decision-making, and can reduce preparation time for spatial information. And it has some demonstration in the application of GPT.

Acknowledgment

This work was supported in part by a grant from National Natural Science Foundation of China under Grant No.U1304403 and No.61071121, Henan Science and Technology Program under Grant No.132102210398 and No.112102210079, Henan Basic and frontier Technology Research Program under Grant No.132300410349, Henan College Young Teachers Program under Grant No.2010GGJS-177, Xuchang University Young Teachers Program.

References

[1] Mather P M. “Computer Processing of Remotely- Sensed Images: An Introduction (3rd Edition)”. *Chichester: John Wiley & Sons*, 2004.

[2] CHENG Chengqi, REN Fuhu, PU Guoliang, etc. “Introduction to Spatial Information Partition Organization”. *Beijing: Science Press*, 2012.

[3] Guido Lemoine; Martina Giovalli. “Geo-Correction of High-Resolution Imagery Using Fast Template Matching on a GPU in Emergency Mapping Contexts”. *Remote Sens*. vol.5, no.9, pp.4488-4502, 2013.

[4] LI Deren, GONG Jianya, SHAO Zhenfeng. “From Digital Earth to Smart Earth”. *Geomatics and Information Science of Wuhan University*. vol.35, no.2, pp.127-132, 2010.

[5] LI Deren, Zhu Qing, Zhu Xinyan, etc. “Task-oriented focus on remote sensing information service”. *Beijing: Science Press,* 2010.

[6] LI Deren, YI Huarong, JIANG Zhijun. “Introduction and Analysis of Grid Technology”. *Geomatics and Information Science of Wuhan University*, vol.30, no.9, pp.757-761, 2005.

[7] Goodchild M. “Discrete Global Grids for Digital Earth”. *International Conference on Discrete Global Grids*, California: Santa Barbara, 2000.

[8] CHENG Cheng-qi, SONG Shu-hua, WAN Yuan-wei. “Preliminary Studies on Geospatial Information Code Model Based on Global Partition Model”. *Geography and Geo-Information Science*. vol.25, no.4, pp.8-11, 2009.

[9] TONG Xiaochong. “The Principles and Methods of Discrete Global Grid Systems for Geospatial Information Partition Organization”. *Acta Geodaetica et Cartographica Sinica,* vol.40, no.4, pp.536, 2011.

[10] Sahr K, White D, Kimmerling A. “Geodesic discrete global grid systems”. *Cartography and Geographic Information Science*, vol.30, no.2, pp.121-134, 2003.

[11] Dutton G. “A Hierarchical Coordinate System for Geoprocessing and Cartography: Working Through the Scales”. *Lecture Notes in Earth Sciences*, vol.79, Berlin: Springer-Verlag, 1999.

[12] YUAN Wen, ZHUANG Da-fang, YUAN Wu. “Some essential questions in remote sensing science and technology”. *Journal of Remote Sensing*. vol.13, no.1, pp.103-111, 2009.

[13] LI De-ren. “On Generalized and Specialized Spatial Information Grid”. *Journal of Remote Sensing*, vol.9, no.5, pp.513-520, 2005.

[14] DONG Fang, CHENG Chengqi, GUO Shide. "Research on Spatial Relationships Calculation Model Based on EMD Partition Architecture", *Acta Scientiarum Naturalium Universitatis Pekinensis*, vol.48, no.3, pp.444-450, 2012.
[15] CHI Zhanfu, CHENG Chengqi, GUAN Li, XIAO Qia. "Subdivision Integration Cataloguing Model of Geospatial Information Based on the Extended Model of Mapping Division". *Geography and Geo-Information Science*, vol.25, no.6, pp.26-29, 2009.
[16] CHENG Cheng qi, GUAN Li ."The Global Partition Grid Based on Extended Mapping Division and Its Address Coding". *Acta Geodaetica et Cartographica Sinica*, vol.39, no.3, pp.295-302, 2010.
[17] GUAN Li, LV Xuefeng. "Properties Analysis of Geospatial Partition Grid Framework for Spatial Data Organization". *Acta Scientiarum Naturalium Universitatis Pekinensis*, vol.48, no.1, pp.123-132, 2012.
[18] Xiong Delan, Du Genyuan. "Research on Remote Sensing Image Template Processing Based on Global Partition Theory". *International Journal of Computer Science Issues*, vol.10, no.1, pp.388-392, 2013.
[19] DU Gen-yuan, MIAO Fang, XIONG De-lan. "Service Model of Spatial Data Storage Scheduling Based on Partition Theory". *Computer Science*, vol.39, no.8, pp.263-267, 2012.
[20] Craig A. Lee, Samuel D. Gasster, Antonio Plaza, Chein-I Chang, Bormin Huang. "Recent Developments in High Performance Computing for Remote Sensing: A Review". *IEEE Journal Of Select Topics In Applied Earth Observations And Remote Sensing*, vol.4, no.3, pp.508-527, 2011.
[21] A. Plaza, J. Plaza, H. Vegas. "Improving the performance of hy-perspectral image and signal processing algorithms using parallel, distributed and specialized hardware-based systems". *Signal Process System*, vol.61, pp.293-315, 2010.
[22] Hongping Wang, Juan Zhang, Xiuguo Liu, Xiaodong Huang. "Parallel algorithm design for remote sensing image processing in the PC cluster environment".*10th International Conference on Geoinformatics*, pp.1-5, 2010.
[23] M. Li, M. Chen, J. Xie. Cloud computing: "A synthesis models for resource service management". *2nd International Conference On Communication Systems, Networks and Applications*, vol.2, pp.208-211, 2010.

Gen-yuan Du was born in PR China, in1974. He is currently an Associate Professor in the college of Computer Science and Technology at Xuchang University. He received P.D. degree in Earth Exploration and Information Technology from Chengdu University of Technology, PR China, in 2011, and the M.E. degree in Signal and Information Processing from Chengdu University of Technology, PR China, in 2005, and the B.S. degree in Computer Science and Technology from Henan Normal University, PR China, in 1997. His research interests include remote sensing image processing, remote sensing and computer networks.

Mr. DU Gen-yuan is a member of the CCF.

Delan Xiong was born in PR China, in1980, Female, Master Degree achieved in 2006, Instructor, member of China Computer Federation, more than 10 papers published in Chinese journals, mainly research in Spatial Information Technology, Compute and Information Technology Education.

Mrs. Xiong Delan is a member of the CCF.

Huolin Zhang was born in PR China, in1980, Male, Master Degree achieved in 2005, Instructor, member of China Computer Federation, mainly research in Spatial Information Technology, Parallel Computing.

Mr. Zhang Huolin is a member of the CCF.

A Novel Sink Mobility Off-line Algorithm for Avoiding Energy Hole in Wireless Sensor Network

Qing-hua Li, Qiao-ming Pan, Fu-ping Xie
Institute of Technology, Lishui University, Lishui 323000, Zhejiang China;
Email: netow@163.com

***Abstract*—In multi-hop data collection sensor network, nodes near the sink need to relay remote data, thus, have much faster energy dissipation rate and suffer from premature death. This phenomenon cause energy hole near the sink, seriously damaging the network performance. In this paper, we propose sink mobility with adjustable communication range to avoid the energy hole. First of all, we compute energy consumption of each node when sink is set at any point in the network through theoretical analysis. Based on detailed analysis of factors that affect the network life, the paper proposes an off-line centralized algorithm to compute the theoretically optimal track of the movements of sink, the number of halt positions, as well as the available maximum network lifetime. Theoretical analysis and experimental results show that the proposed algorithms improve significantly the lifetime. It lowers the network residual energy by more than 30% when it is dead. Moreover, the cost for moving the sink is relatively smaller.**

***Index Terms*—wireless sensor networks; energy hole; mobile sink; network life; load balancing**

I. INTRODUCTION

Wireless sensor nodes usually cannot be replaced or re-allocated energy in wireless sensor network, and most applications need to ensure long-term monitoring of certain areas (Most applications have pre-specified lifetime requirements), for example, the application mentioned in reference [1, 2] require that the effective monitoring time for the network should be greater than 9 months. To extend the life of sensor network, thus, is of great significance.

However, researching to improve the network life is of great challenges. There is a sensor network-specific "energy hole" phenomenon, which refers to premature death of those nodes in the hotspot. In multi-hop data collection sensor network, nodes near the sink have to suffer more routing load [3], so the energy consumption level is higher than nodes in other regions. This is known as the hotspot. Those nodes die because of earlier running out of energy and will form energy hole [3]. Consequently, nodes near the energy hole are required to bear the data load of those death nodes so that the energy consumption level will increase more rapidly, leading to extension of the hole, which is called funneling effect [3], and finally premature death or standstill of the entire network. Study shows that because of the impact of the energy hole, the network residual energy is as high as 90% [4, 5, 6] when the network is out of function.

Different from the general network with static sink, intelligent mobile robots can act as a mobile sink in the network to collect data. when the residual energy near sink become small, sink repeatedly move to the location with more abundant remaining energy so as to achieve a balanced energy consumption rate among the entire network ,avoiding the energy hole and obtaining longer network lifetime.

There are many existing researches handling energy hole problem. They can be divided into two categories based on the sink mobility: static sink network (for short, static sink) and mobile sink network (for short, mobile sink).The research in mobile sink can be summarized into the following categories:

(A) Relay nodes: Such method is to use relay node in hotspot to avoid energy hole. Relay nodes can be both stationary and mobile. The role of mobile relay nodes is essentially similar with that of mobile sink. Related research can be found in the literature [1].

(B)Single mobile sink: In this kind of network there is only one sink. Luo puts forward a strategy that mobile sink moves along the anchor (anchor points) to collect data in [7]. The main idea is: when sink stays in an anchor it collects data and gets the situation of energy consumption over the whole network in order to determine the interval to stay in every anchor.

Reference [8] presents a mobile sink trajectory optimization algorithm and the main idea is: At first, the mobile sink moves along a straight line and collect information about network data and energy consumption information. Mobile sink then adjust the trajectory using the latest information collected in the process of data collection so that the mobile sink move near the nodes in order to reduce the cost of data communication, and thus to form an optimal trajectory of sink. The paper discusses random movement, forecast movement as well as the network performance of different modes of data collection patterns (passive, multi - hop, limited multi-hop).

(C) Multiple mobile sinks [9]: Compared with single mobile sink, multiple mobile sinks will increase the cost of the network, but the network performance (network

doi:10.4304/jcp.9.6.1454-1461

lifetime, network delays) can be greatly improved and, therefore, is subject to a wide range of research. However, mobile sinks requires mutual cooperation and mutual coordination of movement between several sinks, and thus the study is more complicated than research of single mobile sink.

Despite of a lot of research on the mobile sink, different from previous studies, the main contribution of this paper is as follows:

Based on accurate analysis of energy consumption, we propose a better mobile sink strategy. Previous study indicates that areas near the sink suffer relatively higher energy consumption. Therefore, it is only needed to consider energy consumption within the scope of the one-hop distance from current sink for locations of choice [10]. However, we cannot simply believe that. As shown below in Figure 1 (A) and (B), when located at point (x, y), the actual energy consumption map of network is a changeable surface with various shape after conducting one round of data collection. Therefore, the map of total energy consumption after sink moving to different locations is the superposition of cost energy in every single round. Figure 1 (C) is a total energy expenditure map after sink move through five different anchors. So when choosing the location of next sink, it is needed to consider the network energy consumption not only before moving, but also after sink is at its new location, rather than only near the sink(Or within one hop distance). Accordingly, hotspots may appear in arbitrary area in the network. This paper propose centralized sink mobile strategy which consider the energy consumption of the entire network to get optimal trajectory, location of sink as well as the maximal network lifetime.

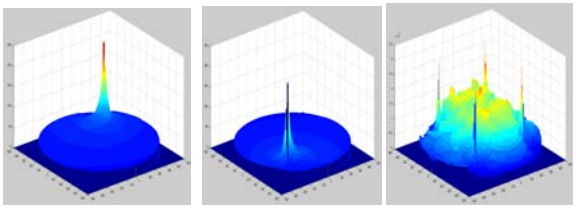

(A) (B) (C)

Figure 1. Energy consumption of mobile sink network

The organization of this paper is as follows: Section 2 introduces relevant research. Section 3 presents discussion of the network model and describes the problem. Section 4 introduces characteristics of data forwarding and energy consumption. It is the basis of theoretical research of our paper. Section 5 discusses the centralized sink mobile strategy. Section 6 discusses performance and experimental comparison. Section 8 is a summary of the whole paper.

II. Network Model and Problem Description

Network architecture model: we apply the module similar with reference [6, 7], a typical wireless sensor network for cyclical data collection, a circle with radius of R, see Figure 2. In this network, there are n nodes, $\{N_0, N_1, N_2, N_3, \ldots N_n\}$, N_0 stands for sink and it can move throughout the network, others represent work nodes and cannot move after initially deployed. Communication range of nodes, is noted with r, the difference from general sensor networks is that the transmission range is changeable, and nodes automatically adjust its communication range based on the distance between two nodes, for example, Berkeley Motes node has 100 transmission levels [6, 10]. Each work node will sense data in each cycle. We use the mature shortest path protocol for collecting data [11] and sending them to sink with multi-hop [11, 12].

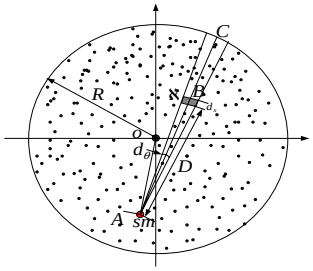

Figure 2. Network computing model

Energy consumption model: We use typical energy consumption model, the cost of moving mobile sink is calculated according to formula 1 , cost for sending data is calculated according to formula 2, cost for receiving data see formula 3, specific details can be found in literature [5].

$$E_{\sin k}(s) = sE_e \quad (1)$$

$$\begin{cases} E_{member} = lE_{elec} + l\varepsilon_{fs}d^2 \ \ if d < d_0 \\ E_{member} = lE_{elec} + l\varepsilon_{amp}d^4 \ \ if d > d_0 \end{cases} \quad (2)$$

$$E_{Rx}(l) = lE_{elec} \quad (3)$$

The cost for sending l bit of data can refer to 2. E_{elec} stands for the energy loss of firing circuit. If the transmission distance is less than the threshold d_0, power amplifier loss is based on free-space model; when the transmission distance is greater than or equal to the threshold value, it uses of multi-path attenuation model. ε_{fs}, ε_{amp} represent the power for these two models' amplification respectively. Energy for receiving l bit of data refers to formula 3. In this paper, the above specific parameters come from the literature [5].

Problem Description: For a given mobile sensor networks shown in Figure 2, the problem can be described as: how to choose the anchors of mobile sink to maximize the network lifetime. Here we term the rounds of data collection till the first node die as the network lifetime [5, 10].

III. Analysis of Energy Consumption

A. Data Load Computing

When the sink moves to an arbitrary location such as (x_0, y_0), if it is able to calculate the data load of each node , it then will be easy to calculate the energy consumption of each node based on formula 2 and 3 so as to learn energy consumption of the entire network.

Therefore, this paper will compute data load for each sensor node when sink is located at arbitrary (x_0, y_0).To the best of our knowledge, this paper gives derivation of data load in the network. It is also the basis for sink strategy in this paper.

Theorem 1: *Suppose the center of network be O (0,0), sink has moved to A(x_0, y_0), an optional sensor node B at (x_b, y_b), and the intersection point of AB extension with the network border is (x_c, y_c), then the data load for B node is as follows:*

$$\begin{cases} D_t^x = 1+\{(a-1-i)c + \frac{(a-i-1)(a+i)r}{2}\}/(ir+c) \quad \text{// if} \\ D = ir+c \mid i \in \{0..a\},\ c \in \{b..r\} \text{ // data sent} \\ D_r^x = \{(a-1-i)c + \frac{(a-i-1)(a+i)r}{2}\}/(ir+c) \quad \text{// if} \\ D = ir+c \mid i \in \{0..a\},\ c \in \{b..r\} \text{ //data receive (4)} \\ D_t^x = 1+((a-i)c + \frac{(i+1+a)(a-i)r}{2})/(ir+c) \quad \text{// if} \\ D = ir+c \mid i \in \{0..a\},\ c \in \{0..b\} \text{ //data send} \\ D_r^x = ((a-i)c + \frac{(i+1+a)(a-i)r}{2})/(ir+c) \quad \text{// if} \\ D = ir+c \mid i \in \{0..a\},\ c \in \{0..b\} \text{ // data receive} \end{cases}$$

Note: $R_1 = |AC|, \alpha = \left\lfloor \frac{R_1}{r} \right\rfloor, R_1 = \alpha r + b \mid b \le r$.

$D = |AB| = ir + c \mid i \in \{0..\alpha\}, i = \left\lfloor \frac{D}{r} \right\rfloor, c = D - ir, c \in \{0..r\}$.

$|AC| = \sqrt{(x_c - x_0)^2 + (y_c - y_0)^2}$,

$|AB| = \sqrt{(x_b - x_0)^2 + (y_b - y_0)^2}$.

Proof: This paper applies the shortest path routing protocol to transmit data to sink through multi-hop. For an arbitrarily node $B(x_b, y_b)$,see Figure 2, C represents intersection point of AB extension with the network border, the data load for B is the amount of data whose distance from B is integer multiple of r on line BC. First, we calculate the coordinates of C (x_c, y_c).

Equation of line AB: $y = \frac{y_b - y_0}{x_b - x_0}(x - x_0) + y_0$ (5)

Equation of the circle: $x^2 + y^2 = R^2$ (6)

Formula 5 can be simplified as: $y = \frac{y_b - y_0}{x_b - x_0}(x - x_0) + y_0 =$

$\frac{y_b - y_0}{x_b - x_0} x - \frac{y_b - y_0}{x_b - x_0} x_0 + y_0$

Let $g_1 = \frac{y_b - y_0}{x_b - x_0}, g_2 = -\frac{y_b - y_0}{x_b - x_0} x_0 + y_0 = y_0 - g_1 x_0$

$y = g_1 x + g_2$, we can work out (x_c, y_c) by substituting it in formula (6):

$$(1 + g_1^2)x^2 + 2g_1 g_2 x + g_2^2 - R^2 = 0$$

Solving the coordinates of C can be divided into several situations as follows:

First: when $x(i) \neq x_0$

coordinates of C is as follow:

$$\begin{cases} x_c = \frac{-2g_1g_2 \pm \sqrt{(2g_1g_2)^2 - 4(1+g_1^2)(g_2^2 - R^2)}}{2(1+g_1^2)} \\ y_c = g_1 \frac{-2g_1g_2 \pm \sqrt{(2g_1g_2)^2 - 4(1+g_1^2)(g_2^2 - R^2)}}{2(1+g_1^2)} + g_2 \end{cases}$$

Note: $g_1 = \frac{y_b - y_0}{x_b - x_0}$, $g_2 = -\frac{y_b - y_0}{x_b - x_0} x_0 + y_0$

if $x_b < x_0$ *then*

$$x_c = \frac{-2g_1g_2 - \sqrt{(2g_1g_2)^2 - 4(1+g_1^2)(g_2^2 - R^2)}}{2(1+g_1^2)}$$

$$y_c = g_1 \frac{-2g_1g_2 - \sqrt{(2g_1g_2)^2 - 4(1+g_1^2)(g_2^2 - R^2)}}{2(1+g_1^2)} + g_2$$

if $x_b > x_0$ *then*

$$x_c = \frac{-2g_1g_2 + \sqrt{(2g_1g_2)^2 - 4(1+g_1^2)(g_2^2 - R^2)}}{2(1+g_1^2)}$$

$$y_c = g_1 \frac{-2g_1g_2 + \sqrt{(2g_1g_2)^2 - 4(1+g_1^2)(g_2^2 - R^2)}}{2(1+g_1^2)} + g_2$$

Second: when $x_b = x_0$

if $y_b = y_0$ *then* this is the sink itself, no data needs to be sent

if $y_b \neq y_0$ *then* $x_c = x_0$ $x_c^2 + y_c^2 = R^2$

if $y_b > y_0$ *then* $y_c = \sqrt{R^2 - x_c^2}$

if $y_b < y_0$ *then* $y_c = -\sqrt{R^2 - x_c^2}$

According to coordinate of C, the length of line AC is:

$|A\overline{C}| = \sqrt{(x_c - x_0)^2 + (y_c - y_0)^2}$

the length of line AB is:

$|A\overline{B}| = \sqrt{(x_b - x_0)^2 + (y_b - y_0)^2}$.

Let: $R_1 = |AC|, \alpha = \left\lfloor \frac{R_1}{r} \right\rfloor, R_1 = \alpha r + b \mid b \le r$.

$D = |AB| = ir + c \mid i \in \{0..\alpha\}, i = \left\lfloor \frac{D}{r} \right\rfloor, C = D - ir, c \in \{0..r\}$.

Data load of B is calculated as follows. Its distance from sink is: $D = |A\overline{B}| = ir + c \mid i \in \{0..a\}, x \in \{0..b\}$.

Then check sector area $\aleph$ with angle of $d\theta$, width of dx (See figure 2).The dimensions of this area is approximately: $\aleph_s = Dd\theta dx$ .The number of nodes in

this ring is: $\rho\ Dd\theta dx$ .If it is located in the $\{ir\ ..\ ir+b\}|i\in\{0..a\}^{th}$ ring,that is to say, the location is :D=$ir+c \mid i\in\{0..a\}$, $c\in\{0..b\}$, then data load of ℵ is:

It is responsible to forward all the remote data in sector area whose width is dx and is integer multiple of r away from ℵ . The dimension of these areas can be computed as:

$$d\theta((i+1)r+c)dx+d\theta((i+2)r+c)dx+$$
$$d\theta((i+3)r+c)dx+\ldots d\theta(\mathrm{a}r+c)dx$$
$$=d\theta\ dx((\mathrm{a}\text{-}i)c+(\frac{(i+1+a)(a-i)r}{2}))$$

This is the dimension of area ℵ is responsible to forward data. Then data load of ℵ is:

$$d\theta\ dx((\mathrm{a}\text{-}i)c+(\frac{(i+1+a)(a-i)r}{2}))\rho .$$

Data sent is: $\{(d\theta\ dx((\mathrm{a}\text{-}i)c+(\frac{(i+1+a)(a-i)r}{2}))+d\theta(ir+c)dx\}\rho$.

It can be assumed that the data load is uniformly shared by each node in a very small region. Then data load of each node is:

$$d\theta\ dx((a\text{-}i)c+(\frac{(i+1+a)(a-i)r}{2}))\rho/d\theta\ (ir+c)$$
$$dx\ \rho=((a\text{-}i)c+(\frac{(i+1+a)(a-i)r}{2}))/(ir+c).$$

Data sent is:$\{(d\theta\ dx(\mathrm{a}c+(\frac{(1+a)ar}{2}))+d\theta(ir+c)dx\}\rho/$
$d\theta(ir+c)dx\}\rho=1+((a\text{-}i)c+$
$(\frac{(i+1+a)(a-i)r}{2}))/(ir+c)$

If D=$ir+c \mid i\in\{0..\mathrm{a}\}, c\in\{\mathrm{b}..r\}$ is located in the $\{ir+b, ir+r\}^{th}$ ring data load of ℵ can be computed as following:

It is responsible to forward all the remote data in sector area whose width is dx and is integer multiple of r away from ℵ . The dimension of these areas can be computed as:

$$d\theta((i+1)r+c)dx+d\theta((i+2)r+c)dx+d\theta((i+3)$$
$$r+c)dx+\ldots d\theta((\mathrm{a}\text{-}1)r+c)dx$$
$$=d\theta\ dx((a\text{-}i\text{-}1)c+(\frac{(a-i-1)(a+i)r}{2}))$$

Then data received by ℵ is:

$$d\theta\ dx((a\text{-}i\text{-}1)c+(\frac{(a-i-1)(a+i)r}{2}))\rho .$$

Data sent:

$$\{(d\theta\ dx((a\text{-}i\text{-}1)c+(\frac{(a-i-1)(a+i)r}{2}))$$
$$+d\theta\ c\ dx\}\rho$$

It can be assumed that the data load is uniformly shared by each node in a very small region. Then received data of each node is:

$$\{(a\text{-}1\text{-}i)c+(\frac{(a-i-1)(a+i)r}{2})\}/(ir+c).$$

Data sent is:

$$1+\{(a\text{-}1\text{-}i)c+(\frac{(a-i-1)(a+i)r}{2})\}/(ir+c)$$

B. Computing Node Energy Consumption

Corollary 1: *Note the transmission range r with $f_r^i(x)$,sink has moved to A(x_0, y_0),an arbitrary node B(x_b, y_b),then the energy consumption of node B is:*

$$\begin{cases} f_r^i(x)=\mathrm{D_r}\times E_{elec}+\mathrm{D_t}\times E_{elec}+\mathrm{D_t}\times\varepsilon_{fs}\ x^2 \\ \quad if\ \ x<d_0\ and\ i=0 \\ f_r^i(x)=\mathrm{D_r}\times E_{elec}+\mathrm{D_t}\times E_{elec}+\mathrm{D_t}\times\varepsilon_{amp}\ x^4 \\ \quad if\ \ x\ge d_0\ and\ i=0 \\ f_r^i(x)=\mathrm{D_r}\times E_{elec}+\mathrm{D_t}\times E_{elec}+\mathrm{D_t}\times\varepsilon_{fs}\ r^2 \\ \quad if\ \ r<d_0\ and\ i\neq 0 \\ f_r^i(x)=\mathrm{D_r}\times E_{elec}+\mathrm{D_t}\times E_{elec}+\mathrm{D_t}\times\varepsilon_{amp}\ r^4 \\ \quad if\ \ r\ge d_0\ and\ i\neq 0 \end{cases} \quad (7)$$

Proof: According to Theorem 1, the amount of received data of nodes D=$ir+x$ away from the sink is D_r, the amount of sent data is D_t=D_r+1.Substituting them in energy formula 1 and 2 will lead to ***Corollary 1***.

Based on *Theorem 1* and *Corollary 1*, Figure 3 shows the energy consumption under different sink locations and different r . As we can be seen from the figure, the energy consumption of mobile sink is very complex. So it requires careful planning for moving sink.

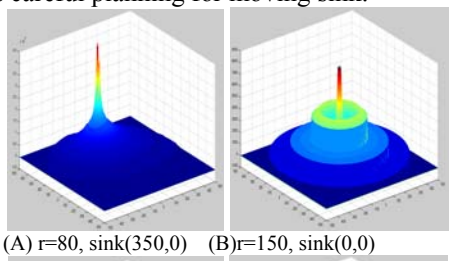

(A) r=80, sink(350,0) (B)r=150, sink(0,0)

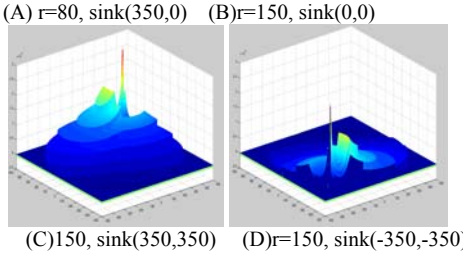

(C)150, sink(350,350) (D)r=150, sink(-350,-350)

Figure 3. Energy consumption of network (R = 500)

IV. OFF-LINE ALGORITHM FOR MOBILE SINK

From our analysis on factors affecting the network lifetime, many factors interfacing with each other make the mobile sink very complex NP-complete problem. Therefore, this section presents an off-line heuristic

algorithm to compute the movement of mobile sink. The central idea of the algorithm is:

First of all, we can obtain the network lifetime as *rounds* under optimal parameters when sink is located in the center. It is obvious that the network life will not be worse than *rounds* regardless of the mobile sink strategy. Sink moving along the circle trajectory has proven to be the best. If sink only collects data for one round at each anchor, the number of anchor is equal to the network life. If we can calculate the largest life of each trajectory, then parameters allows the largest lifetime is the result.

In this paper the idea of the heuristic algorithm is: For each mobile trajectory (trajectory will be divided into discrete value in accordance with the application requirements) compute the largest network lifetime under each transmission radius as the *r* energy, then the maximum of *r* energy is the result.

Method for calculating is: set the current track radius as Rm, transmission range r, uniformly choose *rounds* node on current track, *rounds* is the best lifetime under optimal parameters when sink is located in the center. Sink conduct one round of data collection at each anchor. If the largest energy consumption is greater than the initial energy of nodes, it indicates no better lifetime of the network can be obtained under such r and Rm settings. Select the next transmission level and continue testing, if the largest energy consumption is less than the initial energy of nodes, it indicates better lifetime can be obtained under such r and Rm values. Algorithm will seek the next stop and conduct a new round of data collection. If the largest energy consumption is less than the initial energy, then the largest network lifetime *rounds* = *rounds* +1, then algorithm continues to calculate the next stop. Repeat the above process until the largest energy consumption is not less than the initial energy of nodes, and then choose the next r, to continue testing until all r are tried, then we get the maximum network lifetime under trajectory Rm. Repeating the process can obtain lifetime under different Rm trajectory in order to get the greatest life of the whole network. *Algorithm 1* gives the description of optimizing mobile sink.

***algorithm 1*:**

Sink-Move_optimal (R, rbest, rounds,Rm) //pausing anchors for sink
1: compute lifetime rounds when sink static in centre
//compute the lifetime when sink is located at the center of network
2: Rtj = R; //the initial track is on the circumference
3: while Rtj>0;
4: r= r_{min}
5: while r<r_{max}
6: **Compute_**xy(rounds, R_{traj}, xy(n)) //caculate the pausing ahchor *rounds*
7: **trajectory_**Energy_compute(Rtj, r, xy(n), E(m,n))
//compute the energy consumption of the network
8: max_energy =max(E(m,n)) //get the location for largest energy consumption
9: if max_energy>Einit //lifetime under current parameters is less than *rounds* stop considering these parameters
10: r=next(r)
11: break;
12: end
13: while max_energy<Einit
14: **Compute_nextxy**(rounds, R_{traj}, xy(n+1)) //energy left, sink move to next anchor abd conduct new data collection
15: compute_energy(R,x(n+1),y(n+1),r,energy(m,n))
//add the energy of ne round data collection
16: E(m,n)= E(m,n)+ energy(m,n) //energy consumption for data collection
17: max_energy= max(E(m,n))
18: if max_energy<Einit
19: rounds = rounds +1 //this is the current maximum lifetime *rounds*
20: rbest=r // this is the current best r
21: Rm=Rtfj // this is the current best Rm
22: End if
23: end do
24: r=next(r) //try next r level for lifetime incensement
25: end do //end (4)
26: Rtj= Rtj-rtj // move track inside, try next Rm level for lifetime incensement
27: end do

Algorithm explanation: Compute_xy (rounds, Rtraj, xy(rounds)) is to get the *rounds* docking points on the trajectory of Rtraj, all the points are stored in xy(n) vector, the locations are requested to be evenly distributed on the trajectory, and this can be implemented by *algorithm 2*. Compute_nextxy (rounds, Rtraj, xy (rounds +1)) is the function for adding a new docking point to the already *rounds points* on the trajectory, the generated points are uniform and symmetric, due to space limitations, we omit it here. The complexity of the algorithm is |R| * |r| * m * n, of which |R| is the number of track, |r| is the number of node transmission level, m * n is the number of grid after meshing the network. |r| is affected by the physical characteristics of the network. Other parameters are relevant with accuracy of actual application. If the application needs high precision, then number of grid and |R| increase and the algorithm complexity become higher and vice versa.

algorithm 2:

Compute_xy(rounds, R_{traj}, xy(rounds)) //compute the *rounds* anchors
1: i=1
2: Do While (i <= rounds)
3: x = R_{traj} * Sin(aa)
4: y = R_{traj} * Cos(aa)
5: xy(i)=(x,y)
6: end do

V. Performance Analysis and Experimental Results Comparison

This paper apply OMNET ++ to carry out experiments, OMNET + + is an open network simulation platform

which is open source, component-based and modular for large network and has been widely recognized by the academic community [13]. Experimental parameters are shown at table 1 from the literature [5], if there is no special note.

A. Mobile Sink Network Performance Analysis and Experimental Comparison

LUO [7] claims that the optimal mobile trajectory is along the circle. We will justify the assertion and analyze the performance of sink on different route through theoretical and experimental verification. The main parameters of first scenes are as follows: Network radius R = 500m; the number of anchor is 20; the number of nodes is 3000. It is easy to meet the conditions of 20 anchors in some applications. For example: Network radius R = 500m, each node generate 100bits of data in each cycle, sink conducts 100 round of data gathering for each anchor point. we can get 20 anchors and life expectancy of the network is about 2000.

Figure 4 shows the theoretical calculated value based on *Theorem 1* and *Corollary 1*. The experimental results show that energy cost for R_m =400m is less than that of R_m =500m, this indicates the circumference is not necessarily the best migrating route, and it is determined by real application.

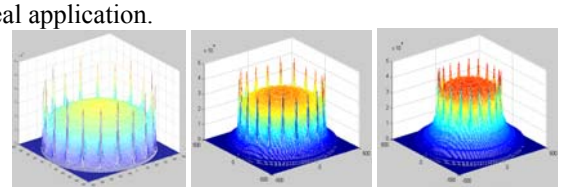

(A)R=500,Rm=500 r=85, anchors=20 max energy=50597
(B)Rm=400 max energy=45749
(C) Rm=300 max energy= 46619

Figure 4 Optimal network lifetime when sink track is in the circle (theoretical results)

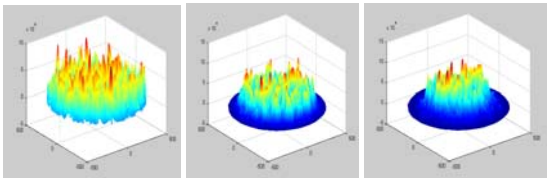

(A)R=500,Rm=500 r=85, anchors=20, max energy=58692
(B)Rm=400 max energy=53068
(C) Rm=300 max energy=54078

Figure 5. Optimal network lifetime when sink track is in the circle (experimental results)

Figure 5 is experimental results under the same scene. The experimental results are accordant with theoretical results. The theoretical results are based on the assumption that nodes are evenly deployed. However, nodes are randomly deployed in the experimental network. In fact the nodes are usually unevenly distributed. Therefore, data load of particular nodes may be higher and the actual energy they spend is correspondently larger than theoretical calculation. In addition, the maximum energy cost is not as smooth and concentrated as the theoretical values. Instead, they are sporadic. This is because: nodes are discretely deployed, there are only 20 anchors in scene one, resulting in unbalanced energy consumption among nodes. Figure 5 is formed by numerically interpolating energy consumption of discrete node, thus, there are a series of small protrusions in areas of high energy consumption. However, the difference between experimental and theoretical results is about 10%, which is in line with reality.

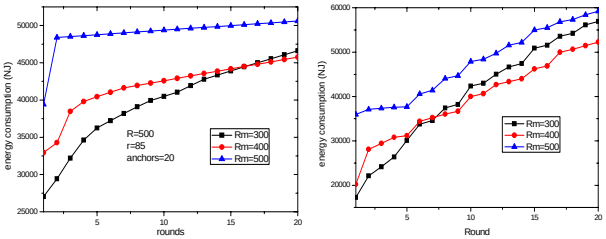

Figure 6. Maximum energy consumption under different trajectory (theoretical value, scene one)

Figure 7. Maximum energy consumption under different trajectory (experimental value, scene one)

Figure 6 shows the statistical chart of maximum energy consumption after each round of data collection .It can be seen from the chart that when sink moves along the circle, the maximum energy consumption after each round of data collection are all large. There is a cross between chart of R_m =400m and R_m =300m and the reason is: based on *Corollary 1*, the maximum energy consumption of R_m =300m is the smallest. So when the number of rounds is few, the maximum energy consumption is smaller. when the number of rounds is many, the energy consumption of nodes near the network centers after each round is high, so its energy consumption grows faster and finally is even higher than that of R_m =400m. Figure 7 shows experimental results, the overall trends and theoretical analysis are consistent.

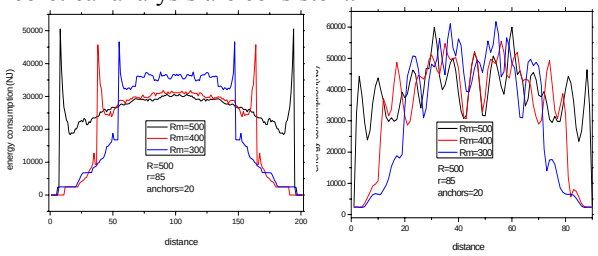

Figure 8. Profiles of energy consumption under different track (theoretical value, scene one)

Figure 9. Profiles of energy consumption under different track (experimental value, scene one)

Figure 8 shows the energy consumption of nodes on the diameter. From this figure it can be seen: in scene one, when sink move along the circle, nodes inside the track spend less energy than nodes on the track. As the track moves inward, energy consumption inside the track become higher. There is a best track to maximum the network lifetime. Figure 9 shows the experimental result. As the energy consumption in Figure 9 is of a selected diameter from figure 5 and Figure 5 is obtained by grid interpolation on the 3000 discrete values after gathering original data from 3000 nodes in experiment. Therefore the results of Figure 9 cannot include infinitely values as theoretically calculation in Figure 8 and some value is

generated by interpolation. If the selected straight line do not pass through the node with maximum energy cost, energy consumption of nodes on the trajectory is not necessarily the highest. In sum, The overall trend in Figure 9 is accordant with the theoretical results.

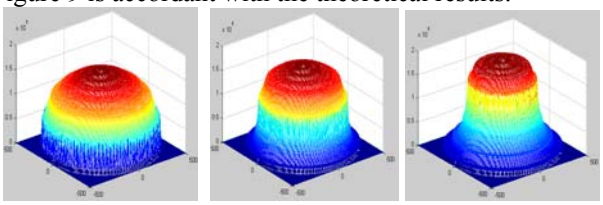

(A)R=500,r=85,Rm=500,rounds=100 max energy=157100
(B)Rm=400 max energy=170000
(C)Rm=300 max energy=191970

Figure 10. Optimal network lifetime when sink track is in the circle (theoretical result)

Figure 10 shows the energy consumption when sink trajectory respectively as R_m =500m,400m,300m and 100 anchors, sink gathers data for one round at each pausing anchor. As can be seen from the chart, when the sink is on the circular trajectory of the mobile network energy consumption of the network is the minimum and the network lifetime is the largest. Figure 11 shows the corresponding experimental results. When the number of the anchor increases, the experimental results get closer to the theoretical results. Although the experimental results of energy consumption is larger than the ideal theoretical calculation, but the difference between them is less than 10%, so it is in line with the theoretical calculation.

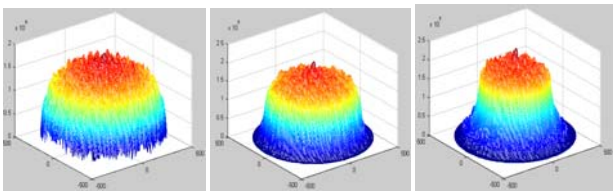

(A) R=500,r=85,Rm=500,rounds=100 max energy=165390
(B)Rm=400 max energy=185440
(C)Rm=300 max energy=209664

Figure 11. Optimal network lifetime when sink track is in the circle (experimental result)

Figure 11 shows the maximum energy consumption after each round of data gathering. The result shows that at the beginning of data collection, the smaller R_m is, the smaller maximum energy consumption and total energy consumption will be. However, with the number of round exceeding certain degrees, energy dissipation rate of node in the middle of the network become rapid when sink get closer to the center of the network. At this time, energy consumption is lower when sink moves along the circumference. Here we get maximum energy expenditure shown in Figure 12. Figure 13 shows the experimental result which is in line with the analysis.

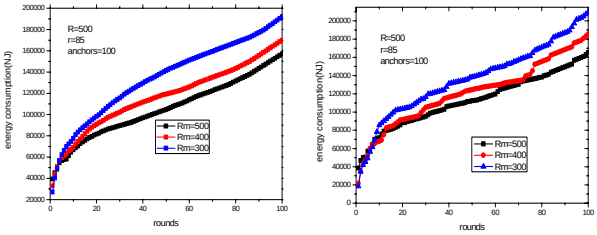

Figure 12. Maximum energy consumption under different trajectory (theoretical value, scene two)

Figure 13. Maximum energy consumption under different trajectory (experimental value, scene two)

B. Net Work Performance Comparison with Existing Mobile Sink Strategy

Next, we compare and analyze the efficiency of our mobile sink algorithm through experiments. Strategies discussed here include: 1) static sink [3]; 2) sink moves along the fixed circumference [7]; 3) Strategy proposed in this paper. We were referred to these three respectively as A, B and C strategy.

In order to fully contrast the effectiveness of experiment, all the algorithms should under the circumstances of optimal parameters. If only random settings of the parameters are compared, the comparison may be between the optimal performances of our algorithm with others' non-optimal state, and then the result is unconvincing. We first analyze the optimal parameters for static sink network.

The life span of the network depends on the lifetime of those nodes consuming the highest energy. Therefore, in order to prolong the life expectancy, measures have to be taken to minimize the energy cost of nodes that dissipate the most energy. This section analyzes how to choose a transmission range to minimize the maximum energy consumption among nodes in static sink network, which is to achieve longest life span.

In this paper, C is similar with B, the most crucial discrepancy between them is: strategy B consider that the best mobile track in circumference, while C proposed in this paper choose the optimal trajectory according to the case of the network. So, if the optimal trajectory is indeed in the circle, the strategy of this paper will track the movement of the sink in the circle election. Bu if the circle is not the best, strategy C will choose other optimal track, rather than circumference whose performance is worse. In theory, strategy C performs no worse than in the literature [7]. Next, we compare through experiment.

Figure 14 shows the results conducted in scene three: network radius R = 500m, 150 anchors, sink conducts one round of data gathering in each anchor. For strategy A, sink is fixed at the center, it consume the least when the transmission range is r = 170. Strategies B and C spend the least energy when sink moves along the circumference and the best communication radius is 85. Therefore the two strategies are the same. Figure 14 shows the theoretical experimental comparison between static sink and mobile sink. It can be seen from the figure, even when static sink is under the best network configurations, its energy consumption is much higher than the mobile sink .If the static sink communicate with the same radius 85 as mobile sink, energy consumption

will become higher. This indicates mobile sink network is much better than static sink network.

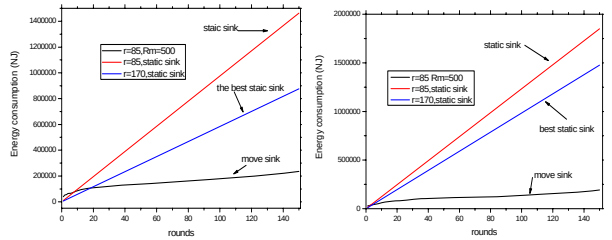

(A) Theoretical results (B) Experimental results

Figure 14. Energy consumption of different strategies (Scene three)

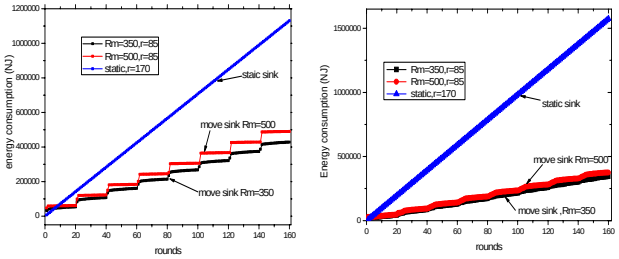

(A) Theoretical results (B) Experimental results

Figure 15. contrast between static sink, mobile sink (along circle) (Scene four)

Figure 15 shows the experimental results in scene four: network radius R = 500m, 20 anchors, sink conducts eight rounds of data collection at each anchor. For strategy A it is equal to sink collecting data for 160 rounds at the center, and strategy B migrates along the circular ,strategy C , however, moves along the track of Rm = 350m. The comparing chart between theory and experiment is shown in Figure 15. The strategy proposed in this paper, performs better than the other two strategies.

CONCLUSION AND DISCUSSION

The main contribution of this paper are: 1) presents a method to accurately calculate energy expenditure of the network when sink is located anywhere; 2) proposes a preferable off-line centralized mobile sink algorithms which can achieve better balanced energy consumption; In experiment section, we analyze the factors that affect network life in detail. The conclusion is of more general significance. As far as we know, there is no similar detailed analysis as in this article at present.

Although this article can present a more precise calculation of the energy consumption of the network, but the complexity of both of the centralized mobile algorithm and distributed mobile algorithm is still relatively large. Although we can calculate through unlimited sink energy, reducing the complexity of algorithm is worth further study.

ACKNOWLEDGMENT

This work was supported by China Postdoctoral Science Foundation 2012M511756

REFERENCES

[1] Wei Wang, Vikram Srinivasan, and Kee-Chaing Chua. Extending the lifetime of wireless sensor networks through mobile relays, IEEE/ACM Transactions on Networking, 2008,16(5):1108-1120.

[2] Ioannis Chatzigiannakis, Athanasios Kinalis,Sotiris Nikolets. Efficient data propagation strategies in wireless sensor networks using a single mobile sink, Computer Communications ,2008, 31(2):896–914.

[3] Anfeng Liu, Xin Jin, Guohua Cui, Zhigang Chen. Deployment Guidelines for Achieving Maximal Lifetime and Avoiding Energy Holes in Sensor Network, Information Sciences, 2013, 230:197–226.

[4] Olariu S, Stojmenovic I. Design guidelines for maximizing lifetime and avoiding energy holes in sensor networks wit h uniform distribution and uniform reporting .Proceedings of the IEEE INFOCOM. Barcelona , Spain , 2006 : 1-12

[5] Anfeng Liu, Zhongming Zheng, Chao Zhang, Zhigang Chen, and Xuemin (Sherman) Shen. Secure and Energy-Efficient Disjoint Multi-Path Routing for WSNs, IEEE Transactions on Vehicular Technology, 2012, 61(7):3255-3265.

[6] Hossain A, Chakrabarti S, Biswas P K. Equal energy dissipation in wireless image sensor network: A solution to energy-hole problem. Computers & Electrical Engineering, 2013, 39(6):1789-1799.

[7] Luo J, Hubaux J P. Joint sink mobility and routing to maximize the lifetime of wireless sensor networks: the case of constrained mobility[J]. IEEE/ACM Transactions on Networking, 2010, 18(3): 871-884.

[8] Ming Ma, Yuanyuan Yang.SenCar: An Energy-Efficient Data Gathering Mechanism for Large-Scale Multihop Sensor Networks, IEEE Transactions on Parallel and Distributed Systems, 2007,18(10):1476-1488.

[9] Mirela Marta, Mihaela Cardei. Improved sensor network lifetime with multiple mobile sinks,Pervasive and Mobile Computing, 2009, 5(5):542–555.

[10] Jian Li, Prasant Mohapatra. Analytical modeling and mitigation techniques for the energy hole problem in sensor networks[J],Pervasive and Mobile Computing, 2007,3(3):233-25

[11] EKICI E, GU Y, BOZDAG D. Mobility-based communication in wireless sensor networks. IEEE Communications Magazine, 2006,44(7): 56-62.

[12] C. Intanagonwiwat, R. Govindan, D. Estrin, J. Heidemann, and F. Silva, Directed diffusion for wireless sensor networking, *IEEE/ACM Trans .on Networking*, 2003,11(1):2–16.

[13] Varga A. The OMNET + + Discrete Event Simulation System. http://www.omnetpp.org,version 3.3

A Robust and Efficient Evolutionary Algorithm based on Probabilistic Model

Caichang Ding
School of Computer Science, Yangtze University, Jingzhou 434023, China
Email: hamigua_ping@hotmail.com

Wenxiu Peng
School of Computer Science, Yangtze University, Jingzhou 434023, China
Email: dianxin_1999@qq.com

***Abstract*—Evolutionary algorithms commonly search for the best solutions by maintaining a population of individuals that evolves from one generation to the next. The evolution consists of selecting a set of individuals from the population and applying, to some subsets of it, recombination operators that create new solutions. In this paper, Estimation of distribution algorithms arise as an alternative to genetic algorithms. Instead of exchanging information between individuals through genetic operators, Estimation of distribution algorithms use machine learning methods to extract relevant features of the search space through the selected individuals of the population. The replacement of crossover and mutation operators by probabilistic models can bring some benefits. The most important benefit could be that the structural component of the probabilistic model can provide explicit information about the interactions among the variables used to codify the problem solutions.**

***Index Terms*—interaction, machine learning, optimization, probabilistic model.**

I. Introduction

Looking for the best solutions to problems is not only a fundamental task for the development of mankind but also seems to be inherent to natural processes, and researchers have been able to see this. Proof of this is the emergence of evolutionary algorithms (EAs) to solve optimization problems regardless of the domain of application. This type of algorithms is mainly inspired by the way in which, according to Darwin [1], the adaptation of species to the environment is accomplished by nature. Nonetheless, other sources of inspiration from nature, such as the behaviors of ant colonies [2] or swarms [3], have also motivated the development of different EAs. Reciprocally, besides the inspiration of algorithms through the observation of nature, the study of such algorithms could provide us with a better understanding of nature.

EAs commonly search for the best solutions by maintaining a population of individuals (solutions) that evolves from one generation to the next. The evolution consists of selecting a set of individuals from the population and applying, to some subsets of it, recombination operators that create new solutions. A huge number of methods conforming to this framework have been developed. Therefore, the choice of the appropriate alternative for a particular application results in an important matter, as it may determine whether the problem is solved efficiently or, even, if the best solution is found at all.

Mathematically, optimization is the minimization or maximization of a given function. Hence, optimization problems can be formulated as,

$$x^* = \arg\max_x f(x), \tag{1}$$

where $f : S \to \mathrm{R}$ is called the objective function or fitness function, $x = (x_1, \ldots, x_n) \in S$ represents a possible solution of the problem and S is called the search space. The optimum x^* is not necessarily unique. We will assume that S is an n-dimensional discrete search space.

This paper is devoted to study a relatively new class of EAs: Estimation of distribution algorithms (EDAs) [4]. Based on the same principles of natural selection and evolution of populations, EDAs use explicit probability distributions to lead the search to promising areas of the search space instead of applying genetic operators of crossover and mutation used in genetic algorithms [5]. Throughout the paper, we will try to shed light on different open issues regarding EDAs. The final motivation is essentially to achieve a deeper understanding of this type of algorithms and their relationship with the optimization problems. To this end, novel methodological approaches and analyses have been conducted. The basic questions that have guided the elaboration of this work can be summarized as follows.

Firstly, the learning of probabilistic models to extract the relevant information that the selected individuals can contain about the problem is a fundamental step of the algorithm. Regarding this issue, we wonder how the search and the behavior of the EDA is influenced by the accuracy of the learning method.

Secondly, one of the most interesting properties of EDAs is their ability to capture and explicitly represent

doi:10.4304/jcp.9.6.1462-1469

interactions among the variables of the problems by means of the probabilistic models. Thus, investigating the relationship between the interactions of the problem variables and the structure of the probabilistic model is a question that arises naturally. Following this idea, we also wonder how the topology that these interactions provide determines the difficulty of the problem. More generally, the question of what makes a problem difficult for EDAs is an open question of undoubted interest.

Thirdly, a utopian goal is to know the limits of effectiveness of any search algorithm. Among other things, this type of knowledge would allow us to select the most adequate algorithm depending on the problem at hand. Coming back to more affordable issues, we wonder where the learning limits of EDAs are. We want to better understand when and why the learning step is not able to extract from the population the needed information to reach the optimum.

Fourthly, another fundamental issue regarding EDAs that we consider of special interest is to better understand how the probability of the optimum evolves during the generations. This is an essential characteristic of the algorithm which reflects how the problem is being solved. And finally, a more general issue that we keep in mind is the relationship that emerges between an EDA and the space of optimization problems. Regarding this issue, we consider the possibility of creating taxonomies of problems according to the different behaviors that an EDA can exhibit.

This introductory part will treat, as directly and briefly as possible, the theoretical background related with the paper. Thus, only Bayesian networks and EDAs are formally presented. Further details of any topic or scientific discipline related with the aforementioned elements, but not directly used throughout the paper, can be consulted in different works that will be cited in the appropriate places. In turn, the specific theoretical background that the different chapters could need, will be introduced in the corresponding points.

The rest of this paper is organized as follows. Estimation of distribution algorithms are introduced in section II. Section III presents Bayesian networks. Section IV discusses the parameters of the EDAs. At last, the summary is given in section V.

II. Estimation of Distribution Algorithms

Estimation of distribution algorithms [4][6] are a population-based optimization paradigm in the field of evolutionary computation [7]. Initially, a random sample of solutions is generated. These solutions are evaluated using the objective function, and a subset of candidate solutions is selected based on this evaluation. Hence, solutions with better function values have a higher chance of being selected. Then, a probabilistic model from the selected set is built and a new population is sampled from that model. The process is iterated until the optimum has been found or another termination criterion is fulfilled. The general scheme of the EDA approach is shown in Figure 1.

EDAs arise, in part, as an alternative to genetic algorithms [5]. Instead of exchanging information between individuals through genetic operators, EDAs use machine learning methods to extract relevant features of the search space through the selected individuals of the population. The replacement of crossover and mutation operators by probabilistic models can bring some benefits. For example, EDAs reduce the number of parameters involved and hence, the tune of the algorithm could become simpler depending on the scenario of application. Nevertheless, the most important benefit could be that the structural component of the probabilistic model can provide explicit information about the interactions among the variables used to codify the problem solutions.

$D_{t=0} \leftarrow$ Generate N individuals randomly
do
  $D_t \leftarrow$ Evaluate individuals
  $D_t^{Se} \leftarrow$ Select $M \leq N$ individuals from D_t according to a selection method
  $p_t(\boldsymbol{x}) = p(\boldsymbol{x}|D_t^{Se}) \leftarrow$ Estimate the joint probability distribution by means of a probabilistic model
  $D_{t+1} \leftarrow$ Sample M individuals from $p_t(\boldsymbol{x})$ and create the new population
  $t \leftarrow t+1$
until Stopping criterion is met

Figure 1. The general scheme of estimation of distribution algorithms.

With the aim of finding the optimal solution x^* and solving Problem in (1), EDAs use explicit probability distributions. At each iteration, the algorithm manages a probability distribution $p(X = x)$ of the random variable X taking values from the search space S. Thus, each of the possible problem solutions has an associated probability of being sampled which varies during the optimization process. The probability values assigned to the solutions are the main source in determining which one will be returned by the algorithm. Consequently, given a problem, the main goal is to get higher probability values for the highest quality solutions throughout an iterative process.

In the last decade, EDAs have acquired special relevance. Proof of this popularity is the development of new and more complex EDAs [8][9], the applications for these EDAs in different domains such as engineering [10], biomedical informatics or robotics [11] and the works which study fundamental issues in order to better understand how these algorithms perform [12].

Although there is a wide variety of EDA implementations, as an example, we present below the pseudocode of the univariate marginal distribution algorithm (UMDA), the tree-based estimation of distribution algorithm (Tree- EDA) and the estimation of Bayesian networks algorithm (EBNA). These algorithms will be considered in subsequent sections of the paper.

A. Univariate Marginal Distribution Algorithm

The univariate marginal distribution algorithm was introduced in [13]. This algorithm assumes that all the variables are independent. That is, the value of variable

X_i does not depend on the state of any other variable. Then, $p(x)$ can be factorized as follows:

$$p(x) = \prod_{i=1}^{n} p(x_i) \quad (2)$$

Figure 2 shows the steps of the UMDA. This algorithm has been successfully applied to different problems such as feature subset selection [14], learning of Bayesian networks from data [15], optimization of a composite video processing system [16], or to solve some linear and combinatorial problems using Laplace correction [17].

Theoretical results derived from the UMDA [4] expose its relationship with GAs, particularly with GAs that use uniform crossover. [18] have investigated some of the issues that explain the success of UMDA in the optimization of a wide class of functions. Other theoretical results have been obtained for UMDA in [19].

$D_{t=0} \leftarrow$ Generate N individuals randomly
do
  $D_t \leftarrow$ Evaluate individuals
  $D_t^{Se} \leftarrow$ Select $M \leq N$ individuals from D_t according to a selection method
  Calculate the univariate marginal frequencies $p_t^s(x_i)$
  $D_{t+1} \leftarrow$ Sample N individuals from $p_t(\boldsymbol{x}) = \prod_{i=1}^{n} p_t^s(x_i)$
  $t \leftarrow t+1$
until Stopping criterion is met

Figure 2. Pseudocode for UMDA.

B. Tree-based Estimation of Distribution Algorithms

Tree-based estimation of distribution algorithms [20] use factorizations that can be expressed by means of trees or forests. In particular, we will focus on the implementation. The pseudocode of this algorithm is shown in Figure 3 and will be called Tree-EDA. Although other methods can also be employed, the factorization is constructed using the algorithm introduced in [21] that calculates the maximum weight spanning tree from the matrix of mutual information between pairs of variables. Additionally, a threshold for the mutual information values is used when calculating the maximum weight spanning tree in order to allow disconnected components in the structural model.

$D_{t=0} \leftarrow$ Generate N individuals randomly
do
  $D_t \leftarrow$ Evaluate individuals
  $D_t^{Se} \leftarrow$ Select $M \leq N$ individuals from D_t according to a selection method
  Calculate the univariate and bivariate marginal frequencies $p_t^s(x_i)$ and $p_t^s(x_i, x_j)$ from D_t^{Se}
  Calculate the mutual information and learn the tree structure
  $D_{t+1} \leftarrow$ Sample N individuals from the tree
  $t \leftarrow t+1$
until Stopping criterion is met

Figure 3. Pseudocode for Tree-EDA.

C. EDAs based on Bayesian Networks

Throughout the paper, we pay special attention to EDAs that learn Bayesian networks. There are different implementations of this type of EDAs. The best known algorithms could be the following, such as learning factorized distribution algorithm (LFDA), Bayesian optimization algorithm (BOA) or estimation of Bayesian networks algorithm (EBNA). We mainly focus on the EBNA implementation whose pseudocode is presented in Figure 4.

$BN_{t=0} \leftarrow (\boldsymbol{s}_0, \boldsymbol{\theta}_{\boldsymbol{s}_0}^0)$ where $\boldsymbol{s}_0$ is an arc-less structure and $\boldsymbol{\theta}_{\boldsymbol{s}_0}^0$ is uniform
$D_{t=0} \leftarrow$ Generate N individuals from BN_0
do
  $D_t \leftarrow$ Evaluate individuals
  $D_t^{Se} \leftarrow$ Select $M \leq N$ individuals from D_t according to a selection method
  $\boldsymbol{s}_t \leftarrow$ Obtain a network structure
  $\boldsymbol{\theta}^t \leftarrow$ Calculate θ_{ijk}^t using D_t^{Se} as the data set
  $BN_t \leftarrow (\boldsymbol{s}_t, \boldsymbol{\theta}_{\boldsymbol{s}_t}^t)$
  $D_{t+1} \leftarrow$ Sample N individuals from BN_t and create the new population
  $t \leftarrow t+1$
until Stop criterion is met

Figure 4. Pseudocode for EBNA

In order to better understand how EDAs based on Bayesian networks perform, the characteristics of the learned probabilistic models are a rich source of information which has been studied in several works [22-25]. A straightforward form of analysis is through the explicit dependences between the variables they capture. Thus, it has been shown how different parameters of the algorithm influence the accuracy of the structural models [24], how the dependencies of the probabilistic models change during the search and, how the networks learned can provide information about the problem structure [23]. Moreover, the structural component of the model can be used to introduce available information of the structural characteristics of the problem [26].

III. Bayesian Networks

All the algorithms considered throughout the paper use factorizations that can be encoded by means of Bayesian networks . Bayesian networks, also called belief networks, are a class of probabilistic graphical model. This type of models have become a very popular paradigm to efficiently deal with probability distributions in modeling uncertain knowledge. One of the most important sources of the development of Bayesian networks was the field of expert systems. In addition, over the last few years, Bayesian networks have received considerable attention from the machine learning community. As a result of this interest, many publications and tutorials have appeared. Thus, besides expert systems, the applications of Bayesian networks include classification problems, optimization or bioinformatics.

As any other probabilistic graphical model, Bayesian networks are the result of combining probability and graph theory. The graphical component of the model encodes a list of conditional independences [27-28]

associated to the probability distribution. Let $X=(X_1,\ldots,X_n)$ be an n-dimensional discrete random variable. A Bayesian network is a graphical representation of the factorization of the joint probability distribution for X, $p(X=x)$, where $x=(x_1,\ldots x_n)$ denotes an assignment of the variable X. More specifically, a Bayesian network can be defined as a pair (s,θ_s) where s is a directed acyclic graph (model structure) and θ_s is the set of parameters associated to the structure (model parameters). The structure s determines the set of conditional (in)dependences among the random variables of X. According to the structure s, the joint probability distribution $p(x)$ can be factorized by means of marginal and conditional probability functions. Specifically, the probability distribution factorizes according to the graph as,

$$p(x)=\prod_{i=1}^{n} p(x_i \mid pa_i) \tag{3}$$

where pa_i denotes a value of the variables Pa_i, the parent set of X_i in the graph s.

The local probability distributions of the factorization are those induced by the terms of the product that appears in (3). We assume that these local distributions depend on the parameters $\theta_s=(\theta_1,\ldots,\theta_n)$. Equation (3) can be rewritten specifying the parameters:

$$p(x \mid \theta_s)=\prod_{i=1}^{n} p(x_i \mid pa_i,\theta_i) \tag{4}$$

Assuming that the variable X_i has r_i possible values, the local distribution $p(x_i \mid pa_i^j,\theta_i)$ is an unrestricted discrete distribution:

$$p(x_i^k \mid pa_i^j,\theta_i)=\theta_{ijk} \tag{5}$$

where $pa_i^1,\ldots,pa_i^{q_i}$ denote the q_i possible values of the parent set Pa_i. The parameter θ_{ijk} represents the probability of variable X_i being in its k-th value, knowing that the set of its parents' variables is in its j-th value. Therefore, the local parameters are given by $\theta_i=((\theta_{ijk})_{k=1}^{r_i})_{j=1}^{q_i}$.

A. Bayesian Network Learning

In order to obtain a Bayesian network which allows us to represent and manage the uncertain knowledge of a specific domain, it is necessary to set both the structure and the parameters. The structure and conditional probabilities necessary for characterizing the Bayesian network can be provided either externally by experts, by automatic learning from datasets or by mixing both of these. We focus on the second approach. Moreover, when the model is automatically learned, it can provide us with insights into the interactions between the variables of the domain.

The learning task can be separated into two subtasks: structural learning and parameter learning. Although there are different strategies to learn the structure of a Bayesian network, we focus on the so-called score+search approach. This type of techniques deals with the structure learning as an optimization problem. Therefore, learning a Bayesian network can be enunciated as follows. Given a data set D with N cases, $D=\{x_1,\ldots,x_N\}$, searching the structure s^* such that,

$$s^*=\arg\max_{s\in S^n} g(s,D) \tag{6}$$

where $g(s,D)$ is the score or metric which measures the goodness of any given structure s with respect to the data set D, and S_n is the set of all possible directed acyclic graphs with n nodes. Some of the most relevant and used heuristic techniques such as greedy search, simulated annealing, genetic algorithms, estimation of distribution algorithms or ant colony optimization have been applied to this task.

One of the desirable properties of a metric or score is the decomposability in presence of complete data sets. These metrics can be decomposed in sub-metrics associated to each node X_i and its parents Pa_i in the graph s. Formally, any decomposable metric can be expressed as:

$$g(s,D)=\sum_{i=1}^{n} g_D(X_i,Pa_i) \tag{7}$$

where the function g_D is the sub-metric. Due to the decomposability, the local search methods are computationally more efficient because after adding an arc, we only need to evaluate the family of nodes affected by this change.

Although different learning methods are considered throughout the paper, a specific search algorithm will be generally used. It is Algorithm B [29]. This is a greedy search algorithm and the pseudocode is presented in Figure 5, where A is a data structure that stores the information needed to manage the addition of the candidate arcs. Basically, Algorithm B starts with an arcless structure and, at each step, adds the arc which improves the score the most. The algorithm finishes when there is no arc whose addition improves the score.

Start with an arcless structure
Compute $A[X_j \to X_i] = g_D(X_i, X_j) - g_D(X_i)$ for all distinct X_i, X_j
do
  Look for the largest $A[X_j \to X_i]$ and add that arc $X_j \to X_i$ to $\boldsymbol{s}$
  $A[X_j \to X_i] = g_D(X_i, \boldsymbol{Pa}_i \bigcup X_j) - g_D(X_i, \boldsymbol{Pa}_i)$ for all distinct X_i, X_j not belonging to $\boldsymbol{Pa}_i$
  $A[X_j \to X_i] = -\infty$
until Every $A[X_j \to X_i] < 0$

Figure 5. Pseudocode for Algorith B

Regarding the implementation of the score $g(s, D)$, different alternatives can be considered. Among the most used families of scores we can find marginal likelihood, penalized log-likelihood or information theory based scores. In the current section we will use the Bayesian Information Criterion score (BIC) [30] based on penalized maximum likelihood. This metric is obtained as follows. Given a dataset $D = \{x_1, \ldots, x_N\}$, we might calculate for any Bayesian network structure s the maximum likelihood estimate $\hat{\theta}_s$ for the parameters θ_s and the associated maximized log likelihood:

$$\begin{aligned} \log p(D \mid s, \theta_s) &= \log \prod_{w=1}^{N} p(x_w \mid s, \theta_s) \\ &= \log \prod_{w=1}^{N} \prod_{i=1}^{n} p(x_{w,i} \mid pa_i, \theta_i) \\ &= \sum_{i=1}^{n} \sum_{j=1}^{q_i} \sum_{k=1}^{r_i} \log(\theta_{ijk})^{N_{ijk}} \end{aligned} \quad (8)$$

where N_{ijk} denotes the number of cases in D in which the variable X_i has the value x_i^k and Pa_i has its j-th value. Since the maximum likelihood estimate for θ_{ijk} is given by $\hat{\theta} = \frac{N_{ijk}}{N_{ij}}$ where $N_{ij} = \sum_{k=1}^{r_i} N_{ijk}$, we obtain:

$$\log p(D \mid s, \hat{\theta}) = \sum_{i=1}^{n} \sum_{j=1}^{q_i} \sum_{k=1}^{r_i} N_{ijk} \log \frac{N_{ijk}}{N_{ij}} \quad (9)$$

The log-likelihood function is not used to guide the search process due to two main problems. Firstly, the log-likelihood is a monotonous increasing function with respect to the complexity of the model structure. Therefore, the use of this score to evaluate the quality of the structures during the search could lead us towards complete Bayesian networks. Secondly, as the number of parameters for each node increases, the error in the parameter estimation also increases. In order to overcome these difficulties, a penalty term is added to the log-likelihood. A general formula of the penalized log-likelihood is given by:

$$\sum_{i=1}^{n} \sum_{j=1}^{q_i} \sum_{k=1}^{r_i} N_{ijk} \log \frac{N_{ijk}}{N_{ij}} - h(N) dim(S) \quad (10)$$

where $dim(S)$ is the dimension (number of parameters needed to specify the model) of the Bayesian network with a structure s, i.e. $dim(S) = q_i(r_i - 1)$. $h(N)$ is a non-negative penalization function. The Jeffreys- Schwarz criterion, which is usually called BIC [30], takes into account $h(N) = \frac{1}{2} \log N$. Thus, the BIC score can be written as follows:

$$\begin{aligned} &BIC(s, D) \\ &= \log \prod_{w=1}^{N} \prod_{i=1}^{n} p(x_{w,i} \mid pa_i, \hat{\theta}_i) - \frac{1}{2} \log N \sum_{i=1}^{n} q_i (r_i - 1) \end{aligned} \quad (11)$$

On the other hand, parameter learning is the numerical assessment of the parameters θ_S that specify the conditional and marginal probability distributions of the factorization given by s. Although this task can be done by means of different approaches such as the Bayesian model averaging or the maximum a posteriori criterion [31], we use the maximum likelihood estimation. Specifically, once the structure has been learned, the parameters of the Bayesian network are calculated by using the Laplace correction as follows:

$$\hat{\theta}_{ijk} = \frac{N_{ijk} + 1}{N_{ij} + r_i} \quad (12)$$

B. Simulation

Once a Bayesian network is obtained, this model is able to provide us with specific probabilistic information of interest. Usually, the information that the practitioner wants to know is the probability of a certain event in the light of particular observations or evidence. The probabilities of interest are not usually stored in the Bayesian network at hand, they need to be computed. This process is known as probabilistic inference and, in the general case, it is an NP-complete problem [32].

Simulation (also called stochastic sampling) of Bayesian networks can be considered as an alternative to the exact inference. The simulation of any probabilistic graphical model consists of obtaining a sample from the probability distribution for X that the model encodes. Then, the marginal or conditional probabilities of interest can be estimated from the sample.

For our purposes regarding EDAs, the objective of the simulation of Bayesian networks is to obtain a dataset (new population) in which the probabilistic relationships between the random variables of the model are underlying. Particularly, in order to sample the Bayesian network, we consider a forward sampling method. A variable is sampled once all its parents have been sampled. This method is known as probabilistic logic

sampling (PLS). Figure 6 shows a pseudocode of this method.

$\pi \leftarrow$ Ancestral ordering of the nodes in the Bayesian network
for $j = 1$ to N
  for $i = 1$ to n
    $x_{j,\pi(i)} \leftarrow$ Randomly generate a value from $p(x_{\pi(i)}|pa_{\pi(i)})$
  done
done

Figure 6. Pseudocode of the probabilistic logic sampling method.

IV. Parameters of the EDAs

We have set a configuration of the EDA parameters which is often used throughout the paper. Therefore, this standard configuration is introduced here to avoid unnecessary repetitions.

According to the main scheme of the EDA, it works with populations of N individuals. The initial population is generated according to a uniform distribution, and hence, all the solutions have the same probability of being sampled. Each iteration starts by selecting a subset of promising individuals from the population. In this step we use truncation selection with a threshold of 50%. Thus, the $N/2$ individuals with the best fitness value are selected. The next step is to learn a probabilistic model from the subset of selected individuals. This is the only step where the algorithms that we will consider differ. Once the model is built, the new population can be generated. In order to do that, N new solutions are sampled from the probabilistic model and then they are added to the N individuals of the current population. The N best individuals, among the $2N$ available, constitute the new population.

As previously commented, every EDA considered in the paper uses factorizations that can be encoded by means of Bayesian networks. Therefore, the same approaches can be used both to obtain the corresponding parameters and to sample the new solutions. As explained above, the parameters are estimated by maximum likelihood and the new population is generated by PLS (see Figure 6).

V. Summary

This paper has been devoted to increase our comprehension about EDAs.

The relationship between the structure that the interactions of the problem variables provide and the structural models learned by the algorithm has been a issue. In this regard, we have seen that the structures that the algorithm learns during the search provide valuable information about the interdependences among the variables of the problem. This fact has been observed in other related works and it is considered as a distinctive feature of EDAs compared with other types of evolutionary algorithms. However, it has also been noticed that introducing a learning method that obtains the best Bayesian networks at each generation does not necessarily improve the performance of the algorithm. Nevertheless, with enough population size, this type of algorithm is able to obtain structures that provide much more information about the problem than the approximate learning.

When the algorithm is studied from the perspective of the probability of the optimum and the most probable solution, novel insights can be provided. The main elements of the algorithm that we have considered, which are the structural model and the population size, clearly influence the probability of the optimum and the most probable solution. Moreover, the patterns of behavior are constant in every optimization problem analyzed. For instance, using an adequate population size or an accurate structural model increases the probability of the optimum during the search in relation to the most probable solution, even in runs where the optimum is not reached. In addition, the function values of the most probable solution also reflect the influence of the population size and the structural model accuracy. The properties of the problem at hand, such as the multimodality, or even the difficulty that it entails for the algorithm, are reflected in this type of analysis. The experimental framework designed is not only useful to better understand EDAs but also to devise new improvements of the algorithm.

As previously commented, the relationship between the structure of the problem and the structural models used by EDAs is a issue. In this regard, different adjectives such as benign, malign, strong or deceptive have been used to describe the interactions among the variables of the problem and then, study their effect both in EDAs and other evolutionary algorithms. Although some attempts to formalize this type of concepts have been presented, we clearly need to conduct more research in order to understand and specify all the aforementioned terms in the context of optimization by means of EDAs.

Regarding the limits of effectiveness in EDAs, a more in-depth study should be carried out in order to increase the soundness of the conclusions. Thus, more accurate learning techniques, more sophisticated EDAs aided by niching or local searches, or even other approaches such as mixtures of evolutionary algorithms, should be tested under the same worst-case scenario. Then, analyzing the levels of problem difficulty that this type of algorithms successfully reaches, would be useful to better understand both the learning limits of EDAs and the limits of other search techniques. To complement the results obtained by using functions based on deceptive sub-functions, similar experiments could be conducted with other classes of functions such as Max-SAT or Ising. The role of the population in the limits of effectiveness of the algorithm was also discussed. We argue that a given population size can only contain useful information to solve problems to a certain degree of interaction among their variables. However, studies related with the information that the populations contain about the problem have hardly been considered. We believe that the formalization and study of this notion would be worthwhile.

The taxonomy of problems opens new research lines. First of all, some generalization such as the introduction of non-injective functions and general Bayesian networks could be developed. In addition, providing the needed definitions to deal with any type of selection scheme could also be considered. Other important extensions are related to the connection between the characteristics of the problems and the equivalence classes to which they belong. We have shown the connection of the classes with the neighborhood system induced by the Hamming distance for univariate EDAs. This connection can be studied for more complex probabilistic models. For example, preliminary results indicate that, if we add an arc to the univariate model, then it is possible to include functions with one and two local optima in the same class. This implies that some functions with two local optima can entail the same difficulty as functions with one local optimum (the global optimum). This agrees with that using higher order statistics could improve the chance of finding the global optimum. Moreover, we hypothesize that it is possible to discover new links with other problem characteristics or descriptors. For instance, we have very preliminary results regarding the additive decomposition of the functions and its relationship with the equivalence classes. In turn, the classes could also be tagged in terms of the difficulty of the problems they contain. In an ideal scenario, the information available about the problem at hand could be used to identify the class to which it belongs to and then try to advance, for example, whether for a given factorization the algorithm will reach the optimum. In fact, knowing if a determined factorization will converge to the optimum for a given function is one of the most important issues in EDAs.

ACKNOWLEDGMENT

This paper is supported in part by National Natural Science Foundation of China(Grant no.60975050), Research Fund for the Doctoral Program of Higher Education(Grant no.20070486081) and Fundamental Research Funds for the Central Universities(Grant no.6081014). The authors are grateful to the four anonymous referees for their insightful and constructive comments, which greatly improved the quality of the paper.

REFERENCES

[1] C. Darwin, The Origin of Species by Means of Natural Selection or the Preservation of Favoured Races in the Struggle for Life, 1859.

[2] M. Dorigo, and T. Stützle, Ant Colony Optimization. MIT press, 2004.

[3] J. Kennedy, and R. Eberhart, Particle swarmoptimization. In Proceedings of the IEEE International Conference on Neural Networks, volume 4, pp. 1942–1948. IEEE Press, 1995.

[4] H. Mühlenbein, and G. Paaß, From recombination of genes to the estimation of distributions I. Binary parameters. In Voigt, H.-M., Ebeling, W., Rechenberg, I., and Schwefel, H.-P., editors, Parallel Problem Solving from Nature (PPSN IV), volume 1141 of Lectures Notes in Computer Science, pp. 178-187, Berlin. Springer Verlag, 1996.

[5] D. E. Goldberg, Genetic Algorithms in Search, Optimization, and Machine Learning. Addison-Wesley, Reading, MA, 1989.

[6] P. Larrañaga, and J. A. Lozano, editors, Estimation of Distribution Algorithms: A New Tool for Evolutionary Computation. Kluwer Academic Publishers, Boston/Dordrecht/London, 2002.

[7] E. A. Eiben, and J. E. Smith, Introduction to Evolutionary Computing (Natural Computing Series). Springer, 2003.

[8] P. A. Bosman, The Anticipated Mean Shift And Cluster Registration In Mixture-Based EDAs For Multi-Objective Optimization. In Proceedings of the Genetic and Evolutionary Computation Conference (GECCO-2010), pp. 351 – 358. ACM Press, 2010.

[9] M. Hauschild, M. Pelikan, K. Sastry, , and Goldberg, D. E. (2012). Using previous models to bias structural learning in the hierarchical BOA. Evolutionary Computation, 20(1): pp. 135–160, 2012.

[10] P. A. Simionescu, D. Beale and G. V. Dozier, Teeth-number synthesis of a multispeed planetary transmission using an estimation of distribution algorithm. Journal of Mechanical Design, 128(1): pp. 108–115, 2007.

[11] B. Yuan, M. E. Orlowska and S. W. Sadiq, Finding the optimal path in 3D spaces using EDAs - the wireless sensor networks scenario. In Proceedings of the Adaptive and Natural Computing Algorithms, 8th International Conference (ICANNGA-2007), pages 536–545, Warsaw, Poland. Springer Verlag, 2007.

[12] J. L. Shapiro, Drift and scaling in estimation of distribution algorithms. Evolutionary Computation, 13(1): pp. 99–123, 2005.

[13] H. Mühlenbein, The equation for response to selection and its use for prediction. Evolutionary Computation, 5(3): pp. 303–346, 1998.

[14] R. Blanco, P. Larrañaga, I. Inza and B. Sierra, Selection of highly accurate genes for cancer classification by estimation of distribution algorithms. In Proceedings of the Workshop Bayesian Models in Medicine held within (AIME-2001), pp. 29-34, 2001.

[15] R. Blanco, I. Inza and P. Larrañaga, Learning Bayesian networks in the space of structures by estimation of distribution algorithms. International Journal of Intelligent Systems, 18(2): pp. 205-220, 2003.

[16] W. Ali and A. P. Topchy, Memetic optimization of video chain designs. In Proceedings of the Genetic and Evolutionary Computation Conference (GECCO-2004), pp. 869–882, Seattle, WA, USA. Springer, 2004.

[17] T. Paul and H. Iba, Linear and combinatorial optimizations by estimation of distribution algorithms. In Proceedings of the 9th MPS Symposium on Evolutionary Computation, pp. 99–106, 2003.

[18] H. Mühlenbein and T. Mahnig, Evolutionary computation and beyond. In Y. Uesaka, P. Kanerva and H. Asoh, Eds, Foundations of Real-World Intelligence, pp. 123–188. CSLI Publications, Stanford, California, 2001.

[19] C. González, J. A. Lozano and P. Larrañaga, Mathematical modeling of UMDAc algorithm with tournament selection. Behaviour on linear and quadratic functions. International Journal of Approximate Reasoning, 31(4): pp. 313–340, 2002.

[20] S. Baluja and S. Davies, Using optimal dependency-trees for combinatorial optimization: Learning the structure of the search space. In Proceedings of the 14th International Conference on Machine Learning, pp. 30–38. Morgan Kaufmann, 1997.

[21] C. K. Chow and C. N. Liu, Approximating discrete probability distributions with dependence trees. IEEE

Transactions on Information Theory, 14(3): pp. 462–467, 1968.
[22] M. Hauschild, and M. Pelikan, Enhancing efficiency of hierarchical BOA via distance-based model restrictions. MEDAL Report No. 2008007, Missouri Estimation of Distribution Algorithms Laboratory (MEDAL), 2008.
[23] M. Hauschild, M. Pelikan, K. Sastry, and C. Lima, Analyzing Probabilistic Models in Hierarchical BOA. IEEE Transactions on Evolutionary Computation, 13(6): pp. 1199–1217, 2009.
[24] C. F. Lima, M. Pelikan, D. E. Goldberg, F. G. Lobo, K. Sastry and M. Hauschild, Influence of selection and replacement strategies on linkage learning in BOA. In Proceedings of the 2007 Congress on Evolutionary Computation (CEC-2007), pp. 1083–1090. IEEE Press, 2007.
[25] H. Mühlenbein and R. Hőns, The factorized distributions and the minimum relative entropy principle. In Pelikan, M., Sastry, K., and Cantú-Paz, E., editors, Scalable Optimization via Probabilistic Modeling: From Algorithms to Applications, Studies in Computational Intelligence, pp. 11–38. Springer-Verlag, 2006.
[26] M. Hauschild, M. Pelikan, K. Sastry and D. E. Goldberg, Using previous models to bias structural learning in the hierarchical BOA. Evolutionary Computation, 20(1): pp. 135–160, 2012.
[27] A. P. Dawid, Conditional independence in statistical theory. Journal of the Royal Statistical Society Series B, 41: pp. 1–31, 1979.
[28] A. P. Dawid, Conditional independence for statistical operations. Annals of Statistics, 8(3): pp. 598–617, 1980.
[29] W. Buntine, Theory refinement on Bayesian networks. In Proceedings of the Seventh Conference on Uncertainty in Artificial Intelligence, pp. 52–60, 1991.
[30] G. Schwarz, Estimating the dimension of a model. Annals of Statistics, 7(2): pp. 461–464, 1978.
[31] D. Heckerman, D. Geiger and D. M. Chickering, Learning Bayesian networks: The combination of knowledge and statistical data. Machine Learning, 20: pp. 197–243, 1995.
[32] G. F. Cooper, The computational complexity of probabilistic inference using belief networks. Artificial Intelligence, 42: pp. 393–405, 1990.

Caichang Ding received the B.Sc. degree from the School of Mechanical & Electronic Information, China University of Geosciences, Wuhan, China, in 2003, and the M.Sc. degree from the School of Computer, Wuhan University, Wuhan, China, in 2006. He is currently a lecturer in the School of Computer Science, Yangtze University, Jingzhou, China. His main research interests include computational learning theory, statistical learning, basic theory of evolutionary computation and optimization theory.

Wenxiu Peng received the B.Sc. and M.Sc. degrees from Hubei University, Hubei, China, in 2003 and 2006. She is currently a lecturer in the School of Computer Science, Yangtze University, Jingzhou, China. Her main research interests include computational learning theory, statistical learning, basic theory of evolutionary computation and optimization theory.

Tasks Distribution Strategy based on Cluster in MWfSCC

Xiuguo Wu
Shandong University of Finance and Economics/School of Management Science and Engineering, Jinan, China
Email: xiuguosd@163.com

***Abstract*—Cloud computing technology offers a new way to develop workflow system. Migrating workflow system based on cloud computing paradigm (MWfSCC) can obtain high system performance and service quality in cloud computing environment, where an agent (called CMI) is deployed to fulfill several tasks by migrating to other computers (called work machines). In general, task execution involves several input data sets usually placed on distributed work machines. On the other hand, task execution will also generate some data sets, which may be regard as input data sets for other tasks. Traditionally, CMI moves to work machines one by one for the reason that tasks execution places are also distributed. In this way, it is very important to arrange the tasks on different work machines in order to reduce CMI's movements. In this paper, we propose a tasks distribution strategy based on cluster in MWfSCC, which contains tasks classifications and arrangements. Simulations show that tasks distribution strategy based on cluster can effectively reduce CMIs movements during workflow execution, and hence can significantly improve the performance of MWfSCC.**

***Index Terms*—workflow, cloud computing, tasks distribution**

I. Introduction

Cloud computing technology offers a new way to enable massive amounts of data sets to work together, since it supplies a pool of abstracted, virtualized, dynamically-scalable, highly available, and configurable and reconfigurable computing resources (e.g., networks, servers, storage, applications, data) [1]. However, as solving problems becomes more and more complex, especially the exponential growth of data sets, the data movements is a challenge for the sake of network bandwidth limitation. In this way, migrating workflow is an emerging technology that applies mobile agent technology to workflow management, which deploys an agent (called CMI) to fulfill several tasks by migrating to other computers (called work machines) [2-4]. By taking advantage of cloud computing technology, migrating workflow system based on cloud computing paradigm (MWfSCC) could gain a wider utilization. MWfSCC obtains so many advantages in system performance, such as easy interaction, intelligent decision making, especially in distributed, dynamic and unpredictable environment [5-6].

Yet there are still some new challenges have to face, and the tasks distribution is one of them [7]. There are many tasks in MWfSCC, and each task can be bound to a certain work machines for execution, where store a large amount of data sets. Similarly, each task execution usually includes several input data sets, which are usually placed on distributed work machines. On the other hand, a series of output data sets will be generated after tasks completed, which may be required by other tasks as input data sets. Traditionally, a CMI's tasks execution involves many work machines; and it needs to move on these machines one by one for the reason that tasks are also distributed. However, if one work machine can fulfill one or more tasks, then CMI's movements can be reduced effectively during workflow execution, and the performance of cloud workflow system can be significantly improved in this way.

Based on the above analysis, it is an urgent question to find the tasks relations and arrange them in a suitable work machine in order to reduce the CMI movements. So, in this paper, we propose a tasks distribution strategy based on cluster in MWfSCC. In our strategy, we try to classify the different tasks into sub-classes, which are linked by input and output data sets. In this way, the performance of cloud workflow system will be greatly improved when some tasks are distributed on the same machine.

The remainder of the paper is organized as follows: Section II presents the related works, including migrating workflow system based on cloud computing paradigm and tasks scheduling in traditional distributed system, Section III gives models for task distribution in MWfSCC, including models of task and other related conceptions, and Section IV demonstrates the strategy for tasks distribution based on cluster using a simple example. Section V presents the simulation results and the evaluation. Finally, Section VI addresses our conclusions and future work.

II. Related Work

In this section, we will briefly introduce the existing literatures related to this research. There are two parts, including migrating workflow system based on cloud computing paradigm, and tasks management about workflow in traditional distributed system.

A. Migrating Workflow System based on Cloud Computing Paradigm

A framework of MWfSCC is shown in Figure 1. There are four components, including cloud workflow engine,

doi:10.4304/jcp.9.6.1470-1477

service cloud server, service cloud network and cloud migrating instance (CMI) [2].

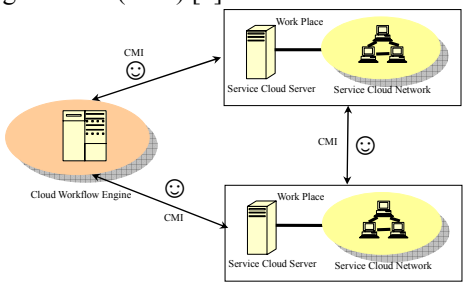

Figure 1. Framework of MWfSCC.

- Cloud workflow engine (CWfE). The main function of cloud workflow engine is to administrate the execution of whole system, including the management of service cloud servers and service cloud networks. It has the capabilities to create, to call and to kill a cloud migrating instance. Also, it controls the generation and elimination of CMIs.
- Service cloud server (SCS). Service cloud server is the main place of cloud migrating instance. It accepts the queries and requests from CMI, and supplies the service once an instance arrives. In special circumstances, it can also create and kill cloud migrating instance.
- Service cloud network (SCN). Service cloud network is the provider of resource and service.
- Cloud migrating instance (CMI). Cloud migrating instance is the main body of workflow execution, which is assigned a task description before execution. And CMI also manages and monitors tasks execution process.

According to the framework of MWfSCC, the core question of SCS is to administrate a table of tasks list, which is associated with a task description, input and output data. Figure 2 describes the architecture of service cloud server.

- Task engine: the main function of task engine is to administrator the task list table, such as adding, deleting and updating the service of SCS, and to take over the execution of a CMI.
- Task list table: the list of service is stored in task list table, indicating the capability of SCS. Each element in task list table includes task description, its input data and output data.
- Migrating tree: once a CMI decides to achieve its goals in SCS, migrating tree will tell the routine of how to find the nearest (most appropriate) work machine.
- Tasks directory: a blue print of service list table.
- Tasks lib: a library containing all the tasks description.

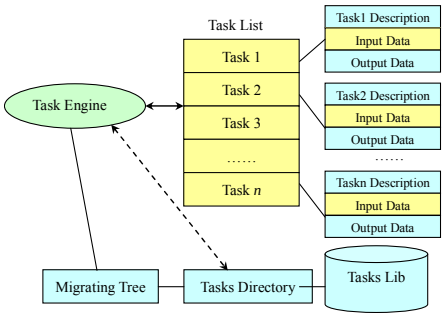

Figure 2. Architecture of service cloud server.

B. Task Scheduling in Traditional Distributed System

Task managements in the traditional distributed computing system include tasks scheduling and tasks placement strategy. As for cloud workflow systems, scheduling is a very important component similar to many other workflow systems. It directly determines the performance of the whole system. According to [8], there are two major types of workflow scheduling: best-effort based and QoS constraint based. Best-effort based scheduling attempts to minimize the execution time without considering other factors such as the cost of accessing resources and various users' QoS satisfaction levels.

Generally speaking, the algorithms usually are designed for scheduling a single workflow instance. However, for instance-intensive workflows on a cloud computing platform, fierce competition on servers/services may occur and failures may happen from time to time. Thus scheduling strategy needs to incorporate these situations accordingly. In addition, scheduling algorithm needs to consider the characteristics of cloud computing in order to accommodate instance-intensive cost-constrained workflows by compromising execution time and cost with user intervention, which is not considered in other strategies [9-12].

In cloud computing system, the infrastructure is hidden from users. Hence, for most of the application tasks, the system will decide where to perform them. Dependencies exist among these tasks via input and output data sets [13-15]. In this paper, we initially adapt the cluster algorithms for tasks distribution in order to reduce the number of CMIs movements.

III. MODELS FOR TASKS DISTRIBUTION IN MWFSCC

In this section, we will define some models related to research, including migrating workflow system based on cloud computing paradigm, cloud migrating instance, data set, etc.

Definition 1. Migrating Workflow System based on Cloud Computing Paradigm (MWfSCC).

Migrating workflow system based on cloud computing paradigm is a 4-tuple: (*Wid*, *CMI*, *SC*, *Eng*), where,

(1) *Wid* is an identifier of MWfSCC;

(2) $CMI=\{CMI_1, CMI_2,\ldots, CMI_n\}$, representing a set of cloud migrating instances (CMIs). Each CMI pursues a certain goal on behalf of an independent business process;

(3) $SC=\{sc_1, sc_2, \ldots, sc_n\}$, representing a set of servers in cloud computing environment, where CMIs fulfill tasks;

(4) *Eng* is an engine of MWfSCC, which administers the whole workflow system, including creating, killing or suspending CMIs and monitoring the activities, etc.

Definition 2. Cloud Migrating Instance (CMI).

A CMI can be described with a 8-tuple: (*cmiid*, *TL*, *t*, SC_{cmi}, *p*, S_{cmi}, *ToL*, *MC*), where,

(1) *cmiid* is an identifier of a *CMI*, which is exclusive in the whole system;

(2) $TL=(\{\langle t_1, R_1, S_1\rangle, \langle t_2, R_2, S_2\rangle, \ldots, \langle t_n, R_n, S_n\rangle\}$, *Schedule*), representing sub-task specifications in CMI, including two parts: task list table $\{\langle t_1, R_1, S_1\rangle, \langle t_2, R_2, S_2\rangle, \ldots, \langle t_n, R_n, S_n\rangle\}$ and task scheduler *Schedule*. And task *t* is corresponds to the activities a_i in business process, R_i is the resource requirements for task completion, S_i is the service requirements of tasks. *Schedule* is the dependency relationship of sub-tasks $t_1, t_2 \ldots t_n$;

(3) *t* is the a task that CMI is processing, equal to one of t_i;

(4) SC_{cmi} is the set of available service cloud, $SC_{cmi} \in SC$;

(5) *p* is the service cloud that CMI is deployed;

(6) S_{cmi} describes CMI's current state;

(7) *ToL* is CMI's life cycle;

(8) *MC* is the machine that supplies services or resources CMI requires, including task performing and halting, multi-tasks coordination, detecting resource and service, migrating places query.

Definition 3. Service Cloud (SC).

A service cloud (SC) can be described by a 4-tuple: (*scid*, *S*, *R*, *Svr*), where,

(1) *scid* is an identifier of service cloud;

(2) $S=\{s_1, s_2, \ldots, s_n\}$ represents a set of services that a service cloud can supply;

(3) $R=\{r_1, r_2, \ldots, r_m\}$ is a set of resources that a service cloud can supply;

(4) *Svr* is a service engine, which can coordinate the running of cloud system.

Definition 4. Data set type (DST) .

Data set in MWfSCC can be divided two types: DS_{ini}, and DS_{gen}, where,

(1) $DS_{ini}=\{d_{i1}, d_{i2}, d_{i3},\ldots\}$, representing the original data sets uploaded by users, which are usually collected from the devices in experiments. And the most important feature of these data sets is that they can't be regenerated again if they are deleted;

(2) $DS_{gen}=\{d_{g1}, d_{g2}, d_{g3},\ldots\}$, representing the data sets produced in the cloud computing system after tasks completion. They are the intermediate or final computation results of the applications.

Definition 5. Task (T).

A task in MWfSCC can be defined as a 3-tuple $<t_i, d_{in}, d_{out}>$, where,

(1) t_i means the identifier of a task;

(2) d_{in} means input data sets for performing a task t_i;

(3) d_{out} means output data sets after a task t_i execution.

A task model can be described as Figure 3.

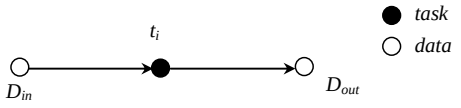

Figure 3. Model of task in MWfSCC.

Definition 6. Use relation matrix R_u.

Given a data set $D=\{d_1, d_2, .., d_n\}$, and a task set $T=\{t_1, t_2, \ldots, t_m\}$, then using relation matrix R_u can be defined as follows: $R_u=(r_{ij})_{m\times n}$, where,

$$r_{ij}=\begin{cases}1 & \text{where executing task } t_i \text{ using data } d_j;\\ 0 & \text{else}\end{cases}$$

Definition 7. Generation relation matrix R_c.

Generation relation matrix R_c can be defined as follows: $R_c=(r_{ij})_{m\times n}$, where,

$$r_{ij}=\begin{cases}1 & \text{where executing task } t_i \text{ generating data } d_j;\\ 0 & \text{else}\end{cases}$$

Definition 8. Task data graph (TDG).

A task data graph can be defined as a 4-tuple $<T, D, C_i, Da_i>$, where,

(1) *T* is a task set;

(2) *D* is a data set;

(3) C_i represents the control flow between task t_i;

(4) Da_i refers to data flow relation.

According to the above definition, we can depict a graph including tasks, data sets and their relations. Figure 4 shows a simple task data graph, where each node in the graph denotes a data set. In Figure 4, data set d_1 points to task t_4, which means that d_1 is an input data set of task t_4; and task t_3 points to data set d_4, which means the data set d_4 can be acquired by performing task t_3.

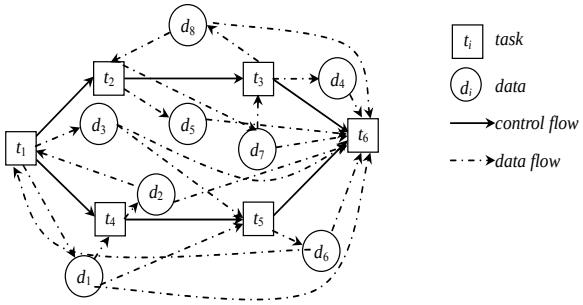

Figure 4. An example of task data graph.

In this way, the use relation matrix and generation relation matrix can be represented as follows:

$$R_u=\begin{pmatrix}0&1&0&0&0&0&1&0\\0&0&0&0&0&0&0&1\\0&0&0&0&0&0&1&0\\1&0&0&0&0&0&0&0\\1&0&1&0&0&0&0&0\\1&1&1&1&1&1&1&1\end{pmatrix}, \text{ and}$$

$$R_c = \begin{pmatrix} 1 & 0 & 1 & 0 & 0 & 0 & 0 & 0 \\ 0 & 0 & 0 & 0 & 1 & 0 & 1 & 0 \\ 0 & 0 & 0 & 1 & 0 & 0 & 0 & 1 \\ 0 & 1 & 0 & 0 & 0 & 0 & 0 & 0 \\ 0 & 0 & 0 & 0 & 0 & 1 & 0 & 0 \\ 0 & 0 & 0 & 0 & 0 & 0 & 0 & 0 \end{pmatrix}.$$

Definition 9. Work machine.

A work machine can be defined as a 4-tuple <w_i, p_i, s_i, D>, where,

(1) w_i means the identifier of work machine;

(2) p_i is the performance value related to the CPU speed, memory size and other hardware factors;

(3) s_i is the size for data storage;

(4) D is a data sets stored in work machine w_i.

A work machine can fulfill a number of tasks; also, each task can perform on many work machines.

Definition 10. Dependency relation.

R$\rightarrow$ denotes that two data sets have a generation relationship, where $d_i \rightarrow d_j$ means that d_j can be acquired by calculation from data set d_i, that d_i is the predecessor of d_j. Also, we can define relation $\neg\rightarrow$ denotes that the two data sets do not have a generation relationship, where d_i and d_j are in different branches in TDG.

IV. Algorithm for Tasks Distribtion Based on Cluster

In workflow modeling stage, all the data sets should be logically assigned to different work machines, which can optimize the distribution schema.

Use relation matrix describes the using relation between data sets and tasks; and we will calculate the relativity using matrix R_u in the succeeding paragraph. An element r_{ij} means a data set d_j can be used in fulfilling a task t_i directly.

A. Algorithm for Tasks Distribution

In this section, we will present task distribution algorithm based on cluster.

Algorithm 1: Tasks distribution algorithm based on Cluster

Input: A set of tasks T;

Output: Tasks subset for distribution on work machines.

01. Construction input data set D_{in} from task t_i, $D_{in}=\{t_i.d_{in} | t_i \in T\}$;
02. Construction output data set D_{out} from task t_i, $D_{out}=\{t_i.d_{out} | t_i \in T\}$;
03. Calculate the use relation matrix R_u;
04. Calculate generation relation matrix R_c;
05. Calculate the one-step arrival matrix G
06. i=2;
07. While i<|T| Do //multi-steps arrival matrix
08. Begin
09. $G^i=G^{i-1}\times G^1$;
10. $i=i+1$;
11. End;
12. $G= G^1\vee\ldots\vee G^{|T|-1}\vee G^{|T|}$
13. Calculate the mutual accessibility among data sets;
14. Calculate sub-strong mutual accessibility matrix;
15. Row adjustment;
16. Column adjustment;
17. Acquire the classification of task sets;
18. End.

In Algorithm 1, function |T| means the number of tasks in cloud environment. Here, we will analyze the time complexity of Algorithm 1. An adjacent matrix is used to represent task data graph. And the Line 09 will execute less than n^3 times, where n is the tasks number. So, the total time complexity of tasks distribution algorithm based on cluster is $O(n^3)$. A simple example will be shown in the following sub-section.

B. A Simple Example

In this section, we will present the proposed tasks distribution algorithm step by step using a simple example. The tasks are described in Table I. And there are eight data sets, representing as d_1, d_2, d_3, d_4, d_5, d_6, d_7, d_8, and six tasks, representing as $task_1$, $task_2$, $task_3$, $task_4$, $task_5$, $task_6$.

TABLE I
TASKS DESCRIPTIONS

Tasks	Input Data	Output Data
t_1	$\{d_2, d_6\}$	$\{d_1, d_3\}$
t_2	$\{d_8\}$	$\{d_5, d_7\}$
t_3	$\{d_7\}$	$\{d_4, d_8\}$
t_4	$\{d_1\}$	$\{d_2\}$
t_5	$\{d_1,d_3\}$	$\{d_6\}$
t_6	$\{d_1,d_2,d_3,d_4, d_5,d_6,d_7,d_8\}$	Ø

Step 1

The use relation matrix R_u can be obtained from Table I using Definition 6. And the matrix R_u is described as follows:

$$R_u = \begin{pmatrix} 0 & 1 & 0 & 0 & 0 & 1 & 0 & 0 \\ 0 & 0 & 0 & 0 & 0 & 0 & 0 & 1 \\ 0 & 0 & 0 & 0 & 0 & 0 & 1 & 0 \\ 1 & 0 & 0 & 0 & 0 & 0 & 0 & 0 \\ 1 & 0 & 1 & 0 & 0 & 0 & 0 & 0 \\ 1 & 1 & 1 & 1 & 1 & 1 & 1 & 1 \end{pmatrix}.$$

Step 2

The generation relation matrix R_c can be obtained from Table I using Definition 7. And the matrix R_c is described as follows:

$$R_c = \begin{pmatrix} 1 & 0 & 1 & 0 & 0 & 0 & 0 & 0 \\ 0 & 0 & 0 & 0 & 1 & 0 & 1 & 0 \\ 0 & 0 & 0 & 1 & 0 & 0 & 0 & 1 \\ 0 & 1 & 0 & 0 & 0 & 0 & 0 & 0 \\ 0 & 0 & 0 & 0 & 0 & 1 & 0 & 0 \\ 0 & 0 & 0 & 0 & 0 & 0 & 0 & 0 \end{pmatrix}.$$

Step 3

Calculate one-step arrival matrix G using the following formula:

$$G = R_c \cdot R_u^T = (g_{i,j})_{m*m} = (\vee_{k=1}^{n}(R_c(i,k) \wedge R_u^T(k,j)),$$

i=1, 2… m, and j=1, 2 …n.

$$G = \begin{pmatrix} 1 & 0 & 1 & 0 & 0 & 0 & 0 & 0 \\ 0 & 0 & 0 & 0 & 1 & 0 & 1 & 0 \\ 0 & 0 & 0 & 1 & 0 & 0 & 0 & 1 \\ 0 & 1 & 0 & 0 & 0 & 0 & 0 & 0 \\ 0 & 0 & 0 & 0 & 0 & 1 & 0 & 0 \\ 0 & 0 & 0 & 0 & 0 & 0 & 0 & 0 \end{pmatrix} \cdot \begin{pmatrix} 0 & 1 & 0 & 0 & 0 & 1 & 0 & 0 \\ 0 & 0 & 0 & 0 & 0 & 0 & 0 & 1 \\ 0 & 0 & 0 & 0 & 0 & 0 & 1 & 0 \\ 1 & 0 & 0 & 0 & 0 & 0 & 0 & 0 \\ 1 & 0 & 1 & 0 & 0 & 0 & 0 & 0 \\ 1 & 1 & 1 & 1 & 1 & 1 & 1 & 1 \end{pmatrix}^T$$

$$= \begin{pmatrix} 1 & 0 & 1 & 0 & 0 & 0 & 0 & 0 \\ 0 & 0 & 0 & 0 & 1 & 0 & 1 & 0 \\ 0 & 0 & 0 & 1 & 0 & 0 & 0 & 1 \\ 0 & 1 & 0 & 0 & 0 & 0 & 0 & 0 \\ 0 & 0 & 0 & 0 & 0 & 1 & 0 & 0 \\ 0 & 0 & 0 & 0 & 0 & 0 & 0 & 0 \end{pmatrix} \cdot \begin{pmatrix} 0 & 0 & 0 & 1 & 1 & 1 \\ 1 & 0 & 0 & 0 & 0 & 1 \\ 0 & 0 & 0 & 0 & 1 & 1 \\ 0 & 0 & 0 & 0 & 0 & 1 \\ 0 & 0 & 0 & 0 & 0 & 1 \\ 1 & 0 & 0 & 0 & 0 & 1 \\ 0 & 0 & 1 & 0 & 0 & 1 \\ 0 & 1 & 0 & 0 & 0 & 1 \end{pmatrix}$$

$$= \begin{pmatrix} 0 & 0 & 0 & 1 & 1 & 1 \\ 0 & 0 & 1 & 0 & 0 & 1 \\ 0 & 1 & 0 & 0 & 0 & 1 \\ 1 & 0 & 0 & 0 & 0 & 1 \\ 1 & 0 & 0 & 0 & 0 & 1 \\ 0 & 0 & 0 & 0 & 0 & 0 \end{pmatrix}.$$

Step 4

Two-step arrival matrix G can be obtained by calculation using following formula:

$$G^2 = G \cdot G = \left(\bigvee_{k=1}^{m} (G(i,k) \wedge G(k,j)) \right),$$

i=1, 2… m, and j=1, 2 …n.

So,

$$G^2 = \begin{pmatrix} 0 & 0 & 0 & 1 & 1 & 1 \\ 0 & 0 & 1 & 0 & 0 & 1 \\ 0 & 1 & 0 & 0 & 0 & 1 \\ 1 & 0 & 0 & 0 & 0 & 1 \\ 1 & 0 & 0 & 0 & 0 & 1 \\ 0 & 0 & 0 & 0 & 0 & 0 \end{pmatrix} \cdot \begin{pmatrix} 0 & 0 & 0 & 1 & 1 & 1 \\ 0 & 0 & 1 & 0 & 0 & 1 \\ 0 & 1 & 0 & 0 & 0 & 1 \\ 1 & 0 & 0 & 0 & 0 & 1 \\ 1 & 0 & 0 & 0 & 0 & 1 \\ 0 & 0 & 0 & 0 & 0 & 0 \end{pmatrix}$$

$$= \begin{pmatrix} 1 & 0 & 0 & 0 & 0 & 1 \\ 0 & 1 & 0 & 0 & 0 & 1 \\ 0 & 0 & 1 & 0 & 0 & 1 \\ 0 & 0 & 0 & 1 & 1 & 1 \\ 0 & 0 & 0 & 1 & 1 & 1 \\ 0 & 0 & 0 & 0 & 0 & 0 \end{pmatrix}.$$

Similarly, we can calculate the three-step arrival matrix G^3, four-step arrival matrix G^4 and five-step arrival matrix G^5. Then the arrival matrix R can be obtained using following formula:

$$R = G \vee G^2 \vee G^3 \vee G^4 \vee G^5;$$

$$R = \begin{pmatrix} 1 & 0 & 0 & 1 & 1 & 1 \\ 0 & 1 & 1 & 0 & 0 & 1 \\ 0 & 1 & 1 & 0 & 0 & 1 \\ 1 & 0 & 0 & 1 & 1 & 1 \\ 1 & 0 & 0 & 1 & 1 & 1 \\ 0 & 0 & 0 & 0 & 0 & 1 \end{pmatrix}.$$

Step 5

In order to calculate the accessible relationship among data sets, we will first give definitions of accessibility and mutual accessibility.

Definition 11. Accessibility.

In matrix R, if there is an element $R(i, j)$=1, we call task t_i is accessible to task t_j. In other words, accessibility means the t_i's output data sets are also the input data sets for task t_j.

For example, in matrix R, the element $R(4, 5)$ =1, we can see from Figure 1 that the output data set of t_4 (d_2) is also the input data set of task t_1. On the same way, task t_1's output data set d_3 is also the input data set of task t_5.

Definition 12. Mutual accessibility.

If a data set d_i is accessible to data set d_j, and d_j is also accessible to d_i, then these two data sets are mutual accessible.

As is shown in Figure 5, where data set d_i and d_j are mutual accessible.

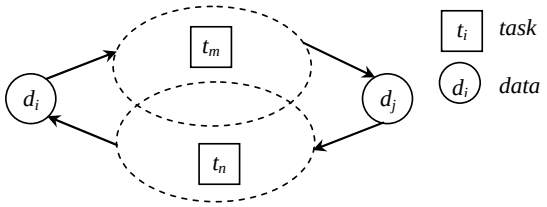

Figure 5. Mutual accessibility of two data sets.

We use Q=$R \wedge R^T$ to calculate the mutual accessibility. As is shown in Figure 6.

$$Q = \begin{pmatrix} 1&0&0&1&1&1 \\ 0&1&1&0&0&1 \\ 0&1&1&0&0&1 \\ 1&0&0&1&1&1 \\ 1&0&0&1&1&1 \\ 0&0&0&0&0&1 \end{pmatrix} \wedge \begin{pmatrix} 1&0&0&1&1&0 \\ 0&1&1&0&0&0 \\ 0&1&1&0&0&0 \\ 1&0&0&1&1&0 \\ 1&0&0&1&1&0 \\ 1&1&1&1&1&1 \end{pmatrix}^T$$

$$= \begin{pmatrix} 1&0&0&1&1&0 \\ 0&1&1&0&0&0 \\ 0&1&1&0&0&0 \\ 1&0&0&1&1&0 \\ 1&0&0&1&1&0 \\ 0&0&0&0&0&1 \end{pmatrix}.$$

	t_1	t_2	t_3	t_4	t_5	t_6
t_1	1	0	0	1	1	0
t_2	0	1	1	0	0	0
t_3	0	1	1	0	0	0
t_4	1	0	0	1	1	0
t_5	1	0	0	1	1	0
t_6	0	0	0	0	0	1

Figure 6. Mutual accessibility among data sets.

Step 6

Sub-strong mutual accessibility matrix can be obtained by adjusting the rows and columns order. And there are three steps.

Step 6.1

Create a set of random sequence numbers, which can be a Fibonacci sequence. In this paper, we use a number list as follows:

a_1=1,

a_2=3,

a_3=a_1+a_2+1=5,

a_j=2a_j□1 (j≥4).

In this way, random sequence numbers can be calculated as: 1, 3, 5, 10, 20, 40, 80 …

Step 6.2

Adjust the columns using random sequence numbers. Each element $Q[i][j]$ is multiplied by corresponding sequence number, then a series values can be obtained for adjusting the columns. As is shown in Figure 7(a) and (b).

	t_1	t_2	t_3	t_4	t_5	t_6	
t_1	1	0	0	1	1	0	1
t_2	0	1	1	0	0	0	3
t_3	0	1	1	0	0	0	5
t_4	1	0	0	1	1	0	10
t_5	1	0	0	1	1	0	20
t_6	0	0	0	0	0	1	40
	31	8	8	31	31	40	

(a)

	t_2	t_3	t_1	t_4	t_5	t_6	
t_1	0	0	1	1	1	0	1
t_2	1	1	0	0	0	0	3
t_3	1	1	0	0	0	0	5
t_4	0	0	1	1	1	0	10
t_5	0	0	1	1	1	0	20
t_6	0	0	0	0	0	1	40
	8	8	31	31	31	40	

(b)

Figure 7. Adjustment the column of Matrix(i).

Step 6.3

Adjust the rows using random sequence numbers. Each element $Q[i][j]$ is multiplied by corresponding sequence number, then a series values can be obtained for adjusting rows. As is shown in Figure 8.

	t_2	t_3	t_1	t_4	t_5	t_6	
t_1	0	0	1	1	1	0	35
t_2	1	1	0	0	0	0	4
t_3	1	1	0	0	0	0	4
t_4	0	0	1	1	1	0	35
t_5	0	0	1	1	1	0	35
t_6	0	0	0	0	0	1	40
	1	3	5	10	20	40	

(a)

	t_2	t_3	t_1	t_4	t_5	t_6	
t_2	1	1	0	0	0	0	4
t_3	1	1	0	0	0	0	4
t_1	0	0	1	1	1	0	35
t_4	0	0	1	1	1	0	35
t_5	0	0	1	1	1	0	35
t_6	0	0	0	0	0	1	40
	1	3	5	10	20	40	

(b)

Figure 8. Adjustment the column of Matrix(ii).

Step 7

The last step is to acquire the classification of tasks sets. As is shown in Figure 9.

	t_2	t_3	t_1	t_4	t_5	t_6
t_2	1	1				
t_3	1	1				
t_1			1	1	1	
t_4			1	1	1	
t_5			1	1	1	
t_6						1

Figure 9. Result of classification Matrix.

In this way, we have divided all the tasks into three sub sets, including $\{t_2, t_3\}$, $\{t_1, t_4, t_5\}$ and $\{t_6\}$. In the tasks distribution, these tasks in one sub sets should be arranged in the same work machine for reducing the CMIs movements. And the classification result can be seen in Figure 10.

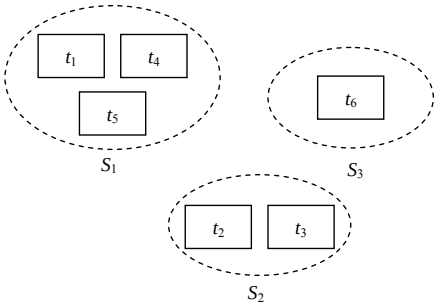

Figure 10. Result of tasks distribution.

V. Experimental Details and Comparisons

MWfSCC (Migrating Workflow System Model based on Cloud Computing Paradigm) is developed on migrating workflow system. The prototype is designed in Java and currently running on the simulation environment. As is shown in Figure 11.

To simulate the cloud computing environment, we set up VMware software on the physical servers and PCs as work machines. In order to testify the validity of task classification strategy, we design an experiment of sorting random numbers. The main object is to compare mean execution time between task classification and no task classification.

In experiments, each CMI is assigned a task to arrange 2,000 random numbers into a sequence. In task classification, most of tasks are stored on the same work machine, while each task is arranged in different work machines with no task classification. Table II recorded the execution time among different number of CMIs.

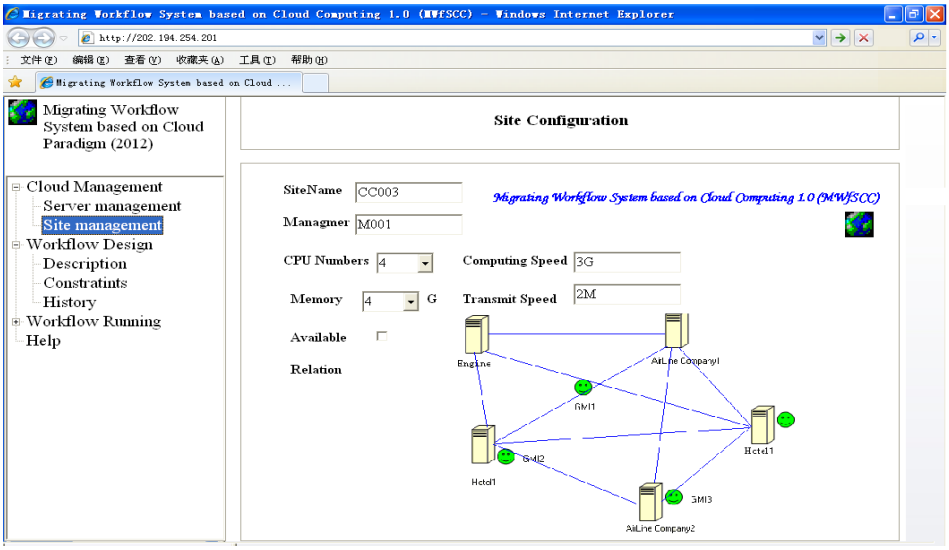

Figure 11. Prototype of MWfSCC.

Table II.

Execution Time among Different Number of CMIs

Number of CMIs	*Execution Time with No Tasks classification*	*Execution Time with Tasks classification*
100	1.156	0.756
150	1.239	0.839
250	1.508	1.008
300	1.602	1.202
350	2.676	1.376
400	3.889	1.667
450	6.581	2.743
500	9.541	4.652

Figure 12 describes the execution time for workflows across scheduling with different number of CMIs. From Figure 12, we can see that the execution time with tasks classification has gradually deceased compared with the time without tasks classification. In addition, the execution time will be saved up to half of the whole time with CMIs number 500.

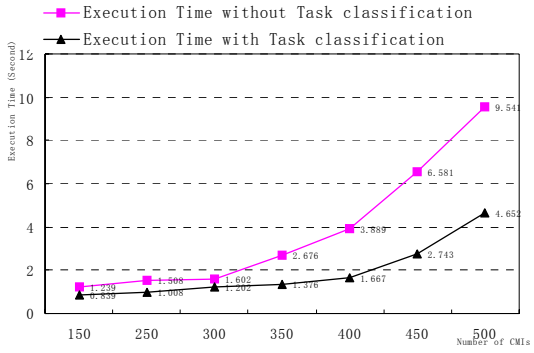

Figure 12. Execution time for workflow among different number of CMIs

VI. Conclusions and Future Works

Large scale sophisticated workflow applications are commonly seen in both *e*-business and *e*-science areas.

Workflow system built on high performance computing infrastructures such as p2p and grid computing are often applied to support the process automation of large scale workflow applications. MWfSCC is not built from scratch but from its predecessor GoMWfS (goal oriented migrating workflow system). The practical applications show the simplicity and validity of our prototype system in modeling and executing cloud computing transactions. Traditional scheduling strategy usually emphasize on the data place, not involving the tasks distribution.

In this paper, a novel task distribution strategy based on cluster has been presented. Simulations in our MWfSCC indicated that our task distribution strategy can effectively reduce execution time.

In the future, more functional components will be designed and deployed to enhance the capability of MWfSCC. And different types of tasks should be performed many times to guarantee the task classification reliability. Also, we will develop some efficient replication strategies for data sets placements according different types of tasks, which could balance the data sets and tasks storage usage.

ACKNOWLEDGMENTS

This work presented in this paper is partly supported by Project of Shandong Province Higher Educational Science and Technology Program (No.J12LN33), China; the Doctor Foundation of Shandong University of Finance and Economics under Grant (No.2010034), and the Project of Jinan High-technology Independent and Innovation (No.201303015), China.

REFERENCES

[1] Raghavan B., Ramabhadran S., Yocum K. and Snoeren A. C. "Cloud control with distributed rate limiting". In *Proceedings of the 2007 conference on Applications, technologies, architectures, and protocols for computer communications (ACM SIGCOMM)* , Kyoto, Japan, 2007, pp.337–348.

[2] WFMC, *Workflow management coalition terminology and glossary*, Workflow Management Coalition, Brussels: Technical Report WFMC-TC-1011, 1996.

[3] Zeng Guangzhou and Dang Yan, "The study of migrating workflow based on the mobile computing paradigm," *Chinese Journal of Computers*, Vol.26,(10), pp.1343-1349, 2003.

[4] Wu Xiuguo, "MWfSCC: A migrating workflow system based on cloud computing paradigm," *Journal of Convergence Information Technology*, Vol. 7(23), pp. 537-547, 2012.

[5] Wu Xiuguo and Zeng Guangzhou, "Goals description and application in migrating workflow system". *Expert Systems with Application*, Vol.37(12), pp.8027-8035, 2010.

[6] Zhuangjun Wu, Xiao Liu, Zhiwei Ni, Dong Yuan and Yun Yang, "A market-oriented hierarchical scheduling strategy in cloud workflow system," *The Journal of Supercomputing*, Vol. 63(1), pp.256-293, 2011.

[7] D. Yuan, Y. Yang, X, Liu and Jinjun Chen, "A cost-effective strategy for intermediate data storage in scientific cloud workflow systems," in *Proceedings of 24th International parallel & Distributed Processing Symposium*, Atlanta, USA, pp.1-12, 2010.

[8] R. Barga and D.Gannon, "Scientific versus business workflows," in *Workflows for e-Science*, pp.9-16, 2007.

[9] Yu J, Buyya R and Ramamohanarao K. "Workflow scheduling algorithms for grid computing", *Metaheuristics for scheduling in distributed computing environments*. Springer Berlin Heidelberg, pp.173-214, 2008.

[10] Y. Yang, K. Liu, J. Chen, X. Liu, D. Yuan and H. Jin, "An algorithm in SwinDeW-C for scheduling transaction-intensive cost-constrained cloud workflows," in *proceedings of 4th IEEE International Conference on e-Science*, pp. 374-375, 2008.

[11] J. Yan, Y. Yang and G. K. Raikundalia, "SwinDeW- A P2P-based decentralized workflow management system", *IEEE Transactions on Systems, Man and Cybernetics*, Part A, Vol. 36, pp.922-935, 2006.

[12] Liu K, Chen J, Yang Y and Jin H, "A throughput maximization strategy for scheduling intensive workflows on SwinDeW-G," Concurrency and Computation: Practice & Experience - *2nd International Workshop on Workflow Management and Applications in Grid Environments (WaGe2007)*, vol.10(15), pp. 1807-1820, 2008.

[13] Ludscher, B., Altintas, I., Berkley, C., Higgins, etc. "Scientific Workflow Management and the Kepler System". In: *Concurrency and Computation: Practice and Experience*, vol.18, pp.1039–1065, 2006.

[14] D. Ardagna and B. Pernici, "Adaptive service composition in Flexible Processes", *IEEE Trans. on Software Engineering*, vol.33(6), pp. 369-384, 2007.

[15] Wang M, Kotagiri R and Chen J, "Trust-based robust scheduling and run time adaptation of scientific workflow". *Concurrency Computation: practice and experience*, vol.21(16), pp: 1982-1998, 2009.

Xiuguo Wu received the BEng degree from Shanghai University of Electric Power, Shanghai, China, in 1999, the MEng and PhD degrees from Shandong University, Jinan, China, in 2002 and 2010, respectively, all in computer science. He is currently an associate professor in School of Management Science and Engineering at Shandong University of Finance and Economics (SDUFE). His research interests include workflow and distributed data management for cloud computing, service computing.

A P2P Traffic Management Model Based on an ISP Game

Chunzhi Wang, Shuping Wang, Hui Xu, *Hongwei Chen
School of Computer Science, Hubei University of Technology, Wuhan, China
Email: chw2001@sina.com

***Abstract*—While P2P applications enrich the network application, they consume huge network bandwidth and have a great impact on ISP. As for current traffic optimization problem, maybe the most effective analysis tool is the game theory. This paper proposes an ISP-involved P2P network traffic management framework, builds a game model and its equilibrium solution, then from the perspective of evolution, performs convergence analysis on the equilibrium solution, based on this, generates a traffic management optimization algorithm, and discusses the fairness of the algorithm. Finally, the simulation experiments show that, the model can reach the purpose of optimizing traffic management.**

***Index Terms*—Traffic Management, ISP, P2P, Game Theory**

I. INTRODUCTION

P2P (Peer-to-Peer) is a distributed network, and a peer in the P2P network acts as the role of both a server and a client. While P2P applications enrich the network application, they consume huge network bandwidth and have a great impact on ISP (Internet Service Provider). In addition, the mismatch between the overlay networks and underlay networks leads to large redundant traffic, which strengthens the tension between P2P content providers and ISPs.

Many researchers try to solve this problem with such methods as cache management and traffic localization. GuoQiang Zhang etc. survey the P2P traffic optimization technologies from three aspects: P2P cache, traffic locality-awareness and data scheduling [1]. Literature [2] summarizes ISPs' P2P traffic management schemes: p2p blocking, p2p caching, Localization (peers), Localization (ISPs). In order to minimize the total amount of P2P traffic, Noriaki Kamiyama etc. present an optimum design for capacity and location of caches based on dynamic programming method, assuming that a transit ISP provides caches at transit links to access ISP networks [3]. Miyoshi etc. present a new method for P2P traffic localization, featuring the insertion of an additional delay into each P2P packet based on the geographic location of its destination [4]. Byungryeol Sim etc. have assessed the impacts of ALTO (Application-Layer Traffic Optimization Protocol) on P2P applications from the respects of network traffic optimization [5]. However, researches show that residential ISPs can actually lose money when localization is employed, and some of them will not see increased profitability until other ISPs employ localization [6]. So, it's necessary to reduce traffic and increase ISP profit through cooperation between P2P and ISPs. Recently, some scholars study P2P traffic optimization problem from the cooperation between P2P and ISPs. Literature [7] has studied whether a cooperative caching scheme could help ISPs to decrease traffic costs caused by P2P applications. Literature [8] provides a ranking service that applies the ISP's own policies to the P2P peer selection flexibly. Through the peer selection policy, it can effectively control download traffic. Peng Yang etc. propose a rate allocation mechanism for achieving a balance between the cross-ISP P2P traffic and the P2P streaming performance [9].

As for current traffic optimization problem, maybe the most effective analysis tool is the game theory. From a theoretical perspective, it is feasible to achieve the purpose of traffic optimization if the ISP manages content through certain game strategy. There are many researchers apply game theory to P2P and ISP. Literature [10,11] describe a game theoretic framework for scalable video streaming over a P2P network. Literature [12] optimizes the non-cooperative P2P network from the game theory point of view. Literature [13] provides a new framework based on spatial evolutionary game theory for incentive mechanism to encourage cooperation among peers in P2P networks. Literature [14] presents a game theoretic framework to help the design of techniques encouraging the ISP cooperation in P2P streaming applications and decreasing unnecessary inter-ISP streaming traffic. Literature [15] formulates the interaction among ISPs and subscribers in a local market with two ISPs competing with each other as a two-stage game, and studies the influence of different traffic patterns on the Nash Equilibrium of the market. Literature [16] studies two games that model the adoption of ISP-driven locality promotion and of ISP-owned caches that intervene in the overlay.

In this paper, we apply game theory to P2P traffic optimization. The remaining of this paper is organized as follows: Section 2 proposes a P2P traffic management framework involved with ISPs. Section 3 establishes a game theory model and solves the Nash equilibrium, and analyzes convergence property of the Nash equilibrium from respect of evolution. On the basis of above, a P2P traffic optimization algorithm is presented, and its fairness is discussed. In section 4, the simulative result shows that the model can achieve the effect on traffic

doi:10.4304/jcp.9.6.1478-1483

optimization. Finally, section 5 concludes the work and points out future research directions.

II. BASIC HYPOTHETICAL FRAMEWORK

There are two hypotheses for the model.

(1) The P2P networks may possibly be of great differences between topologies of the underlying network and the carrying network, and the span of ISP domains may also be very great. Here, we assume that in this paper, the peer and ISP domains are relatively concentrated, without consideration of the marginal situation. Based on this hypothesis, some additional overhead and delay of resources during a request can be ignored. This is reasonable and critical for analysis of the core problem.

(2) Assume that, the resource request and transmission process of the peer node is controllable in a certain range. This helps to build and analyze the model conveniently when analyzing the activity process of a node.

When the peer node in this paper requires a resource, the required traffic request information is submitted to the P2P Resource Management System (RMS), according to related information of the task type and the ISP domain of the request, RSM divides the traffic request into sub-tasks corresponding to the ISP services, and then delivers them to the ISP for processing, finally in the part of ISP service provision, sets up links for peers and resources, in response to the request.

This is a two-level management model of mutual cooperation for P2P resource management system and ISP service provider. P2P RMS is the core part of the system, including not only Tracker but also the ability of dividing task requests into various sub-tasks, which can appear in the form of links or part resources. For example, when a node sends a resource request to the RMS, the Tracker finds that many places (ISP Cache or nodes in the domain) have the resources, and in order to select the optimal traffic path, the task is divided by RMS into multiple sub-requests to each ISP having the resources, and according to certain strategy to select and manage the path, the purpose of optimizing the traffic will be realized. According to the basic assumptions and analysis, the basic framework of the system can be obtained, as shown in Figure 1.

The framework of the system is divided into three layers. The bottom layer is a set of peers that are nodes with both the upload and download capabilities. The middle layer is a RMS, in which the system behaves as multiple sub-systems distributed in different places, with the functions of both Tracker and splitting the request. The top layer is a set of ISPs, which is direct interaction and choice with the RMS layer and the peer layer.

We assume that, in the whole controllable analysis network, there are n peer nodes, m RMS sub-systems and k ISP service processing parts. And assume that, i_th sub-RMS can divide peer traffic request information into t sub-tasks. Among them, the roles of each layer in this model should meet requirements as follows.

(1) Peer: provider and requester of the resource, which can generate a request for a resource, relatively independent of each other to generate the traffic task request. Assume that, average traffic request generated by the peer i is ω_i. The resource request generated by peer is divided into sub-tasks to ISP partly processing by P2P RMS system.

(2) RMS: the core of the system, which can receive the task request from the peer, the Tracker part is responsible for the inquiry of distribution of the resources, and then the request is divided into sub-tasks, sent to the corresponding ISP processing part. Assume that traffic request receiving by RMS i is γ_j, and requested traffic for RMS i sent to ISP j is φ_{ij}.

(3) ISP: the executor of requested task traffic, which is responsible for request routing and traffic management. The network topology that is actually owned by ISP can have the resource transmission path with optimal strategy choice optimization. Assume that, the average traffic for sub-tasks in the ISP j is Θ_j, the requested task is $\varphi_j = \sum_{i=1}^{t} \varphi_{ij}$.

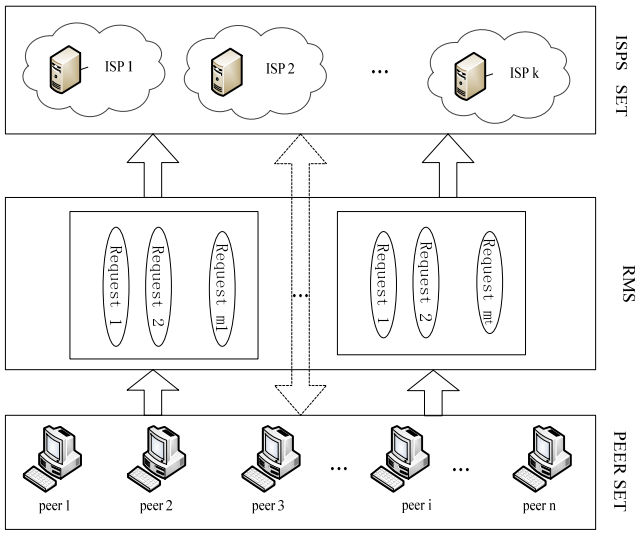

Figure 1. An ISP-involved P2P network traffic management framework

III. MODELING ON OPTIMAL NUMBERS OF CLUSTER HEADS

This section first analyzes and establishes a cooperative game model and its equilibrium solution, then from the perspective of evolution, performs convergence analysis on the equilibrium solution, finally generates a traffic management optimization algorithm based on the above, and discusses the fairness of the algorithm.

A. Basic Game Model

Assume that, a set of peer nodes in P2P network is set as N ($|N| = n$), and these nodes are owned by k ISPs. If

the set P_1 , P_2 , …, P_k meet requirements i , j , $1 \le i, j \le k$, $P_i \subseteq N$, $P_i \ne \phi$, $P_i \bigcap P_j = \phi$, $\bigcup_{i=1}^{k} P_i = N$, so that N nodes are assigned to k ISPs. p_i^k means that p_i^k i_th node belongs to the domain of P_k , which is $p_i^k \in P_k$. Here, it can be considered that P_i is an ISP set domain. In the network model as shown in Figure 1, the ISP processing sections by mutual cooperation, in accordance with the principle of optimal allocation, complete each task by RMS decomposition. When RMS decomposes the sub-tasks, each ISP provides a minimum of resources traffic load and fairness of task allocation. Based on this analysis, the ISP request processing section for the game model of the cooperation of the participants can be built.

The objective function of cooperative game is ISPs overall response to all traffic provided by peer requesting resources. Assume φ_j is the request traffic RMS sent to ISP j , the average traffic response of ISP j resource requested is

$$Q_j = 1 \Big/ \left(\Theta_j - \varphi_j \right) \tag{1}$$

, and it also meet the following conditions.

$$\varphi_j \ge 0 \tag{2}$$

$$\varphi_j < \Theta_j \tag{3}$$

$$\sum_{j=1}^{k} \varphi_j = \sum_{i=1}^{t} \gamma_i \tag{4}$$

1 in the numerator of Formula (1) means that all traffic requests can be seen as a whole unit. Formula (2) means that the response of ISP j traffic request should be greater than 0, in other words, ISP j is in the active state. Formula (3) means that the response capability of ISP j should be less than the average traffic. Formula (4) means that all requests from the peer to the RSM and ISP ends should be equal.

B. Solving the Model

From the Nash equilibrium solution of the bargaining model, cooperative game defined by Formula (1) has a unique bargaining equilibrium solution, which is the optimal solution of

$$\max_{\varphi} T = \prod_{j=1}^{k} \left(\Theta_j - \varphi_j \right) \tag{5}$$

, and the constraint conditions are Formula (2) ~ (4). From the mathematical knowledge, the optimization problem of Formula (5) is equivalent to the optimal solution defined by

$$\max_{\varphi} T = \max_{\varphi} \prod_{j=1}^{k} \ln \left(\Theta_j - \varphi_j \right) \tag{6}$$

, in which Formula (6) does logarithm operations for each element, and the constraint conditions are still Formula (2) ~ (4). So Formula (1) is equivalent to Formula (6), with the solution as follows.

Taking into account $\partial Q / \partial \varphi_j \le 0$ and $\partial^2 Q / \partial {\varphi_j}^2 \le 0$, Q is a non-convex function, and the constraint conditions of Formula (2) ~ (4) is non-linear, so optimal solutions of Formula (6) satisfies the first-order Karush-Kuhn-Tucker (KKT) conditions. With Lagrange function, there is

$$L\left(\varphi_j, \alpha \right) = \prod_{j=1}^{k} \ln \left(\Theta_j - \varphi_j \right) + \alpha \left(\sum_{j=1}^{p} \varphi_j - \sum_{i=1}^{q} \gamma_i \right) \tag{7}$$

Assume $\partial Q / \partial \varphi_j = 0$, then

$$-1 \Big/ \left(\Theta_j - \varphi_j \right) + \alpha = 0 \tag{8}$$

After further re-organization, there is

$$\varphi_j = \Theta_j - 1/\alpha \tag{9}$$

Put Formula (9) into the constraint equation (4), then

$$\sum_{j=1}^{k} \left(\Theta_j - \frac{1}{\alpha} \right) = \sum_{i=1}^{t} \gamma_i \tag{10}$$

Further, according to Formula (10), there is

$$\alpha = k \Big/ \left(\sum_{j=1}^{k} \Theta_j - \sum_{i=1}^{t} \gamma_i \right) \tag{11}$$

Finally, put Formula (11) into Formula (9), there is

$$\varphi_j^* = \Theta_j - \left(\sum_{j=1}^{k} \Theta_j - \sum_{i=1}^{t} \gamma \right) \Big/ k \tag{12}$$

According to the obtained result, the traffic equalization solution of ISP j in response to the request is φ_j^* . If only two ISPs are considered, $\left(\varphi_1^*, \varphi_2^* \right)$ is the optimal strategy solution. Similarly, the optimal strategy can be obtained by k ISPs.

C. Analysis of φ_j from the View of Evolution

In the process of solving the B part, after the requesting peer initiates the resource request, through a split and assignment, optimization is directly realized. But in fact, this is a process of dynamic convergence. From the evolutionary point of view, there are the fluctuation of iterations, repeated allocation and choice, gradually tending to a certain value, and eventually converging to the optimal strategy solution. By introducing parameter λ as evolution control parameter, the evolution iterative formula can be

$$\varphi_j^{s+1} = \begin{cases} \varphi_j^s \left(1 - \lambda \right) \\ \varphi_j^s + \lambda \Theta_j \quad otherwise \end{cases} \tag{13}$$

, in which $0 < \lambda < 1$, and assumes that the initial iterative value is from the beginning of φ_j^0 .

D. Algorithm Design

Through the analysis of B and C solutions, from Formula (12) and (14), when Θ_j satisfies

$$\Theta_j < \left(\sum_{j=1}^{k} \Theta_j - \sum_{i=1}^{t} \gamma \right) \Big/ k \tag{14}$$

, $\varphi_j < 0$. At this point, take $\varphi_j = 0$, the traffic has reached the maximum bandwidth, and can't handle the new resource request. Then, the best traffic management algorithm (BTMA) is as follows:

TABLE I.
THE BEST TRAFFIC MANAGEMENT ALGORITHM (BTMA)

for $j = 1$ to k

$$\tau_j = \left(\sum_{j=1}^{k} \Theta_j - \sum_{i=1}^{t} \gamma \right)$$

while φ_j not converge φ_j^*

Iterative φ_j^{s+1} until converge

end while

if $\tau_j > \varphi_j$ then

$$\varphi_j = 0$$

else

$$\varphi_j = \Theta_j - \tau_j$$

end if

end for

E. Algorithm Evaluation

Fairness is an important measurement index of the algorithm, mainly inspecting the differences of the response time of each participant with an algorithm. If the response time of each participant is smaller, it illustrates the fairness of the algorithm is better; otherwise, the fairness of the algorithm is poorer. The opportunity for all participants to obtain the response for the request should be same and fair.

In order to measure fairness of the algorithm, take the following Formula (15) as the fairness index.

$$F = \left(\sum_{j=1}^{k} Q_j \right)^2 \Big/ \left(k \times \sum_{j=1}^{k} Q_j^2 \right) \tag{15}$$

Put Formula (12) into Formula (1), the average traffic of response to ISP j resource request is

$$\Theta_j = k \Big/ \left(\sum_{j=1}^{k} \Theta_j - \sum_{i=1}^{t} \gamma_i \right) \tag{16}$$

Put Formula (16) into Formula (15) for the fairness index, $F = 1$ can be obtained. Here the fairness index value 1 indicates that, in the cooperative game, each player is fair in the cost of traffic treatment.

IV. SIMULATION RESULTS AND ANALYSIS

This section is divided into two parts, which do simulation and verification of the model and algorithm in Section 2 and Section 3.

(1) Assume that, average traffic processing capabilities of ISPs are equal, possibly as 0.45Gb/s, then the traffic distribution management results is shown in Figure 2. As shown in Figure 2, the white histogram chart means the result without doing the optimal traffic management algorithm, and black columnar part is the results of ISP treatment by reasonable orientation and segmentation using the optimal traffic management algorithm.

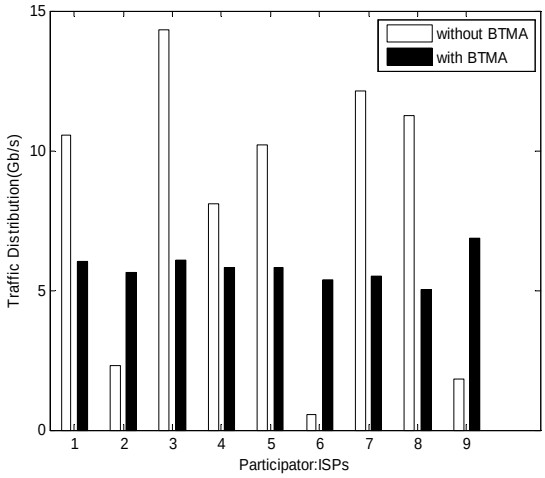

Figure 2. Traffic distribution management with same processing ability of ISPs

It can be seen that, traffic is random obviously without the BTMA algorithm, although the traffic management capabilities of ISPs are the same, but the resource request results reflect that, traffic of final treatment by each ISP is not the same, obviously in traffic management, such as ISP 1, 3, 4, 5, 7, 8 bear a larger load, and the traffic loads ISP 2, 6, 9 are very light, and the gap among traffic distribution is unfair to all the parties in the set of ISPs.The traffic distribution of BTMA algorithm has a small distribution fluctuation in the ISPs, which shows that in the process of cooperation, under the conditions of the same processing ability, traffic burden and its processing capacity of each ISP is roughly the same, with better fairness.

(2) Assume that there are 9 ISPs processing parts in the model, average processing capacity of each ISP part is shown in Table 2. Introduce the load coefficient ρ to measure load condition of the system, then the task request of RMS i is

$$\kappa_i = \rho \omega_i \sum_{j=1}^{k} \varphi_j \tag{17}$$

, in which ω_i is the average request traffic for peer i .

TABLE II.

AVERAGE TRAFFIC PROCESSING CAPACITY OF EACH ISP FOR PROCESSING RESOURCE REQUEST

ISP	Average traffic processing capacity (Gb/s)
1	0.12
2	0.49
3	0.96
4	0.34
5	0.59
6	0.22
7	0.75
8	0.26
9	0.50

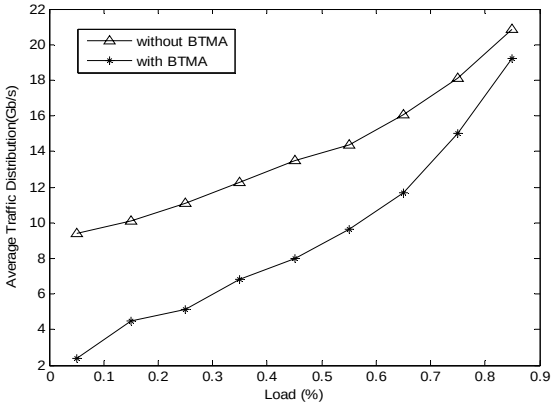

Figure 3. The distribution of average traffic cost of ISPs under different loads

For different load coefficients, the test results for average traffic handling of all ISP participants are shown in Figure 3. As seen from the Figure 3, when the load is small, the two have great differences, and when the load is more and more big, the gap between the two is reduced, but on the whole, the application of BTMA algorithm is better than non-usage, and obvious in the early time.

V. CONCLUSION

This paper proposes an ISP-involved P2P network traffic management framework based on the game theory, and analyzes and solves the model. Finally, the simulation results show that, this model can achieve the expectation of P2P network traffic optimization. This paper focuses on the relationship of cooperation between IPS and RMS. The next step of work is to improve the RMS, in order to realize engineering of traffic management.

ACKNOWLEDGMENT

This work has been supported by the General Program for National Natural Science Foundation of China (No. 61170135), the National Natural Science Foundation of China for Young Scholars (No. 61202287), the Key Project for Natural Science Foundation of Hubei Province in China (No. 2010CDA011), the General Program for Natural Science Foundation of Hubei Province in China (No.2013CFB020, No.2011CDB075), the Key Project for Scientific and Technological Research of Wuhan City in China (No. 201210421134).

REFERENCES

[1] GuoQiang Zhang, MingDong Tang, SuQi Cheng, GuoQing Zhang, HaiBin Song, JiGuang Cao, Jing Yang. P2P traffic optimization. Science China Information Sciences, vol. 55, no. 7, pp. 1475-1492, 2012.

[2] Jessie Hui Wang, Chungang Wang, Jiahai Yang, Changqing An. A study on key strategies in P2P file sharing systems and ISPs' P2P traffic management. Peer-to-Peer Networking and Applications, vol. 4, no. 4, pp. 410-419, 2011.

[3] Noriaki Kamiyama, Ryoichi Kawahara, Tatsuya Mori, Shigeaki Harada, Haruhisa Hasegawa. Optimally designing caches to reduce P2P traffic. Computer Communications, vol. 34, no. 7, pp. 883-897, 2011.

[4] Miyoshi T., Shinozaki Y., Fourmaux O. A P2P Traffic Localization Method with Additional Delay Insertion. 2012 4th International Conference on Intelligent Networking and Collaborative Systems (INCoS), pp. 148-154, 2012.

[5] Byungryeol Sim, Yeonhee Lee, Youngseok Lee. A simulation study of application-layer traffic optimization protocol for P2P applications. 2011 IEEE 36th Conference on Local Computer Networks (LCN), pp. 279-282, 2011.

[6] Jeff Seibert, Ruben Torres, Marco Mellia, Maurizio M. Munafo, Cristina Nita-Rotaru, Sanjay Rao. The internet-wide impact of P2P traffic localization on ISP profitability. IEEE/ACM Transactions on Networking (TON), vol. 20, no. 6, pp. 1910-1923, 2012.

[7] Dan G. Cache-to-Cache: Could ISPs Cooperate to Decrease Peer-to-Peer Content Distribution Costs? IEEE Transactions on Parallel and Distributed Systems, vol. 22, no. 9, pp. 1469 - 1482, 2011.

[8] Shibuya M., Hei Y., Ogishi T. ISP-friendly peer selection mechanism with ALTO-like server.2011 13th Asia-Pacific Network Operations and Management Symposium (APNOMS), pp. 1- 8, 2011.

[9] Peng Yang, Lisong Xu. On tradeoffs between cross-ISP P2P traffic and P2P streaming performance. Computer Networks, vol. 55, no. 18, pp. 4033-4042, 2011.

[10] Stefano Asioli, Naeem Ramzan, Ebroul Izquierdo. A game theoretic approach to minimum-delay scalable video transmission over P2P. Signal Processing: Image Communication, vol. 27, no. 5, pp. 513-521, 2012.

[11] Ehsan Maani, Zhaofu Chen, Aggelos K. Katsaggelos. A game theoretic approach to video streaming over peer-to-peer networks. Signal Processing: Image Communication, vol. 27, no. 5, pp. 545-554, 2012.

[12] Rozario F., Zhu Han, Niyato D. Optimization of non-cooperative P2P network from the game theory point of view. 2011 IEEE Wireless Communications and Networking Conference (WCNC), pp. 868- 873, 2011.

[13] Guanghai Cui, Mingchu Li, Zhen Wang, Linlin Tian, Jianhua Ma. Analysis and Evaluation Framework Based on

Spatial Evolutionary Game Theory for Incentive Mechanism in Peer-to-Peer Network. 2012 IEEE 11th International Conference on Trust, Security and Privacy in Computing and Communications (TrustCom), pp. 287-294, 2012,.

[14] V. Bioglio, R. Gaeta, M. Grangetto, M. Sereno, S. Spoto. A game theory framework for ISP streaming traffic management. Performance Evaluation, vol. 68, no. 11, pp. 1162-1174, 2011.

[15] Jessie Hui Wang, Dah Ming Chiu, John C.S. Lui. A game-theoretic analysis of the implications of overlay network traffic on ISP peering. Computer Networks, vol. 52, no. 15, pp. 2961-2974, 2008.

[16] Papafili I., Soursos S., Stamoulis G. D. A novel game-theoretic framework for modeling interactions of ISPs anticipating users' reactions. 2012 6th International Conference on Performance Evaluation Methodologies and Tools (VALUETOOLS), pp. 204 -213, 2012.

Chunzhi Wang (1963-), female, from Hubei province of China, PHD, Professor of Hubei University of Technology, Dean of School of Computer Science, interested in the security of network and computer network, Computer supported cooperative work. The Chairman of Wuhan of CCF Young Computer Scientists & Engineers Forum (2010).

Shuping Wang (1988-), male, from Hubei Province, master candidate of Hubei University of Technology, interested in Peer-to-Peer, Game Theory and Information Security.

Hui Xu (1983-), PHD, Lecturer of Hubei University of Technology, interested in network and service management. Since 2006, she has been a certified computer system analyst in P.R. China. In July 2008, her biography was selected for inclusion in the 26th edition (2009) of the Marquis Who's Who in the World, California, USA.

Hongwei Chen (1975-), male, from Hubei Province, PHD, Associate Professor of Hubei University of Technology, interested in Wireless Sensor Networks, Peer-to-Peer, Cloud Computing.

Study of Scraping Guide Ways Inspection

Ching Wei Wu, Ying Shing Shiao and Ching Feng Chang
Department of Electrical Engineering,Chang-hua University of Education, Changhua, Taiwan
Email: r37@mail.buffalo.com.tw, shiaoing@cc.ncue.edu.tw, paul07@mail.buffalo.com.tw

***Abstract*—Based on the image morphology technology and takes IEEE 1394 digital camera as the image catching tool, which is to be able to check the number of the actual contacts of each area on the box guide ways and the distribution uniformity of each area of machine. By setting from an experienced scraping technician as example, there should be around 16~24 points on the bearing surface per square inch which is considered as an acceptable level of its tolerance. The performance of tolerance of the box guide ways can be secured to ensure the precision requirement of machine. The evenly distributed lubrication on the surface of box guide ways can be assured to prolong the machine life of usage. This study can eliminate the disadvantage by the inspections with naked eyes of quality control inspectors. After practical tests, the contact points on the box guide ways can be firmly check, it will be a big amount of reduction of machine producing cost which is generated by lack of inspection by eyes and the repeat scraping job. The computerized inspection record will be great benefit for supporting after sales service**

***Index Terms*—scraping, guide ways inspection, image processing, machine tool**

I. Introduction

The mass production of linear guide way effectively improved the production speed of traditional machines and the rapid speed of linear motion. Many machines guide ways perform high precision and low anti-resistance, while high rigidity is still required, such as bridge type grinding machine or gantry Milling machine, it can still be adopted by box guide ways. The main reason is that the linear guide way is unable to reach the thrust force and radius force, and its bearing capacity is still insufficient for large size machine. Thus, box guide way is still the main stream mechanical structure of heavy duty machine.

But the number of contacting points and surface finish acceptance of box guide way is still depends on the naked eyes of scraping technician to examine if the box guide ways are qualified, as shown in fig. 1. However, examining the contact point with naked eyes is a controversial way. To determine whether the contact points are evenly distributed and if the area of each contact point is made within the allowable range, which meets the requirements for the uniform forces exerted on the guide way surface, is a critical key factor to determine the precision and its life running time of machine. Unfortunately, inspections with naked eyes are kind of job which is time-consuming, and in general, many experienced technicians are gradually retiring while only a few people in young generation are willing to do machine scraping inspection. Although motorized scraping machines have been invented, but it is normally used on the last step for scraping only, and the guide way is still unable to be assured whether the precision of machine is qualified. There have been further researches for the theories, among which CAD/CAPP/CAM software technologies are introduced. Practically, considering the assembly after each component is completed; this design is a great advantage to meet the precision requirement and also convenient to consider the nature of scraping, improving the quality of machines [1-4]. However, it can't be assured that the life and duration of machine because the research neglected the importance of the contact point of box ways surface and the uniform lubrication. For the straightness of guide way of machine, Profile Matching Method is adopted for measurement. Despite it is helpful to the inspection of new machine and the compliance of tolerance [5,6], it is still unable to assure to maintain the precision of machine in the long term. Fundamentally, the basis is to precisely inspect the uniformity and control the area of each contact point of bearing surface. This is the most important issue, considering the quality of machine

Figure 1. Reagents on the surface of guide way

The image morphology is applied to extract the geometric features of binary images, such as noise treatment of image or intensification of object structure. The basic image morphology includes four functions as following: (1) Dilation is an algorithm in binary image to escalate or thicken objects. The way and degree of escalation are controlled by the shape of structuring element, usually it's used to fill small caves of objects or thicken lines. (2) Erosion is an algorithm in binary image which is used to shrink or thin objects. The way and

doi:10.4304/jcp.9.6.1484-1490

degree of shrink are also controlled by structure of physical object, usually it's used to clear noises or thin lines. (3) Morphological opening is to use erosion algorithm on image first, and then expansion algorithm is applied, usually it's used to eliminate small details in image to maintain most of the shapes of objects. (4) Morphological closing is to use expansion algorithm on image first, and then erosion algorithm, usually it's used to connect adjacent objects, fill seams, and smoothen the edges of objects [7-12].

The data in image segment for different objects is applied. There are four different common technologies for the segmentation of gray-scale image, The description as following: (a) Threshold-based segmentation which is to utilize the gray-scale statistical bar chart to figure out the suitable threshold values to segment objects from background [13-14]. (b) Boundary-based segmentation; it is to utilize the obvious variations of brightness in between object and background, which is to figure out the edges of objects [10]. (c) Region-based segmentation; it is to set the similar brightness in adjacent image with the same tag for segmentation [15]. (d) Hybrid segmentation; this is to combine all the above three methods for segmentation to achieve better segmentation. Among these, the watershed segmentation is representative [16].
Following ISO inspection standard for machine manufacturing industry, the contact point requirement of bearing surface is around 16-24 points evenly distributed in the area of one square inch. The inspection method is to apply reagents on the surface of guide way and move the scraped sliding elements back and forth on the surface which is scraped. Thus, the surface of the sliding element has obvious reagents, as shown in fig. 1, which is applicable for the quality controller to identify the number of bearing point and ensure it meets the requirement. Unlike the method with reagent that determined by naked eyes, this adopts CCD camera is to identify the sliding element, which is not applied with reagent. Though the calibration of image, it can convert the image coordinate system to the world coordinate system to further recognize the number, area, and uniformity of the bearing point within each square inch, which can be analyzed by computer.

This image analyst system is a PC-based structure, consisting of IEEE 1394 digital camera, video extraction card, and light regulator. The processes and analyses of image are completed done by LabVIEW and MATLAB of National Instrument. The transmission speed of IEEE 1394 digital camera is fast and precise, the maximum shooting speed is up to 400Mbit/s, and the parameters of camera can be adjusted by software, such as shutter speed, white balance, and gain values, etc. Figure 2 shows the mechanism drawings of the scraping guide ways inspection device. Figure 2(a) and 2(b) are the side view and top view of the scraping guide ways inspection device respectively. "B" is light regulator as shown in figure 2(b), which is used to adjust the reflective brightness on the scraped surface, it is to stabilize the algorithm for image processing. "C" is a hand wheel, which is to drive the gear rotation on the rack, so that the whole inspection platform can be moved upward and downward with a stroke distance for 280mm. Combined with the lens of range 8mm-48mm is applied, this device is able to catch the ranged view area from the farthest 500 cm2 to the nearest 230cm2. The turret design will be able to do angle adjustment for the camera and the light regulator for a range of ±65°. Even the 60°V shape guide way slope can be inspected. The linear guide way can be used to control the movement of inspection platform, both in back and forth with movable stroke for 200mm. "A" is the front edge in Figure 2(a), which meets the requirement that the inspection platform can easily move. The total movement is 325mm. This range meets most inspection requirements of guide way surface.

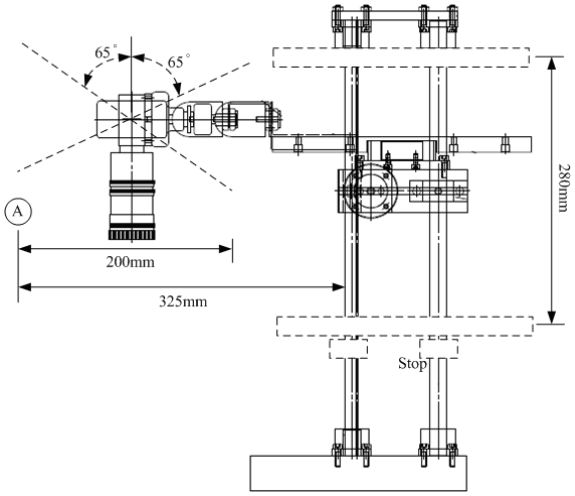

(a) side view

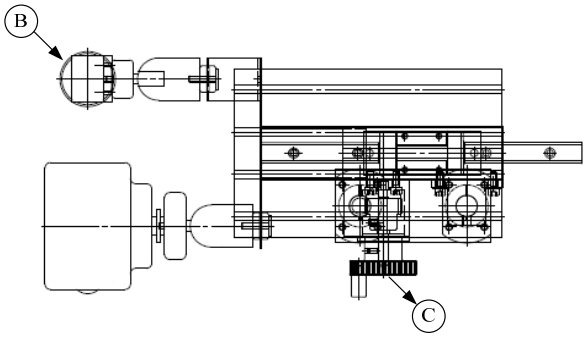

(b) top view

Figure 2. The prototype scraping inspection machine.

II. IMAGE CALIBRATION

The realization of this work supposes the availability of a great number of repetitions of samples responding to the same known theoretical model. In practice, as the theoretical model is unknown, we use the Monte-Carlo method based on the generation of the data by computer according to a fixed theoretical model.

In the image plane, the unit seen used to represent the image element is in pixel. To realize the size in the image plane, it needs to calibrate images to convert the image coordinate system to the world coordinate system. In this

experiment, a calibration plate is distributed with points in various colors. The interval of each point is within one inch. Thus, every 4 points is circled one square inch. Figure 3(a) shows the image calibration plate. Figure 3(b) shows the range of figure 3(a) Region of Interest (ROI) and convert to HSI color space. This can easily extract red, which is more saturated. HSI color space illustration is shown as figure 4. HSI color space represents colors with Hue, Saturation, and Intensity. Hue indicates the wave length of the light reflected from object. Different wave lengths represent different colors. In HSI color space, Hue indicates the object color, such as $H = 0°$ represents red, $H = 120°$ represents green, $H = 240°$ represents blue. Saturation indicates the sharpness of color. When S=0, it is the location of center point. S value is closer to the point of center, the color is lighter, such as light blue, light red, light green, and so on. The closer to the edge, the color is darker, such as dark blue, dark red, dark green, and so on. Intensity indicates the relative shading in the grey-scale image. $I = 0$ represents as dark (black). $I = 1$ represents as bright (white).

Thus, the red points can be extracted as the higher saturated values which are reserved. This study selects the range of saturation within 200~255. The data of red points is shown as table 1. The mass center and the area of red point 1 are located at (17.2, 16.6) and 154 pixels respectively, red point 2 are located at (135, 17.2) and 149 pixels, red point 3 are located at (17.4, 135.5) and 152 pixels, red point 4 are located at (136.7, 136.1) and 150 pixels. As shown in table 1, even though the sizes of the four points are the same, the results obtained in the image plane are a little bit different. The reasons are as following; 1. The distortion caused by the camera itself, 2. The difference of saturation happened due to uneven lighting. The maximum difference of red point is 5 pixels, which is negligible since there is almost no influence. The distances of red points can be obtained from following equation. X=118.5, Y=118.9, each point is the length of the image plane in 1 inch. Thus, the region of interest (ROI) to check the scarping image is an area with 119 pixels long and 119 pixels width.

$$X = \frac{\sqrt{(x_2 - x_1)^2 + (y_2 - y_1)^2} + \sqrt{(x_4 - x_3)^2 + (y_4 - y_3)^2}}{2}$$
$$Y = \frac{\sqrt{(x_3 - x_1)^2 + (y_3 - y_1)^2} + \sqrt{(x_4 - x_2)^2 + (y_4 - y_2)^2}}{2} \quad (1)$$

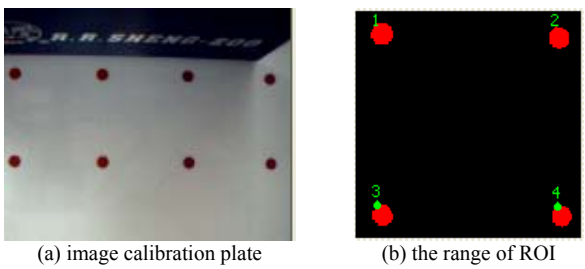

(a) image calibration plate (b) the range of ROI

Figure 3. Image calibration plate

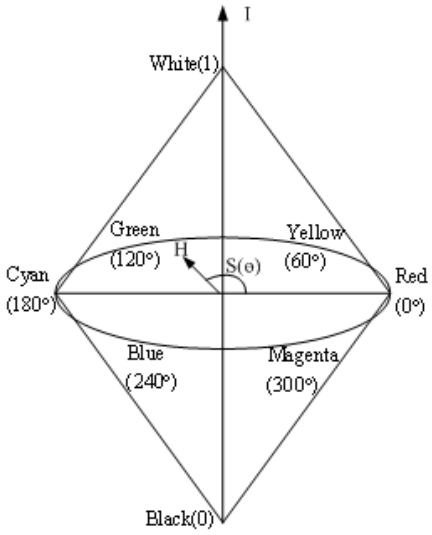

Figure 4. HSI color space

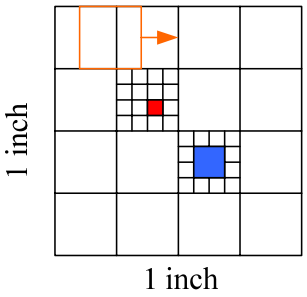

Figure 5. Scanning images method

TABLE1
IMAGE DATA OF CALIBRATION PLATE (UNIT: PIXEL)

	1	2	3	4
Center of Mass X	17.2	135	17.4	136.7
Center of Mass Y	16.6	17.2	135.5	136.1
Area	154	149	152	150

III. IMAGE ANALYSIS

Through the image calibration, the size of one square inch can be obtained in the image plane, which is assigned as ROI of image, and the image in ROI is calculated if complying with the requirement of scraping. Several questions will be encountered when determined with images; such as (1) it is difficult to have identical size at crest, due to manually scraping these days; (2) In the area of each square inch, there are many incomplete

points around the edges. To solve the questions, the contact of 16 points in each square inch is set as standard. Therefore, 1/16 of 1 square inch is used as a mask for scanning images. Meanwhile, convolution algorithm is used with images. The size of the scraping crest should be larger than 1/16 and smaller than 1/4 of mask, as shown in Figure 5. If there is no crest found in the convolution algorithm, it is determined as disqualified. The disqualified area will be marked for reference.

This study uses threshold segmentation to segment the disqualified scraping area. Threshold segmentation is a method to find the suitable critical values through histogram. Figure 6(a) shows the original image of scraping, and the red frame is a scanning area with 1/16 square inch. The scanning procedure is started from left to right and from top to bottom. Figure 6(b) shows the histogram of the scraping image. The numbers of the brightness values with 100 are the maximum quantity in the image while the image for looking for the reflective surface in Figure 6(a) can be found, which shows that the brightness value is a little bit high.

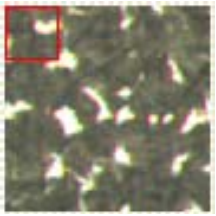

(a) original image

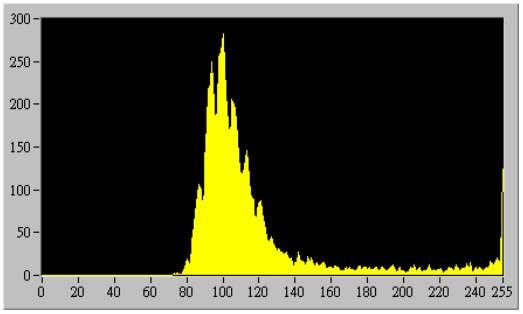

(b) histogram of scraping image

Figure 6. Image processing by histogram

Therefore, Threshold is set between 100 and 255. The binary image as shown in Figure 7(a) is obtained. Figure 7(a) shows the most crests that need scraping which can be segmented with Threshold segmentation. However, there are still some tiny noises that must be filtered out. And the effective crest size defined above, in the image of 119×119 images in this experiment, it is defined to be between the value of 55 and 221. Therefore, the crest which is not within this range will be deemed as noises and filtered out. Figure 7(b) shows the result that the noises are cleared

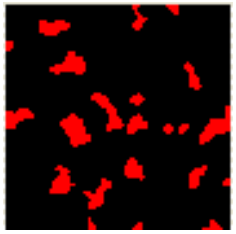

(a) threshold segmentation result

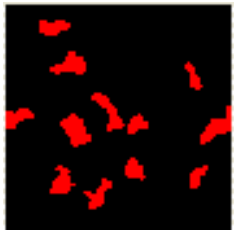

(b) noises removed result

Figure 7. Threshold segmentation result

Through the image processing procedures as mentioned in above, the crests in scraping image can be segmented. Next, the whole image is checked with the 1/16 square inch area which is set as described above. The method is to carry out convolution algorithm through this area with image. And the searched area where is disqualified will be marked as 1. Set the image of m×n as f, and mask T is value of matrix m×m = 1. The calculation of equation convolution can be given as following equation and the result is shown in Figure8(a).

$$f'(x,y)=\sum_{i=0}^{m-1}\sum_{j=0}^{m-1}T(i,j)f\left(x+i-\frac{m-1}{2},y+j-\frac{m-1}{2}\right)=T*f(x,y)$$

(x=0,1,…,M-1; y=0,1,…,N-1; i=0,1,…,m-1;j=0,1,…,m-1)

$$\begin{cases}T*f(x,y)\le 0, & f'(x,y)=1\\ T*f(x,y)>0, & f'(x,y)=0\end{cases} \quad (2)$$

The image f' is a binary image. The position marked with "1", which represent the location that is determined by mask "T" as disqualified. The image f' is convolution through morphology with another mask "G". All the disqualified area can be extracted as following equation. Figure8(b) shows the result of convolution. It can clearly confirm that the disqualified areas are located.

$$f''(x,y)=\sum_{i=0}^{n-1}\sum_{j=0}^{n-1}G(i,j)f\left(x+i-\frac{n-1}{2},y+j-\frac{n-1}{2}\right)=G*f'(x,y)$$

(x=0,1,…,M-1; y=0,1,…,N-1; i=0,1,…,n-1;j=0,1,…,n-1)

$$\begin{cases}G*f'(x,y)\ge 1, & f''(x,y)=1\\ G*f'(x,y)<1, & f''(x,y)=0\end{cases} \quad (3)$$

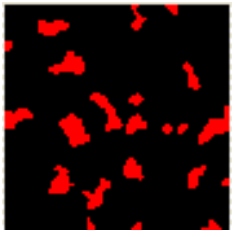

((a) $T*f(x,y)$ result

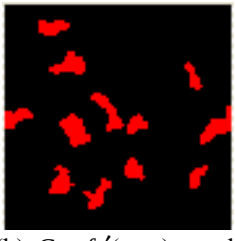

(b) $G*f'(x,y)$ result

Figure 8. Convolution result

IV. EXPERIMENT

Figure 9 shows the prototype of scraping guide ways inspection device. The design of the stand can be varied along with the range of movement where the inspected items are stored and different angles may be applied. The tripods with various lengths can be replaced. The fixture of camera can be adjusted upward or downward with travel distance 280mm, which is to obtain the best focus range. This fixture can be also moved forward or backward for a range of 200mm, which meet the request of purpose for wide range of inspection.

Figure 9. Prototype of scraping guide ways inspection device

Figure 10 shows the result of processing scraping image. To illustrate the fact of each shot, the detail is described as following:

(1) Figure10 (a1) is the first original scraping image. Through the image processing method as described above, first point can be found that the brightness is larger than 100 with Threshold segmentation. The results are shown in figure 10 (a2), there are 21 scraping points found. However, the sizes of the points are different. All the points are either too big or too small which is deemed to be ineffective crest. Thus, through the sieve of effective crests, Figure 10 (a3) is obtained. The effective crests are 10 points. The image is format with convolution algorithm with 1/16 square inch mask. The disqualified location will be marked as 1. The red part as shown in Figure 10(a4) those are all the marked locations. The image shows in Figure 10(a4) is format with convolution algorithm. The purpose is to spread the points marked as 1 to areas, as shown in figure 9(a5). Eventually, the disqualified areas are marked in figure 10(a3). The inspectors can find which one is the disqualified area, as shown in figure 10 (a6). From the results, there are a number of 10 points of scraping contact, which is not meet the requirement. As for the uniformity inspection, apparently, there are four areas disqualified.

(2) Figure10(b1) shows the second scraping original image. Through Threshold segmentation, 19 scraping points can be found. The result is as shown in Figure 10(b2). Through the procedure, the sieve of effective crest, Figure10(b3) is obtained. The effective crests are 13 points. Through twice of convolution algorithms, the disqualified locations are marked, and the points are spread to different areas, shown as Figure 10(b4) and figure 9(b5). Eventually, the disqualified areas are marked in 10(b3). The inspectors can find which one is the disqualified area. The result is shown as Figure 10(b6). It's confirmed that the number of scraping contact point is only 13 points, which is not meet the requirement. As for the uniformity inspection, it is obviously found that a large area is disqualified.

(3). Figure 10(c1) shows the third scraping original image. Through Threshold segmentation, 24 scraping points can be found, among which 12 points are effective crests. And the results as shown in Figure 10(c6), the number of scraping contact point is only 12 points, which does not meet the requirement, too. As for the uniformity inspection, it is obviously found that 3 large areas are disqualified.

(4). Figure 10(d1) shows the fourth scraping original image. Through Threshold segmentation, 19 scraping points are found, among which there are 14 points which is effective crests. From the result as shown in Figure 10(d6), the number of scraping contact point is 14 points, which does not meet the requirement. As for the uniformity inspection, it is obviously found that an area is disqualified.

(5). Figure 10(e1) shows the fifth scraping original image. Through Threshold segmentation, 16 scraping points are found, among which there are 10 points which is effective crests. From the result in Figure 10(e6), the number of scraping contact point is 10 points, which does not meet the requirement. As for the uniformity inspection, it is obviously found that 3 areas are disqualified.

From the results as mentioned above, it's realized that all disqualified numbers of bearing points and the areas can be clearly found. This is also verified the methods for image processing adopted in this research have excellent effects. Figure 11 shows the human machine interface. The image on the left is the original image caught by camera. The red frame in the photo is the scanning area of 1/16 square inch. Through the image processing methods as described above, the image on the right is obtained. When the area of disqualified block is 0, and the number of effective contact point is between 16~24, it is determined as qualified, and the OK indicator will be lit up. On the contrary, if one of the conditions does not meet, it is determined as disqualified, and NG indicator will be lit up. Through the information of coordinate and area, the locations and the sizes of all points can be found. The smallest one is at point (11.68, 7.24) with area of 2.56 mm^2; the largest one is at point (17.84, 7.87) with area of 6.14 mm^2. As shown in Figure 11, which shows the analysis result of Figure10(e6). This research takes the inspection item as an example to input LabView system for analysis. From the analysis report, it can be found that the area of disqualified block is 297.392 mm^2, and the effective contact points are only 10 points, which does not meet the standard. Thus, the result is determined

as NG. Figure 11 shows that X and Y mark the coordinate location of the inspected point respectively. The area of the inspected point is calculated by computer. Meanwhile, the qualification can be determined by checking if this area is larger than the set area.

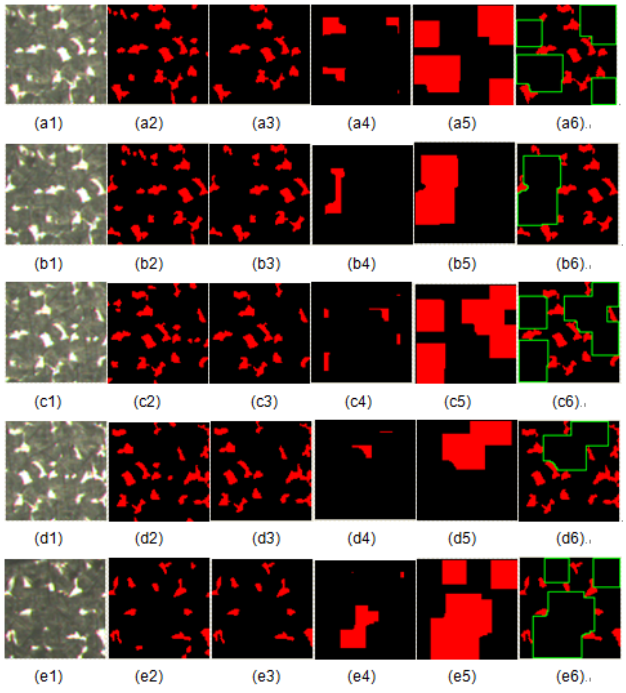

Figure 10. Result of processing scraping image

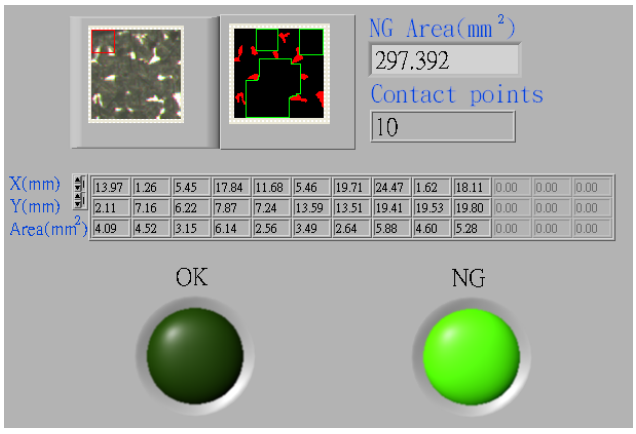

Figure 11. LabView system analysis report

V. Conclusion

The scraping guide ways inspection device can accurately inspect the contact points of the guide way of machine, as concluded as the following:

The study can accurately inspect the contact points of the sliding surface on the guide ways with optical methods to ensure the precision and quantity of contact point of guide way.

The digitized inspection data are obtained. In addition to the number of contact points and the uniformity, the area of each point can be calculated to eliminate the possible errors by determinations with naked eyes.

The eyes inspection mistakes can be avoided and prevent the time wasting from the assembly of machine, which is to be dismantled to improve the production margin.

Acknowledgment

Thanks to funds sponsored by Challenger Company, which support us to complete this research, scraping inspection machine has been implemented in the production line in Challenger Company for product inspection since mid of 2010.

References

[1] J. Gao, D.T. Zheng, N. Gindy, D. Clark, Extraction/conversion of geometric dimensions and tolerances for machining features, Int J Adv Manuf Technol Vol. 26(2005) pp. 405-414.

[2] J. Y. Lee, K. Kim, Generating alternative interpretation of machining features. Int J Adv Manuf Technol Vol. 15(1999), pp. 38–48

[3] J. Gao, D. T. Zheng, J. Sun, Study on mathematical model of feature conversion in domains between design and manufacturing. Chin J Mech Eng Vol. 8(1998), pp. 4–11

[4] J. J. Shah, Y. Yan, B. C. Zhang, Dimension and tolerance modeling and transformations in feature based design and manufacturing. J Intell Manuf Vol. 9(1998), pp. 475–488

[5] H. J. Pahk, J. S. Park, I. Yeo, Development of straightness measurement technique using the profile matching method, Int J Mach Tools Manuf Vol. 37(1997), pp.135-147.

[6] M. Burdekin, H. Pahk, The application of a micro computer to the on-line calibration of the flatness of engineering surfaces. Proc. Instn Mech. Engrs Vol. 203(1989), pp. 127-137.

[7] R. M. Haralick, S. R. Sternberg, X. Zhuang, Image Analysis using mathematical morphology, IEEE Trans Pattern Anal Mach Intell Vol. PAMI-9(1987), pp. 532-550.

[8] S. Godbole, A. Amin , Mathematical morphology for edge and overlap detection for medical images, R Time Imag Vol. 1(1995), pp. 191-201

[9] J. Yang, X. Li, Boundary detection using mathematical morphology, Pattern Recogn Lett Vol. 16(1995), pp.1277-1286

[10] F. Y. Shih, S. Cheng, Adaptive mathematical morphology for edge linking , Inform Sci Vol. 167(2004), pp.9-21

[11] M. Nachtegael, E. E. Kerre, Connections between binary, gray-scale and fuzzy mathematical morphologies, Fuzzy Set Syst Vol. 124 (2001), pp. 73-85

[12] L. Yu, R. Wang, Shape representation based on mathematical morphology, Pattern Recogn Lett Vol. 26(2005), pp.1354-1362

[13] H. D. Cheng, X. H. Jiang, J. Wang, Color image segmentation based on homogram thresholding and region merging, Pattern Recogn Vol. 35(2002), pp. 373–393.

[14] P. K. Saha, J. K. Udupa, Optimum image threshold via class uncertainty and region homogeneity, IEEE Trans Pattern Anal Mach Intell Vol. 23(2001), pp. 689–706.

[15] S. A. Hojjatoleslami, J. Kittler, Region growing: a new approach, IEEE Trans Image Process, Vol. 7(1998), pp.1079–1084.

[16] L. Vincent, P. Soille, Watershed in digital spaces: An efficient algorithm based on immersion simulations, IEEE Trans Pattern Anal Mach Intell, Vol.13(1991), pp. 583-598.

Ying-Shing Shiao received the Ph.D. in Electrical Engineering from National Cheng Kung University in 1992. He is a Professor in Department of Electrical Engineering, National Changhua University of Education, Changhua, Taiwan. His research interest includes computer vision, digital image processing, control engineering, and intelligent robot.

Ching-Wei Wu received the M.S. in Electrical Engineering from National Changhua University of Education. He is pursuing the Ph.D. degree in Department of Electrical Engineering, National Changhua University of Education, Changhua, Taiwan. His current research interests include visual control and computer vision.

Ching-Feng Chang graduated in electrical engineering from National KaoHsiung University of Applied Sciences, Kaohsiung, Taiwan in 1975. And Received the M.S. degree of Electric Engineering in National ChangHua University of Education, ChangHua, Taiwan, in 2006. He continues his PH D degree study in electric enginee- ring, major items are motorized spindle and torque motor.

From 1977-1979, he was serving in his family company, there are mainly in producing metal cutting machines, including Turning machine and Planning Mills. He then found his own company in 1980, as a trading house and specally in marketing CNC metal working machines, and to increase the quality and service, he decided to start the production plant of CNC metal turning machines and CNC machining centers in 1996, main markets are N.A and European market, very successfully introduce his own brand into this market. He is now only the shareholder of his company, no more running the business daily basis.

Stereo Matching Using Iterative Dynamic Programming Based on Color Segmentation of Images

Fuzhi Wang
Key Laboratory of Manufacturing and Automation of Xihua University, Chengdu, China
redfires_789@163.com

Changlin Song and Qiang Du
School of Mechanical Engineer & Automation of Xihua University, Chengdu, China
clsong@126.com, duqiang2007@hotmail.com

***Abstract*—The traditional dynamic programming stereo matching algorithms usually adopt the disparity assumption based on the intensity change of images; With the development of stereo matching technique, the disparity assumption based on image color segmentation is proved to meet better the need of true scenes. The paper introduces the disparity assumption into the stereo matching using dynamic programming, proposes a new global energy function, which not only resolves the problem of traditional dynamic programming stereo matching algorthm that the energy function is short of intensity and disparity constraints between scan lines but also can be computed more exactly because the adopted dissimillarity function propsed by Birchfield is extended from 2-connect neighborhood to 8-connect neighborhood. The energy function can converge fast because of the proposed pruning algorithm based on color segmentation. The experiments show that the proposed method produces competitive results with the 2-dimensional energy function minimized algorithm but has the much lower computing cost than them.**

***Index Terms*—stereo matching, dynamic programming, color segmentation, energy function, visual disparity.**

I. INTRODUCTION

Stereo matching, which is to find the corresponding relationship between the pixels of two or more images taken from different viewpoints, is one of the most basic and important problems in computer vision and widely used in fields such as robot vision, autonomous vehicle navigation, visual inspection and tracking, etc.

According to whether using global reasoning or not, the stereo matching algorithm is usually divided into two types [1]: local optimal stereo matching based on WTA and global optimal stereo matching based on minimization of energy function. Dynamic planning stereo matching belongs to global optimal stereo matching algorithm, its matching process is easy to introduce sequence constraint of disparity. However, for traditional dynamic programming stereo matching, the visual disparity is determined only according to the two corresponding polar lines; therefore the dynamic planning stereo matching is called the one-dimensional energy algorithm and the matching error at a certain point is easy to spread down; In addition, the disparities between adjacent scan lines in traditional dynamic planning stereo matching algorithm are short of constraints. To solve these problems, Bobick A F proposed a dynamic programming algorithm based on GCP (Ground Control Point) [2], but the number and correctness of GCP will affect the matching performance; Leung S. C. proposed an algorithm called IDP to strengthen disparity continuity constraint between scanning lines [3]; Zhang H. F. furthermore combined the GCP with the IDP algorithm [4]; Jae C. K. proposed a two-pass dynamic programming technique combined with GCPs for a dense stereo matching [5]; The common feature of these methods is that they all adopt such a disparity assumption that the image intensity variation corresponds to disparity change. However, the assumption is workable only to a certain extent, therefore, the performance of the traditional dynamic planning stereo matching is still not ideal even relative to the best local stereo matching algorithm.

Besides matching accuracy, matching efficiency is another important question. Image segmentation is an efficient method to improve simultaneously matching efficiency and matching efficiency. For example, Cheng L. proposed a region-tree based stereo matching algorithm using dynamic planning [6]. Recently, a number of color segmentation based stereo matching algorithms confirmed the following assumptions: disparities of pixels within same color region changes continuously, discontinuous changes of disparity appear only on color segmentation region boundaries. It can be said that almost all the best stereo matching experiment results are obtained by segmentation-based global optimal algorithm such as Graph-cut, BP, etc [7-10]. However, such 2-dimensional global optimal algorithm's calculating cost is very huge, this limits its practical applications.

The paper introduces the disparity assumption based on color segmentation into the dynamic programming stereo matching and extends the dissimilarity measure function proposed in Ref.11 from 2-neighborhood to 8-

doi:10.4304/jcp.9.6.1491-1496

neighborhood, on these two points a new global energy function is proposed, which can be minimized iteratively to obtain high-quality disparity map. Because the iterative process is implemented by the forward pruning algorithm based on segmentation, the iterative process converges quickly. Therefore, the proposed method has good performance on both matching efficicency and matching accuracy.

II. Color Segmentation of Image

Applying color segmentation to stereo matching is because that there is a correspondence relation between the disparity change and the color change of stereo image, this assumption has been proved to basically meet the needs of the real scenes. In stereo-matching, Mean-shift based color segmentation algorithm has been widely used, this algorithm selects Epanechnikov kernel function to make a non-parameter estimation of the probability density distribution of the color mode by iteratively calculating the mean shift vector distribution to implements. This segmentation method requires little prior knowledge and has a high robustness and a high segmentation speed [12]. Figure 1 shows the results of color segmentation for Tsukuba image based on Mean-shit algorithm.

(a)Tsukuba image

(b) the color segmentation of Tsukuba image

Figure 1 color segmentation of Tsukuba image based on mean-shift

III. Iterative Dynamic Planning Stereo Matching Based on Color Segmentaion

Stereo correspondence is an inherently ambiguous problem. One reasonable and commonly made solution is to assume that visual scene is piecewise smoothting. The methods of obtaining piecewise smooth disparity map can be divided into two types: global optimal method and local optimal method. In global optimal stereo matching, the constraints on the disparity map are formulated into an objective function E(d) which is then minimized over all image pixels. A typical objective function has the following form:

$$E(d) = E_{\text{data}}(d) + E_{\text{smooth}}(d) \tag{1}$$

Where, $E_{\text{data}}(d)$ is called data item, used to measure the similarity degree between the pixels on corresponding polar lines of left image and right image ; $E_{\text{smooth}}(d)$ is called smoothing item, used to obtain the piecewise smoothing disparity map. The paper introduces the disparity assumption based on segmentation into the dynamic planning stereo matching and makes a new construction of data item and smoothing item.

A. Data Item

Data item measures how well the disparity function agrees with the input image pair and can be defined as follows:

$$E_{\text{data}}(d) = \sum_{i=1}^{N_p} c((x_i, u), d) - N_m K_m \tag{2}$$

Where, $c(x_k, u, d(x_k, y))$ represents the dissimilarity measurement of pixel (x_i, u) on left image with disparity d ; N_p represents the number of all pixels on the u row of left image; N_m represents the number of matching region (same disparity area), K_m represents the matching reward value, which can be interpreted as the maximum allowed of the dissimilarity between the corresponding points.

B. Smoothing item

Smoothing term encodes the smoothing assumptions of disparity made by the algorithm. The smoothing assumption states that disparity varies smoothly almost everywhere except at depth boundaries. Smoothing term is defined as :

$$\begin{aligned} E_{\text{smooth}}(d) = &\sum_k e_h\left(d(x_k, u) - d(x_{k-1}, u)\right) + \\ &\sum_k e_v\left(d(x_k, u) - d(x_k, u-1)\right) \end{aligned} \tag{3}$$

In above formula, the first term represents the disparity smoothness on polar lines, the second represents the disparity smoothness between polar lines. Where, e_h according to the Pots model is defined as:

$$e_h(\Delta d_h) = \begin{cases} 0 & \Delta d_h = 0 \\ K_{occ} + \lambda_h & \Delta d_h \neq 0 \end{cases} \tag{4}$$

According to the Pots model e_v is defined as follows:

$$e_v(\Delta d_v)=\begin{cases}0 & \Delta d_v=0,\pm 1\\ \lambda_v & else\end{cases} \quad (5)$$

Where, K_{occ} represents the punishment constant of occlusion. $\Delta d_h, \Delta d_v$ represents the disparity difference between the adjacent pixels in the horizontal and vertical directions. According to the relationship between the intensity changes and the disparity changes [11], it can be inferred that: on the left polar line (scanning line), occlusion area must be located on the left side of the boundary of the color segmentation region, and on the right scanning line, occlusion area is located on the right side of the boundary of segmentation region. The paper adopts the matching method from left to right. Provided y_j as the arbitrary pixel of right image, y_{j-1} is the pixel left to y_j and y_{j+1} is the pixel right to y_j, the corresponding pixel in the left image is $x_i = y_j + \delta$, δ is the disparity variable. Now in the case of Δd_h, Δd_v taking non-zero value , we discusses the determination method of the e_h, e_v i.e. λ_h, λ_v :

1) In the case that left image is continuous and right image is occlusive, the pixel left to occlusive region of the right image is considered. If the pixel point is the change point of color, $e_h(\Delta d_h)$ is rewarded by letting $\lambda_h = 0$ else $e_h(\Delta d_h)$ is punished by letting $\lambda_h = T_1$, which makes the changes of color are consistent with the changes of disparity.

2) In the case that right image is continuous and the left image is occlusive, the pixel right to occlusive region of the left image is considered. If the pixel is change point of color, $e_h(\Delta d_h)$ is rewarded by letting $\lambda_h = 0$ else $e_h(\Delta d_h)$ is punished by making $\lambda_h = T_1$, which makes the changes of color are consistent with the changes of disparity. Parameter λ_h can be determined according to the same as follows:

$$\lambda_h = \begin{cases}T_1 \ if \ (x_i,u)\in seg(x_{i-1},u)\,\&\,(x_i,u)\in seg(x_{i+1},u)\\ 0 \ if \ ((x_i,u)\notin seg(x_{i-1},u)\,\&\,(x_i,u)\in seg(x_{i+1},u))\\ \| \ ((x_i,u)\in seg(x_{i-1},u)\,\&\,(x_i,u)\notin seg(x_{i+1},u))\end{cases} \quad (6)$$

The parameter λ_v can be determined according to the same reason:

$$\lambda_v = \begin{cases}0 \ if \ (x_i,u)\in seg(x_i,u-1)\,\&\,(x_i,u)\in seg(x_i,u+1)\\ T_2 \ if \ (x_i,u)\notin seg(x_i,u-1)\end{cases} \quad (7)$$

From the definitions of parameters λ_h, λ_v it can be seen that because of using color segmentation instead of the conventional intensity change to indicate the variation of the disparity, a more accurate judgment of disparity change can be obtained.

Equ.1, Equ.2 and Equ.3 provide an iterative structure of dynamic planning stereo matching. If the $E(d)$ doesn't converge using dynamic planning, it can be minimized iteratively.

IV. Two Important Questions of Iterative Dynamic Planning Stereo Matching

A. 8-neighborhood Dissimilarity Measure Function Insensitive to Sample

Due to sampling, dissimilarity between pixels can not been measured simply by the intensity differences of pixels because the intensity differences becomes very large where grayscales change sharply and the disparity is not an integral number of pixels. The Ref.11 has proposed a dissimilarity measurement method which uses linear interpolation of the intensities of adjacent pixels to get the intensity function to calculate the dissimilarity; this method is proved to be not sensitive to the sampling.

Let I_1, I_r respectively denote the grayscale function of the left and right corresponding polar lines, x_i, y_i are the two pixel points to be calculated dissimilarity, and $\hat{I}_r$ is linear interpolation function of the sampling points on polar lines of right image, Ref.11 first definition:

$$\bar{c}(x_i,y_i,I_1,I_r)=\min_{y_i-\frac{1}{2}\le y\le y_i+\frac{1}{2}}\left|I_1(x_i)-\hat{I}_r(y)\right| \quad (8)$$

Dissimilarity between pixels x_i, y_i can be obtained by the following formula:

$$c(x_i,y_i)=\min\left\{\bar{c}(x_i,y_i,I_1,I_r),\bar{c}(y_i,x_i,I_r,I_1)\right\} \quad (9)$$

From Equ.8 and Equ.9 it can be seen that Ref.11 defined dissimilarity at the left and right neighborhoods of pixel so that the upper and lower adjacent polar lines lost constraint of intensity. Because of this, the paper makes the definitions as follows:

$$\bar{c}_{lr}(x_i,y_i,I_1,I_r)=\min_{-\frac{1}{2}\le\delta x,\delta y\le\frac{1}{2}}\left|I_1(x_i,y_i)-\hat{I}_r(x_i+\delta x,y_i+\delta y)\right|^2 \quad (10)$$

$$\bar{c}_{rl}(y_i,x_i,I_r,I_1)=\min_{-\frac{1}{2}\le\delta x,\delta y\le\frac{1}{2}}\left|I_r(x_i,y_i)-\hat{I}_l(x_i+\delta x,y_i+\delta y)\right|^2 \quad (11)$$

Where, $\hat{I}_l, \hat{I}_r$ are linear piecewise continuous fitting function, the maxima or the minimal point of linear piecewise continuous function must be the breakpoints of function, thus:

$$I_r^{\max} = \max_{\delta x,\delta y=-1,0,1} \frac{1}{2}\{I_r(x,y)+I_r(x+\delta x, y+\delta y)\}$$
$$I_r^{\min} = \min_{\delta x,\delta y=-1,0,1} \frac{1}{2}\{I_r(x,y)+I_r(x+\delta x, y+\delta y)\} \quad (12)$$

Then, $\bar{c}_{lr}(x_i, y_i, I_l, I_r)$ can be computed as follows:

$$\bar{c}(x_i, y_i, I_l, I_r) = \max\{0, I_l(x,y)-I_r^{\max}(x,y), I_r^{\min}(x,y)-I_l(x,y)\} \quad (13)$$

For $\bar{c}(y_i, x_i, I_r, I_l)$, it can be treated in the same way. Thus, the measure of the dissimilarity between the two pixels of the left and right images can be defined as follows:

$$c(x_i, y_i) = \min\{\bar{c}(x_i, y_i, I_l, I_r), \bar{c}(y_i, x_i, I_r, I_l)\} \quad (14)$$

Dissimilarity measurement obtained by the Equ.13 still maintains the sampling-insensitive advantage because it still uses the linear interpolation method. At the same time, the new measurement function is computed over 8-connected neighborhood, this strengthens intensity constraint between polar lines, the dissimilarity calculation and energy function can be computed accurately.

Figure 2 shows the experimental results. We can see that the 8-neiborhood Birchfield function has the better performance of measuring the dissimilarity between pixels.

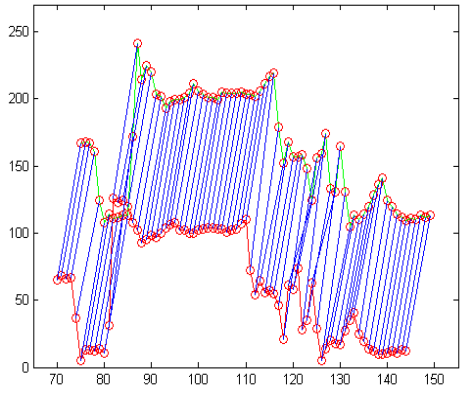

(a) Pixel corresponding between the left and right images

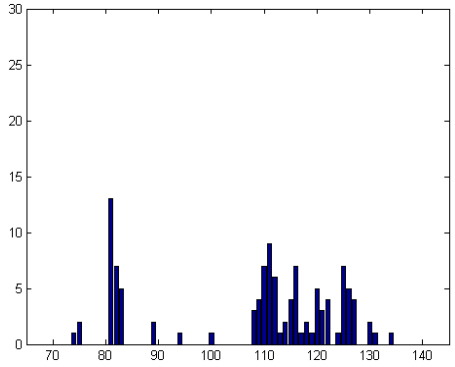

(b) The dissimilarity measurement by 2 neiborhood Birchfield function

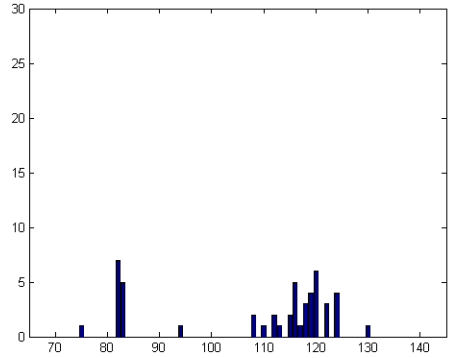

(c) The dissimilarity measurement by 8-neiborhood Birchfield function

Figure 2 The dissimilarity measurement between pixels

B. Fast Implementation of Iiterative Dynamic Programming Stereo Matching Based on Color Segmentation

The dynamic planning has the disadvantage of "curse of dimensionality", how to make the energy function converge fast has become a key issue. G. Van Meerbergen proposed a hierarchical symmetric stereo algorithm [13]; Olga Veksler proposed a fast algorithm based on tree structure decomposition [14]. The Ref.11 proposed a pruning algorithm, but the algorithm adopts disparity assumption based on intensity change, therefore, although this algorithm has a high matching efficiency, the matching accuracy is not ideal.

In order to obtain ideal matching accuracy and matching speed, the paper proposed the forward pruning algorithm based on color segmentation, i.e Figure 3. In this algorithm, $\varphi[\delta, y]$ is the cost of the best match sequence (so far) ending at match $(y+\delta, y)$; m_y represents the minimum matching cost of certain column of the $x-y$ searching grid. $m_x[x]$ represents the minimum matching cost of certain row of the $x-y$ searching grid. update_path represents the updating function of the matching path and cost . The key to the new algorithm is at the 4, 8, 9, 10, 13 row. At the rows 8 and 10, the change of disparity is judged by the boundary of segmentation region in place of the change of intensity. This method not only protects the image edges but also enhances the piecewise smoothness

of disparity of image. At the rows: 4, 9 and 13, the disparity constraint between the scanning lines is introduced and the dissimilarity is measured on the 8-connected neighborhood, the two methods make the energy function more exact. When the energy function is minimized iteratively, an accurate disparity map can be obtained.

Seen from the Figure.3, the proposed algorithm is established on the fact that there are not the disparity changes within the same segmentation region (called sub-segmentation). Therefore, it is better to select over-segmentation.

01 for $y_p \leftarrow 0$ to $n-2$
02 $m_y \leftarrow \min\{\varphi[0, y_p], \varphi[1, y_p], \cdots, \varphi[\Delta, y_p]\}$
03 for $\delta_p \leftarrow 0$ to Δ
04 update_path$(\delta_p, y_p, \delta_p, y_p+1)$
05 if $\varphi[\delta_p, y_p] \le m_y$ then
06 $y \leftarrow y_p + 1$
07 for $\delta \leftarrow \delta_p + 1$ to Δ
08 *if* $(y+\delta-1) \notin \text{seg}_x(y+\delta)$
09 update_path$(\delta_p, y_p, \delta_p, y)$
10 if $\varphi[\delta_p, y_p] \le \text{m}_x[\delta_p + y_p]$ and $(y_p+1) \notin \text{seg}_y(y_p)$
11 for $\delta \leftarrow 0$ to $\delta_p - 1$
12 $y \leftarrow y_p + \delta_p - \delta + 1$
13 update_path$(\delta_p, y_p, \delta, y)$

Figure 3 pruning algorithm based on image segmentation

V. Experiment Results and Analysis

The experiments are done with the stereo images from Middlebury University. Some parameters are introduced into the energy function, these parameters are set as follows: the matching award $K_m = 15$, $K_{occ} = 50$, T_1=80, $T_2 = 7$.

The experimental results are shown in Figure 4. It can be seen from Figure 4 that the proposed method can protect better the edges of the image because the disparity change is judged by color segmentation; it also can be seen that the proposed algorithm overcomes basically the foreground expansion drawback of usual dynamic programming stereo matching algorithms such as Ref.11.

Table 1 shows the quantitative comparison results of the proposed algorithm's performance indicators with other algorithms'. The three performance indicators are respectively the nnoc, all, disc proposed in the Ref.1. Where, DP represents the experiment results of the classic dynamic programming stereo matching [1]. Adaptweight represents the experiment results of one of the best stereo matching algorithm based on area matching [15]. AdaptingBP represents the experiment results of one of the best stereo matching algorithm based on the two-dimensional energy function [16].

Computational efficiency comparison of various matching algorithm has currently no literature to refer to, we can only make a rough comparison. Such two-dimension energy function algorithms as Graph-cut, BP need a few minutes to complete matching for the standard stereo images [10]. Even optimized by the image segmentation technique, these algorithms still need tens of seconds machine. However, the proposed algorithm takes only 4.723s to completes stereo matching for Tsukuba image pair on the computer with configuration: CPU 2.67G.

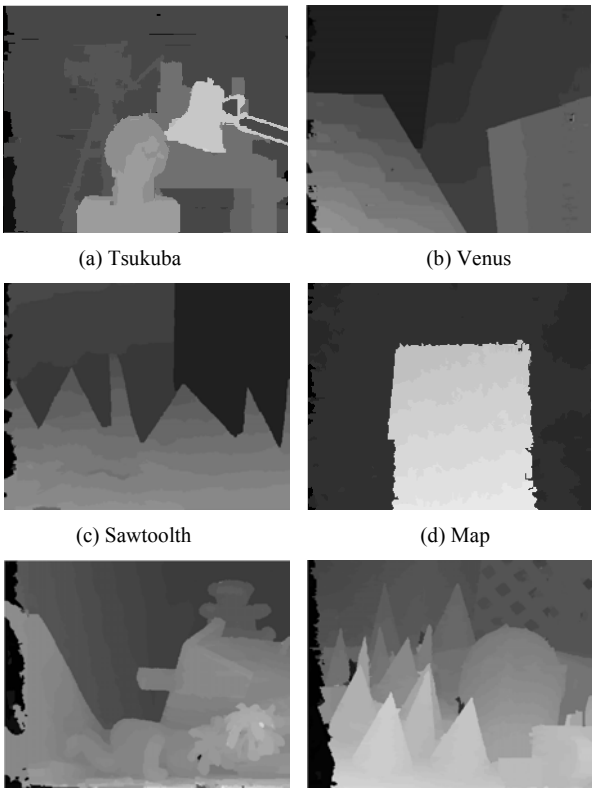

(a) Tsukuba (b) Venus

(c) Sawtoolth (d) Map

(e) Teddy (f) Cones

Figure 4 The experimental results of the proposed iterative dynamic planning stereo matching

TABLE 1

COMPARISON RESULTS OF THE PROPOSED ALGORITHM WITH OTHER ALGORITHMS

Algorithm		Proposed method	DP	Adaptive-Weight	Adaptive-BP
Tsukuba	nnoc	1.17	4.12	1.38	1.11
	all	1.50	5.04	1.85	1.37
	disc	5.43	12.0	6.90	5.79
Venus	nnoc	0.64	10.0	0.71	0.10
	all	0.88	11.0	1.19	0.21
	disc	5.23	21.0	6.13	1.44
Teddy	nnoc	6.87	14.0	7.88	4.22
	all	9.76	21.6	73.3	7.06
	disc	16.8	20.6	18.6	11.8
Cones	nnoc	3.52	10.5	3.97	2.48
	all	8.57	19.1	9.79	7.92
	disc	8.14	21.1	8.26	7.32

ACKNOWLEDGMENT

This research was supported in part by Chunhui project of The Ministry of Education of China (NO. 12202528), important project of Xihua University (NO. Z1120223) and the Open Research Fund of Key Laboratory of Manufacturing and Automation (NO.SZJJ2011-019) , Xinhua University.

REFERENCES

[1] D. Scharstein, and R. Szeliski, "A taxonomy and evaluation of dense two-frame stereo correspondence algorithms," *Int. J. Comput. Vision*, vol. 47, no. 1-3, pp. 7-42, 2002.

[2] A. F. Bobick, and S. Sintille, "Large occlusion stereo," *Int. J. Comput. Vision (S0920-5691)*, vol. 33, no. 3, pp. 181-200, 1999.

[3] S. C. Leung, B. Appleton, and C. Sun, "Fast stereo matching by iterated dynamic programming and quadtree subregioning," in *Proc. Conf. British Mach.Vision*, London: British Mach. Vision Assoc. Press, 2004, pp. 97-106.

[4] H. F. Zhang, and C. X. Zhao, "Ground control point based stereo matching via iterative dynamic programming," *Chinese J. Sci. Instrum.*, vol. 29, no. 8, pp.1665-1669, 2008.

[5] C. K. Jae, M. L. Kyoung, and T. C. Byoung, etc., "A dense stereo matching using two-pass dynamic programming with generalized ground control points," in *Proc. Comput. Vision. Pattern Recogn.*, New York: IEEE Comput. Soc., 2005, pp. 1075-1082.

[6] C. Lei, J. Seizer, and Y. H. Yang, "Region-tree based stereo using dynamic programming optimization," in *Proc. IEEE Conf. Comput. Vision Pattern*, New York: IEEE Comput. Soc., 2006, pp. 378-385.

[7] H. Li, and G. Chen, "Segment-based sereo matching using graph cuts," in *IEEE Comput. Soc. Conf. Comput. Vision Pattern Recogn.*, Washington: IEEE Press, 2004, pp. 74-81.

[8] H. Tao, H. S. Sawhney, "Global matching criterion and color segmentation based stereo," *Proc. IEEE Workshop Appl. Comput. Vision*, Palm Springs: IEEE Press, 2000, pp. 246-253.

[9] M. Bleyer, and M. Gelauta, "Graph_cut_based stereo matching using image segmentation with symmetrical treatment of occlusions," *Signal Process.: Image*, vol. 22, no. 2, pp. 127-143, 2007.

[10] J. Sun, N. N. Zheng, and H. Y. Shum, "Stereo matching using belief propagation," *IEEE Trans. Pattern Anal. Mach. Intell.*, vol. 25, no. 7, pp. 787-800, 2003.

[11] S. Birchfield, and C. Tomasi, "Depth discontinuities by pixel to pixel stereo," in *Proc. Int. Conf. Comput. Vision*, USA: IEEE Press, 1998, pp. 1073-1080.

[12] D. Comanicin and P. Meer, "Mean shift: a robust approach toward feature space analysis," *IEEE Trans. Pattern Anal. Mach. Intell.*, vol. 24, no. 5, pp. 603-619, 2002.

[13] G. Van Meerbergen, M. Vergauwen and M. Pollefeys, etc. "A hierarchical symmetric stereo algorithm using dynamic programming," *Int. J. Comput. Vision*, vol. 47, no. 1, pp. 275-285, 2002.

[14] O. V. Eksler, "Stereo correspondence by dynamic programming on a tree," in *Proc. of the IEEE Conference on Computer Vision and Pattern Recognition*, New York: IEEE Comput. Soc., 2005, pp.384-390.

[15] K. J. Yoon, and I. S. Kweon, "Adaptive support-weight approach for correspondence search," *Pattern Anal. Mach. Intell.*, vol. 28, no. 4, pp. 650-656, 2006.

[16] A. Klaus, M. Sormann and K. Karner, "Segment-based stereo matching using belief propagation and a self-adapting dissimilarity measure," in *Int. Conf. Pattern Recogn.*, pp. 15-18, 2006.

Fuzhi Wang, received a Ph.D. degree from UESTC in 2010, now works in School of Machanical Engineer & Automation of XiHua University. His research Interests mainly concentrate on the automation technology based on machine vision.

Changlin Song, received a Ph.D from SWJTU in 2004, now works in School of Machanical Engineer & Automation of XiHua University.

Qiang Du，born in Zigong, China, in 1969. He received the Ph.D. degree from the University of Electronic Science and Technology of China, China, in 2011.He is currently a lecturer with the Xihua university, China. His research interests include the digital design and CFD application.

A SVD Feature based Watermarking Algorithm for Gray-level Image Watermark

Wei Wang
College of Computer Science and Technology, Jilin University, Changchun, China
Computer School, Dalian Nationalities University, Dalian, China
Email: wangwei@dlnu.edu.cn

Wenhui Li
College of Computer Science and Technology, Jilin University, Changchun, China
Email:wang09@mails.jlu.edu.cn

Yongkui Liu
Computer School, Dalian Nationalities University, Dalian, China
Email: ykliu@dlnu.edu.cn

Borut Žalik
Computer School, University of Maribor, Maribor, Slovenia
Email: borut.zalik@um.si

***Abstract*—In this paper, a novel gray-level image watermarking algorithm based on Singular Value Decomposition (SVD) feature and neural network is presented for copyright protection. Firstly, a new method which encodes the gray-level secret information into bit string is used. It uses the eigenvalues of SVD to extract the most valuable features of the watermark image and reduces lots of redundant information. Then based on human visual system's characteristic, the SVV (Singular Value and Variance) method is adopted to analyze the host image and choose the regions suitable for watermark embedding. Finally, the back propagation neural network is utilized for watermark recovery. Relying on the information contained in the extracted eigenvalues, the neural network is trained to recognize the original watermark. The application of the proposed scheme makes the gray-level watermark capable of transparent hiding. Results demonstrate that our method is robust to the intentional attacks and performs better than traditional methods.**

***Index Terms*—SVD, Neural Network, Watermarking, Singular Value**

I. INTRODUCTION

Digital watermarking is a technique that embeds secret information, such as identifiers, words, image logos and so on imperceptibly into multimedia data to prove data ownership. The special application of digital watermarking technique requires that the embedded watermark should be not only transparent to observers, but also robust enough so that it cannot be easily destroyed or removed after some digital image processing or attacks [1].

According to the practical application, the digital watermarking technologies can be classified into three types including image watermarking algorithm [1], audio watermarking algorithm [2] and video watermarking algorithm [3]. More recent research have turned their attention to image watermarking algorithms and developed many methods including spatial domain method, frequency domain method, physiological model method and so on [4-6].

According to the watermark detection method whether needs original host image, image digital watermarking algorithms can be classified into non blind watermarking algorithm and blind watermarking algorithm [7-9]. Non blind watermarking technology refers to the detection method needs original host image, while blind watermarking algorithm means that the watermark extraction doesn't need original image. In the process of non blind watermark extraction, it is hard to find the original image rapidly and accurately in the massive image database, so it affects the efficiency of watermark extraction. Therefore, blind watermarking algorithm has great research significance and practical value in the current research region of image digital watermark. In this paper, a blind watermark algorithm is developed to realize the digital copyright protection.

Nowadays there are many existing watermarking algorithms based on image watermarks [10-12]. Some methods embed the watermark information through changing the relative relationships of pixel values in spatial domain or the coefficient values of frequency domain [13]. Yoo et al. [13] has proposed a method

This work was supported by the Fundamental Research Funds for the central Universities of China and the National Natural Science Foundation of China (NO.61300089)
Corresponding author: Wenhui Li

doi:10.4304/jcp.9.6.1497-1502

which chooses some intermediate frequency coefficients after discrete wavelet transform and changes the average value of these neighboring coefficients to embed the BCD code of student identifier. The other methods are using coefficient quantization to realize the hiding of watermark. In literature [14], the DCT coefficients are quantified firstly and then be modified according to the value of embedded watermark.

In fact, the visual masking effect is also an important evaluation index of watermarking algorithm. Many algorithms only pay attention to specific watermark information hiding method, while ignoring the position of information hiding. According to Human Visual System (HVS) [15], embedding information in texture areas with high visual masking effect, can not only realize the watermark information hiding, but also can improve the robustness of information hiding. In [16] the authors present a watermarking approach which embeds the singular values (SVs) of the original image into the watermark to attain the lossless objective. The scheme degrades the quality of the embedded watermark image by replacing SVs of the watermark image with those of the original one to some acceptable degree in advance [1]. So in this paper a novel algorithm which uses the characteristics of the Singular Values (SV) to adaptively select watermark hiding position suitable for information hiding in the host image is proposed. The algorithm can not only achieve the purpose of information hiding, but also has large quantitative range of coefficients value changing to ensure the robustness of the algorithm. In addition, because more and more watermarks are gray-level images, this paper proposes a grayscale image watermark algorithm based on the scheme of literature [1]. The overview of the algorithm is shown in Figure 1.

The rest of this paper is organized as follows: Section II introduces our algorithm of watermark preprocessing and host image analyzing in detail. In Section III, we describe the watermark embedding algorithm, extraction algorithm and watermark recovery algorithm respectively. Experimental results are exhibited in Section IV. Finally, conclusions are given in Section V.

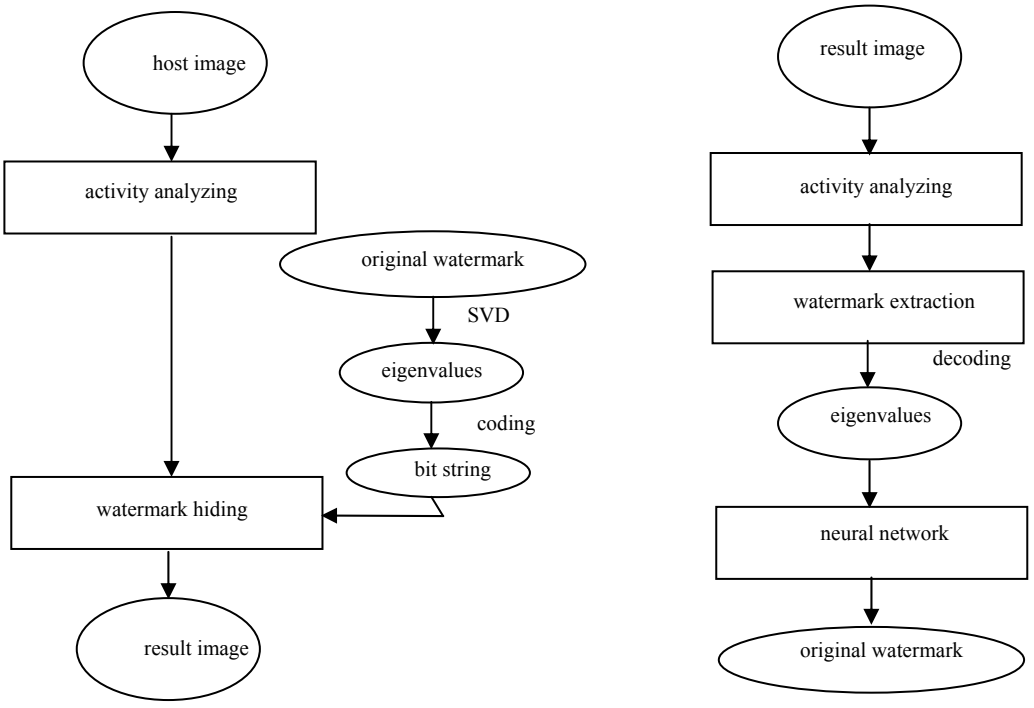

(a) (b)

Figure 1. An overview of the proposed watermarking scheme. (a) embedding scheme. (b) extraction scheme

II. IMAGE PREPROCESSING

2.1 Singular Value Decomposition

Singular Value Decomposition (SVD) is one of the most powerful numeric analysis techniques and its application in image compression and image watermarking field is also compelling [17-18].

Let A be a grayscale image with size of m×n. Every real matrix A can be decomposed into three matrices as $A = USV^T$ by SVD, where U and V are orthogonal matrices with size of m×m and n×n respectively, S is a diagonal matrix with the same size as A and with larger singular value entries in decreasing order satisfying $\lambda_{1,1} \geq \lambda_{2,2} \geq \cdots \geq \lambda_{r,r} > \lambda_{r+1,r+1} = \cdots = \lambda_{t,t} = 0$, r is the rank of A ($r \leq t,\ t = \min(m,n)$).

$$A=\begin{bmatrix} u_{11} & \cdots & u_{1m} \\ u_{21} & \cdots & u_{2m} \\ \vdots & & \vdots \\ u_{n1} & \cdots & u_{nm} \end{bmatrix}\begin{bmatrix} \lambda_{11} & 0 & \cdots & 0 \\ 0 & \lambda_{22} & \cdots & 0 \\ & & \lambda_{rr} & \\ 0 & 0 & & 0 \end{bmatrix}\begin{bmatrix} v_{11} & \cdots & v_{1n} \\ v_{21} & \cdots & v_{2n} \\ & \vdots & \\ v_{n1} & \cdots & v_{nn} \end{bmatrix}^T=\sum_{i=1}^{r}\lambda_i u_i v_i^T \quad (1)$$

2.2 Watermark Preprocessing

Most existing digital watermarking methods concentrated on the embedding methods of binary image as the watermark. Along with the development of multimedia and digital watermarking technique, more and more gray-level image watermark algorithms are needed because the gray-level image can take more information. In this paper we improve the method described in [1] and embed the watermark into the host image. The detail of the method is as follows.

Step 1: Perform SVD on the watermark image and extract the first 20 values of matrix S which are called eigenvalues in this paper [1].

Step 2: For every eigenvalue marked as Xi(1<=i<=20), firstly we use the floor(X) function to get the greatest integers less than or equal to X, and then we convert every decimal bit of Xi into binary number[1].

For example, if the eigenvalue Xi is '5379', the result will be '0101 0011 0111 1001' after the operation of step 2.

Step 3: Because most eigenvalues are no more than 10000, we make a length limitation of the encoded eigenvalue to 16 bits. If there are some encoded strings more than 16 bits, from left to right, we mark the first bits which are not belong to the 16 bits as W_high, the length of W_high is recorded as N, and then the first N bits of the encoded minimal eigenvalue is replaced by W_high. The W_high and the original code are separated by the string of '1111' which is not equal to any decimal bit form 0 to 9[1].

For example, if there is an eigenvalue '25379' and its bit string is '0010 0101 0011 0111 1001', a minimal eigenvalue '14' and its bit string is '0000 0000 0001 0100', after Step 3, W_high is marked as '0010', the two eigenvalues are marked as '0101 0011 0111 1001' and '0010 1111 0001 0100' separately.

Step 4: Horizontally concatenates the corresponding binary bit string according to the descending order of the 20 eigenvalues and save as W_encoded which will be embedded into the host image as secret information [1].

2.3 Host Image Analyzing

Based on human visual system's characteristic, the human eyes have different sensitivity to noise in areas with different luminance and texture. So we analyze the host image before watermark embedding to ensure the imperceptibility of the proposed watermarking scheme. In this paper we adopt the SVV (Singular Value and Variance) method to analyze the host image. The method is described as follows:

Step 1: Divide the host image into 8×8 sub-blocks in spatial domain.

Step 2: Compute each sub-block's variance V1 and find the maximum value V_max among them. Define the normalized variance as $A1 = V1 / V\_\max$.

Step 3: Perform singular value decomposition (SVD) on each sub-block and then computer E of the obtained S matrix.

$$[U\ S\ V] = svd(A), \qquad E = S(1,1)/S(2,2) \quad (2)$$

where A stands for the matrix of the sub-block, svd denotes the operation of SVD, U, S and V are the three result components of SVD transformation. S(1,1) and S(2,2) denote the two maximum values in the diagonal matrix S.

Step 4: Find the maximum value of E marked as E_max and define the normalized E as $A2 = E / E\_\max$.

Step 5: Calculate activity factor AF of each sub-block as

$$AF = \alpha 1 \times A1 + \alpha 2 \times A2 \quad (3)$$

where $\alpha 1$ and $\alpha 2$ are the weights of A1 and A2 with $\alpha 1 + \alpha 2 = 1$.

Step 6: Sort all the sub-blocks' activity factors in decreasing order. The sub-blocks which have large magnitude of activity factors have complex texture and median luminance and are suitable for embedding watermark with imperceptibility.

After analyzing the host image using our method, we have obtained the activity factors of all the sub-blocks. The high magnitude of activity factor means the corresponding sub-block is not only suitable for embedding watermark but also robust to the attacks. So we select the best sub-blocks which have large values of activity factors and good visual masking effect to embed watermark.

III. WATERMARKING ALGORITHM

3.1 Embedding Algorithm

In this sub-section, we employ singular value decomposition to embed watermark into the selected sub-blocks of host image after the preprocessing of the SVV method. Our algorithm is robust because the maximum SV is stable to the attacks that always encountered in digital image processing. SVD_based algorithm is described as follows:

Step 1: Perform SVD on each selected 8×8 sub-block.

Step 2: Choose the maximum SV marked as S(1, 1) in the diagonal matrix S.

Step 3: Use dither modulation method to insert one bit watermark signal into each sub-block according to Formula (4).

$$\begin{aligned} &L = fix(S(1,1), Q) \\ &if \quad W\_encoded(i) == 1 \quad S(1,1) = L \times Q \\ &else \quad W\_encoded(i) == 0 \quad S(1,1) = L \times Q + Q/2 \end{aligned} \quad (4)$$

where L denotes the integer part of the result of S(1, 1)/Q, W_encoded denotes the watermark bit and Q denotes the quantization step.

Step 4: Perform the inverse SVD on each sub-block to get the modified sub-image.

Step 5: Embed the watermarked sub-image back into the original host image.

3.2 Extraction Algorithm

Watermark extraction algorithm is the exact inverse process of embedding algorithm. Watermark could be extracted without the original host image as soon as we get the secret keys.

Step 1: The value of extracted bit for a given sub-block is calculated according to Formula (5).

$$Z = \mathrm{mod}(S*(1,1), Q)$$
$$\begin{aligned} &if\ (Z - Q/2) < Q/4 \quad && W\_recover\ (i) = 0 \\ &else && W\_recover\ (i) = 1 \end{aligned} \tag{5}$$

where Z stands for the modulus after division of S*(1, 1) and Q, Q is transmitted as secret key.

Step 2: Decode the obtained W_recover according to the inverse order of coding and record the result as W_Decoded. W_Decoded denotes the eigenvalues of the watermark.

Step 3: Use Neural Network to regain the hidden watermark.

In this paper, we utilized the method based on back propagation (BP) neural network (NN) for watermark recovery [19-20]. Relying on the information that the extracted eigenvalues contained, the neural network is applied to recognize the original watermark. This method is able to associate the accurate content of watermark, which contributes a lot to the work of tracing multimedia data distribution.

3.3. Neural Network Training

In this sub-section, the work of training neural network is done to make it possess the capability of memorizing the characteristics of different watermarks. First, a huge number of watermarks are collected as the training set which we have performed different kinds of attacks on them with distinct factors. Then we take each watermark as data matrix X and get the first 20 eigenvalues after performing SVD as the neural network input feature. Every unique output node is assigned to every different watermark. The 20 eigenvalues marked as $B_k = (a_1, a_2, \cdots, a_p)$ while the NN output marked as $Y_k = (y_1, y_2, \cdots y_q)$ form the training-pair patterns, where p stands for the number of input nodes, q denotes the number of output nodes and k is the total number of training patterns of training set. The structure of the BP neural network is three layers including an input layer with 20 nodes, a hidden layer with 35 nodes, and an output layer with q nodes which can be easily changed in the training process according to the actual number of different watermarks.

3.4. Watermark Recovery based on the BPNN

The trained neural network performs a highly adaptive ability of recognition. Take the regained 20 eigenvalues which were extracted from the host image following the instruction of the former sections as input pattern and feed them to the BP neural network. The exact original watermark will be recognized by the network according to the identifier of output pattern.

IV. RESULTS AND DISCUSSION

Figure 2 and Figure 3 are the result images of test images 'Barbara' and 'Baboon' of size 512×512. Figure 4 and Figure 5 show the original gray-level watermark of size 64×64， 128×128. Taking 'Baboon' image for example, in the experiment we first calculate each sub-block's activity factor according to the image's texture and gray information. The watermarks as shown in Figure 4(a) and Figure 5(a) are respectively embedded into the selected sub-blocks using our algorithm. In the process of embedding, the weights value of $\alpha 1$ and $\alpha 2$ used in the experiments are set to 0.1 and 0.9 respectively, and the quantization step used is set to 55.

The PSNR (peak signal-to-noise ratio) is used in this paper to access the imperfectability of our algorithm, as follows:

$$PSNR = 10 \times \log_{10}\left(\frac{M \times N \times \max(I^2(i,j))}{\sum_{i=1}^{M}\sum_{j=1}^{N}[I(i,j) - I^*(i,j)]^2}\right) \tag{6}$$

where I(i, j) denotes the gray value of host image pixel, I*(i, j) denotes the gray value of watermarked image pixel, M and N are the height and width of host image.

Because of the encoding processing for the watermarks of the proposed algorithm, the sizes of the watermarks are independent on our embedding scheme. Table 1 shows the PSNR results of different watermarked host images which have hidden different sizes of watermarks. All the results of PSNR are capable to insure the fidelity of the watermarked host images.

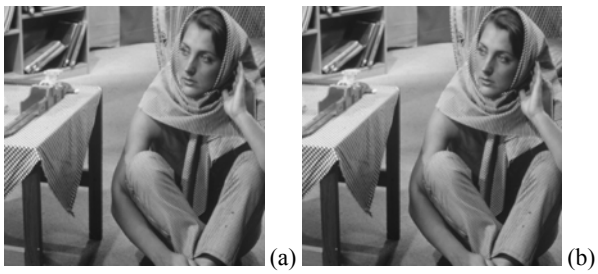

(a) (b)

Figure 2. (a) Original host image 'Barbara'. (b) Watermarked image

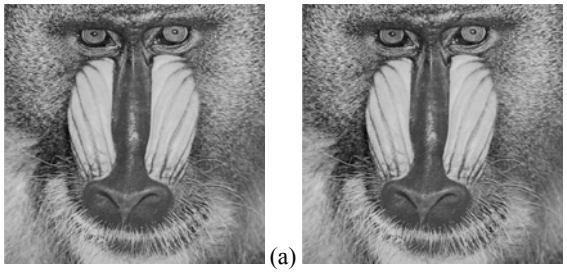

(a) (b)

Figure 3. (a) Original host image 'Baboon'. (b) Watermarked image

(a) (b)

Figure 4. (a) Original watermark 'Logo' of size 64×64. (b) Watermark extracted from Figure 3(b) after watermark recovery

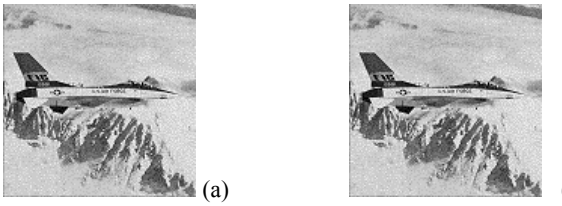

(a) (b)

Figure 5. (a) Original watermark 'Airplane' of size 128×128. (b) Watermark extracted from Figure 3(b) after watermark recovery

TABLE 1.
THE PSNR OF DIFFERENT WATERMARKED HOST IMAGES FREE OF ANY ATTACKS

Host image / Watermark		Barbara	Baboon
Logo	64×64	41.7439	42.4396
Airplane	128×128	41.6653	42.8744

TABLE 2.
THE RESULT OF WATERMARK RECOVERY AFTER JPEG 30% ATTACK BASED ON BPNN

after JPEG 30% attack	Barbara	Baboon
Watermark total number	20	20
Right recognized number	20	19
Wrong recognized number	0	1
Precision	100%	95%

TABLE 3.

THE RESULT OF WATERMARK RECOVERY AFTER MULTIPLE ATTACKS BASED ON BPNN

after crop 50% + Noise 2%	Barbara	Baboon
Watermark total number	20	20
Right recognized number	18	19
Wrong recognized number	2	1
Precision	90%	95%

In the watermark recovery sub-section, the extraction results are first decoded into the regained eigenvalues of the watermark, and then fed to the BPNN. Figure 4 (b) and Figure 5 (b) show the result original watermarks that recognized by the NN. In the experiment, the eigenvalues of 20 gray-level watermark images are extracted and trained in the proposed BPNN. Table 2 and Table 3 shows the watermark recovery results after different attacks based on BPNN, where 'JPEG 30%' means JPEG compression with quality factor of 30% , 'crop 50% + Noise 2%' means crop the watermarked image with the ratio of 50%, and then add the Pepper and Salt noise with the density of 2%. The precision for different attacks indicates that the proposed algorithm is robust and the watermark recovery for gray-level watermark images is flexible and applicable.

V. CONCLUSION

In this paper, a novel technique of digital image watermarking has been discussed. Our method is a new algorithm that employs the SVD to encode the gray-level watermark and extract watermark. We have utilized the characteristics of singular values and variance to preprocess the host image and then embed the watermark into the selected sub-blocks. Results demonstrate the excellent performance on both robustness and transparency of our scheme.

REFERENCES

[1] Wei Wang, Chengxi Wang, "A Watermarking Algorighm for Gray-level Watermark based on Local Feature Region and SVD", *International Congress on Image and Signal Processing*, 2008, 650-654.

[2] Shuo-Tsung Chen, Huang-Nan Huang, Chur-Jen Chen, Kuo-Kun Tseng, Shu-YiTu, "Adaptive audio watermarking via the optimization point of view on the wavelet-based entropy", *Digital Signal Processing*, 23 (2013) 971–980.

[3] Th. Rupachandra Singh, Kh. Manglem Singh, Sudipta Roy, "Video Watermarking Scheme based on Visual Cryptography and Scene Change Detection", *International Journal of Electronics and Communications*, Volume 67, Issue 8, August 2013, Pages 645–651.

[4] Frederic Lusson, Karen Bailey, Mark Leeney, Kevin Curran. "A Novel Approach to Digital Watermarking, exploiting Colour Spaces", *Signal Processing*, 93 (2013) 1268–1294.

[5] F. Qi, J. Wu, G. Shi, "Extracting Regions of Attention by Imitating the Human Visual System", *Proceedings of the IEEE International Conference on Acoustics, Speech and Signal Processing*, 2009, 1905–1908.

[6] S.P. Mohanty, P. Guturu, "A Novel Invisible Color Image Watermarking Scheme using Image Adaptive Watermark Creation and Robust Insertion-Extraction", *ACM Transactions on Multimedia Computing Communications and Applications*, 5(2), 2008, 1–24.

[7] Yong C Kim, et al. "Two-Step Detection Algorithm in a HVS-based Blind Watermarking of Still Images". *Lecture Notes in Computer Science*, Springer-Verlag Heidelberg, 2003, 2613: 235-248.

[8] Huang Jiwu, G F Elmasry. "An Algorithm for Meaningful Watermarks Based on Matched Filtering", *ACTA ELECTRONICA SINICA*, 2001, 29 (4), 447-451.

[9] Yongwon Jang, Intaek Kim, et al. "Blind Watermarking Algorithm Using Complex Block Selection Method". *Lecture Notes in Computer Science*, Springer-Verlag Heidelberg, 2001, 2195: 996.

[10] M.V.S.S. BABU. "A Robust Watermarking Algorithm for Image Authentication", *International conference of information and network technology*, 2012, 200-207.

[11] Wei Wang, Wenhui Li, Chengxi Wang, Huijie Xin. "A Novel Watermarking Algorithm based on SURF and SVD", *TELKOMNIKA*, VOL. 11, No 3, 2013, 1560-1567.

[12] Tai-yue Wang, Hong-wei Li, "A Novel Robust Color Image Digital Watermarking Algorithm Based on Discrete Cosine Transform", *Journal of Computers*, VOL.8, NO.10, 2013, 2507-2511.

[13] Kil-Sang Yoo, et al. "A Wavelet-based Blind Watermarking Technique for Real-time Watermark Interpretation". *Lecture Notes in Computer Science*, Springer-Verlag Heidelberg, 2003, 2668: 348-355.

[14] Piva A, Barni M, et al. “DCT-based Watermark Recovering without Resorting to the Uncorrupted Original Image”. *Proceedings of International Conference on Image Processing*, USA, 1997. 520-523.
[15] Huiyan Qi, Dong zheng, Jiying Zhao, “Human visual system based adaptive digital image watermarking”, *Signal Processing*, 88(2008) 174-188.
[16] Jieh Ming Shieh, Der Chyuan Lou, Ming Chang Chang. "A semi-blind digital watermarking scheme based on singular value decomposition". *Computer Standards & Interfaces*, 28(2006), 428-440
[17] E. Ganic, A. M. Eskicioglu. "Robust DWT-SVD domain image watermarking: embedding data in all frequencies". *Proceedings of the 2004 Multimedia and Security Workshop on Multimedia and Security*, 2004, 166-174
[18] CAI Yong-mei, GUO Wen-qiang, DING Hai-yang, "An Audio Blind Watermarking Scheme Based on DWT-SVD", *Journal of Software*, VOL.8, NO.7, 2013, 1801-1808.
[19] Yinghua Lu, Wei Wang, Jun Kong. "A robust watermarking algorithm based on SVD and neural network". *2005 Asia-Pacific workshop on visual information processing, IEEE SMC Society Hong Kong Chapter*, Hong Kong, 165-170.
[20] HE Dong-xiao, ZHOU Chun-guang, LIU Miao, MA Jie, "Approach for Constructing Neural Network Ensemble Applied to Handwritten Digit Recognition", *Journal of Jilin University*, 2009, 47(6), 1211-1216.

Wei Wang was born in 1981. She is a lecturer in College of Computer Science and Technology, Dalian Nationalities University, Dalian, China. Her major research interests include computer vision, image processing and information security.

Wenhui Li was born in 1961. He is a Professor and doctor supervisor in College of Computer Science and Technology, Jilin University, Changchun, China. His major research interests include computer vision, image processing and computer graphics.

Yongkui Liu was born in 1961. He is a professor in Computer Science Department, Dalian Nationalities University, Dalian, China. He obtained his PhD degree in CAD and computer graphics from Zhejiang University in 1999. His research interests include computer Graphics, pattern recognition and image processing.

Borut Žalik is a professor of Computer Science in University of Maribor, Slovenia. He obtained PhD degree in computer science in 1993 from the University of Maribor, Slovenia. He is the head of Laboratory for Geometric modeling and multimedia algorithms. His research interests include computational geometry, geometric data compression, scientific visualization and geographic information systems. He is an author or co-author of more than 70 journal and 90 conference papers.

Object Tracking via Tensor Kernel Space Projection

Jiashu Dai
College of Computer Science and Technology, Harbin Engineering University, Harbin, China
Email: daijiashu2008@163.com

Tingquan Deng[a] Tianzhen Dong[a] Kejia Yi[b]
a. Laboratory of Fuzzy Information Analysis and Intelligent Recognition, Harbin Engineering University, Harbin, China
b. Science and Technology on Underwater Acoustic Antagonizing Laboratory, Systems Engineering Research Institute of CSSC, Beijing, China
Email: {tq_deng, tianzhen.d, yikejia2007}@163.com

***Abstract*—Although there has been significant progress in the past decade, object tracking under complex environment is still a very challenging task, due to the irregular changes in object appearance. To alleviate these problems, this research developed an object tracking algorithm via tensor kernel space projection. In the initial stage of tracking, a template matching algorithm was used to obtain a priori images of the appearance of the object. The steps taken were as follows: define the tensor kernel function based on a multi-linear singular value decomposition, view the object appearance color image as tensor data, calculate the kernel matrix for the priori appearance image samples, use KPCA to obtain the projection matrix of the image samples in kernel space, and finally, obtain an optimal estimate of the object state through Bayesian sequence interference. Meanwhile, the projection matrix in kernel space was updated on-line. Experiments on two real video surveillance sequences were conducted to evaluate the proposed algorithm against two classical tracking algorithms both qualitatively and quantitatively. Experimental results demonstrate that the proposed algorithm is robust in handing occlusion and object scale changes.**

***Index Terms*—object tracking, tensor kernel, SVD, kernel pace, projection**

I. INTRODUCTION

Object tracking as an important research area in computer vision and pattern recognition, has many applications, such as: object recognition, video surveillance, traffic monitoring, human-computer interaction, video compression, weapon automatic tracking, *etc*. [1-3].

The chief challenge in object tracking is how to adapt to appearance variability in the object. The appearance variability includes the effects of: camera motion, camera viewpoint changes, illumination change, pose variation, shape deformation and occlusions [4]. To solve this problem, there are two types of methods based on different appearance models: generative and discriminative methods.

Supported by the Natural Science Foundation of Inner-Mongolia Autonomous Region China under grant 2012M0931.
Corresponding author: Jiashu DAI
E-mail:daijiashu2008@163.com

Generative methods model appearance of targets use gray value or other features, and predict the target state by find the image patch most similar to the target. The classical mean-shift [5-6] tracking method using the kernel function forms a weighted model of the color histogram, and defining the similarity measure by its Bhattacharyya coefficient, seeks the most similar region to the reference template by a first-order gradient descent algorithm. The CBWH tracker [7] transforms only the object model but not the object candidate model. Ross [4] uses an incremental sub-space model combined with a particle filter to adapt to appearance changes. Gao [8] uses a Mexican hat wavelet to change the mean-shift tracking kernel and embedded a discrete Kalman filter to achieve satisfactory tracking. The ℓ_1-tracker [9] uses a visual tracking problem as a sparse approximation, obtains sparse representation by solving ℓ_1 regularisation, and finally finds the minimum reconstruction error region. Gao [10] fused multi-feature weights through DS evidence theory and combined with a particle filter achieves better results when considering the particle degeneration phenomenon.

Discriminative methods formulate object tracking as a binary classification problem for separates the target from the background. The Support Vector Tracking [11] integrates SVM into optical flow classifier for object tracking. Avidan [12] combined weak classifiers into a strong classifier to distinguish the object with background. The online boosting tracker [13] selects features using boosting classifier. The MIL tracker [14] using Multiple Instance Learning to overcome slight inaccuracies in labeled training examples can cause drift, the samples are considered within positive and negative bags.

The authors proposed an algorithm that uses tensor kernel space projection for object tracking to estimate the object state in real-world scenarios. For the purpose of highlighting the real differences between color images, a tensor kernel based on multi-linear singular value decomposition was defined. The Bayesian sequence interference framework was combined therewith to project the observe image samples in kernel space using a kernel matrix. Experimental results showed that the

doi:10.4304/jcp.9.6.1503-1510

proposed algorithm could achieve object tracking in real-world and occlusion environments, it was also adaptive to object scale changes.

II. Tensor Kernel Based on Multi-linear Singular Value Decomposition

A. Tensor Algebra

A tensor can be seen as a multi-order array which exists in multiple vector space, meanwhile, tensor algebra forms the mathematical basis of the multi-linear analysis [15]. A scalar is a zero-order tensor, a vector is a first-order tensor and a matrix is a second-order tensor. It is obviously that a color image is a third-order tensor. An *N*-order tensor can be denoted by $\tilde{\boldsymbol{X}} \in \mathrm{R}^{I_1 \times I_2 \times \cdots \times I_N}$, the element of $\tilde{\boldsymbol{X}}$ is $x_{i_1,\cdots,i_n,\cdots,i_N}$, where $1 \le i_n \le I_n$.

Definition 1: The n-mode unfolding matrix of a tensor data $\tilde{\boldsymbol{X}}$ is denoted as

$$\tilde{\boldsymbol{X}}_{(n)} \in \mathbb{R}^{I_n \times (I_1 \times \cdots \times I_{n-1} \times I_{n+1} \times \cdots \times I_N)} \tag{1}$$

The element $x_{i_1,\cdots,i_n,\cdots,i_N}$ of $\tilde{\boldsymbol{X}}$ in $\tilde{\boldsymbol{X}}_{(n)}$ at i_n-*th* row and at $[(i_{n+1}-1)I_{n+2}\cdots I_N I_1 \cdots I_{n-1} + \cdots + (i_N - 1)I_1 \cdots I_{n-1} + (i_1 - 1)I_2 \cdots I_{n-1} + \cdots i_{n-1}]$-*th* column.

Definition 2: The n-mode product of a tensor data $\tilde{\boldsymbol{X}} \in \mathbb{R}^{I_1 \times I_2 \times \cdots \times I_N}$ and a matrix $\boldsymbol{U} \in \mathbb{R}^{J_n \times I_n}$ denoted as $\tilde{\boldsymbol{X}} \times_n \boldsymbol{U} \in \mathbb{R}^{I_1 \times \cdots \times I_{n-1} \times J_n \times I_{n+1} \cdots \times I_N}$. The element of $\tilde{\boldsymbol{X}} \times_n \boldsymbol{U}$ is

$$\left(\tilde{\boldsymbol{X}} \times_n \boldsymbol{U}\right)_{i_1 \cdots i_{n-1} j_n i_{n+1} \cdots i_N} = \sum_{i_n} x_{i_1 i_2 \cdots i_N} u_{j_n i_n} \tag{2}$$

Definition 3: The inner product of two tensors $\tilde{\boldsymbol{X}}, \tilde{\boldsymbol{Y}} \in \mathbb{R}^{I_1 \times I_2 \times \cdots \times I_N}$ denoted as

$$\left\langle \tilde{\boldsymbol{X}}, \tilde{\boldsymbol{Y}} \right\rangle = \sum_{i_1} \sum_{i_2} \cdots \sum_{i_N} x_{i_1 \cdots i_n \cdots i_N} y_{i_1 \cdots i_n \cdots i_N} \tag{3}$$

B. Tensor Kernel Based on Multi-linear Singular Value Decomposition

Tensor data can retain the original spatial structure of an object. Viewing the object color image as tensor data can help us exploit the intrinsic geometric relationships of object classes. The object image data belong to the same class reside in a low-dimensional manifold embedded in high-dimensional vector space.

The purpose of the kernel method is to identify and learn the relationship in a data set.

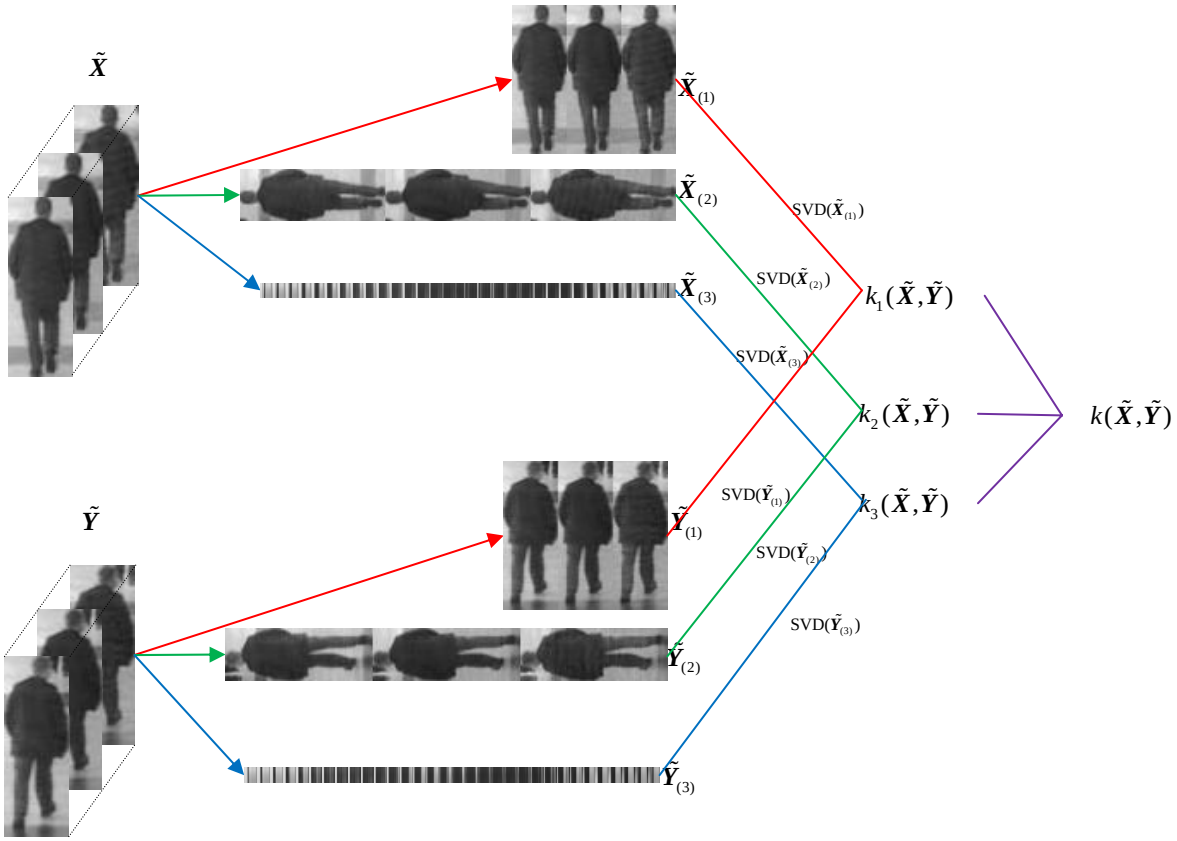

Fig.1 The schematic diagram of tensor kernel based on multi-linear SVD.

The original data can be embedded in high-dimensional feature space through a nonlinear mapping φ. The traditional kernel function $k(x, y)$ for vector data is known as: $\mathrm{R}^N \times \mathrm{R}^N \to \mathrm{R}$ and

satisfied $k(\tilde{\boldsymbol{X}},\tilde{\boldsymbol{Y}})=\left\langle \varphi(\tilde{\boldsymbol{X}}),\varphi(\tilde{\boldsymbol{Y}})\right\rangle$, so the kernel function $k(x,y)$ for tensor data must obey the rule: $\mathrm{R}^{I_1\times I_2\times\cdots\times I_N}\times\mathrm{R}^{I_1\times I_2\times\cdots\times I_N}\to\mathrm{R}$.

Kernel methods for non-linear models have proven successful in many computer vision fields[16]. So it is feasible to improve the discriminatory power of supervised tensor-based models using a tensor kernel. The most recent tensor-based techniques are based on matrix unfolding. The multi-linear singular value decomposition of tensor data $\tilde{\boldsymbol{X}}$ can be reduced to the SVD of $\tilde{\boldsymbol{X}}_{(n)}$, where $\tilde{\boldsymbol{X}}_{(n)}$ is the matrix unfolding of $\tilde{\boldsymbol{X}}$, $n\le I_N$,

$$\tilde{\boldsymbol{X}}_{(n)}=U_{\tilde{X}_{(n)}}\Sigma_{\tilde{X}_{(n)}}V_{\tilde{X}_{(n)}}{}^{T} \tag{4}$$

where $U_{\tilde{X}_{(n)}}$, $\Sigma_{\tilde{X}_{(n)}}$, $V_{\tilde{X}_{(n)}}{}^{T}$ are the three components of this SVD, and can be sated in block-partitioned form,

$$U_{\tilde{X}_{(n)}}=\begin{pmatrix}U^1_{\tilde{X}_{(n)}} & U^2_{\tilde{X}_{(n)}}\end{pmatrix} \tag{5}$$

$$\Sigma_{\tilde{X}_{(n)}}=\begin{pmatrix}\Sigma^1_{\tilde{X}_{(n)}} & 0\\ 0 & 0\end{pmatrix} \tag{6}$$

$$V_{\tilde{X}_{(n)}}{}^{T}=\begin{pmatrix}V^1_{\tilde{X}_{(n)}}{}^{T}\\ V^2_{\tilde{X}_{(n)}}{}^{T}\end{pmatrix} \tag{7}$$

Definition 4: Given a dataset $\boldsymbol{X}:\tilde{\boldsymbol{X}}_1,\tilde{\boldsymbol{X}}_2,\cdots,\tilde{\boldsymbol{X}}_m\in\boldsymbol{X}$, the kernel matrix of this set is an $N\times N$ matrix K , and the element k_{ij} is

$$k_{ij}=k(\tilde{\boldsymbol{X}}_i,\tilde{\boldsymbol{X}}_j) \tag{8}$$

A simple template matching object tracking method used in the first m frame images, then we can get the prior acquisition object sample tensor dataset $\{\tilde{\boldsymbol{X}}_1,\tilde{\boldsymbol{X}}_2,\cdots,\tilde{\boldsymbol{X}}_m\}$.

Because $k_{ij}\ge 0$, the kernel matrix K is non-negative, and positive semi-definite.

$k_i(\tilde{\boldsymbol{X}},\tilde{\boldsymbol{Y}})$ correspond to the kernel function in mode i of the two tensors, and can be calculated by:

$$k_i(\tilde{\boldsymbol{X}},\tilde{\boldsymbol{Y}})=\exp\left(-\frac{\left\|V^1_{\tilde{X}_{(i)}}V^1_{\tilde{X}_{(i)}}{}^{T}-V^1_{\tilde{Y}_{(i)}}V^1_{\tilde{Y}_{(i)}}{}^{T}\right\|}{2\sigma^2}\right) \tag{9}$$

Where σ indicates an appropriate bandwidth.

Then the kernel function between tensors is defined as:

$$k(\tilde{\boldsymbol{X}},\tilde{\boldsymbol{Y}})=k_1(\tilde{\boldsymbol{X}},\tilde{\boldsymbol{Y}})k_2(\tilde{\boldsymbol{X}},\tilde{\boldsymbol{Y}})k_3(\tilde{\boldsymbol{X}},\tilde{\boldsymbol{Y}}) \tag{10}$$

The kernel function of colour image tensor data is showed as Figure1.

III. TENSOR KERNEL SPACE PROJECTION

Principle component analysis can only handle the linear information in a dataset, a kernel trick may be used in kernel space to distinguish object and background [17].

Given a training dataset $\alpha_1,\alpha_2,\cdots,\alpha_m$, using kernel mapping φ projecting them into kernel space, we get $\varphi(\alpha_1),\varphi(\alpha_2),\cdots,\varphi(\alpha_m)$, Let $\aleph=[\alpha_1,\alpha_2,\cdots,\alpha_m]$ and $\varphi(\aleph)=[\varphi(\alpha_1),\varphi(\alpha_2),\cdots,\varphi(\alpha_m)]$. Projecting $\varphi(\alpha_i)$ in kernel space along projection direction p ,

$$\beta_i=p^T\varphi(\alpha_i) \tag{11}$$

The total dispersion of the projected training dataset is

$$\begin{aligned}D&=\frac{1}{m}\sum_{i=1}^{m}(\beta_i-\bar{\beta})(\beta_i-\bar{\beta})^T\\&=p^T\left[\frac{1}{m}\sum_{i=1}^{m}(\varphi(\alpha_i)-\bar{\alpha})(\varphi(\alpha_i)-\bar{\alpha})^T\right]p\\&=p^TSp\end{aligned} \tag{12}$$

Where $\bar{\varphi}=\left[\sum_{i=1}^{m}\varphi(\alpha_i)\right]\Big/m$ is the mean value of the dataset in kernel space.

The purpose of this kernel space projection is to find the optimal projection direction p by maximizing the total dispersion of the projected training dataset D . Thus,

$$J(p)=\arg\max_{p}p^TSp \tag{13}$$

To maximize the objective function, we need to find the Eigen-value decomposition to S .

$$\begin{aligned}\lambda p=Sp&=\frac{1}{m}\sum_{i=1}^{n}(\varphi(\alpha_i)-\bar{\varphi})^T(\varphi(\alpha_i)-\bar{\varphi})p\\&=\sum_{i=1}^{m}\left[\frac{1}{m}(\varphi(\alpha_i)-\bar{\varphi})^Tp\right](\varphi(\alpha_i)-\bar{\varphi})\end{aligned} \tag{14}$$

Here p can be regarded as the feature vector of S . It can also be seen that the projection direction p is the linear composition of $(\varphi(\alpha_i)-\bar{\varphi})$, Namely that

$$\psi(\aleph)=\left[(\varphi(\alpha_1)-\bar{\varphi}),(\varphi(\alpha_2)-\bar{\varphi}),\cdots,(\varphi(\alpha_m)-\bar{\varphi})\right] \tag{15}$$

That is

$$p=\sum_{i=1}^{m}c_i(\varphi(\alpha_i)-\bar{\varphi})=\psi(\aleph)C \tag{16}$$

Where $C=\left[c_1,c_2,\cdots,c_l\right]^T$ is the matrix which comprising the linear combination coefficients. Now, solving for the optimal projection direction was transformed into a problem whereby solving the combination coefficient matrix was required, the objective function became:

$$J(C)=\arg\max_{C}\frac{1}{m}C^T\left[\psi(\aleph)^T\psi(\aleph)\right]^2C \tag{17}$$

Let A_m is a $m\times m$ matrix with all entries equal to $1/m$, $\widehat{K}=\psi(\aleph)^T\psi(\aleph)$. Then,

$$\widehat{K} = K - A_m K - K A_m + A_m K A_m \tag{18}$$

Eigen-value decomposition to S,

$$Sp = (\lambda/m)\, p \tag{19}$$

Then

$$\psi(\aleph)^T S \psi(\aleph) C = (\lambda/m)\widehat{K} C \tag{20}$$

$$\widehat{K} C = (\lambda/m) C \tag{21}$$

It is can be seen that C is the matrix composed of the Eigen-vectors corresponding to the first l maximum Eigen-values of $\widehat{K}$.

The tensor kernel space projection algorithm works as shown in Table1:

TABLE 1.
TKSP ALGORITHM

1) Define tensor kernel function $k(\alpha, \beta)$.

2) Compute kernel matrix K and matrix $\widehat{K}$.

3) Eigen-value decomposition to $\widehat{K}$ to obtain Eigen-values and Eigen-vectors, and sort Eigen-values in descending order $\lambda_1 \geq \cdots \geq \lambda_l \geq \cdots \geq \lambda_m$, v_i is the eigenvector corresponding to λ_i. Take the first l Eigen-values, let $c_i = v_i / \sqrt{\lambda_i}\ (i = 1, 2, \cdots, l)$. Then, the projection matrix $C = [c_1, c_2, \cdots, c_l]$.

4)The projected data in kernel space are $\beta = C^T k(\aleph, \alpha)$

IV. Bayesian Sequence Interference Framework For Object Tracking

A. Bayesian Sequence Interference

In the problem of object tracking, the object state in the current frame only related to the object state in the prior frame. Define o_t as the state variables of the object at time *t*. Let $o_t = (x_t, y_t, w_t, h_t)$, where x_t, y_t, w_t, h_t denotes the center coordinate, the width and height of the tracking rectangle.

Given a set of targets $Z_t = \{z_1, z_2, \cdots, z_t\}$, the objective of object tracking is to obtain the optimal estimate value of the hidden state variables o_t. According to Bayesian theorem, it can be obtained in a similar fashion as that of the object state:

$$P(o_t | Z_t) \propto P(z_t | o_t) \int P(o_t | o_{t-1}) P(o_{t-1} | Z_{t-1}) do_{t-1} \tag{22}$$

Where $P(o_t | o_{t-1})$ refers to the state transition model and $P(z_t | o_t)$ refers to the observation model. It can be seen that the observation model $P(z_t | o_t)$ determine the tracking results.

State transition model: This was used to model the object motion between consecutive frames. Because of the irregular movement of object, the state o_t is modeled by independent Gaussian distribution around its counterpart in state o_{t-1}. Described as

$$P(o_t | o_{t-1}) = N(o_t; o_{t-1}, \Delta) \tag{23}$$

Where Δ means the diagonal covariance matrix of x_t, y_t, w_t, h_t, and the element is $\sigma_x^2, \sigma_y^2, \sigma_w^2, \sigma_h^2$. Point to Gaussian distribution, N particles can be randomly generated. According to the particle can obtain multiple states $\{o_t^i, i = 1, 2, \cdots, N\}$. During the computing process, with the increase in the number of particles, the *a posteriori* probability estimate was more accurate, but at the same time, the computational efficiency was low, so a balance was sought between these factors.

Observation model: this was used to measure the similarity between the appearance observation and the object appearance model. Given a drawn particle state o_t^i and a cropped version of the corresponding image patch z_t^i from the frame image I_t. The probability of an image patch being generated from the kernel space is inversely proportional to the difference between image patch and the appearance model, and could be calculated between the negative exponential distance of the projected data and the center of dataset

$$p(z_t^i | o_t) = \exp\left\{ -\left\| s_t^i - \overline{s} \right\|_F / \sigma \right\} \tag{24}$$

Where σ indicates an adjustment factor, $\|\bullet\|_F$ is the Frobenius norm, $s_t^i = C^T k(X, z_t^i)$, $\overline{s} = C^T k(X, \overline{x})$, C is the projection matrix in kernel space, and $\overline{x}$ is the center of dataset in kernel space.

The state o_t^i corresponding to the maximum $p(z_t^i | o_t)$ is the optimal object state at time *t*.

B. Projection Matrix Online Update

Along with the movement of the object in scenarios, the object appearance also changed. The projection matrix in kernel space must be updated on-line so that at time *t*, we have obtained the former *t - 1* time object states. When *t - 1* is the times used as initial training dataset numbers, we recalculated the projection matrix in kernel space using the newly acquired *t - 1* object tensor data points.

The flow chart of whole proposed object tracking algorithm is shown as figure 2.

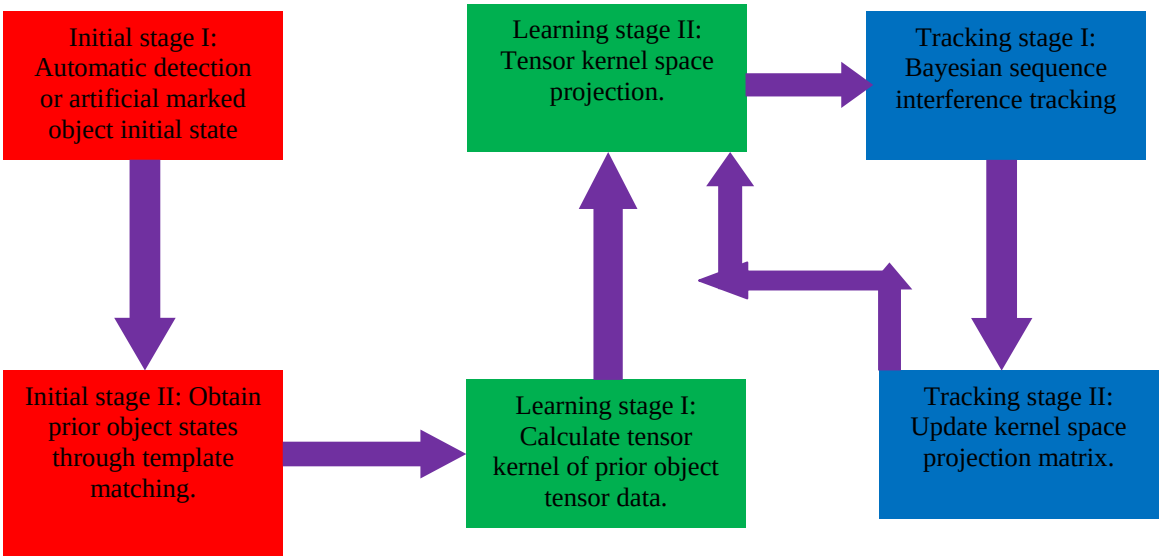

Fig.2 The flow chart of the proposed visual tracking algorithm.

V. Comparative Experiments And Analysis

All the experiments were carried out in the MATLAB® 2010a environment running on a Pentium® Dual-Core E5200 processor with a clock-speed of 2.50 GHz.

In these experiments, we use Portuguese shopping center video monitoring data to test. The video frame image size was $388 \times 284 \times 3$, and the experimental data were compared with classical CBWH, and MIL, tracking algorithms. The CBWH tracking algorithm select 16×16×16 bin histogram. In MIL tracking algorithm, the feature pool is 250, weak classifiers number is 50 and the learning rate is 0.85. The variance of Gaussian distribution is [2, 2, 0.5, 0.5] in the proposed tracking algorithm. In the initial frame, the object tracking rectangle was manually/artificially marked, and a template matching tracking algorithm was used to get the previous twenty frame object states.

A. *Expeiment A*

We first selected scale changes in an environment of complex surveillance scenario, meanwhile the movement of object was irregular. The object was walking toward the camera. The length of this video was 200 frames.

The tracking results of experiment A are shown as Figure 3. It can be seen from the pictures that when a similar object appeared around the target, the CBWH and MIL tracking algorithms cannot achieve well tracking; our tracking algorithm could adapt thereto. In the tracking progress, the size of the object changed from 28 × 79 to 44 × 111.

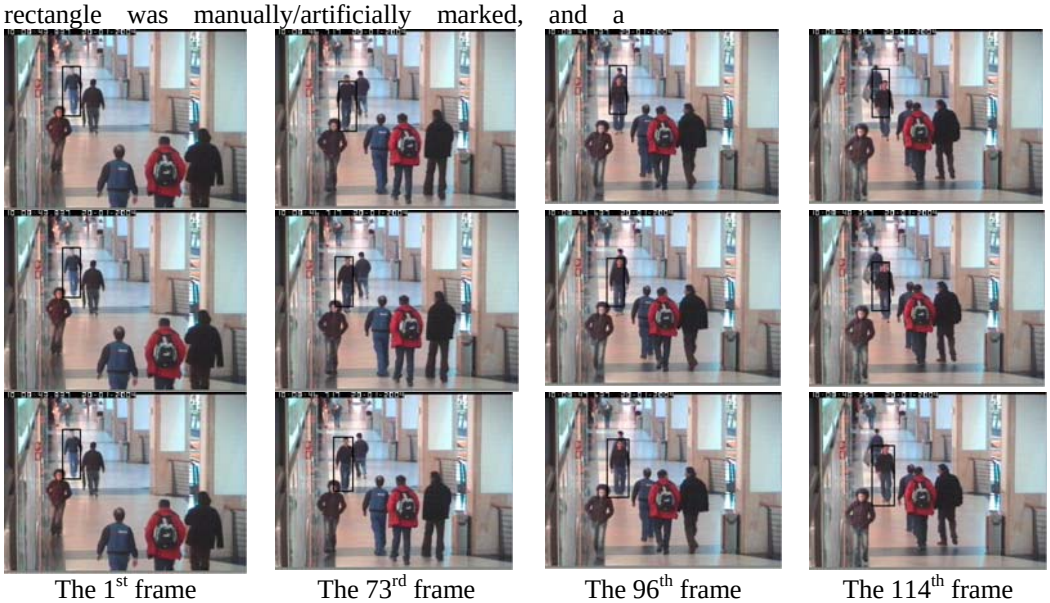

Fig.3 The tracking results of experiment A.

B. Expeiment B

The second video had scale changes and occlusion in the surveillance scenarios studied. The object was walking away from the camera. The object was walking away from the camera. The length of this video was 300 frames.

The tracking results from experiment B are shown in Figure 4. It can be seen from the pictures that when the object was almost occluded by other moving objects, the CBWH and MIL tracking algorithms suffered interference from the other objects, and could not have tracked the target. Our tracking algorithm overcame the problem of occlusion and tracked the target.

In the tracking progress, the size of object changed from 39× 112 to 21× 64.

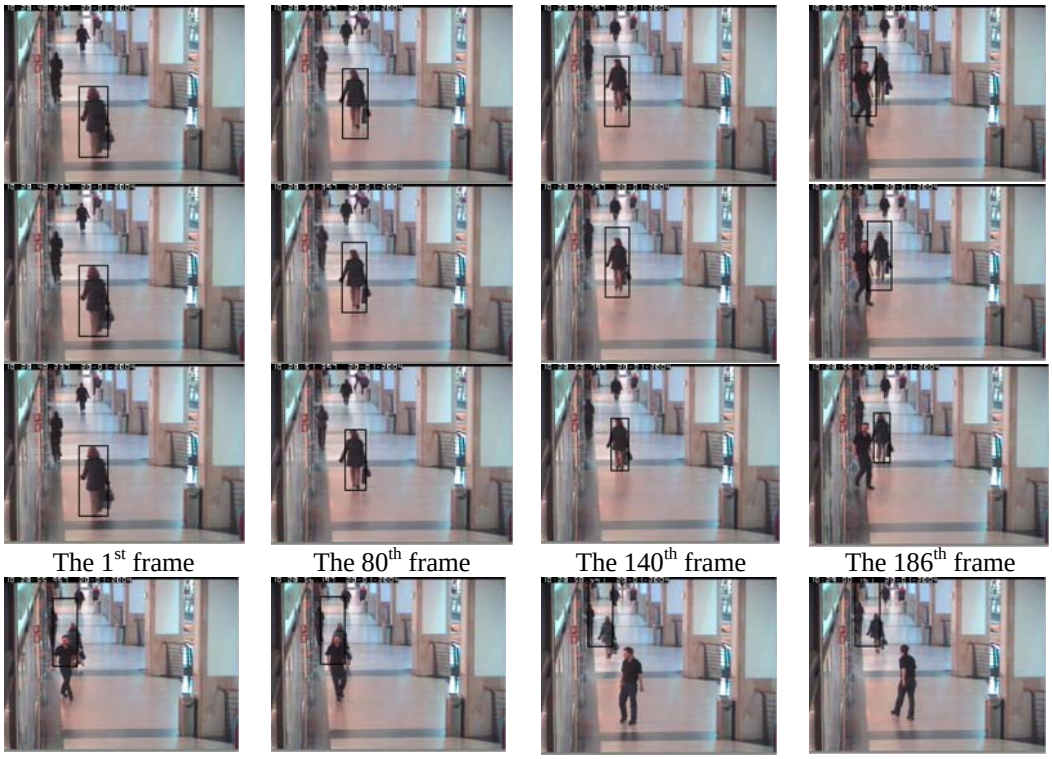

Fig.4 The tracking results of experiment B.

C. *The Evaluation of Tracking*

To quantitatively compare the experimental results of the tracking algorithms, we used two metrics to describe it: *Tracking errors* and *Tracking correct ratio*. We initially hand-labelled the object state in each experimental scenario.

The error in X-axis e_x is

$$e_x = \left| x_e - x_g \right| \tag{25}$$

Where x_e, x_g are the X-axis coordinates of the center of the experiment tracking rectangle and the ground truth rectangle.

The error in Y-axis e_y is

$$e_y = \left| y_e - y_g \right| \tag{26}$$

Where y_e, y_g are the Y-axis coordinates of the center of the experiment tracking rectangle and the ground truth rectangle.

The error in center coordinate e_c is

$$e_c = \sqrt{(x_e - x_g)^2 + (y_e - y_g)^2} \tag{27}$$

The error in experiment A and B are shown as Table 2 and 3. The data in bold refer to optimal results.

TABLE 2
THE ERRORS OF EXPERIMENT A

Items(pixels)	x-errors	y-errors	c-errors
Proposed Method	**1.7145**	**2.3905**	**3.2788**
CBWH	4.0725	15.6325	16.9349
MIL	4.2025	5.0400	6.8776

TABLE 3
THE ERRORS OF EXPERIMENT B

Items(pixels)	x-errors	y-errors	c-errors
Proposed Method	**1.8276**	**2.4318**	**3.2209**
CBWH	7.0183	19.1450	21.0142
MIL	12.7800	19.4817	23.5559

The tracking correct ratio r is

$$r = \frac{area(R_e \cap R_g)}{area(R_e \cup R_g)} \tag{28}$$

Where R_e is the experiment tracking rectangle, R_g is the ground truth rectangle, $area()$ means the area of the region. It was thought that if the tracking correctly ratio was greater than 0.5, the tracking in this frame was successful. The tracking correctly ratios in two scenarios are shown as Figures 5 and 6. The red line indicates the results of the proposed tracking algorithm, the green line indicates the CBWH tracking algorithm and the blue line indicates the MIL tracking algorithm. It can be seen that our proposed tracking algorithm had better results than the other two tracking algorithms. Also, the tracking correctly ratio of our algorithm was almost always greater than 0.5, implying that the algorithm was successful.

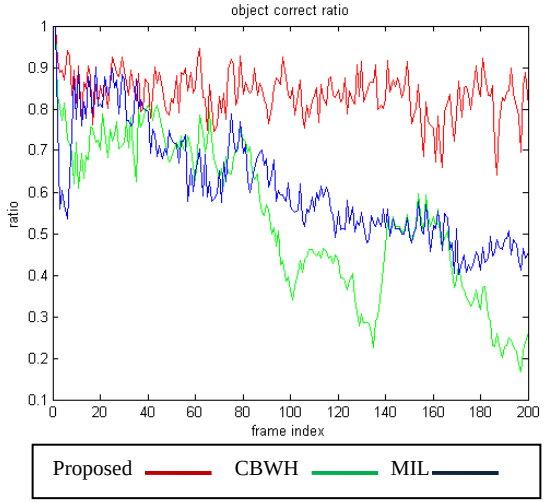

Fig.5 The tracking correct ratio in experiment A.

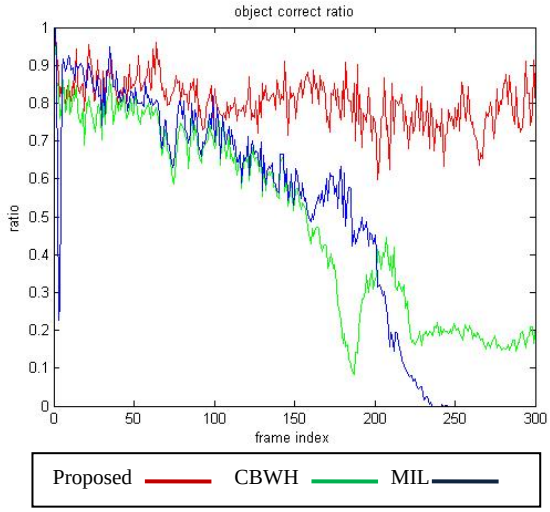

Fig.6 The tracking correct ratio in experiment B.

V I. CONCLUSION

In this work, we proposed the use of a tensor kernel space projection for object tracking in video surveillance scenarios. Considering the spatial structure of the object image, we defined a tensor kernel function based on multi-linear singular value decomposition. We projected the object image tensor data into kernel space, and combined this with a Bayesian sequence interference tracking framework to achieve object tracking. To adapt to the object appearance changes, we updated the projection matrix on-line and also analyzed the performance of our proposed tracking algorithm in an assessment against challenging real-world video surveillance scenarios and compared the output with two classical tracking algorithms. The experimental results demonstrated the accuracy and robustness of the proposed tracking algorithm.

REFERENCES

[1] A. Yilmaz, O. Javed and M. Shah, "Object tracking: a survey," *ACM Computing Surveys*, vol. 38, pp. 1-45, 2006.
[2] H. Yang, L. Shao, F.Zheng, L. Wang and Z. Song, "Recent advances and trends in visual tracking: a review," *Neurocomputing*, vol. 74, pp. 3823-3831, 2011
[3] Z. Feng, B. Yang, Y. Zheng, H. Tang and Y. Li, "Initialization of 3D human hand model and its applications in human hand tracking," *Journal of Computers*, vol. 7, pp. 419-426, February 2012.
[4] D.A. Ross, J. Lim, R. Lin and M. Yang, "Incremental learning for robust visual tracking," *International Journal of Computer Vision*, vol. 77, pp. 125-141, 2008.
[5] D. Comaniciu, V. Ramesh and P. Meer, "Kernel-based object tracking," *IEEE Transactions on Pattern Analysis and Machine Intelligence*, vol. 25, pp. 564-577, 2003.
[6] H. Zhou, Y. Yuan and C. shi, "Object tracking using sift features and mean shift," *Computer Vision and Image Understanding*, vol. 113, pp. 345-352, 2009.
[7] J. Ning, L. Zhang, D. Zhang and C. Wu, "Robust mean shift tracking with corrected background-weighted histogram," *Iet Computer Vision*, vol. 6, pp. 62-69, 2012.
[8] T. Gao, Z. Yao, P. Wang, C. Wang and J. Yang, "Automatic Stable Scene based Moving multi-target detection and tracking," *Journal of Computers*, vol. 16, pp. 2647-2655, Decemble 2011.
[9] X. Mei and H. Ling, "Robust visual tracking and vehicle classification via sparse representation," *IEEE Transactions on Pattern Analysis and Machine Intelligence*, vol. 33, pp. 2259-2272, 2011.
[10] J. Gao, W. Li, D. wu, "Multi-feature fusion tracking based on a new particle filter," *Journal of Computers*, vol. 7, pp. 2939-2947, December 2012.
[11] S. Avidan, "Support vector tracking," *IEEE Transactions on Pattern Analysis and Machine Intelligence*, vol. 26, pp. 1064-1072, 2006.
[12] S. Avidan, "Ensemble tracking," *IEEE Transactions on Pattern Analysis and Machine Intelligence*, vol. 29, pp. 261-271, 2007.
[13] H. Grabner, M. Grabner, and H. Bischof, "Real-time tracking via online boosting," *British Machine Vision Conference*, Edinburgh, British, vol. 1, pp. 47-56, 2006.
[14] B. Babenko, M. Yang and S. Belongie, "Robust object tracking with online multiple instance learning," *IEEE Transactions on Pattern Analysis and Machine Intelligence*, vol. 33, pp. 1619-1632, 2011.
[15] H. Lu, K.N. Plataniotis and A. N. Venetsanopoulos, "A survey of multilinear subspace learning for tensor data," Pattern Recognition, vol. 44, pp. 1540-1551, 2011.
[16] M. Signoretto, L. De. Lathauwer and J. A. K. Suykens, "A kernel-based framework to tensorial data analysis," *Neural Networks*, vol. 24, pp. 861-874, 2011.
[17] B. Scholkopf, A. J. Smola and K. R. Muller, "Nonlinear component analysis as a kernel eigen-value problem," *Neural Computing*, vol. 10, pp. 1299-1319, 1998.

Jiashu Dai received his B.S. degree from Mudanjiang Normal University, Mudanjiang, China, in 2008. He is currently a candidate for Ph.D. degree in College of Computer Science and Technology, Harbin Engineering University. His research interests include computer vision, pattern recognition as well as image processing.

Tingquan Deng received his B.S. degree in Mathematics, M.S. degree in Applied Mathematics, and Ph.D degree in Fundamental Mathematics from Harbin Institute of Technology, Harbin, China, in 1987, 1990 and 2002, respectively. He was a visiting scholar from Center for Mathematics and Computer Science, Amsterdam, the Netherland from 1999 to 2000 for one year and a postdoctoral research fellow in Department of Automation, Tsinghua University, Beijing, China from 2003 to 2005. Currently, he is a professor in College of Science as well as in College of Computer Science and Technology, Harbin Engineering University, Harbin, China. His research interests include uncertainty theory, image processing and pattern recognition, and data mining and machine learning.

A Research of Image Difference Algorithm Based on the Correlation of Color Attributes

Xiangyang Xu [1]
1 School of Media and Communication, Shenzhen Polytechnic, Shenzhen, 518055, China.
Email: xxy0906 @szpt.edu.cn

Qiao Chen *[1], Ziqi Zhao [2], Gang Zhang [2] and Jiang Duan [3]
2 College of Graphic Arts Qufu Normal University, Rizhao, 276800, China
3 School of Economic Information Engineering Southwestern University of Finance and Economics, Chengdu, 610075, China
*Corresponding author Email: qiaochen @szpt.edu.cn

***Abstract*—The CIE color difference formula was developed using simple color patches in controlled viewing conditions. They are not suitable for predicting color differences of spatially complex images. In order to quantify color differences between the original and reproduced images, we present an image difference algorithm based on image contents. This formula uses the Contrast Sensitivity Functions (CSF) to reduce the spatial complexity. The CSF serves to remove information that is imperceptible to the human visual system. This algorithm determines the color attribute weights by means of the correlation analysis between image pairs. Psychophysical experiments confirmed that the metric correlates strongly with the human perception. The proposed algorithm can be used to assess the performance of color image compressions, color image enhancement algorithms, gamut mapping algorithms and so on.**

***Index Terms*—image processing, color vision, color difference, image difference**

I. INTRODUCTION

The goal of research on color differences is to use numeral values to evaluate color differences between two objects. In order to develop easy-to-use color industrial applications, CIE recommended two color difference formulas: 1976CIELAB and 1976CIELUV[1]. These two color difference formulas are used directly to represent the distance between two points in the corresponding color space. Since CIELAB and CIELUV are not completely uniform visual color space, the distance between two points cannot represent the exact visual difference. Then CIE launched CIE DE94[2] and CIE DE2000[3] color difference formulas, which put color difference researches to a new stage. These color difference equations improved the accuracy of the mapping between physically measured stimuli and perceived differences. However, these complex formulas can only predict simple perceptible differences between a pair of color patches under a given viewing condition, they cannot predict color differences between images with spatial complexities.

In order to quantify the color difference between complex images, S-CIELAB[4] was proposed as the first image difference model based on the CIELAB color space and color difference formulas. This model is an extension of traditional color difference formulas, in which image pixels are considered as separate objects, and Contrast Sensitivity Function(CSF) was added before calculating the color difference of image pairs. The use of CSF can remove the information of image that is imperceptible to the human vision. S-CIELAB model has been modularized[5], and the corresponding module can be added or modified to develop a new image color difference formula. Image Color Appearance Model(iCAM)[6,7] which is accomplished as a spatial filtering pre-processing can be used to calculate the image difference before a pixel-by-pixel color difference calculation in an uniform color space IPT[8].

In order to represent the image difference more accurately, this paper proposes a new image difference algorithm based on the S-CIELAB model. In our proposed algorithm, the spatial statistic characteristics of each image have been analyzed and combined with the current image difference model so that the calculated image differences will be more correlated with human vision responses. In this work, we modified the image difference model by adding the CSF function to minimize variation caused by different viewing angles and then further adjusted the color difference by carrying out color attributes correlation analysis on each image. The performance of the proposed algorithm has been evaluated and tested on different types of distorted images, and the results indicate that the image difference calculated by the proposed algorithm is more consistent with the human visual response than the traditional image difference model.

II. THE PROPOSED IMAGE DIFFERNCE ALGORITHM

The framework of image difference model has been proposed in an earlier work[9], in which spatial pre-processing modules are extensible with great flexibilities. Our proposed image difference algorithm is based on the

doi:10.4304/jcp.9.6.1511-1517

current image difference model by adding individual models. Figure 1 illustrates the framework of the calculation process for the color difference of the image pairs.

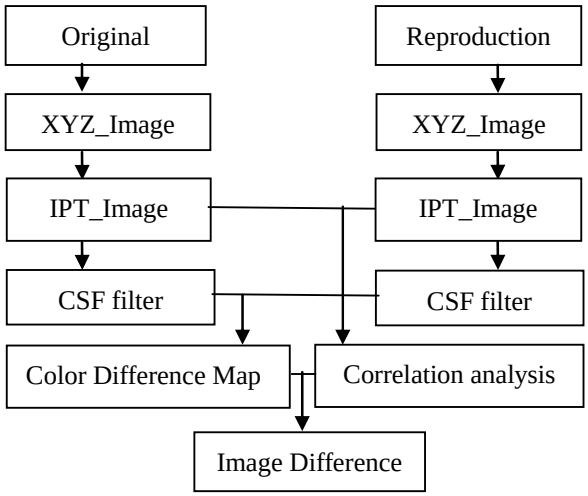

Figure 1. Flowchart of Image Difference Measurement Difference Metric

The calculation of the image difference of an image pair is divided into two parts. The first part is image processing using CSF filter, which is designed to simulate some visual characteristics of human eyes so that the filtered image will meet some aspects of visual features of human eyes. For example, S-CIELAB and iCAM image quality measurements are using CSF functions to simulate spatial frequency behavior of the human vision. The second part is pixel by pixel color difference calculation, which can use color difference formulas recommended by CIE. The calculated image difference can be recorded using statistical methods, such as the average color difference of all pixels, the overall deviation, the maximum value and so on. This framework inherits the characteristics of iCAM image quality measurement, and the color difference is calculated in the uniform color space IPT, which is the key part of the of an image appearance model. This framework allows great flexibility in the choice of color spaces and in this model we also use IPT color space because of its excellent color uniformity.

The proposed image difference algorithm mainly includes three aspects. The first one is CSF filter pre-processing which describes the behavior of the human visual system in regards to spatially complex stimuli. The CSF is described as a post-retinal opponent color space, with a band-pass nature for the luminance channel and low-pass nature for the chrominance channels. More are discussed in details by Johnson and Fairchild[10]. The following equations[11] explains the CSF in this framework:

$$CSF(f,l,i^2) = ((3.23(f^2 i^2)^{-0.3})^5 + 1)^{-0.2} \times A1\varepsilon f e^{-(B_1 \varepsilon f)} \sqrt{1 + 0.06 e^{B_1 \varepsilon f}} \quad (1)$$

$$A1 = 0.801\left(1 + \frac{0.7}{l}\right)^{-0.2} \quad (2)$$

$$B1 = 0.3\left(1 + \frac{100}{l}\right)^{0.15} \quad (3)$$

Where f is spatial frequency in cycles per degree of visual angle(CPD), i^2 is image size, ε is frequency scaling constant, l is the light adaption level(cd/m2).This function is capable of predicting the effects of many changes in the viewing conditions, which contain the image size, viewing distance, environment luminance and so on.

The second aspect is IPT color space conversion, and more details of IPT can be found in the literature[8] in references.

The third aspect is the calculation for the correlation of three attributes of color, which is completed in the IPT color space. The calculation of the correlation of color attributes is the most important part of the proposed algorithm, and will be described in details in the next paragraph.

III. Principle of Image Difference Calculation Based on Color Attributes

The biggest innovation of the proposed image difference algorithm is to add image color attributes correlation analysis and calculation. Image pairs' correlation will be analyzed in the IPT color space, and the respective correlation coefficients of color components will be determined and used as weighting factors to calculate image differences. The color difference between the original and the reproduced images can be understood as a color similarity between two images. The meaning of the similarity includes differences between a pair of images of both color values and spatial distributions. The average color difference value of all pixels is used to represent the overall deviation. The correlation coefficient is calculated to measure the difference of image pixels in spatial distributions. The correlation analysis is carried out in IPT color space which is an orthogonal space, therefore it is equivalent to the analysis of correlation with three attributes of color: hue, lightness and saturation. The problem can be mathematically solved by computing the correlation of two sets of data as Equation 4:

$$r_{xy} = \frac{s_{xy}}{\sqrt{s_{xx}}\sqrt{s_{yy}}} \quad (4)$$

Where r_{xy} is the correlation coefficient of two sets of data. s_{xy} is the covariance of two sets of data, $\sqrt{s_{xx}}$ and $\sqrt{s_{yy}}$ represent the separate variance of two sets of data respectively. r_{xy} is the correlation coefficient and $|r_{xy}| \le 1$. The value of the correlation coefficient can represent the degree of similarities between spatial dichotomous data sets. If the absolute value of the correlation coefficient is 1, it means that the two sets of data is equal, so the associated color component is equal.

Small absolute correlation coefficient values may indicate large distribution differences of the two sets of data and large differences for the image color components, so the color differences between the image pairs should be large as well.

For S-CIELAB and iCAM, during the calculation of the image difference, the average value of color differences of all of image pixels is considered as the image difference. However, the average value can only reflect the variation of concentrated locations of image data, it does not reflect the characteristics of spatial dispersion of those data sets. The color property of images is space-related, to obtain the color difference between image pairs, analyzing of the spatial distribution of the image pairs' color data will be much more significant than obtaining concentrated locations. Because the average value does not fully represent the mean image color difference between a pair of images, so in this work based on the conventional color difference formula between image pairs, modified image difference formula has been established. Weight coefficients are the correlation coefficients for the respective color component plane of image pairs. Therefore, the color difference formula between image pairs based on traditional color difference formula is modified as Equation 5:

$$\Delta E = \sqrt{\frac{\Delta I^2}{I_r} + \frac{\Delta P^2}{P_r} + \frac{\Delta T^2}{T_r}} \qquad (5)$$

Where, ΔE represents the color difference between image pairs, ΔI represents the average value of the brightness component , ΔP and ΔT represent the average value of the chromatic component, I_r represents the correlation coefficient of I plane, P_r represents the correlation coefficient of P plane and T_r represents the correlation coefficient of T plane.

IV. Objective Evaluation

In order to verify the performance of the proposed image difference algorithm, we selected several different types of distorted images from TID2008 database[12]. TID2008 is designed for the evaluation of full-reference image visual quality assessment metrics, and it allows estimating how a given metric corresponds to the mean human perception. TID2008 contains 25 reference images and 1700 distorted images (25 reference images x 17 types of distortions x 4 levels of distortions). Mean human perception (MOS, Mean Opinion Score) is used to represent average visual image quality, and higher value of MOS (0 - minimal, 9 - maximal) corresponds to higher visual quality of the image. In our evaluation experiment we chose three distorted type of images: Gaussian blur, JPEG compression and Contrast change, and all images are chosen randomly. Each distorted type is divided into four levels, so there are 36 pairs in the trials. The MOS values are shown in Table 1.

TABLE 1.
THE EVALUATION DATAS OF OBJECTIVE

Distorted types		Test images					
		Image 1		Image 2		Image 3	
		MOS	ΔE	MOS	ΔE	MOS	ΔE
Gaussian blur	L1	4.7353	0.012	5.7931	0	5.4063	0.004
	L2	3.9143	0.016	5.2414	0	4.6875	0.006
	L3	3.2778	0.021	4.0000	0.003	3.5313	0.007
	L4	2.1765	0.023	3.0690	0.007	2.7500	0.008
Jpeg compression	L1	5.9444	0.003	6.3929	0.002	5.8667	0.002
	L2	5.1667	0.007	5.4138	0.002	5.3438	0.002
	L3	3.3056	0.044	3.1667	0.016	3.2813	0.043
	L4	1.4571	0.041	2.2667	0.021	1.2581	0.069
Contrast change	L1	6.5000	0.104	7.2000	0.122	7.2188	0.051
	L2	4.9714	0.081	5.5333	0.100	5.2258	0.042
	L3	6.1944	0.181	7.0667	0.163	7.2813	0.132
	L4	3.9722	0.131	4.5333	0.163	3.7742	0.072

Color differences between the source images and the corresponding distorted images are calculated and the results are also shown in Table 1: small ΔE values indicate the difference between two images is small, and bigger ΔE values indicate larger color differences for image pairs.

In this table the MOS is arranged in the descending order for each distortion. It is clear that the calculated image difference values are in ascending orders. With the decrease of the MOS values, the trend of image difference values increases for each type of distortion. This result confirms that the proposed image difference algorithm can predict the effect of image distortion, and is consistent with human visual perceptions.

Testing images are shown in Figure 2. Image quality is in descending order with the MOS.

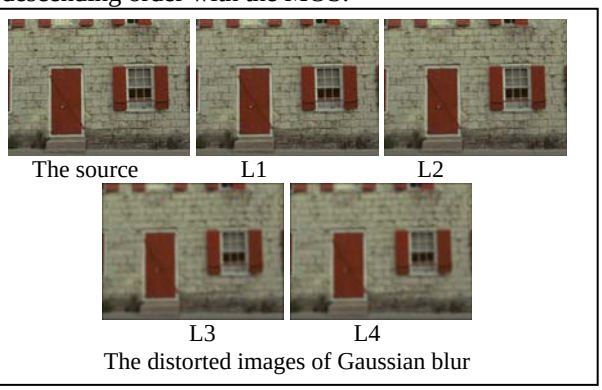

The distorted images of Gaussian blur

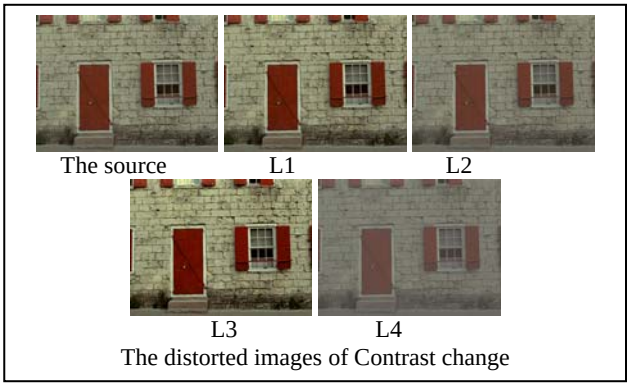

Fig.2 Testing image in this objective evaluation

Because of the limited space, here we only give testing image1 as an example, others images can be found in TID2008 database.

TABLE 2.

THE CORRELATION COEFFICIENT EVALUATION

Distorted types	Test images		
	Image 1	Image 2	Image 3
Gaussian blur	0.96521	0.96452	0.96944
Jpeg compression	0.8997	0.97795	0.9919
Contrast change	0.211205	0.09247	0.367274

Table 2 shows the correlations between the image difference and MOS. For the 'Gaussian blur' and 'Jpeg compression' distortion, correlation coefficients are bigger, which means that the calculation result of the image difference and the MOS is in a good consistency. The framework of image difference is used to evaluate the image quality. But the predicted results of the 'contrast change' distortion is poor. The result suggests the framework has been improved, especially the spatial filtering module.

V. PSYCHOPHYSICAL EVALUATION

In order to further verify the performance of the proposed algorithm for the image color difference, a psychophysical experiment was also carried out [13-15]. five typical images were selected from image database recommended by ISO SCID 400 Standards. They are Grey Neutrals (N1), Memory Colors (N2), Painting Kids (N3), Red Couch (N4) and Ski (N5). These 5 images represent different types and contents, which include memory colors (sky, grass, color, etc.), bright colors (bright clothing, color, etc.) and neutral colors (cloth, etc.), so human visual sense of color differences between images with different contents can be tested. The mode of original images is RGB, and sRGB profile is embedded within the image file. In sRGB space different power functions are used for color adjustments as Equation 6:

$$Out = \max(in) \times \left(\frac{in}{\max(in)}\right)^{\alpha} \qquad (6)$$

In Equation 6, Out is an output of the calculation, in represents an input value, α is adjustment parameter. In this experiment α value was chosen in the sequence of: 0.95, 0.85, 0.80, 0.75, therefore visual differences of 20 image pairs were obtained. Each image was adjusted through different power functions, so the results were four images, given serial number img1, img 2, img 3, img 4 respectively. Testing images are shown in Figure 3.

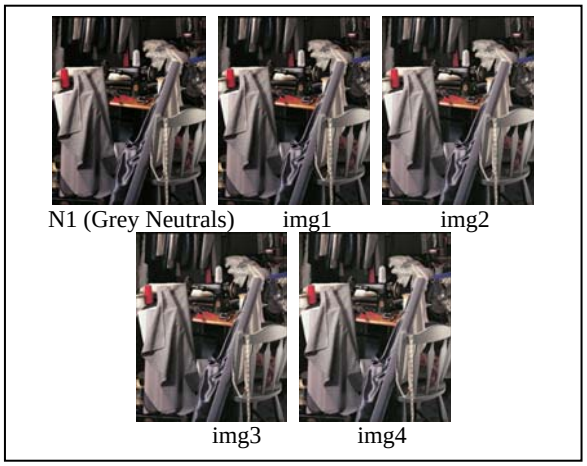

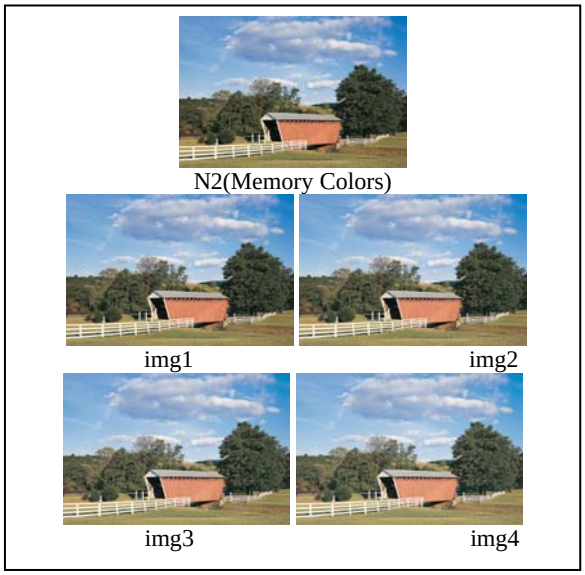

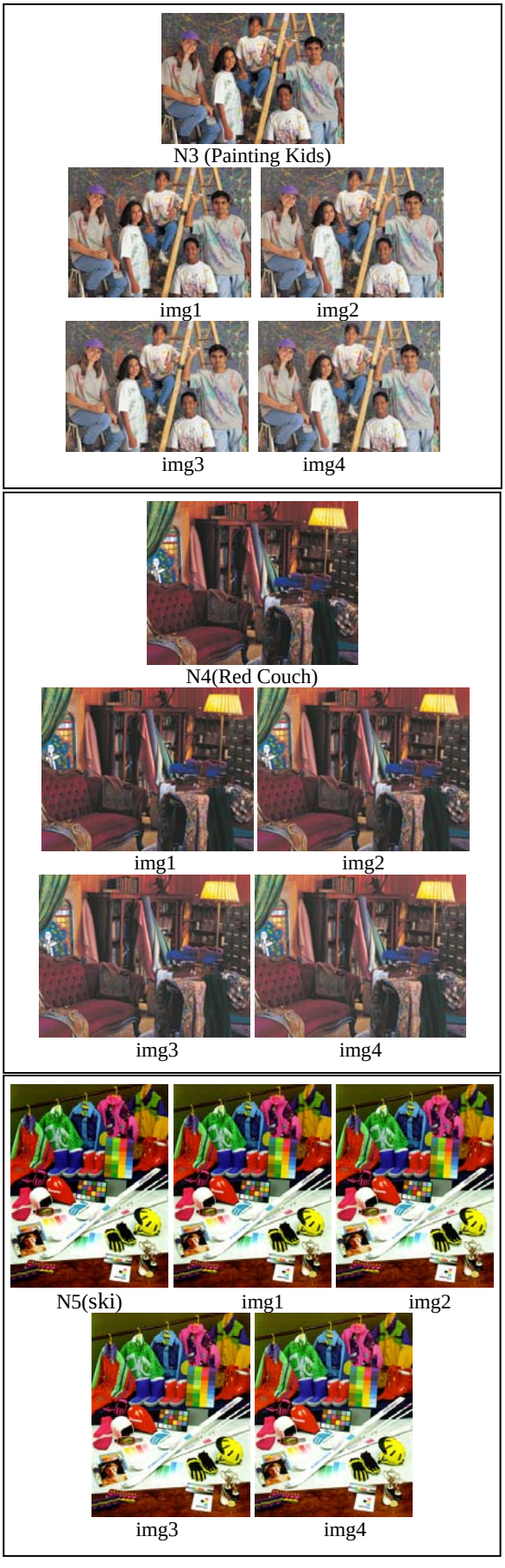

Fig.3 Testing image in this Psychophysical evaluation

EIZO ColorEdge CG21 LCD monitor was used in the subjective evaluation, and the setup of the experiment is as follows: r=2.2, white point D56, the monitor was calibrated with ProfileMaker5.0, color measurement instrument was GretagMacbeth Eye-One, the average color difference (CIELAB), the maxim color difference, ambient illumination is 200Lx-300Lx, observation background is neutral gray. 10 observers were recruited, each observer repeated experiment for three times, the monitor was warmed up for half an hour before each observation, each observer stayed in the observation environment for an adaptation for half an hour in advance, and the monitor color difference was calibrated. All evaluation images for observation are correspond to the source image, and the processed images were displayed as slide show using ACDSee software in a random order. Judgments on visual color difference are divided into five levels as Table 3:

TABLE 3.

THE VISION LEVEL OF SUBJECTIVE OBSERVATION

Visual experience	Score
No sense of perceived differences	0
A sense of barely perceptible differences, indistinctly, obscure or uncertain	1
Differences are in a weak sense of presence, but can be determined	2
Slightly significant sense of difference, but in an acceptable range	3
Significant sense of difference , the difference is not acceptable	4

Four test images were created for each of five images, each observation was repeated three times, and the average scores are shown in Table 4. The average scores of 10 observers represent the discrimination level for image color differences between image pairs, the bigger the average score, the larger the difference of images, and the smaller the differences in average scores, the smaller the difference between the two images.

TABLE 4:

THE EVALUATION DATAS OF SUBJECTIVE

Testing image	The Score of subjective evaluation			
	img1	img2	img3	img4
N1	1.17	1.47	1.9	2.63
N2	1.4	1.57	2.07	2.73
N3	1.1	1.57	2.07	4.13
N4	1.33	1.93	2.3	2.83
N5	0.97	1.4	1.97	2.4

Color differences between five source images and the corresponding 4 resulting images are calculated and shown in Table 5: small color difference indicates the difference between two images is small, and large color difference of images indicates big difference.

TABLE 5:
THE EVALUATION DATA OF OBJECTIVE

Testing image	The color difference data of image pairs (IPT)			
	img1	img2	img3	img4
N1	0.66	1.34	2.04	2.78
N2	0.43	0.87	1.32	1.78
N3	0.51	1.01	1.52	2.06
N4	0.66	1.34	2.04	2.78
N5	0.42	0.86	1.33	1.84

To further evaluate the performance of the proposed algorithm, S-CIELAB color difference values of test image pairs are listed in Table 6.

TABLE 6:
THE EVALUATION DATAS OF S-CIELAB

Testing image	The color difference of S-CIELAB			
	img1	img2	img3	img4
N1	2.16	4.27	6.61	9.15
N2	2.05	3.96	5.97	8.05
N3	3.78	7.00	9.75	12.67
N4	1.95	4.10	6.12	8.68
N5	2.49	4.93	7.52	10.11

By comparing above tables, it is clear, that color difference values from the new color difference algorithm and color difference values from S-CIELAB algorithm are showing the same trend: in the accordance with the image number img1, img2, img3, img4, color difference values are changing in an increasing order, and the trend of data is consistent with each other. The results of objective and subjective evaluations are more correlative, which means that the performance of the algorithm is better. Analysis results of the correlation are shown in Figure 4.

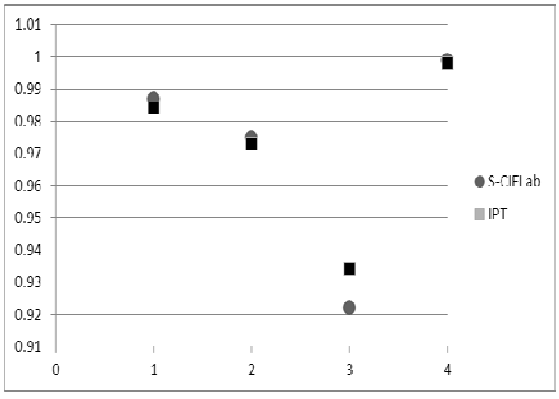

Fig.4 The Correlation Analysis Results of Subjective and Objective

From Figure 4 it can be found that the correlation of the results using two algorithms are basically the same, except for img3 the proposed algorithm performs relative better than that S-CIELAB. The result of color difference algorithm using S-CIELAB is generally larger than the proposed algorithm color difference. Most resulting color differences ΔE calculated by S-CIELAB are larger than 4, in that case, majority of the images are falling in category of "significant sense of difference, the difference is not acceptable", which is contrary to the judgments of subjective scoring. The average scores of subjective evaluation analyzed with visual levels as criteria show that color difference values calculated by the proposed algorithm are relative more consistent with the human visual than S-CIELAB results.

VI. CONCLUSION

The experimental results of the objective evaluation show that the color difference algorithm based on image contents has better results in terms of consistency with perceptual difference with human eyes than the traditional image difference algorithm. The proposed algorithm can be used to evaluate the performance of a number of distorted image processing algorithms, such as JPEG image compression methods, image blur algorithms, gamut mapping algorithms, etc. However, to achieve a better result and a more accurate consistency between the calculated color difference value and the human visual perception, a number of images with different characteristics should also be chosen, and a lot of visual psychophysical experiments should be carried out to establish an effective subjective evaluation data set. In order to establish a more reasonable model of visual image difference, further works will be focused on the improvement of space pre-processing functions based on human vision, and color difference calculation model with image pairs will be constantly adjusted.

ACKNOWLEDGEMENT

This work was supported by National Natural Science Foundation of China (Grant No.61108087), the Program for New Century Excellent Talents in University of State Education Ministry, and Excellent Youth Foundation of Sichuan Scientific Committee (2012jq0017).

REFERENCES

[1] CIE. Colorimetry. 2nd Ed. CIE Publ. No. 15.2. Central Bureau of the CIE: 1986.
[2] CIE. Technical report: Industrial color-difference evalution. CIE Pub. No. 116. Vienna: Central Bureau of the CIE: 1995.
[3] CIE. Technical report: Improvement to Industrial color-difference Evalution. CIE Pub. No. 142-2001. Vienna: Central Bureau of the CIE: 2001.
[4] X. Zhang, B.A. Wandell, A spatial extension to CIELAB for digital color image reproduction, in: Proceedings of the SID Symposiums, vol. 27, 1996, pp. 731–734.
[5] G.M. Johnson and M.D. Fairchild, On Contrast Sensitivity in an Image Difference Model, Proc. of IS&T PICS Conference, 18-23 (2001).

[6] Fairchild, M.D. and Johnson, G.M, The iCAM framework for image appearance, image differences, and image quality, J. of Electronic Imaging, 13, 126-138, 2004.
[7] M.D Fairchild. G.M. Johnson, Image appearance modeling, in: Proc. SPIE/IS& T Electronic Imaging Conference, SPIE, vol. 5007, 2003, pp. 149–160.
[8] F. Ebner, and M.D. Fairchild, “Development and Testing of a Color Space (IPT) with Improved Hue Uniformity,” IS&T/SID 6th Color Imaging Conference, Scottsdale, 8-13 (1998).
[9] G.M. Johnson and M.D. Fairchild, Darwinism of Color Image Difference Models, Proc. of IS&T/SID 9th Color Imaging Conference, 108-112 (2001).
[10] G.M. Johnson and M.D. Fairchild, On Contrast Sensitivity in an Image Difference Model, Proc. of IS&T PICS Conference, 18-23 (2001).
[11] S.Daly, A. B. Watson, Ed., MIT Press,The Visible Differences Predictor: An algorithm for the assesssment of image fidelity, ch. 13 in Digital Images and Human Vision. Cambridge MA(1993).
[12] N. Ponomarenko, V. Lukin, A. Zelensky, K. Egiazarian, M. Carli, F. Battisti, "TID2008 - A Database for Evaluation of Full-Reference Visual Quality Assessment Metrics", Advances of Modern Radioelectronics, Vol. 10, pp. 30-45, 2009.
[13] YU Hui,LIU Zhen. Research of Image Color Difference Model Based on Mixed Chromatic Adaptation Transform[J]. PACKAGING ENGINEERING. 2013,34(3):21-25.
[14] Liu Shi-wei,YU Hui.Image Quality Evaluation Model Based on Hue Angle Algorithem[J]. PACKAGING ENGINEERING. 2012,33(17):941-97.
[15] LIU Hao- xue, H UANG Min, WU Bing, XU Yan- fang. Test of Validity of Color Difference Formulae in Evaluating Color Accuracy of Displayed Images[J]. Journal o f Beijing Institute of Graphic Communication. 2008.16(6):27-40.

Xiangyang Xu He was born in 1979, PhD, lecturer. He received his master degree in Nanjing forestry University (China), during the three years he working hard at gamut mapping. Now he is a teacher in Shenzhen Polytechnic. He is working hard at color management. Since 2012, he is studying for PhD in South China University. He is committed to study the visual image.
E-mail: xxy0906@szpt.edu.cn

Qiao Chen He received his BSc degree in Computer Science and Technology from Southwest Jiaotong University (China) in 2000 and his MSc degree in Colour Imaging from the Colour Imaging Institute at the University of Derby (UK) in 2001 and his PhD degree in colour and imaging science from the University of Leeds (UK) in 2006. Now he is work as an associate professor at School of Media and Communication, Shenzhen Polytechnic (China). His research interests include spectral reflectance modelling, multispectral imaging, human spatial vision and Colour management.

Ziqi Zhao He was born in 1989, Male, Shandong, Master, Qufu Normal University graduate, Main research direction is Multispectral image acquisition system.
E-mail: qsyszzq@163.com

Gang Zhang He was born in 1989, Male, Shandong, Master, Qufu Normal University graduate, Main research direction is color copy based on the spectral.
E-mail: haoyue_95@163.com

Jing Duan He is a Professor in the Computer Science Department of Southwestern University of Finance and Economics, China. He received his Ph.D. from the University of Nottingham, UK. In 2005, he worked as an intern at Xerox Research Centre Europe (XRCE), Grenoble, France. His research interests mainly focus on high dynamic range imaging.

Call for Papers and Special Issues

Aims and Scope.

Journal of Computers (JCP, ISSN 1796-203X) is a scholarly peer-reviewed international scientific journal published monthly for researchers, developers, technical managers, and educators in the computer field. It provide a high profile, leading edge forum for academic researchers, industrial professionals, engineers, consultants, managers, educators and policy makers working in the field to contribute and disseminate innovative new work on all the areas of computers.

JCP invites original, previously unpublished, research, survey and tutorial papers, plus case studies and short research notes, on both applied and theoretical aspects of computers. These areas include, but are not limited to, the following:

- Computer Organizations and Architectures
- Operating Systems, Software Systems, and Communication Protocols
- Real-time Systems, Embedded Systems, and Distributed Systems
- Digital Devices, Computer Components, and Interconnection Networks
- Specification, Design, Prototyping, and Testing Methods and Tools
- Artificial Intelligence, Algorithms, Computational Science
- Performance, Fault Tolerance, Reliability, Security, and Testability
- Case Studies and Experimental and Theoretical Evaluations
- New and Important Applications and Trends

Special Issue Guidelines

Special issues feature specifically aimed and targeted topics of interest contributed by authors responding to a particular Call for Papers or by invitation, edited by guest editor(s). We encourage you to submit proposals for creating special issues in areas that are of interest to the Journal. Preference will be given to proposals that cover some unique aspect of the technology and ones that include subjects that are timely and useful to the readers of the Journal. A Special Issue is typically made of 10 to 15 papers, with each paper 8 to 12 pages of length.

The following information should be included as part of the proposal:

- Proposed title for the Special Issue
- Description of the topic area to be focused upon and justification
- Review process for the selection and rejection of papers.
- Name, contact, position, affiliation, and biography of the Guest Editor(s)
- List of potential reviewers
- Potential authors to the issue
- Tentative time-table for the call for papers and reviews

If a proposal is accepted, the guest editor will be responsible for:

- Preparing the “Call for Papers” to be included on the Journal’s Web site.
- Distribution of the Call for Papers broadly to various mailing lists and sites.
- Getting submissions, arranging review process, making decisions, and carrying out all correspondence with the authors. Authors should be informed the Instructions for Authors.
- Providing us the completed and approved final versions of the papers formatted in the Journal’s style, together with all authors’ contact information.
- Writing a one- or two-page introductory editorial to be published in the Special Issue.

Special Issue for a Conference/Workshop

A special issue for a Conference/Workshop is usually released in association with the committee members of the Conference/Workshop like general chairs and/or program chairs who are appointed as the Guest Editors of the Special Issue. Special Issue for a Conference/Workshop is typically made of 10 to 15 papers, with each paper 8 to 12 pages of length.

Guest Editors are involved in the following steps in guest-editing a Special Issue based on a Conference/Workshop:

- Selecting a Title for the Special Issue, e.g. “Special Issue: Selected Best Papers of XYZ Conference”.
- Sending us a formal “Letter of Intent” for the Special Issue.
- Creating a “Call for Papers” for the Special Issue, posting it on the conference web site, and publicizing it to the conference attendees. Information about the Journal and Academy Publisher can be included in the Call for Papers.
- Establishing criteria for paper selection/rejections. The papers can be nominated based on multiple criteria, e.g. rank in review process plus the evaluation from the Session Chairs and the feedback from the Conference attendees.
- Selecting and inviting submissions, arranging review process, making decisions, and carrying out all correspondence with the authors. Authors should be informed the Author Instructions. Usually, the Proceedings manuscripts should be expanded and enhanced.
- Providing us the completed and approved final versions of the papers formatted in the Journal’s style, together with all authors’ contact information.
- Writing a one- or two-page introductory editorial to be published in the Special Issue.

More information is available on the web site at http://www.academypublisher.com/jcp/.

(Contents Continued from Back Cover)

Design of Wind-solar Complementary Power System Based on Progressive Fuzzy Control 1378
Ning Chen, Xiao Qu, Weibing Weng, and Xing Xu

Adaptive Control based Particle Swarm Optimization and Chebyshev Neural Network for Chaotic Systems 1385
Zhen Hong, Xile Li, and Bo Chen

Relay Node Scheduling Model Based on Improved Discrete Markov Chain 1391
Chaoyi Zhang, Yandong Zhao, and Junguo Zhang

Multiplexing Periodic CSI with HARQ-ACK on PUCCH Format 3 in LTE-A 1397
Dan Wang, Xuemei Deng, Xiaowen Li, and Xin Ni

Restricted Nussbaum Gain Control Method and Its Application in One Order System 1402
Jinyong Yu, Junwei Lei, Yuqiang Jin, and Hongchao Zhao

Chinese Sentiment Analysis Using Appraiser-Degree-Negation Combinations and PSO 1410
Wen Xiong, Yaohong Jin, and Zhiying Liu

Image Denoising via Robust Simultaneous Sparse Coding 1418
Lei Li, Jiangming Kan, and Wenbin Li

DDoS: Flood vs. Shrew 1426
Zhijun Wu, Guang Li, Meng Yue, and Hualong Zeng

A Dynamic Load-balancing Scheme for XPath Queries Parallelization in Shared Memory Multi-core Systems 1436
Xiaocheng Huang, Xujie Si, Xiaojie Yuan, and Chao Wang

Research on Template Computing Mode of Remote Sensing Image Based on Partition Model 1446
Gen-yuan Du, De-lan Xiong, and Huo-lin Zhang

A Novel Sink Mobility Off-line Algorithm for Avoiding Energy Hole in Wireless Sensor Network 1454
Qing-hua Li, Qiao-ming Pan, and Fu-ping Xie

A Robust and Efficient Evolutionary Algorithm based on Probabilistic Model 1462
Caichang Ding and Wenxiu Peng

Tasks Distribution Strategy based on Cluster in MWfSCC 1470
Xiuguo Wu

A P2P Traffic Management Model Based on an ISP Game 1478
Chunzhi Wang, Shuping Wang, Hui Xu, and Hongwei Chen

Study of Scraping Guide Ways Inspection 1484
Ching Wei Wu, Ying Shing Shiao, and Ching Feng Chang

Stereo Matching Using Iterative Dynamic Programming Based on Color Segmentation of Images 1491
Fuzhi Wang, Changlin Song, and Qiang Du

A SVD Feature based Watermarking Algorithm for Gray-level Image Watermark 1497
Wei Wang, Wenhui Li, Yongkui Liu, and Borut Žalik

Object Tracking via Tensor Kernel Space Projection 1503
Jiashu Dai, Tingquan Deng, Tianzhen Dong, and Kejia Yi

A Research of Image Difference Algorithm Based on the Correlation of Color Attributes 1511
Xiangyang Xu, Qiao Chen, Ziqi Zhao, Gang Zhang, and Jiang Duan